ERDC/ITL TR-11-1

Information Technology Laboratory

US Army Corps of Engineers®
Engineer Research and Development Center

Navigation Systems Research Program

Dynamic Structural Flexible-Beam Response to a Moving Barge Train Impact Force Time-History Using Impact_Beam

Robert M. Ebeling, Abdul N. Mohamed, Jose R. Arroyo,
Barry C. White, Ralph W. Strom, and Bruce C. Barker

August 2011

Winfield Full-Scale Impact Tests

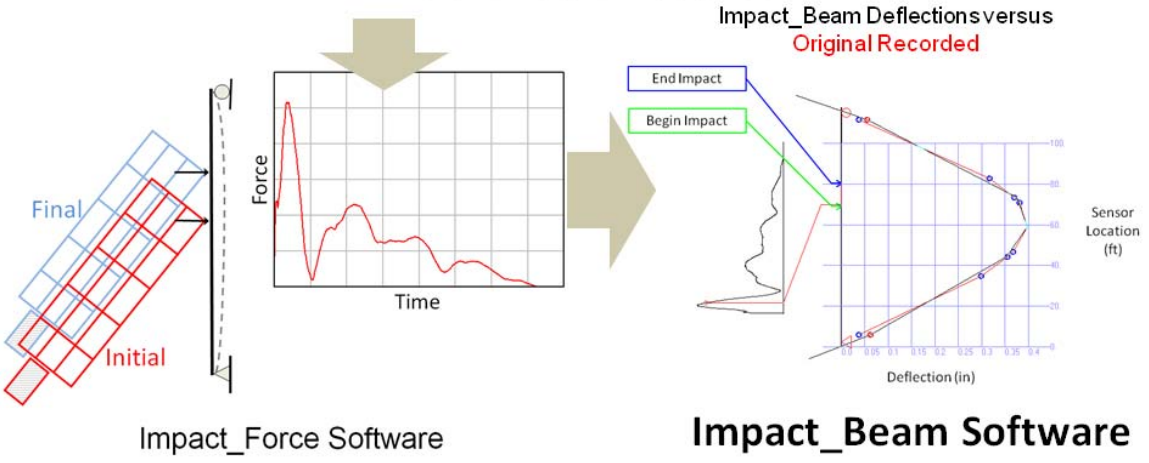

Impact_Force Software

Impact_Beam Software

Report Documentation Page

Form Approved
OMB No. 0704-0188

1. REPORT DATE	2. REPORT TYPE	3. DATES COVERED
AUG 2011		

4. TITLE AND SUBTITLE	5a. CONTRACT NUMBER
Dynamic Structural Flexible-Beam Response To A Moving Barge Train Impact Force Time-History Using Impact_Beam	5b. GRANT NUMBER
	5c. PROGRAM ELEMENT NUMBER
6. AUTHOR(S)	5d. PROJECT NUMBER
	5e. TASK NUMBER
	5f. WORK UNIT NUMBER
7. PERFORMING ORGANIZATION NAME(S) AND ADDRESS(ES) **U.S. Army Engineer Research and Development Center,Information Technology Laboratory,3909 Halls Ferry Road,Vicksburg,MS,39180**	8. PERFORMING ORGANIZATION REPORT NUMBER
9. SPONSORING/MONITORING AGENCY NAME(S) AND ADDRESS(ES)	10. SPONSOR/MONITOR'S ACRONYM(S)
	11. SPONSOR/MONITOR'S REPORT NUMBER(S)

12. DISTRIBUTION/AVAILABILITY STATEMENT
Approved for public release; distribution unlimited.

13. SUPPLEMENTARY NOTES
The original document contains color images.

14. ABSTRACT

15. SUBJECT TERMS

16. SECURITY CLASSIFICATION OF:			17. LIMITATION OF ABSTRACT	18. NUMBER OF PAGES	19a. NAME OF RESPONSIBLE PERSON
a. REPORT	b. ABSTRACT	c. THIS PAGE			
unclassified	**unclassified**	**unclassified**		**302**	

ERDC/ITL TR-11-1
August 2011

Dynamic Structural Flexible-Beam Response to a Moving Barge Train Impact Force Time-History Using Impact_Beam

Robert M. Ebeling, Abdul N. Mohamed, Jose R. Arroyo, Barry C. White, Ralph W. Strom, and Bruce C. Barker

Information Technology Laboratory
U.S. Army Engineer Research and Development Center
3909 Halls Ferry Road
Vicksburg, MS 39180-6199

Final report

Prepared for U.S. Army Corps of Engineers
441 G. Street, NW
Washington, DC 20314-1000

Under Work Unit G99180

Abstract: To design simply-supported, flexible impact beams spanning between cells or bents for lock approach walls, a dynamic structural analysis of the beam under impact time-history loads for design- specific barge trains is required. At several locks, this flexible structural feature is the primary structural member resisting the glancing-blow impact event of a barge train as it aligns itself with a lock. This technical report describes an engineering methodology used to conduct this dynamic structural analysis and visualize the resulting deflections, moments, and shears. This engineering methodology is implemented with a PC-based FORTRAN program and visual modeler named Impact_Beam. The engineering formulation for Impact_Beam uses time-history force data that are scaled for design specific barge trains to perform a dynamic structural response analysis for either a single degree of freedom system or a modal time-history analysis for the simply supported beam subjected to a impact load that is travelling along the beam. Time-history force data has been collected from the interpretation of the results from the 1997 full-scale barge train impact prototype experiments conducted at Old Lock and Dam 2 just north of Pittsburgh, PA, and of the 2008 full-scale barge train impact experiments conducted at Winfield Lock and Dam, Winfield, WV. This database of pulse time-history can be scaled for site specific design barge trains with approach angle and velocity using the companion software Impact_Force. It is also possible to use force time-histories from other impact simulation software (e.g., dBEAS). The engineering formulation for Impact_Beam is verified against the original Winfield experiments using modal time-history analysis and dBEAS simulations using single degree of freedom analysis.

Contents

Figures and Tables

Figures

Tables

Preface

This technical report describes an engineering methodology for the dynamic response analysis of a simply supported, flexible impact beam to barge train impact loading. This engineering methodology is implemented in a PC-based FORTRAN program and Visual Modeler named Impact_Beam, which is also discussed in this report. The engineering formulation for Impact_Beam uses an impact force time-history acting on the flexible impact beam to characterize the impact event. This impact force time-history may be obtained using a companion program Impact_Force (Ebeling, et al. 2010). Included in this effort is the interpretation of the results from the 2008 full-scale impact experiments conducted on a flexible approach wall at Winfield Lock and Dam, Winfield, WV.

The investigation reported herein was authorized by the Headquarters, U.S. Army Corps of Engineers and was performed during the period of October 2009 to September 2011 under the Navigation Systems Research Program. The research was performed under Work Unit G99180, entitled "Vessel/Barge Impact". Jim Walker is the HQUSACE Navigation Business Line Manager.

The Program Manager for the Navigation Systems Research Program is Charles Wiggins in the Coastal and Hydraulics Laboratory (CHL), U.S. Army Engineer Research and Development Center (ERDC). Dr. John Hite, CHL, was the Inland Focus Area Leader. Jeff Lillycrop is the Technical Director for Navigation in CHL. The research is being led by Dr. Robert M. Ebeling of the Information Technology Laboratory under the general supervision of Dr. Reed L. Mosher, Director ITL: Dr. Deborah F. Dent, Deputy Director ITL; Dr. Robert M. Wallace, Chief of the Engineering and Informatic Systems Division, ITL. Dr. Ebeling is the Principal Investigator of the Navigation Systems "Vessel/Barge Impact" work unit under which this research was performed.

This report was authored by Dr. Ebeling, Abdul N. Mohamed and Barry C. White of ITL, Professor Jose R. Arroyo of the University of Puerto Rico Mayaguez, Ralph W. Strom, consultant, and Bruce C. Barker of ITL. White is in the Computational Analysis Branch, ITL. Mohamed is in the Data Analysis and Assessment Branch, ITL. Impact_Beam PC-based software

development and Winfield full-scale impact data interpretation were made by Dr. Ebeling, Mohamed, Professor Arroyo, Strom and White. Bruce C. Barker, Branch Chief of the Sensor Measurement and Instrumentation Branch, ITL, collected the 2008 Winfield Lock approach wall full-scale impact experiment data and beam response data discussed in this report.

COL Kevin J. Wilson was Commander and Executive Director of ERDC. Dr. Jeffery P. Holland was Director.

Unit Conversion Factors

Multiply	By	To Obtain
feet	0.3048	meters
pounds (force) per square inch	6.894757	kilopascals
pounds (mass) per cubic inch	2.757990 E+04	kilograms per cubic meter
tons (2,000 pounds, mass)	907.1847	kilograms

1 Dynamic Structural Time-History Response Analysis of a Simply Supported, Flexible Approach Wall Beam During Barge Train Impact

1.1 Introduction - glancing impact blows and flexible approach wall structural systems

A glancing blow impact event of a barge train impacting an approach wall as it aligns itself with a lock is an event of short duration; the contact time between the impact corner of the barge train and the approach wall can be as short as a second or as long as several seconds. In order to reduce construction costs as well as to reduce damage to barges during glancing blow impacts with lock approach walls, the next generation of Corps approach walls are more flexible than the massive, stiff-to-rigid structures constructed in the past. A flexible approach wall or flexible approach wall system is one in which the wall has the capacity to absorb impact energy by deflecting or "flexing" during impact, thereby affecting the dynamic impact forces developing during the impact event. This report summarizes an engineering methodology and corresponding software for performing a dynamic structural response analysis of a simply supported, flexible impact beam to a barge impact event. The results of the analysis are used to size and to design the structural member. A comparison to an equivalent static loading is included so as to gage the level of dynamic behavior occurring during the impact event.

1.2 Examples of the next generation flexible approach walls

Examples of this next generation of Corps flexible approach walls are shown in Figures 1.1 through 1.9 for the three locks at Marmet, London and Winfield (courtesy of Huntington District).

Marmet Lock: The Marmet Locks and Dam are located about 68 miles above the mouth of the Kanawha River at Marmet, W.V. The twin locks, built in 1934, measured 56 feet by 360 feet. The addition of the new, larger lock, adjacent to the existing lock, will accommodate the increased traffic at Marmet. The new upstream guide wall is straight, approximately 1,600 feet long, and has conventional steel wall armor (left wall in Figure 1.1 plan

view). The Figure 1.2 wall consists of 14 drilled shaft piers, spaced at 105 feet on center, and a concrete-filled nose cell (not shown). This substructure supports 15 post-tensioned concrete box beams. Each pier is constructed of two drilled shafts with cast-in-place concrete cap beams to support the precast concrete wall beams. Refer to Figures 1.1 through 1.4. A thrust block (Figure 1.1) is provided at the cap beam to transfer the barge impact from the beam into the shafts and nose cell. The hollow, rectangular beams have an outside dimension of 10 feet by 10 feet. The weight of each of the precast beams is approximately 500 tons. The new upstream approach guard wall is also straight, approximately 950 feet long, and has conventional steel wall armor (right wall in Figure 1.1 plan view). The wall consists of seven piers spaced at 122 feet on center, concrete-filled nose cell. This substructure supports 8 post-tensioned concrete box beams. These beams are shown in Figure 1.3 during transport to the site. Figure 1.4 shows the placement of one of these beams. Each pier is a concrete-filled sheet pile cell, approximately 31 feet in diameter. The hollow, rectangular beams have an outside dimension of 10 feet wide by 8 feet deep.

London Lock: The structure consists of five concrete-filled sheet-pile cells spaced at 32 m (105-ft) center to center and a concrete-filled sheet-pile nose cell, which support five precast concrete beams. An example of this flexible impact beam is shown in Figures 1.5 during placement and in Figure 1.6

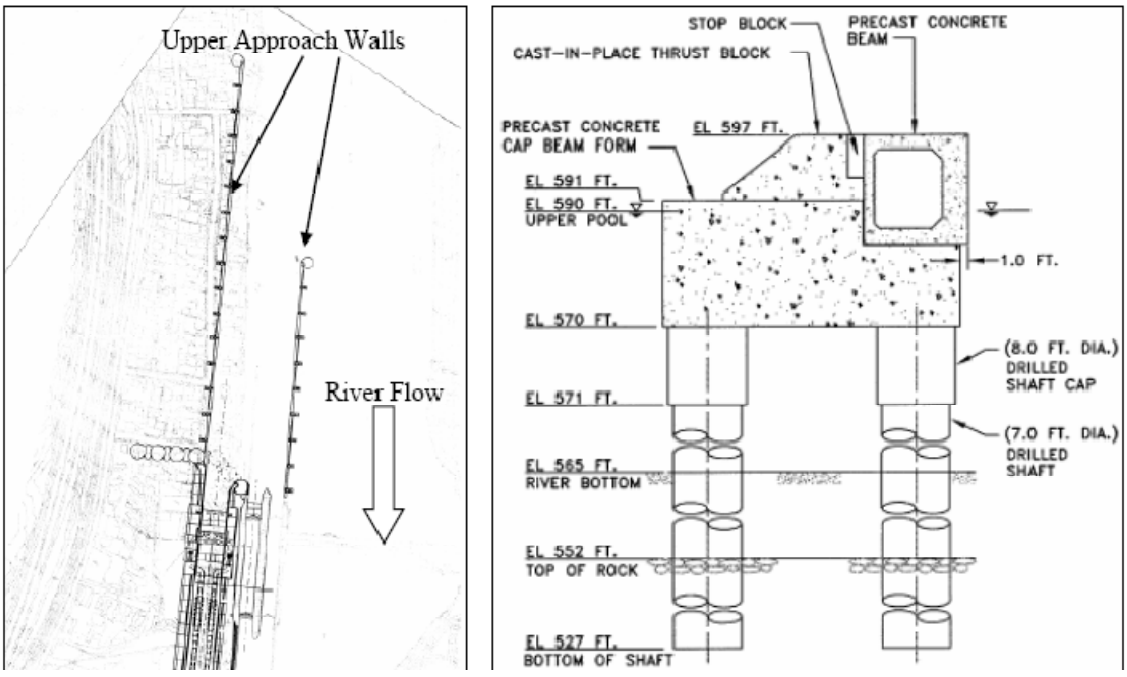

Figure 1.1 Marmet Flexible Upper Approach Walls (courtesy of Huntington District)

Figure 1.2 Marmet Lock Upper Guide Wall Intermediate Piers during construction (courtesy of Huntington District)

Figure 1.3 Transporting the Post-tensioned Beams to Marmet Lock (courtesy of Huntington District)

Figure 1.4 Lifting and setting the Marmet approach wall beams (courtesy of Huntington District)

Figure 1.5 Lifting the Post-tensioned Beams at London Lock (courtesy of Huntington District)

Figure 1.6 Transporting the Post-tensioned Beams to London Lock (courtesy of Huntington District)

Figure 1.7 Winfield Lock Approach Wall Beam at Placement (courtesy of Huntington District)

Figure 1.8 End view of the match-cast guide wall box beams at the fabrication yard (courtesy of Huntington District)

Figure 1.9 Side view of one of three match-cast guide wall box beams at the fabrication yard (courtesy of Huntington District)

during transport. The London Locks and Dam upstream guard wall is on the Kanawha River at London, West Virginia. Each sheet-pile cell is constructed with a thrust block to transfer the barge impact from the beam into the cell. The hollow, rectangular precast wall beams are each 105 ft long, and have an outside dimension of 10 ft by 8 ft high. The weight of each of the precast concrete beams is approximately 340 tons.

Winfield Lock Guard Wall: Figure 1.7 shows a flexible Winfield Approach (Guard) wall precast concrete beam during placement. Each approximately 112 feet long, 10 feet by 10 feet hollow beam was match cast in three segments and then post-tensioned to form one beam. They are hollow to save weight and cost and to allow them to be inspected.

Winfield Lock Guide Wall: The 10 feet wide by 8 feet deep hollow post-tensioned concrete box beams used to form the Guide wall in the approach area to the old lock are approximately 118' long. Figures 1.8 and 1.9 shows end and side views at the casting yard. The top is 1'-3" thick, the bottom is 1'-3" thick, the impact face is 2'-6" thick and the back face is 1'-0" thick. The beams were match-cast in 3 sections then were post-tensioned using

10 tendons, each being jacked to 192.7 ksi and seated at 188.2 ksi after seating losses. The beams rest on concrete filled sheet pile cells and thrust blocks. The beams bear on two (2) - 1'-6" x 2'-4" x 2" thick bearing pads on either end. The beams are tied back to the thrust block using (2) 1 3/8" diameter threadbar on each end. The threadbar are installed inside grease filled conduits cast into the thrust block and beams. The threadbar are not tensioned, only snugged hand tight. The impact is transferred into the thrust block through one (1) 1'-4" x 3'-6" x 2" thick bearing pad at each end of the beam. All bearing pads have a durometer hardness of 50+/- and all concrete is 5000 psi at 28 days.

1.3 Static versus dynamic loading for approach wall impacts

A static or quasi-static load is one that is applied in such a way that the impulse of the load can be modeled as a single force acting in equilibrium with the resisting force of the simply supported impact beam, and therefore the velocity of the structure is constant. A problem becomes dynamic when the inertial forces (d'Alembert forces) of the structure vary rapidly and significantly. As such, the load is not in equilibrium with the resisting forces when the maximum deflection of the body mass is reached. An instantly applied load for an elastic response under ideal conditions will produce twice the stress and deformation demands of a statically applied load. This aspect of dynamic behavior is commonly demonstrated in books on structural dynamics by equating external work to internal strain energy (e.g., Chopra, 1995).

Barge impact testing (e.g., interpretation presented for the 2008 Winfield test results in Appendix A and for the 1997 Pittsburgh Prototype test results in Appendix B of Ebeling, et al., 2010) indicates the collision of a barge train with an approach wall can be represented as a short duration pulse. It suggests that the amount of external work done by the pulse over the approach wall can be greater than that it would experience if the same external work is applied in a zero velocity (i.e. static loading) environment, producing higher internal strain energy in the approach wall. The engineering methodology and supporting Impact_Beam PC-based software described herein is intended to capture this aspect of dynamic behavior. An impact factor is used to represent the ratio of the deformation from a load applied dynamically divided by the deformation occurring as a result of a load applied statically. With the internal restoring force being proportional to the displacement by the structural stiffness for elastic beams, this ratio also reflects the ratio of dynamic to static internal structural restoring

forces. A noteworthy observation is that in the Chapter 4 study by Chopra (1995) of the dynamic response of linear elastic, single-degree-of-freedom (SDOF) systems subjected to various types of pulse excitations, the displacement (and thus the internal structural restoring force) experienced by the SDOF system can be up to, but not exceed, twice that it would experience if the load were applied statically (i.e., a maximum impact load factor of two, as shown in Chopra's Equation 4.3.4). For the generalized single-degree-of-freedom system used for the mathematical model of the impact beam of the approach wall (discussed in Chapter 2), this also infers an upper bound of two for the ratio of dynamic-to-static deformations (and for the ratio of dynamic-to-static internal restoring forces) for a linear elastic flexible impact beam. This is an integral part of the time-history modal response procedure of analysis.

A glancing blow impact event of a barge train impacting an approach wall as it aligns itself with a lock is an event of less than 4 seconds (see Table A.1 in Ebeling, et al., 2010); the contact time between the impact corner of the barge train and the approach wall can be as short as a second or as long as several seconds. For the 1997 Pittsburgh Prototype field test data of Patev, Barker and Koestler (2003b), and Ebeling, White, Mohamed and Barker (2010) found that for the eighteen impact tests of interest the duration of contact during impact by the 2-by-2 barge train with the stiff-to-rigid wall at Old Lock and Dam 2 (just north of Pittsburgh, PA) to have a mean impact time of 3.05 seconds with a standard deviation of 0.34 seconds (coefficient of variation, COV, of 0.11). The 2008 impact tests at the flexible Guide wall of Winfield provides additional time of impact data.

When an impact event occurs, the flexible beam starts from an at-rest position of zero displacement. As the impact event progresses the beam's deflection changes with time, thereby creating a velocity within the beam. Since the displacement of the beam will not be constant with time of impact, neither will the beam's velocity be a constant with time. Consequently, with the velocity of the flexible impact beam varying with time, the beam will accelerate and decelerate during its translatory motion during and after the impact event concludes, exhibiting a free vibration behavior.

1.4 Overview of dynamic time-history response analysis of a flexible, simply supported beam

Due to the flexibility and the mass of the new generation flexible approach walls, the impact event can be a dynamic event from the point of view of the

mathematical structural model.[1] In structural dynamics the mathematical model of bodies of finite dimensions undergoing translatory motion are governed by Newton's Second Law of Motion, expressed as

$$\sum F = m \bullet a \tag{1.1}$$

at each time step t during motion. In the mathematical model, the forces acting on the flexible wall mass at each time step t include (1) the impact force at time step t, (2) the elastic restoring forces (of the beam), and (3) the damping forces (of the beam). This report discusses an engineering methodology that uses Equation 1.1 to compute the dynamic structural response of the mass of the Figure 1.10 simply supported, flexible impact beam mathematical model to the impact force time history (impact applied at a fixed position along the beam). The impact event is idealized as shown in Figure 1.11 for the mathematical beam and impact event model as the force time history $F_{normal\text{-}wall}(t)$ by creating a synthetic time history or by scaling of existing pulse force time-histories recorded during the full-scale barge impact experiments conducted at Winfield Lock & Dam (Barker, et al., 2010) and the Pittsburgh Prototype tests (Patev, et al., 2003b). The Figure 1.11 force time history denotes the component of the pulse force time history acting normal to the wall.[2] Initial barge train contact with the wall starts at time t_1 and ends at time t_2. The solution to this dynamic problem will be a succession of solutions at user specified time steps starting at time t_1. These solution time steps are dictated by the time step the user selects for the barge train impact force time history, created using the PC-based software Impact_Force (Ebeling, White, Mohamed and Barker, 2010). Due to the nature of dynamic structural response of some types of beams[3] with consideration of both the duration and frequency characteristics of the impact force time history, the peak response of the simply supported, flexible impact beam may occur during impact (i.e., between times t_1 and t_2) or after impact concluded (i.e., after time t_2). The engineering methodology discussed in this report and corresponding software is capable of addressing both types of dynamic structural systems responses.

---

[1] As observed by Paz (1985, page 10), a mathematical model is the symbolic designation for the substitute idealized system that includes all key structural features, characteristics, boundary conditions and assumptions imposed on the physical system.

[2] The solid arrow in Figure 1.10 represents the impact pulse force time history acting on the beam while the dashed arrow represents the impact pulse force time history acting on the impact corner of the barge; equal and opposite forces.

[3] The structural (beam) characteristic used to determine when peak structural response occurs is the natural period of the simply supported impact beam and is discussed in Chapter 2.

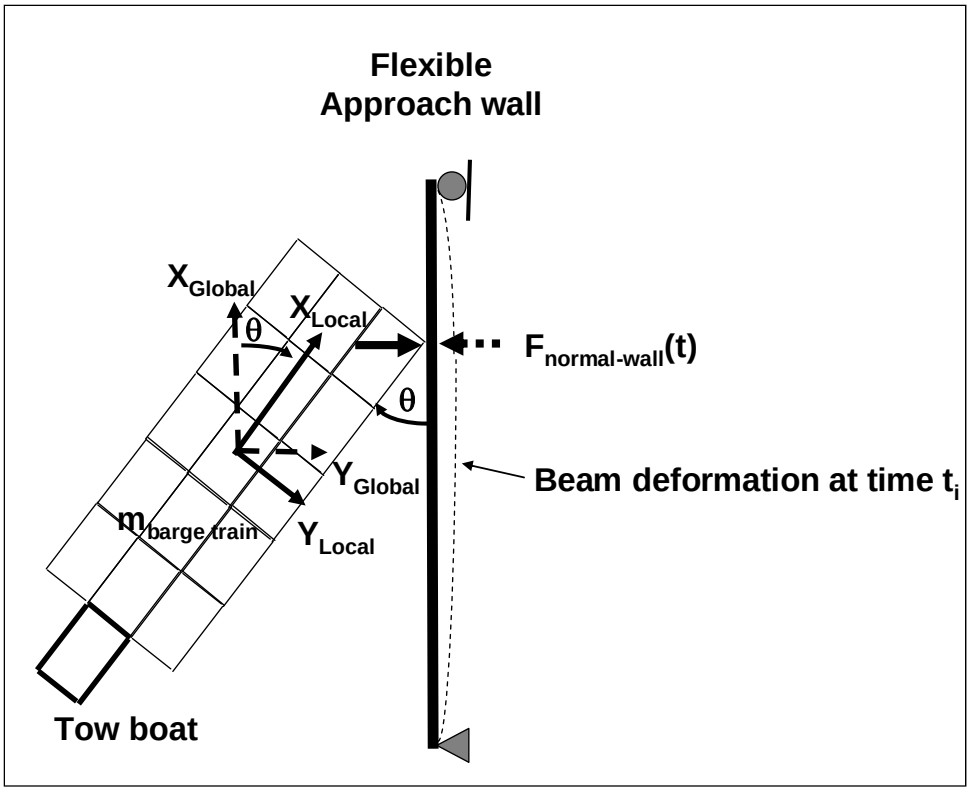

Figure 1.10. Barge train impacting at a fixed impact position along the simply supported, flexible impact beam mathematical model with the barge train oriented at an approach angle θ to the wall's X_{Global} axis (plan view)

An alternative formulation incorporated within the PC-based program Impact_Beam allows for the specification of a barge train having an initial contact with the impact beam at position designated X_Impact (in PC-program Impact_Beam input terminology) at time t_1 and moving in contact at a constant velocity V along the beam as shown in Figure 1.12.[1] The position of the impact point force moves with time after contact. Time after contact is designated as an increment in time, Δt_i , and occurs at an absolute time of $[t_1 + \Delta t_i]$. The change in position of the contact force is designated a distance ΔX from initial contact point X_Impact and is given by

$$\Delta X = V \bullet \Delta t_i \tag{1.2}$$

The position of the point load along the beam at time t_i is

$$[x_{\text{point load}}]_{t_i} = X\_\text{Impact} + \Delta X \tag{1.3}$$

[1] The Velocity, V, of the barge train in the direction of the X_{Global} axis is along the line of the beam and it's user provided value to PC-program Impact_Beam is designated as X_Impact_velocity.

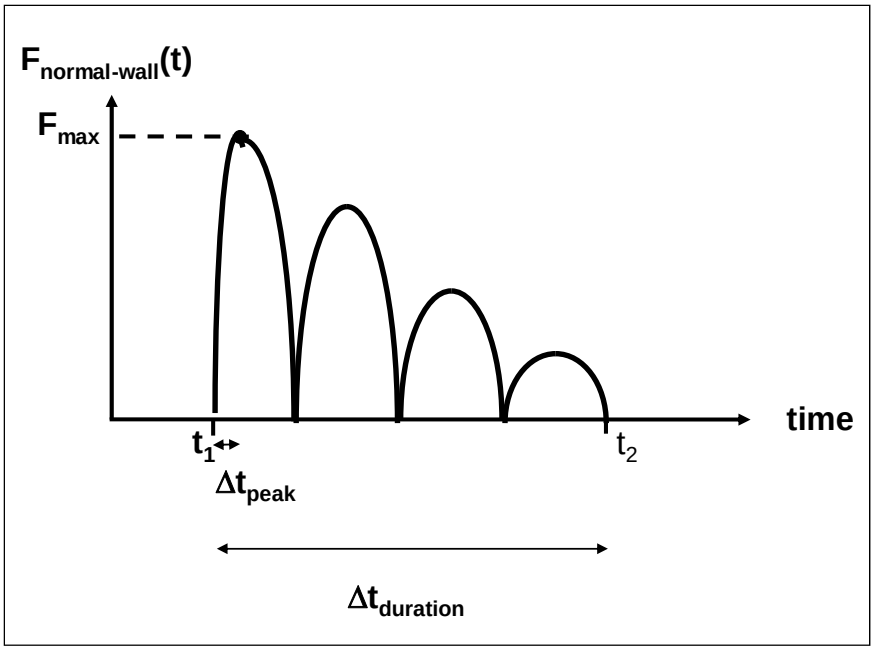

a) Idealized synthetic pulse force time history

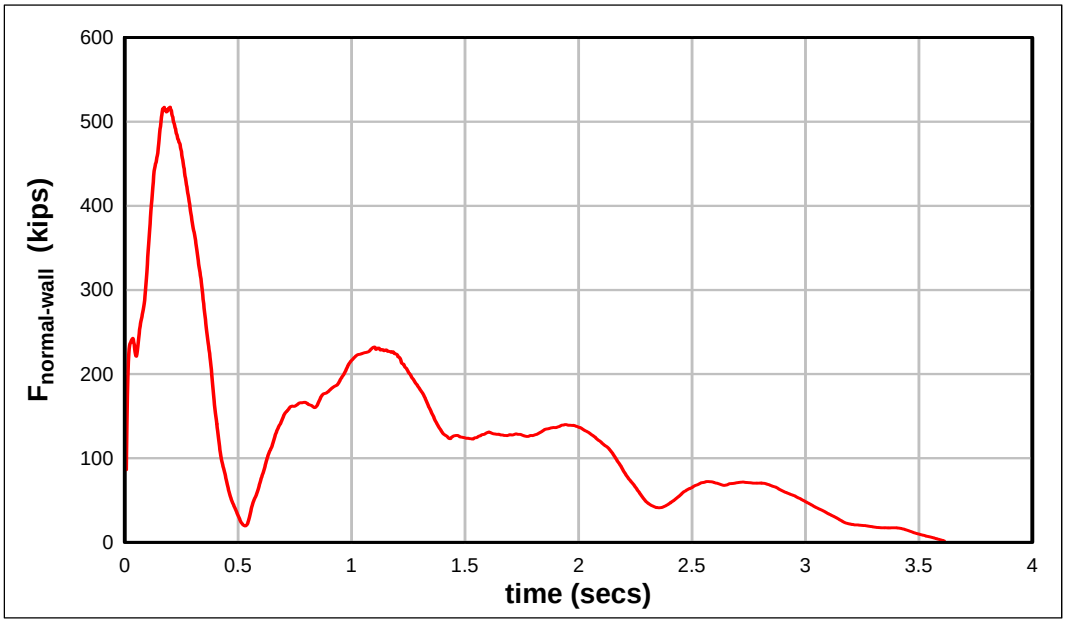

b) Scaling of an existing pulse force time history recorded at the full-scale impact experiment conducted at Winfield Lock & Dam by Barker, et al. (2010)

Figure 1.11 Idealized Examples of an impact pulse force time history created using Impact_Force

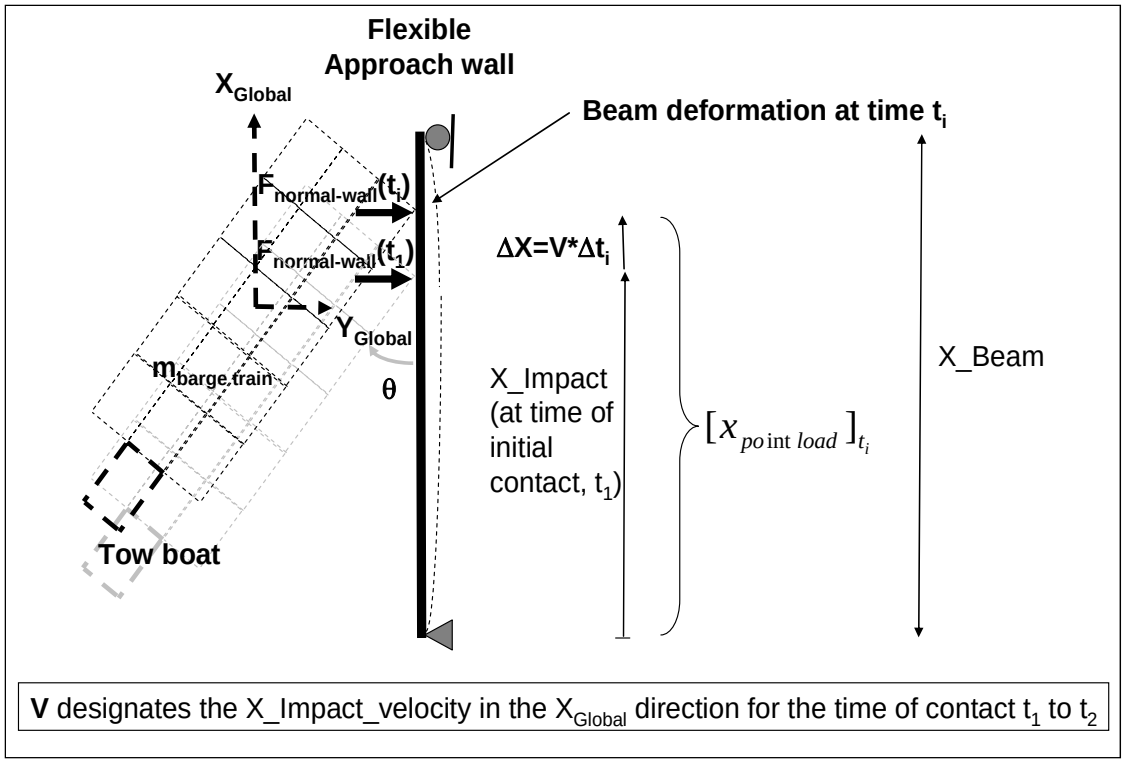

Figure 1.12Barge impact point force moving along the wall from initial contact time t_1 to final contact time t_2

Introducing Equation 1.2, Equation 1.3 becomes

$$[x_{\text{point load}}]_{t_i} = [X\_\text{Impact} + V \bullet \Delta t_i] \tag{1.4}$$

Thus, the Figure 1.11b normal force time history moves along the beam from time t_1 to time t_2 according the user specified velocity V.

1.5 Dynamics of a distributed-mass and –stiffness system of a simply supported beam; an infinite-degree-of-freedom system

Considering the long spans and distribution of mass and stiffness along the length of this one category of flexible impact beam, i.e., the simply supported, flexible impact beam[1], an infinite-degree-of-freedom system mathematical model is used to compute its transverse vibration. The mathematical model of a beam of this type has an infinite number of degrees of freedom because its mass is evenly distributed.

[1] Simply supported impact beams are used at Marmet, London and Winfield Locks to name a few.

1.6 Impact factors

Because it is a dynamic event the structural response of approach wall mass at every time step t to the impact load imparted (at each time step t) to the flexible wall mass is not the same as if the force at each time step is applied statically (i.e., with acceleration equal to zero in Equation 1.1).[1] Therefore, included within the response computations of the infinite-degree-of-freedom system (infinite-DOF system) engineering methodology for the impact beam is the computation of;

- a Displacement Impact Factor (DIF), defined as the ratio of the deflection during dynamic vibration divided by its static deflection,
- a Moment Impact Factor (MIF), defined as the ratio of the internal moment during dynamic vibration divided by the static internal moment, and
- a Shear Force Impact Factor (SFIF), defined as the ratio of the shear force during dynamic vibration divided by its static shear force.

These ratios reflect the level of dynamic amplification (or attenuation) during dynamic response of the mass of the flexible impact beam. This factor gives the engineer a sense of the level of dynamic response taking place within the beam's mass during its vibration resulting from the impact by the barge train.

1.7 Report contents

This engineering methodology is implemented in a PC-based FORTRAN program and Visual Modeler named Impact_Beam, which is also discussed in this report. A pulse force time history (normal to the flexible approach wall) is used in this dynamic time-history response analysis to represent the demand made of the simply supported, flexible beam mass during the impact event. The impact force time history to be used in the Impact_Beam analysis is created by the companion PC-based program Impact_Force (Ebeling, White, Mohamed and Barker, 2010). The engineering formulation for Impact_Force uses the impulse momentum principle to convert the linear momentum of a barge train into a pulse force time history acting normal to the approach wall.

[1] As observed by Clough and Penzien (1993, page 4), because the loading is not applied slowly, noteworthy inertial forces result from the structural time-varying displacements of the (distributed) mass of the Figure 1.8 flexible beam which in turn are influenced by the magnitude of inertial forces; it's a closed cycle of cause and effect.

The engineering formulation developed for and implemented in Impact_Beam assumes that the District engineer will have knowledge of

1. the length, modulus of elasticity, moment of inertia and mass per unit length (equal to the weight per unit length divided by the gravitational constant) (including hydrodynamic added mass for the beam) of the simply supported, flexible impact beam ,
2. the point of initial impact,
3. the velocity, V, the barge train moves along the approach wall during impact (distributed – mass and –stiffness system of a simply supported beam case) , and
4. the impact pulse force time history normal to the impact beam.

The engineering formulation developed for Impact_Force assumes that the District engineer will have knowledge of

1. the size, the weight (and mass) of the barge train (including hydrodynamic added mass),
2. the barge approach velocity (often expressed in local barge coordinates), and
3. approach angle (the angle measured from the face of the wall to the side of the barge train).

This information will be required for the usual, unusual and extreme design load cases.

Chapter 2 describes the relationships that comprise the engineering formulation used to solve Newton's Second Law of Motion for the dynamic response of a simply supported, flexible impact beam subjected to a pulse force time-history used to represent the impact at the point of contact between the barge train and the flexible approach wall. Because the mass of the beam is distributed continuously along its length, the displacements and acceleration will be defined for each point along the axis of the Figure 1.10 simply supported, flexible impact beam.[1] In this initial engineering formulation implemented in Impact_Beam, the numerical solution of the Newton's Second Law of Motion for the impact pulse force time history

[1] An alternative formulation used in structural dynamics is to create a mathematical model of the Figure 1.8 impact beam in which the continuous mass of the beam is concentrated at discrete points with the displacements and accelerations determined at these discrete locations during the course of the dynamic analysis; commonly referred to as a lumped-mass model.

applied to the simply supported, flexible impact beam makes use of Duhamel's Integral. This formulation (evaluated using numerical methods) makes use of the superposition principle and as such, is restricted to linear systems. Note: Future enhancements to be proposed for Impact_Beam include an upgrade to nonlinear structural response during extreme impacts, at which time the numerical solution of Newton's Second Law of Motion would be changed.

Chapter 3 summarizes the computation of transverse beam displacements, shears and internal moments to a long, simply supported, flexible impact beam due to static point loading. Computed results for these three beam response parameters, compared to computations made using the Chapter 2 structural dynamic response formulation provide insights into if dynamic amplification occurs for the flexible impact beam being analyzed. Dynamic to static responses expressed in terms of "Impact Factors" are also presented in this chapter.

Chapter 4 will present an overview of the Visual Modeler Graphical User Interface (GUI) for Impact_Beam. The Impact_Beam Visual Modeler is capable of creating two types of input data files: 1) Input data file for a Dynamic Response Analysis of a Simply Supported Beam and 2) Input data file for a Dynamic response analysis of a Single Degree of Freedom system. For the Dynamic Response Analysis, the Impact_Beam Visual Modeler has the capability to perform two types of plots; 1) Individual Sensor Plot and 2) Animated Beam Response. The Input for the Impact_Beam Visual Modeler force time history comes from the Impact_Force Visual Modeler.

Chapter 5 will present some numerical examples based on the elastic simply supported beam used during Winfield experiments and some examples based on a SDOF system. The first numerical example is the comparison of the results of a simply supported beam subjected to a non-moving dynamic load based on Impact_Beam and SAP2000. This example provides the validation for Impact_Beam. Then, this chapter discusses the interpretation of the structural response of the Winfield flexible guide wall impact beam for Winfield Experiment Test # 10. Comparisons are made in this chapter between the results computed for these impact events using PC-program Impact_Force and the corresponding data recorded during the impact events. The Impact_Beam software is used to estimate the dynamic modulus of elasticity of the simply supported beam used during

Winfield Experiments. The SDOF numerical examples presented in Chapter 5 are the following; 1) a SDOF model obtained from Paz (1985); 2) a numerical example of a SDOF model of Winfield experiment for Test # 10; 3) a numerical example of a SDOF model of Winfield experiment for Test # 10 using a bilinear stiffness but assigning the same stiffness for each section of the force-displacement relationship; 4) a numerical example of a SDOF model of Winfield Experiment for Test # 10 for a linear stiffness model calculated using the average total deflection of the beam between sensor LD3 and LD4; 5) a set of examples presented to compare the results obtained with the computer program dBEAS and Impact_Beam. Force time histories generated by dBEAS were used as the input forcing function of Impact_Beam and the responses of both systems (dBEAS – 2DOF and Impact_Beam – SDOF) were compared. These comparisons were made changing the damping ratio of the base isolators under the dBEAS and the approach velocity of the barge train.

Chapter 6 presents the results of the analysis done to the Winfield simply supported elastic beam using Impact_Beam to estimate the dynamic modulus of elasticity. The results presented in this chapter follow the same procedure done in Chapter 5 for Winfield Experiment Test # 10.

Chapter 7 presents the conclusions of this report based on the Impact_Beam computer software.

Appendix A summarizes the traditional single-degree-of-freedom system response in free vibration.

Appendix B summarizes the application of Duhamel's Integral to calculate the displacement response of a single degree of freedom system. In addition, an alternate or explicit solution of the Duhamel's integral is presented as an additional formulation to determine the response of a SDOF system subjected to initial conditions and an arbitrary dynamic load. Finally, this appendix presents the modification of the equation of motion of underdamped SDOF systems that exhibits a spring bilinear force-displacement relationship. The equation of motion results the same as if the spring is linear but with a change in the dynamic load.

Appendix C summarizes the numerical procedure used to solve for the dynamic response (displacement and velocity) using Duhamel's Integral applied to a generalized SDOF system model.

Appendix D describes the ASCII input data file to the PC-based FORTRAN program Impact_Beam which performs a dynamic structural response evaluation of the simply supported, flexible impact beam of distributed mass. This ASCII input data file (Impact_Beam.IN) is created by a Visual Modeler.

Appendix E describes the ASCII output file of the PC-based FORTRAN program Impact_Beam which performs a dynamic structural response evaluation of the simply supported, flexible impact beam of distributed mass. The name of this output file is Impact_Beam_Simulation.OUT.

Appendix F presents in detail derivation of the equations to calculate the deflection of a simply supported beam under the action of a concentrated static load at a specified distance “a” from the left support reaction.

Appendix G presents the results of the estimation of the Dynamic Modulus of Elasticity Considering the Axial and Bending Deformation for the Winfield Experiment Test # 10 using Impact_Beam computer program.

Appendix H presents the methodology for determining the mass per unit length of the simply-supported beam at Winfield. Hydrodynamic added mass is taken into account.

Appendix I discusses the effects of selecting the total number of frequency modes for analysis of the simply supported beam under dynamic loads. Recommendations for the appropriate number of modes are given.

Appendix J discusses the location of laser deflection and strain gage sensors for the barge impact tests at Winfield. These locations are used when deflections and moments are captured for comparison with the Winfield test data in the Impact_Beam computer program.

Appendix K discusses the efforts to recapture neoprene pad compression secant stiffness from the reaction points on the Winfield simply-supported beam using the Impact_Beam computer program. Discussions of literature definitions for neoprene compression stiffness are included.

2 Engineering Methodology to Compute the Dynamic Structural Time-History Response of a Simply Supported, Flexible Approach Wall Beam During an Impact Event

2.1 Introduction

In structural dynamics the mathematical model of bodies of finite dimensions undergoing translatory motion are governed by Newton's Second Law of Motion, expressed as

$$\sum F = m \bullet a \qquad \text{(1.1 bis)}$$

at each time step *t* during motion. In the mathematical model of transverse vibration, the forces acting on the flexible impact beam mass at each time step *t* include:

1. the impact force at time step t,
2. the elastic restoring forces (of the beam), and
3. the damping forces (of the beam).

The mathematical model of the beam in the engineering formulation described in this chapter has an infinite number of degrees of freedom because its mass is distributed. In this initial engineering formulation implemented in the PC-based program Impact_Beam, the numerical solution of dynamic transverse beam deflections, beam moments and shear force responses to the impact pulse force time-history applied to the simply supported, flexible impact beam of distributed mass and flexural stiffness makes use of modal response analyses as a function of position along the beam combined with a generalized coordinate solution for dynamic response with time for each mode considered. Superposition of modal responses is evoked to obtain the total dynamic beam responses. The generalized coordinate solution for dynamic response with time is solved using Duhamel's Integral. Duhamel's Integral is outlined in Appendix B and is evaluated using numerical methods by Impact_Beam that are outlined in Appendix C. This chapter discusses the various

relationships used in this engineering methodology that are implemented in Impact_Beam.

2.2 Dynamics of a distributed-mass and –stiffness system of a simply supported beam; an infinite-degree-of-freedom system

Considering the long spans and distribution of mass and stiffness along the length of one category of flexible impact beam, i.e., the simply supported, slender,[1] flexible impact beam of the type shown in Chapter 1, an infinite-degree-of-freedom system mathematical model is used for its transverse vibration. Applying D'Alembert's Principle[2], the sum of forces in the transverse direction of the beam shown in Figure 2.1 is

$$V - \left[V + \frac{\partial V}{\partial x} \bullet dx\right] + p(x,t) \bullet dx - m(x) \bullet dx \bullet \frac{\partial^2 u}{\partial t^2} = 0 \qquad (2.1)$$

Note that a damping force is not included in Equation 2.1 but will be accounted for at a later stage in the dynamic beam response formulation using the generalized coordinate solution for dynamic response with time.

Introducing the three equations listed in the left-hand side of Figure 2.1 and simplifying, the Equation 2.1 partial differential equation governing the motion $u(x,t)$ subjected to external dynamic forces $p(x,t)$ becomes

$$m(x) \bullet \frac{\partial^2 u}{\partial t^2} + \frac{\partial^2}{\partial x^2}\left[EI(x) \bullet \frac{\partial^2 u}{\partial x^2}\right] = p(x,t) \qquad (2.2)$$

with a distributed mass $m(x)$ and flexural rigidity $EI(x)$ per unit length both as a function of position x along the beam. The solution to Equation 2.2 is based on imposing a boundary condition of zero displacement and zero

---

[1] A slender beam implies that during beam flexure the plane cross-section of a beam remains plane, i.e., the Bernoulli-Euler theory. That is, shear deformations are negligible for a slender beam and are not accounted for in the formulation discussed in this chapter.

[2] Chopra (1995, 2001), Paz (1985) and Clough and Penzien (1993) all observe that D'Alembert's Principle of dynamic equilibrium is commonly applied to this simply supported, slender beam problem and is based on the concept of a fictitious inertia force (f_i), a force equal to the product of mass times acceleration that acts in a direction opposite to the acceleration. In Figure 2.1 the beam is assumed to be accelerating in the direction of positive displacement $u(x,t)$ at time t so f_i acts as shown, in the opposite direction to $u(x,t)$. D'Alembert's Principle states that with inertia forces (e.g., f_i in the Figure 2.1 insert figure box) included via the last term in Equation 2.1, a system is in equilibrium at each time instant. Thus a free-body diagram of a moving mass can be drawn as shown in Figure 2.1 and principles of statics can be used to develop the equation of motion as is done here.

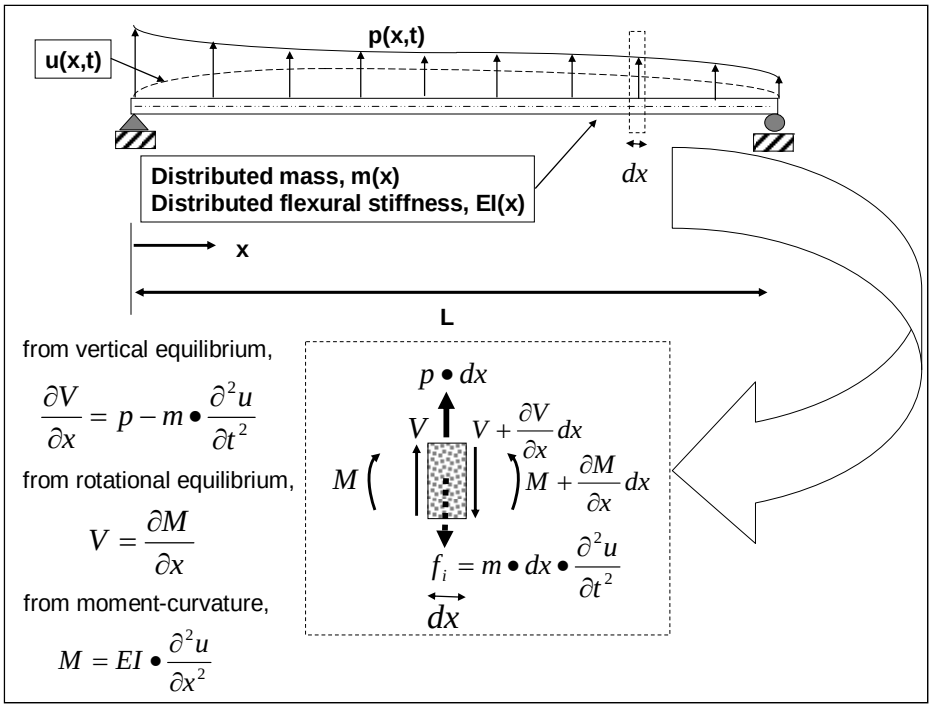

Figure 2.1. Simply-supported flexible beam with distributed mass and flexural stiffness, equations of equilibrium and forces and moments on a beam element.

moment at each end of the Figure 2.1 simply supported beam as well as imposing the initial displacement $u(x,0)$ and initial velocity $\dot{u}(x,0)$ along the entire beam at time $t = 0$.

2.2.1 Free vibration response for a single mode of an infinite-degree-of-freedom system - a solution in two parts

In the case of free vibration for the slender beam, Equation 2.2 simplifies to

$$m(x) \bullet \frac{\partial^2 u}{\partial t^2} + \frac{\partial^2}{\partial x^2}\left[EI(x) \bullet \frac{\partial^2 u}{\partial x^2}\right] = 0 \qquad (2.3)$$

For this model, the displacements and acceleration will be defined for each point along the longitudinal axis of the simply supported, flexible impact beam as depicted in Figure 2.1. In this formulation, the transverse displacements $u(x,t)$ at all locations along the beam are defined by two terms:

- the shape function $\phi(x)$, and
- the generalized coordinate $q(t)$

The equation for the transverse beam displacement at position x along the beam and at time t is

$$u(x,t) = \varphi(x) \bullet q(t) \tag{2.4}$$

Substitution of Equation 2.4 into Equation 2.3 and collecting terms, numerous structural dynamics books including Chopra (1995, 2001), Paz (1985, 1991), and Clough and Penzien (1993), all show that the partial differential equation becomes two ordinary differential equations, one governing the time varying function $q(t)$,

$$\ddot{q} + \omega^2 q = 0 \tag{2.5}$$

and a second governing the spatial function $\phi(x)$,

$$\left[EI(x) \bullet \varphi''(x)\right]'' - \omega^2 \bullet m(x) \bullet \varphi(x) = 0 \tag{2.6}$$

Observations:

- The dynamic transverse beam displacement response $u(x,t)$ is the product of two terms; $\varphi(x)$ and $q(t)$. Thus, the solution for $u(x,t)$ is achieved in two parts; the first solution is made for $\phi(x)$ and the second solution is made for q(t).
- The first term, $\varphi(x)$, in Equation 2.4 is a function (only) of position along the simply supported beam and the second term, $q(t)$, is a function (only) of time.
- There are two ordinary differential equations governing dynamic beam response; one governing position response and a second governing time response. Their solutions combine to the total response.
- Equation 2.5 has the same form as the equation governing the free vibration of a SDOF system with a natural frequency ω (refer to Equation A.2 in Appendix A, but without its second term, i.e., the damping term).

Note that, for any user specified mass and stiffness distributions along the beam, there are infinite sets of frequencies ω and associated mode shapes $\phi(x)$ that satisfy Equation 2.6 for the simply supported beam boundary

conditions of zero displacements and zero moments at each end of the slender beam.

The next sub-section addresses the solution of mode shapes $\phi(x)$; the first term of the two terms in Equation 2.4 for transverse beam displacement $u(x,t)$. Sub-section 2.2.3 will address the solution of $q(t)$; the second term in Equation 2.4 for $u(x,t)$.

2.2.2 Mode shapes $\phi(x)$ and natural vibration frequencies ω for a uniform beam

For the special case of a slender, simply supported beam of uniform (i.e., constant) mass designated $\bar{m}$ per unit length and uniform flexural stiffness, EI, along a simply supported beam, Equation 2.6 becomes

$$\varphi^{iv}(x) - \beta^4 \bullet \varphi(x) = 0 \tag{2.7}$$

with

$$\beta^4 = \frac{\omega^2 \bullet \bar{m}}{EI} \tag{2.8}$$

and (the real form of) the general solution for the spatial function $\varphi(x)$ is

$$\begin{aligned} \varphi(x) = C_1 \bullet \sin(\beta \bullet x) + C_2 \bullet \cos(\beta \bullet x) + C_3 \\ \bullet \sinh(\beta \bullet x) + C_4 \bullet \cosh(\beta \bullet x) \end{aligned} \tag{2.9}$$

The solution for the four constants C_1, C_2, C_3, and C_4 and for the eigenvalue parameter β are determined by applying the boundary conditions of zero displacements and zero moments to each end of the simply supported beam. Applying the boundary conditions $u(0,t) = 0$ and moment $M(0,t)=0$ at $x = 0$ results in constants C_2 and C_4 both equal to zero. Similarly, applying the boundary conditions $u(L,t) = 0$ and moment $M(L,t)=0$ at $x = L$ results in constant C_3 equal to zero and leads to the frequency equation

$$C_1 \bullet \sin(\beta \bullet L) = 0 \tag{2.10}$$

Equation 2.10 is satisfied for the cases of

$$\beta \bullet L = n \bullet \pi \tag{2.11}$$

for n equal to 1, 2, 3, ...

Introducing Equation 2.8, Equation 2.11 becomes

$$\omega_n = \frac{n^2 \bullet \pi^2}{L^2} \bullet \sqrt{\frac{EI}{\bar{m}}} \tag{2.12}$$

By setting C_1 equal to unity, this makes the maximum amplitude of the spatial function $\varphi(x)$ equal to unity as well, and Equation 2.9 reduces to

$$\varphi(x) = \sin\left(\frac{n \bullet \pi \bullet x}{L}\right) \tag{2.13}$$

Recognizing that, for a simply supported beam with uniform distributed mass, there are an infinite number of frequencies and mode shapes, Equation 2.13 is re-written as

$$\varphi_n(x) = \sin\left(\frac{n \bullet \pi \bullet x}{L}\right) \tag{2.14}$$

and thereby acknowledges via the (subscript) notation that the spatial function $\varphi(x)$ is in actuality the mode shape $\varphi_n(x)$ for mode n with a natural frequency ω_n . The mode shapes and (undamped) natural frequencies for a uniform simply supported beam are idealized in Figure 2.2 for the first three modes, i.e., n = 1, 2 and 3.

Observations:

- There are infinite sets of mode shapes $\phi_n(x)$ and associated frequencies ω_n that satisfy Equation 2.7 for this simply supported uniform beam, from mode number n equal to one to mode number n equal to infinity.
- Equation 2.12 defines the natural frequency ω_n for each mode n, and
- Equation 2.14 defines the mode shape $\phi_n(x)$ for each mode n.

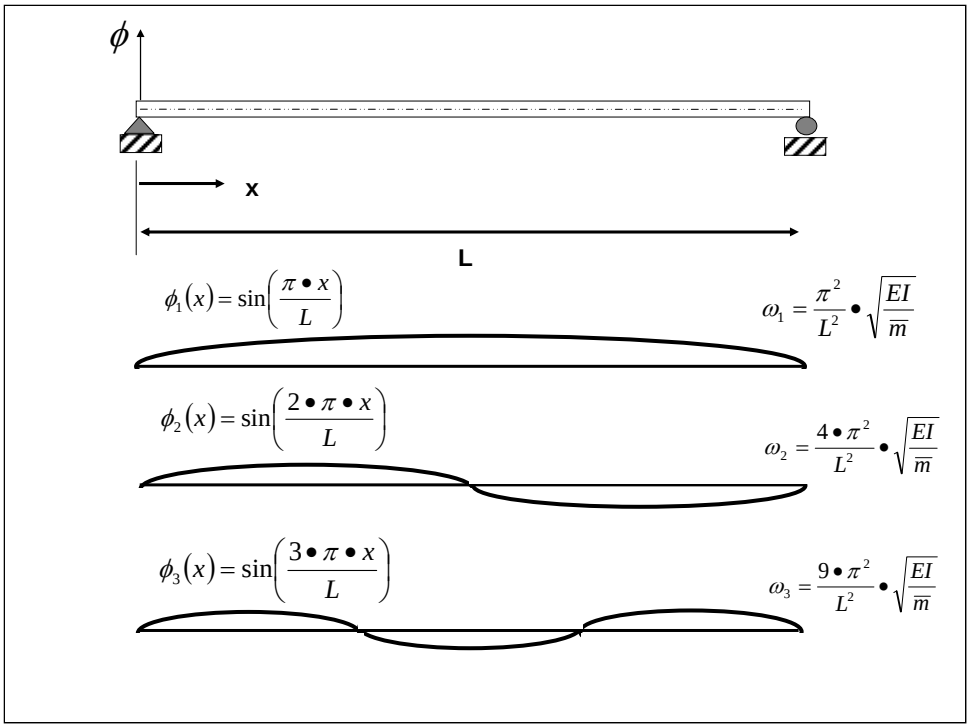

Figure 2.2. Idealization of the first three (undamped) natural vibration mode shapes and frequencies of a simply supported flexible beam with uniform mass and flexural stiffness.

2.2.3 Definition of modal variables for a simply supported uniform beam with an infinite-DOF system subject to dynamic loading *p*(*x*,*t*) - a solution in two parts

The displacement response of the mathematical model of a simply supported uniform beam (with a distributed mass and stiffness) to a dynamic external force $p(x,t)$ applied transverse to the beam is

$$u(x,t) = \sum_{n=1}^{\infty} \varphi_n(x) \bullet q_n(t) \tag{2.15}$$

Observations:

- Equation 2.15 expresses the superposition of the contribution of individual (orthogonal) modes (from mode number n equal to one to mode number n equal to infinity); superposition is restricted to linear beam response problems.
- The solution is made at each user specified point x along the beam.
- The solution for the (mode shape) term $\phi_n(x)$ for mode n is given by Equation 2.14.

- The solution for the (generalized coordinate) term $q_n(t)$ for mode n is obtained by numerically solving Duhamel's Integral (Appendix B).
- Note that a solution for $\phi_n(x)$ and for $q_n(t)$ is determined each for mode n and the solutions for $\phi_n(x)$ and for $q_n(t)$ will each differ from one mode to the next.

Substituting Equation 2.15, Equation 2.2 after some mathematical manipulations as described, e.g., by Chopra (1995, 2001) or Paz (1985, 1991), becomes

$$M_n \bullet \ddot{q}_n(t) + K_n \bullet q_n(t) = P_n(t) \tag{2.16}$$

where the mode n mass is given by

$$M_n = \int_0^L m(x) \bullet \left[\varphi_n(x)\right]^2 dx \tag{2.17}$$

For a uniform beam $m(x)$ is set equal to a constant mass $\overline{m}$ per unit length, and Equation 2.17 becomes

$$M_n = \overline{m} \bullet \int_0^L \left[\varphi_n(x)\right]^2 dx \tag{2.18}$$

Introducing Equation 2.14 and performing the integration, Equation 2.18 becomes

$$M_n = \frac{\overline{m} \bullet L}{2} \tag{2.19}$$

The mode n stiffness (as implemented in the PC-based program Impact_Beam) is

$$K_n = \omega_n^2 \bullet M_n \tag{2.20}$$

Introducing Equations 2.12 and 2.19, Equation 2.20 for mode n becomes

$$K_n = \frac{n^4 \bullet \pi^4}{2 \bullet L^3} EI \tag{2.21}$$

And the mode n external force is given by

$$P_n(t) = \int_0^L p(x,t) \bullet \varphi_n(x) dx \tag{2.22}$$

This external forcing function $P_n(t)$ for mode n is used as the forcing function to the SDOF system, whose response is designated as $q_n(t)$ and solved using Duhamel's Integral as summarized in Appendix B for each mode n = 1 to the highest mode specified in the analysis (theoretically, up to infinity).

2.2.4 Definition of dynamic modal *n* force $P_n(t)$ for loads at a fixed point on a beam or travelling along the beam

For a user specified, time varying point load $p(x_{\text{point load}},t)$ applied at a (fixed) position of x set equal to $x_{\text{point load}}$ along the beam, Equation 2.22 for mode n becomes

$$P_n(t) = p\left(x_{\text{point load}},t\right) \bullet \varphi_n\left(x_{\text{point load}}\right) \tag{2.23}$$

with $\phi_n\left(x_{\text{point load}}\right)$ for mode n is given by

$$\varphi_n\left(x_{\text{point load}}\right) = \sin\left(\frac{n \bullet \pi \bullet x_{\text{point load}}}{L}\right) \tag{2.24}$$

From the initial time that the barge train contacts the impact beam from contact time t_1 through final contact time t_2 (Figure 2.3), the point load $p(x_{\text{point load}},t)$ remains fixed at position $x_{\text{point load}}$ along the beam. The initial impact point position $x_{\text{point load}}$ is designated by the variable *X_Impact* as user input data as shown in the Appendix D.

An alternative formulation incorporated within the PC-based software Impact_Beam allows for the specification of a barge train having an initial contact with the impact beam at position $[x_{\text{point load}}]_{t_1}$ (i.e., *X_Impact* in the Impact_Beam software input terminology) at time t_1 and moving in contact at a constant velocity V along the beam as shown in Figure 2.3[1]. The

[1] The Velocity, *V*, of the barge train in the direction of the X_{Global} axis is along the line of the beam and its user provided value to PC-program Impact_Beam, which is designated as *X_Impact_velocity*.

position of the impact point force $p\left([x_{\text{point load}}]_{t_i}, [t_1 + \Delta t_i]\right)$ moves with time t_i. Its change, in distance ΔX from initial contact point *X_Impact* at time t_i, is given by

$$\Delta X = V \bullet \Delta t_i \tag{1.2 bis}$$

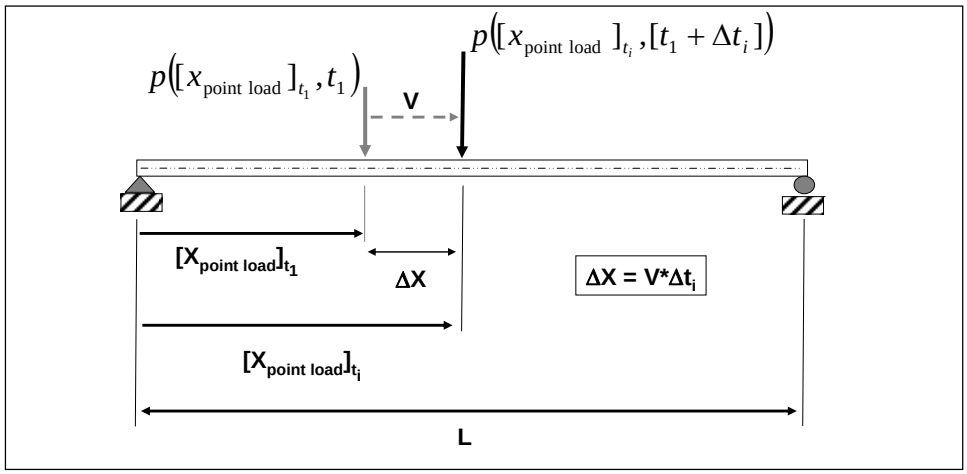

Figure 2.3. Barge impact point force moving along the wall from initial contact time t_1 to final contact time t_2.

The position of the point load along the beam at time t_i is

$$[x_{\text{point load}}]_{t_i} = X\_\text{Impact} + \Delta X \tag{1.3 bis}$$

Recall that by introducing Equation 1.2, Equation 1.3 becomes

$$[x_{\text{point load}}]_{t_i} = \left[X\_\text{Impact} + V \bullet \Delta t_i\right] \tag{1.4 bis}$$

For a user specified, time varying point load $p\left([x_{\text{point load}}]_{t_i}, [t_1 + \Delta t_i]\right)$ that moves with a velocity V along the beam, substituting Equation 1.4 for $x_{\text{point load}}$, Equation 2.23 for mode n becomes

$$\begin{aligned} P_n(t) = p\left([X\_\text{Impact} + V \bullet \Delta t_i], t\right) \bullet \\ \varphi_n\left([X\_\text{Impact} + V \bullet \Delta t_i]\right) \end{aligned} \tag{2.25}$$

with $\phi_n\left(x_{\text{point load}}\right)$ for mode n given by

$$\varphi_n\left(x_{\text{point load}}\right) = \sin\left(\frac{n \bullet \pi \bullet [X\_\text{Impact} + V \bullet \Delta t_i]}{L}\right) \tag{2.26}$$

2.2.5 Dynamic mode n displacements $u_n(x,t)$, modal moments $M_n(x,t)$ and modal shears $V_n(x,t)$ for a simply supported uniform beam subject to dynamic loading $p(x,t)$ and a solution to part one of two parts

For a slender, uniform beam (with $m(x)$ equal to a constant mass $\overline{m}$ per unit length), the (undamped) natural frequency ω_n for mode n is given by Equation 2.12. The displacement for mode n is

$$u_n(x,t) = \varphi_n(x) \bullet q_n(t) \tag{2.27}$$

Recall the spatial function $\phi_n(x)$ is the mode shape for mode n with a natural frequency ω_n, given by Equation 2.14 for the user specified point x along the beam. The solution for the (generalized coordinate) term $q_n(t)$ for mode n is obtained by numerically solving Duhamel's Integral (Appendix B). The solution for $u_n(x,t)$ for each mode n is accomplished by the PC-based software Impact_Beam. In theory, there are an infinite number of modes for a uniform beam. In actuality, only a finite number of modes provide a practical contribution to beam response (i.e., displacements, moments and shear forces). Impact_Beam allows the user to specify the maximum number of modes, designated mode r, to be used in the transverse displacement, moment and shear force response analyses. For the user specified number of modes one through r, the total uniform beam displacement is

$$u(x,t) = \sum_{n=1}^{r} u_n(x,t) \tag{2.28}$$

with each mode n displacement defined by Equation 2.27. The bending moment along the uniform beam (for the user defined one to r modes) is

$$M(x,t) = \sum_{n=1}^{r} M_n(x,t) = \sum_{n=1}^{r} EI(x) \bullet \varphi_n''(x) \bullet q_n(t) \tag{2.29}$$

which for a uniform beam $EI(x)$ equals a constant value EI, Equation 2.29 becomes

$$M(x,t) = \sum_{n=1}^{r} EI \bullet \varphi_n''(x) \bullet q_n(t) \tag{2.30}$$

The second derivative of the Equation 2.14 mode shape is

$$\varphi_n''(x) = -\frac{n^2 \bullet \pi^2}{L^2} \sin\left(\frac{n \bullet \pi \bullet x}{L}\right) \tag{2.31}$$

Shear is the partial of the moment with respect to x. The shear along the uniform beam (for the user defined one to r modes) is

$$V(x,t) = \sum_{n=1}^{r} V_n(x,t) = \sum_{n=1}^{r} \left[EI(x) \bullet \varphi_n''(x)\right]' \bullet q_n(t) \tag{2.32}$$

which for a uniform beam $EI(x)$ equals a constant value EI, Equation 2.32 becomes

$$V(x,t) = \sum_{n=1}^{r} EI \bullet \varphi_n'''(x) \bullet q_n(t) \tag{2.33}$$

The third derivative of the Equation 2.14 mode shape is

$$\varphi_n'''(x) = -\frac{n^3 \bullet \pi^3}{L^3} \cos\left(\frac{n \bullet \pi \bullet x}{L}\right) \tag{2.34}$$

2.2.6 Generalized coordinate solution $q_n(t)$ for dynamic response with time for each mode n considered - a solution to part two of two parts

Although Equation 2.15 expresses the transverse beam displacement $u(x,t)$ as the superposition of an infinite number of modes, in actuality, the solution is based on a user specified finite number of modes. So, for user specified r modes, the Impact_Beam software computes the dynamic transverse displacement along the uniform beam as equal to

$$u(x,t) = \sum_{n=1}^{r} \varphi_n(x) \bullet q_n(t) \tag{2.35}$$

Similarly, the dynamic moments for a uniform beam are given by

$$M(x,t) = \sum_{n=1}^{r} EI \bullet \varphi_n''(x) \bullet q_n(t) \qquad (2.30 \text{ bis})$$

and the shear forces for a uniform beam are given by

$$V(x,t) = \sum_{n=1}^{r} EI \bullet \varphi'''(x) \bullet q_n(t) \qquad (2.33 \text{ bis})$$

Observe, in these three equations, that the dynamic transverse displacements, moments and shear forces are all a product of two terms:

- the shape function and its derivatives, and
- a generalized coordinate $q_n(t)$ for each mode n.

The previous sub-sections describe the solution for the first term and the shape function (with its derivatives). Note that the shape function solely is a function of position. This sub-section describes the solution for the second term, the generalized coordinate $q_n(t)$. Note that the generalized coordinate solely is a function of time.

Along with others, Paz (1985) observes that the equation of motion for each mode, e.g., mode n, of the generalized coordinate $q_n(t)$ is analogous to the modal equation for a discrete (i.e., lumped mass) system and as such, that the modal damping can simply be added to Equation 2.16 to become

$$M_n \bullet \ddot{q}_n(t) + C_n \bullet \dot{q}_n(t) + K_n \bullet q_n(t) = P_n(t) \qquad (2.36)$$

where the fraction of critical damping for mode n, ζ_n , is equal to

$$\zeta_n = \frac{C_n}{C_{n,critical}} \qquad (2.37)$$

Dividing through by modal Mass M_n and introducing Equation 2.37, Equation 2.36 becomes

$$\ddot{q}_n(t) + 2 \bullet \zeta_n \bullet \omega_n \bullet \dot{q}_n(t) + \omega_n^2 \bullet q_n(t) = \frac{P_n(t)}{M_n} \qquad (2.38)$$

Equation 2.36 for each specified mode n (i.e., from mode one up to the user specified mode r) has the same form as the equation governing the forced vibration of a SDOF system with a natural frequency ω; refer to the lower right equation in Figure B.1. The solution for the generalized coordinate $qn(t)$ for mode n is obtained by solving Duhamel's Integral for a classically damped system.

2.2.7 Duhamel's Integral solution for the generalized coordinate solution $q_n(t)$ for dynamic response with time for each mode n

One approach to the solution of the equation of motion for the generalized coordinate term $q_n(t)$ for mode n in Equation 2.38 is Duhamel's Integral, as discussed in Craig (1981).[1] Duhamel's Integral is based on representing the applied force time-history as a sequence of infinitesimally short impulses. Note that, because superposition is used, application of Duhamel's Integral is limited to linear elastic systems.

The displacement response $q_n(t)$ for mode n to a time-varying modal force applied to mode n, is obtained by adding the responses to all of the individual impulses up to the time t of interest for mode n. Appendix B summarizes a traditional derivation of Duhamel's Integral for a SDOF system. Key to this derivation is the observation that the magnitude of the impulse is equal to the change in momentum. This allows for the introduction of the force time-history into the free vibration response relationship, Equation A.9, for a SDOF system.

The Appendix B Duhamel's Integral derivation has been adapted in this sub-section to the solution of the generalized coordinate solution $q_n(t)$ for each mode n. The solution to the generalized coordinate solution $q_n(t)$ for mode n which starts at rest, i.e., with zero initial displacement and zero initial velocity at time t equal to 0, is expressed as

$$q_n(t) = \frac{1}{M_n \bullet (\omega_D)_n} \int_0^t P_n(\tau) \bullet e^{-\zeta_n \omega_n (t-\tau)} \bullet \sin\left[(\omega_D)_n \bullet (t-\tau)\right] d\tau \quad (2.39)$$

[1] Appendix B discusses the application of Duhamel's integral to the solution of the dynamic response of a SDOF system. Note that both Equation 2.38 and the equation given in the lower right of Figure B.1 are both second order differential equations of the same form.

for a critical damping ratio value ζ_n[1], undamped natural circular frequency ω_n, and damped natural circular frequency $(\omega_D)_n$. The modal forcing function time-history $P_n(t)$ is expressed as $P_n(\tau)$ in Equation 2.39 and is based on the user defined impact pulse force time-history. Equation 2.39 is analogous to Equation B.4 for the dynamic response of a SDOF system starting at-rest and subjected to a time-varying, external forcing function. This equation is solved numerically using the procedure outlined in Appendix C.

The slender, uniform beam possesses for each mode n a unique value for the undamped natural frequency ω_n and equal to

$$\omega_n = \frac{n^2 \bullet \pi^2}{L^2} \bullet \sqrt{\frac{EI}{m}} \qquad \text{(2.12 bis)}$$

and damped natural frequency $(\omega_D)_n$ defined for mode n as

$$\left(\omega_D\right)_n = \omega_n \bullet \sqrt{1 - \zeta_n{}^2} \qquad \text{(2.40)}$$

In addition, each mode n of a slender beam with constant mass $\overline{m}$ per unit length will possess a unique modal mass M_n

$$M_n = \frac{\overline{m} \bullet L}{2} \qquad \text{(2.19 bis)}$$

and a unique (to mode n) modal forcing function time-history $P_n(t)$

$$P_n(t) = p\left(x_{\text{point load}}, t\right) \bullet \varphi_n\left(x_{\text{point load}}\right) \qquad \text{(2.23 bis)}$$

for a user specified, time varying point load $p(x_{\text{point load}}, t)$ applied at a (fixed) position $x = x_{\text{point load}}$ along the beam. The value for $\varphi_n\left(x_{\text{point load}}\right)$ for mode n in Equation 2.23 is

$$\varphi_n\left(x_{\text{point load}}\right) = \sin\left(\frac{n \bullet \pi \bullet x_{\text{point load}}}{L}\right) \qquad \text{(2.24 bis)}$$

[1] The user specifies the fraction of critical damping ξ_n for mode n as well as all other user specified modes, and is typically a value between 0.0 and 0.1.

The user defined, time varying point load $p(x_{\text{point load}},t)$ may be developed using the companion PC-based software Impact_Force. It is important to recognize that values for ω_n, $(\omega_D)_n$ and M_n, and time-history $P_n(t)$, will each vary with mode number.

In the case of a point force moving along the beam, a unique (to mode n) modal forcing function time-history $Pn(t)$ is given by

$$P_n(t) = p([X\_\text{Impact} + V \bullet \Delta t_i], t) \bullet \varphi_n([X\_\text{Impact} + V \bullet \Delta t_i]) \quad \text{(2.25 bis)}$$

with $\phi_n(x_{\text{point load}})$ for mode n given by

$$\varphi_n(x_{\text{point load}}) = \sin\left(\frac{n \bullet \pi \bullet [X\_\text{Impact} + V \bullet \Delta t_i]}{L}\right) \quad \text{(2.26 bis)}$$

Recall that x point load moves along the beam and for a given time increment Δt_i after initial contact (t_1) is

$$[x_{\text{point load}}]_{t_i} = [X\_\text{Impact} + V \bullet \Delta t_i] \quad \text{(1.4 bis)}$$

The time-history response for each SDOF system for each mode n, $q_n(t)$, in Equation 2.39 is solved for the forcing function $P_n(t)$ applied to mode n.

2.3 Summary of PC-based program Impact_Beam computation of dynamic beam Displacements *u*(*x,t*), Moments *M*(*x,t*) and Shears *V*(*x,t*) for a slender, simply supported, uniform beam subject to dynamic loading *p*(*x point load,t*)

The PC-based computer program Impact_Beam solves for the dynamic beam displacements, moments and shears for a slender, simply supported, uniform beam subject to a time-varying point load $p(x_{\text{point load}},t)$. Section 2.2 described the derivation of the engineering methodology implemented in Impact_Beam for a slender, simply supported, uniform beam case. The solution is accomplished in two parts for each mode, summing the products of the two solutions from mode one up to the user specified maximum mode r. In response to the user specified, time varying point load $p(x_{\text{point load}},t)$

applied at a (fixed) position $x = {}^{x_{\text{point load}}}$ along the beam, the dynamic beam transverse displacements are

$$u(x,t) = \sum_{n=1}^{r} \varphi_n(x) \bullet q_n(t) \qquad \text{(2.35 bis)}$$

The first part of the solution is made for the mode shape term $\phi_n(x)$ for mode n using Equation 2.14. The second part of the solution is made for the generalized coordinate $q_n(t)$ using Equation 2.39 for mode n.

The dynamic moments for a uniform beam (of constant EI) are given by

$$M(x,t) = \sum_{n=1}^{r} EI \bullet \varphi_n''(x) \bullet q_n(t) \qquad \text{(2.30 bis)}$$

The first part of the solution is made for the second derivative of the shape function for mode n, $\phi_n''(x)$, using Equation 2.31. The second part of the solution is made for the generalized coordinate $q_n(t)$ using Equation 2.39 for mode n.

The dynamic shear forces for a uniform beam (of constant EI) are given by

$$V(x,t) = \sum_{n=1}^{r} EI \bullet \varphi'''(x) \bullet q_n(t) \qquad \text{(2.33 bis)}$$

The first part of the solution is made for the third derivative of the shape function for mode n, $\varphi_n'''(x)$, using Equation 2.34. The second part of the solution is made for the generalized coordinate $q_n(t)$ using Equation 2.39 for mode n.

The left and right vertical support reactions can be calculated using Equations 2.33 and 2.34

$$V(x,t) = \sum_{n=1}^{r} EI \bullet \varphi_n'''(x) \bullet q_n(t) \qquad \text{(2.33 bis)}$$

where

$$\varphi_n'''(x) = -\frac{n^3 \bullet \pi^3}{L^3}\cos\left(\frac{n \bullet \pi \bullet x}{L}\right) \tag{2.34 bis}$$

for $x = 0$ and $x = L$. The resulting expressions are the following;

$$\begin{aligned} R_A(t) &= V(x=0,t) = \sum_{n=1}^{r} EI \bullet \varphi_n'''(x=0) \bullet q_n(t) \\ R_B(t) &= V(x=L,t) = \sum_{n=1}^{r} EI \bullet \varphi_n'''(x=L) \bullet q_n(t) \end{aligned} \tag{2.41}$$

and

$$\begin{aligned} \varphi_n'''(x=0) &= -\frac{n^3 \bullet \pi^3}{L^3} \\ \varphi_n'''(x=L) &= -\frac{n^3 \bullet \pi^3}{L^3}\cos(n \bullet \pi) \end{aligned} \tag{2.42}$$

where the magnitudes of R_A and R_B are the left and right vertical supports reactions time-history, respectively.

Observations:

- Chopra (1995), Paz (1985), and Clough and Penzien (1993) observe that higher modes contribute more to the dynamic moment response for a simply supported uniform beam than to its displacement response.
- Chopra (1995), Paz (1985), and Clough and Penzien (1993) also observe that higher modes contribute more to the dynamic shear force response for a simply supported uniform beam than to its moment response.
- Experience with the application of this uniform mass and uniform stiffness slender beam solution process dictates that more modes must be included for accurate solutions compared to the number of modes considered adequate in a lumped mass modal solution.

3 Computation of Transverse Beam Displacements, Internal Shears and Moments Impact Factors

3.1 Introduction

Long, slender flexible beams such as those used for impact beams (i.e., flexible approach walls) as shown in Chapter 1, can respond to an impact pulse force time-history with intensities that can be larger, the same, or smaller than if that same load is applied as a sequence of static loadings.[1] This chapter summarizes the computation of transverse beam displacements, shears and internal moments to a long, simply supported, flexible impact beam due to static point loading. Computed results for these three beam response parameters, compared to computations made using the Chapter 2 structural dynamic response formulation provide insights into whether or not dynamic amplification occurs for the flexible impact beam being analyzed. Dynamic to static responses are expressed in terms of "Impact Factors."

3.2 Impact factors used in Impact_Beam

Because a barge train impact with a flexible impact beam (i.e., a flexible approach wall) is a dynamic event, the structural response of this flexible approach wall mass at every time step t to the impact load imparted to the flexible wall mass is not the same response as if the force at the same time step t is applied statically (i.e., with acceleration equal to zero in Equation 1.1).[2] Therefore, included in Impact_Beam is the computation of three Impact Factors; the first is for transverse beam displacements, the second for shear forces, and the third for bending moments. They are defined as:

- Displacement Impact Factor DIF; the ratio of the dynamic deflection at any position along the beam at each time step divided by its static deflection calculated at the same position along the beam due to a

[1] Note that structural amplification is influenced by, among other factors, the span of the flexible beam and the cross-sectional geometry of a prestressed concrete beam.

[2] As observed by Clough and Penzien (1993, page 4), because the loading is not applied slowly, noteworthy inertial forces result from the structural time-varying displacements of the (distributed) mass of the Figure 2.1 flexible beam which in turn are influenced by the magnitude of inertial forces; it's a closed cycle of cause and effect.

static force applied at the same position as the dynamic load.[1] It will be shown in section 3.3 that the point of maximum static deflection lies within a narrow region; within 8 percent of beam length, either side of the mid-span of a simply supported impact beam when subjected to a point load.

- Shear Force Impact Factor SFIF; the ratio of the dynamic shear force at any position along the beam at each time step divided by its static shear force calculated at the same position along the beam due to a static force applied at the same position as the dynamic load . The point of maximum static shear occurs anywhere between the position of the point load and the reaction that is closest to the point load (i.e., the shear force is uniform within this region).
- Moment Impact Factor MIF; the ratio of the dynamic moment at any position along the beam at each time step divided by its static moment calculated at the same position along the beam due to a static force applied at the same position as the dynamic load. For a simply supported beam, the point of maximum static moment is at the position of the point load.

Since the (internal) restoring force of the beam is proportional to the beam's deflection (by a stiffness term), the DIF ratio also reflects the level of dynamic restoring force amplification (or attenuation) during dynamic response of the mass of the flexible impact beam. This and the other two impact factors give the engineer a sense of the level of dynamic response taking place within the beams' mass.

3.3 Beam deflection under an eccentric static load *P*

This sub-section summarizes the deflection equations for a simply supported beam subjected to a static load *P* applied anywhere along the beam. The deflection relationships are derived in numerous books. The beam response to a static point load applied to any point along a simply supported beam can be derived by integration, moment area or by other methods (as described in references on Strength of Materials and Structural Analysis, including Cernica (1966)). Figure 3.1 shows a simply supported beam subjected to a static point load *P* with the length of beam and load position definitions.

[1] Chopra (1995) refers to this displacement ratio as the" impact factor" and Paz (1985) refers to this ratio as the "dynamic load factor. "

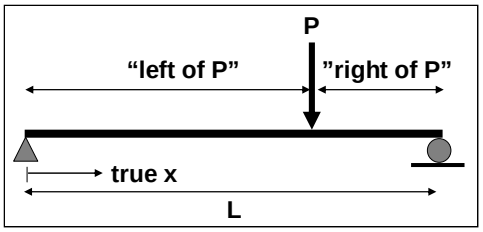

Figure 3.1. Simply supported beam – static load *P*.

Figure 3.2 provides a definition of terms for the equations cited in this sub-section to compute deflection of this simply supported beam.[1]

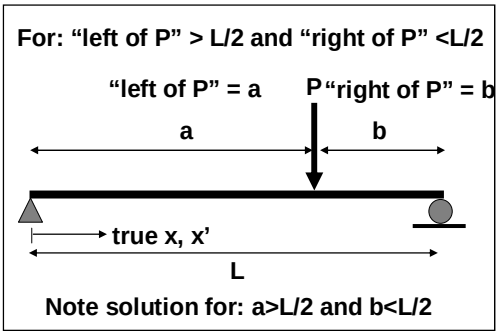

Figure 3.2. Distance definitions *a* and *b* for Equations 3.1 through 3.4 for a simply supported beam with the distance "left of *P*" > *L*/2.

The maximum deflection for a static load *P*:

$$\delta = \frac{P \bullet b \bullet \left(L^2 - b^2\right)^{3/2}}{9 \bullet \sqrt{3} \bullet L \bullet EI} \tag{3.1}$$

occurs at the position

$$x' = \sqrt{\frac{L^2 - b^2}{3}} \tag{3.2}$$

The following deflection equations are based upon the distances *a* and *b* from the support to the static point load *P*, where the value for distance *a* is always greater than or equal to the distance *b*, as shown in Figures 3.2 and 3.3. Deflections at any point *x'* where $0 < x' < a$ are

[1] After Table 4-1 on page 253 of Cernica (1966).

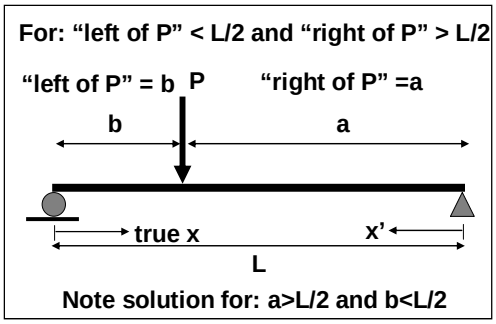

Figure 3.3. Distance definitions *a* and *b* for Equations 3.1 through 3.4 for a simply supported beam with the distance "left of P" < *L/2*.

$$\delta_1 = \frac{P \bullet b \bullet x'}{6 \bullet L \bullet EI} \bullet \left[L^2 - (x')^2 - b^2 \right] \tag{3.3}$$

And deflections at any point *x'* where $a < x' < L$ are

$$\delta_2 = \frac{P \bullet b}{6 \bullet L \bullet EI} \bullet \left[\frac{L}{b} \bullet (x' - a)^3 + \left(L^2 - b^2 \right) \bullet x' - (x')^3 \right] \tag{3.4}$$

To use the above equations when the static point load *P* is at a position where the "left of *P*" distance is less than *L/2* (as measured from the left-hand-side reaction point), the transformation depicted in Figure 3.3 is required.

The general equations for the transversal deflection of a simply supported beam as presented in Figure 3.1 is as follows

$$v(x) = \frac{P}{EI} \left[\frac{bx^3}{6L} + \left(\frac{a^2}{2} + \frac{L^2}{6} - \frac{bL}{6} - \frac{aL}{2} - \frac{a^3}{6L} \right) x \right]; \quad 0 \le x \le a \tag{3.5}$$

and

$$v(x) = \frac{P}{EI} \left[\frac{bx^3}{6L} - \frac{x^3}{6} + \frac{ax^2}{2} + \left(\frac{L^2}{6} - \frac{bL}{6} - \frac{aL}{2} - \frac{a^3}{6L} \right) x + \frac{a^3}{6} \right]; \quad a \le x \le L \tag{3.6}$$

where the *x* value is measure from the left support. This solution is helpful because it is not necessary to consider the transformation of the *x* coordinate depicted in Figure 3.3. That is, by using Equations 3.5 and 3.6, no considerations have to be made related to which distance, *a* or *b*, is greater or less. Equations 3.5 and 3.6 were used to calculate the static transverse displacement of the simply supported beam subjected to a static concentrated load in Impact_Beam computer software. These equations are derived in Appendix F.

Parametric calculations summarized in Figure 3.4 show that the point of maximum static deflection depends upon the location of the point load and is only at beam center when a mid-span static point load is applied. The "normalized deflections" summarized in this figure are for a unit static point load and for *EI* equal to unity. Multiply the Figure 3.4 "normalized deflection" values by the value of (*P*/*EI*) to obtain actual deflection values or apply Equations 3.3 and 3.4 according to the distance definitions established in Figures 3.2 and 3.3.

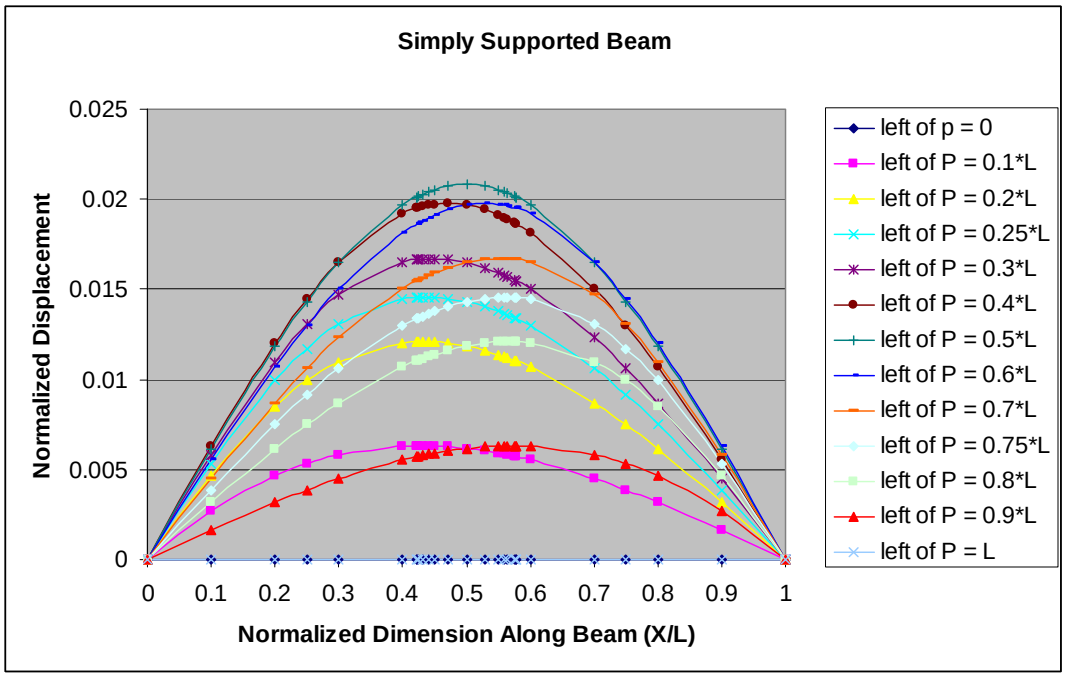

Figure 3.4. Normalized displacements for the 13 unit point load positions along the simply supported beam subjected to a static point load of unity and with a value of unity for *EI*.

These resulting maximum normalized displacements and their corresponding positions along the simply supported beam are summarized in Table 3.1 for each of the 13 static point load *P* positions. These results show that:

a) the point of maximum deflection occurs when the position of the static point load *P* is mid-span of the beam,

b) there is symmetry in computed normalized maximum displacements for equidistant distances for the unit static point load *P* about the center of the beam,

c) the magnitude of the maximum displacements diminishes as the distance to the point load form the center of the beam increases, and

d) with a unit static point load *P* positioned between 0.1**L* and 0.9**L*, the point of maximum displacement falls within a narrow range distance of approximately 0.43**L* and 0.57**L*. A separate calculation (not include in this table) for a unit point load *P* at 0.01**L* results in a maximum displacement computed at approximately 0.42**L*.

Table 3.1. Maximum normalized displacements for each of the thirteen unit point load *P* positions along a simple beam with a value of unity for *EI*.

(a) Continued

(left of *P*)/*L*	0	0.1	0.2	0.25	0.3	0.4	0.5
MAX Deflection	0	0.00632	0.01207	0.01456	0.01671	0.01975	0.02083
point of maximum displacement in (true *x* coordinate/*L*)	0	0.42554	0.4343	0.44098	0.44924	0.47085	0.5

(b) Concluded

(left of *P*)/*L*	0.5	0.6	0.7	0.75	0.8	0.9	1
MAX Deflection	0.02083	0.01975	0.01671	0.01456	0.01207	0.00632	0
point of maximum displacement in (true *x* coordinate/*L*)	0.5	0.52915	0.550757	0.559017	0.565685	0.57446	1

3.4 Displacement impact factor DIF

Parametric studies of the response of SDOF systems summarized in Chapter 4 of Chopra (1995) report that for pulse force time-history duration $\Delta_{duration}$ greater than one-half the natural period of an undamped SDOF system, i.e., $>(½*T_n)$, peak displacement responses occur during the pulse loading.[1] In

[1] When the pulse force time history duration $\Delta_{duration}$ is less than one-half the natural period of an undamped SDOF system, i.e., $<(½*T_n)$, peak dynamic displacement responses occur after the pulse loading.

this case, the comparison of the maximum value for the dynamic displacement $u(x,t)$ occurring along the beam and at any time to static displacement for the pulse time-history $p(x_{point\ load},t)$ applied as a static load becomes a relevant displacement index to the dynamic response of the beam.

Given a pulse force time-history $p(x_{point\ load},t)$ applied at a point $x_{point\ load}$ along the beam; the Displacement Impact Factor DIF is defined as the value of dynamic deflection $u(x,t)$ computed at position x along the beam and during any time step t using Equation 2.33 divided by the static deflection at this same position x along the beam for an applied static point load set equal to the magnitude of the pulse time-history at the same time step used for the dynamic displacement calculation $p(x_{point\ load},t)$ using Equations 3.5 and 3.6. Recall the dynamic deflection is

$$u(x,t) = \sum_{n=1}^{r} \varphi_n(x) \bullet q_n(t) \qquad \text{(2.33 bis)}$$

with r modes considered in the analysis. Then, the Displacement Impact Factor is calculated as

$$DIF = \left(\frac{u_{dyn}}{u_{st}} \right)_{(x_{point\ load},t)} \qquad (3.7)$$

DIF is computed at each point along the beam for each time step of the pulse time-history by the computer program Impact_Beam.

Observations:

- If the point load is applied at a slow rate so that inertial forces resulting from the structural time-varying displacements of the beam mass are negligible, the DIF is unity.
- Based on the response of SDOF systems with $(\Delta_{duration}/T_n) > ½$: At the other extreme (to static loading), if the load is applied instantaneously the DIF can be as large as 2.0, for zero damping (as shown in Chapter 4 of Chopra (1995) for SDOF systems). A limiting value less than two may occur depending upon factors that include the level of damping specified.

- Contributions of higher frequencies in a MDOF system such as a beam with distributed mass may alter this limiting factor of two value since higher frequencies can either add to or subtract from the overall displacement response; by Equation 2.33, the total beam displacement response is equal to the sum of displacements across all user defined frequencies 1 to *r*.
- Based on the response of SDOF systems with $(\Delta_{duration}/T_n) < ½$: The peak response for a time-varying load of finite duration, e.g., a half-sine pulse force time-history is applied to a SDOF system with $(\Delta_{duration}/T_n) < ½$, the peak dynamic response occurs during free vibration response (i.e., after the pulse force time-history concludes). The DIF can be less than unity, even for zero damping, as demonstrated in the upper two figures of Figure 4.8.2 in Chapter 4 of Chopra (1995) for SDOF system responses.

3.5 Shears and internal bending moments of a beam subjected to a concentrated static load

The shear and moment diagrams for a simply supported beam subjected to a static point load of magnitude *P* are given in Figure 3.5.

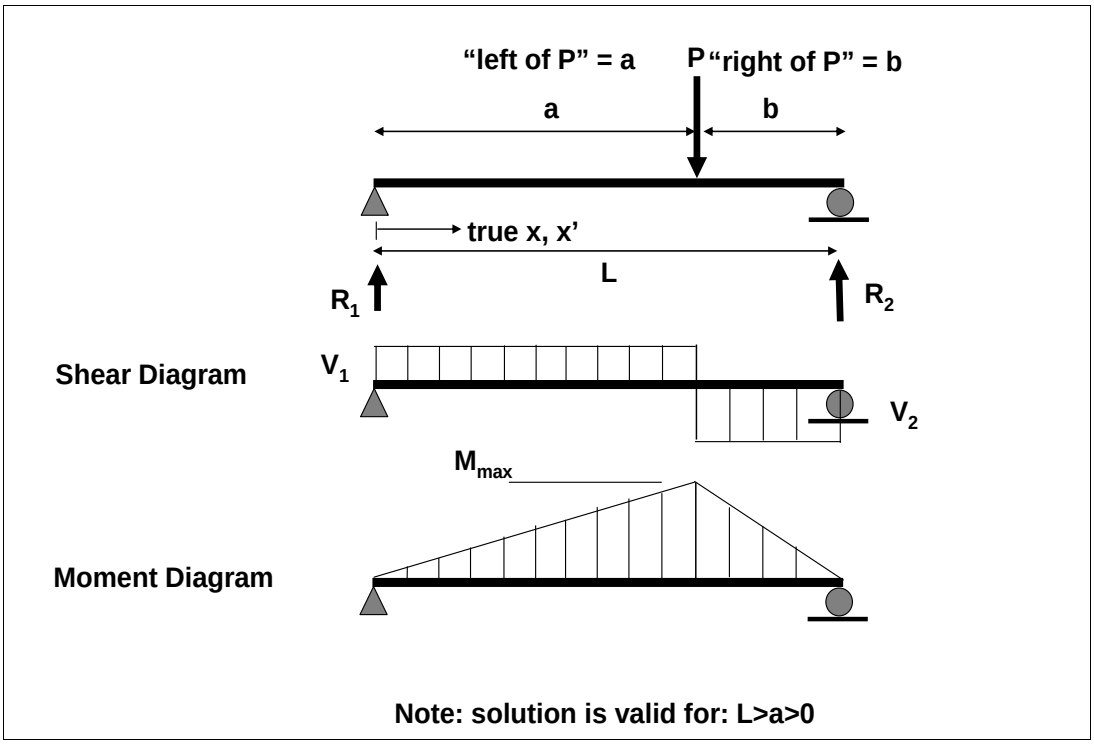

Figure 3.5. Shear and moment diagrams for a simply supported beam with a static point load *P*.

The reaction forces R_1 and R_2 are given as

$$R_1 = P \bullet \frac{b}{L} \tag{3.8}$$

$$R_2 = P \bullet \frac{a}{L} \tag{3.9}$$

and the magnitude of the internal shear force of the beam is equal to

$$V_1 = R_1 \tag{3.10}$$

for $x<a$, and

$$V_2 = -R_2 \tag{3.11}$$

for $x>a$, as shown in Appendix G. That is, the shear distribution is constant along the beam section to the left and to the right of the location of the point load P, as shown in Figure 3.5. For completeness,

$$P = R_1 + R_2 \tag{3.12}$$

The maximum bending moment, located at the point load, is

$$M_{Max} = R_1 \bullet a \tag{3.13}$$

After introducing Equation 3.8, it becomes

$$M_{Max} = P \bullet \frac{a \bullet b}{L} \tag{3.14}$$

The internal bending moment of the beam for $x<a$ is

$$M(x) = M_{Max} \bullet \frac{x}{a} \tag{3.15}$$

and

$$M(x) = M_{Max} \bullet \left[1 - \frac{x-a}{b}\right] \tag{3.16}$$

for $x>a$, as shown in Appendix G.

3.6 Shear force impact factor (SFIF)

Given a pulse force time-history $p(x_{point\ load},t)$ applied at a point $x_{point\ load}$ along the beam; the Shear Force Impact Factor (SFIF) is defined as the value of the dynamic shear force $V(x,t)$ computed at position x along the beam and during any time step t by Equation 2.31 divided by the static shear force calculated at this same position x along the beam for an applied static point load set equal to the magnitude of the pulse time-history at the same time step used for the dynamic shear calculation $p(x_{point\ load},t)$ using Equations 3.10 and 3.11. Recall the dynamic shear force is given by

$$V(x,t)=\sum_{n=1}^{r} EI \bullet \varphi'''(x) \bullet q_n(t) \qquad \text{(2.31 bis)}$$

with r modes considered in the analysis. Then, the Shear Force Impact Factor is calculated as

$$SFIF=\left(\frac{V_{dyn}}{V_{st}}\right)_{\left(x_{point\ load},t\right)} \qquad (3.17)$$

SFIF is computed at each point along the beam for each time step of the pulse time-history by the computer program Impact_Beam. The point of maximum static shear occurs anywhere between the position of the point load and the reaction that is closest to the point load (i.e., the shear force is uniform within this region). Impact_Beam will determine the value for SFIF for the user specified slender, simply supported impact beam and for the applied pulse force time-history.

Observation:

- If the point load is applied at a slow rate, so that inertial forces resulting from the structural time-varying displacements of the beam mass are negligible, the *SFIF* is unity.

3.7 Moment impact factor (MIF)

Given a pulse force time-history $p(x_{point\ load},t)$ applied at a point $x_{point\ load}$ along the beam; the Moment Impact Factor (MIF) is defined as the value

of dynamic moment $M(x,t)$ computed at position x along the beam and during any time step t by Equation 2.28 divided by the static moment calculated at this same position x along the beam for an applied static point load set equal to the magnitude of the pulse time-history at the same time step used for the dynamic moment calculation $(x_{point\ load},t)$ using Equations 3.15 and 3.16. Recall the dynamic moment is given by

$$M(x,t) = \sum_{n=1}^{r} EI \bullet \varphi_n''(x) \bullet q_n(t) \qquad \text{(2.28 bis)}$$

with r modes considered in the analysis. Then, the Moment Impact Factor is calculated as

$$MIF = \left(\frac{M_{dyn}}{M_{st}} \right)_{(x_{point\ load},t)} \qquad (3.18)$$

MIF is computed at each point along the beam for each time step of the pulse time-history by the computer software Impact_Beam. Impact_Beam will determine the value for MIF for the user specified slender, simply supported impact beam and for the applied pulse force time-history.

Observation:

- If the point load is applied at a slow rate so that inertial forces resulting from the structural time-varying displacements of the beam mass are negligible, the MIF is unity.

4 Visual Modeler GUI for Impact_Beam

4.1 Background

To conduct a dynamic structural response analysis of flexible approach walls at Corps locks using structural dynamics engineering computer programs, a force time-history is needed to represent the impact of a barge train with the approach wall. This force time-history can be created with the PC-based software Impact_Force (Ebeling et al. 2010). The engineering formulation for Impact_Force uses existing pulse data or synthetic pulse data and the impulse momentum principle to convert the linear momentum of a barge train into a scaled pulse force time-history acting normal to the approach wall. Included in its software development effort was the interpretation of the results from the 1997 full-scale barge train impact prototype experiments conducted at Old Lock and Dam 2 just north of Pittsburgh, PA, and of the 2008 full-scale barge train impact experiments conducted at Winfield Lock and Dam, Winfield, WV.

This chapter introduces the Impact_Beam graphical user interface. The various inputs and how they should be used are discussed. The Impact_Beam visual modeler has a similar tab-like structure as the Impact_Force visual modeler. The appropriately scaled output force time-history that is generated from the Impact_Force software will serve as the input force time-history for the Impact_Beam visual modeler. Section 4.3.2 will discuss this particular feature. Figure 4.1 shows the Impact_Force units and the barge train input parameters that emulate Winfield Barge Impact Experiment 10.

Figure 4.2 displays the scaled impact time-history normal to the approach wall for Barge Impact Experiment 10. This experiment recorded a maximum force of 517 kips. Four distinct pulses are also noticeable for Experiment 10. The first noticeable pulse occurs with the maximum peak of 517 kips. The second, third, and fourth noticeable pulses have peak values of approximately 232 kips, 139 kips, and 74 kips, respectively. This trend of decreasing amplitude pulses as the impact event proceeds is typical for all of the Winfield field impact tests. (A similar trend was observed in the pulse time-history results for the 1997 full-scale barge train impact prototype experiments conducted at Old Lock and Dam 2 and shown in Appendix B of Ebeling et al. 2010.)

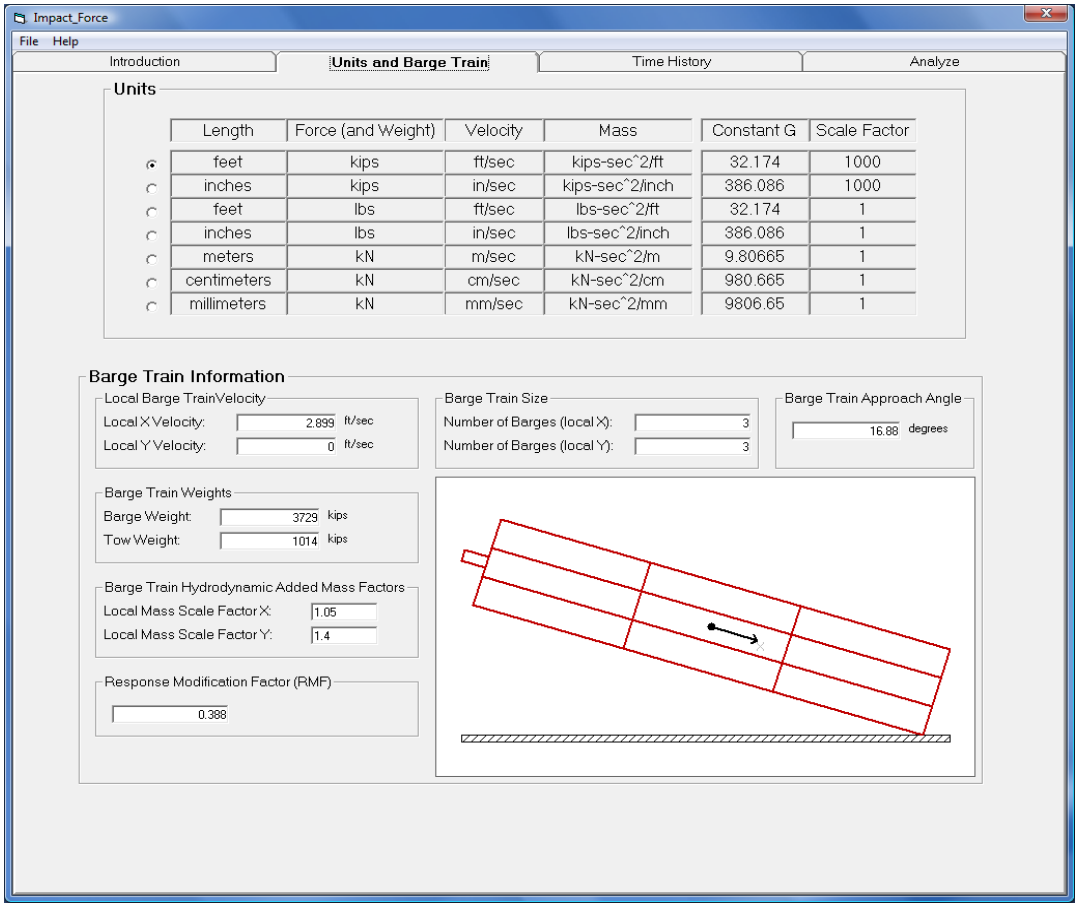

Figure 4.1. Impact_Force units and barge train information tab.

Figure 4.3 shows the frequency information from the Fourier transformation of the Figure 4.2 normal force time-history recorded during Barge Impact Experiment 10. The natural frequencies for this experiment are 1.22 Hz (0.82 second) and 3.42 Hz (0.29 second). The near zero frequency is a long period wave form. It is artificial, introduced by a drift in the recording electronics (i.e., a DC underlying offset). It is not inherent to the structural system and is to be ignored.

4.2 Introduction

Figure 4.4 shows the Introduction tab for Impact_Beam. Also shown on this figure are the titles for the other five tabs; Units and Analysis Type, Time History, Output Parameters, Analyze, and Output. The different subsections of this chapter discuss each tab. Impact_Beam has the capability to perform two types of analysis: 1) Dynamic Response Analysis of a simply supported beam, 2) Single Degree of Freedom (SDOF) Analysis. Section 4.3 will discuss the Dynamic Response Analysis of a simply supported beam. Section 4.4 will discuss the SDOF Analysis.

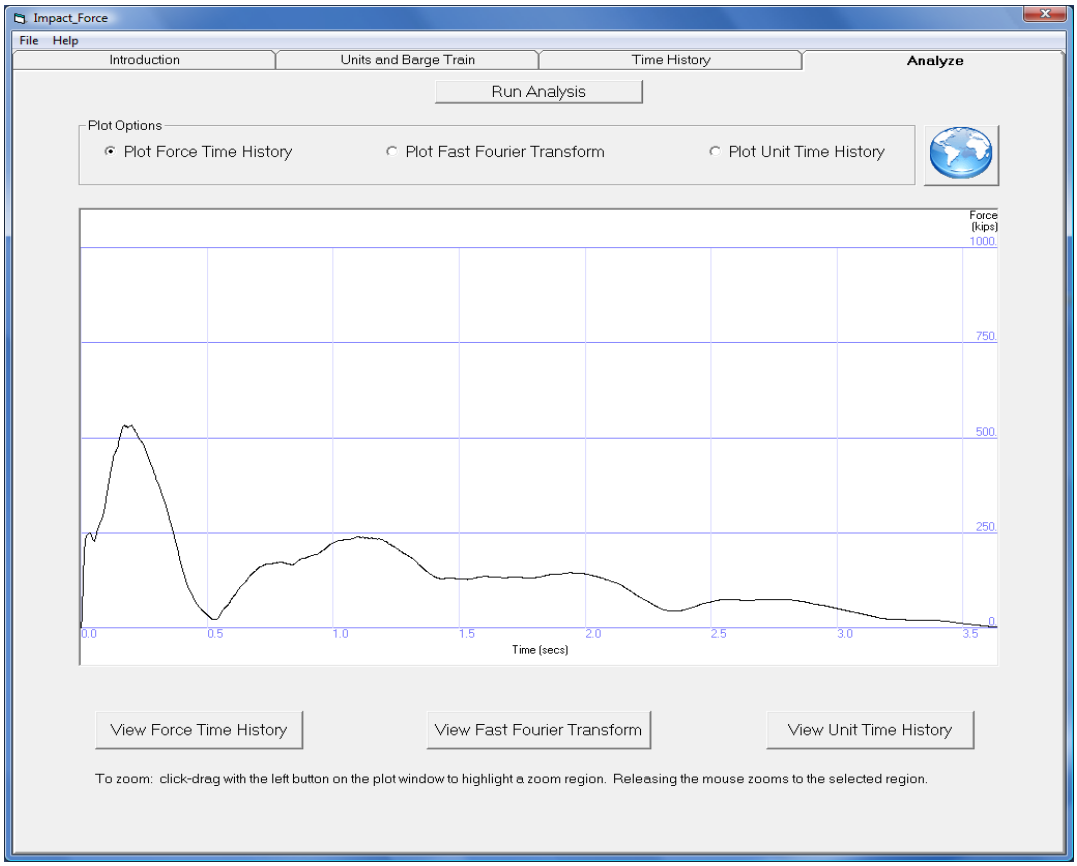

Figure 4.2. Impact_Force plot of force time-history output of barge experiment test 10.

4.3 Dynamic response analysis of a simply supported beam

A glancing blow impact event of a barge train with an approach wall as it aligns itself with a lock is an event of short duration; the contact time between the impacting corner of the barge train and the approach wall can be as short as a second or as long as several seconds. To reduce construction costs, as well as to reduce damage to barges during glancing blow impacts with lock approach walls, the next generation of Corps approach walls are more flexible than the massive, stiff-to-rigid structures constructed in the past. A flexible approach wall or flexible approach wall system is one in which the wall has the capacity to absorb impact energy by deflecting or "flexing" during impact, thereby affecting the dynamic impact forces developing during the impact event. The PC-based software Impact_Beam is used for performing a dynamic structural response analysis of a simply supported, flexible impact beam to a barge impact event. A pulse force time-history is used to represent the impact at the point of contact between the barge train and the flexible approach wall. The results of the analysis may be used to design a new structural member or evaluate the demands made of an existing impact beam.

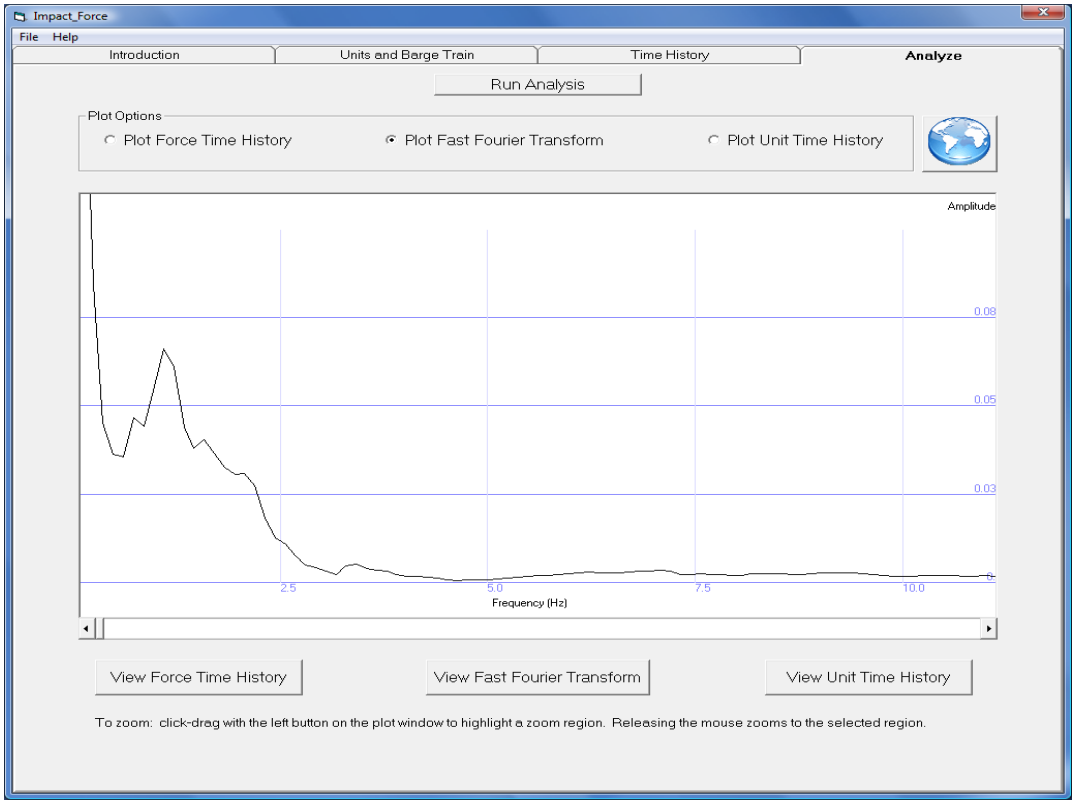

Figure 4.3. Impact_Force plot of Fourier Transformation of barge experiment test 10.

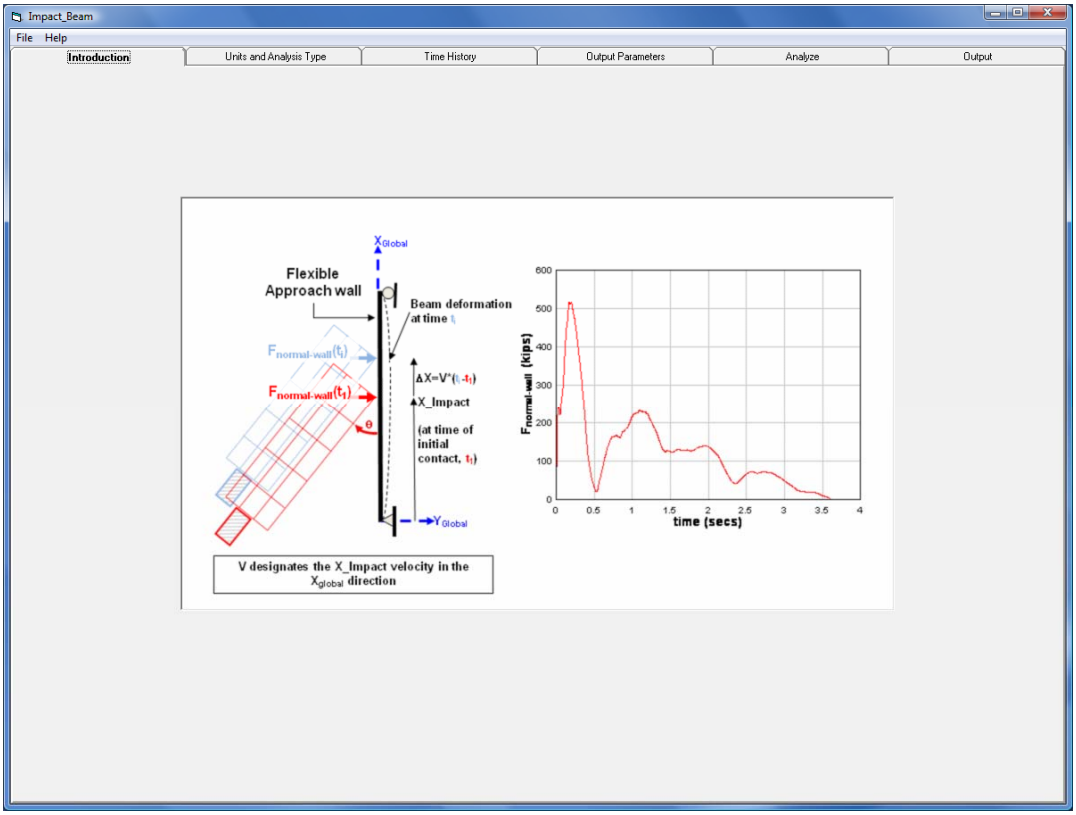

Figure 4.4. Impact_Beam introduction tab.

The PC-based software Impact_Beam is based on an engineering formulation that solves Newton's Second Law of Motion for the dynamic response of a simply supported, flexible impact beam subjected to a pulse force time-history representing the impact force over time at the point of contact between the barge train and the flexible approach wall.

4.3.1 Units and Analysis Type tab

In this tab, the user chooses the units that will be used as input and the type of analysis that will be used for the problem. The interface for the Units and Analysis Type tab is shown in Figure 4.5. The Units frame has a collection of radio buttons next to a chart of units. Selecting the appropriate radio button determines the units that will be used for input and engineering computation, as defined by the charts. The input parameters for the problem depend on what analysis option is selected by the user. Figure 4.5 shows the input parameters when the user selects the Dynamic Response Analysis of simply supported beam option.

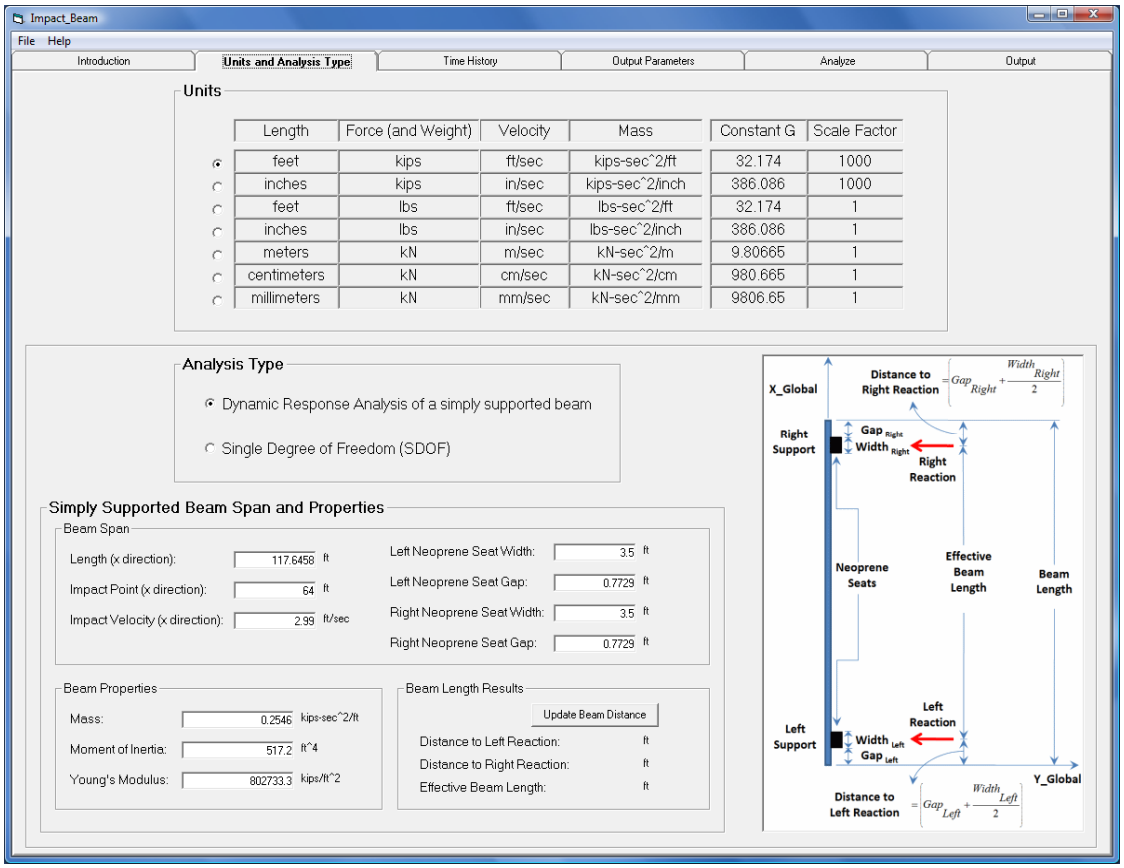

Figure 4.5. Impact_Beam Unit and Analysis Type tab with the Dynamic Response Analysis of a simply supported beam option selected.

For the Dynamic Response Analysis of a simply supported beam option, the user will input data interactively in regards to the following beam span and properties: length (in the *X* direction), impact point (in the *X* direction), impact velocity (in the *X* direction), neoprene seat widths (on the left and right side), neoprene seat gaps (on the left and right side), mass, moment of inertia, and Young's Modulus in the Simply Supported Beam Span and Properties frame. A visual aide showing the beam is provided to assist the user in entering the information for the left and right neoprene seat widths and gaps (between the end of the pad and the end of beam). This information is required to compute the effective beam length, which is discussed in Chapter 5. Effective beam length is defined as the distance from center-to-center of the neoprene pads. After providing the input value for the left and right neoprene seat width and gaps, the user can click the Update Beam Distance button, located in the Beam Length Results frame, to confirm the results for the effective beam length, the distance to the left reaction point of the beam, and the distance to the right reaction point of the beam.
Figure 4.7 shows the result of the user clicking the Update Beam Distance button in the Beam Length Results frame.

***<u>Note</u>: The units to the right of the input text boxes change in correspondence to the units selected in the table, as shown in Figure 4.6.**

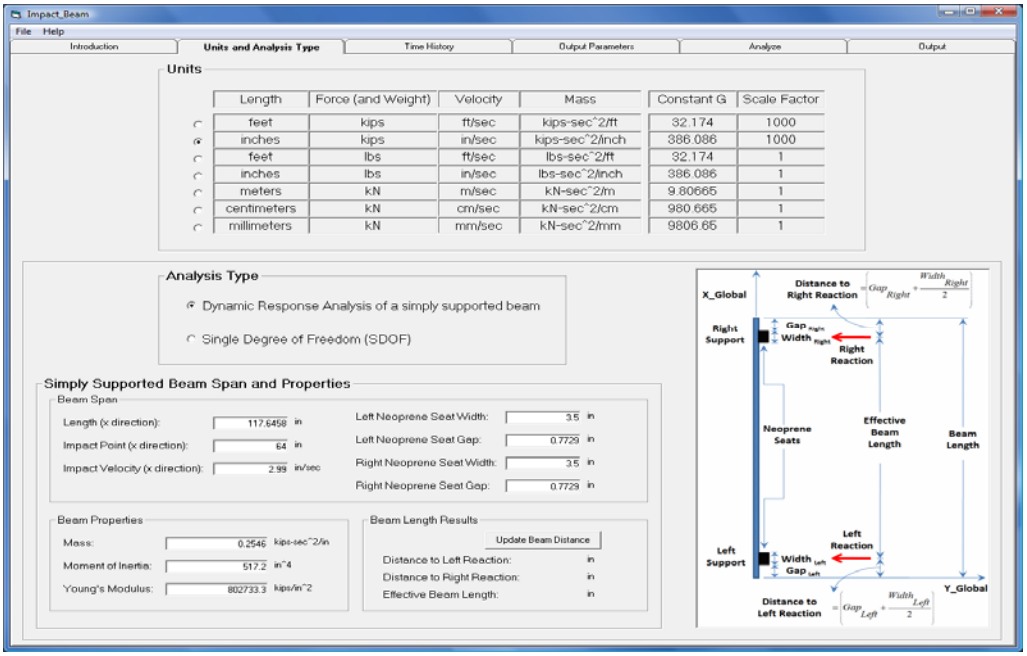

Figure 4.6. Showing that the units to the right of the input text boxes change accordingly to the units selected from the table.

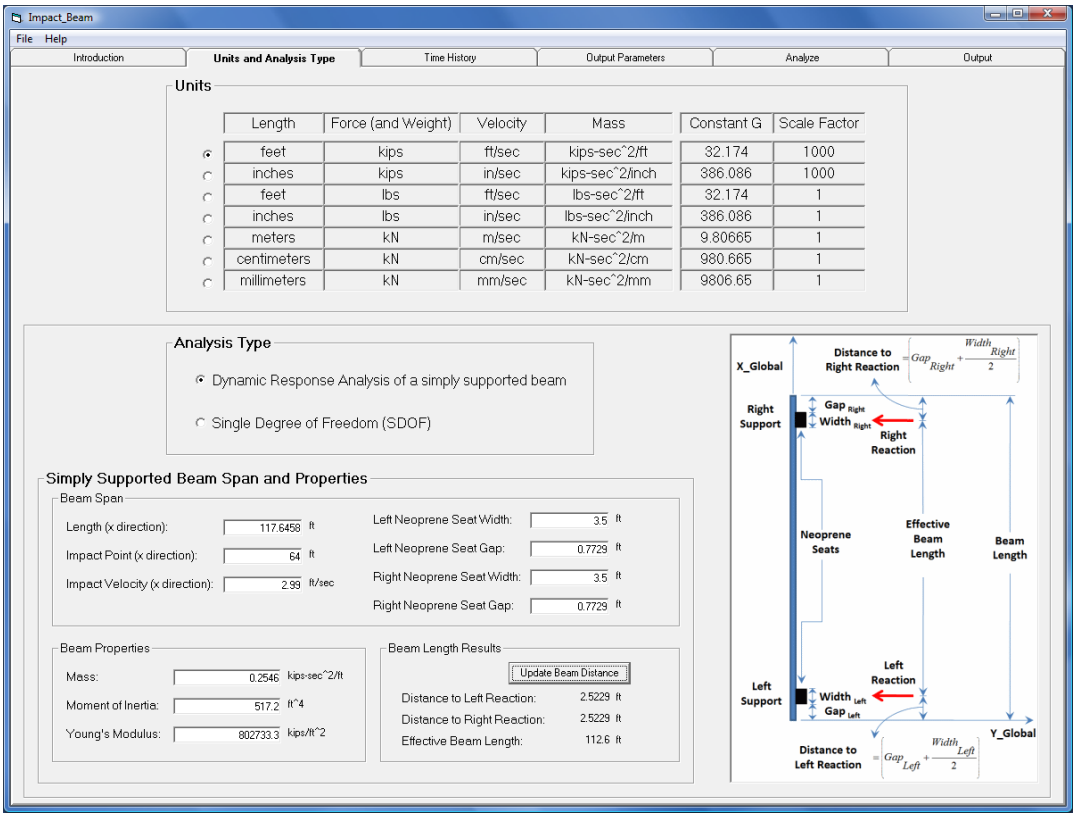

Figure 4.7. Showing the results of clicking the Update Beam Distance button in the Beam Length Results frame.

4.3.2 Time History tab

The Time History tab is more complex than the Unit and Analysis Type tab. Input for this tab is dependent on the force time-history data that is generated from the Impact_Force Visual Modeler. This tab is broken down into two sections: the time history properties section and the time history comparison (optional) section.

To select a file for the force time-history data, click the “Browse” button at the top of the tab. A file open dialog will appear, allowing the user to open force time-history data with an extension of “.frc” (“frc” denotes force time-history). It may be necessary to navigate to the directory where the force time-history data, generated with the Impact_Force software, is stored. The default force time-history file generated by Impact_Force is named “Force.FRC” and stored in the Impact_Force installation directory by default. This is the filename that the user should select as the force time-history data for the Impact_Beam visual modeler. Figure 4.9 shows the user browsing the force time-history data that was generated from the Impact_Force visual modeler.

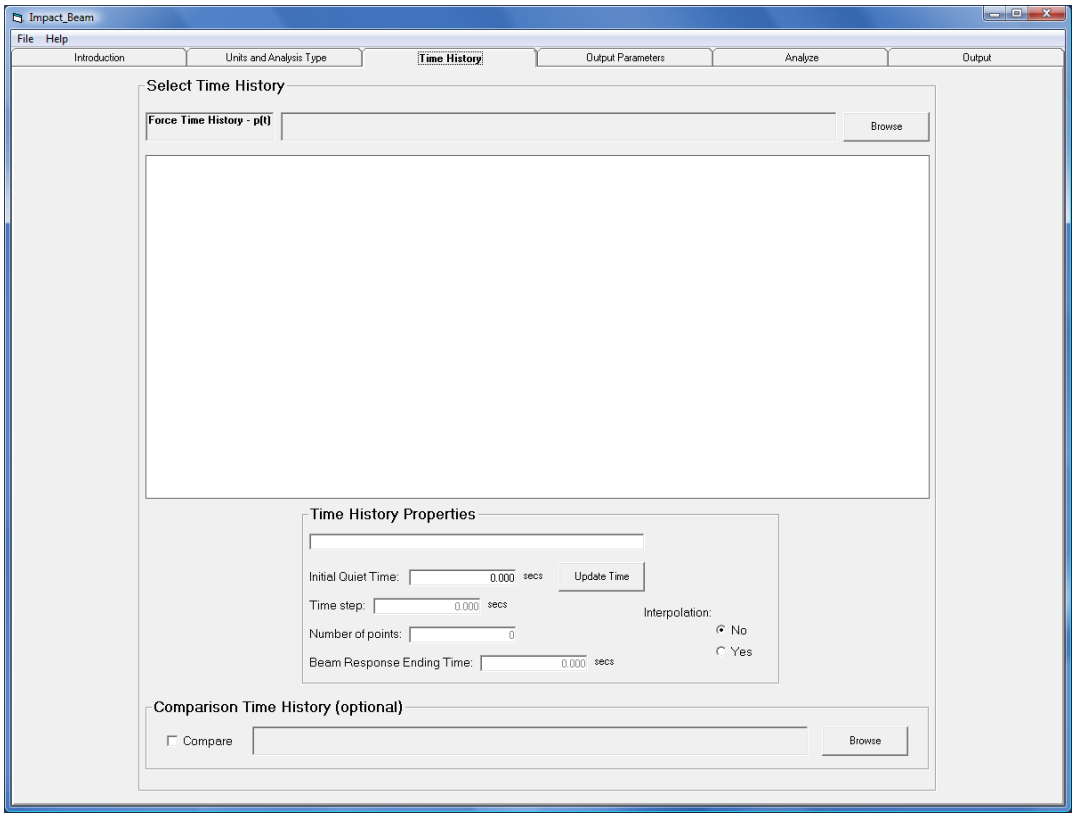

Figure 4.8. The Time History selection window.

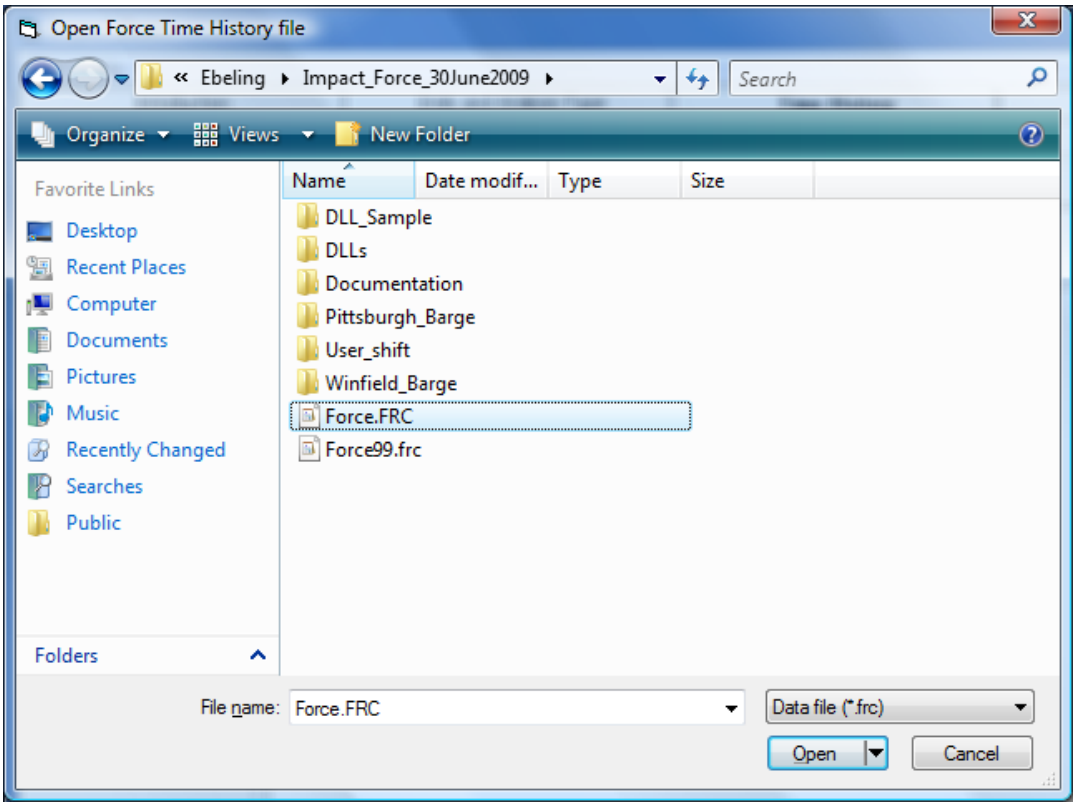

Figure 4.9. Browsing for Force Time-History data.

When a file has been selected, its name is displayed in the label next to the browse button. The window will contain a plot of the selected force time-history data. Figure 4.10 shows the plot of the force time-history data in the window. In the Time History properties frame, four non-editable text boxes will be populated from the force time-history data: the header information describing what force time-history was selected, the time step of the data, the number of points, and the beam response ending time.

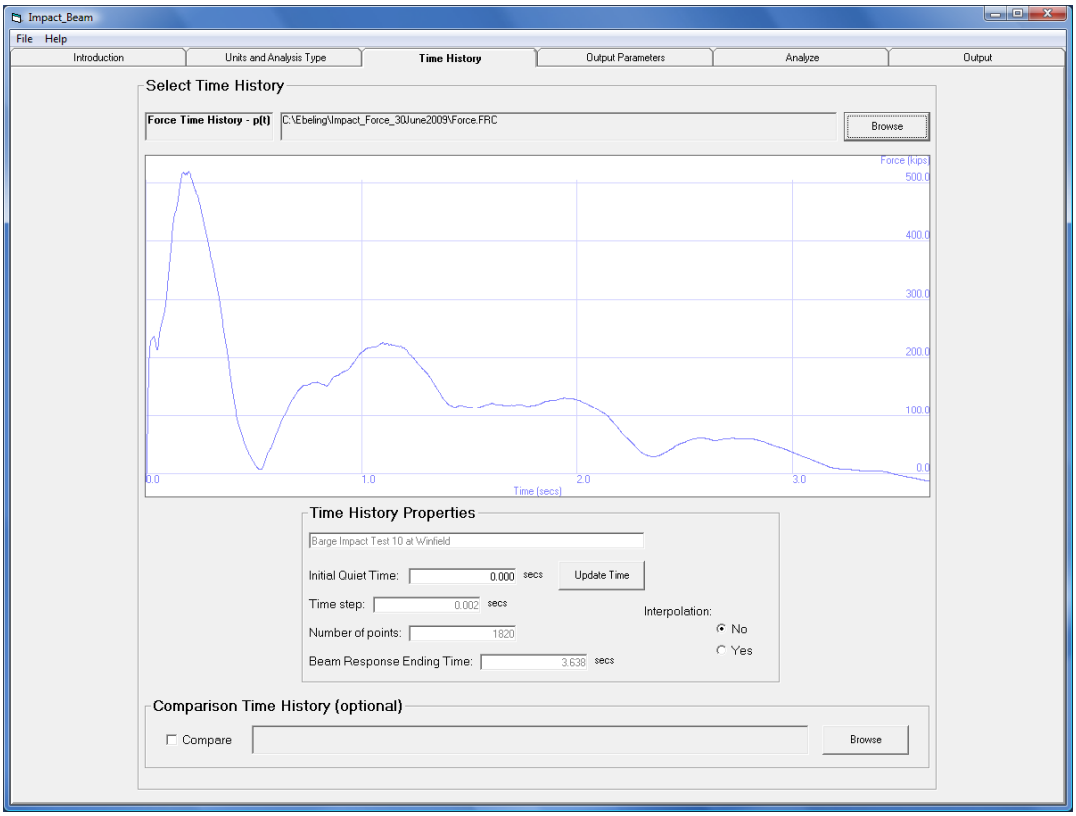

Figure 4.10. Adding a Force Time-History to the window.

The user has the option to add quiet time, as zero force data for a specified time, to the beginning of the force time-history by entering the amount of seconds inside the text box located by the “Initial Quiet Time” label. After entering the desired amount of quiet time, the user has to click the “Update Time” button, which will update the force time-history with the additional quiet time with a corresponding force of zero. If the user elects not to add any quiet time, then a value of 0 seconds should be left in the “Initial Quiet Time” text box. Figure 4.11 shows 1 second of quiet time added to the force time-history.

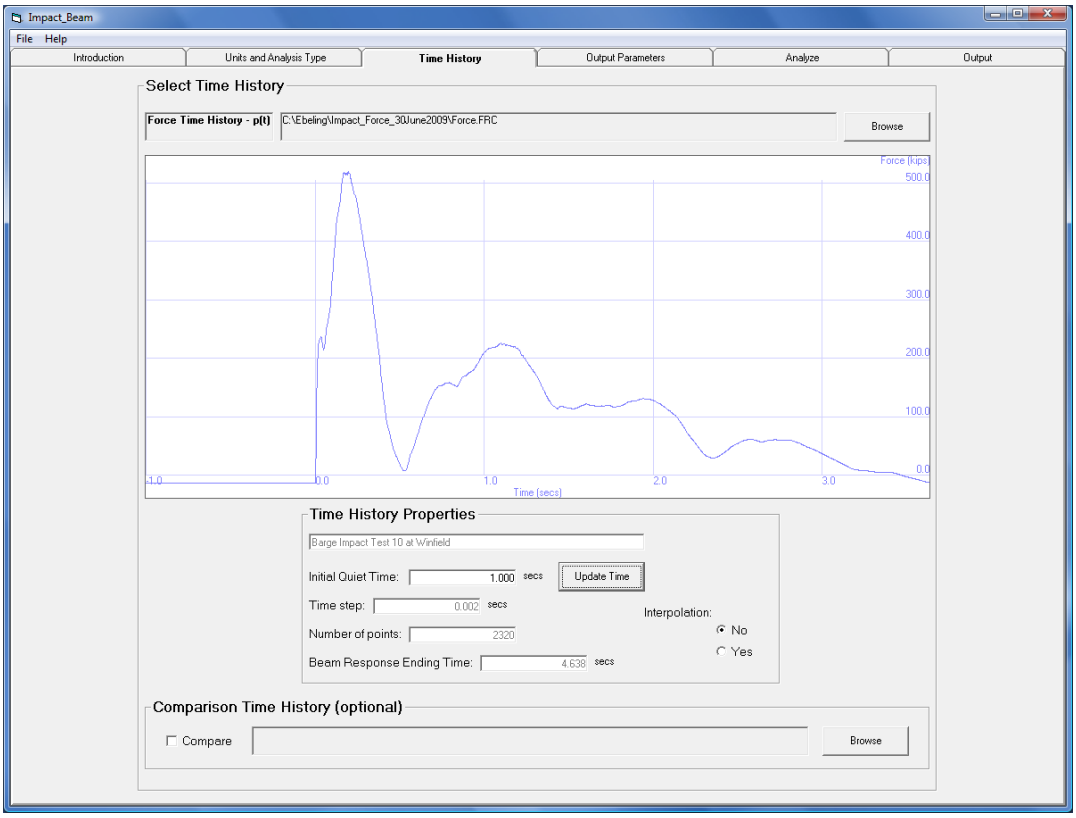

Figure 4.11. Adding 1 second of quiet time to the Force Time-History.

A seldom used resampling option can be selected to interpolate the force time-history data for shorter time steps. The user has the option to resample the data using linear interpolation by selecting the yes or no option buttons, respectively.

The user has the option to compare the results of an Impact_Beam simulation with experimental data recorded at the Winfield Lock in Winfield, West Virginia. To select a file for the comparison time-history, click the “Browse” button at the bottom of the tab. A file open dialog will appear, allowing the user to open a Winfield Barge Impact Beam time-history data with an extension of “.txt” (“txt” denotes a text file). It may be necessary to navigate to the directory where the recorded Winfield Barge Impact Beam data are stored. When the program is installed there should be a directory named “Winfield_Barge_Impact_Beam“ which stores the Winfield Barge Impact Beam time-histories. This directory contains all of the recorded beam deflections, rigid body deflections, and strain gage data from the August 2008 full-scale impact experiments. Figure 4.12 shows the user browsing the Winfield Barge Impact Beam time-history data.

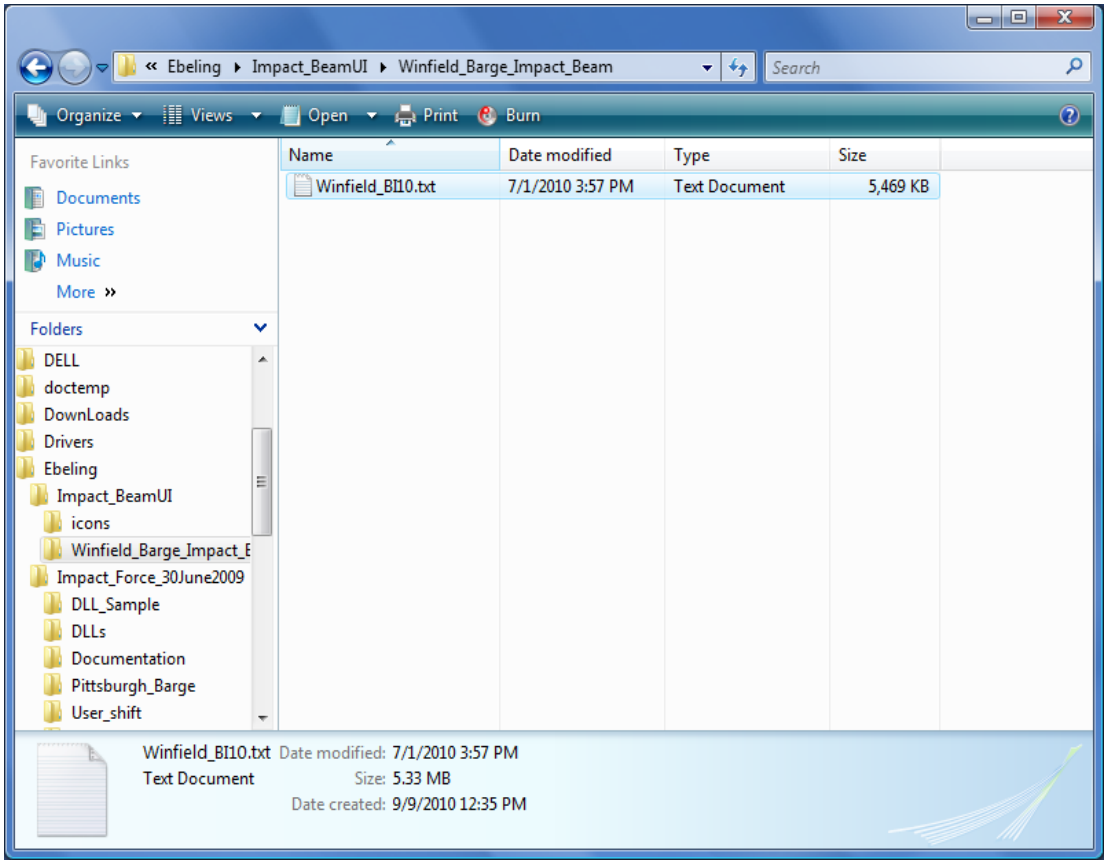

Figure 4.12. Browsing for Winfield Barge Impact Beam Comparison Time-History data.

When a file has been selected for the comparison time-history, its name is displayed in the label next to the browse button. Then, the user has to click a check in the check box that is located next to the label named “Compare”. If the user does not click a check in the check box, then a comparison will not be performed. Figure 4.13 shows the results of selecting the Comparison Time History option.

4.3.3 Output Parameters tab

In this tab, the user will select the output parameters that are required for the analysis of an Impact_Beam problem. The number of beam frequencies, damping ratio, sensor positions along the beam, and desired units for output are examples of the output parameters for Impact_Beam. The output parameters presented to the user are dependent on the analysis option that is selected. Figure 4.14 shows the output parameters for the Dynamic Response Analysis of a simply, supported beam.

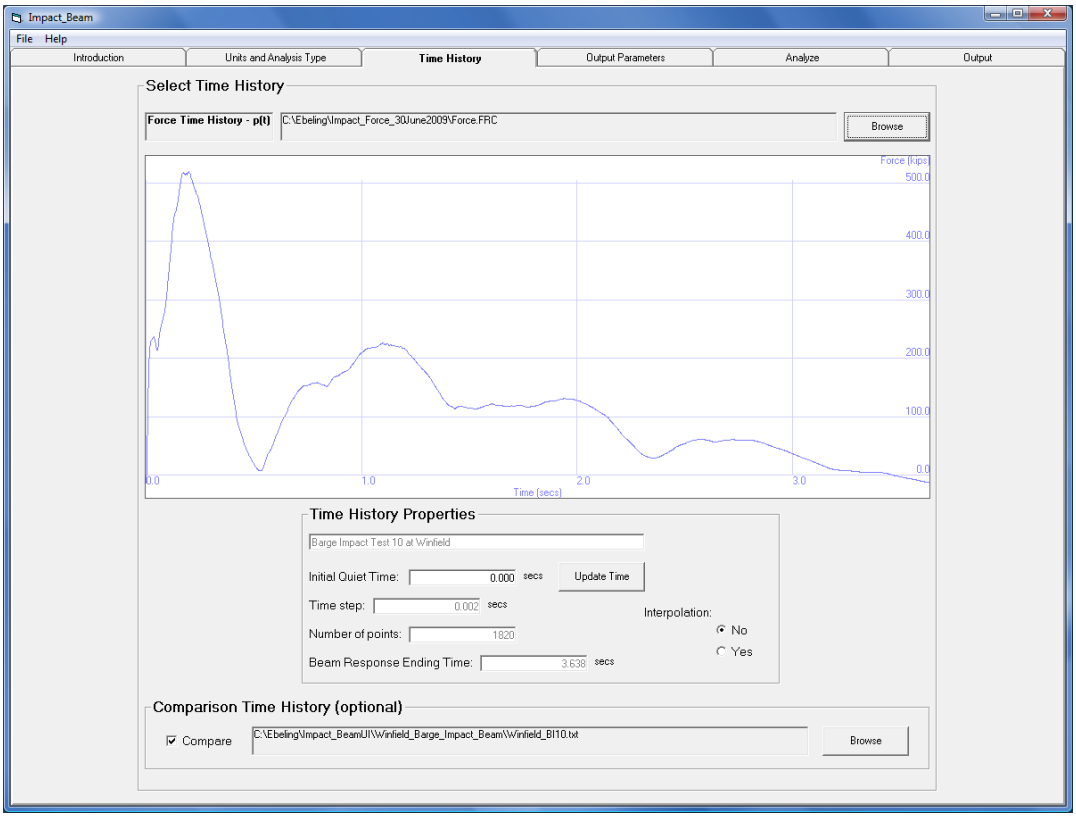

Figure 4.13. Selection of Comparison Time History option.

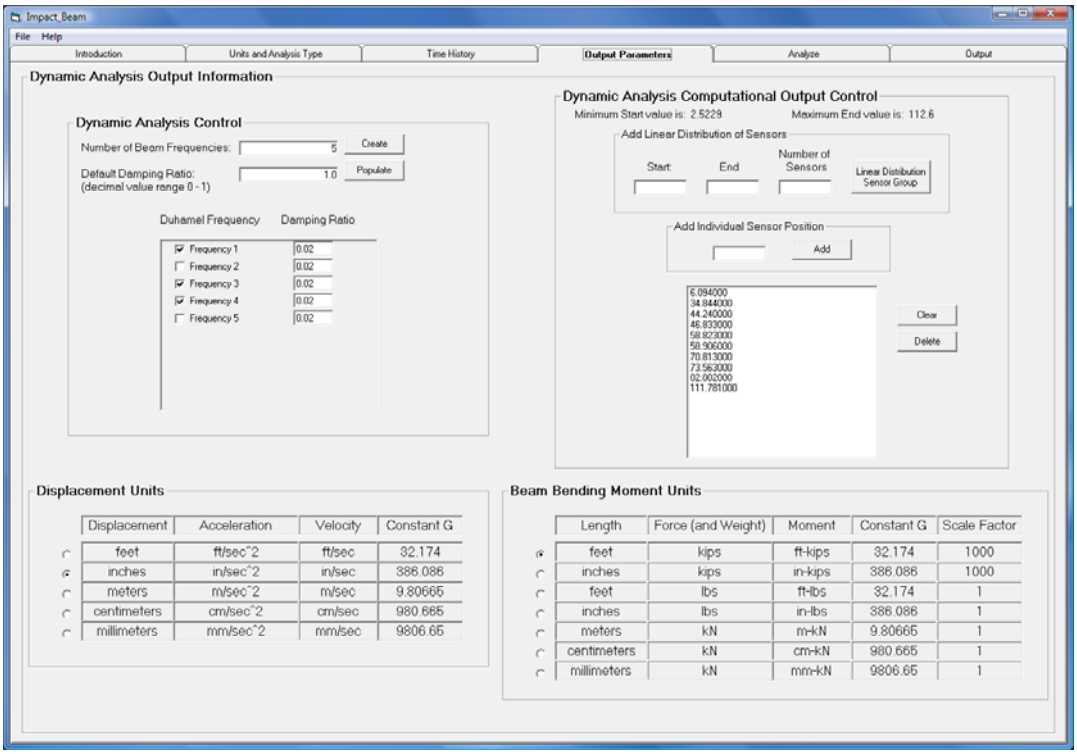

Figure 4.14. Output parameters tab for the Dynamic Response Analysis of a simply, supported beam option.

The number of beam frequencies and the damping ratio for each beam frequency is required for the Dynamic Response Analysis of a simply supported beam. In the Dynamic Analysis Control frame, the user will specify the number of beam frequencies for the problem. Clicking the "Create" button will create the desired amount of frequency check boxes with a corresponding input text box for the damping ratio, initially filled with the default damping ratio. The user will also have the capability to individually modify the damping ratio for each beam frequency. The user is required to check at least one frequency for the output.

Appendix I provides a summary of parametric test results with different values for the total number of input frequencies. From the test results, it is recommended that the user enter at least 5 frequencies to ensure that deflections have converged to consistent results. For moments to converge to consistent results, a total of at least 15 frequencies need to be entered, and for shear forces to converge, a total of at least 30 frequencies need to be entered. The number of frequencies chosen does not have a significant impact on the program run time, which is typically under two minutes.

The sensor positions along the beam are also required for the Dynamic Response Analysis of a simply supported beam. In the Dynamic Analysis Computational Output Control frame, the user can specify the sensor locations along the beam by adding a linear distribution of sensor positions or by adding an individual sensor position. There are two sub-frames for each respective case. To add a linear distribution of sensor positions, the user will specify a start sensor position value, an end value sensor position value, and the number of sensors that will be placed within the start and end values. Clicking the "Linear Distribution Sensor Group" button will place the linear distribution of sensor positions inside of a list box in ascending order. Figure 4.15 shows the result of adding a linear distribution of sensor positions along the beam. In the "Add Individual Sensor Position" sub-frame, a user can specify individual sensor positions along the beam. Clicking the "Add" button will add an individual sensor position to the list box. If the comparison option is selected, the sensor positions stored in the Winfield test data file will be populated in the list box automatically.

The user can delete an unwanted sensor position by selecting it from the list box and clicking the "Delete" button. Also, a multi-delete of unwanted sensor positions works in a similar fashion by selecting sensor positions while pressing the Ctrl key at the same time. Clicking the "Clear" button will remove all of the sensor positions located in the list box.

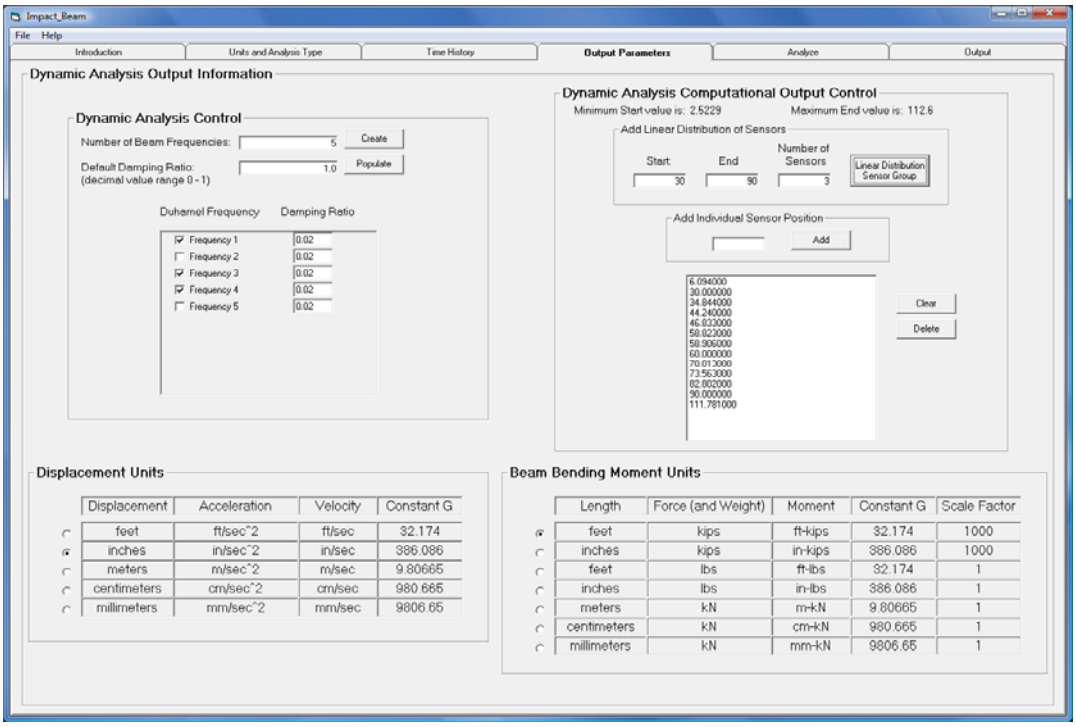

Figure 4.15. Adding a Linear Distribution of Sensor Positions.

In the Displacement Units frame and the Beam Bending Moment Units frame, the user will choose the units that will be used as output for the displacement and the beam bending moments, respectively.

4.3.4 Analyze tab

The Analyze tab serves two major functions for the Impact_Beam Visual Modeler. It first provides a visual confirmation of the user's input for the problem. Figure 4.16 shows a visual confirmation of the user's input for the Dynamic Response Analysis of a simply supported beam. Inside of the window, there is a plot of the beam, a plot of the force time-history (from Section 4.3.2), the start and end impact points along the beam and the sensor locations along the beam (from Section 4.3.3). Each of these elements is color coordinated in the legend in the top left corner of the window.

Secondly, the Analyze tab also allows the user to run the Impact_Beam program and view the consequent output. Before the data can be run, valid input must be entered on the Units and Analysis Type tab and the Output Parameters tab, and a force time-history must be in the TimeHistory window of the Time History tab. If these conditions are met, the "Run Analysis" button is enabled, as shown in Figure 4.16.

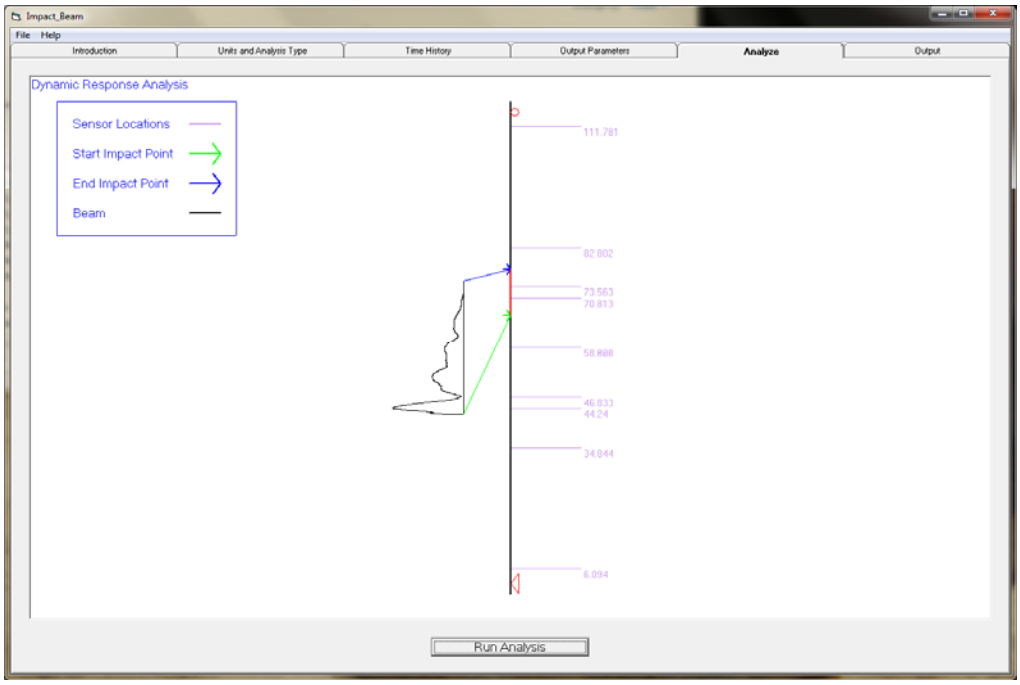

Figure 4.16. Analyze tab.

Clicking Run Analysis will execute the Impact_Beam program on the data that was entered for the Units and Analysis Type tab, the Time History tab, and the Output Parameters tab. After the analysis has been performed, a message box will alert the user that the Impact_Beam program has finished analyzing the data (shown in Figure 4.17).

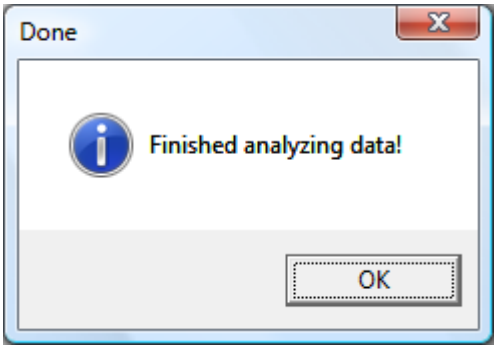

Figure 4.17. Finished analyzing data message box.

Clicking OK will allow the user to proceed in viewing the results of the analysis in the Output tab. The results are stored in a file named "Impact_Beam_Simulation.IBO", and its description is included in Appendix E. It is recommended that the user of the program use the tools in the Output tab to view the output data graphically, as quite a bit of data are stored in the file.

4.3.5 Output tab

The Output tab provides the visualization options that will be used to view the output results of the Impact_Beam simulation. This tab is composed of two visualization options: 1) An animated beam response over time, 2) An individual sensor position response along the beam over time. The two visualization options will not be enabled until the user opens the Impact_Beam output simulation file. Figure 4.18 shows the Output tab in its default state.

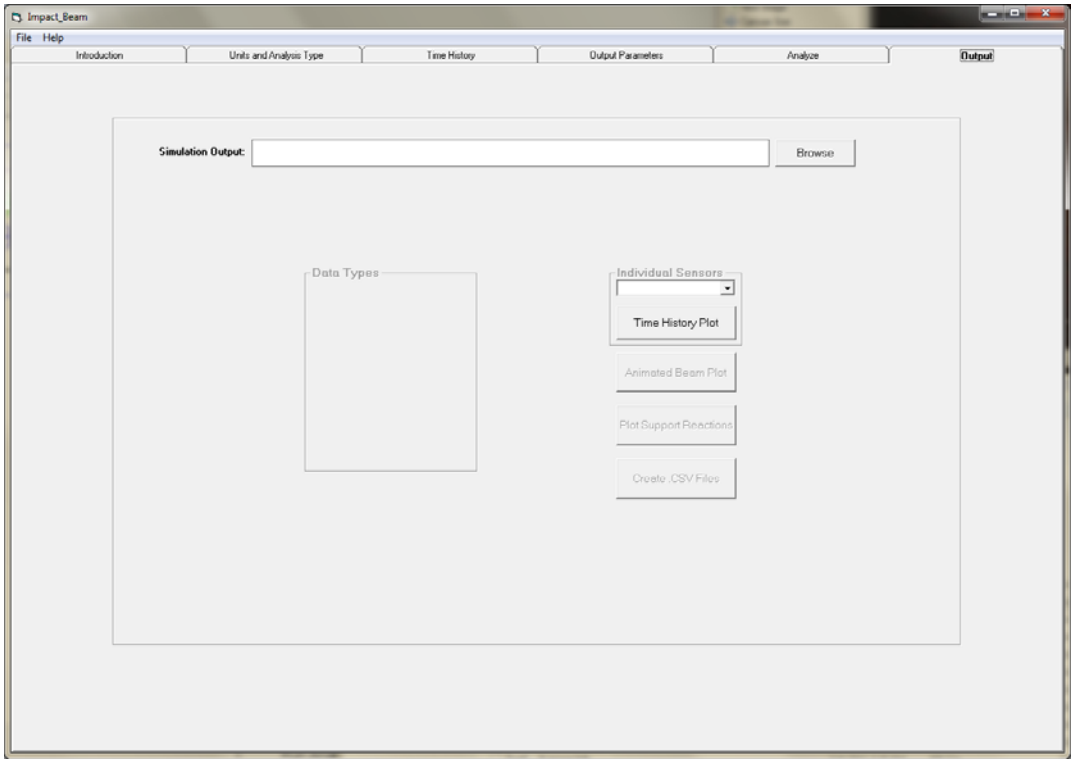

Figure 4.18. Default state for the Output tab.

To select a file for the output simulation data, click the “Browse” button at the top of the tab. A file open dialog will appear, allowing the user to open the output simulation data with an extension of “.out” (“out” denotes output file). After the user has run the analysis, an output simulation file named “Impact_Beam_Simulation.OUT” will be created in the Impact_Beam installation directory. This is the filename that the user should select as the output simulation file for the Impact_Beam visual modeler. Figure 4.19 shows the user browsing for the Impact_Beam output simulation file.

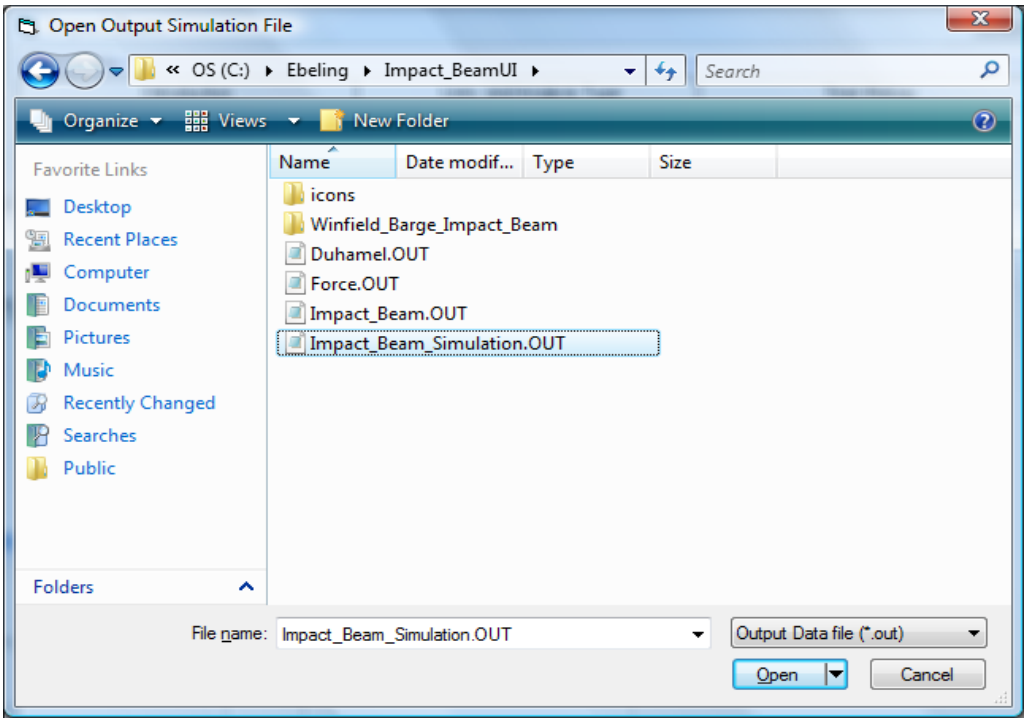

Figure 4.19. Browsing for Output Simulation data.

When the output simulation file has been selected, its name will be displayed in the label next to the browse button. If the comparison option is selected, then the comparison filename will be displayed near the bottom of the frame. If the comparison option is not selected, then the comparison filename will not be displayed. The Impact_Beam output simulation for the Dynamic Response Analysis of a simply supported beam consists of six data types:

- Dynamic Deflection,
- Dynamic Shear Force,
- Dynamic Moment,
- Displacement Impact Factor (DIF),
- Shear Force Impact Factor (SFIF), and
- Moment Impact Factor (MIF).

Each of the data types can be viewed by either of the two visualization options. Clicking the “Beam Plot” button will let the user view the animated beam response over time. Clicking the “Time History” button will let the user view the individual sensor position response along the beam versus time. The sensor positions for the Time History option will be selected from the drop-down box named “Sensors”. If the comparison option was selected, then there will be a sub-frame called “Comparison” that will allow

the user to select which data type will be viewed in the comparison output. Only beam deflections or moments can be viewed for the comparison output, as shown in Tables 4.1 and 4.2. Additional information about sensor locations can be found for the sensors in Appendix J. Sensor names are followed by their location to enable the user to more easily compare values. Figure 4.20 shows the viewing output options being enabled.

Table 4.1. Location along the beam of laser deflection sensors used for Winfield barge impact tests.

Sensor	Location from support (ft)
LD2	111.781
LD3	73.5625
LD4	58.906
LD5	44.24
LD7	6.094
LD1 and LD6 are on the adjacent beams	

Table 4.2. Location along the beam of strain sensors used to determine moments for Winfield barge impact tests.

Sensor	Location from support (ft)
S1	82.802
S2	70.813
S3	58.823
S4	46.833
S5	34.844

4.3.6 Beam Plot

Beam Plot is the viewing option that will display the animated beam response over time. After clicking the “Beam Plot” button, the user will be presented with a plot of the beam, shown in Figure 4.21. The Beam Plot consists of a simply supported beam, the start impact point, and the end impact point. The legend in the top left corner has these elements color-coordinated. Also, the sensor positions along the beam and the force time-history are displayed on the Beam Plot. In this example (shown in Figure 4.21), Dynamic Deflections was selected as the data type and Beam Deflections was selected for the comparison option. The x-axis shows the Deflection (in) value and the y-axis shows the sensor positions along the beam (ft). The blue circles represent the sensor positions specified by the user in the Output Parameters tab (see Section 4.4).

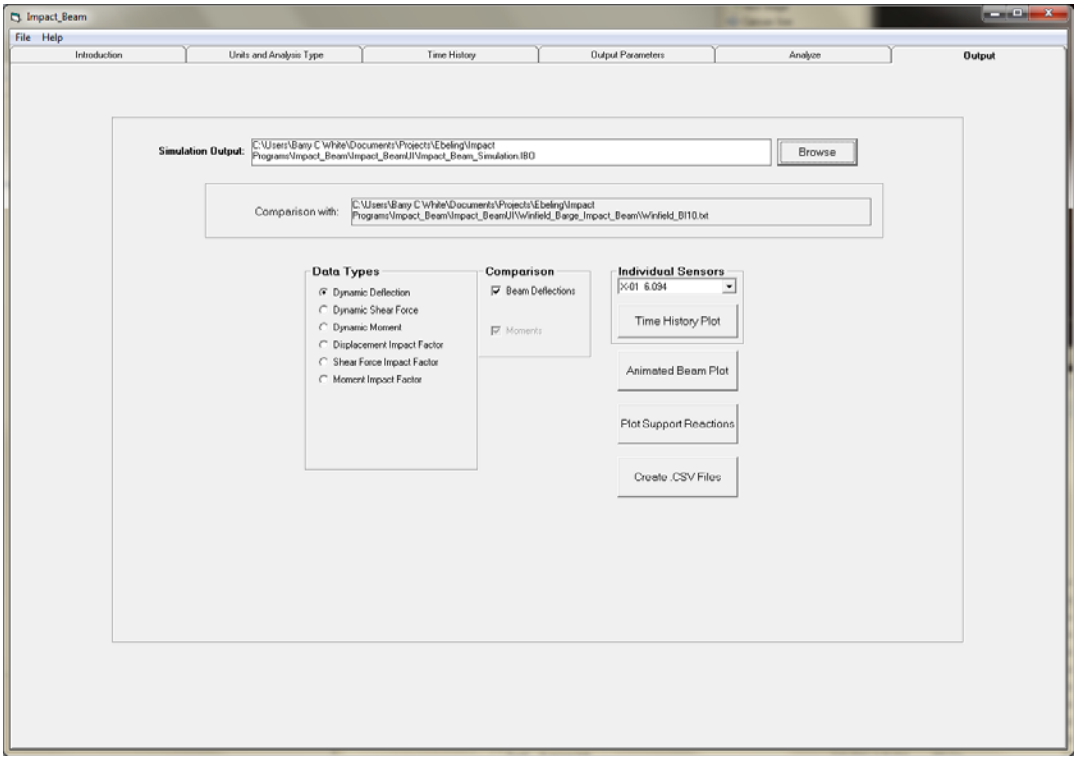

Figure 4.20. Viewing Output Options are enabled.

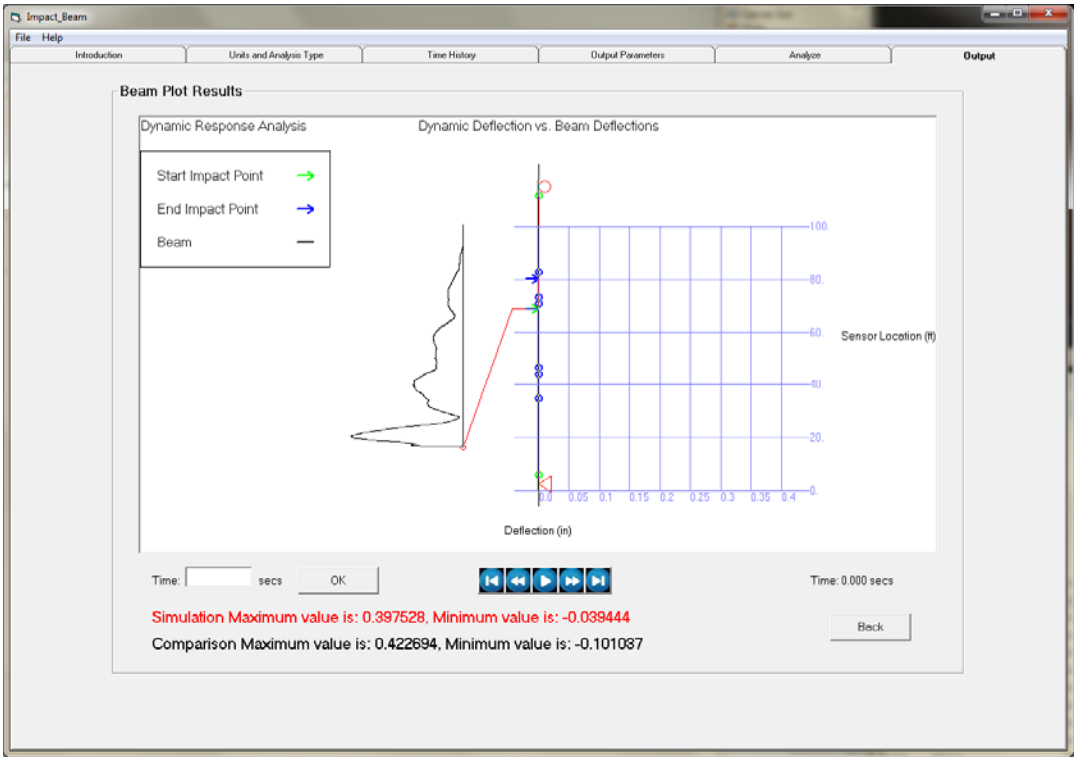

Figure 4.21. Beam Plot Results.

4.3.6.1 *Animation controls*

The animation controls are a set of buttons located directly below the center of the window. A tool tip is provided by scrolling the mouse over each button. A brief description of the buttons that make up the animation controls is listed below.

-  "Begin Data" – steps to the start of the animation
-  "Step Rewind" – steps back one time step
-  ,  "Play/Pause" – plays the animation / pauses the animation
-  "Step Forward" – steps forward one time step
-  "End Data" – steps to the end of the animation

To start the animation, press the "Play" button. The start time and the end time of the animation are respectively the minimum time and the maximum time specified in the force time-history. The time counter, located directly below the right corner of the window, will specify the time step during the animation. While the animation is playing, the user will have an idea of where the impact occurs at a given time step by the following indicators (shown in Figure 4.22):

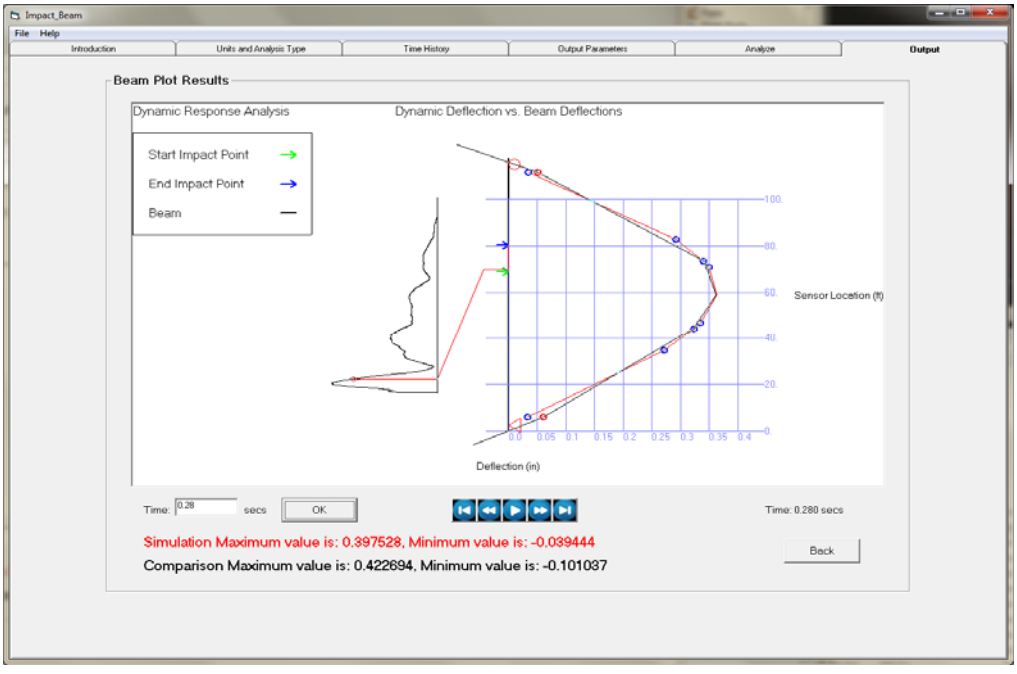

Figure 4.22. Beam Plot Result at 0.28 seconds.

- A red circle will move along the force time-history, giving a sense of the magnitude of the force at a given time.
- A red horizontal line will move from the start impact point to the end impact point, giving the actual position of the load at a given time.

The user will also have the option to view the beam response for a particular time step. By default, the user can specify a time step in the text box located directly below the left corner of the window. Clicking the "OK" button will display the beam response at the specified time step. If the animation is playing, the user will have to click the "Pause" button to pause the animation before specifying the time step of interest. Figure 4.22 shows the beam response at a time step of 0.28 seconds. Clicking the "Back" button will take the user back to the Viewing Options display as shown in Figure 4.20.

4.3.6.2 Time History plot

Time History is the viewing option that will display an individual sensor position response along the beam versus time. After selecting a sensor from the "Sensors" drop-down list and clicking the "Time History" button, the user will be presented with a plot of the time-history, shown in Figure 4.23. In this example, Dynamic Deflections was selected as the data type and Beam Deflections was selected for the comparison option. The x-axis shows the Time (secs) value and the y-axis shows the Deflection (in) value. The values of the x and y coordinates will be displayed by scrolling the mouse over any point in the time-history plot. A plot of the beam along with the start impact point (green arrow), the end impact point (blue arrow) and the selected sensor (red arrow) is displayed on the right side of the window. This will give the user an indication of where the sensor was positioned along the beam. Clicking the "Back" button will take the user back to the Viewing Options display as shown in Figure 4.20.

4.4 SDOF analysis

Since the solution being used is a time-history modal response method of analysis, a SDOF response analysis is fundamental to part of this solution process. The Impact_Beam software allows for user input and analysis of a SDOF system. User input in the Visual Modeler is presented below with pulse force time-history collected from the dBEAS software (Ebeling et al. 2010). The dBEAS software is developed for the purpose of determining impact forces as a barge train collides with a Deformable Bullnose Energy Absorbing System (BEAS), an innovative structure designed to prevent

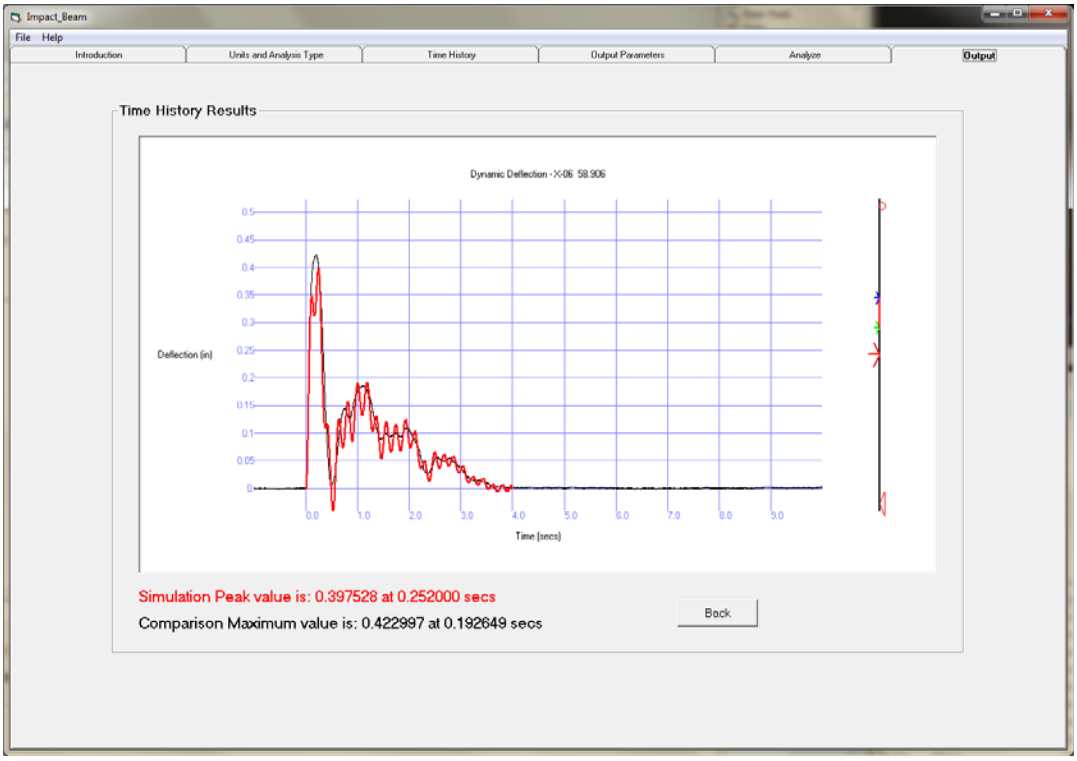

Figure 4.23. Time History plot.

lashing failures resulting in barges that are out of control due to an impact between a tow and a lock approach wall bullnose. Chapter 5 deals with the verification process that was performed between the dBEAS software and Impact_Beam software. It is worthwhile to notice that the Impact_Beam software can deal with pulse force time-histories from other sources than the collected data from Pittsburgh and Winfield.

4.4.1 Units and Analysis Type tab

Refer to Section 4.3.1 for information regarding the Units component of the Units and Analysis Type tab. Figure 4.24 shows the input parameters when the user selects the SDOF Analysis option with a linear slope. Figure 4.25 shows the input parameters when the user selects the SDOF Analysis option with a bi-linear slope.

For the SDOF Analysis option, the user will select the forcing function type (force time-history or acceleration time-history) and the slope type (linear or bi-linear) in their respective sub-frames. In the SDOF Properties sub-frame, the user will interactively input data regarding the mass and the damping ratio of the SDOF system. The input information for the SDOF slope properties is dependent upon what SDOF slope type was selected by

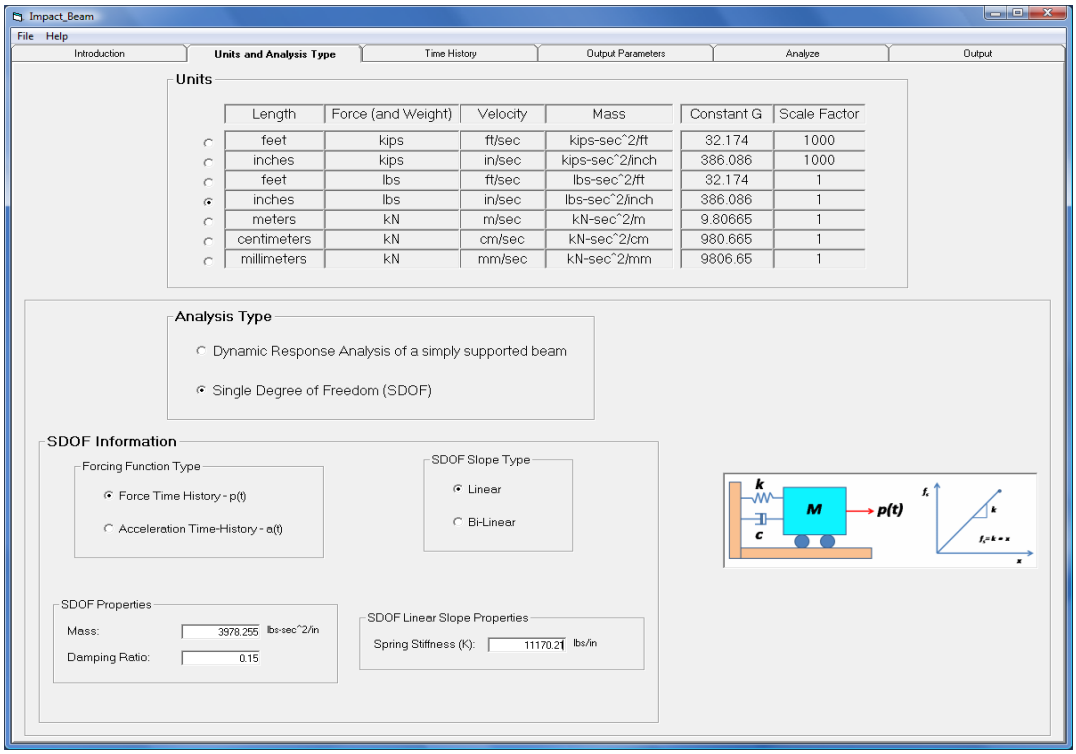

Figure 4.24. Impact_Beam Unit and Analysis Type tab with the SDOF analysis option with a linear slope.

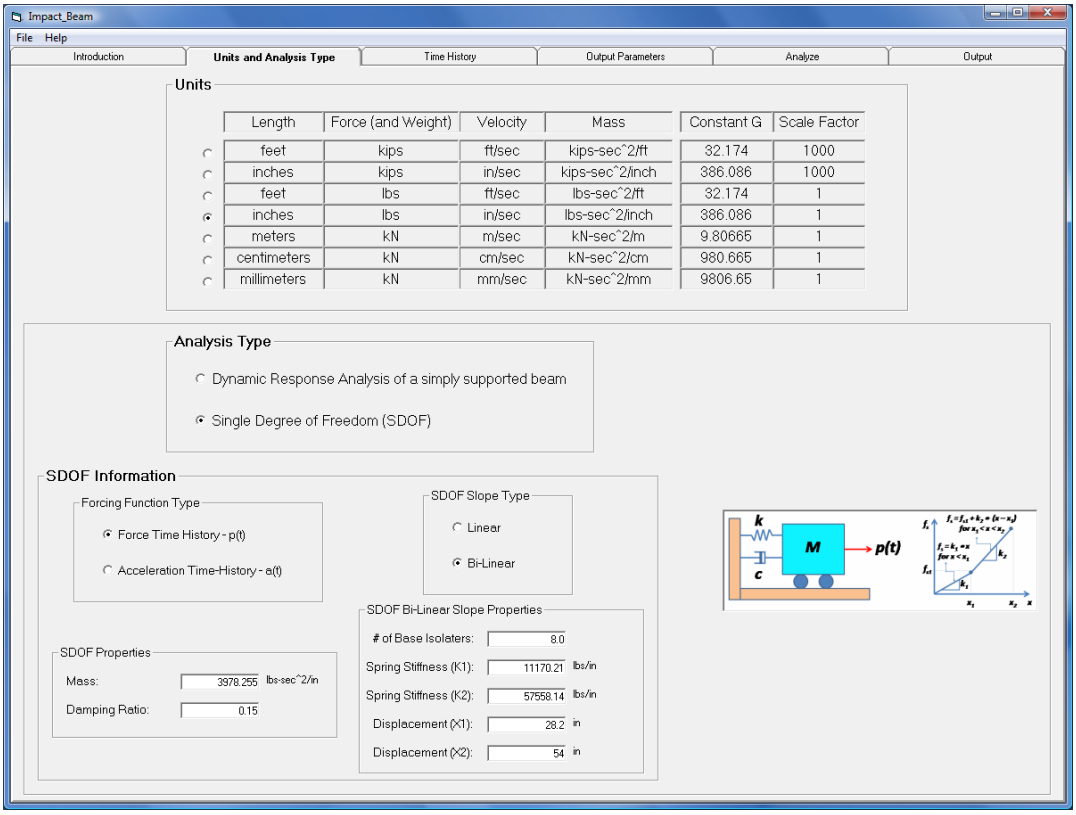

Figure 4.25. Impact_Beam Unit and Analysis Type tab with the SDOF analysis option with a bi-linear slope.

the user; linear or bi-linear. For a linear slope, the user only has to specify the spring stiffness (K). For a bi-linear slope, the user will have to specify the following: number of base isolators, the spring stiffness (K_1 and K_2), and the displacement (X_1 and X_2). A visual aide of the SDOF system and the slope function is provided for each of the SDOF slope types. For a linear slope (shown in Figure 4.24), the visual aid is used to assist the user in entering the information for K. For a bi-linear slope (shown in Figure 4.25), the visual aid is used to assist the user in entering the information for K_1 and K_2 and X_1 and X_2. The SDOF system example problem for the Impact_Beam Visual Modeler will use the bi-linear slope properties, as shown in Figure 4.25.

4.4.2 Time History tab

Refer to Section 4.3.2 for information regarding opening a input force time-history and the time-history properties for the Time History tab. There is not a comparison time-history option for the SDOF Analysis. Figure 4.26 displays a force time-history for a super-barge model as discussed in Chapter 5 (a single barge with the weight of 15 barges+tow).

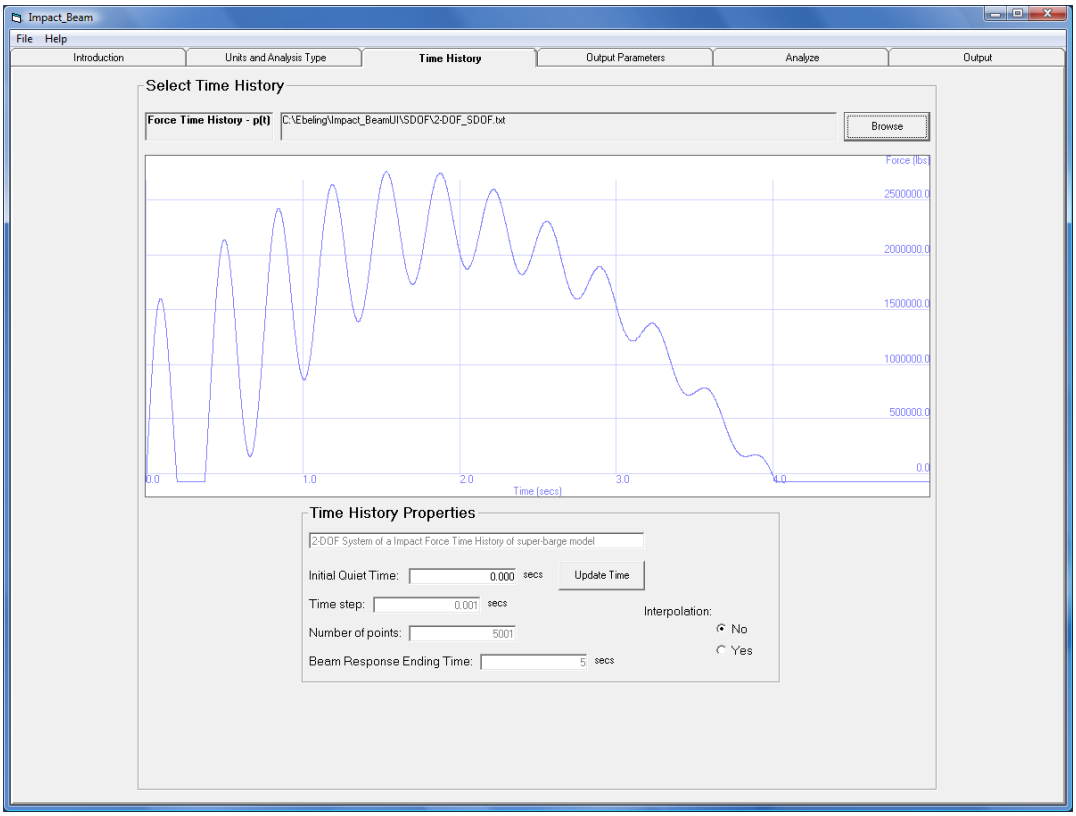

Figure 4.26. Adding a Force Time-History to the window.

4.4.3 Output Parameters tab

In this tab, the user will select the output parameters that are required for the analysis of an Impact_Beam problem. In the Displacement Units frame and the Force Units frame, the user will choose the units that will be used as output for the displacement and the force, respectively. Figure 4.27 shows the output parameters for the SDOF Analysis option.

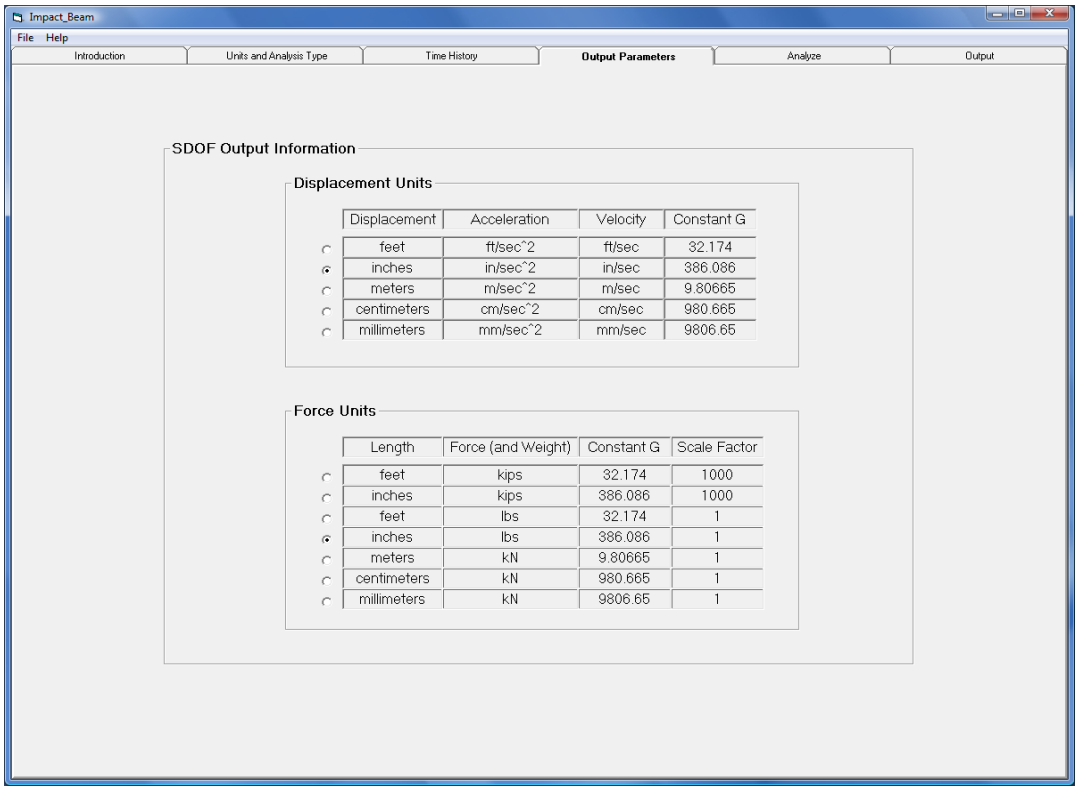

Figure 4.27. Output parameters tab for the SDOF Analysis option.

4.4.4 Analyze tab

The Analyze tab for the SDOF Analysis provides a visual confirmation of the user's input for the force time-history. Figure 4.28 shows a visual confirmation of the user's input of the force time-history for the SDOF system.

The Analyze tab also allows the user to run the Impact_Beam program and view the consequent output. Before the data can be run, valid input must be entered on the Units and Analysis Type tab and the Output Parameters tab, and a force time-history must be in the Time History window of the Time History tab. If these conditions are met, the "Run Analysis" button is enabled, as shown in Figure 4.28.

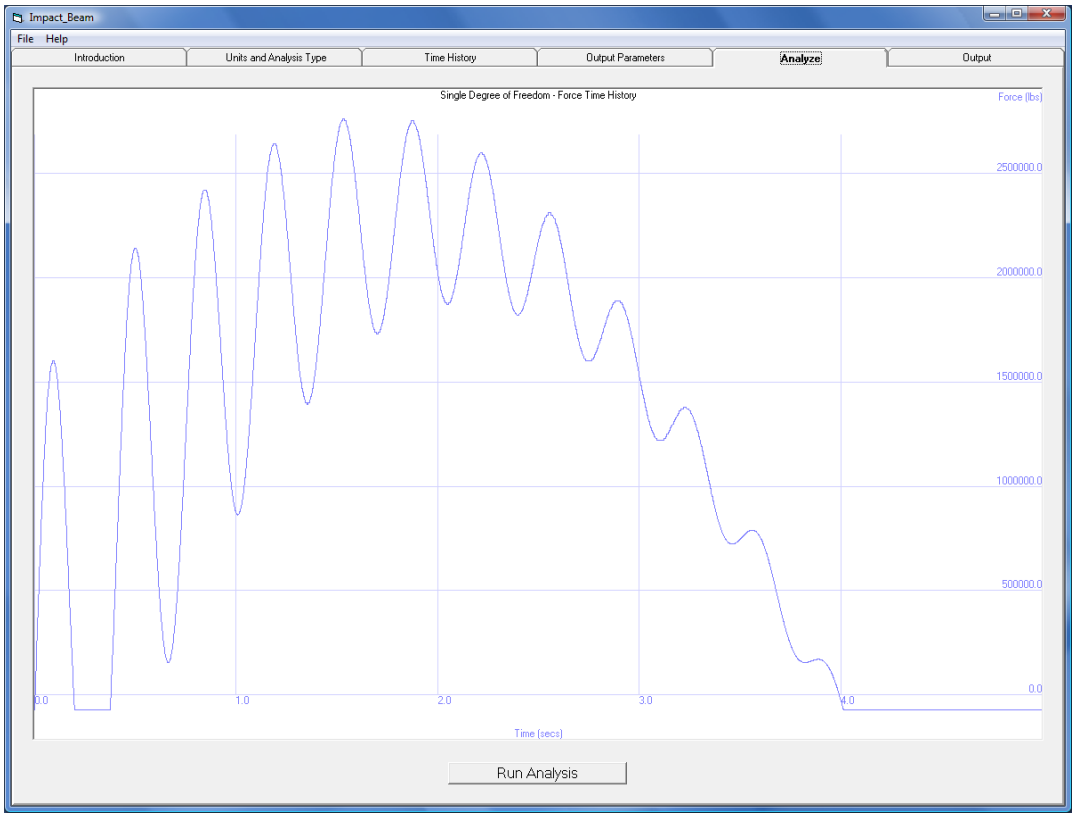

Figure 4.28. Analyze tab.

Clicking Run Analysis will execute the Impact_Beam program on the data that was entered for the Units and Analysis Type tab, the Time History tab, and the Output Parameters tab. After the analysis has been performed, a message box will alert the user that the Impact_Beam program has finished analyzing the data (shown in Figure 4.29). Clicking OK will allow the user to proceed in viewing the results of the analysis in the Output tab.

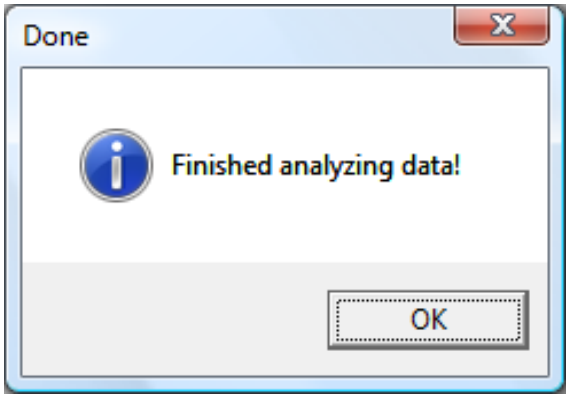

Figure 4.29. Finished analyzing data message box.

4.4.5 Output tab

The Output tab allows the user to view the output results of the Impact_Beam simulation. The user will have a list of data types to choose from to view the output. The Impact_Beam output simulation for the SDOF Analysis is consisted of six data types: Force, Displacement, Velocity, Acceleration, Spring Force, and Damping Force. An output plot of each data type versus time will be displayed in the window of the Output tab. The x-axis is the time (seconds) value and the y-axis is the selected data type value with its respective units. Also, the values of the x and y coordinates will be displayed by scrolling the mouse over any point in the time-history plot. Figures 4.30-4.35 shows the output plot for each of the six data types.

4.5 Conclusions

This chapter has provided an overview of the capabilities of the Impact_Beam visual modeler and postprocessor interface. It has discussed the inputs required to perform both single and multiple degree of freedom analysis of a structure under dynamic loading. It allows the user to input beam specifications and impulse force time-histories that can proceed along the beam for the determination of the dynamic structural response of the simply supported, flexible impact beam. It also allows the user to visualize the deflections, moments, and shear forces internal to the beam during the time of impact either as time-history response at a user-specified point on the beam or as a time-step based animation of the response along the entire beam.

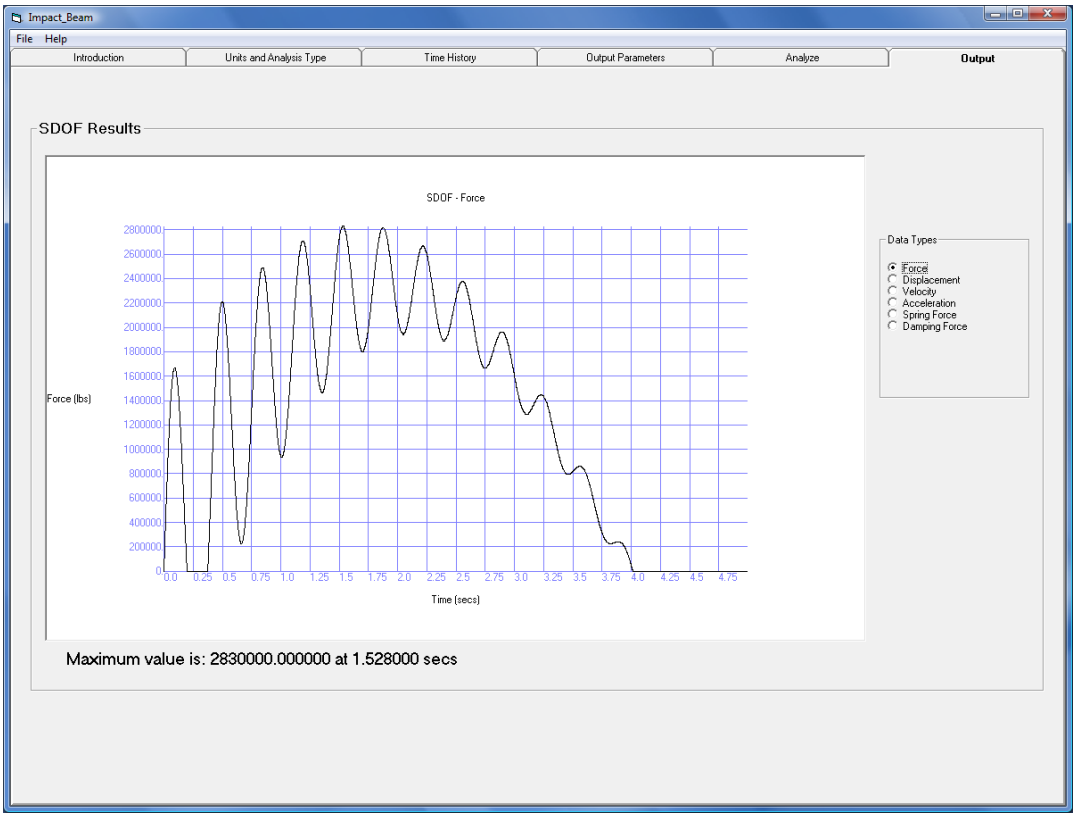

Figure 4.30. Plot of Force vs. Time.

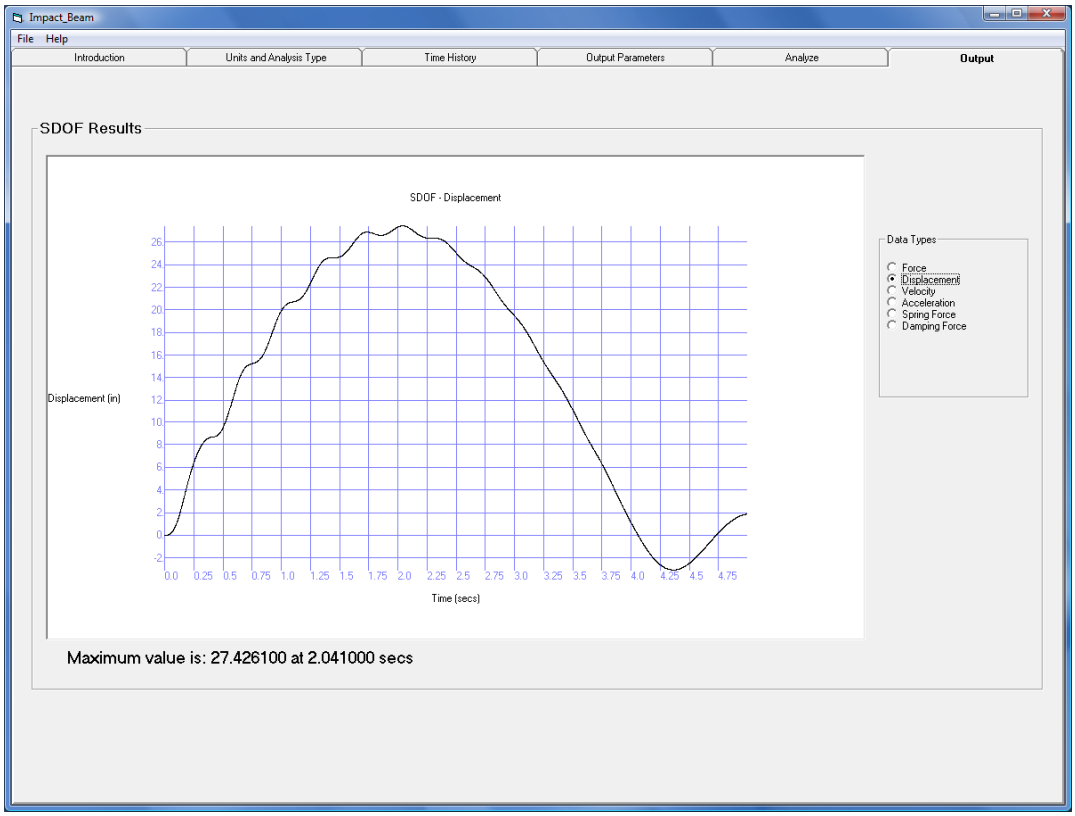

Figure 4.31. Plot of Displacement vs. Time.

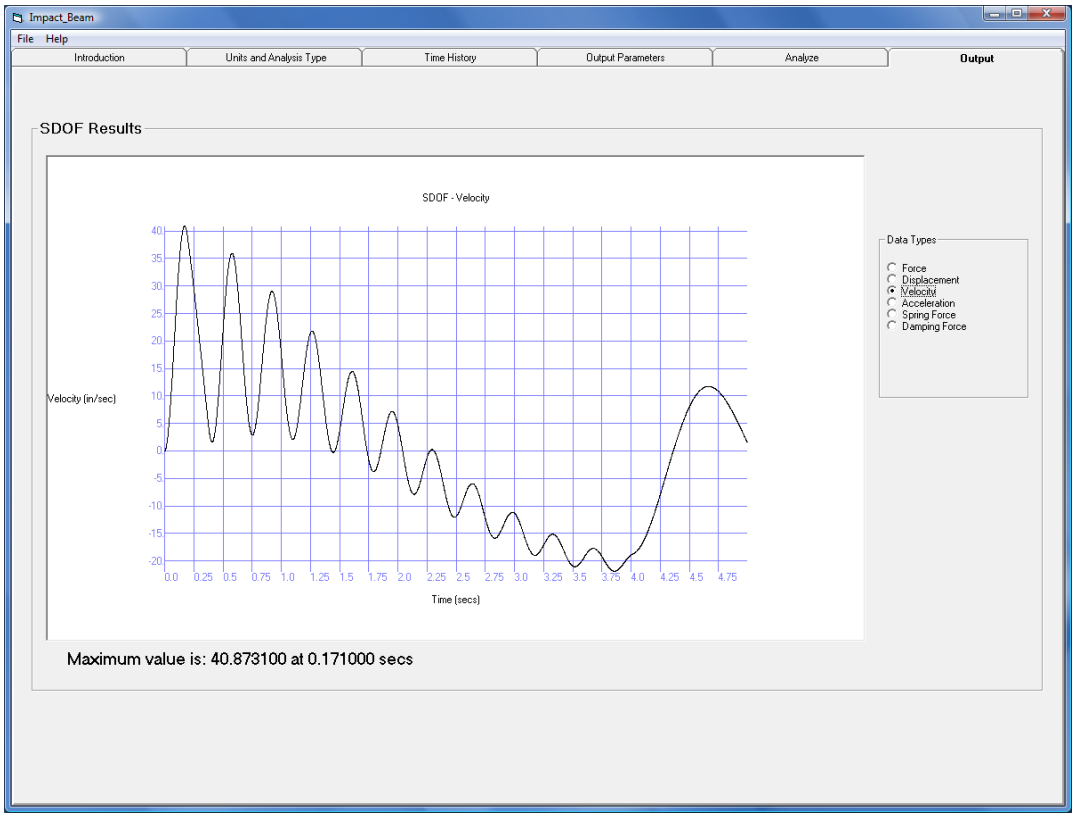

Figure 4.32. Plot of Velocity vs. Time.

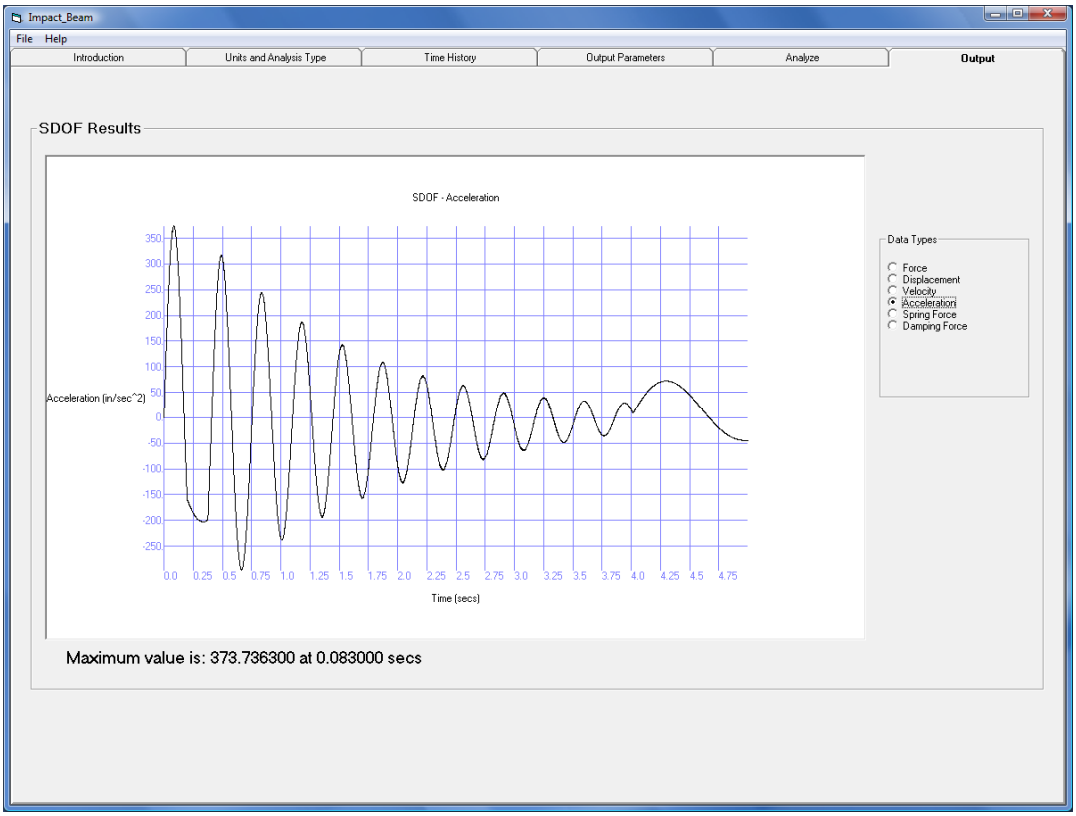

Figure 4.33. Plot of Acceleration vs. Time.

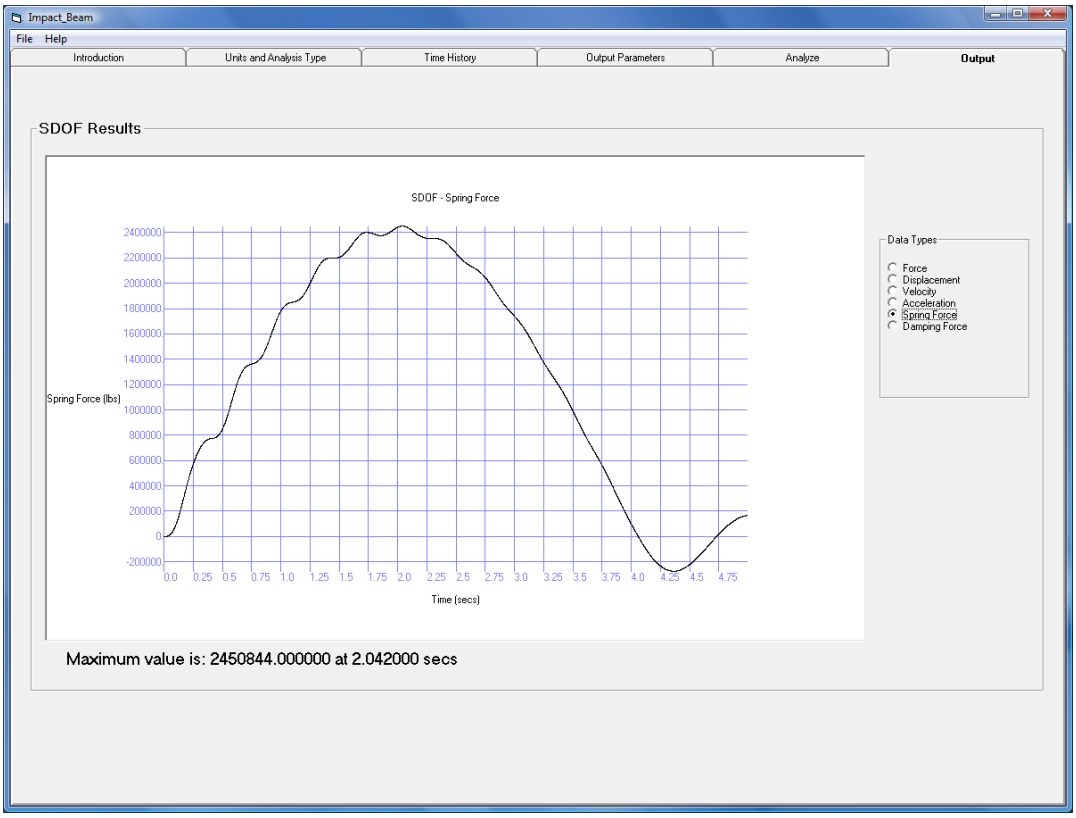

Figure 4.34. Plot of Spring Force vs. Time.

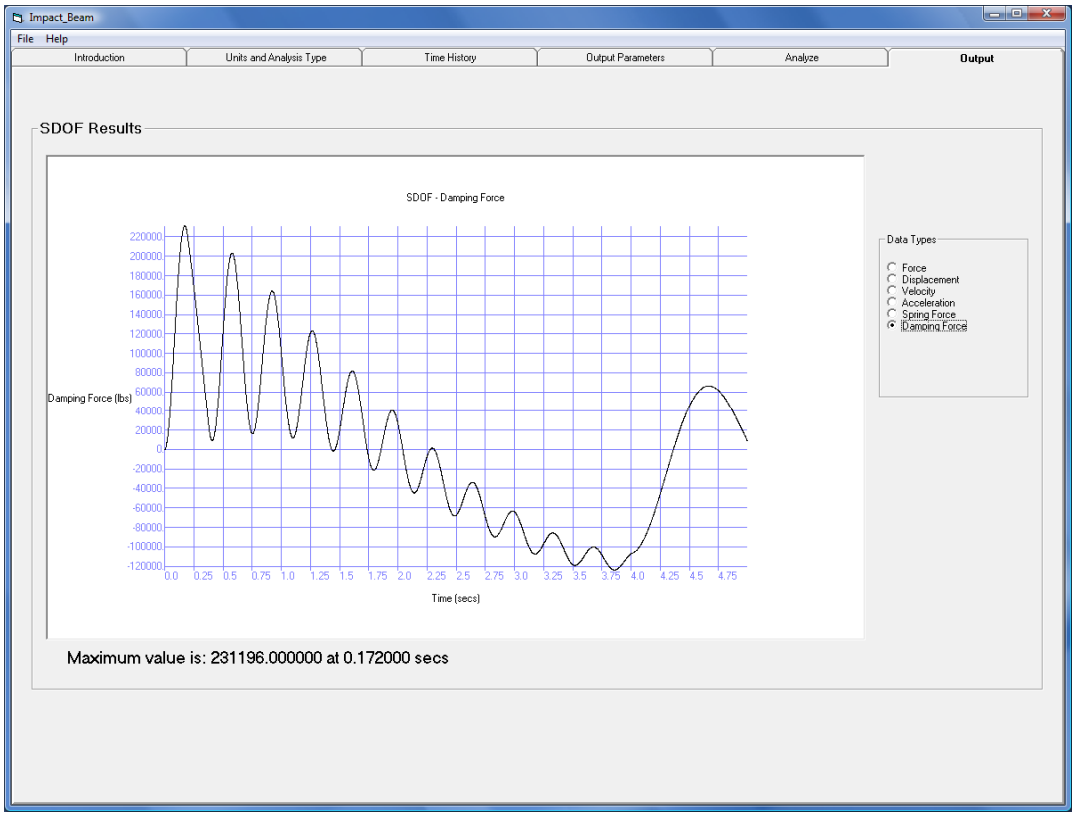

Figure 4.35. Plot of Damping Force vs. Time.

5 Validation and Verification of the Impact_Beam Software

5.1 Introduction to the Impact_Beam software

The Impact_Beam engineering software can solve two different dynamic analyses. Each one of them has a particular sub-case that is also incorporated in Impact_Beam.

In the first dynamic analysis, Impact_Beam can be used to calculate the dynamic response of a Single Degree of Freedom (SDOF) system subjected to an external dynamic load. The SDOF can be a damped or undamped system. The underdamped SDOF model is considered by means of the damping ratio definition ($\beta=c/c_{crit}<1.0$). One feature of this option is that the stiffness can be modeled as a single spring constant ($k=f/x$), or can be modeled as a spring with a bilinear force-displacement relationship. If the bilinear stiffness model is used, the response is calculated using the recursive alternate formulation to solve the Duhamel's integral (explicit formulation), as presented in Appendix C.

The second dynamic analysis Impact_Beam can perform is the calculation of the dynamic transverse beam deflections, beam moments and shear force responses to the impact pulse force time-history applied to the simply supported, flexible impact beam of distributed mass and flexural stiffness that makes use of modal response analyses as a function of position along the beam combined with a generalized coordinate solution for dynamic response with time for each mode considered. The external dynamic load can be located at a specific position along the beam or can be a moving dynamic load with a prescribed initial position and a constant velocity of motion. Superposition of modal responses is evoked to obtain the total dynamic beam responses. The generalized coordinate solution for dynamic response with time is solved using Duhamel's Integral. Duhamel's Integral is outlined in Appendix C and is evaluated using numerical methods similar to those presented in Paz, 1985. If the simply supported, flexible impact beam of distributed mass and flexural stiffness model is used, the Displacement Impact Factor (DIF), the Shear Force Impact Factor (SFIF), and the Moment Impact Factor (MIF) are also calculated.

5.2 Validation of Impact_Beam using SAP2000

The Impact_Beam computer program has the capability to calculate the dynamic response of a continuous elastic beam due to a moving transverse concentrated dynamic load. This section presents the validation of Impact_Beam by comparing its results against the results obtained from the well-known structural analysis computer program SAP2000, Computers and Structures, Inc. 2003. The model in both computer programs has the following input data;

- the effective beam length (from center to center of neoprene pads) is 112.6 ft,
- the moment of inertia of the beam is 517.2 ft^4,
- the cross sectional area is equal to 46 ft^2, and
- the mass per unit length of the beam is 0.25486 kips/ft, which considers the hydrodynamic added mass (discussed in Appendix H).

The force time-history of Winfield Test #10, which has a maximum force of 517.4 kips was used as the excitation. SAP 2000 considers the dynamic load to be applied at a specific position along the beam. For that reason, the force time-history was fixed to act at a position of 64.1 ft from the left support for both software packages. This distance (64.1 ft) is the position of initial contact of the barge train for Winfield Test #10. Impact_Beam has the capability to consider a moving dynamic load. In the Impact_Beam input data, the initial point of contact was also 64.1 ft and the velocity of the moving dynamic load was set to zero. With these values, both programs have the same load conditions. The SAP2000 model had 12 beam elements and no shear energy was considered. The damping ratio was assigned as 2% of the critical damping for each considered mode. Also in Impact_Beam, twelve modes of vibration were considered with a 2% damping ratio for each mode. The resulting fundamental natural period was the same in Impact_Beam and SAP2000 with a value of 0.199 seconds. The maximum displacement at midspan was calculated by SAP2000 to be 0.433 inch and Impact_Beam produced a maximum displacement at midspan of 0.4276 inch. These results produce a 1.2% difference between the Impact_Beam and SAP2000 results. The maximum internal bending moment was calculated by Impact_Beam and SAP2000 as 13,483.41 kip * ft and 13,594.06 kip * ft, respectively. These results produce a 0.8 % difference between the Impact_Beam and SAP2000 results. The output results from Impact_Beam were validated when compared to the SAP2000 results. Figures 5.1 and 5.2 show the moment and displacement time-histories,

respectively, at midspan for SAP2000 and Impact_Beam. Figures 5.3 and 5.4 show the beam deflection and the internal moment diagram for the time step of maximum dynamic force (t = 0.2 seconds), respectively.

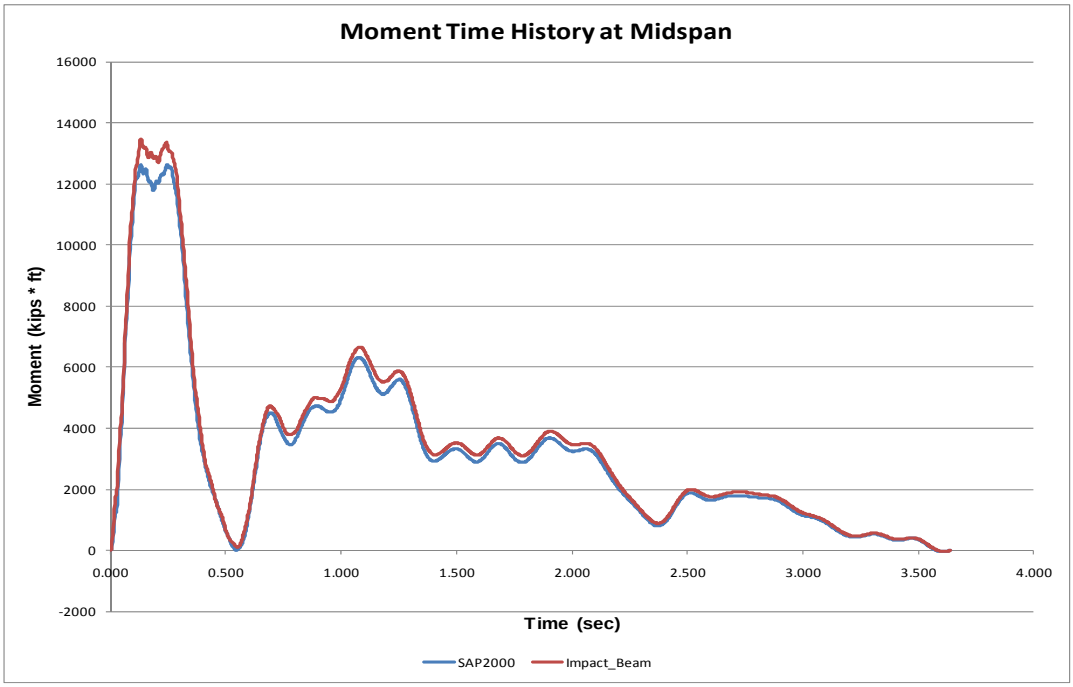

Figure 5.1. Moment time-history at midspan calculated using Impact_Beam and SAP2000.

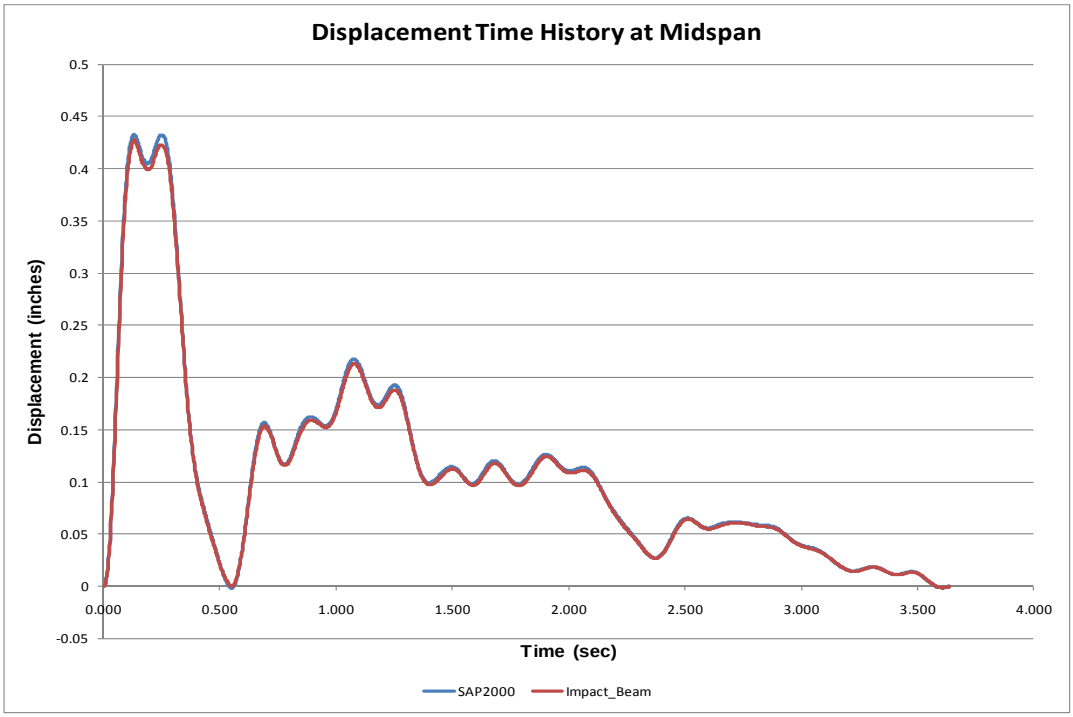

Figure 5.2. Displacement time-history at midspan calculated using Impact_Beam and SAP2000.

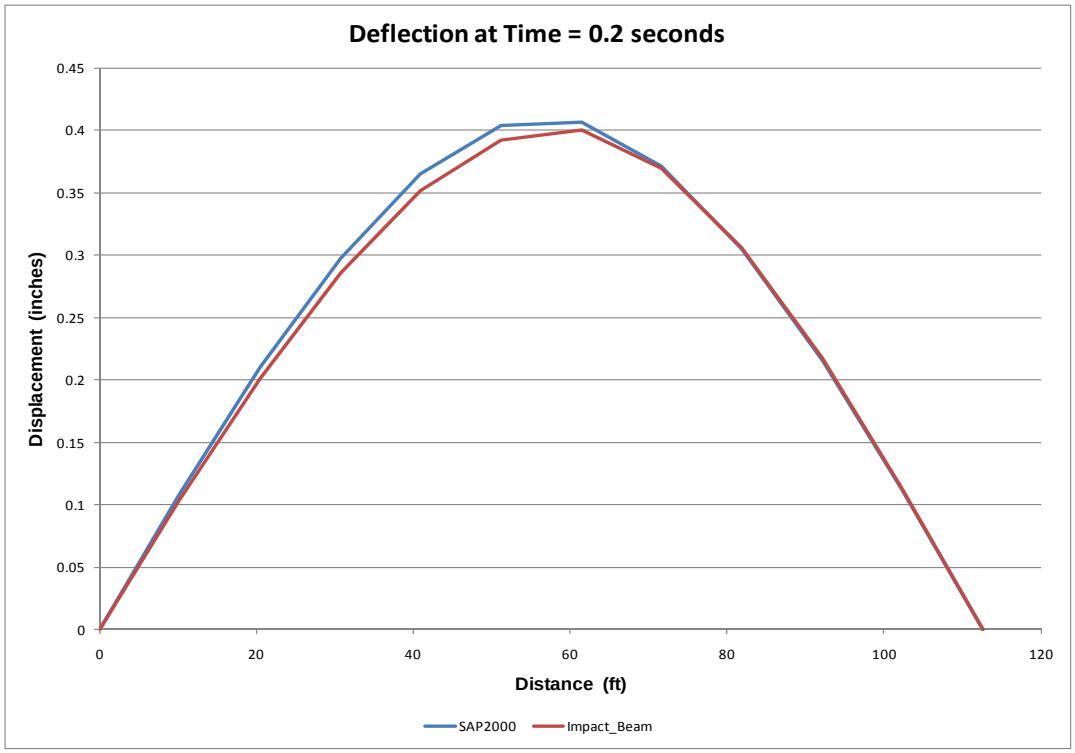

Figure 5.3. Beam deflection at time of maximum dynamic load calculated using Impact_Beam and SAP2000.

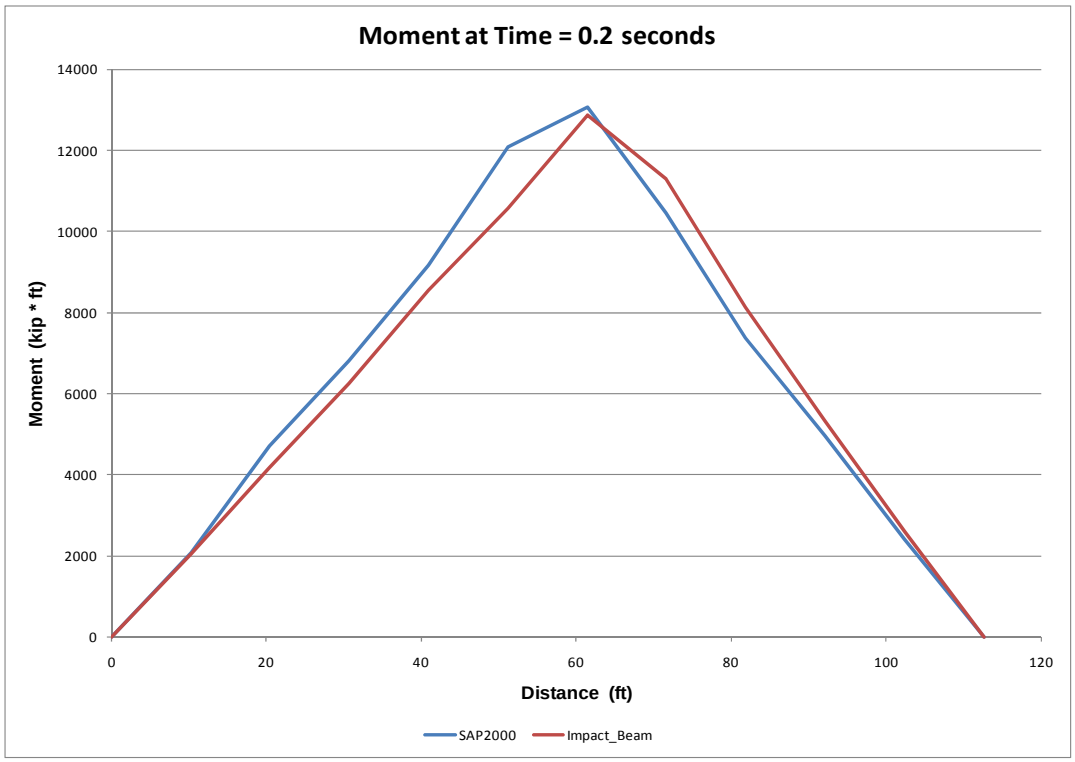

Figure 5.4. Internal bending moment at time of maximum dynamic load calculated using Impact_Beam and SAP2000.

5.3 Continuous beam model from Impact_Beam to estimate the dynamic modulus of elasticity of the simply supported beam used in Winfield Test #10

The full-scale Barge Impact Test #10 conducted at Winfield serves as the template for reducing and interpreting the field data. The simply supported beam possesses a unique value for the dynamic modulus of elasticity, which is necessary for beam response computations. Because a dynamic modulus of elasticity was not captured during the tests at Winfield, it became necessary to estimate a value using the collected sensor data from Winfield. This subsection discusses the procedures for processing and computing this estimate. Different instrumentation provided differing values, which could be used to determine an estimate for the dynamic modulus of elasticity. The following sub-subsections discuss and collate the differing individual estimates for the dynamic modulus of elasticity, and compute an average estimate.

5.3.1 Calculation of the beam deflection based on reference, neoprene and laser deflections

During the Winfield Experiment, several tests were performed and data from displacement, acceleration and strains were gathered. The collections of laser deflections and the neoprene deformations allow the calculation of the beam deflection (elastic curve). The beam experienced some amount of rigid body motion due to base motion that came from displacement of the connection between beam segments and neoprene pad deformation. The laser deflection at Sensors 1 and 6 defines the motion of the reference or base frame. These two sensors are located in the adjacent beams. The Linear Variable Differential Transformer (LVDT) relative displacement sensors at the ends of the beam, named D2-1Y and D6-3Y, account for the in-line displacement of the beam due to deformation of the neoprene pads for tests up through barge impact test #13. After test #13, LVDT sensor D6-3Y was moved. For these calculations, D6-3Y was emulated by linearly interpolating the laser deflections on either side of the sensor D6-3Y location. Then, to calculate the beam deflection, the contribution of each rigid body motion (system and neoprene pads) must be subtracted from the laser deflection at LD3, LD4 and LD5 (total displacements). This concept can be observed in Figure 5.5. The experimental beam deflection at LD3 and LD4 sensor locations was calculated using the laser deflection recorded during the experiment, the neoprene seat deformation and the foundation displacement (displacement time-history at Sensors LD1 and LD6). The neoprene

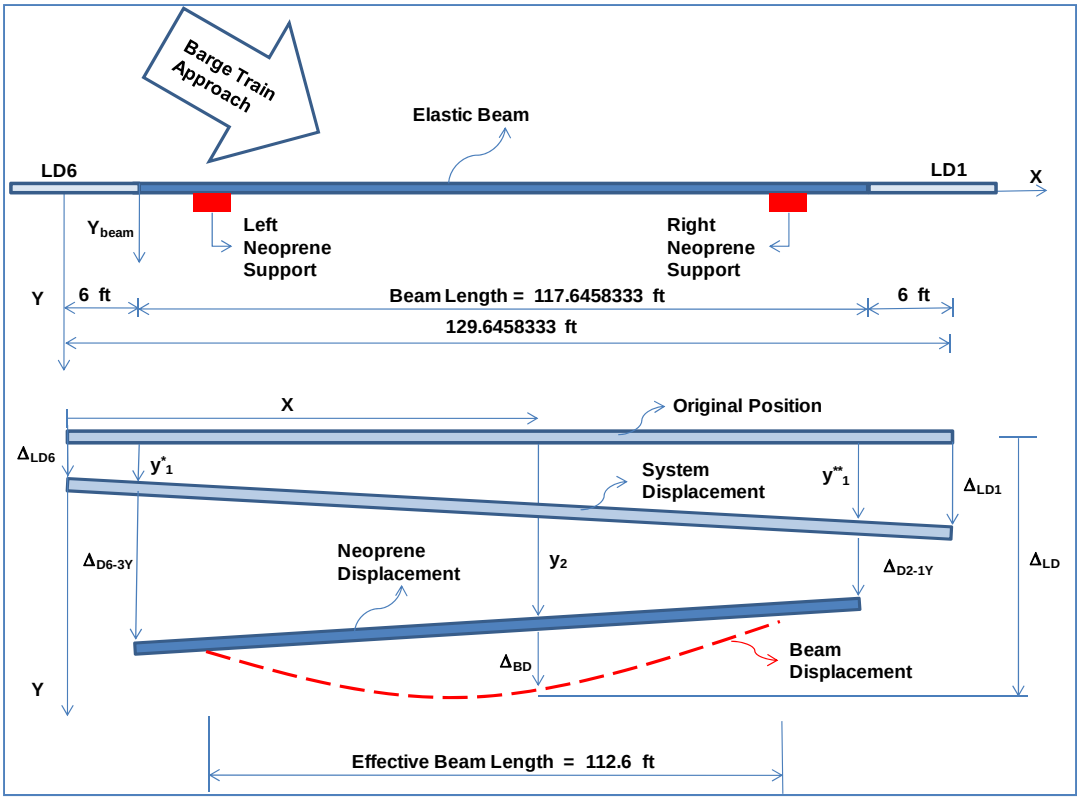

Figure 5.5. Parameters used to calculate the beam deflection based on experimental data.

deformation and foundation displacement produce an in-line displacement of the elastic, simply supported beam. After this in-line motion occurs, the elastic beam starts to deform producing the elastic curve shape. The variables that enter in the calculation of the beam deflection (elastic curve) are the laser deflections LD1, LD3, LD4, LD5 and LD6; the (relative) displacements at the start and end of the impacting beam D2-1Y and D6-3Y; and the x position along the beam where the beam deflection is to be calculated, LD3, LD4, LD5 locations. These parameters are shown in Figure 5.5.

It can be shown from Figure 5.5 that the beam deflection (Δ_{BD}) is equal to the laser deflection (Δ_{LD}) minus the distance y_2. The system displacement and neoprene displacement has to be subtracted from the laser deflection displacement recorded during the experiment. In mathematical notation, the beam deflection (Δ_{BD}) is

$$\Delta_{BD} = \Delta_{LD} - y_2 \tag{5.1}$$

where

$$y_2 = \left[\frac{y_1^{**} + \Delta_{D2-1Y} - y_1^{*} - \Delta_{D6-3Y}}{117.6458333}\right](x-6) + y_1^{*} + \Delta_{(D6-3Y)} \tag{5.2}$$

where

$$y_1^{*} = \left[\frac{\Delta_{LD1} - \Delta_{LD6}}{129.6458333}\right]6 + \Delta_{LD6} \tag{5.3}$$

and

$$y_1^{**} = \left[\frac{\Delta_{LD1} - \Delta_{LD6}}{129.6458333}\right]123.6458333 + \Delta_{LD6} \tag{5.4}$$

Lastly, substituting Equations (5.3) and (5.4) into Equation (5.1), the beam deflection at each sensor location LD3, LD4 and LD5 can be calculated. The distance *x* (in feet) measured along the X-axis in Equation (5.2) has an origin at the labeled Y-axis position as shown in Figure 5.5. For each time step during the experiment, the terms in Equations (5.1) through (5.4) were recorded. During Winfield Test #10, there were three locations where the laser deflections were measured. The location of each of the three sensors were; LD3 at 71.0425', LD4 at 56.38625' and LD5 at 41.7196'. To use Equations (5.1) through (5.4), these positions have to be modified; increased by six feet (the distance between each of the Y axis reference frames). At time equal to 0.20365 seconds, the maximum values for the beam displacements obtained from Equation (5.2) are the following; at LD3 – 0.40 inch, at LD4 – 0.42 inch, and at LD5 – 0.38 inch. Figure 5.6 shows the displacement time-history at sensor LD1 and LD6. They are associated to the displacement the adjacent beams experienced during the Winfield Test #10. Figures 5.7 through 5.9 show the beam and laser displacement time-histories at each sensor location of LD3, LD4 and LD5, respectively. Figure 5.10 shows the beam displacement time histories for each Sensor at LD3, LD4 and LD5.

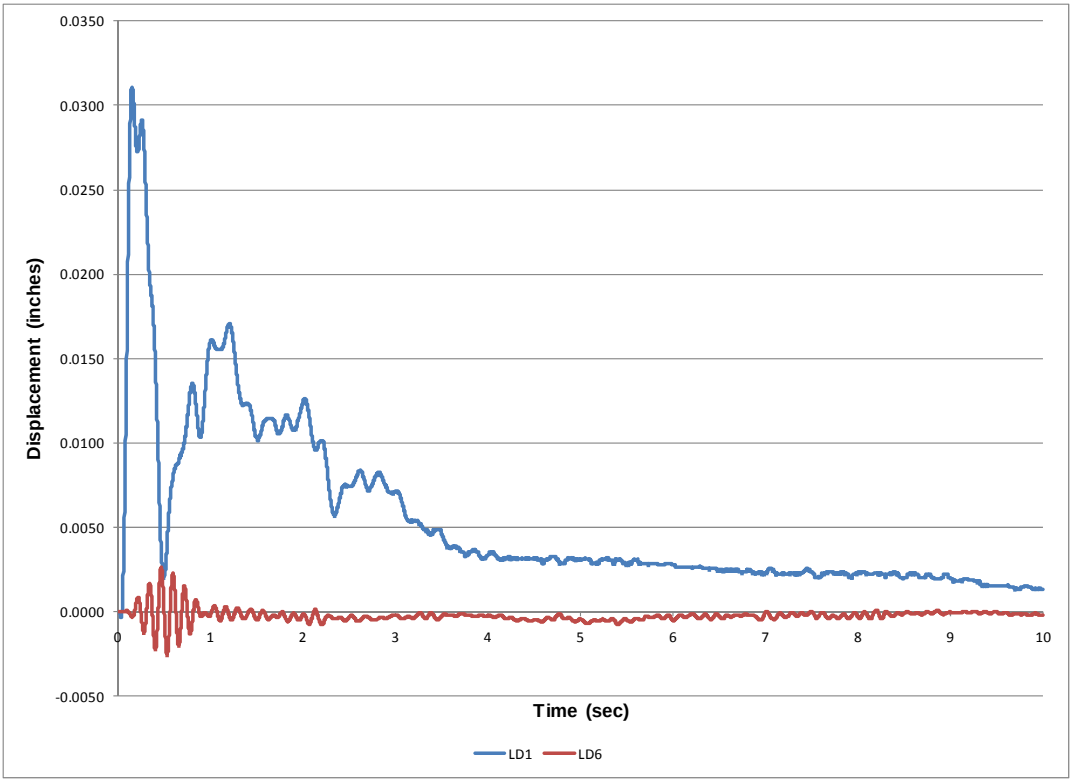

Figure 5.6. Displacement time histories for the Laser displacement LD1 and LD6 sensors mounted on the beams adjacent to the impact beam.

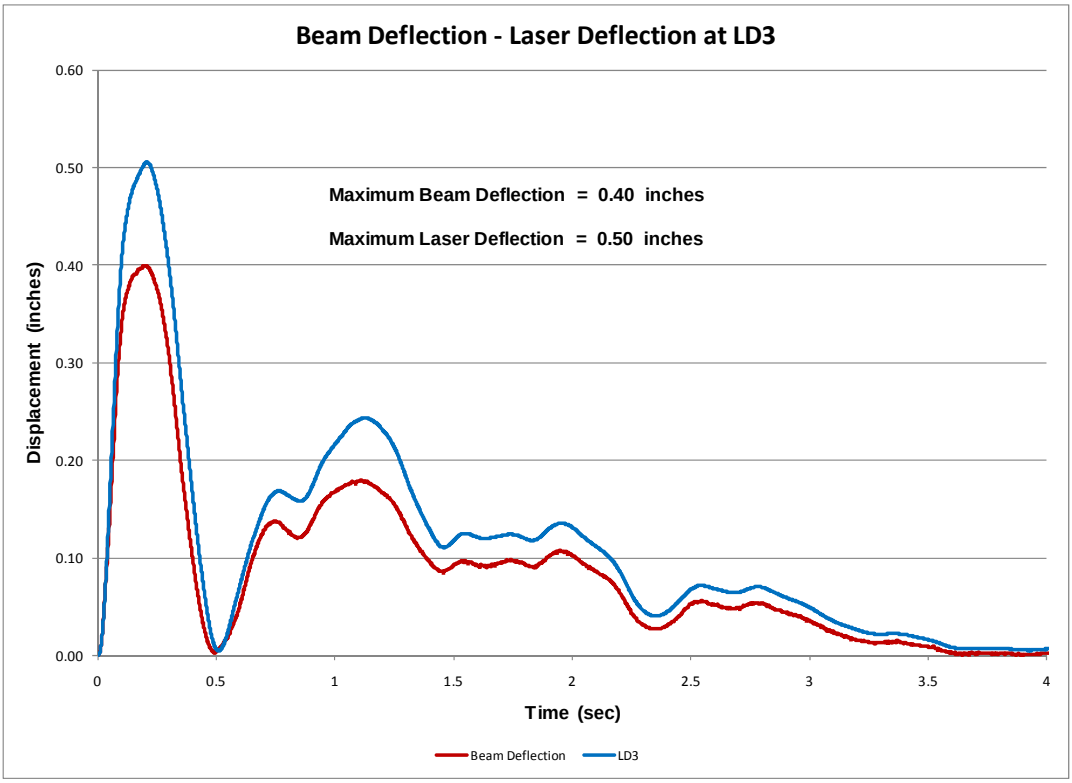

Figure 5.7. Beam and laser displacement time-history at sensor LD3.

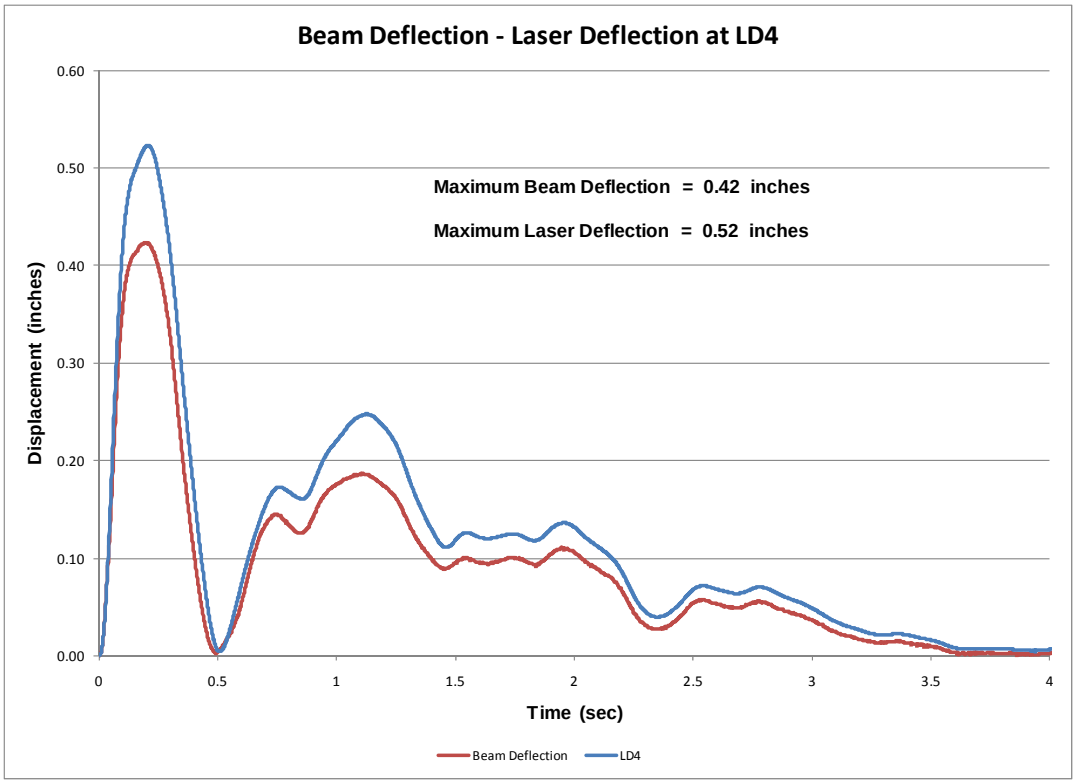

Figure 5.8. Beam and laser displacement time-history at sensor LD4.

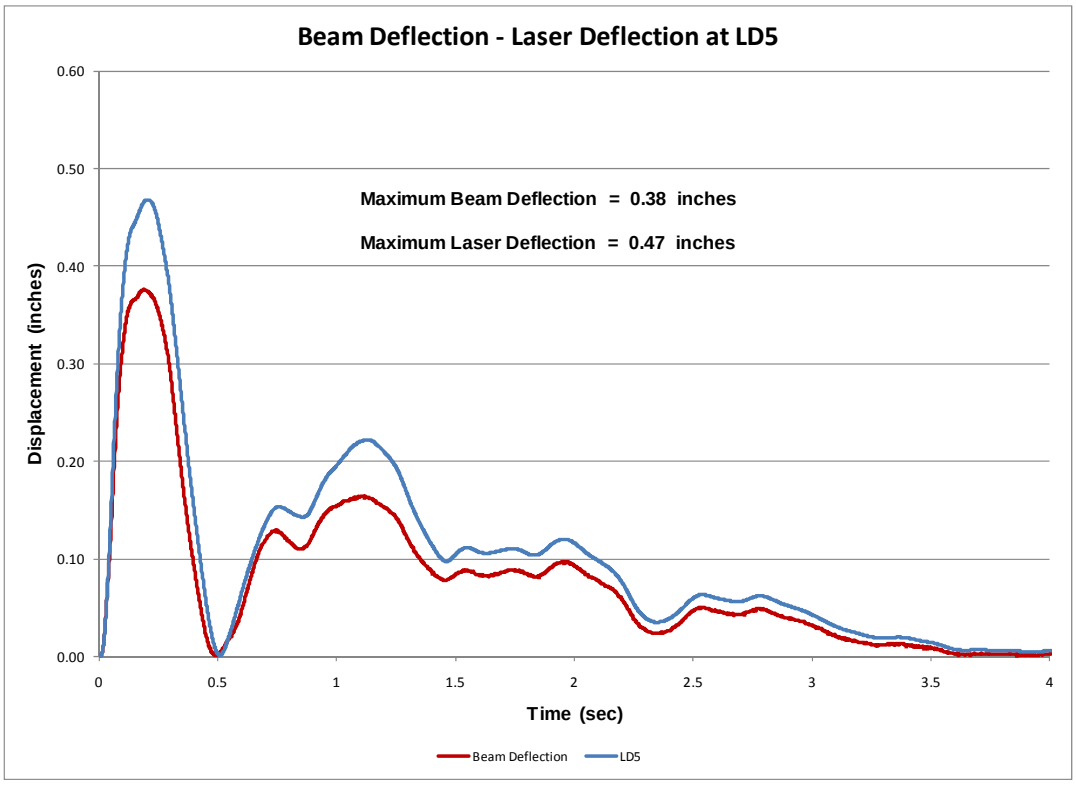

Figure 5.9. Beam and laser displacement time-history at sensor LD5.

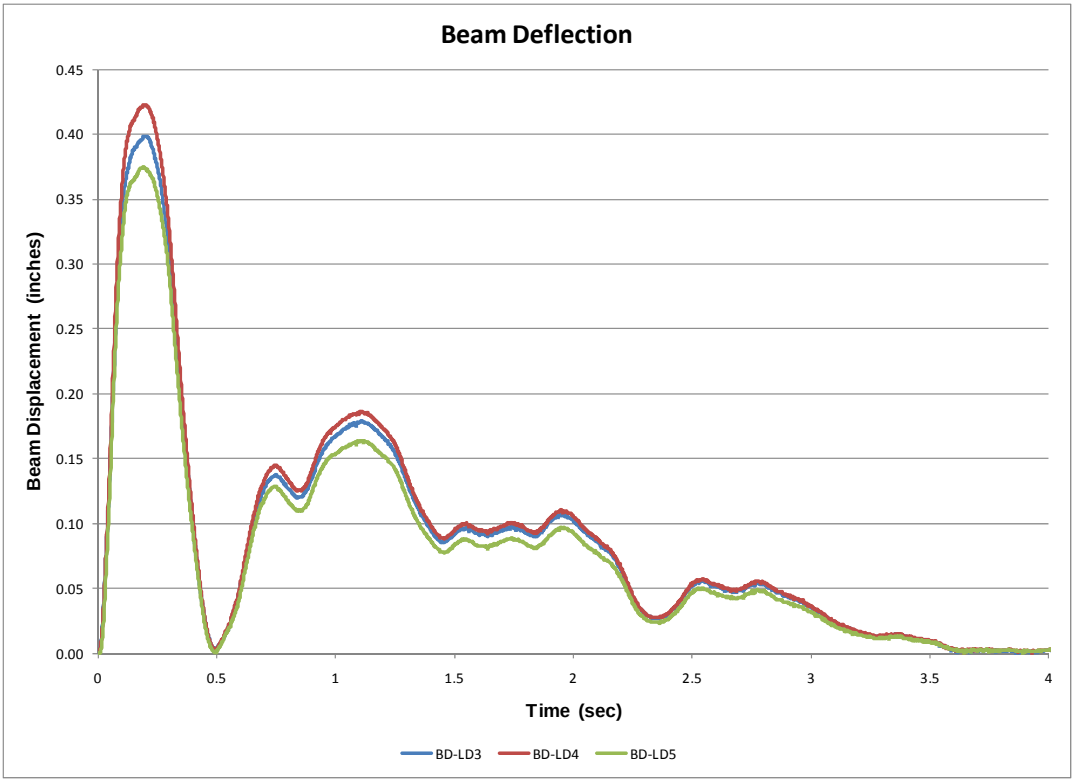

Figure 5.10. Beam deflection time-history at sensor LD3, LD4 and LD5.

5.3.2 Estimation of the dynamic modulus

5.3.2.1 Estimation of the dynamic modulus of elasticity based on calculate experimental beam deflection at LD3, LD4 and LD5 sensor location

Impact_Beam computer program has the capability to calculate the dynamic response (transverse displacement) of a continuous elastic beam due to a moving dynamic load. This feature allows Impact_Beam to estimate the dynamic modulus of elasticity of the concrete continuous beam used during Winfield experiment Test #10. The input for this Impact_Beam analysis is as follows:

- The effective length of the beam (from center to center of neoprene pads) was 112.6 ft,
- The moment of inertia of the beam was 517.2 ft^4,
- The mass per unit length of the beam was 0.25486 kips/ft,
- The barge train was moving at 2.99 ft/s, and
- The first point of contact was at 64.1 ft from the left support.

The procedure for the estimation of the dynamic modulus of elasticity was as follows. First, the location of each sensor LD3, LD4 and LD5 was

calculated as 71.0425, 56.38625 and 41.7196 ft, respectively, as shown in Figure 5.11. At these positions, a sensor was place in the program to obtain results from the program at these specific locations. Ten modes were used and a damping ratio of 0.02 was used for each mode. The elastic modulus is a variable entered as input data in the input file. It was fixed with a lower value (790,000 ksf), that is, a lower value than the one expected for the dynamic modulus of elasticity. Then, a special version of Impact_Beam FORTRAN code was created to iterate from this initial modulus of elasticity until the specified beam deflection at sensor location LD3, LD4 and LD5 was achieved. The values that the computer program had to match were the ones obtained in the previous section; that is, at LD3 – 0.40 inch, at LD4 – 0.42 inch, and at LD5 – 0.38 inch. Following this procedure, the computer program obtained a simulation beam displacement equal to the experimental beam displacement and the value for the modulus of elasticity for this condition is the resulting dynamic modulus of elasticity. The resulting values for the dynamic modulus of elasticity for the LD3, LD4 and LD5 locations were 796,800 ksf (5,533.33 ksi), 812,400 ksf (5,641.67 ksi) and 799,000 ksf (5,548.61 ksi), respectively. Figures 5.12 through 5.14 show the transverse displacement time-history at each sensor location resulting from the analysis done to estimate the dynamic modulus of elasticity. It can be observed that the maximum deflection obtained for the simulation matches with the maximum experimental value.

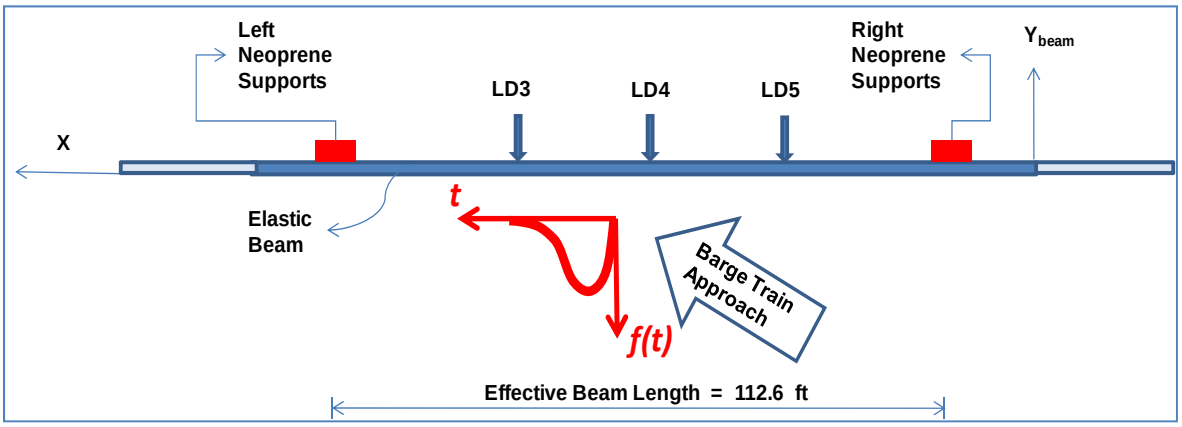

Figure 5.11. Location of LD3, LD4 and LD5 sensors.

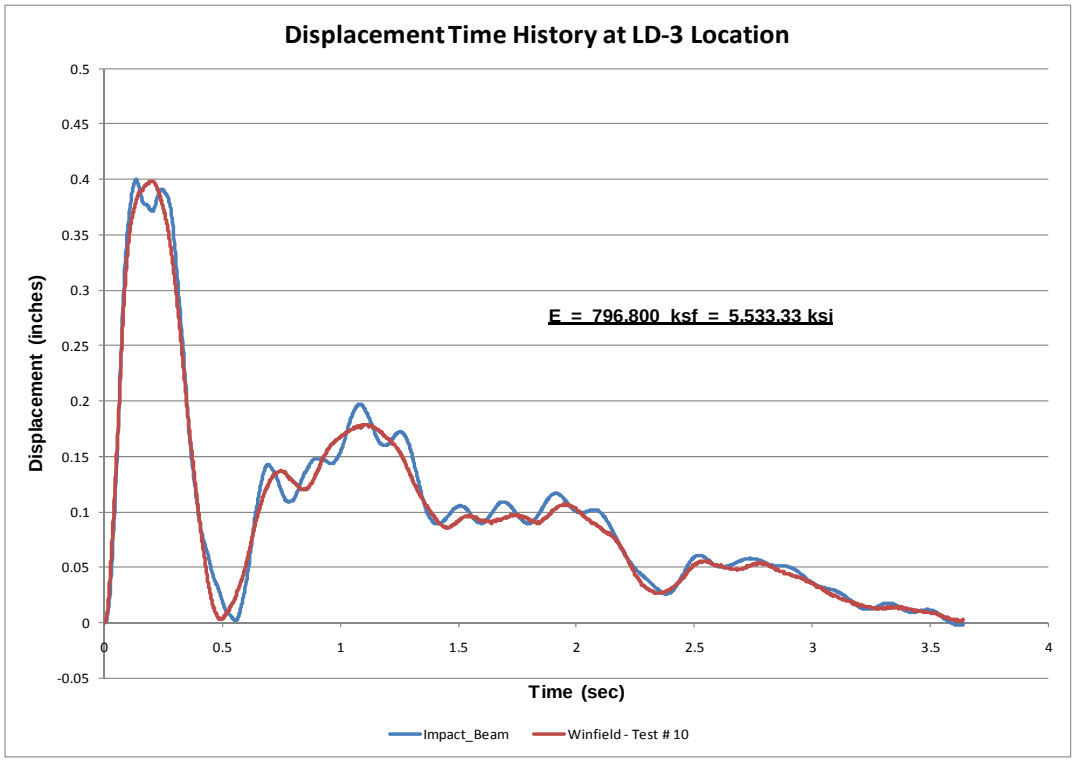

Figure 5.12. Beam displacement time-history for a dynamic modulus of elasticity based on maximum displacement at sensor LD3.

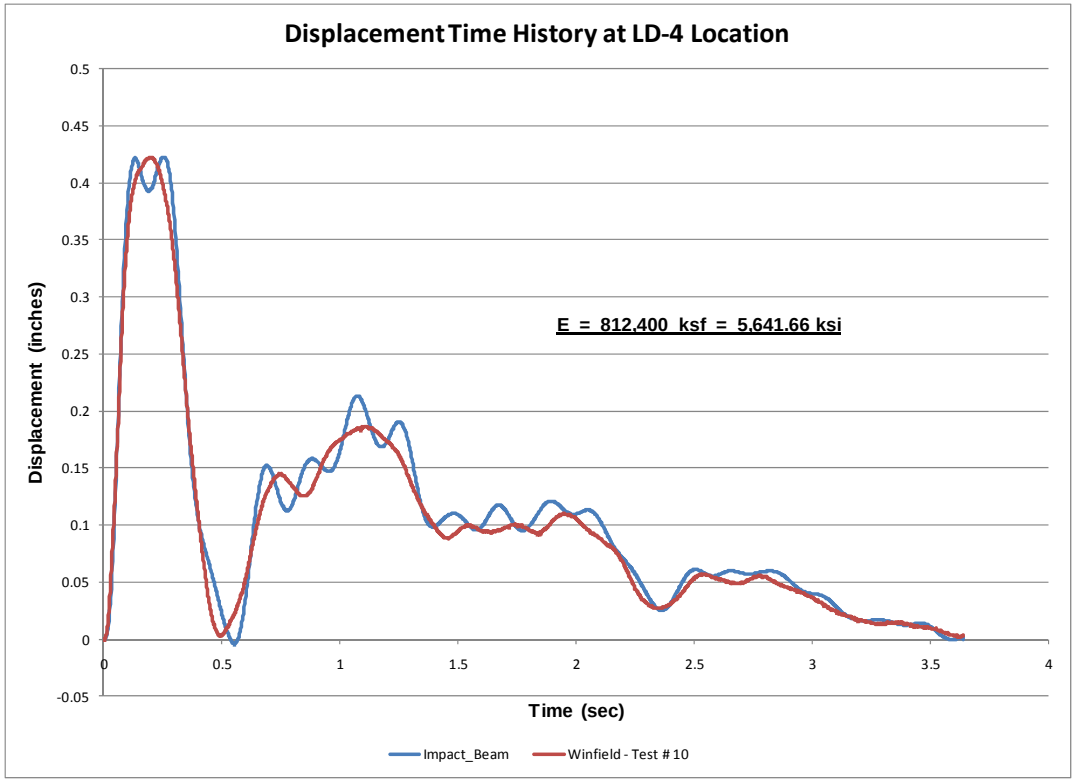

Figure 5.13. Beam displacement time-history for a dynamic modulus of elasticity based on maximum displacement at sensor LD4.

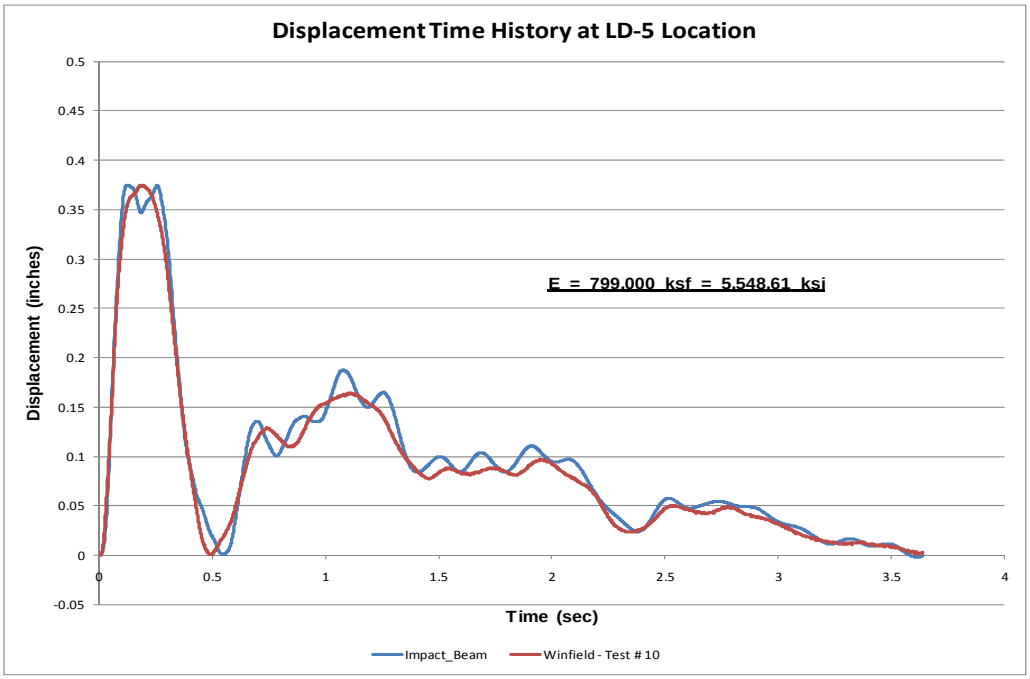

Figure 5.14. Beam displacement time-history for a dynamic modulus of elasticity based on maximum displacement at sensor LD5.

5.3.2.2 *Estimation of the dynamic modulus of elasticity based on experimental curvature at strain gage S1B, S1F, S2B, S2F, S3B, S3F, S4B, S4F, S5B and S5F sensor locations*

The Impact_Beam computer program has the capability to calculate the dynamic internal moment of a continuous elastic beam due to a moving dynamic load. This feature allows Impact_Beam to estimate the dynamic modulus of elasticity of the concrete continuous beam used during Winfield experiment Test #10. The input for this Impact_Beam analysis is as follows:

- The effective beam length (from center to center of neoprene pads) was 112.6 ft,
- The moment of inertia of the beam was 517.2 ft^4,
- The mass per unit length of the beam was 0.25486 kips / ft,
- The barge train was moving at 2.99 ft/s, and
- The first point of contact was at 64.1 ft from right reaction (right neoprene pads, Figure 5.15).

The procedure for the estimation of the dynamic modulus of elasticity was as follows. First, the location of each sensor S1B;S1F, S2B;S2F, S3B;S3F, S4B;S4F and S5B;S5F was calculated as 80.28208 ft, 68.2925 ft, 56.30291667 ft, 44.31333 ft and 32.32375 ft, respectively, as shown in Figure 5.15.

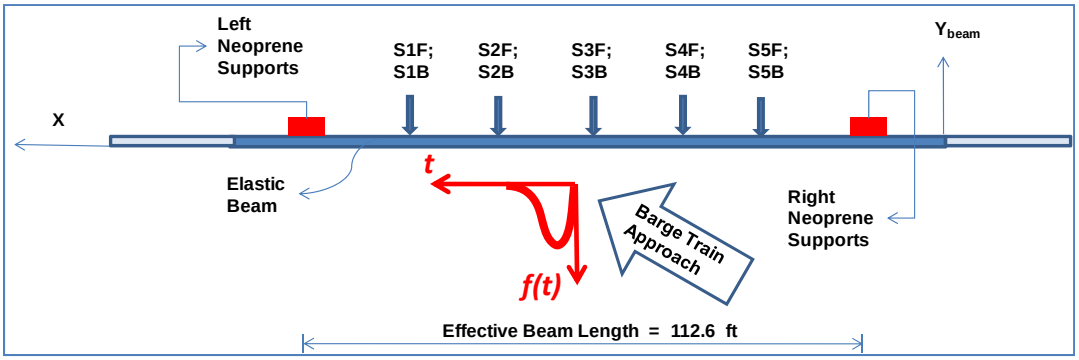

Figure 5.15. Location of S1B;S1F, S2B;S2F, S3B;S3F, S4B;S4F and S5B;S5F sensors.

In the input file for the modified Impact_Beam FORTRAN code, each one of these positions was specified as a location where the results were of interest. Ten modes were used and a damping ratio of 0.02 was used for each mode. The initial modulus of elasticity was assigned a value of 790,000 ksf, which is lower than the expected value for the dynamic modulus of elasticity. Then, the modified Impact_Beam FORTRAN software was iterated from this initial modulus of elasticity until the specified curvature at sensor locations S1B;S1F, S2B;S2F, S3B;S3F, S4B;S4F and S5B;S5F was achieved. Each sensor location represents one run of the computer program and one value for the estimated modulus of elasticity. The maximum curvature at each sensor location was obtained from the experimental curvature time-history. The curvature time-history at each sensor location was obtained from the normal strain recorded during the Winfield Test #10 divided by 4.59 ft for the back sensor and 1.91 ft for the front sensors, as shown in Figure 5.16.

The calculated experimental curvatures (from experimental normal strains) were calculated as; at S1B – 1.65398E-05 rads/ft, S1F – 1.39779E-05 rads/ft, S2B – 2.41901E-05 rads/ft, S2F – 2.72716E-05 rads/ft, S3B – 2.61507E-05 rads/ft, S3F – 2.49923E-05 rads/ft, S4B – 4.43823E-07 rads/ft, S4F – 1.62622E-05 rads/ft, S5B – 1.45119E-07 rads/ft and S5F – 9.47187E-06 rads/ft. The Impact_Beam software calculates the dynamic internal bending moment and, for that reason, the comparison had to be made against the experimental internal moment. The experimental bending moment is calculated by multiplying the curvature at each sensor by the modulus of elasticity and the moment of inertia. Both values change during the process of increasing the modulus of elasticity. The process ends when the experimental and simulation bending moments reach the same results. The modulus of elasticity at this step is the corresponding dynamic modulus of elasticity based on the curvature at this sensor location.

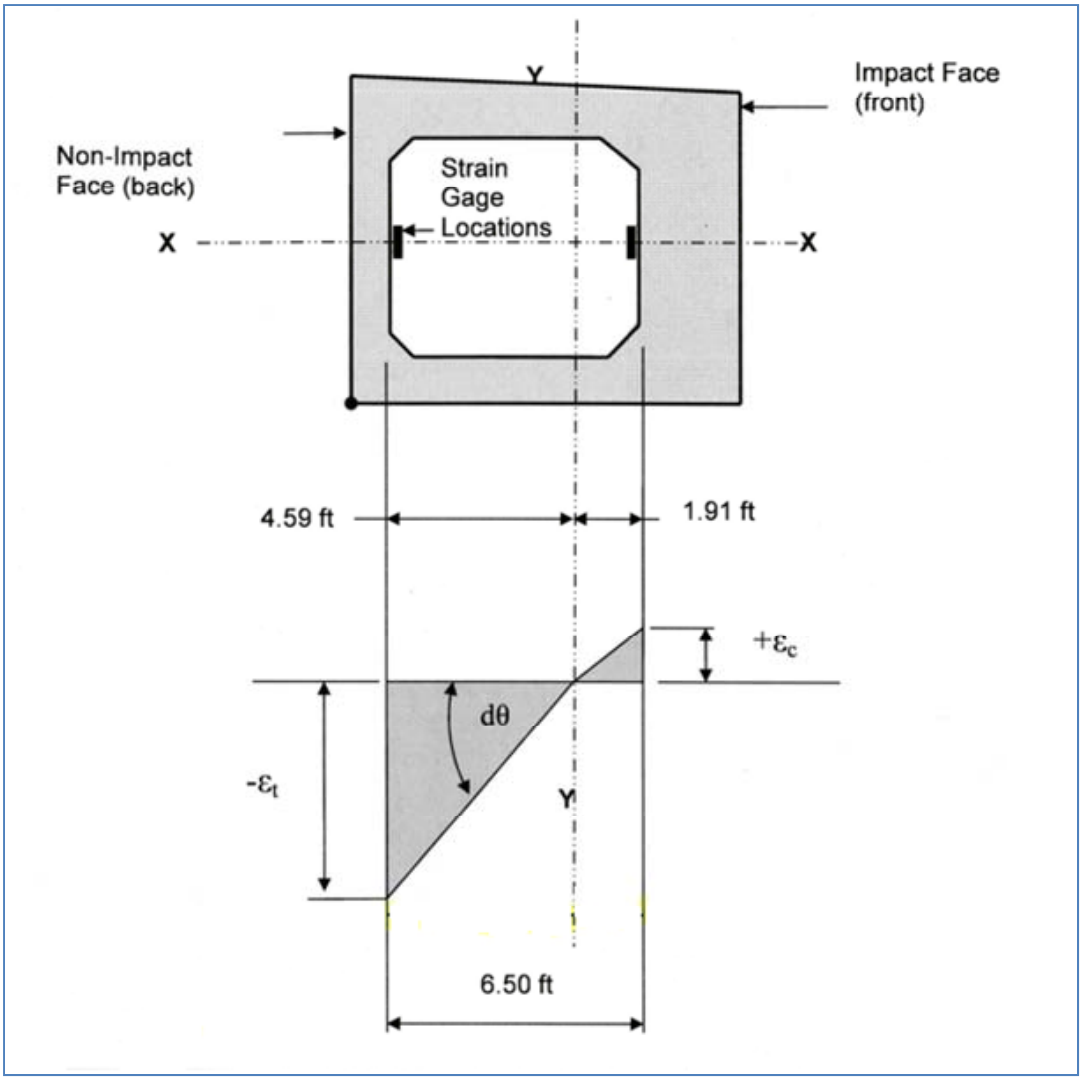

Figure 5.16. Experimental curvature calculation at sensors S1B;S1F, S2B;S2F, S3B;S3F, S4B;S4F and S5B;S5F.

The resulting values for the dynamic modulus of elasticity for S1B, S1F, S2B, S2F, S3B, S3F, S4F, and S5F were 1,522,000 ksf (10,569 ksi), 1,845,000 ksf (12,812 ksi), 1,324,000 ksf (9,194 ksi), 1,059,000 ksf (7,354 ksi), 1,117,000 ksf (7,757 ksi), 1,221,000 ksf (8,479 ksi), 1,688,000 ksf (11,722 ksi), and 2,349,000 ksf (16,313 ksi), respectively. Figures 5.17 through 5.40 show the experimental and simulation moments and curvature time-histories at each specific sensor location. The convergence of the mathematical process to find the dynamic modulus of elasticity at each sensor location is also presented in these sets of figures.

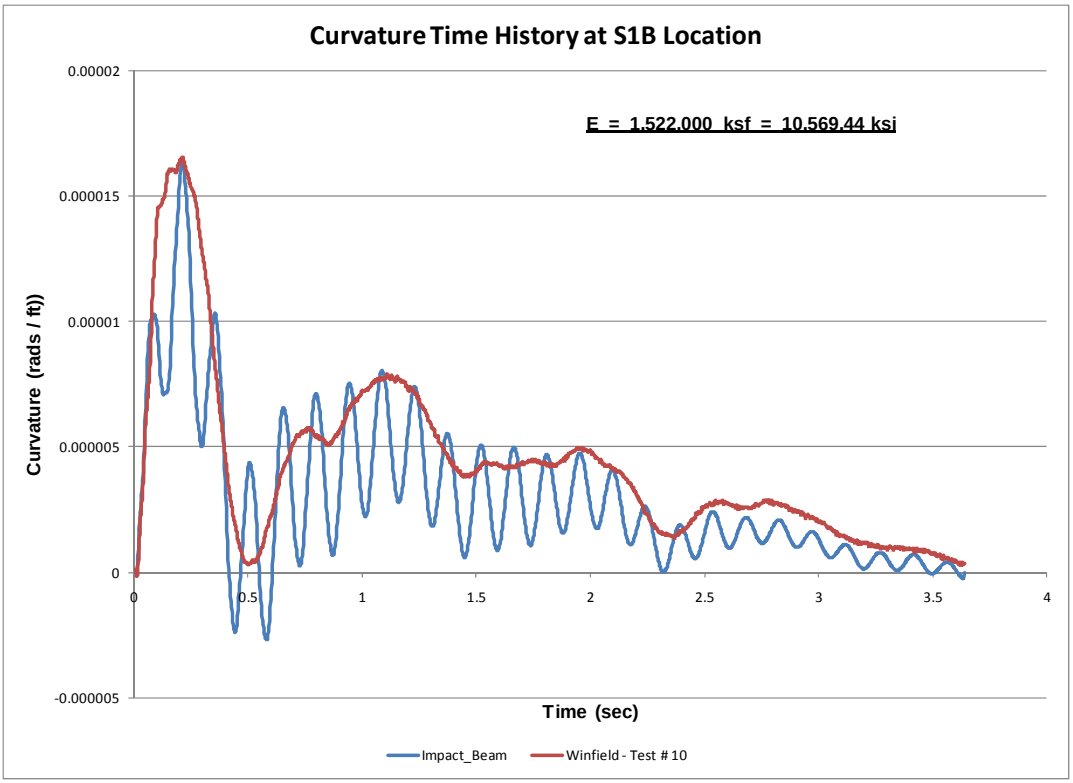

Figure 5.17. Curvature time-history at S1B sensor.

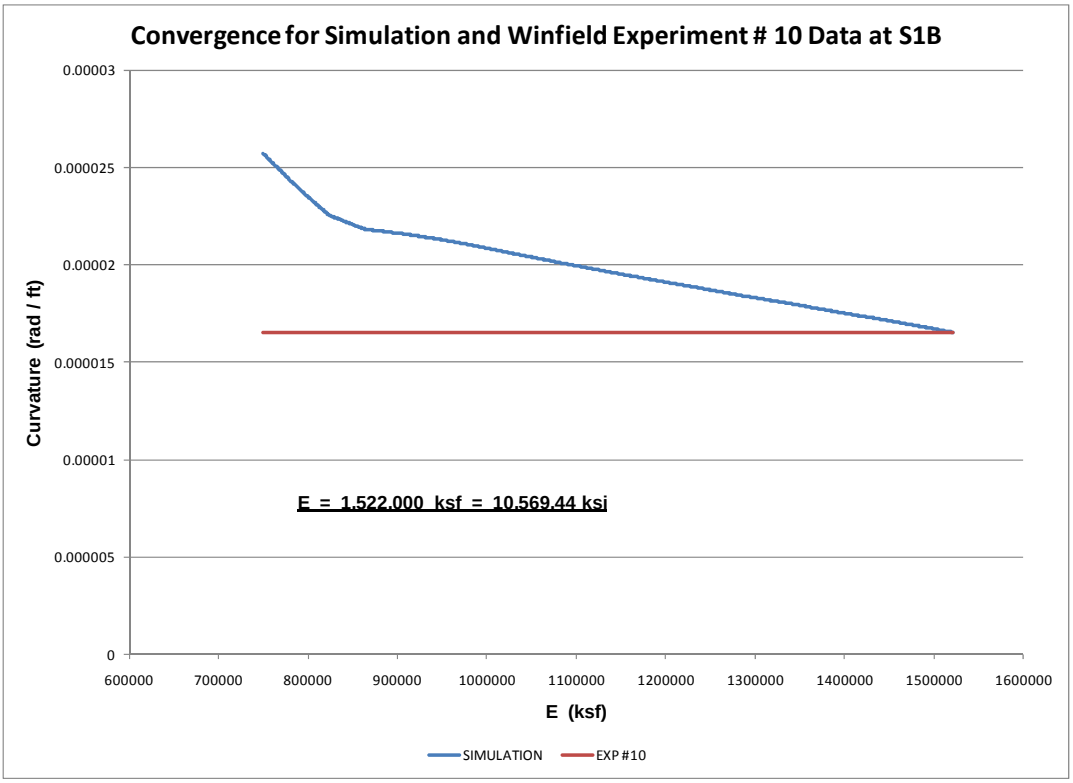

Figure 5.18. Curvature convergence at S1B sensor.

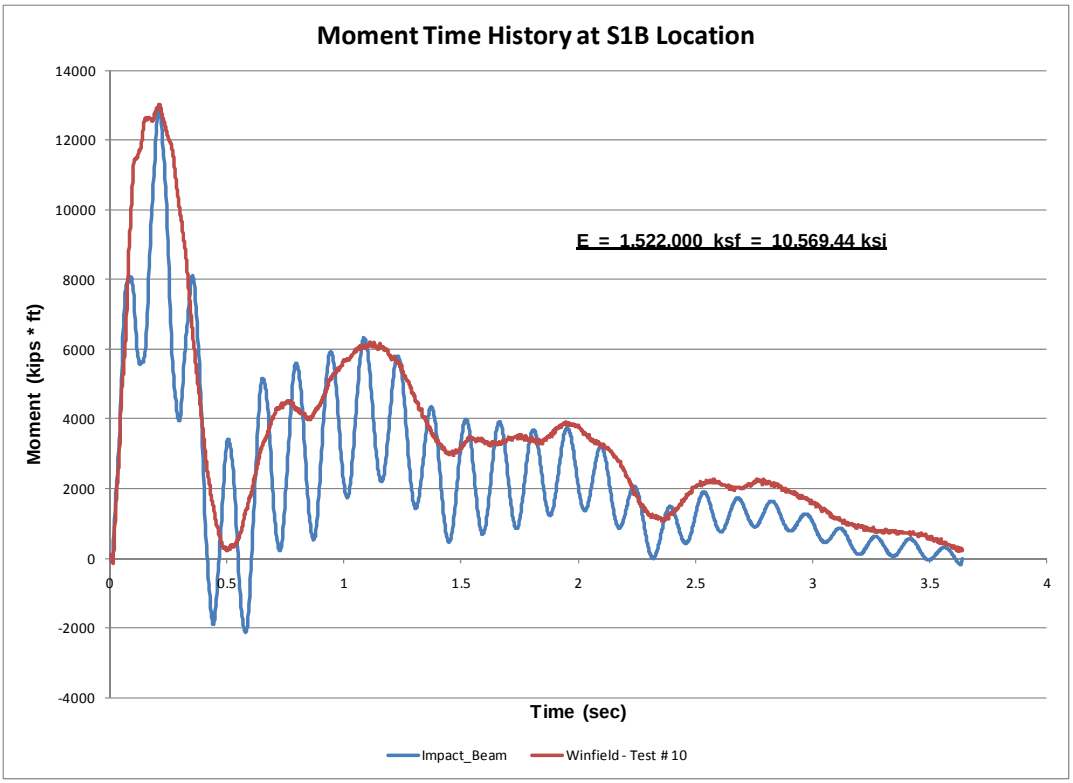

Figure 5.19. Moment time-history at S1B sensor.

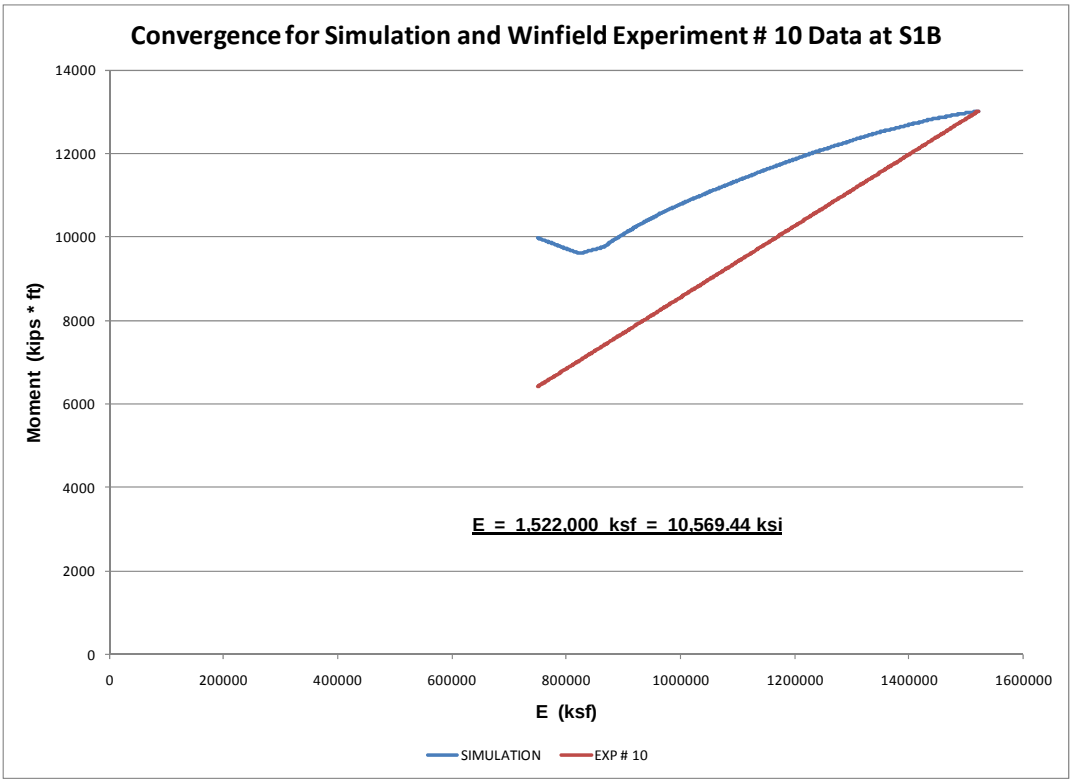

Figure 5.20. Moment convergence at S1B sensor.

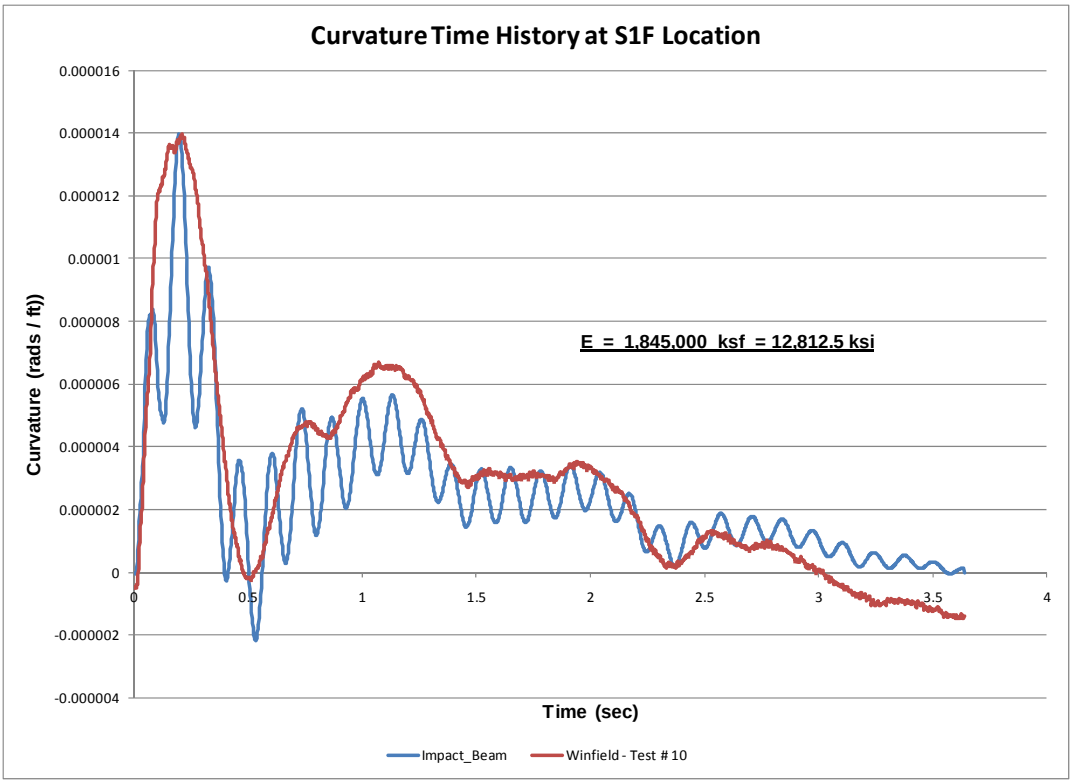

Figure 5.21. Curvature time-history at S1F sensor.

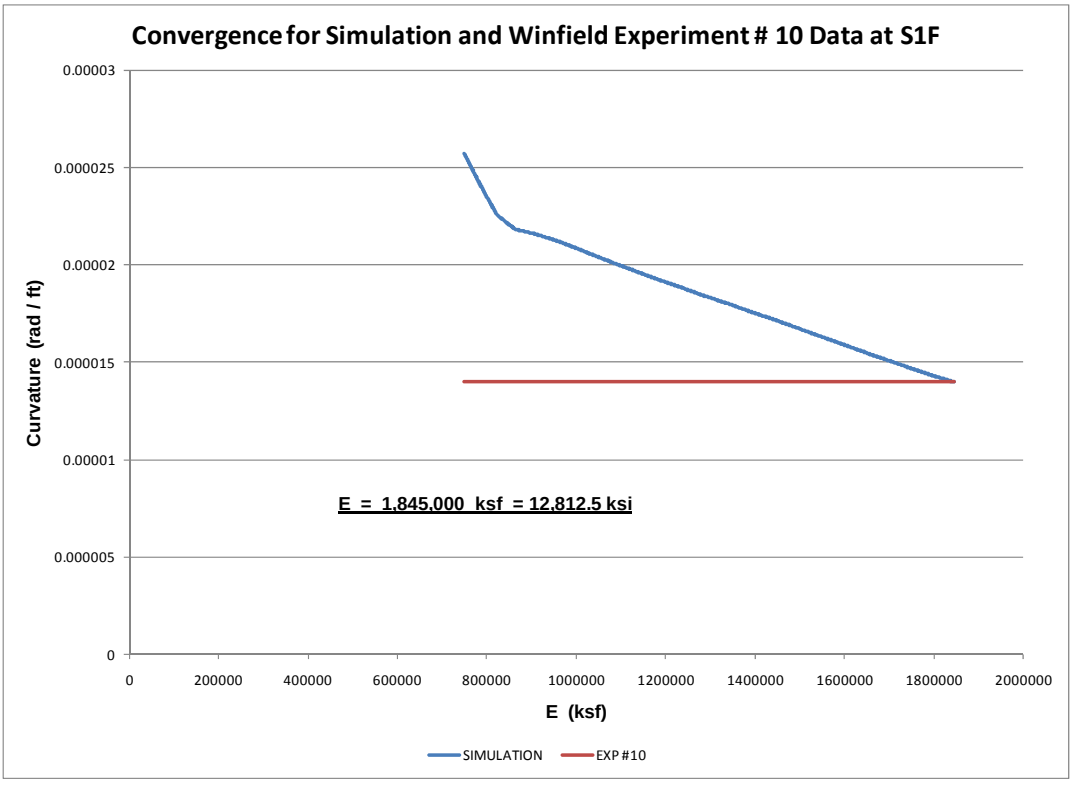

Figure 5.22. Curvature convergence at S1F sensor.

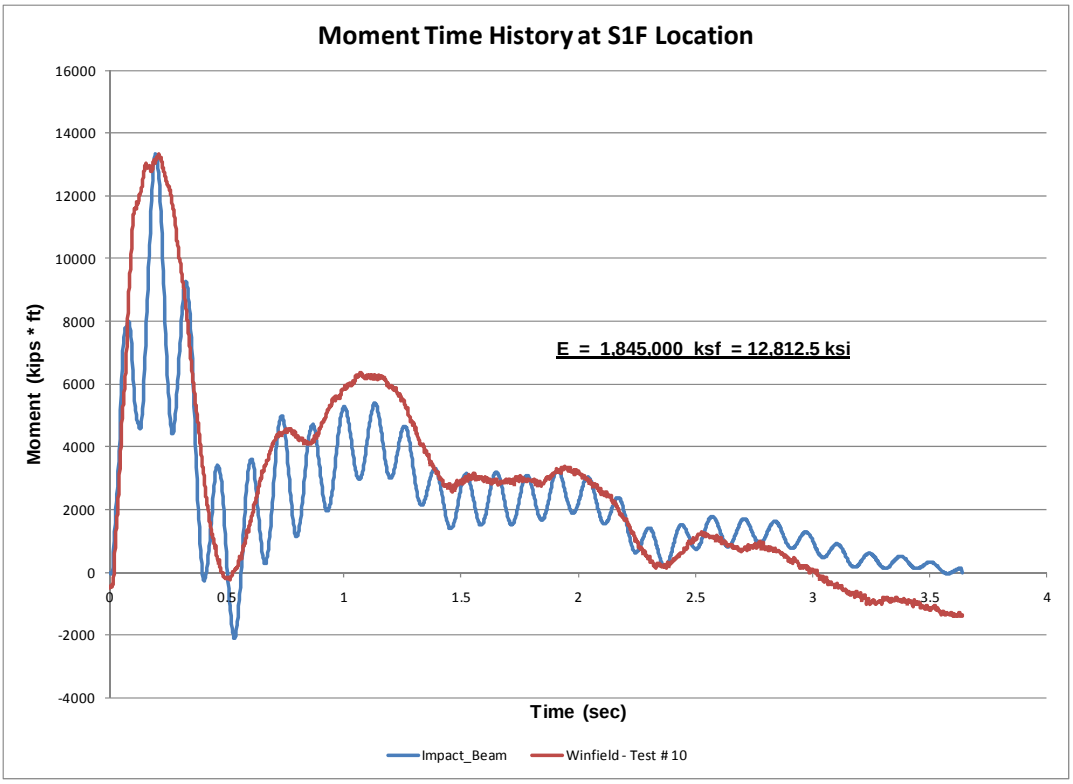

Figure 5.23. Moment time-history at S1F sensor.

Figure 5.24. Moment convergence at S1F sensor.

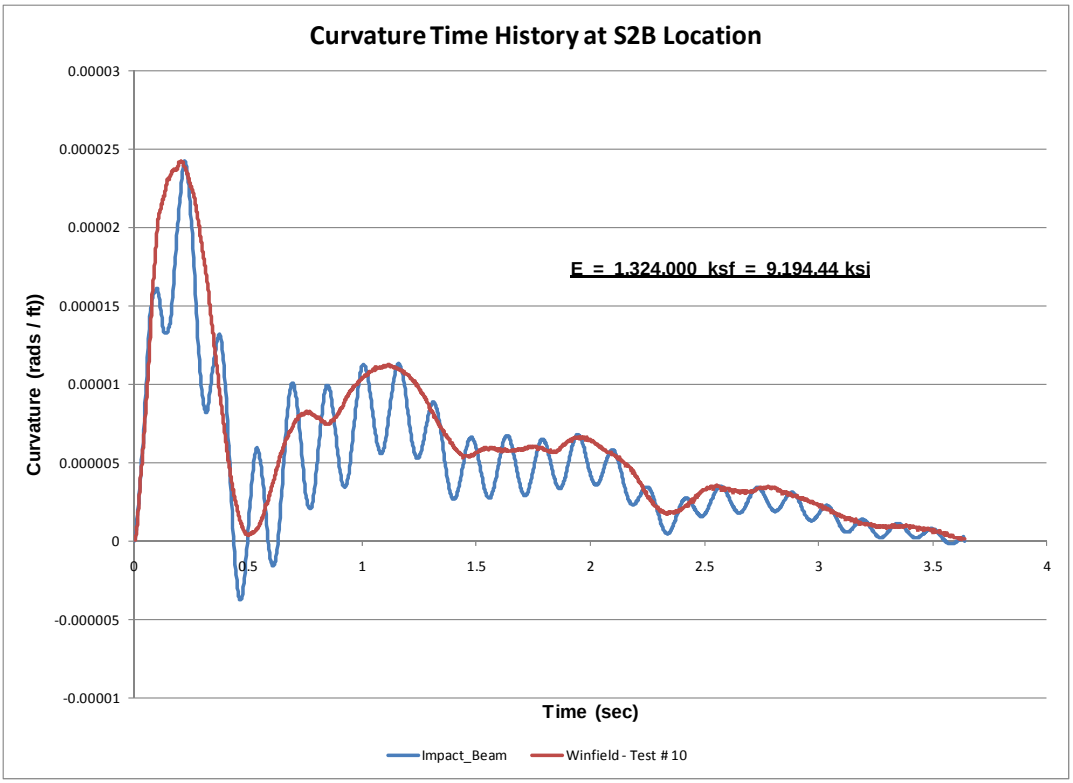

Figure 5.25. Curvature time-history at S2B sensor.

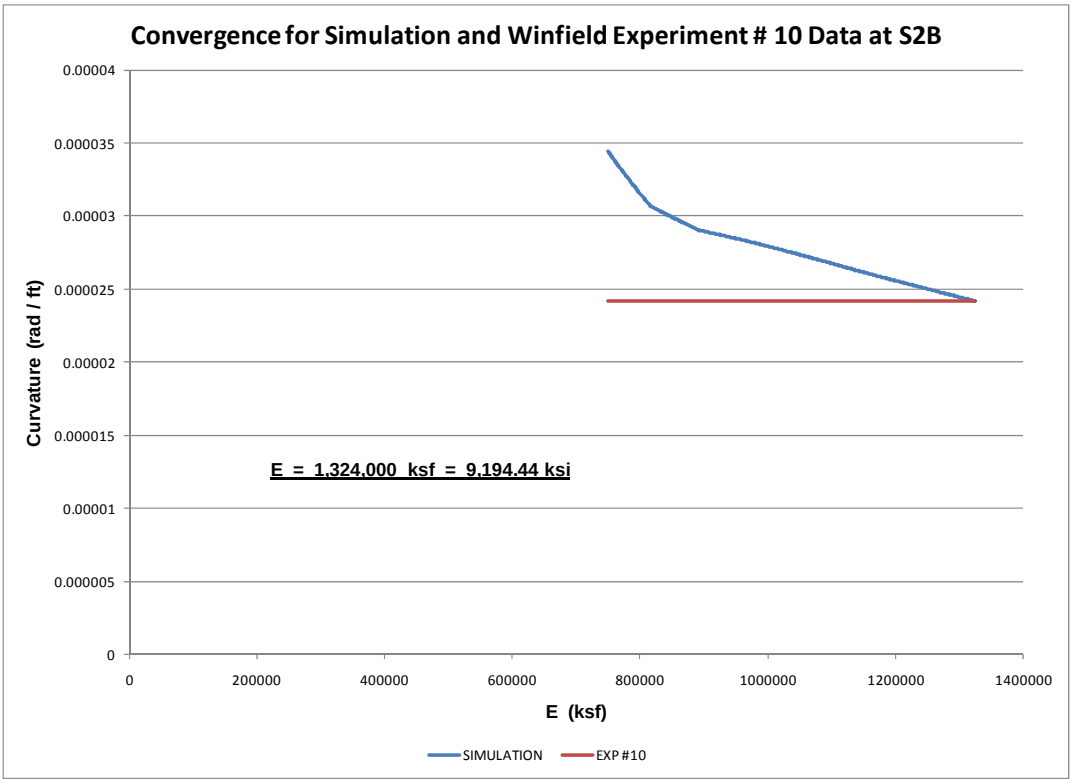

Figure 5.26. Curvature convergence at S2B sensor.

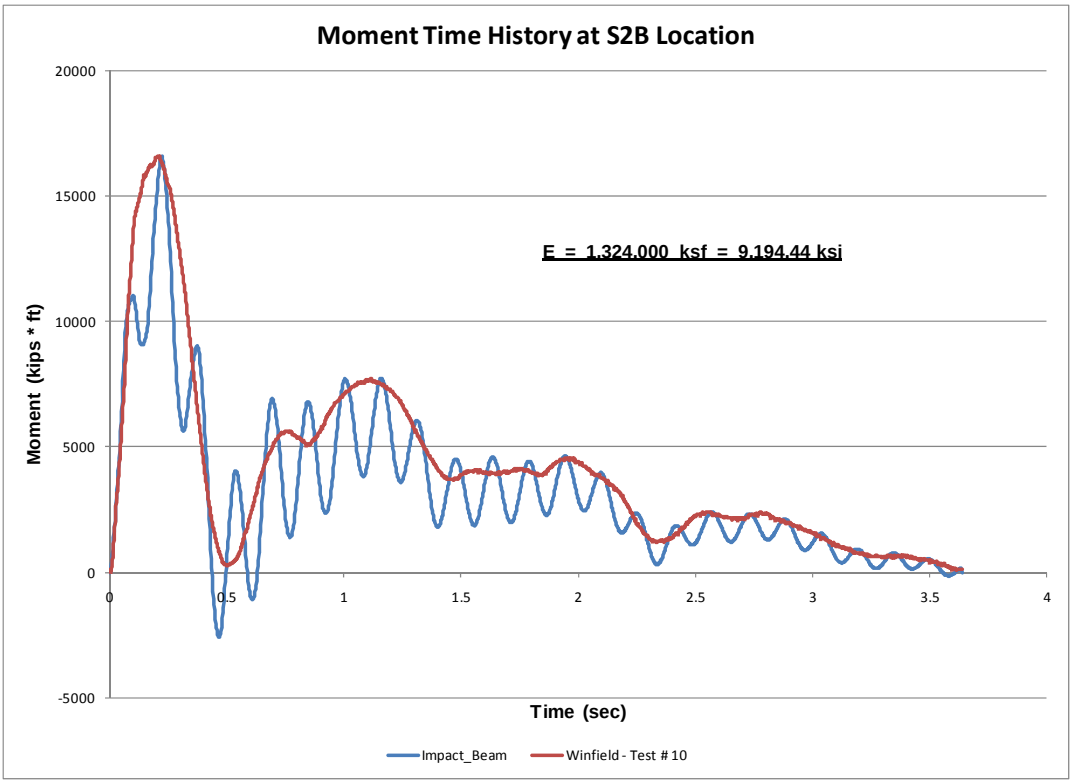

Figure 5.27. Moment time-history at S2B sensor.

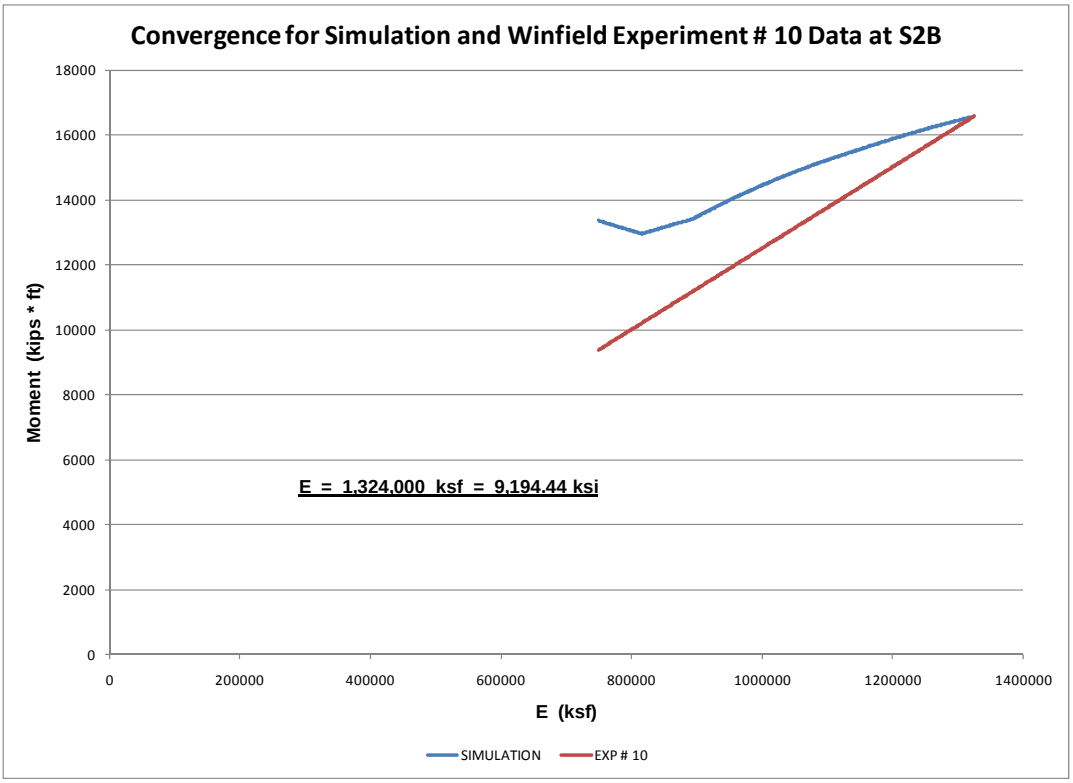

Figure 5.28. Moment convergence at S2B sensor.

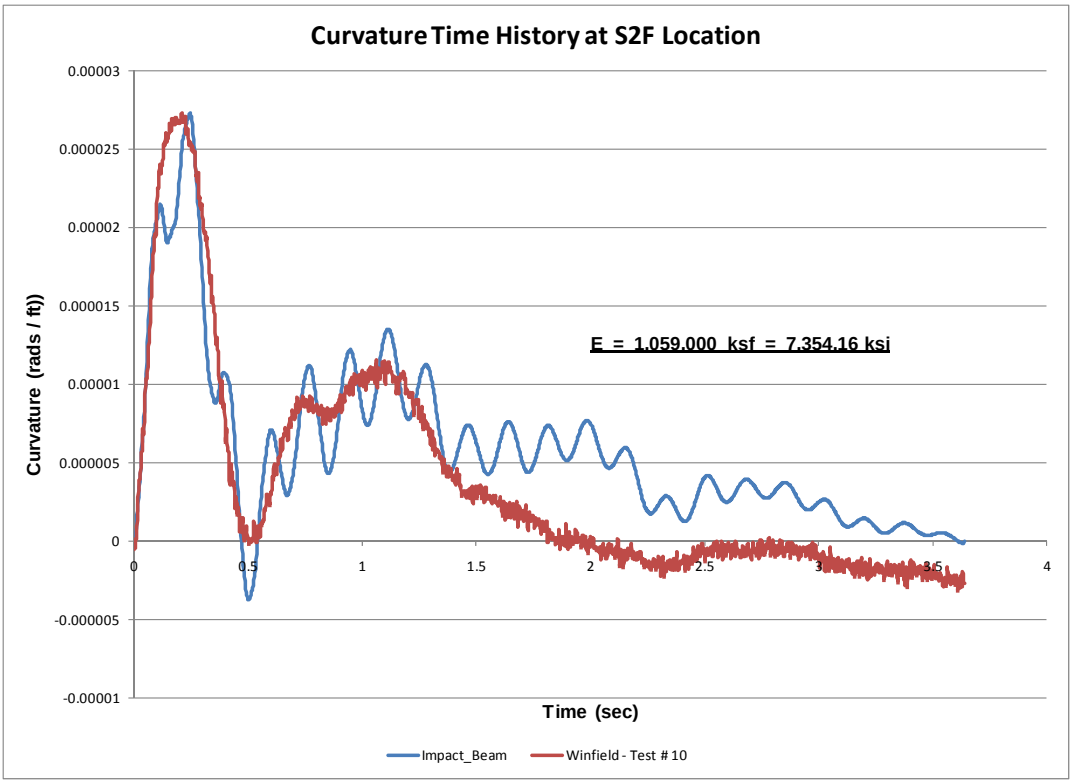

Figure 5.29. Curvature time-history at S2F sensor.

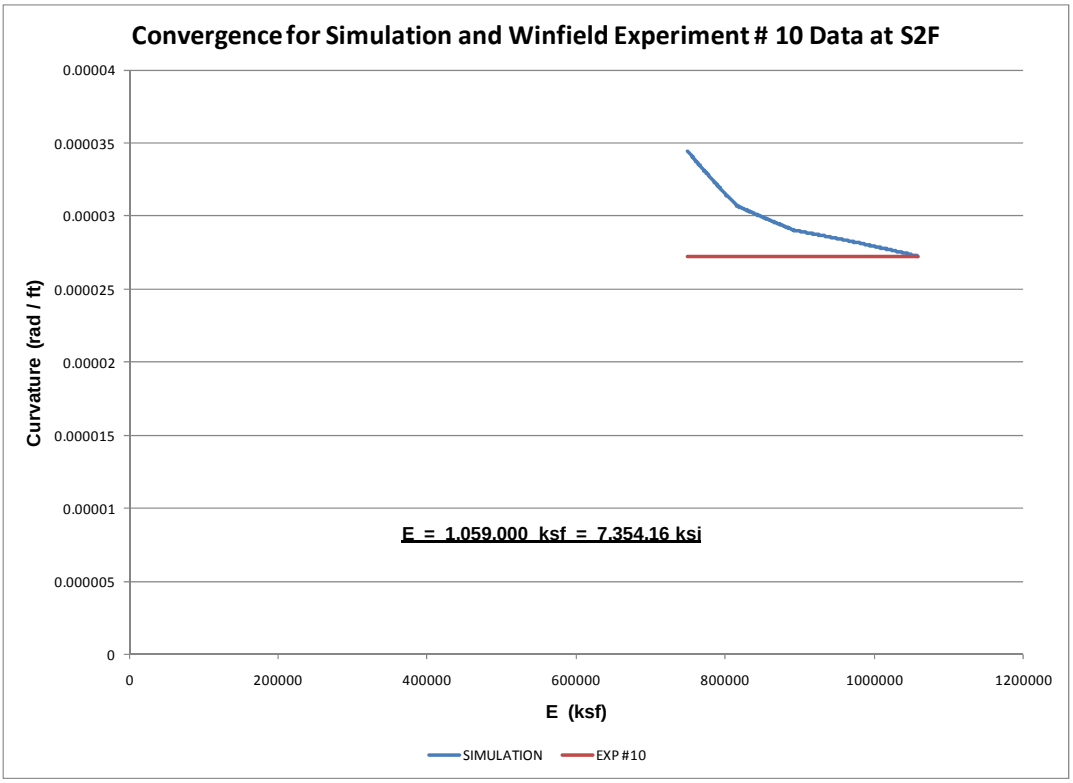

Figure 5.30. Curvature convergence at S2F sensor.

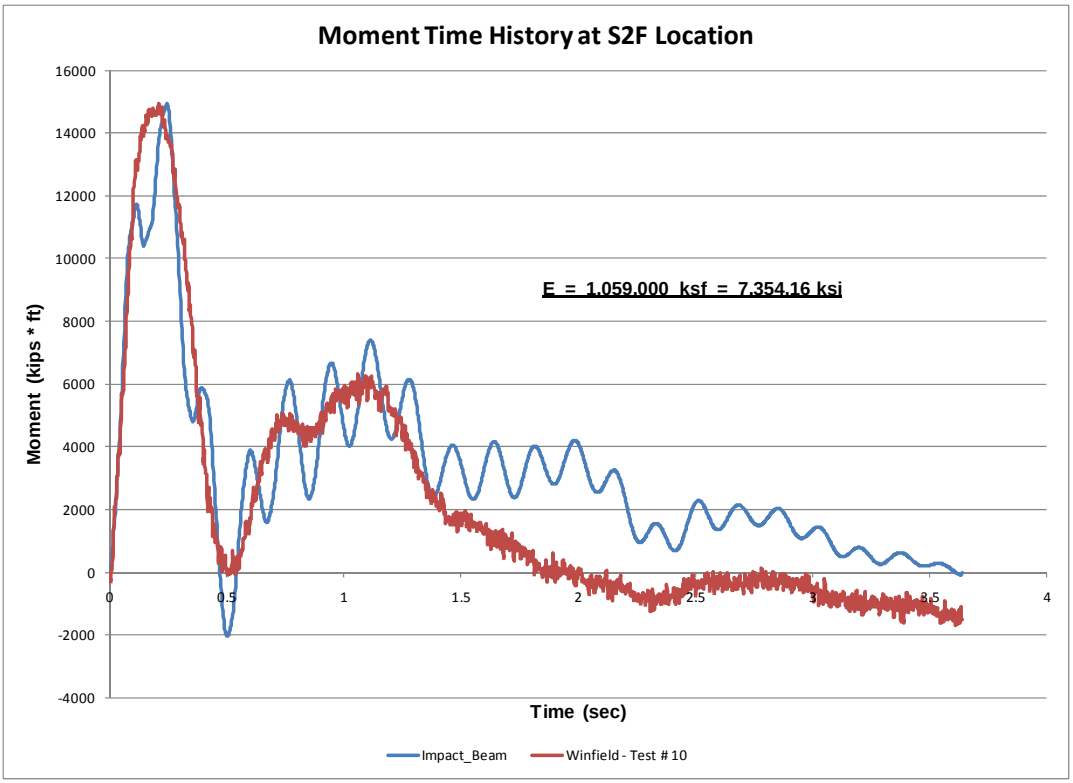

Figure 5.31. Moment time-history at S2F sensor.

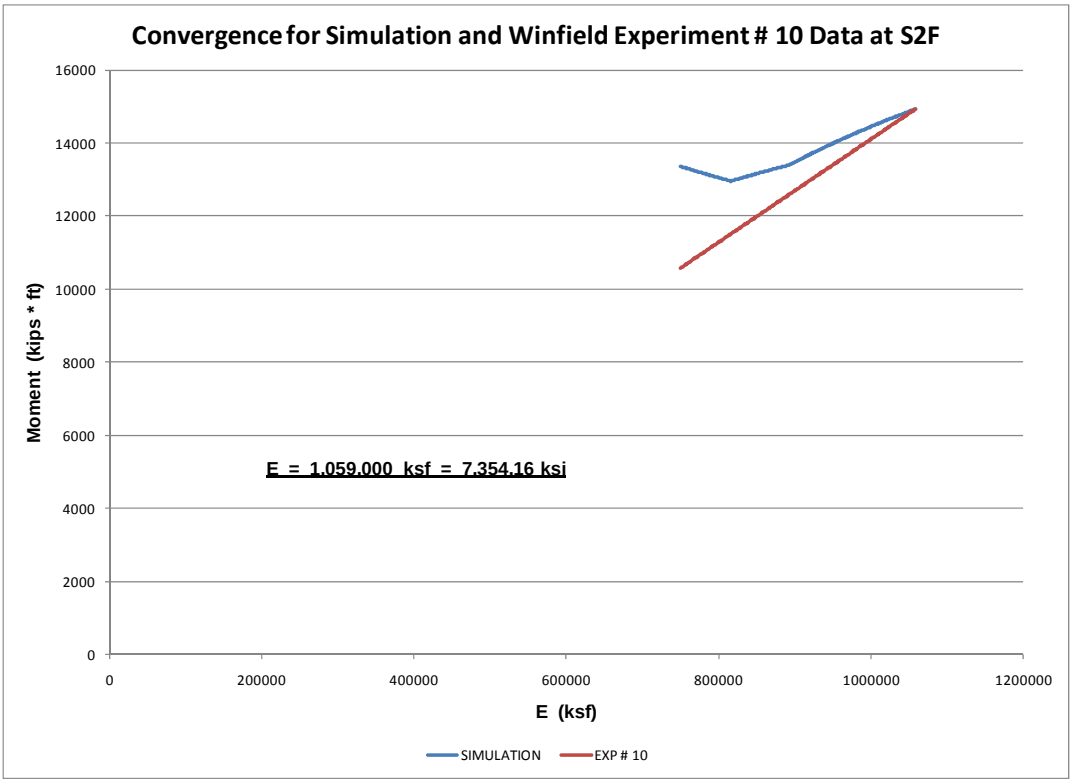

Figure 5.32. Moment convergence at S2F sensor.

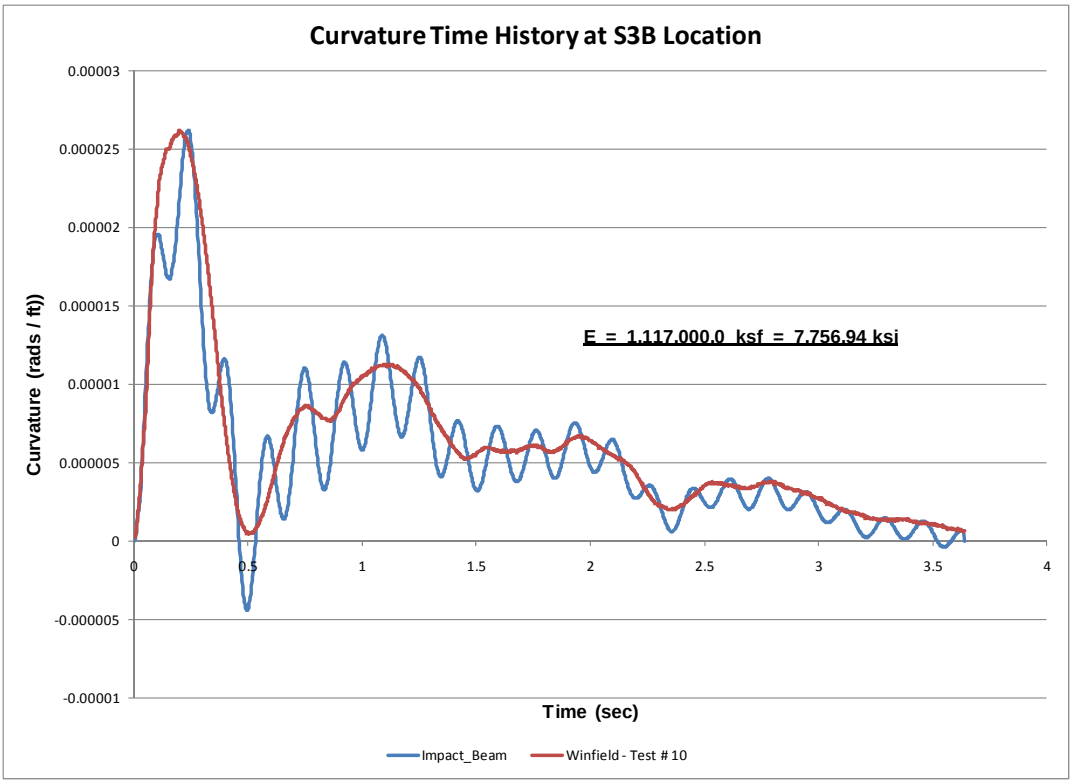

Figure 5.33. Curvature time-history at S3B sensor.

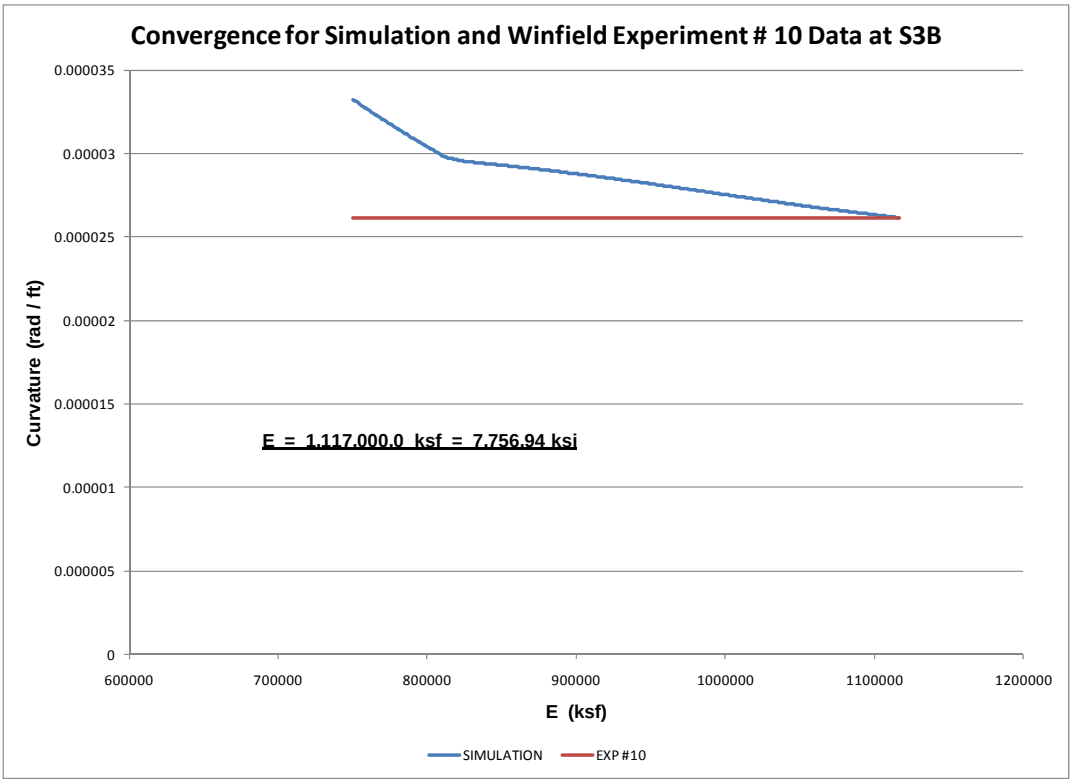

Figure 5.34. Curvature convergence at S3B sensor.

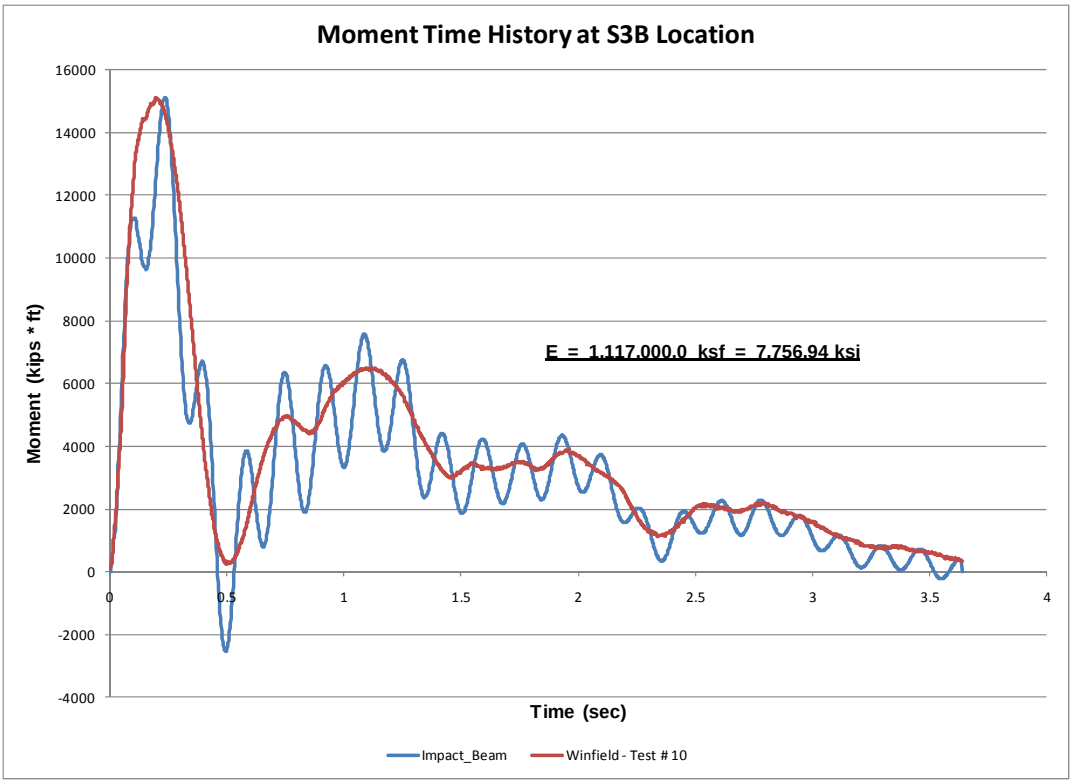

Figure 5.35. Moment time-history at S3B sensor.

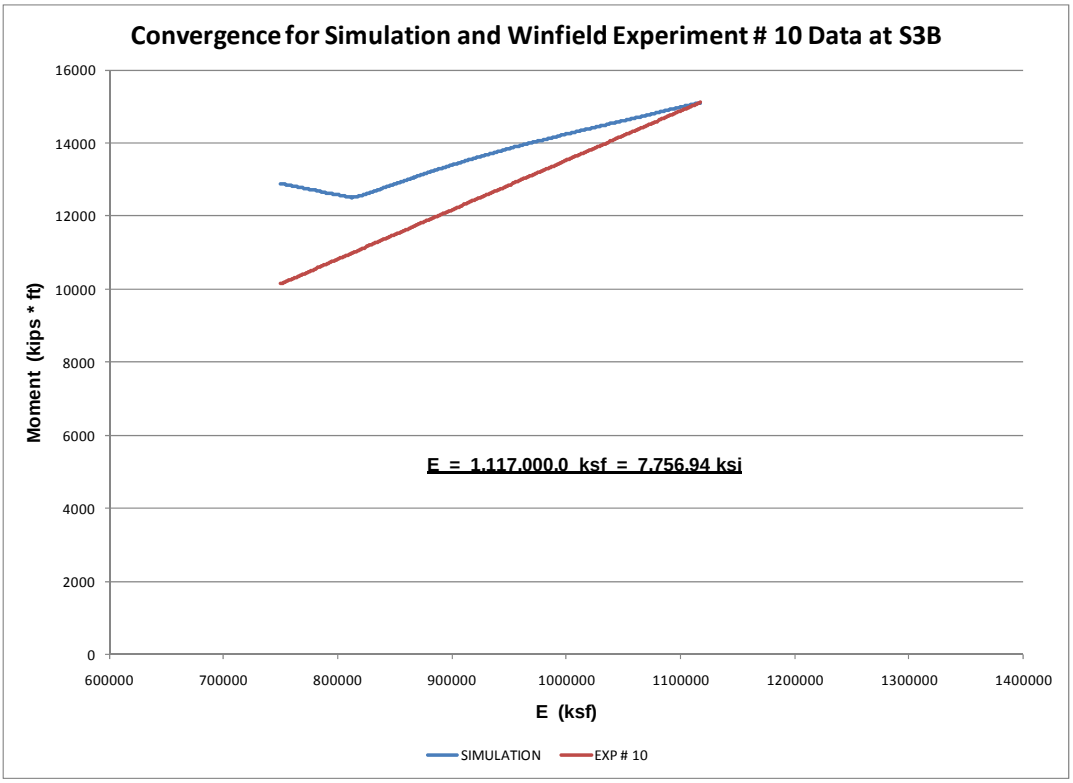

Figure 5.36. Moment convergence at S3B sensor.

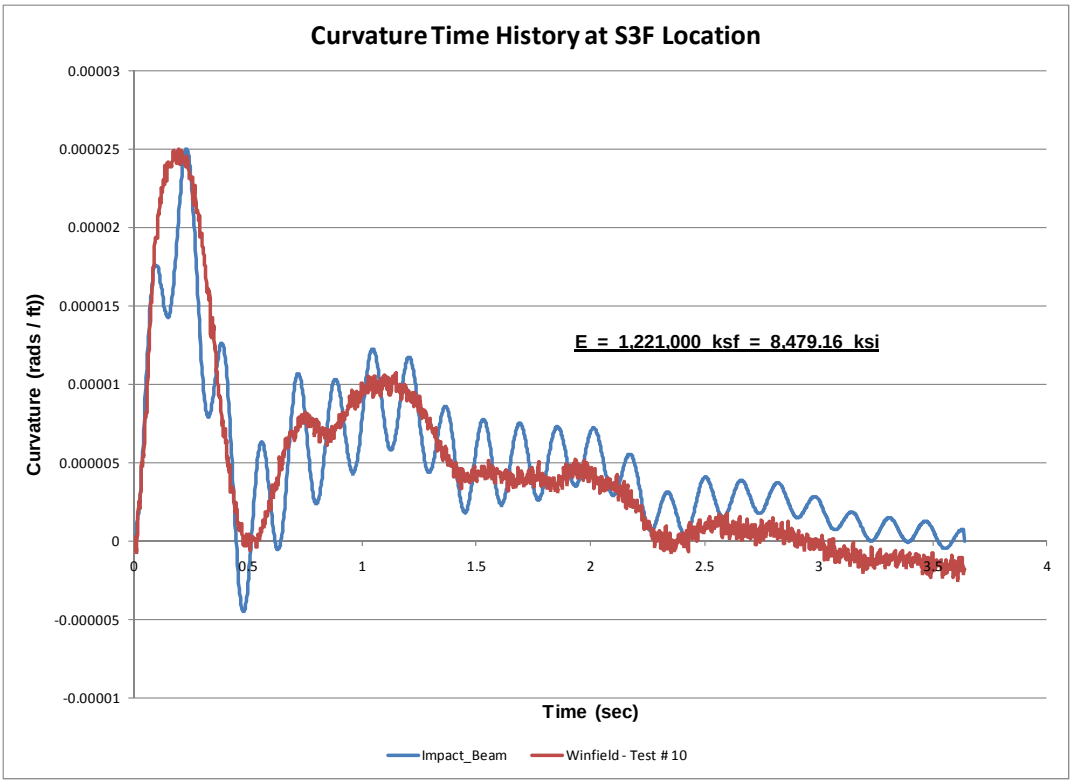

Figure 5.37. Curvature time-history at S3F sensor.

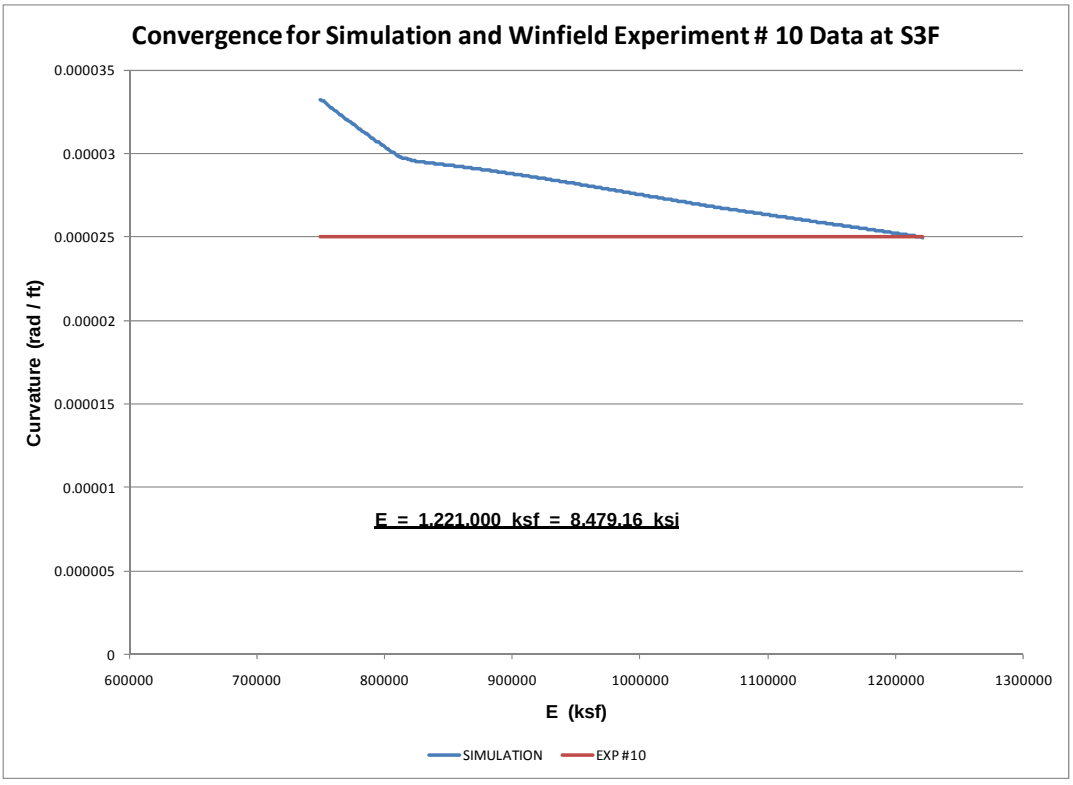

Figure 5.38. Curvature convergence at S3F sensor.

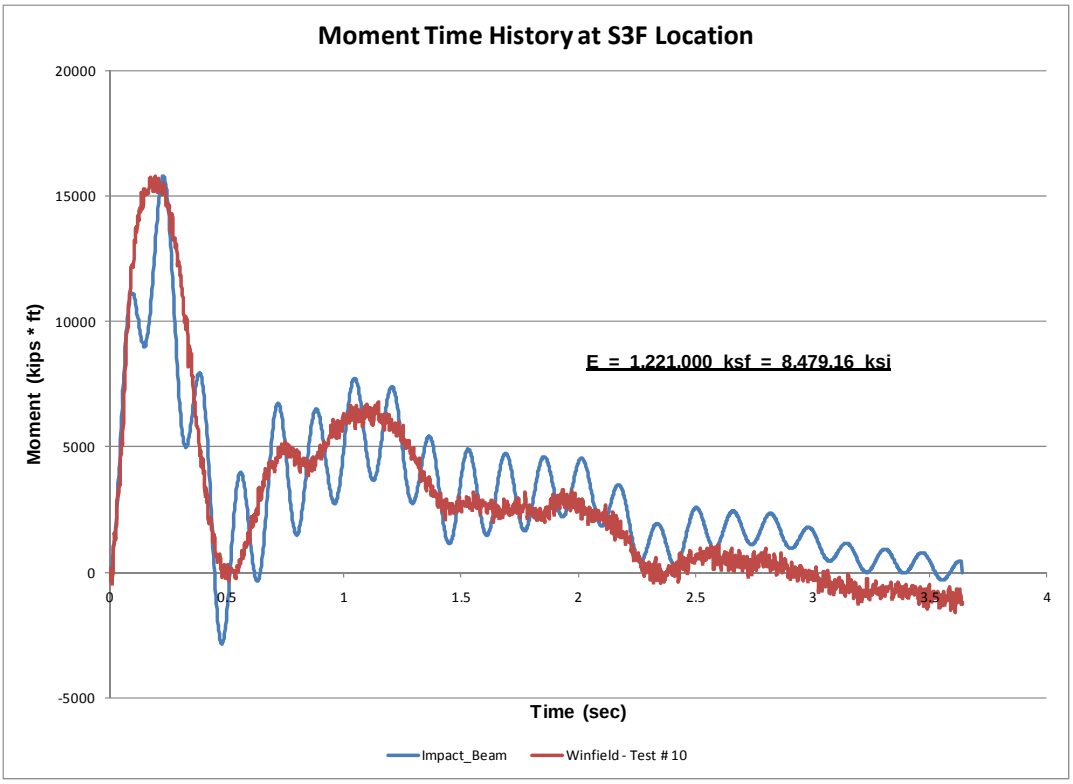

Figure 5.39. Moment time-history at S3F sensor.

Figure 5.40. Moment convergence at S3F sensor.

5.3.2.3 Final remarks on the dynamic modulus of elasticity estimation

The resulting values for the dynamic modulus of elasticity based on experimental beam deflection and experimental curvatures obtained from the experimental normal strains are presented in Tables 5.1 and 5.2.

Table 5.1. Dynamic modulus of elasticity based on experimental beam deflection.

Sensor	LD3	LD4	LD5
Dynamic Modulus of Elasticity, ksf (ksi)	796,800 (5,533)	812,400 (5,642)	799,000 (5,549)
Average Dynamic Modulus of Elasticity = 802,733 ksf (5,574.54 ksi)			

Table 5.2. Dynamic modulus of elasticity based on experimental curvatures.

Sensor	S1B	S1F	S2B	S2F	S3B	S3F	S4B	S4F	S5B	S5F
Dynamic Modulus of Elasticity, ksf (ksi)	1,522,000 (10,569)	1,845,000 (12,812)	1,324,000 (9,194)	1,059,000 (7,354)	1,117,000 (7,757)	1,221,000 (8,479)	N/A	1,688,000 (11,722)	N/A	2,349,000 (16,313)
Average Dynamic Modulus of Elasticity = 1,515,625 ksf (10,525 ksi)										

From the values observed in Table 5.1, the dynamic modulus of elasticity based on experimental beam displacement is very consistent. The resulting average dynamic modulus of elasticity is equal to 802,733 ksf (5,574.54 ksi). The Winfield Impact Beam 28-day design compressive strength was $f_{cd} = f'_c = 5{,}000\ psi$. Based on Tabsh and Aswad, (1995), the static probable 28-day compressive strength is,

$$fcp = 1.11 \cdot fcd = 5{,}550\ psi \tag{5.5}$$

But based on Carrasquillo, Nilson and Slate (1981), the probable 90-day (long term) static compressive strength is,

$$fcpl = 1.15 \cdot fcp = 6{,}382.5\ psi \tag{5.6}$$

Using Branson (1977) equations as per Johns and Belanger (1981) equations, the static modulus of elasticity is,

$$E_c = (39 - 0.0015 f_{cpl}) \sqrt{f_{cpl} \cdot w^3} = 4{,}104{,}708.64\ psi = 591{,}078 ksf \tag{5.7}$$

where $w = 145\ pcf$. Finally, using the dynamic modulus of elasticity definition as per Nam, Compomanes and Kim (1977) and by Johns and Belanger (1981), which establishes a relation between the dynamic and the static modulus of elasticity of 1.3,

$$E_{cd} = 1.3 \cdot E_c = 5{,}336.12\,ksi = 768{,}401.45\,ksf \tag{5.8}$$

The ratio of the average dynamic modulus of elasticity based on experimental beam deflection (Table 5.1) to the static modulus of elasticity of Equation (5.7) produced a value of 1.358. This factor compared to the factor of 1.3 presented by Johns and Belanger (1981).

The resulting values for the dynamic modulus of elasticity based on experimental curvatures obtained from the experimental normal strains are presented in Table 5.2. There exists an inconsistency of the dynamic modulus of elasticity obtained from experimental curvature when compared to the dynamic modulus of elasticity obtained from experimental beam deflections. The dynamic modulus of elasticity obtained from the experimental curvature was above the expected values. The experimental curvatures used in the estimation of the dynamic modulus of elasticity were small values producing high values for the dynamic modulus of elasticity. It can be observed that the curvature values at S4B and S5B were not presented because the experimental curvature at these locations were small values and do not compare to the calculated curvatures at other sensor locations. If these values of curvature are used to estimate the dynamic modulus of elasticity, a very high dynamic modulus is obtained that does not fit the data.

An additional attempt to estimate the dynamic modulus of elasticity was performed by considering the beam under bending and axial effects. Both effects can be included because the impact force applied to the beam by the barge train is not aligned transverse to the beam. If the axial normal strain is to be considered, then the neutral axis of the beam does not lie at the centroid of the cross section. The development of the procedure to calculate the curvature at each sensor location is presented in Appendix G. After considering that the normal strain can be induced by the axial and bending effects, the resulting estimation of the dynamic modulus of elasticity was also high. Table 5.3 shows the dynamic modulus of elasticity based on experimental curvatures calculated considering the axial and bending effects.

Table 5.3. Dynamic modulus of elasticity based on experimental curvatures (axial and bending effects).

Sensor	S1	S2	S3	S4	S5
Dynamic Modulus of Elasticity, ksf (ksi)	1,618,000 (11,236)	1,245,000 (8,645.8)	1,152,000 (8,000)	5,423,000 (37,659.7)	6,980,000 (48,472)
Average Dynamic Modulus of Elasticity = 3,283,600 ksf (22,803 ksi)					

There exists an inconsistency of the dynamic modulus of elasticity obtained from experimental curvature calculated considering the axial and bending effects when compared to the dynamic modulus of elasticity obtained from experimental beam deflections. The dynamic modulus of elasticity obtained from the experimental curvature was above the expected values. The explanation of the behavior of the strain gages (curvatures) during Winfield Test #10 is beyond the scope of this (current) analysis. Additional research is needed to process this normal strain data so that it can be used to estimate the dynamic modulus of elasticity.

5.3.3 Simulation and experimental moment time-history comparison based on average dynamic modulus of elasticity obtained from experimental beam deflection

This section presents the calculation of the simulation moment time-history using Impact_Beam and the experimental moment time-history. To perform this analysis, the Impact_Beam input data must be first presented. For the Winfield Test #10, the effective beam length (from center to center of neoprene pads) was 112.6 ft. The moment of inertia of the beam was 517.2 ft^4. The mass per unit length of the beam was 0.25486 kips/ft. The barge train was moving at 2.99 ft/s and the first point of contact was at 64.1 ft from right reaction (right neoprene pads, Figure 5.41). The location of each sensor S1B;S1F, S2B;S2F, S3B;S3F, S4B;S4F and S5B;S5F was calculated as 80.28208 ft, 68.2925 ft, 56.30291667 ft, 44.31333 ft and 32.32375 ft, respectively, as shown in Figure 5.41.

In the Impact_Beam input file, each one of these positions was specified as a location where the results were of interest. Ten modes were used and a damping ratio of 0.02 was used for each mode. The elastic modulus was assigned a value of 802,733 ksf, which is the average value obtained from the experimental beam deflection analysis in the previous section. This dynamic modulus of elasticity was also used to calculate the dynamic

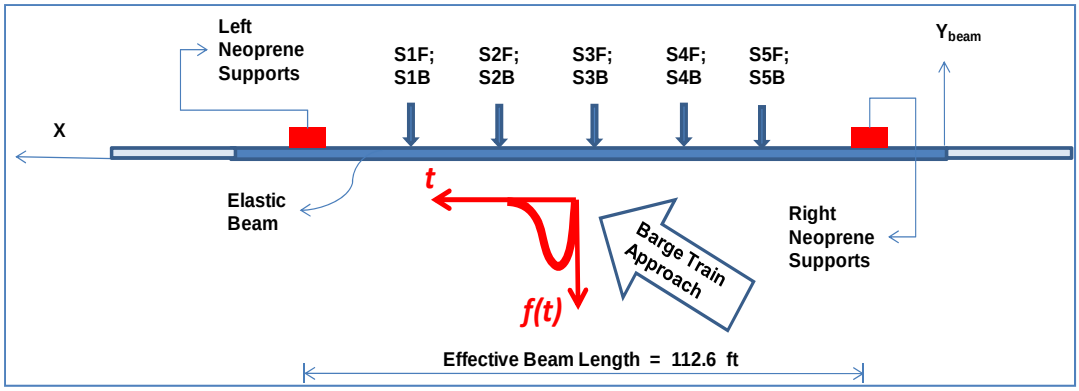

Figure 5.41. Location of S1B;S1F, S2B;S2F, S3B;S3F, S4B;S4F and S5B;S5F sensors.

experimental moment by multiplying this value by the moment of inertia and the experimental curvature. The resulting maximum bending moments obtained with these values and using the experimental curvatures at sensors S1B, S1F, S2B, S2F, S3B and S3F were 6,866.91 kips * ft, 5803.26 kips * ft, 10,043.1 kips * ft, 11,322.46 kips * ft, 10,857.06 kips * ft, 10,376.12 kips * ft, respectively. The maximum bending moment obtained from simulation (Impact_Beam) at sensor locations S1B, S2B and S3B were 9,705.0 kips * ft, 13,037.0 kips * ft and 12,567.2 kips * ft, respectively. The corresponding bending moment time histories are presented in Figures 5.42 through 5.44. It can be observed that the shape of the simulation response is similar to the experimental moment time-history. However, the magnitude of the simulation results is higher than the experimental results. The ratio of the maximum bending moment at each position (S1B;S1F), (S2B;S2F) and (S3B;S3F) to the experimental moment at S1B, S1F, S2B, S2F, S3B and S3F produced values of 1.41, 1.67, 1.30, 1.15, 1.16 and 1.21, respectively. This amplification factor can be explained if it is considered that the dynamic modulus of elasticity used in these calculations was based on the experimental beam displacement and not on the experimental curvature.

5.4 SDOF system numerical examples

This sub-section discusses three groups of SDOF response calculations being made using Impact_Beam. The first compares a SDOF response computed using Impact_Beam to results published by Paz (1985). The second group of calculations, made using three distinct assumptions for spring stiffness, compares Impact_Beam results to Winfield Test #10 results. The third group of calculations, made using five distinct assumptions for spring stiffness based on base isolator characteristics for a Deformable BEAS, compares Impact_Beam results to dBEAS software (Ebeling et al. 2011) results.

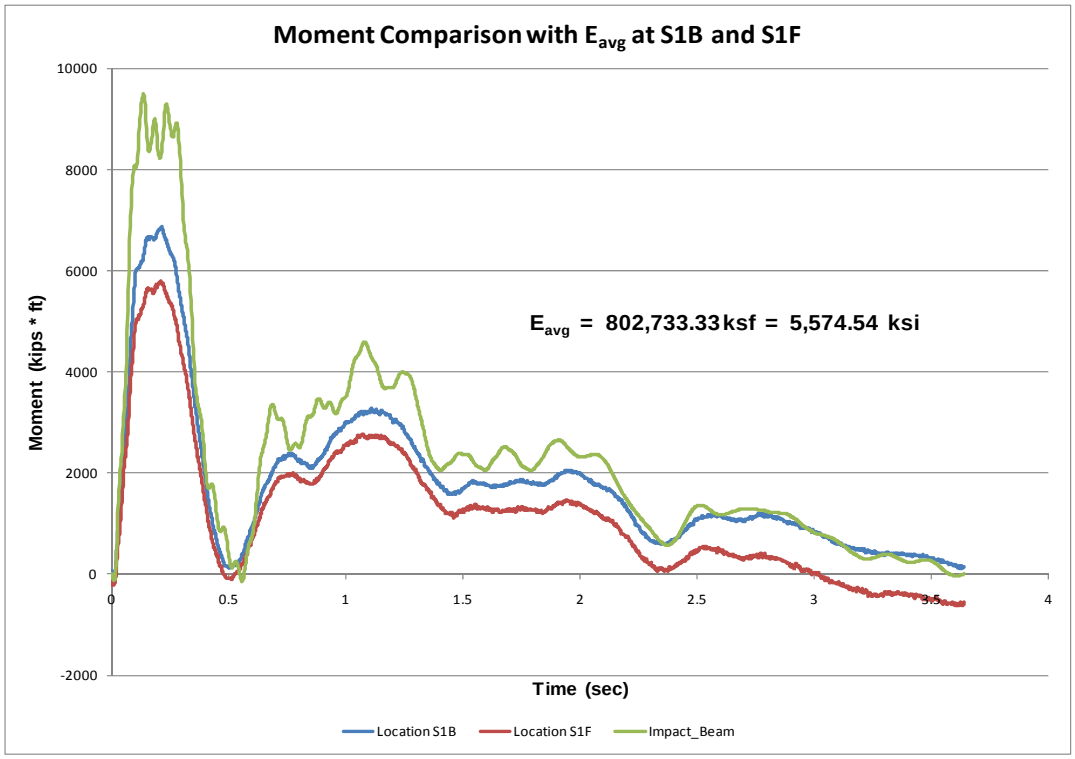

Figure 5.42. Moment comparison at sensor S1B and S1F using the average dynamic modulus of elasticity obtained from experimental beam deflection.

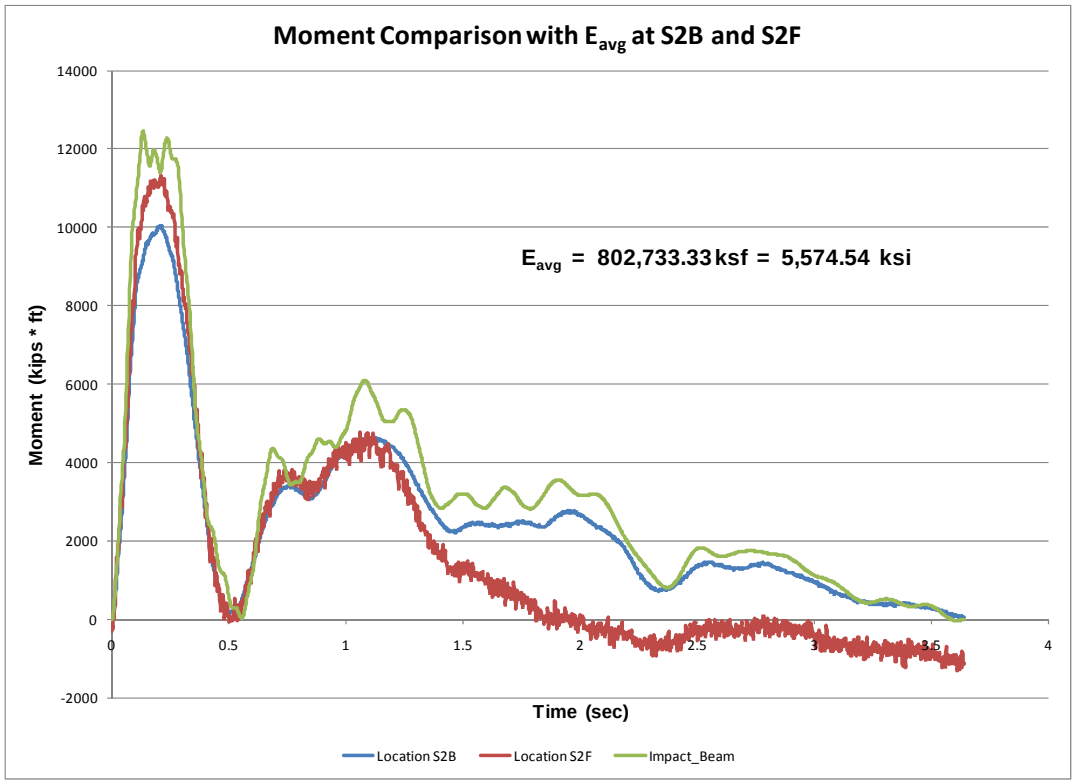

Figure 5.43. Moment comparison at sensor S2B and S2F using the average dynamic modulus of elasticity obtained from experimental beam deflection.

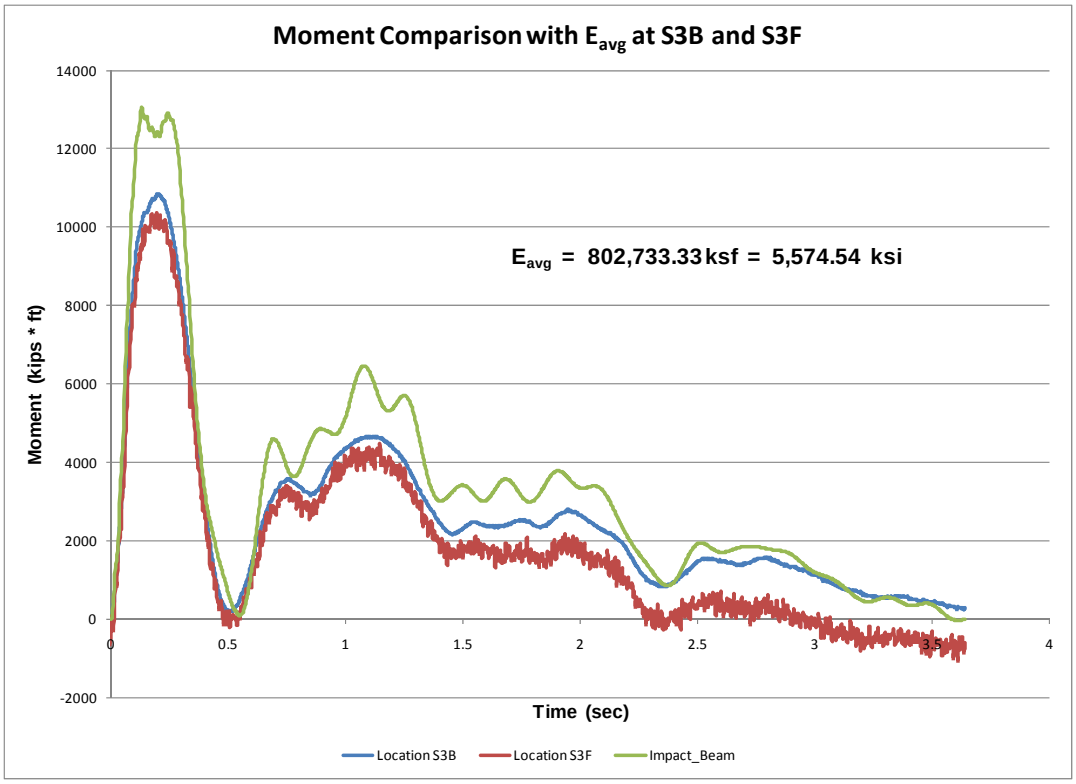

Figure 5.44. Moment comparison at sensor S3B and S3F using the average dynamic modulus of elasticity obtained from experimental beam deflection.

5.4.1 Numerical example obtained from Paz (1985)

Paz (1985) presented an Example 4.2 on page 78 that considers a SDOF subjected to an external dynamic load and calculates the response of the system. The spring in the system is modeled using a linear relation between the internal force of the spring and the displacement the spring undergoes. This SDOF system and the spring force – displacement behavior is presented in Figure 5.45.

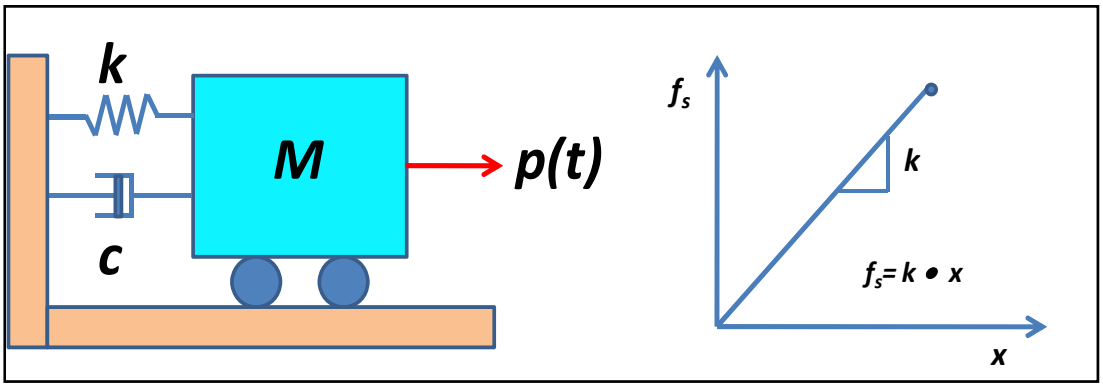

Figure 5.45. SDOF model used in example 4.2 in Paz, 1985.

The input data for the SDOF system example obtained from Paz (1985) is as follows (it is important to mention that the example is presented in consistent units):

- Mass (M)= 100
- Stiffness coefficient(k) = 100,000
- Damping ratio (C)= 5%
- Time step = 0.005
- Dynamic external load as shown in Figure 5.46.

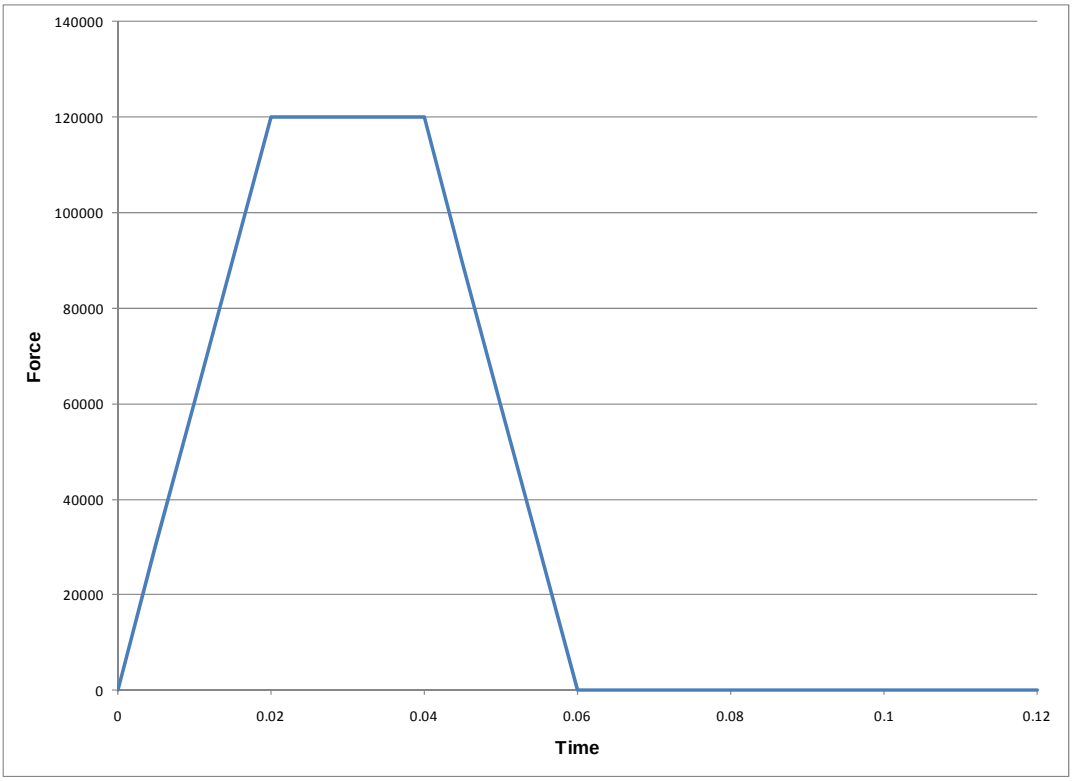

Figure 5.46. Dynamic external force time-history used for numerical example 1.

To use Impact_Beam it is necessary to create an input file with this information. This can be done by using Impact_Beam Visual Modeler. The input file format is described in details in Appendix D and has the following form:

Table 5.4. Impact_Beam input file for Example 4.2 of Paz, 1985.

2 386.086 1
0 100.0 0.05 0
100000.
0.005 4 0.12 1
0. 0.
0.020 120000.
0.04 120000.
0.06 0.0
386.086 386.086 1

It is important to mention that the spring constant is defined by one slope equal to 100,000. After Impact_Beam made the calculations, an output file is obtained, as shown next.

Table 5.5. Results obtained for Example 4.2 of Paz, 1985 using Impact_Beam (continued).

Response of a Single Degree of System Using Duhamel Integral Solution		
SDOF MASS	=	100.000
SDOF Spring Constant	=	100000.00
SDOF Damping Constant	=	316.2278
Undamped Natural Frequency	=	31.623 radians/sec
Damped Frequency	=	31.583 radians/sec
SDOF Damping Constant	=	316.2278
Critical Damping Constant	=	6324.5553
Relative Damping	=	.0500
Undamped Natural Frequency & Period:		Damped Natural Frequency & Period
radians/sec Hertz Seconds :		radians/sec Hertz Seconds
31.623 5.033 .1987 :		31.583 5.027 .1989

The results obtained with Impact_Beam are the same results presented in the numerical example in Paz, 1985. The resulting displacement time-history is presented in Figure 5.47.

Table 5.5. Results obtained for Example 4.2 of Paz, 1985 using Impact_Beam (concluded)

TIME	FORCE	DISPL	VELOCITY	ACC.	SUP. REAC.
.0000	.0000	.000	.000	.00	.00
.0050	30000.0000	.001	.745	296.40	266.26
.0100	60000.0000	.010	2.944	580.82	1356.95
.0150	90000.0000	.033	6.521	846.40	3889.82
.0200	120000.0000	.077	11.366	1086.86	8515.61
.0250	120000.0000	.147	16.594	1000.24	15634.93
.0300	120000.0000	.242	21.329	890.23	25153.09
.0350	120000.0000	.360	25.463	759.91	36847.58
.0400	120000.0000	.496	28.901	612.82	50413.83
.0450	90000.0000	.646	30.825	156.47	65336.24
.0500	60000.0000	.800	30.471	-296.59	80601.41
.0550	30000.0000	.947	27.883	-735.21	95112.86
.0600	.0000	1.076	23.161	-1148.74	107799.47
.0650	.0000	1.177	17.198	-1230.96	117782.91
.0700	.0000	1.247	10.904	-1281.42	124741.06
.0750	.0000	1.285	4.438	-1299.36	128540.42
.0800	.0000	1.291	-2.035	-1284.87	129132.08
.0850	.0000	1.265	-8.358	-1238.80	126550.22
.0900	.0000	1.208	-14.374	-1162.79	120909.47
.0950	.0000	1.122	-19.939	-1059.19	112401.18
.1000	.0000	1.010	-24.924	-931.00	101288.64
.1050	.0000	.874	-29.214	-781.77	87902.56
.1100	.0000	.719	-32.714	-615.54	72639.51
.1150	.0000	.548	-35.349	-436.68	55973.74
.1200	.0000	.367	-37.067	-249.82	38529.60
Maximum (Absolute) SDOF Displacement = 1.29					
Maximum (Absolute) SDOF Velocity = -37.07					
Maximum (Absolute) SDOF Relative Acceleration = -1299.36					
Maximum (Absolute) SDOF Support Force = 129132.08					

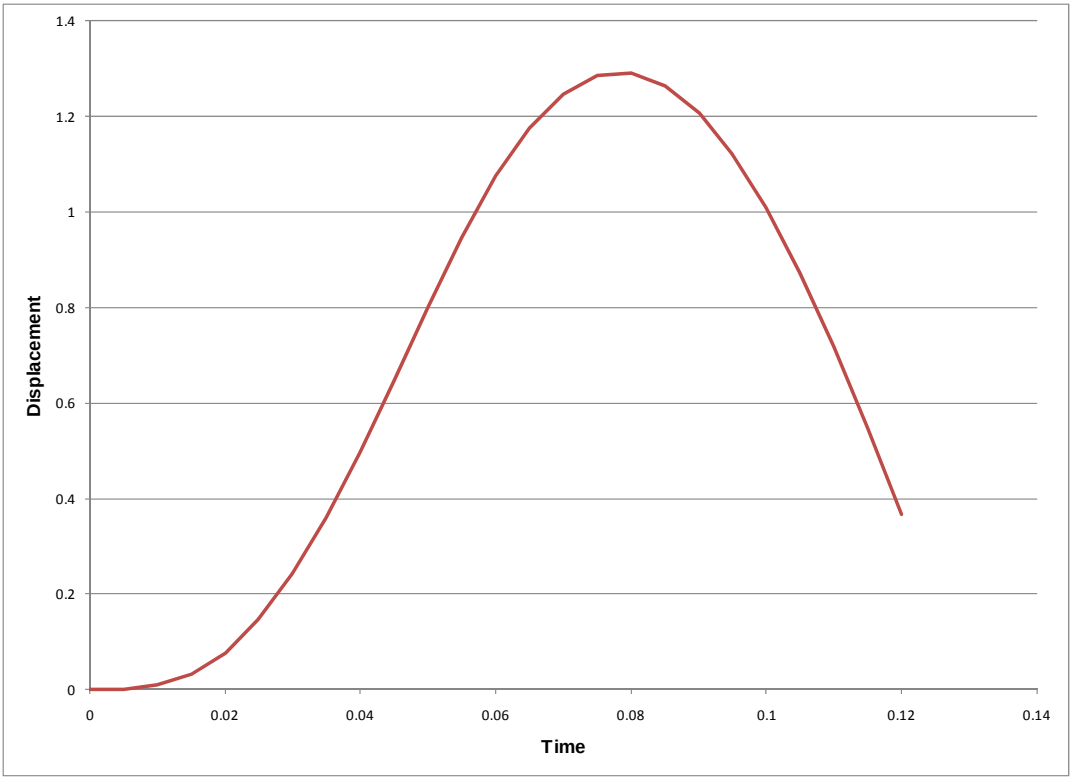

Figure 5.47. Impact_Beam SDOF system response using input data from Paz, 1985.

5.4.2 Winfield Test #10 – Linear spring stiffness

This example represents a simplified model of the elastic beam used at Winfield Test #10. It considers the elastic beam of the field experiment as a SDOF system. Instead of moving an external dynamic load along the beam at a specified velocity, as was the case of the experiment, the external dynamic load has a fixed location for the SDOF model. This numerical example is based on a linear stiffness coefficient obtained from the experimental results of Winfield Test #10. The linear stiffness model used is as idealized in Figure 5.48.

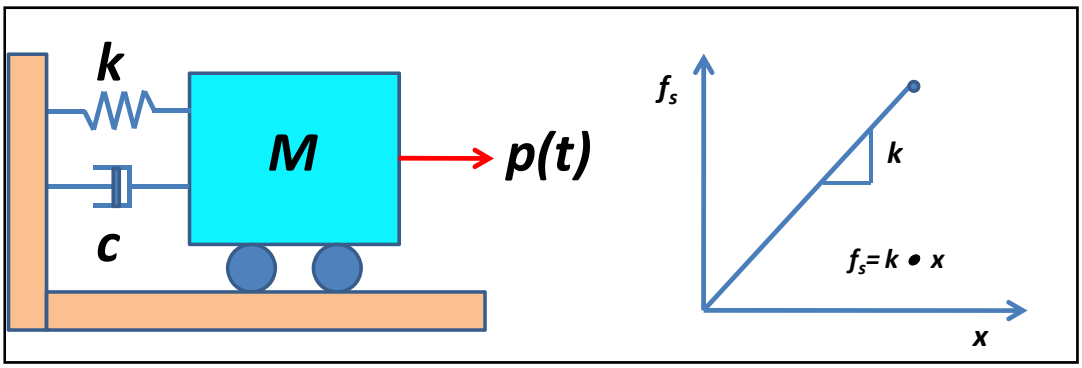

Figure 5.48. SDOF model used for numerical example 5.4.2.

To obtain the equivalent linear stiffness (slope of the force-displacement relationship) for the spring of the SDOF model, the maximum dynamic load recorded during Winfield Test #10 (517,400 lbs) was divided by the corresponding total beam deflection, which is the sum of the foundation displacement, supports (neoprene) displacement and beam elastic curve. The total beam displacement at its midspan was 0.523 inch. This calculation provides the value of the stiffness of the SDOF model, which is 989,292.543 lbs/inch.

Equivalent static force: This stiffness coefficient was calculated using the dynamic maximum force divided by the maximum dynamic deflection. This concept is presented in Chopra (1981) and in El-Tawil, Severino, and Fonseca (2005) as the equivalent static force. The equivalent static force is the static force necessary to produce the same deflection at the point of interest as produced by the dynamic event. Alternatively, the equivalent static force can be interpreted as the external force that will produce the same deformation in the stiffness component of the system as that determined by dynamic analysis. In this example, the unknown is the stiffness of the system. Using the concept of the equivalent static force, the stiffness can be estimated based on the dynamic maximum force and the dynamic maximum displacement. It can be done using the maximum dynamic load and maximum dynamic displacement because at that time step, low magnitude damping and inertia forces are acting in the system. Then, the maximum dynamic force in the spring is transformed to an equivalent static load. Based on the definition of the equivalent static load, the stiffness coefficient can be calculated.

Two cases of damping ratio were considered in this analysis. The damping ratio was fixed first at $\beta = 0.02$, and the second case was for $\beta = 0.05$. The following input data was used in this example:

- Mass (M) = 1,195.985575 lbs • s^2 / inch
- Stiffness coefficient (k) = 517,400 / 0.523 = 989,292.543 lbs/inch
- Damping ratio (c) = 0.02, 0.05
- Time step = 0.002 sec.
- Dynamic external load as shown in Figure 5.49.

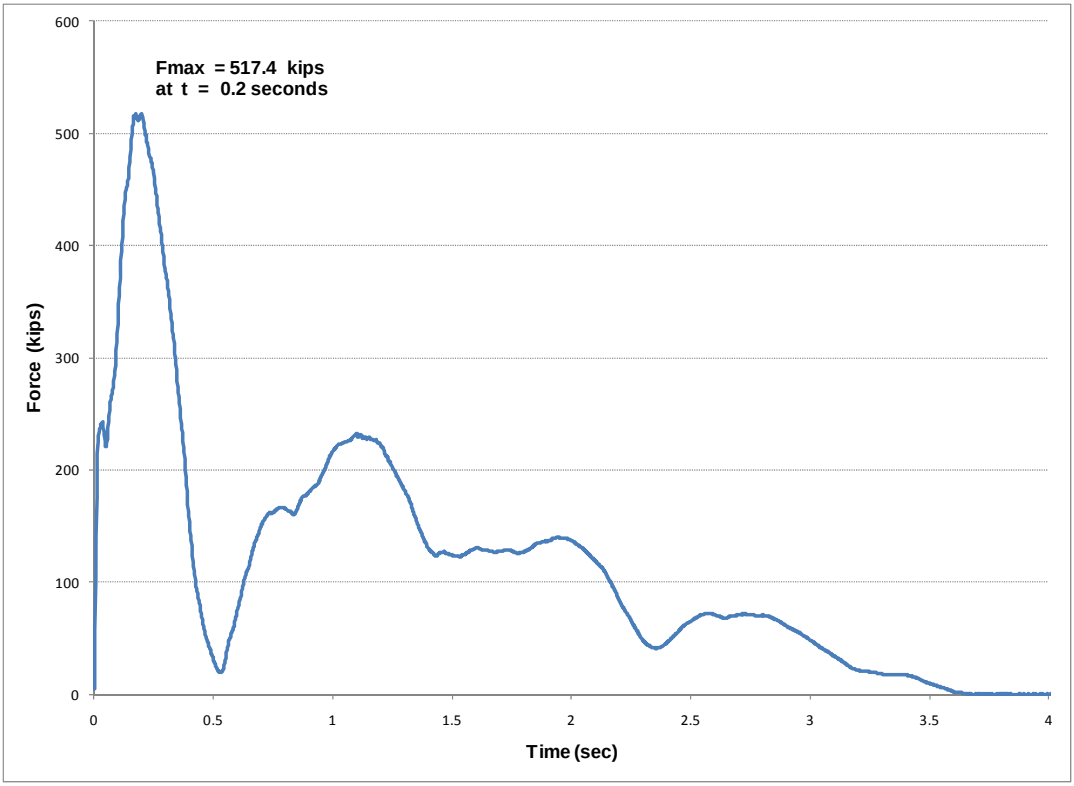

Figure 5.49. Dynamic external force time-history for numerical example 5.4.2.

The maximum value of the force time-history obtained from Winfield Test #10 and used in this example is 517.4 kips. The maximum value for the dynamic response of the SDOF system with $\beta = 0.02$ was 0.56 inch and with $\beta = 0.05$ was 0.54 inch. As a matter of comparison, the maximum beam deflection calculated using the laser measurements and neoprene seats deformation during the experimental procedures was recorded as 0.52 inch. The resulting deflection of the SDOF simulation is in agreement with the Winfield Test #10 recorded data. The whole deflection time-history is presented in Figure 5.50 and the similarity in shape and magnitude of both curves can be observed.

5.4.3 Winfield Test #10 – Bilinear spring Stiffness

This example represents a simplified model of the elastic beam used at Winfield Test #10. It considers the elastic beam of the field experiment as a SDOF system. Instead of moving an external dynamic load along the beam at a specified velocity, as was the case of the experiment, the external dynamic load has a fixed location for the SDOF model. This numerical example is based on a bilinear force-displacement relationship for the spring, as shown in Figure 5.51. The bilinear sloped solution has a

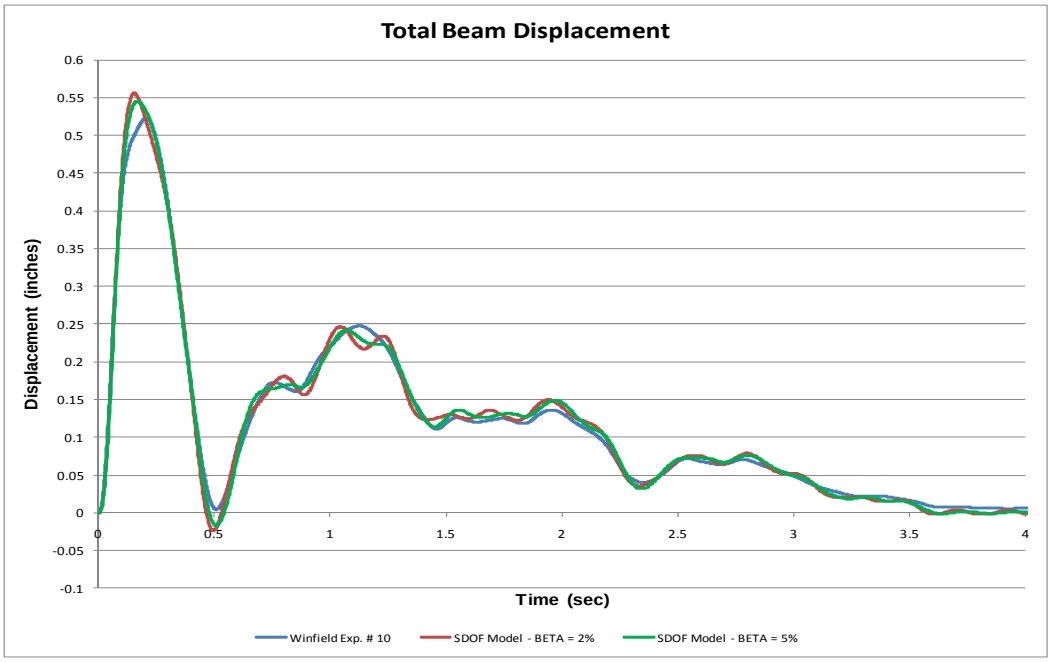

Figure 5.50. Comparison of the dynamic response of the SDOF model and the beam deflection measured during Winfield Test #10.

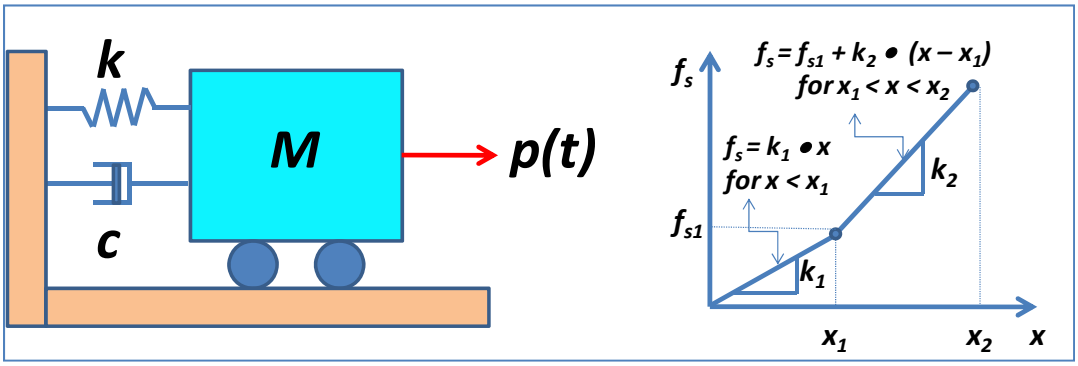

Figure 5.51. SDOF model used for numerical example 5.4.3.

different derivation than the single spring stiffness solution. To verify the bilinear solution, both segments of the stiffness curve will be given the same stiffness coefficient as used for the constant stiffness of the example in subsection 5.4.2. The value of the stiffness coefficient was obtained from the experimental results of Winfield Test #10.

The purpose of this example is to show two concepts: (1) the same results are obtained when both slopes of the two slope spring model are assigned the same slope as the single slope spring model, and (2) the explicit solution of the Duhamel's integral presented in Appendix C and used in the bilinear slope force-displacement relationship is an alternate way to calculate the dynamic response of a SDOF system without using a numerical integration

procedure, as the model of one slope force-displacement relationship does (see example 5.4.2). To obtain the equivalent linear stiffness (slope of the force-displacement relationship) for the spring of the SDOF model, the maximum dynamic load recorded during Winfield Test #10 (517,400 lbs) was divided by the corresponding total beam deflection, which is the sum of the foundation displacement, support (neoprene) displacement and beam elastic curve. The total beam displacement at its midspan was 0.523 inch. This calculation provides the value of the stiffness for each segment of the force-displacement relationship of the SDOF model, which is 989,292.543 lbs/inch. This stiffness coefficient is calculated using the equivalent static force method discussed in sub-subsection 5.4.2.

In addition, the deflection limits where each segment is valid are also provided to Impact_Beam. The first segment of the stiffness curve begins with a deflection of 0.0 and proceeds to location x_1. The second segment begins immediately after deflection x_1 and proceeds along its stiffness curve to deflection x_2. For this example x_1 was selected to be 0.25 inch and x_2 was selected to be 54 inches. This provided the information necessary for Impact_Beam to cover both sections of the force-displacement relationship. In this example two damping ratios were considered, $\beta = 0.02$ and $\beta = 0.05$. The following input data was used in this example:

- Mass (M) = 1,195.985575 lbs • s^2/inch
- Stiffness coefficients ($k_1 = k_2 = k$): 517,400/0.523 = 989,292.543 lbs/inch
- Limits for displacement: x_1 = 0.25 inch; x_2 = 54 inches
- Damping ratio = 0.02, 0.05
- Time step = 0.002 sec.
- Dynamic external load as shown in Figure 5.52.

The maximum value for the time-history used in example 5.4.3 is 517.4 kips, as was obtained during Winfield Test #10. The maximum value for the dynamic response of the SDOF system with $\beta = 0.02$ was 0.56 inch and with $\beta = 0.05$ was 0.54 inch. For comparison, the maximum beam deflection from Winfield was calculated based on laser measurements and neoprene seat deformation during the experimental procedures, and had a value of 0.52 inch. The resulting deflection of the SDOF simulation is in agreement with the Winfield Test #10 recorded data. The whole deflection time-history is presented in Figure 5.53 and the similarity of both curves can be observed.

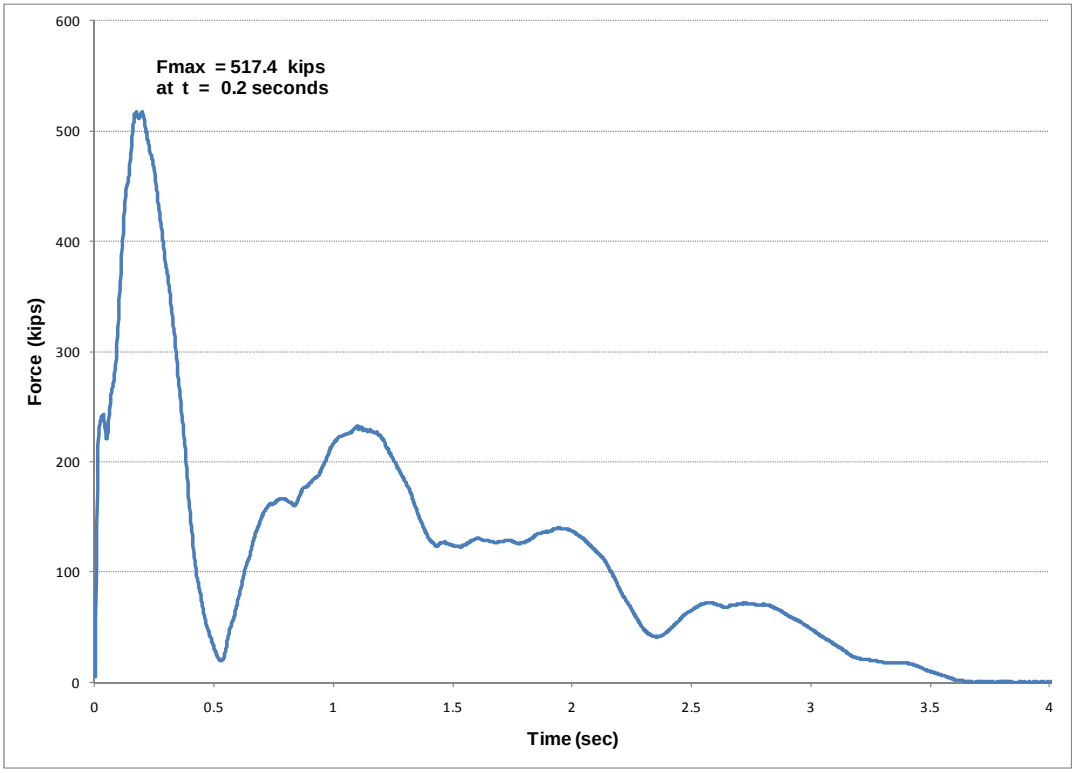

Figure 5.52. Dynamic external force time-history for numerical example 5.4.3.

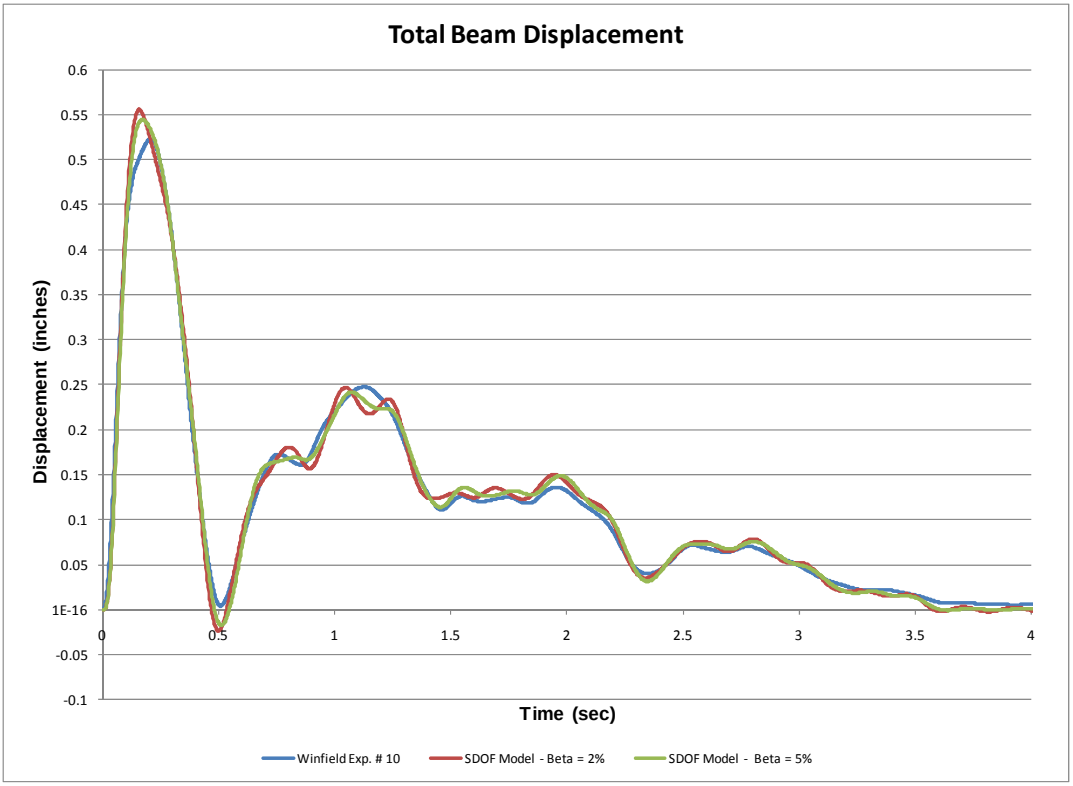

Figure 5.53. Comparison of the dynamic response of the SDOF model and the beam deflection measured during Winfield Test #10, using the bilinear force-displacement spring model.

With the results shown in example 5.4.3 the following points were demonstrated:

- The second slope of the force-displacement relationship was reached because the maximum displacement of the system was approximately 0.54 inch and the displacement where the second slope begins is 0.25 inch;
- The same results are obtained when using the explicit recursive formulas of the Duhamel's integral, as presented in Appendix C, as when using the numerical integration scheme; and
- When the two slope force-displacement relationship spring model has the same stiffness value for each slope; the procedure produces the same dynamic response as when using the single slope force-displacement relationship spring model with that same stiffness.

5.4.4 Winfield Test #10 – Linear spring stiffness – average beam deflection between LD3 and LD4 locations

This example represents a simplified model of the elastic beam used at Winfield Test #10. It considers the elastic beam of the field experiment as a SDOF system. Instead of moving an external dynamic load along the beam at a specified velocity, as was the case of the experiment, the external dynamic load has a fixed location for the SDOF model. This numerical example is based on a linear stiffness coefficient obtained from the experimental results of Winfield Test #10, as idealized in Figure 5.54.

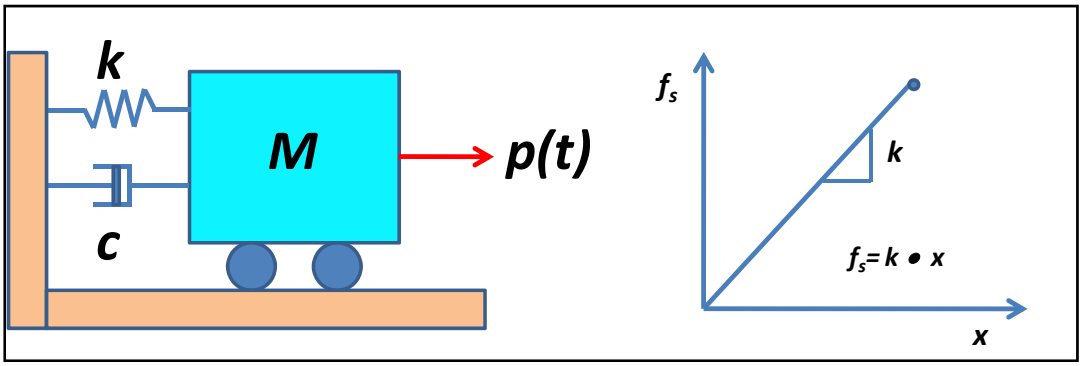

Figure 5.54. SDOF model used for numerical example 5.4.2.

To obtain the equivalent linear stiffness (slope of the force-displacement relationship) for the spring of the SDOF model, the maximum dynamic load recorded during Winfield Test #10 (517.4 kips) was divided by the average of the maximum experimental laser deflection calculated at LD3

and LD4 sensor locations, which produces a value of 0.514295 inch. Using this average deflection and the maximum dynamic load, the value of the stiffness of the SDOF model can be calculated, which results in 1,006,037.4 kips/inch. This concept can be observed in Figure 5.55. This stiffness coefficient is calculated using the equivalent static force method discussed in sub-subsection 5.4.2.

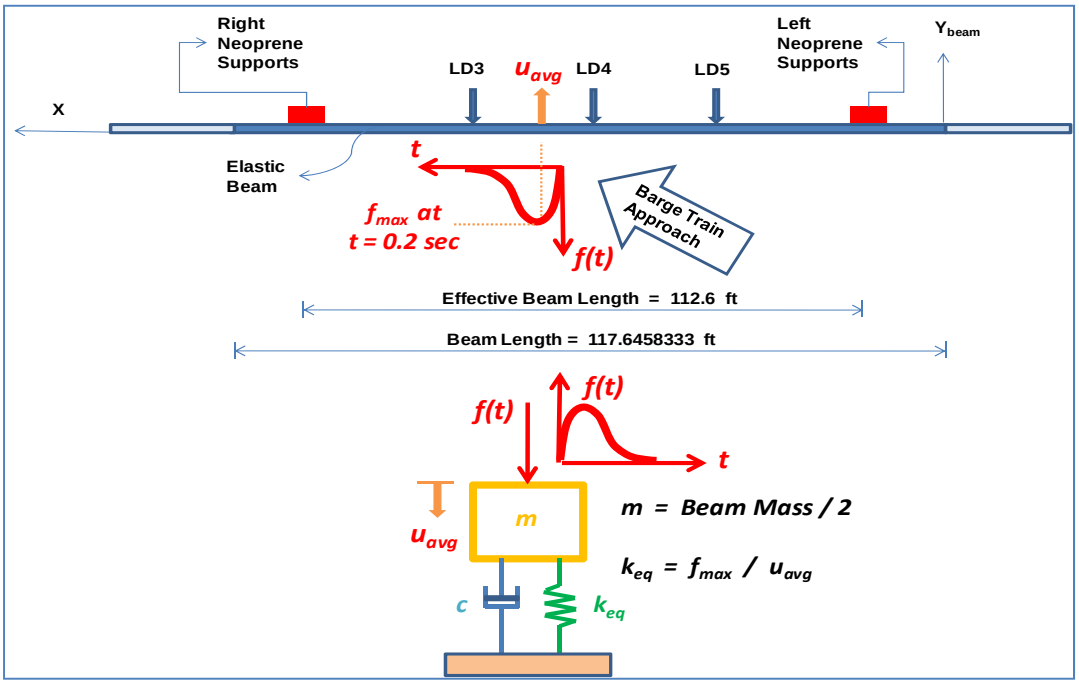

Figure 5.55. Equivalent SDOF system for the Winfield Test #10, using the average of the maximum LD3 and LD4 displacements.

The damping ratio was assumed to be $\beta = 0.02$. The following input data was used in this example:

- Mass (M) = 1,195.985575 lbs • s²/inch
- Stiffness coefficient (k) = 517,400 / 0.514295 = 1,006,037.4 lbs/inch
- Damping ratio (c) = 0.02
- Time step = 0.002 sec.
- Dynamic external load as shown in Figure 5.56.

It can be observed that the value of the equivalent spring stiffness will change if the calculation of k is done in other positions along the beam. If the dynamic load is applied at other locations, the deflection value will be different from 0.514295 inch and therefore the calculated k will be different.

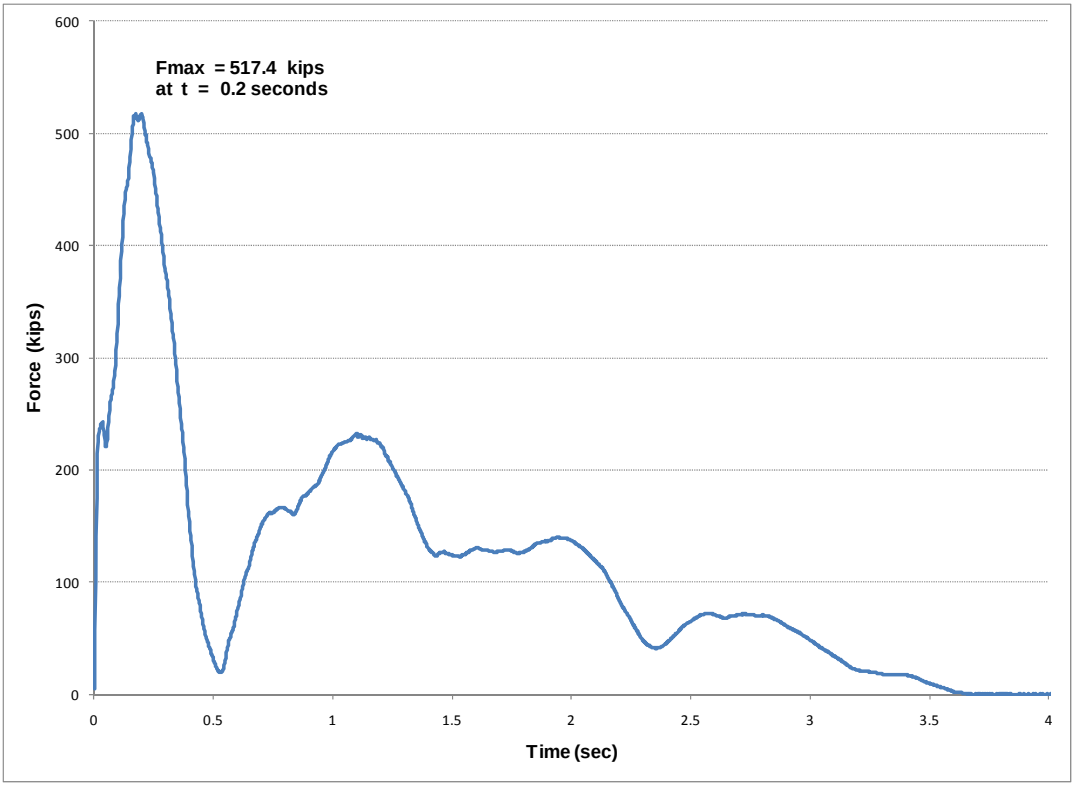

Figure 5.56. Dynamic external force time-history for numerical example 5.4.4.

The maximum value of the force time-history obtained from Winfield Test #10 and used in this example is 517.4 kips. The maximum value for the dynamic response of the SDOF system with $\beta = 0.02$ was 0.54 inch. As a matter of comparison, the maximum average laser deflection recorded during the experiment was 0.51428 inch. The resulting deflection of the SDOF simulation is in agreement with the Winfield Test #10 recorded data. The whole deflection time-history is presented in Figure 5.57 and the similarity in shape and magnitude of both curves can be observed.

Using the equivalent spring stiffness of 1,006,037.4 lbs/inch (12,072.45 kips/ft), the equivalent modulus of elasticity for the system can be calculated. It is well-known that the equivalent spring stiffness for a simply supported beam subjected to a static concentrated force is

$$k = \frac{3\left(E_{system}\right) I \cdot L}{a^2 b^2} \tag{5.9}$$

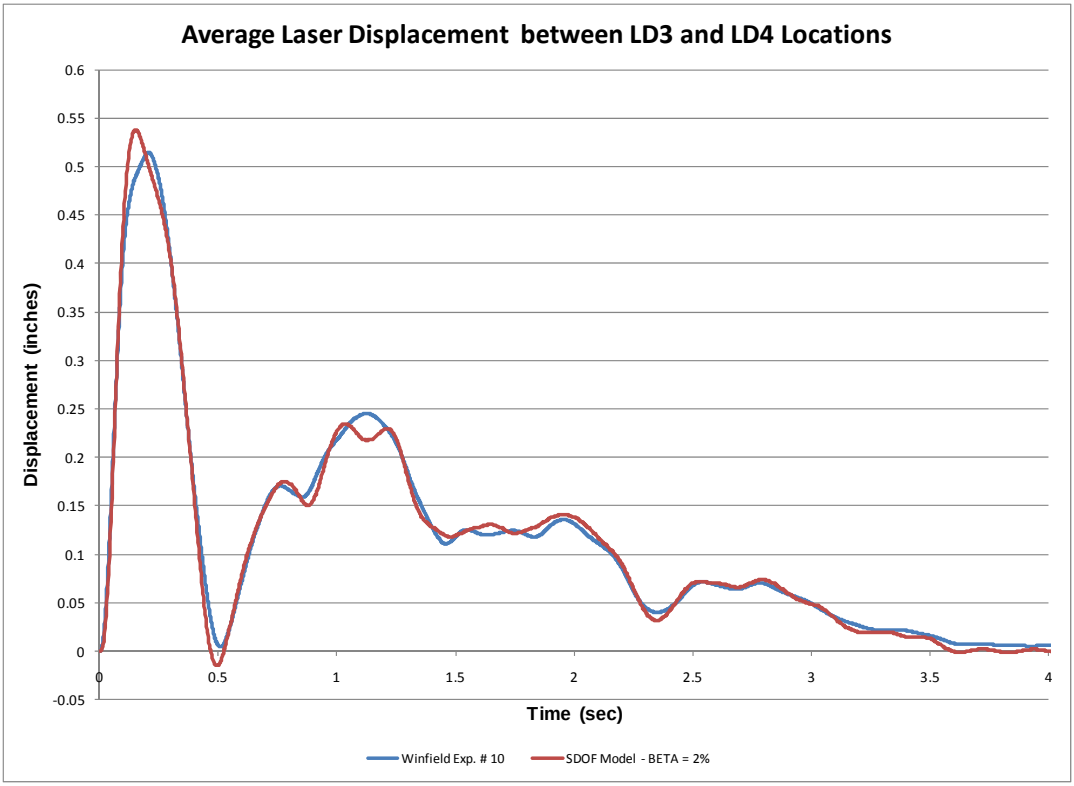

Figure 5.57. Comparison of the dynamic response of the SDOF model and the average laser displacements LD3 and LD4 measured during Winfield Test #10.

where;

E_{system} = modulus of elasticity of the system,
I = moment of inertia about the neutral axis,
L = total span length,
a = distance to the left support from the point of load application, and
b = distance to the right support from the point of load application ($b = L - a$).

The modulus of elasticity calculated from Equation (5.9) is called equivalent modulus of elasticity for the system because the stiffness coefficient used to calculate the E_{system} is based on the average of the maximum displacement of the two adjacent laser deflection sensors to the point of load application. This deflection reflects the displacement of the system (adjacent beams), neoprene pad deformation and elastic curve of the beam. For Winfield Test #10 the approach velocity along the beam was $v = 2.99\ ft/sec$, the point of initial contact was at $7.8\ ft$ to the left of the midspan and the time of maximum force was $t = 0.2\ sec$. The following values can be derived from

this information using Equation (5.1); $I = 517.2\ ft^4$, $L = 112.6\ ft$, $a = L/2 – 7.8 – v \bullet t = 112.6/2 - 7.8 - 2.99 \bullet 0.2 = 47.902\ ft$ from left support, and $b = L – a = 112.6 – 47.902 = 64.698\ ft$. Finally, substituting these values into Equation (5.1) leads to the solution of an equivalent modulus of elasticity for the system, which is $E_{system} = 663{,}434.9\ kips/ft^2 = 4{,}607.2\ kips/in^2$.

The resulting values of $E_{dynamic}$ obtained in sub-section 5.3.2 are greater than the value of E obtained in this sub-section. The value presented in this sub-section ($E_{system} = 663{,}434.9\ kips / ft^2 = 4{,}607.2\ kips / in^2$) was obtained using the average of the total deflection between sensor locations LD3 and LD4 of 0.51428 inch, which includes the system (adjacent beams) deflection, neoprene pad (support) deflection and beam deflection. However, the $E_{dynamic}$ in sub-section 5.3.2 (Average $E_{dynamic} = 802{,}733\ ksf = 5{,}574.54\ ksi$) was calculated with the beam deflection (beam deflection is lower than total deflection) at each sensor location LD3, LD4 and LD5. As the displacement increases, the system becomes more flexible resulting in a lower modulus of elasticity.

5.4.5 Comparison of the response of dBEAS 2-DOF System and a SDOF system of Impact_Beam

This subsection presents a comparison of the response of a Deformable Bullnose Energy Absorbing System (BEAS) using the computer program Impact-Beam and dBEAS (Ebeling et al. 2011). The computer program dBEAS considers a barge train as a multi-degree-of-freedom system which is impacting a deformable bullnose. dBEAS calculates the force time-history a specified barge train generates at the deformable bullnose during impact and the effects (force, displacement, velocity and acceleration) on the barge train and the deformable bullnose. The dBEAS computer program was used to model the impact of a single barge on a deformable bullnose. The weight of the single barge is equivalent to the weight of a barge train consisting of 15 barges plus the tow boat of 52,100 kips. The single super-barge (15-weights+tow) was traveling at 2 ft/sec. The impact force between the super-barge and the deformable bullnose was generated with dBEAS computer program. Then, this force was used as part of the input data for the SDOF model in Impact_Beam to calculate the response of the deformable bullnose and compare the results against the dBEAS computer program results. Next, five examples will be presented where the response of the deformable bullnose was calculated using dBEAS and Impact_Beam computer programs to verify the solution method and accuracy of both mathematical models.

5.4.5.1 *Bilinear force-displacement base isolators stiffness with β = 0, 15 and 30%*

The computer program dBEAS was used to estimate the impact force time-history for the super-barge model (single barge with the weight of 15 barges+tow) and this force was used as input force in the Impact_Beam SDOF model. The responses of both models were compared to observe the behavior of a 2-DOF system and a SDOF system. The dBEAS model is idealized in Figure 5.58. Note as shown in Figure 5.58, that the center of gravity of both systems is coincident with the center of rigidity of the dBEAS and the line of action of the impact force, so all motions will be translational along the line of action (i.e., no rotations). This condition (head-on impact event) can be modeled by a 2-DOF system as shown in Figure 5.59. That is, the 2-DOF system is equivalent to a "super-barge" model impacting the deformable BEAS. The barge train longitudinal stiffness was estimated at 1,200 kips/inch and the deformable bullnose properties are the following; weight of 3,978.255 lbs • s^2/inch, 8 base isolators with bilinear stiffness defined as idealized in Figure 5.60. In this case, the force-displacement relationship is defined by $k_1 = 11{,}170.21$ *lbs/in*, $k_2 = 57{,}558.14$ *lbs/in*, $x_1 = 28.2$ *inches*, and $x_2 = 54$ *inches*. The damping ratio for this example was 0% for each base isolator. Because the group of base isolators are acting in parallel for the impact nosing of the Deformable BEAS, the total stiffness and total damping for the SDOF model of Impact_Beam is calculated by adding the contribution of each single base isolator to obtain an equivalent single stiffness and damping ratio.

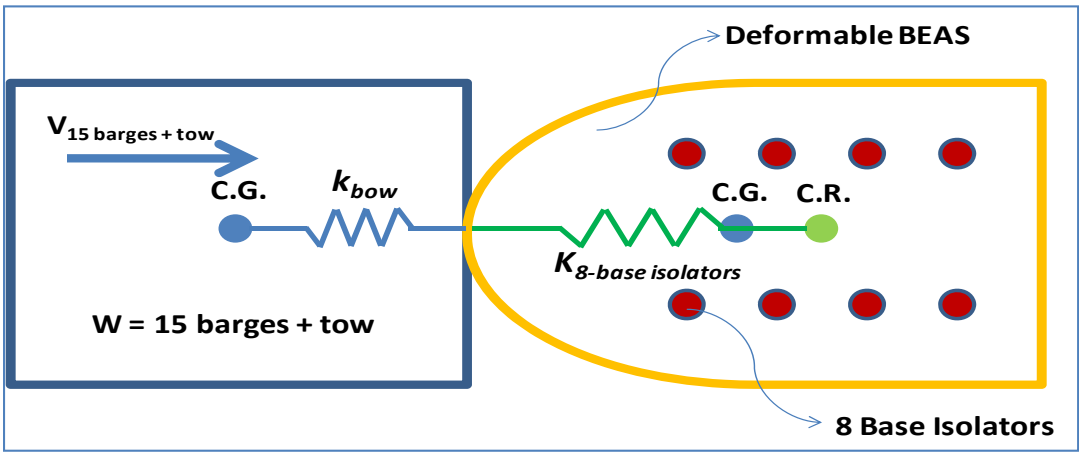

Figure 5.58. Plan View of the 2-DOF system of the super-barge dBEAS model.

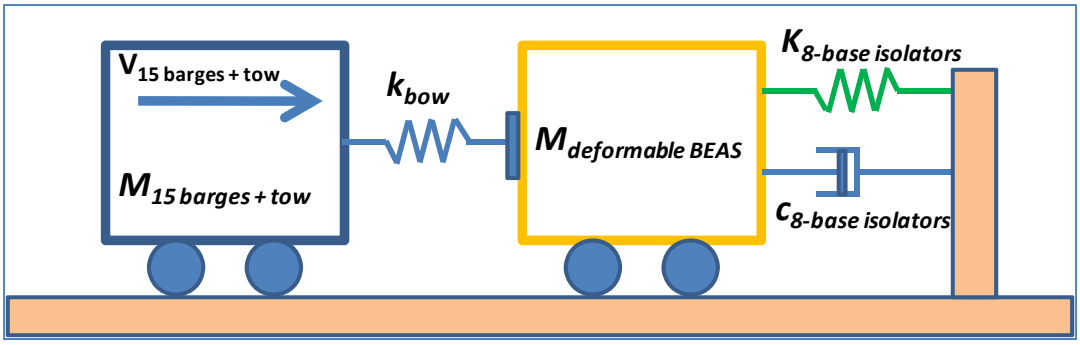

Figure 5.59. 2-DOF system of the super-barge dBEAS model.

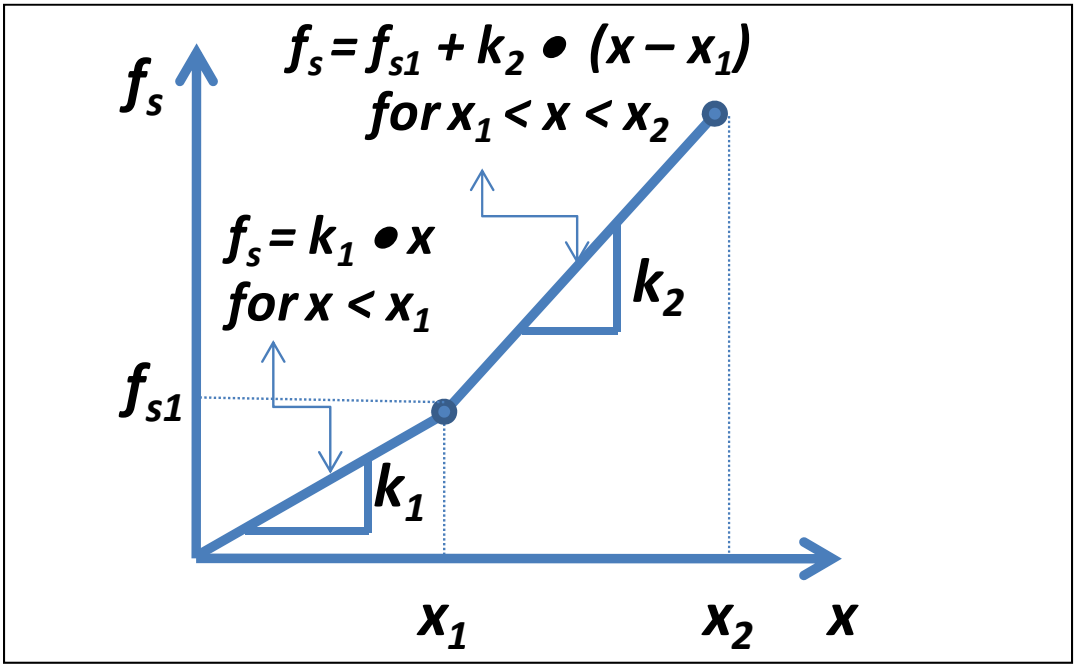

Figure 5.60. Deformable BEAS spring ($k_{8\text{-base isolators}}$) bilinear force-displacement relationship.

The impact force time-history produced by dBEAS is presented in Figure 5.61. This force time-history is used as input force time-history for the SDOF system of Impact_Beam, as shown in Figure 5.62.

The response of the SDOF system of Impact_Beam and the response of the 2-DOF system of dBEAS computer programs are presented in Figure 5.63. The maximum displacement for the SDOF system and the 2-DOF system was 29.8835 inches and 29.8824 inches, respectively. In both cases, the second slope of the force-displacement relationship of the spring was reached ($x_1 = 28.2$ *inches*). It can be observed that the same response was obtained from two independent mathematical tools, Impact_Beam and dBEAS.

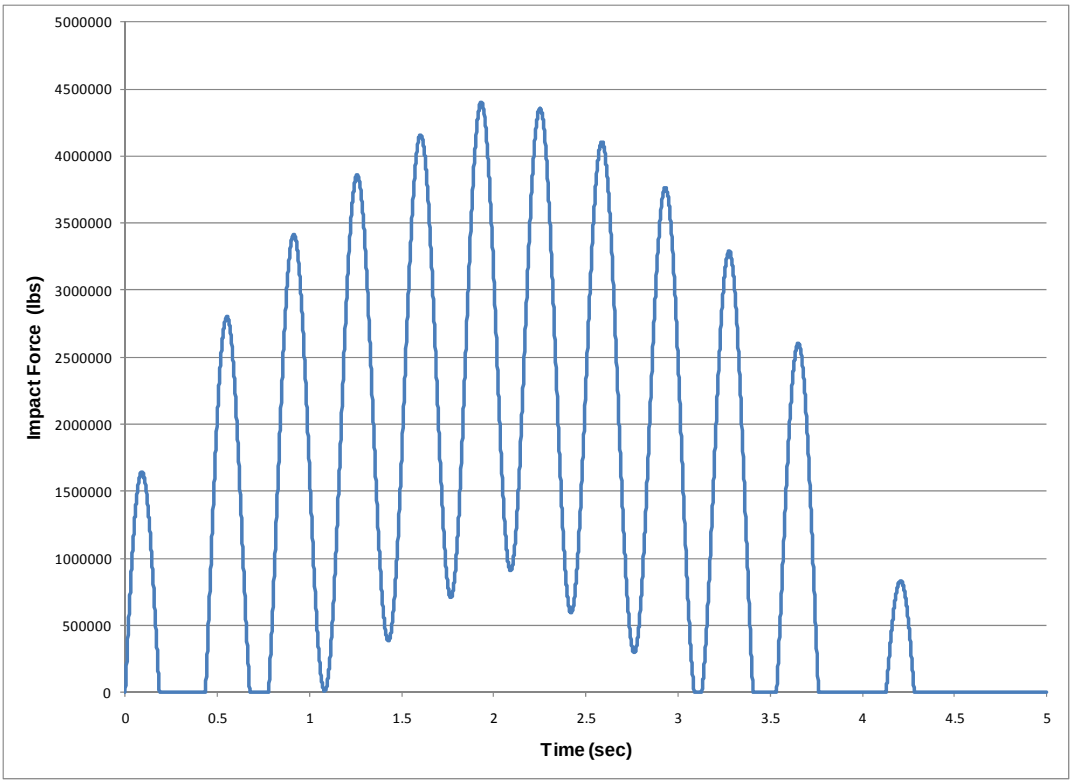

Figure 5.61. Dynamic external force time-history for numerical example in subsection 5.4.5.1 – β = 0%.

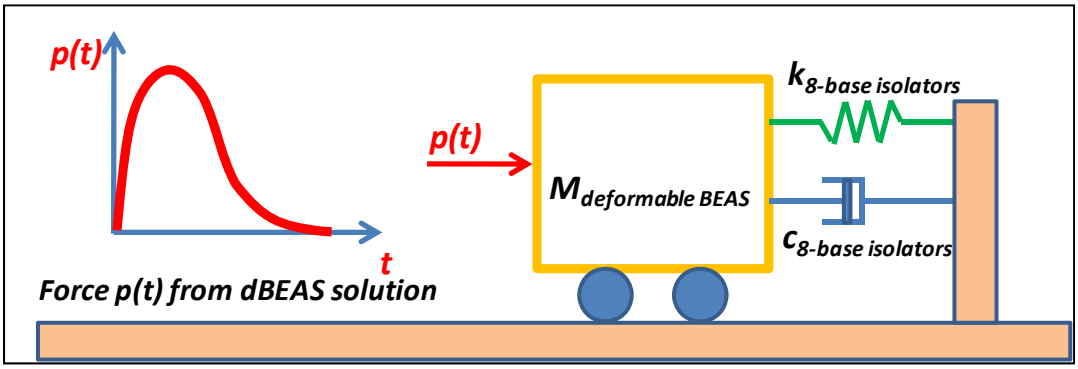

Figure 5.62. SDOF system of Impact_Beam used to calculate the response of a deformable BEAS.

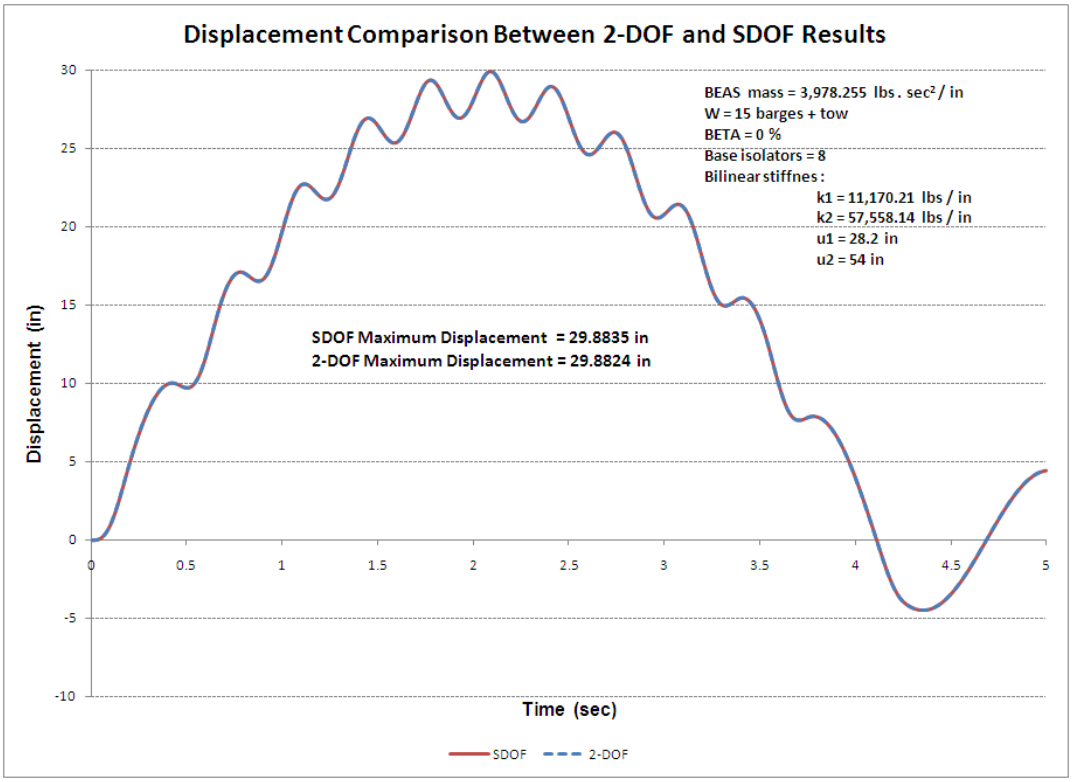

Figure 5.63. Response time-history; dBEAS 2-DOF and Impact_Beam SDOF models, $\beta = 0\%$.

A second case was evaluated using dBEAS with $\beta = 15\%$, and the impact force from dBEAS as shown in Figure 5.64 with all other parameters of the dBEAS remaining the same. The response of the SDOF system of Impact_Beam and the response of the 2-DOF system of dBEAS computer programs are presented in Figure 5.65. The maximum displacement for the SDOF system and the 2-DOF system was 28.1467 inches and 28.1472 inches, respectively. In both cases, the second slope of the force-displacement relationship of the spring was not reached ($x_1 = 28.2$ *inches*). It can be observed that the same response was obtained from two independent mathematical tools, Impact_Beam and dBEAS.

A third case was evaluated with $\beta = 30\%$, impact force from dBEAS, as shown in Figure 5.66, with all other parameters for the dBEAS remaining the same. The response of the SDOF system of Impact_Beam and the response of the 2-DOF system of dBEAS computer programs are presented in Figure 5.67. The maximum displacement for the SDOF system and the 2-DOF system was 27.0217 inches and 27.0192 inches, respectively. In both cases, the second slope of the force-displacement relationship of the spring was not reached ($x_1 = 28.2$ *inches*). It can be observed that the same response was obtained for Impact_Beam and dBEAS.

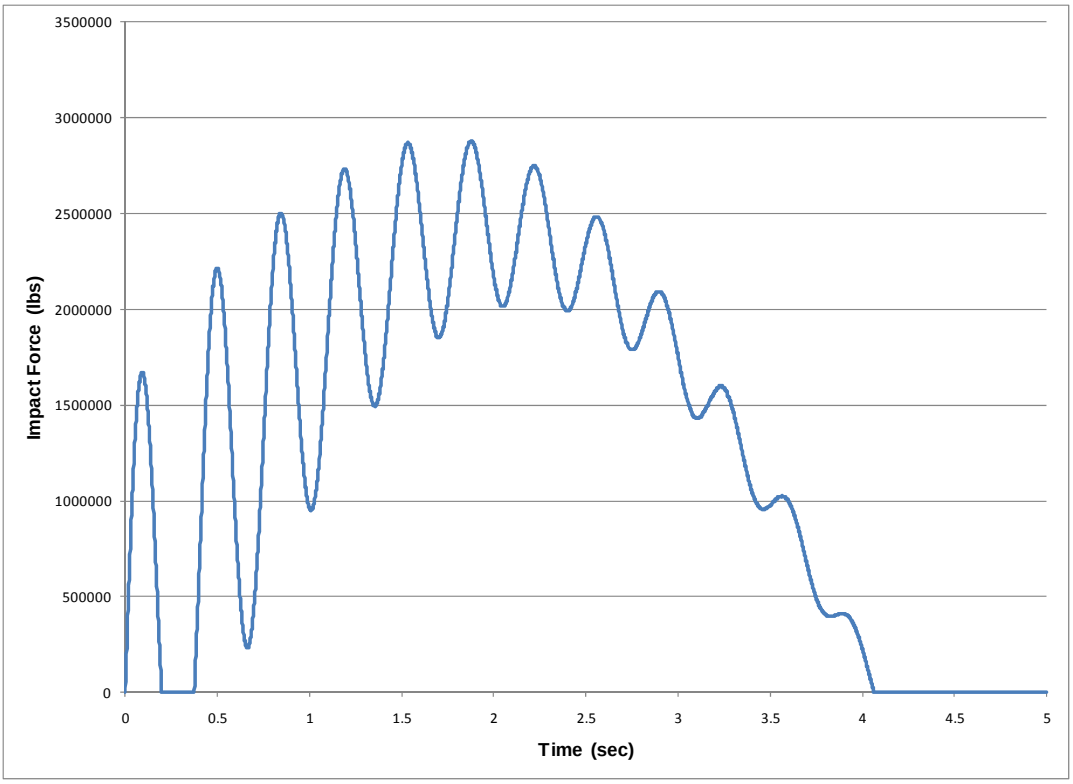

Figure 5.640. Dynamic external force time-history for numerical example in subsection 5.4.5.1 – β = 15%.

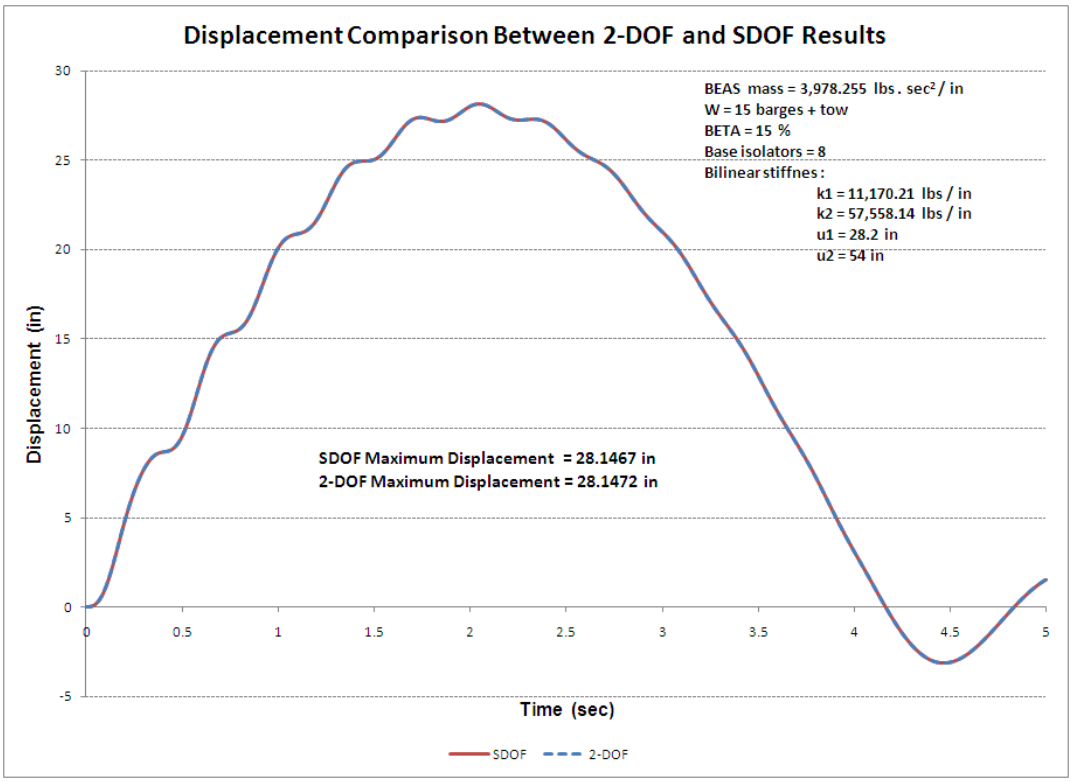

Figure 5.65. Response time-history; dBEAS 2-DOF and Impact_Beam SDOF models, β = 15%.

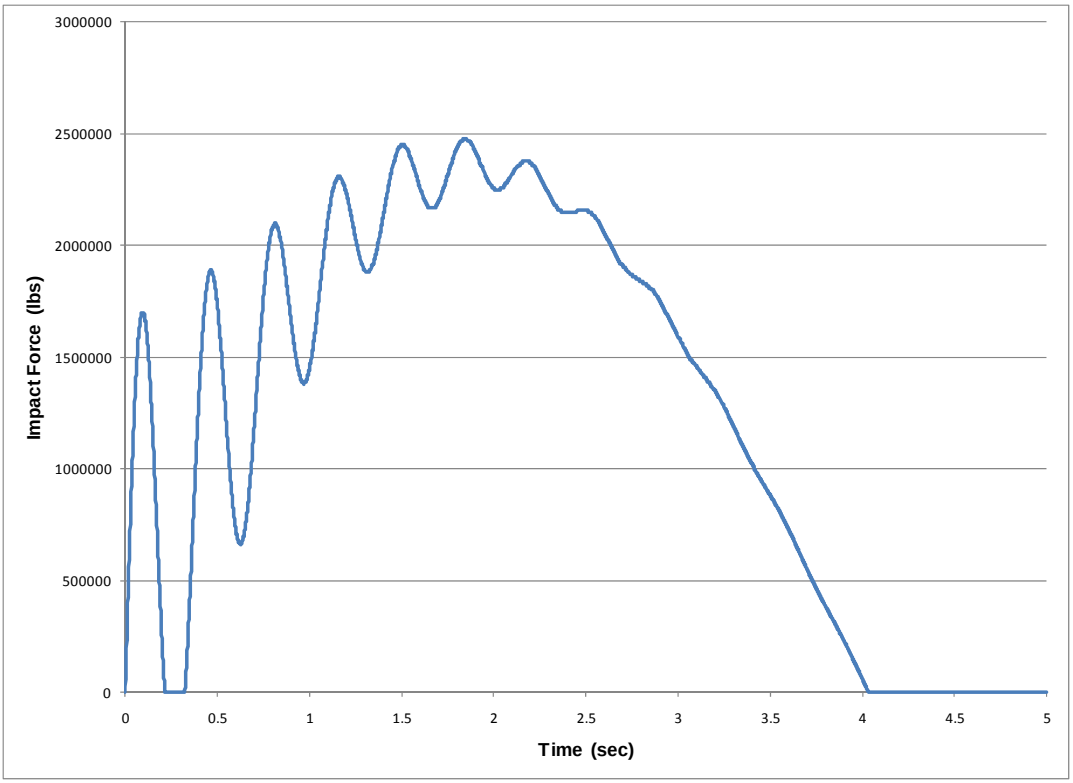

Figure 5.66. Dynamic external force time-history for numerical example in subsection 5.4.5.1 – β = 30%.

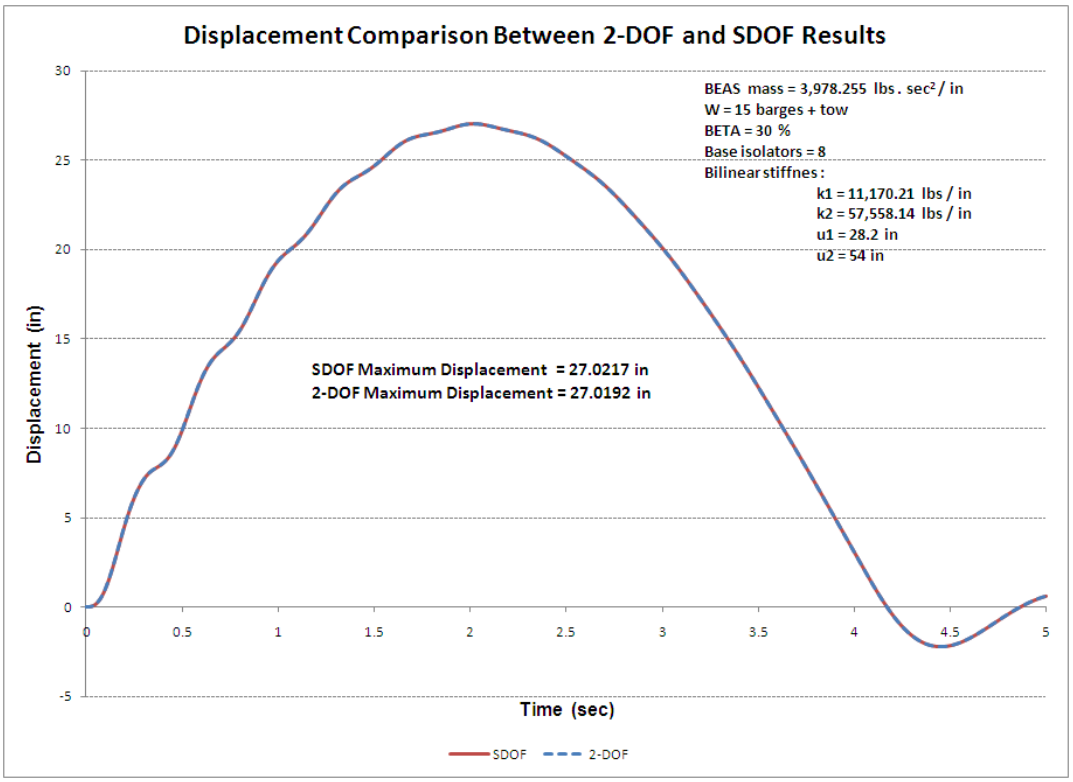

Figure 5.67. Response time-history; dBEAS 2-DOF and Impact_Beam SDOF models, β = 30%.

5.4.5.2 SDOF comparison with low stiffness BEAS

The computer program dBEAS was used to estimate the impact force time-history for the super-barge model (single barge with the weight of 15 barges + tow) and this force was used as input force for the SDOF model in Impact_Beam. The responses of both models are compared by observing the behavior of a 2-DOF system and a SDOF system. The dBEAS model is presented in Figure 5.68. Note, as shown in Figure 5.68, that the center of gravity of both systems is coincident with the center of rigidity of the dBEAS and the line of action of the impact force, so all motions will be translational along the line of action (i.e., no rotations). This condition (head-on impact event) can be modeled by a 2-DOF system as idealized in Figure 5.69. That is, the 2-DOF system is equivalent to a "super-barge" model impacting the deformable BEAS. The barge train longitudinal stiffness was estimated at 1,200 kips/inch and the deformable bullnose properties are the following; weight of 3,978.255 lbs • s^2 / inch, 8 base isolators with linear secant stiffness defined as shown in Figure 5.70. In this case the force-displacement relationship is defined by $k = 129{,}350.0$ *lbs/in* and $x_{ult} = 60$ *inches*. The damping ratio for this example was 0% for each base isolator. Because the group of base isolators are acting in parallel on the impact nosing of the Deformable BEAS, the total stiffness and total damping for the SDOF model of Impact_Beam is calculated by adding the contribution of each single base isolator to obtain an equivalent single stiffness and damping ratio.

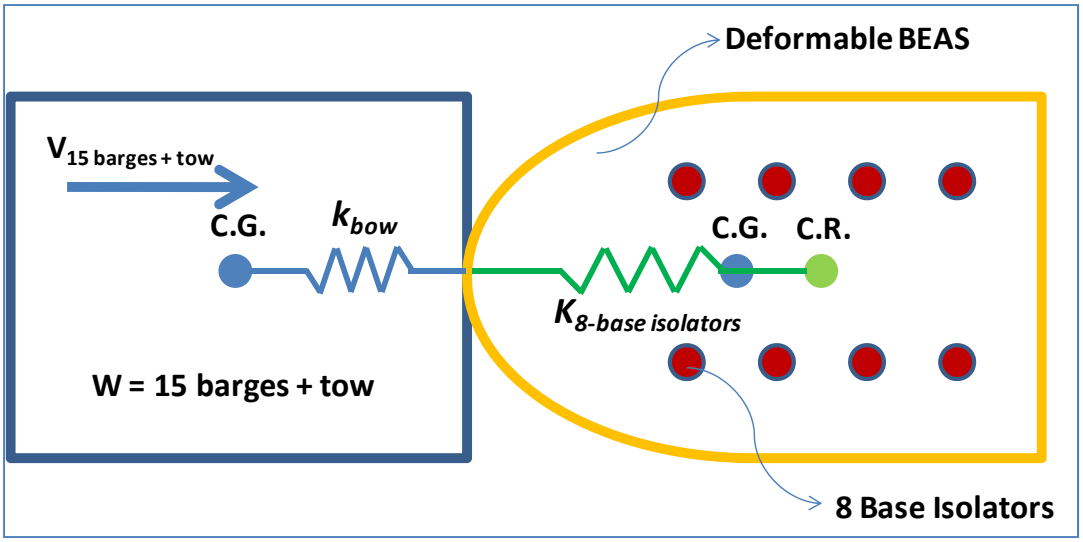

Figure 5.68. Plan View of the 2-DOF system of the super-barge dBEAS model.

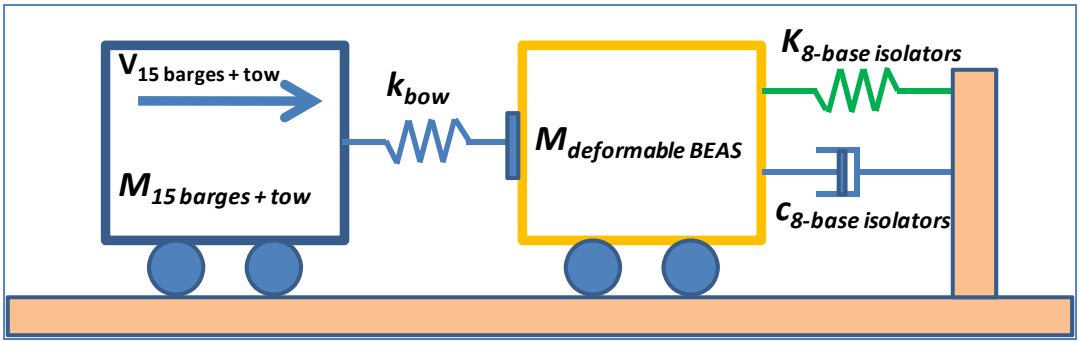

Figure 5.69. 2-DOF system of the super-barge dBEAS model.

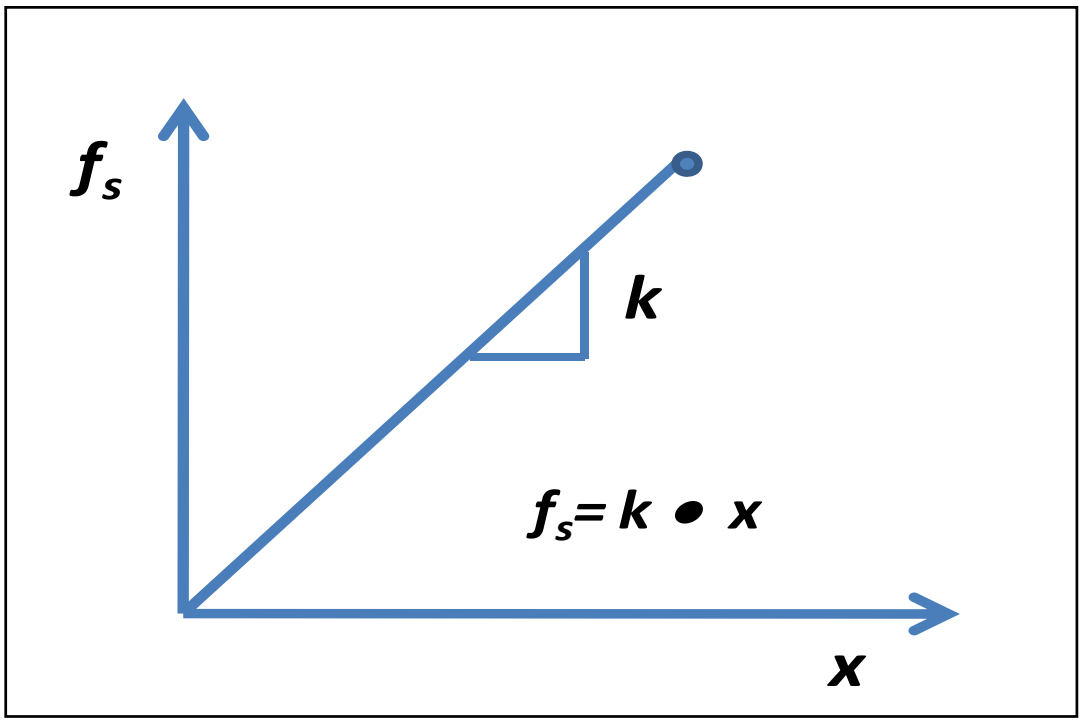

Figure 5.70. Deformable BEAS spring ($k_{8\text{-base isolators}}$) linear secant force-displacement idealized relationship.

The impact force time-history produce by dBEAS is presented in Figure 5.71. This force time-history is used as input force time-history for the SDOF system of Impact_Beam, as shown in Figure 5.72.

The response of the SDOF system of Impact_Beam and the response of the 2-DOF system of dBEAS computer programs are presented in Figure 5.73. The maximum displacement for the SDOF system and the 2-DOF system was 7.0107 inches and 7.0092 inches, respectively. In both cases, the ultimate displacement of the force-displacement relationship of the spring was not reached (x_{ult} = *60 inches*). It can be observed that the same response was obtained for Impact_Beam and dBEAS.

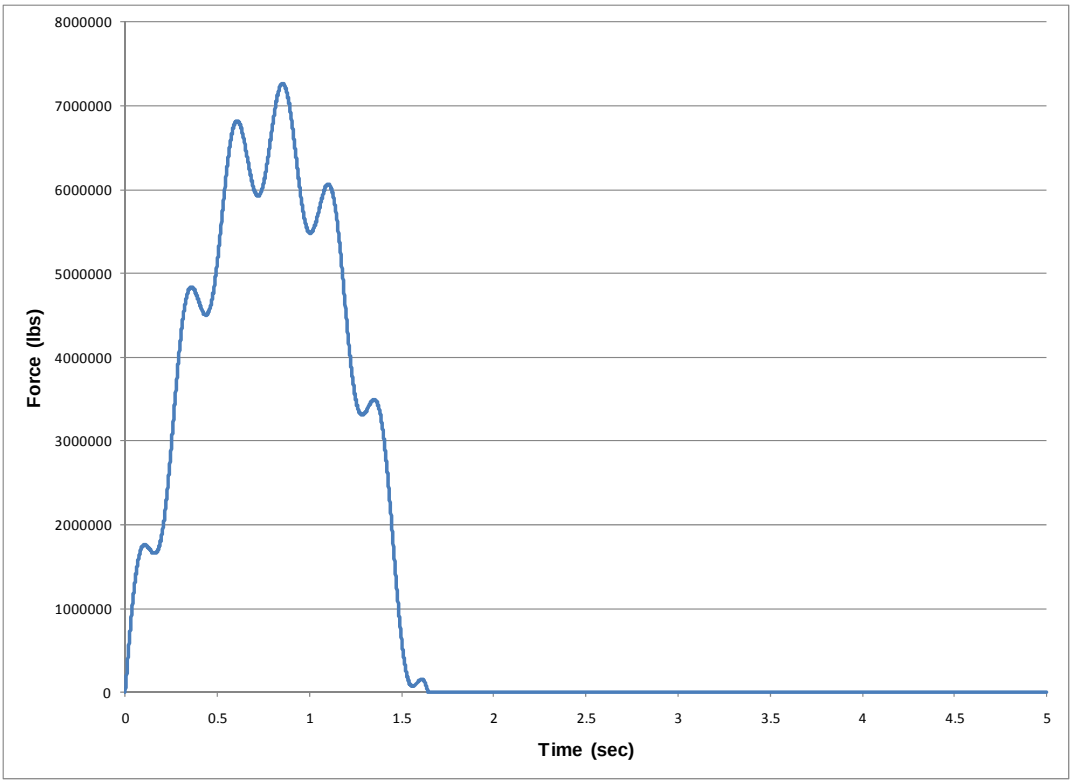

Figure 5.71. Dynamic external force time-history for numerical example in subsection 5.4.5.2 – β = 0%.

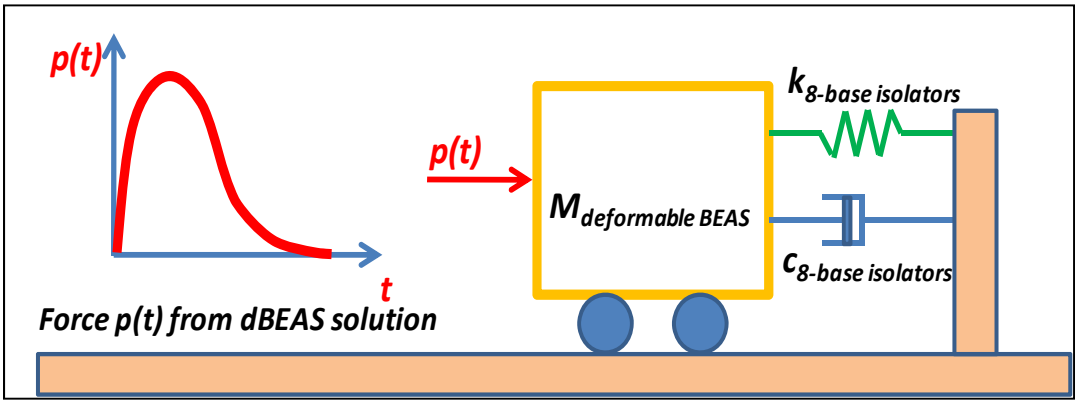

Figure 5.72. SDOF system of Impact_Beam used to calculate the response of a deformable BEAS.

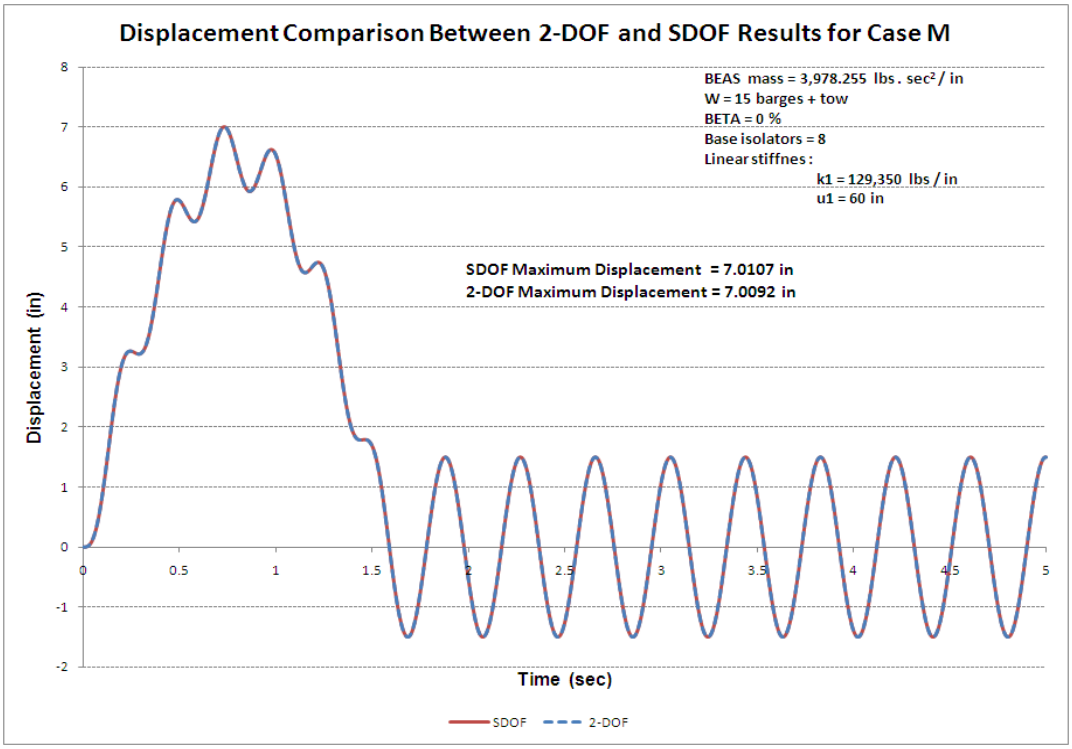

Figure 5.73. Response time-history; dBEAS 2-DOF and Impact_Beam SDOF models, $\beta = 0\%$.

A second case was evaluated using dBEAS with $\beta = 15\%$, the impact force from dBEAS as shown in Figure 5.74, with all other parameters of the dBEAS remaining the same. The response of the SDOF system of Impact_Beam and the response of the 2-DOF system of dBEAS computer programs are presented in Figure 5.75. The maximum displacement for the SDOF system and the 2-DOF system was 6.4840 inches and 6.4824 inches, respectively. In both cases, the ultimate displacement of the force-displacement relationship of the spring was not reached (x_{ult} = *60 inches*). It can be observed that the same response was obtained for Impact_Beam and dBEAS.

A third case was evaluated using dBEAS with $\beta = 30\%$, the impact force from dBEAS, as shown in Figure 5.76, with all others parameters of the dBEAS remaining the same. The response of the SDOF system of Impact_Beam and the response of the 2-DOF system of dBEAS computer programs are presented in Figure 5.77. The maximum displacement for the SDOF system and the 2-DOF system was 6.3356 inches and 6.3360 inches, respectively. In both cases, the ultimate displacement of the force-displacement relationship of the spring was not reached (x_{ult} = *60 inches*). It can be observed that the same response was obtained from Impact_Beam and dBEAS.

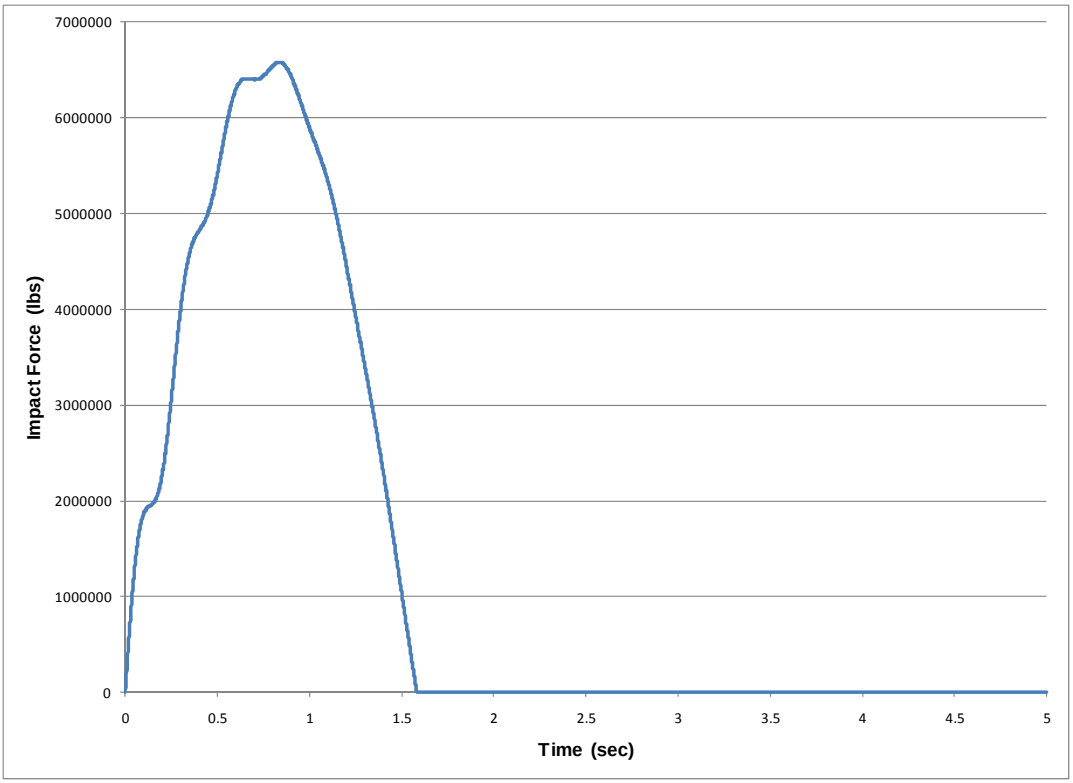

Figure 5.74. Dynamic external force time-history for numerical example in subsection 5.4.5.2 – β = 15%.

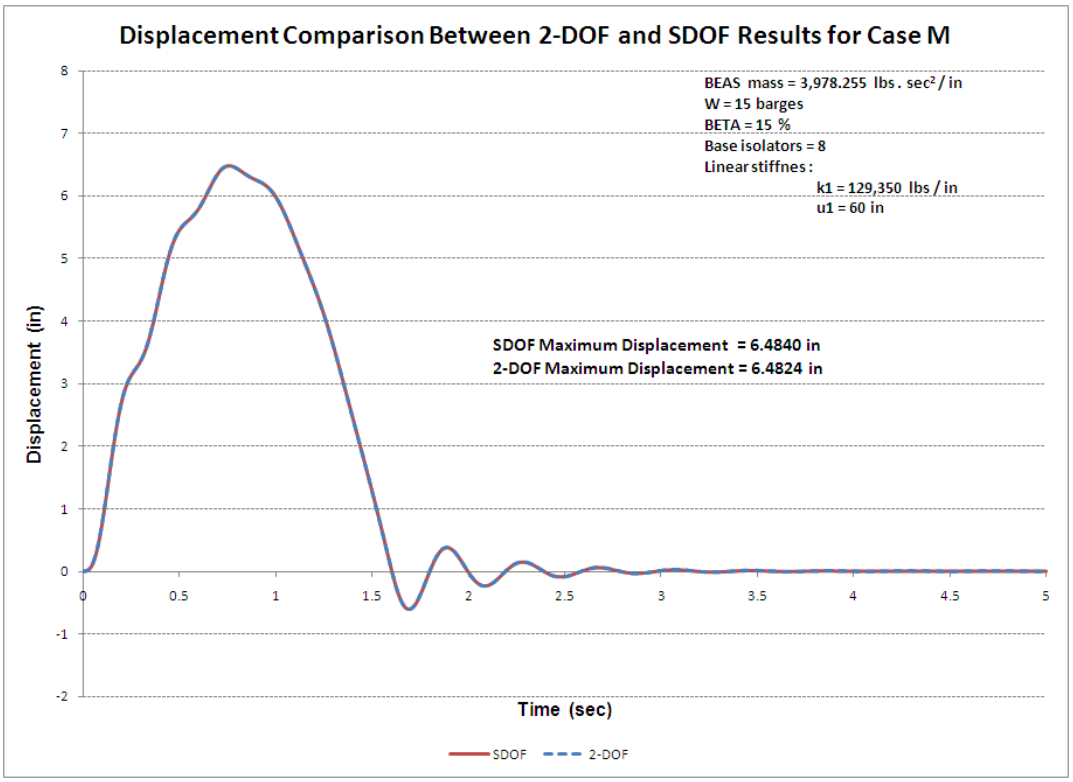

Figure 5.75. Response time-history; dBEAS 2-DOF and Impact_Beam SDOF models, β = 15%.

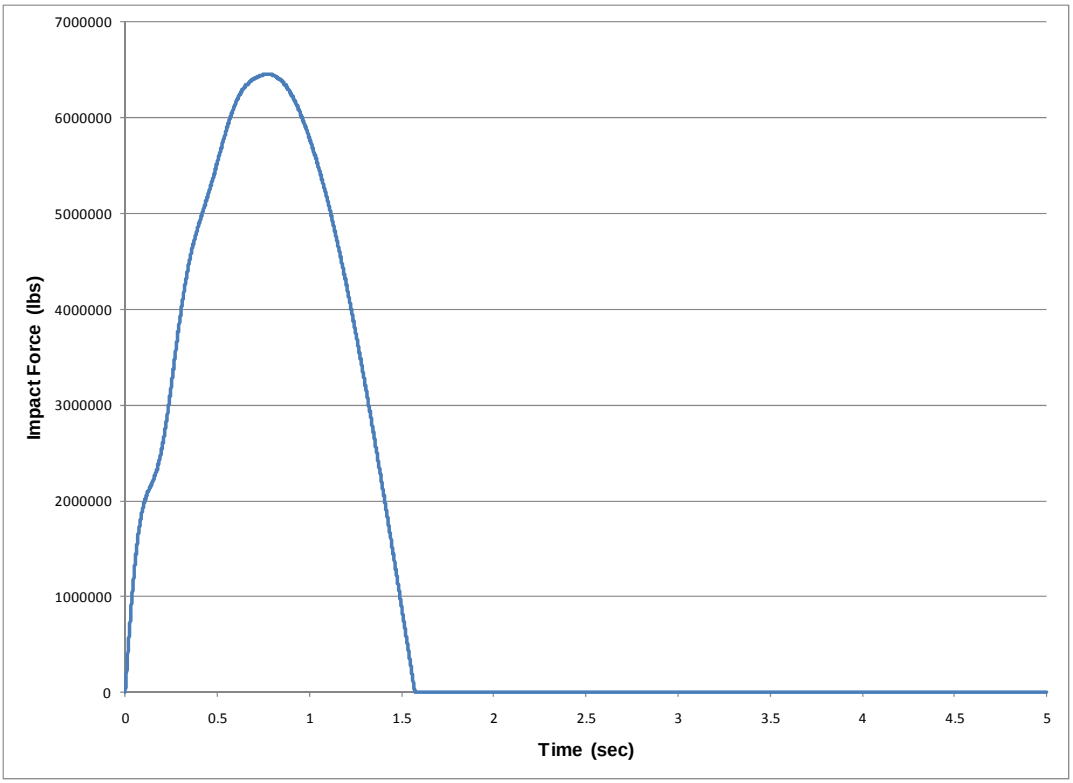

Figure 5.76. Dynamic external force time-history for numerical example in subsection 5.4.5.2 – β = 30%.

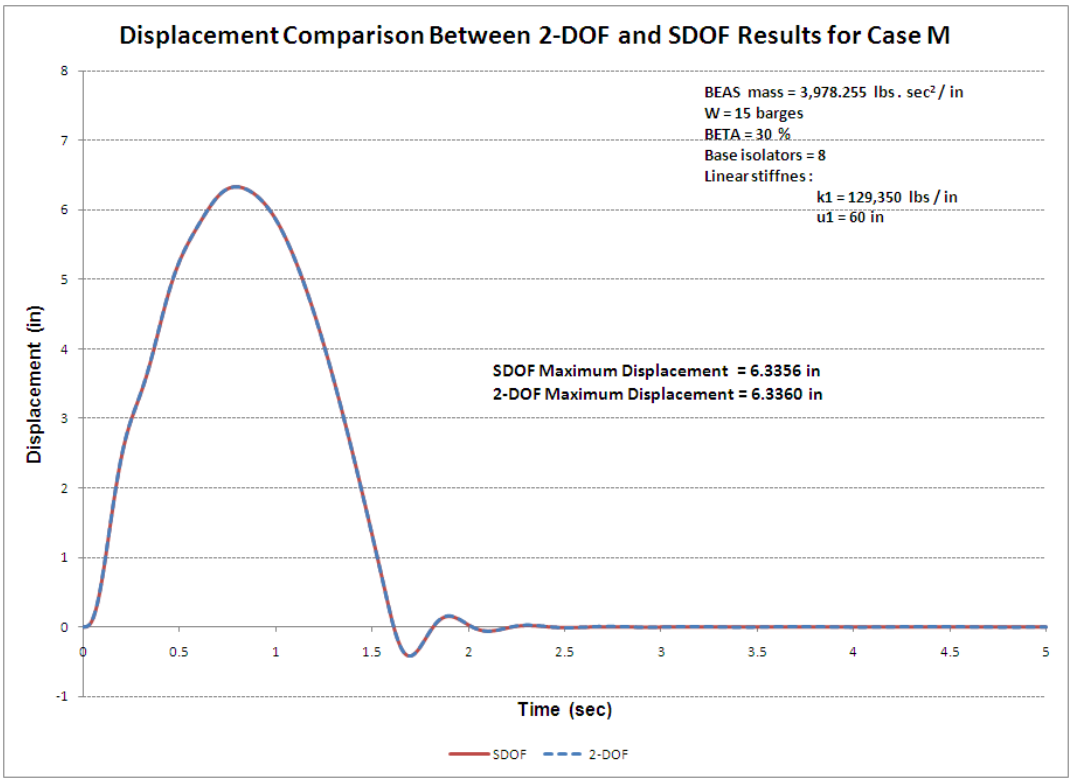

Figure 5.77. Response time-history; dBEAS 2-DOF and Impact_Beam SDOF models, β = 30%.

5.4.5.3 SDOF comparison with high stiffness BEAS

The computer program dBEAS was used to estimate the impact force time-history for the "super-barge" model (single barge with the weight of 15 barges + tow) and this force was used as input force for the SDOF model in Impact_Beam. The responses of both models were observed to compare the behavior of a 2-DOF system and a SDOF system. The dBEAS model is idealized in Figure 5.78. Note as shown in Figure 5.78, that the center of gravity of both systems is coincident with the center of rigidity of the dBEAS and the line of action of the impact force, so all motions will be translational along the line of action (i.e., no rotations). This condition (head-on impact event) can be modeled by a 2-DOF system as idealized in Figure 5.79. That is, the 2-DOF system is equivalent to a super-barge model impacting the deformable BEAS. The barge train longitudinal stiffness was estimated at 1,200 kips/inch and the deformable bullnose properties are the following; weight of 3,978.255 lbs • s^2/inch, 8 base isolators with linear secant stiffness defined as shown in Figure 5.80. In this case the force-displacement relationship is defined by $k = 12{,}935{,}000.0$ *lbs/in* and $x_{ult} = 60$ *inches*. The damping ratio for this example was 0% for each base isolator. Because the group of base isolators are acting in parallel on the impact nosing of the Deformable BEAS, the total stiffness and total damping for the SDOF model of Impact_Beam is calculated by adding the contribution of each single base isolator to obtain an equivalent single stiffness and damping ratio.

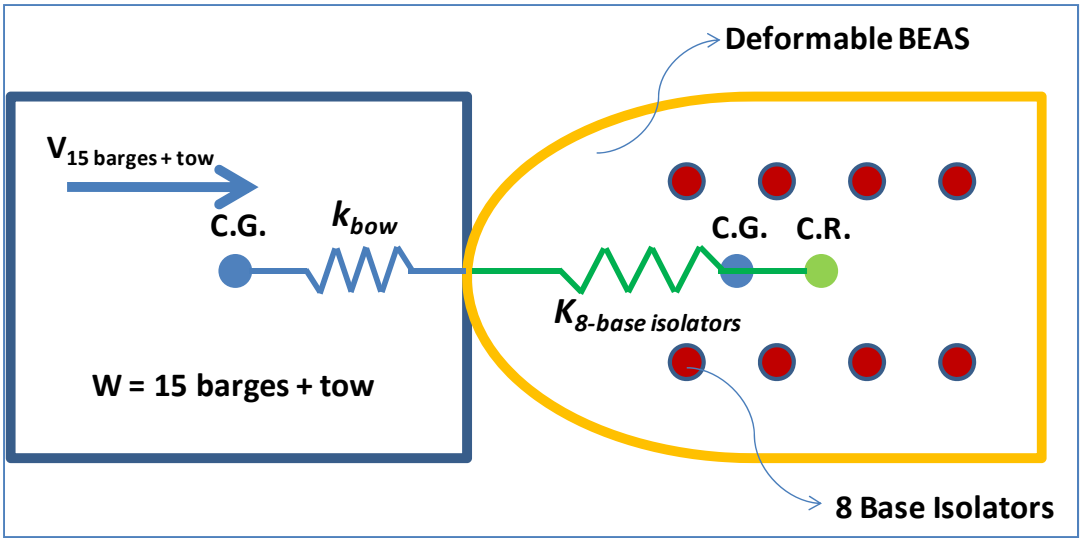

Figure 5.78. Plan View of the 2-DOF system of the super-barge dBEAS model.

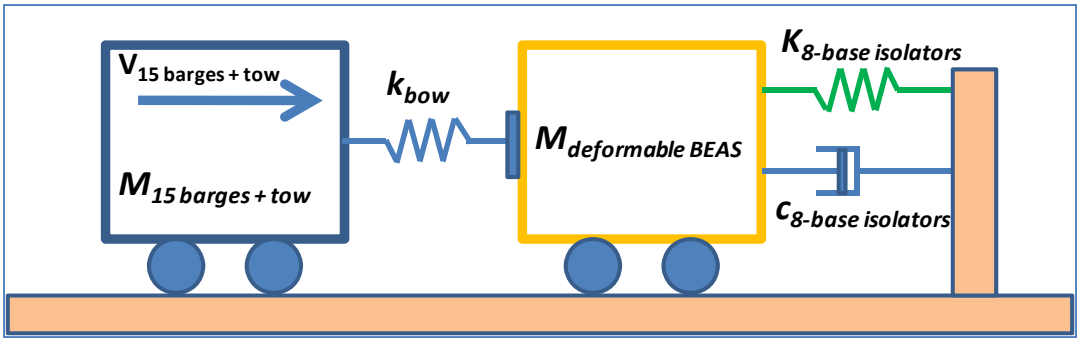

Figure 5.79. 2-DOF system of the super-barge dBEAS model.

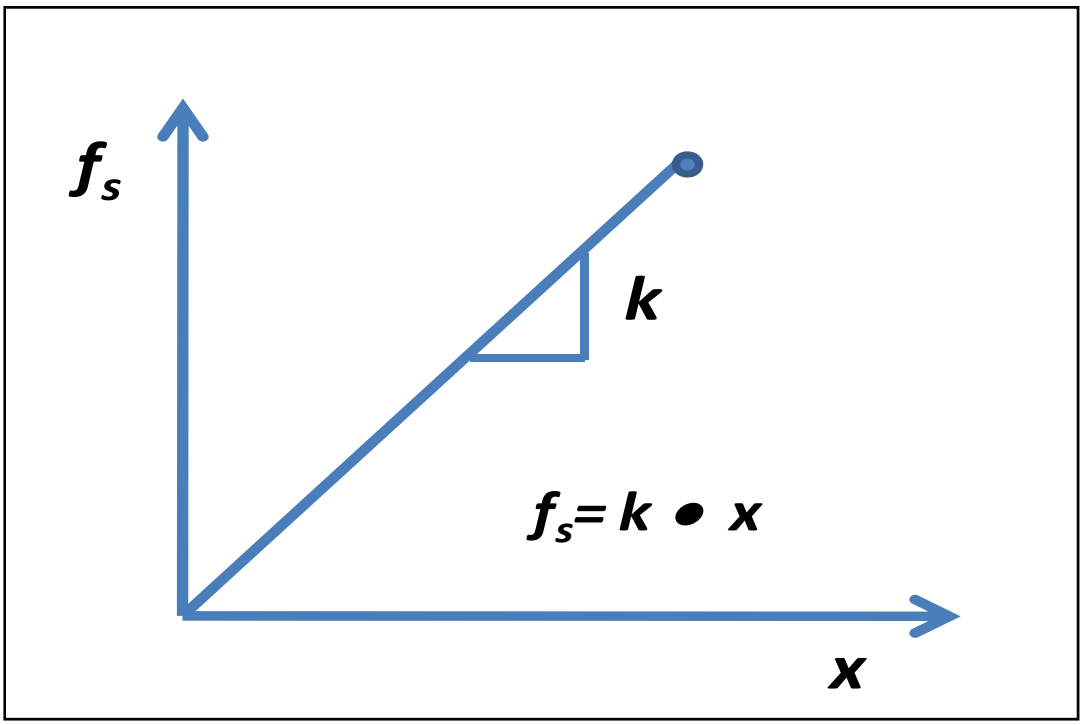

Figure 5.80. Deformable BEAS spring ($k_{8\text{-base isolators}}$) linear secant force-displacement relationship.

The impact force time-history produced by dBEAS is presented in Figure 5.81. This force time-history is used as an input force time-history for the SDOF system of Impact_Beam, as shown in Figure 5.82.

The response of the SDOF system of Impact_Beam and the response of the 2-DOF system of dBEAS computer programs are presented in Figure 5.83. The maximum displacement for the SDOF system and the 2-DOF system was 0.0961 inch and 0.0984 inch, respectively. In both cases, the ultimate displacement of the force-displacement relationship of the spring was not reached (x_{ult} = *60 inches*). It can be observed that the same response was obtained from Impact_Beam and dBEAS.

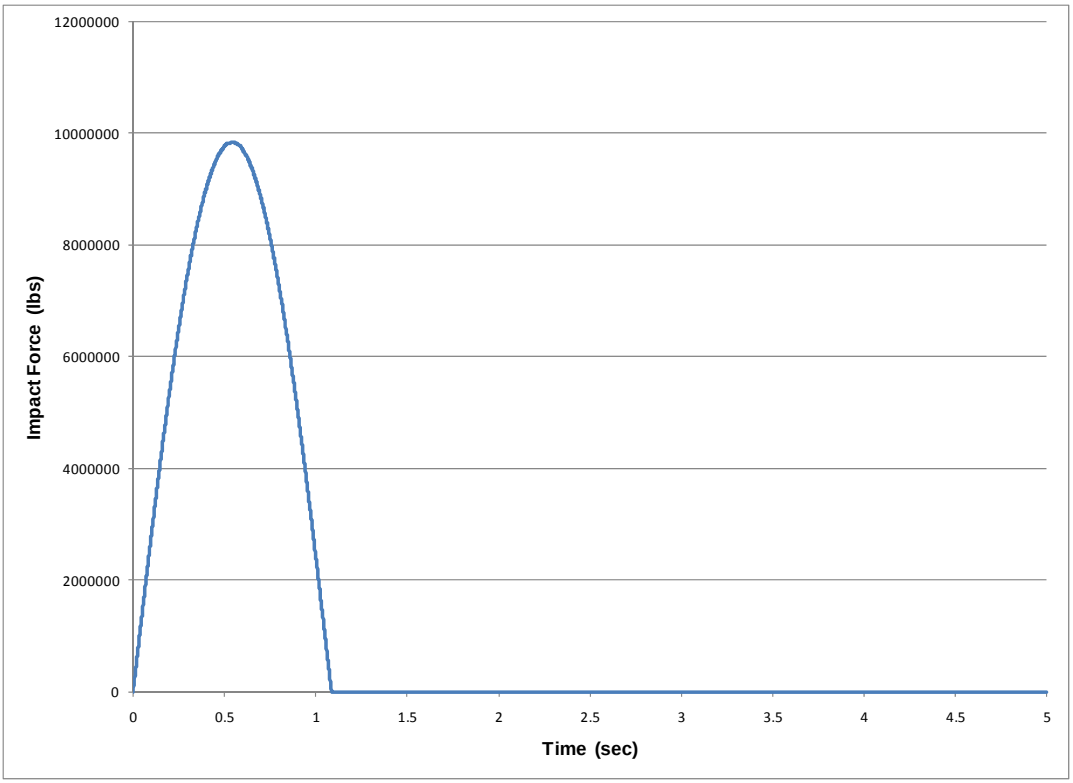

Figure 5.81. Dynamic external force time-history for numerical example in subsection 5.4.5.3 – $\beta = 0\%$.

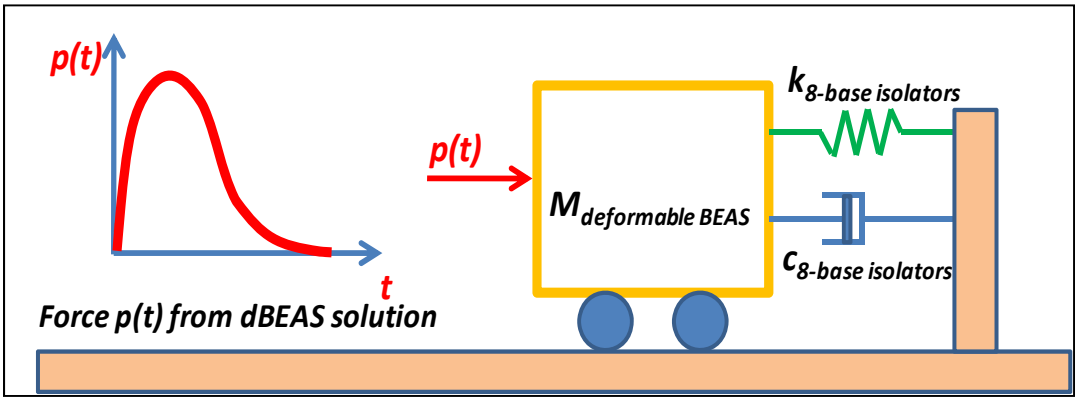

Figure 5.82. SDOF system of Impact_Beam used to calculate the response of a deformable BEAS.

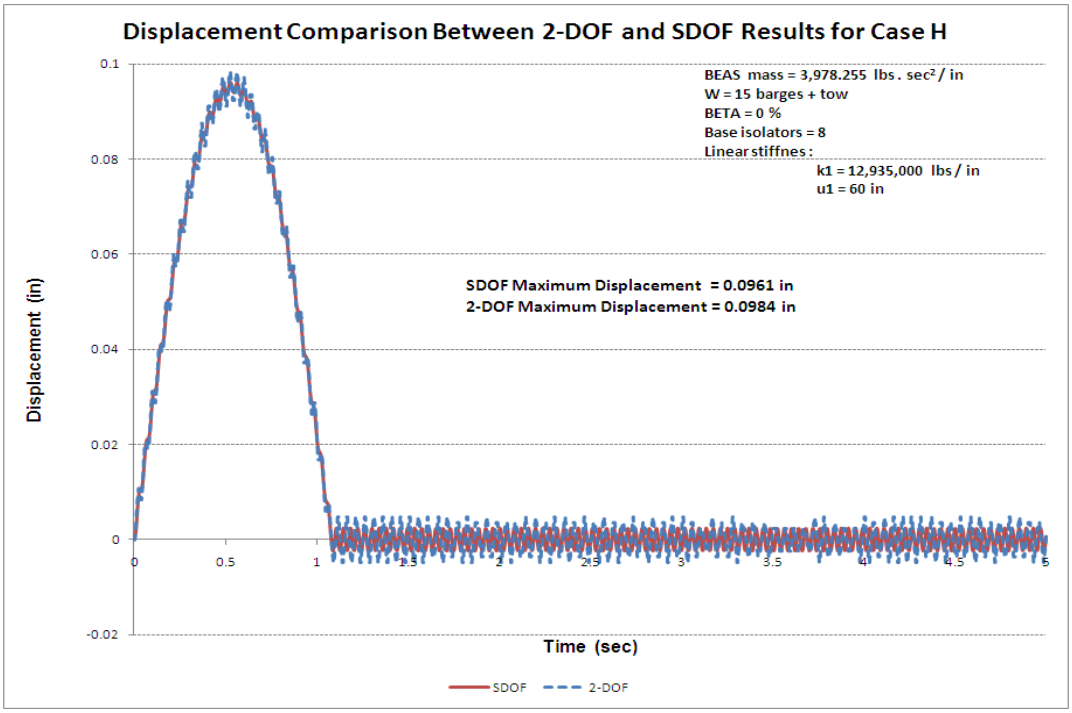

Figure 5.83. Response time-history; dBEAS 2-DOF and Impact_Beam SDOF models, β = 0%.

A second case was evaluated using dBEAS with β = 15%, the impact force from dBEAS as shown in Figure 5.84, with all other parameters of the dBEAS remaining the same. The response of the SDOF system of Impact_Beam and the response of the 2-DOF system of dBEAS computer programs are presented in Figure 5.85. The maximum displacement for the SDOF system and the 2-DOF system was 0.0951 inch and 0.0948 inch, respectively. In both cases, the ultimate displacement of the force-displacement relationship of the spring was not reached (x_{ult} = *60 inches*). It can be observed that the same response was obtained from Impact_Beam and dBEAS.

A third case was evaluated using dBEAS with β = 30%, the impact force from dBEAS as shown in Figure 5.86, with all other parameters of the dBEAS remaining the same. The response of the SDOF system of Impact_Beam and the response of the 2-DOF system of dBEAS computer programs are presented in Figure 5.87. The maximum displacement for the SDOF system and the 2-DOF system was 0.0951 inch and 0.0948 inch, respectively. The maximum response was the same for a system with damping ratios of 15% and 30%. In both cases, the ultimate displacement of the force-displacement relationship of the spring was not reached (x_{ult} = *60 inches*). It can be observed that the same response was obtained from Impact_Beam and dBEAS.

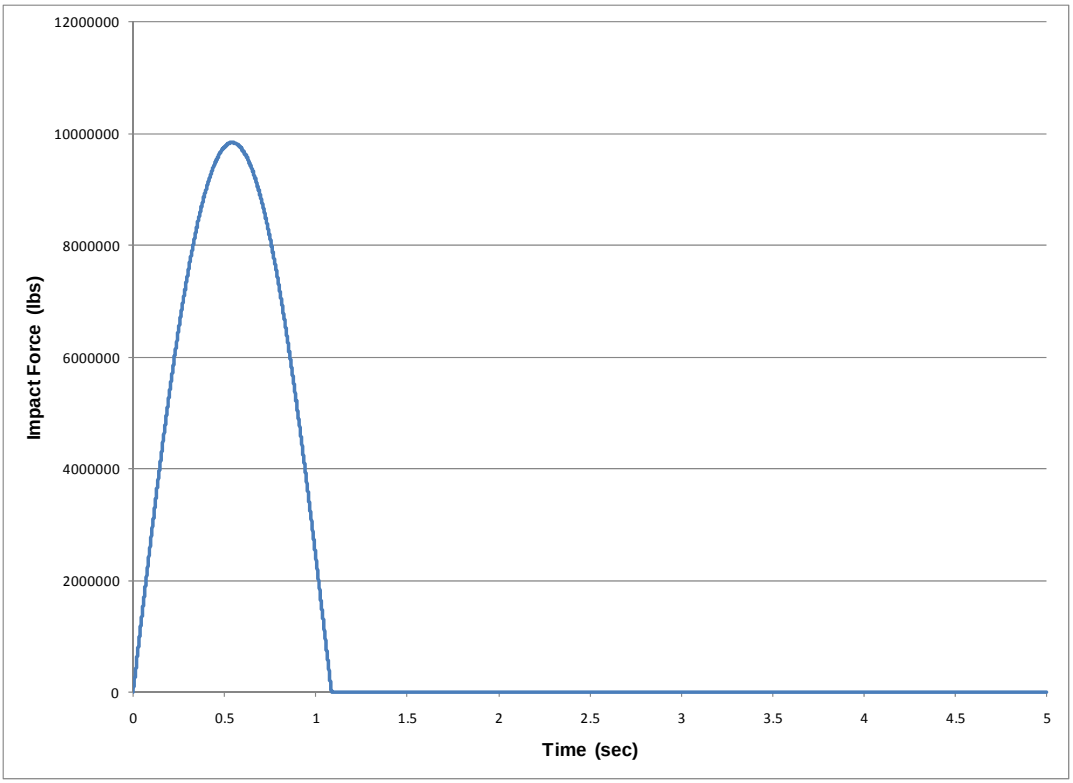

Figure 5.84. Dynamic external force time-history for numerical example in subsection 5.4.5.3 – β = 15%.

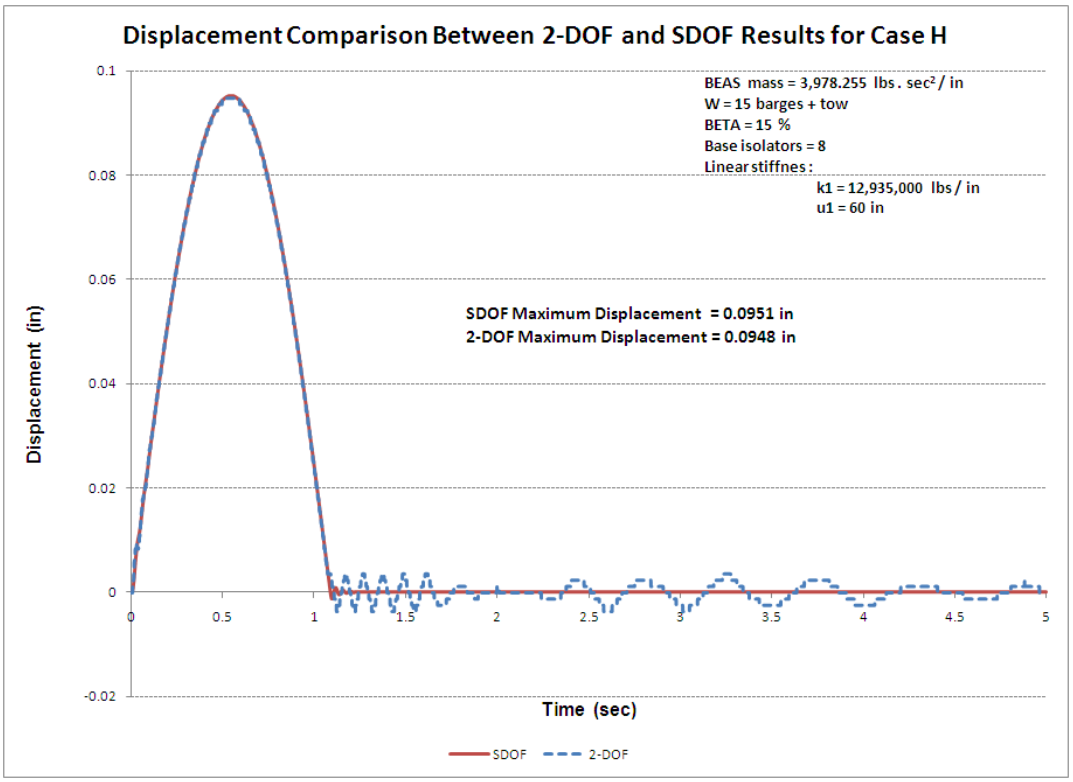

Figure 5.85. Response time-history; dBEAS 2-DOF and Impact_Beam SDOF models, β = 15%.

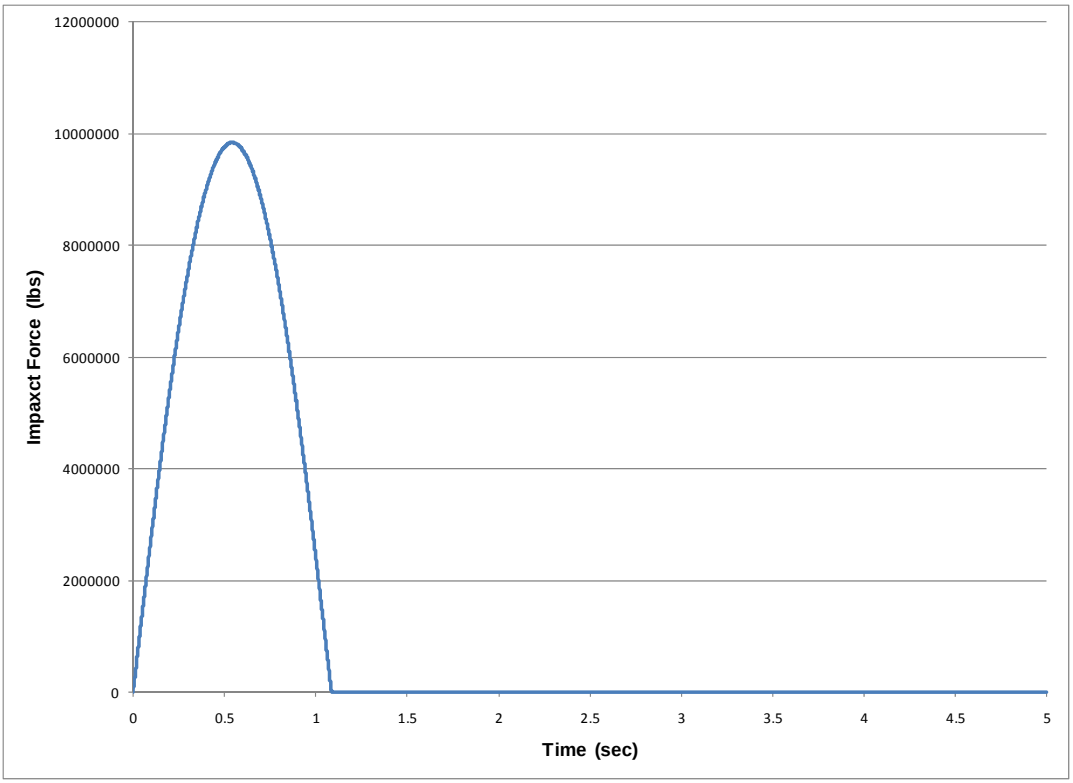

Figure 5.86. Dynamic external force time-history for numerical example in subsection 5.4.5.3 – β = 30%.

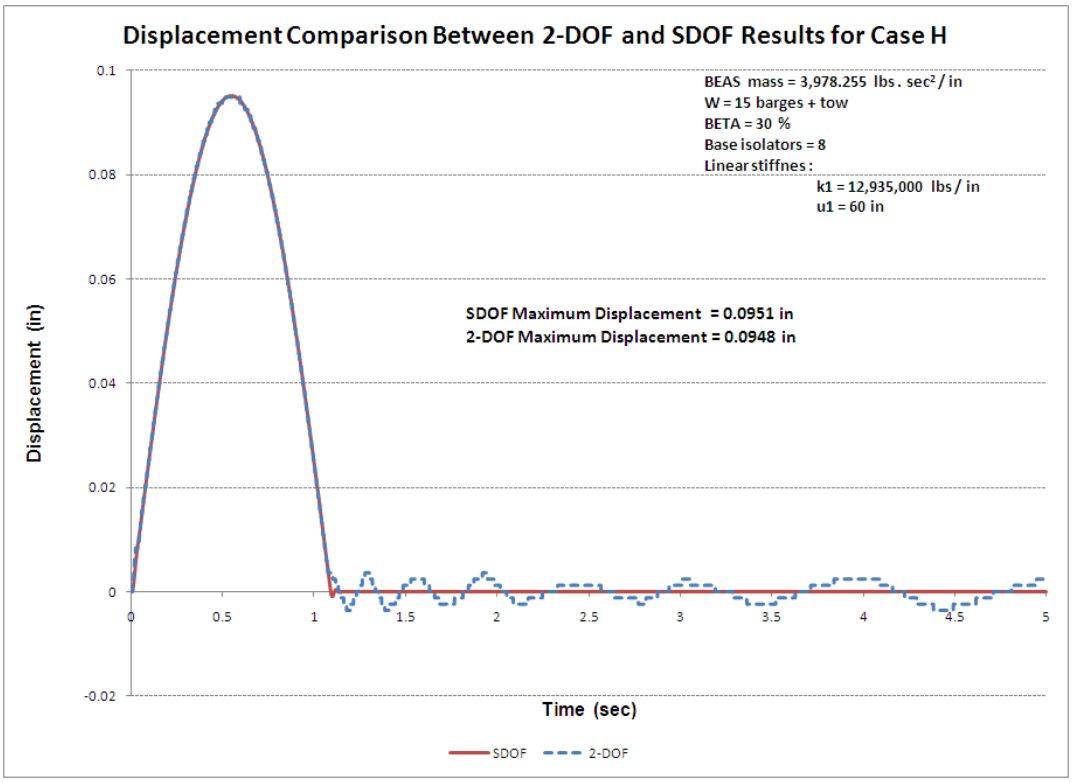

Figure 5.87. Response time-history; dBEAS 2-DOF and Impact_Beam SDOF models, β = 30%.

5.4.5.4 SDOF comparison with high stiffness BEAS and stiff barge model

The computer program dBEAS was used to estimate the impact force time-history for the "super-barge" model (single barge with the weight of 15 barges + tow) and this force was used as input force for the SDOF model in Impact_Beam. The responses of both models were observed to compare the behavior of a 2-DOF system and a SDOF system. The dBEAS model is idealized in Figure 5.88. Note as shown in Figure 5.88, that the center of gravity of both systems is coincident with the center of rigidity of the dBEAS and the line of action of the impact force, so all motions will be translational along the line of action (i.e., no rotations). This condition (head-on impact event) can be modeled by a 2-DOF system as shown in Figure 5.89. That is, the 2-DOF system is equivalent to a super-barge model impacting the deformable BEAS. This example is the same as the example presented in Sub-section 5.4.5.3 but using a stiffer barge train spring constant, that is, the barge train longitudinal stiffness was set equal to the estimated barge train transverse stiffness. In this example, the barge train longitudinal stiffness has a value of 2,100 kips/inch and the deformable bullnose properties are the following; weight of 3,978.255 lbs • s^2/inch, 8 base isolators with linear secant stiffness defined as shown in Figure 5.90. The force-displacement relationship is defined by $k = 12{,}935{,}000.0$ *lbs/in* and $x_{ult} = 60$ *inches*. The damping ratio for this example was 0% for each base isolator. Because the group of base isolators are in parallel on the impact nosing of the Deformable BEAS, the total stiffness and total damping for the SDOF model of Impact_Beam is calculated by adding the contribution of each single base isolator to obtain an equivalent single stiffness and damping ratio.

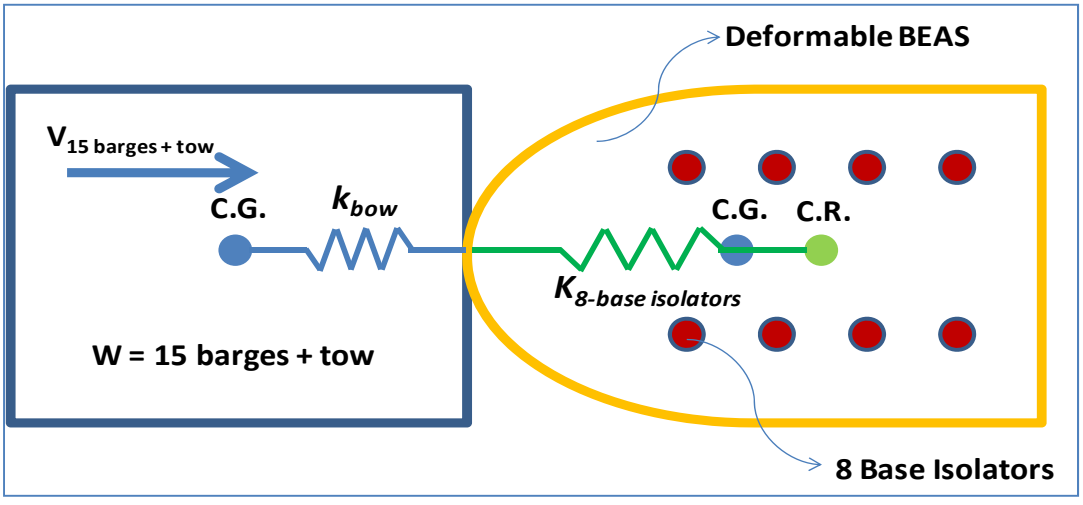

Figure 5.88. Plan View of the 2-DOF system of the super-barge dBEAS model.

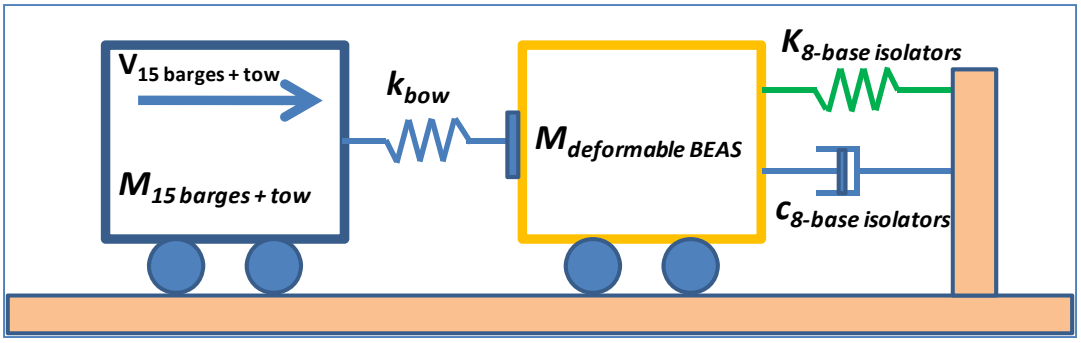

Figure 5.89. 2-DOF system of the super-barge dBEAS model.

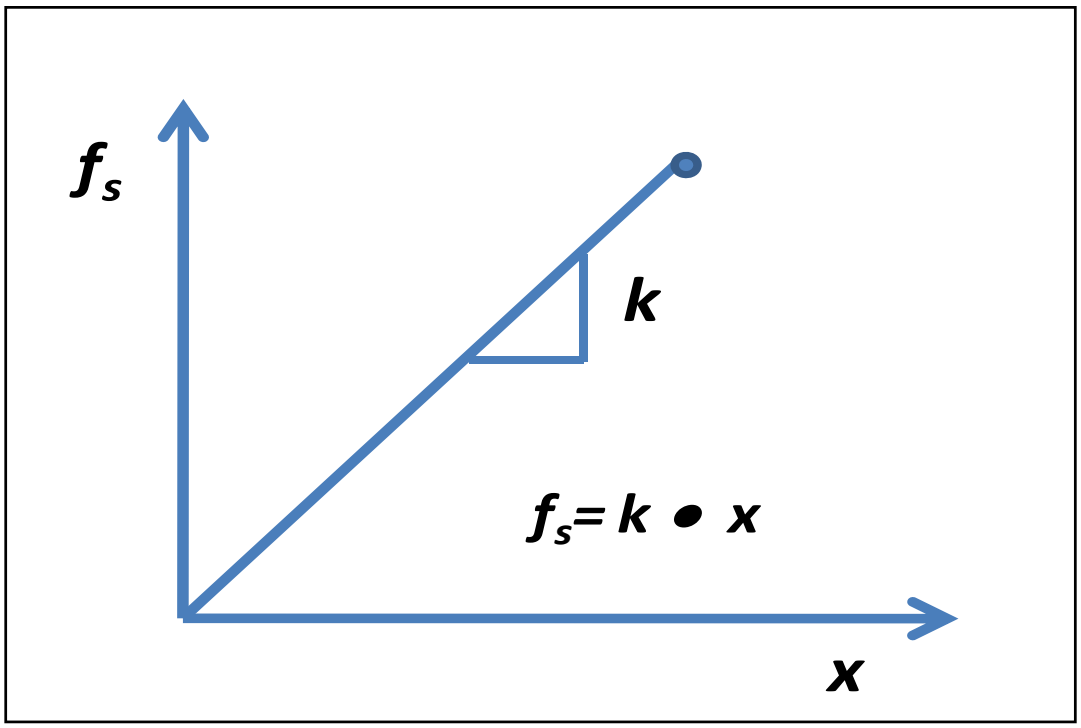

Figure 5.90. Deformable BEAS spring ($k_{8\text{-base isolators}}$) linear secant force-displacement relationship.

The impact force time-history produced by dBEAS is presented in Figure 5.91. This force time-history is used as the input force time-history for the SDOF system of Impact_Beam, as shown in Figure 5.92.

The response of the SDOF system of Impact_Beam and the response of the 2-DOF system of dBEAS computer programs are presented in Figure 5.93. The maximum displacement for the SDOF system and the 2-DOF system was 0.0961 inch and 0.0984 inch, respectively. In both cases, the ultimate displacement of the force-displacement relationship of the spring was not reached (x_{ult} = *60 inches*). It can be observed that the same response was obtained from Impact_Beam and dBEAS.

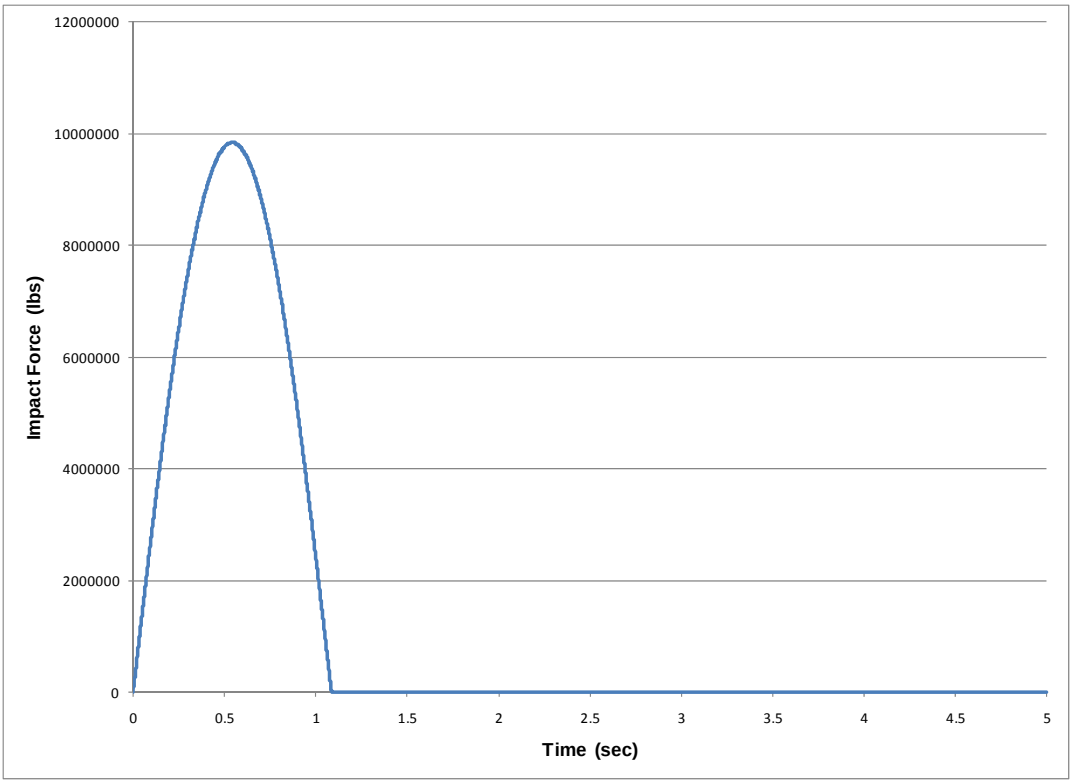

Figure 5.91. Dynamic external force time-history for numerical example in subsection 5.4.5.4 – β = 0%.

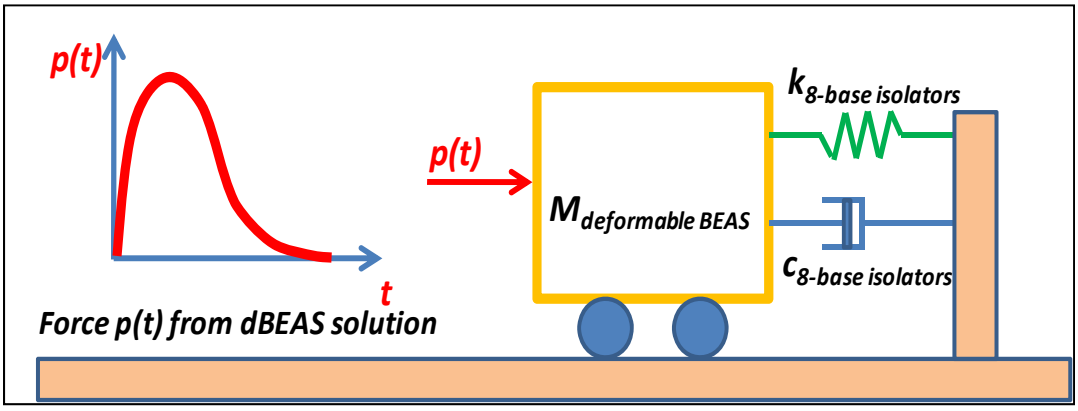

Figure 5.92. SDOF system of Impact_Beam used to calculate the response of a deformable BEAS.

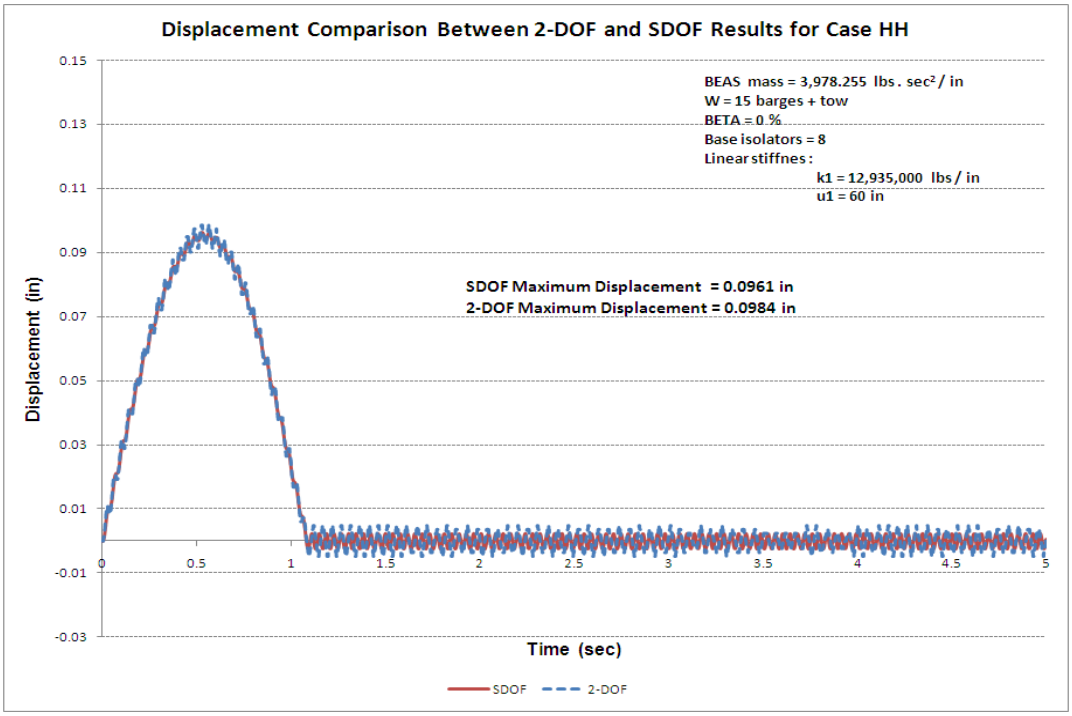

Figure 5.93. Response time-history; dBEAS 2-DOF and Impact_Beam SDOF models, β = 0%.

A second case was evaluated using dBEAS with β = 15%, the impact force from dBEAS as shown in Figure 5.94, with all other parameters of the dBEAS remaining the same. The response of the SDOF system of Impact_Beam and the response of the 2-DOF system of dBEAS computer programs are presented in Figure 5.95. The maximum displacement for the SDOF system and the 2-DOF system was 0.0951 inch and 0.0948 inch, respectively. In both cases, the ultimate displacement of the force-displacement relationship of the spring was not reached (x_{ult} = *60 inches*). It can be observed that the same response was obtained from Impact_Beam and dBEAS.

A third case was evaluated using dBEAS with β = 30%, the impact force from dBEAS as shown in Figure 5.96, with all other parameters of the dBEAS remaining the same. The response of the SDOF system of Impact_Beam and the response of the 2-DOF system of dBEAS computer programs are presented in Figure 5.97. The maximum displacement for the SDOF system and the 2-DOF system was 0.0951 inch and 0.0948 inch, respectively. The maximum response was the same for a system with damping ratio of 15% and 30%. In both cases, the ultimate displacement of the force-displacement relationship of the spring was not reached (x_{ult} = *60 inches*). It can be observed that the same response was obtained from Impact_Beam and dBEAS.

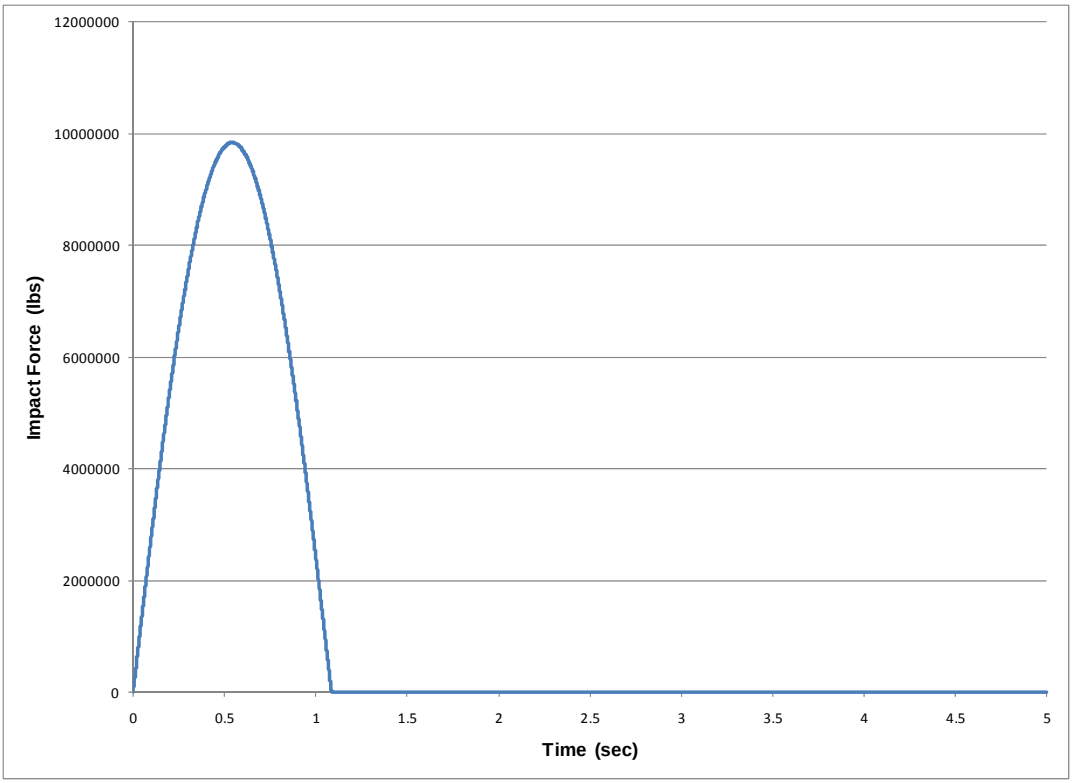

Figure 5.94. Dynamic external force time-history for numerical example in subsection 5.4.5.4 – β = 15%.

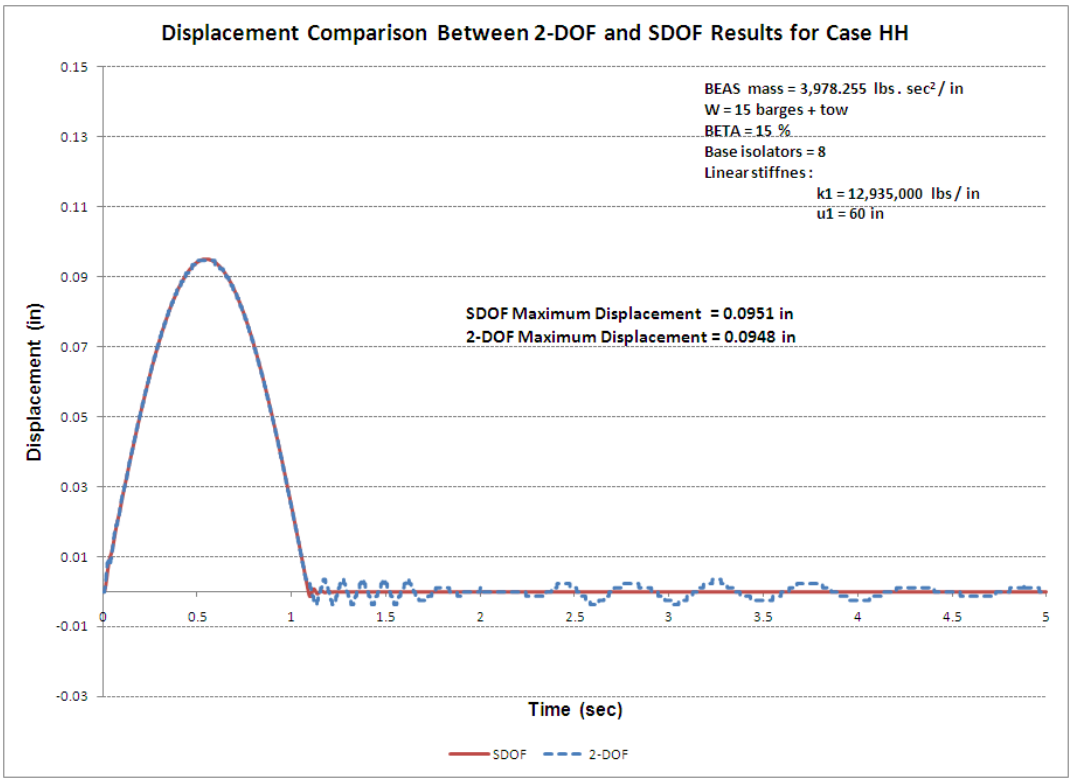

Figure 5.95. Response time-history; dBEAS 2-DOF and Impact_Beam SDOF models, β = 15%.

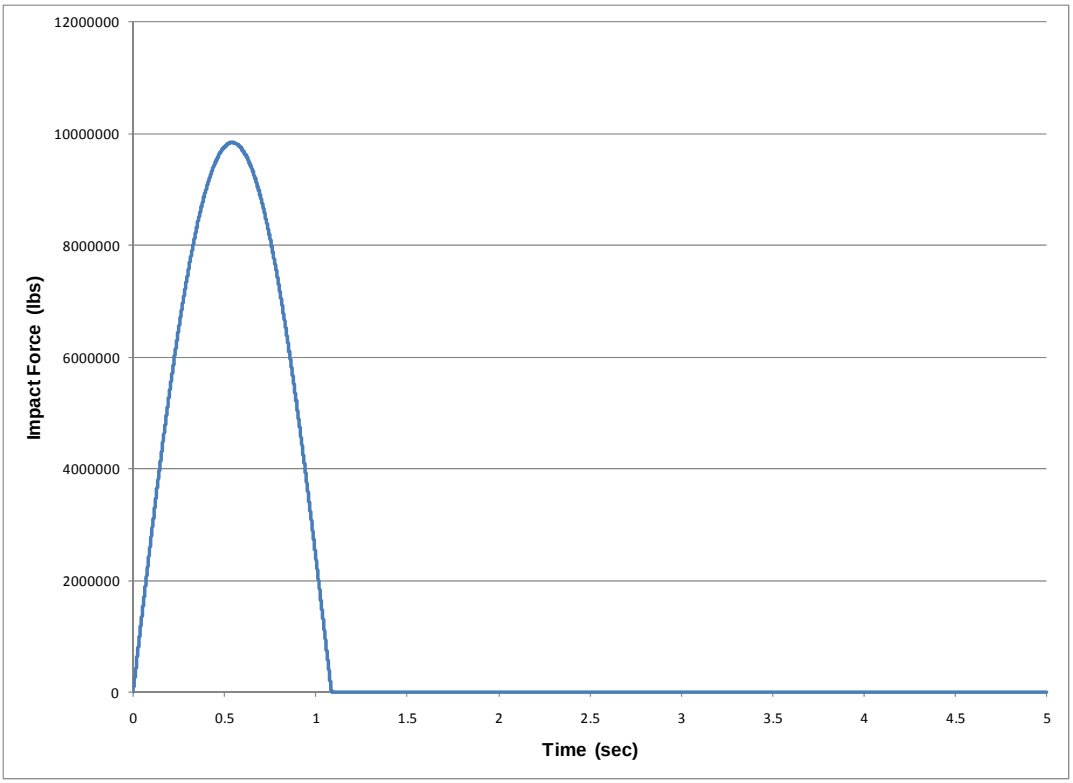

Figure 5.96. Dynamic external force time-history for numerical example in subsection 5.4.5.4 – β = 30%.

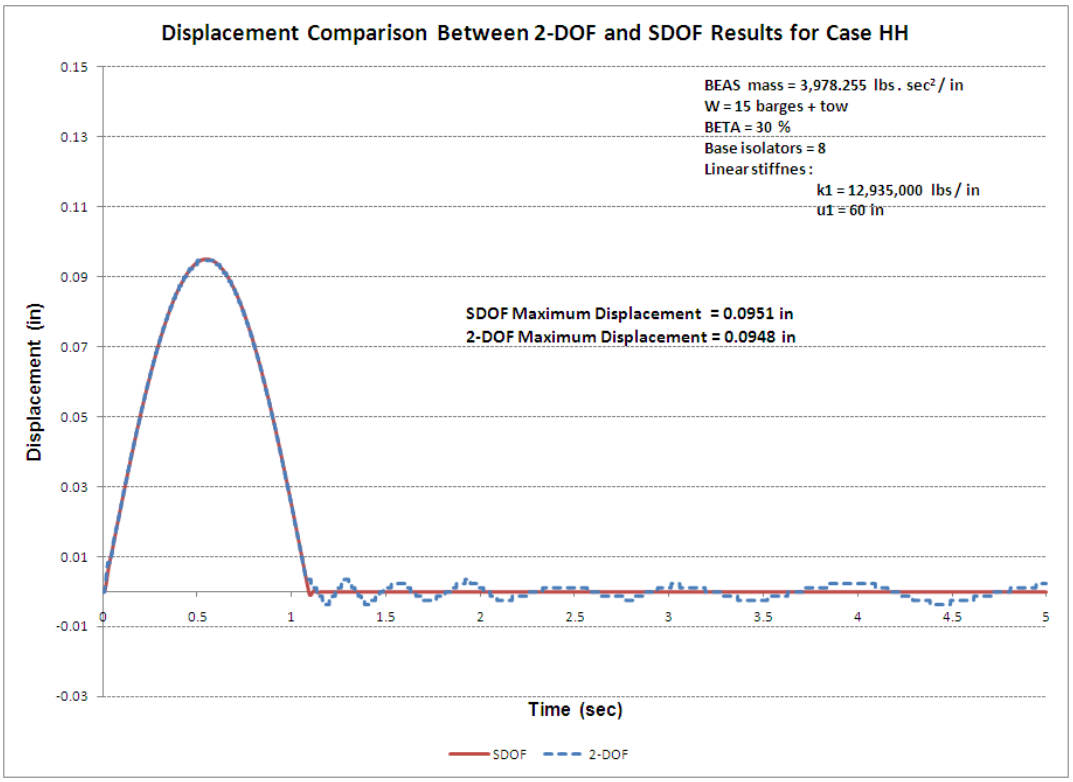

Figure 5.97. Response time-history; dBEAS 2-DOF and Impact_Beam SDOF models, β = 30%.

5.4.5.5 Bilinear force-displacement base isolators stiffness with β = 15%

In the following examples, the same input data as in the example presented in sub -section 5.4.5.1 was used but with a different barge train approach velocity, that is 4 and 6 ft/sec. The results from the example in sub -section 5.4.5.1 (barge train approach velocity equal to 2 ft/s) is repeated here as a matter of comparison. The computer program dBEAS was used to estimate the impact force time-history for the "super-barge" model (single barge with the weight of 15 barges + tow) and this force was used as input force in Impact_Beam SDOF model. The responses of both models were observed to compare the behavior of a 2-DOF system and a SDOF system. The dBEAS model is idealized in Figure 5.98. Note, as shown in Figure 5.98, that the center of gravity of both systems is coincident with the center of rigidity of the dBEAS and the line of action of the impact force, so all motions will be translational along the line of action (i.e., no rotations). This condition (head-on impact event) can be modeled by a 2-DOF system as shown in Figure 5.99. That is, the 2-DOF system is equivalent to a super-barge model impacting the deformable BEAS. The barge train longitudinal stiffness was estimate as 1,200 kips/inch and the deformable bullnose properties are the following; weight of 3,978.255 lbs • s^2/inch, 8 base isolators with bilinear stiffness defined as shown in Figure 5.100. In this case the force-displacement relationship is defined by $k_1 = 11{,}170.21$ *lbs/in*, $k_2 = 57{,}558.14$ *lbs/in*, $x_1 = 28.2$ *inches*, and $x_2 = 54$ *inches*. The damping ratio for this example was 15% for each base isolator. Because the group of base isolators are acting against the impact nosing of the Deformable BEAS in parallel, the total stiffness and total damping for the SDOF model of Impact_Beam is calculated by adding the contribution of each single base isolator to obtain an equivalent single stiffness and damping ratio.

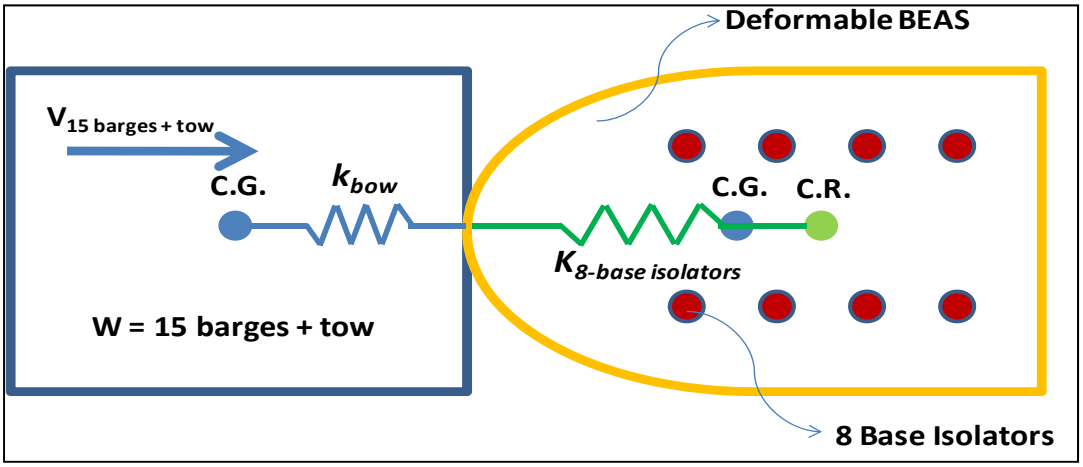

Figure 5.98. Plan View of the 2-DOF system of the super-barge dBEAS model.

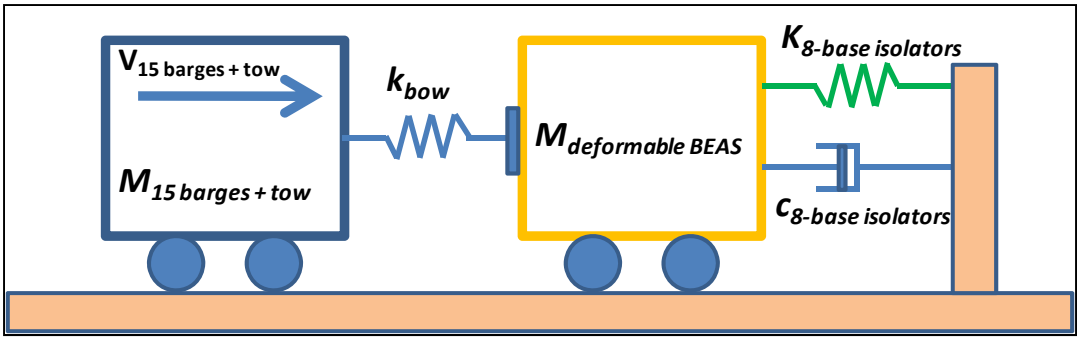

Figure 5.99. 2-DOF system of the super-barge dBEAS model.

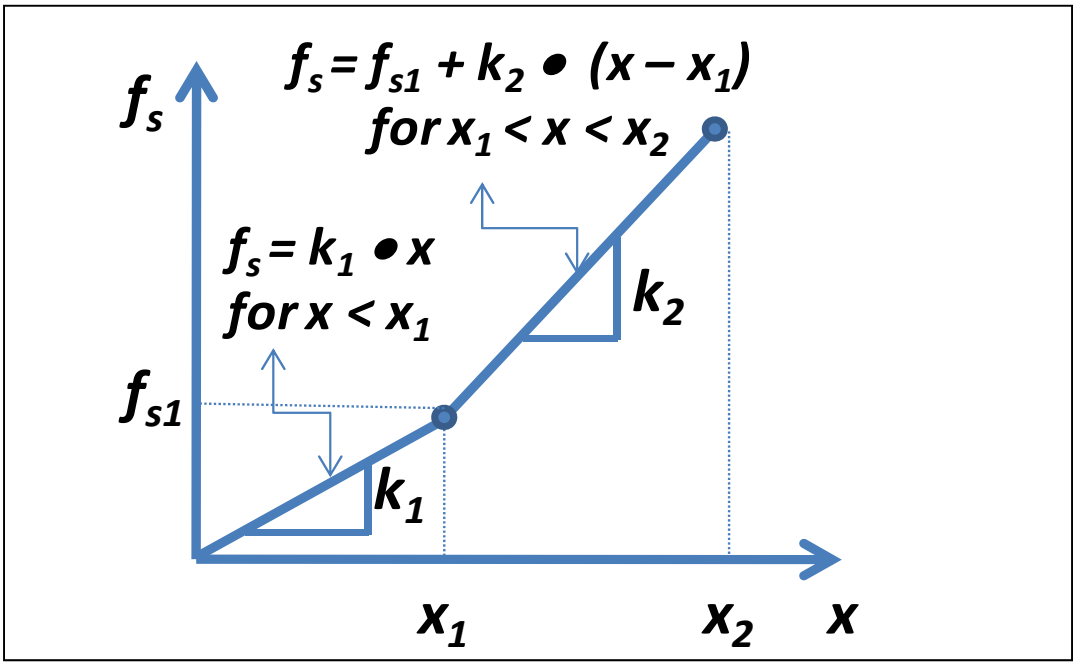

Figure 5.100. Deformable BEAS spring ($k_{8\text{-base isolators}}$) bilinear force-displacement relationship.

The impact force time-history produced by dBEAS is presented in Figure 5.101. This force time-history at the point of contact between the super-barge and the dBEAS is based on a super-barge approach velocity of 2 ft/sec. This force time-history is used as input force time-history for the SDOF system of Impact_Beam, as shown in Figure 5.102.

The response of the SDOF system of Impact_Beam and the response of the 2-DOF system of dBEAS computer programs are presented in Figure 5.103. The maximum displacement for the SDOF system and the 2-DOF system was 28.1467 inches and 28.1472 inches, respectively. In both cases, the second slope of the force-displacement relationship of the spring was not reached ($x_1 = 28.2$ *inches*). It can be observed that the same response was obtained from Impact_Beam and dBEAS.

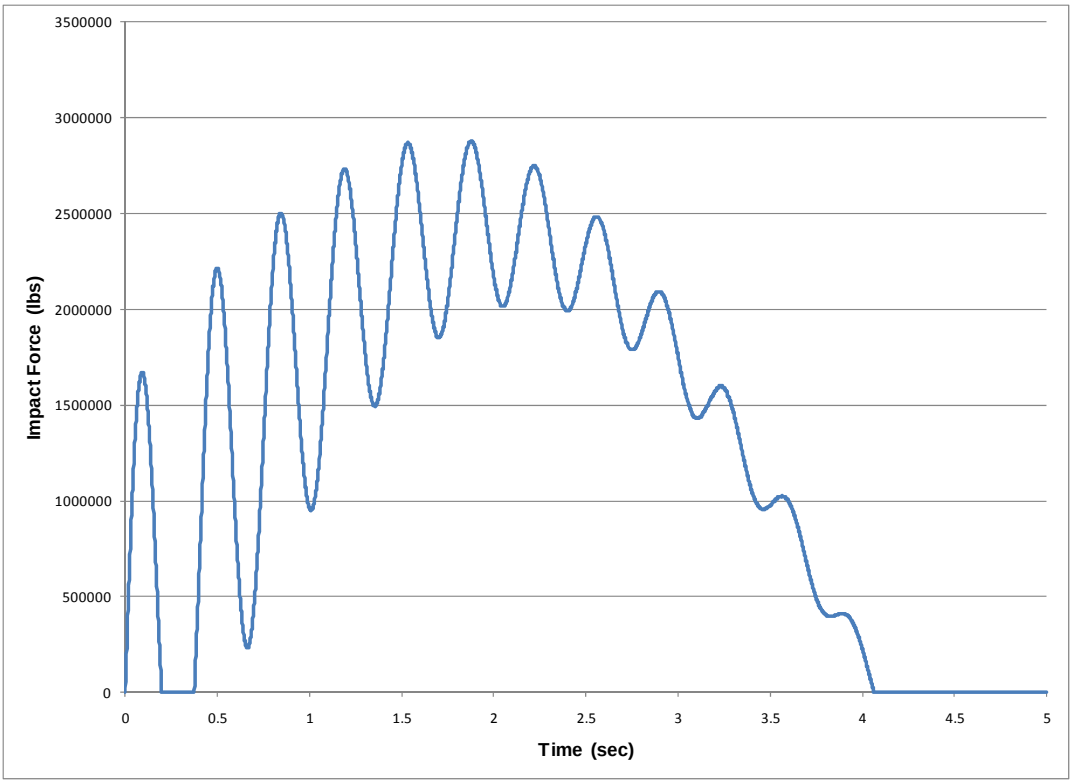

Figure 5.101. Dynamic external force time-history for numerical example in subsection 5.4.5.5 – $\beta = 15\%$, $v = 2$ ft/s.

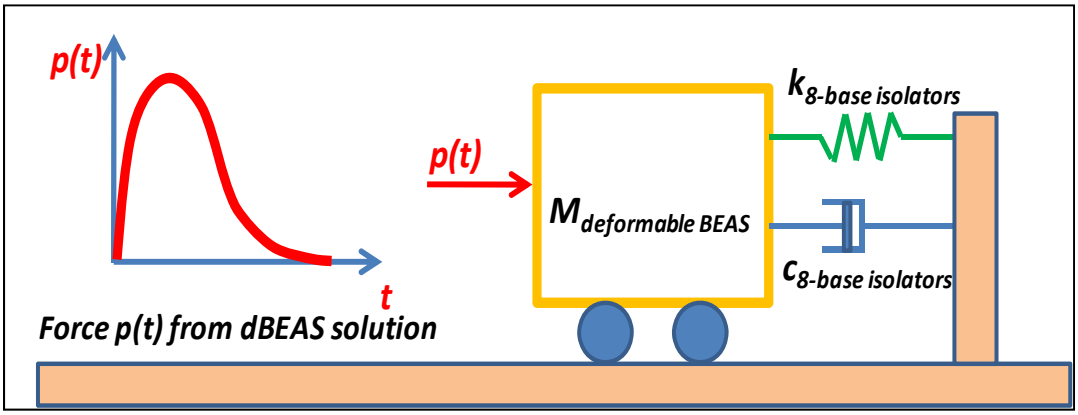

Figure 5.102. SDOF system of Impact_Beam used to calculate the response of a deformable BEAS.

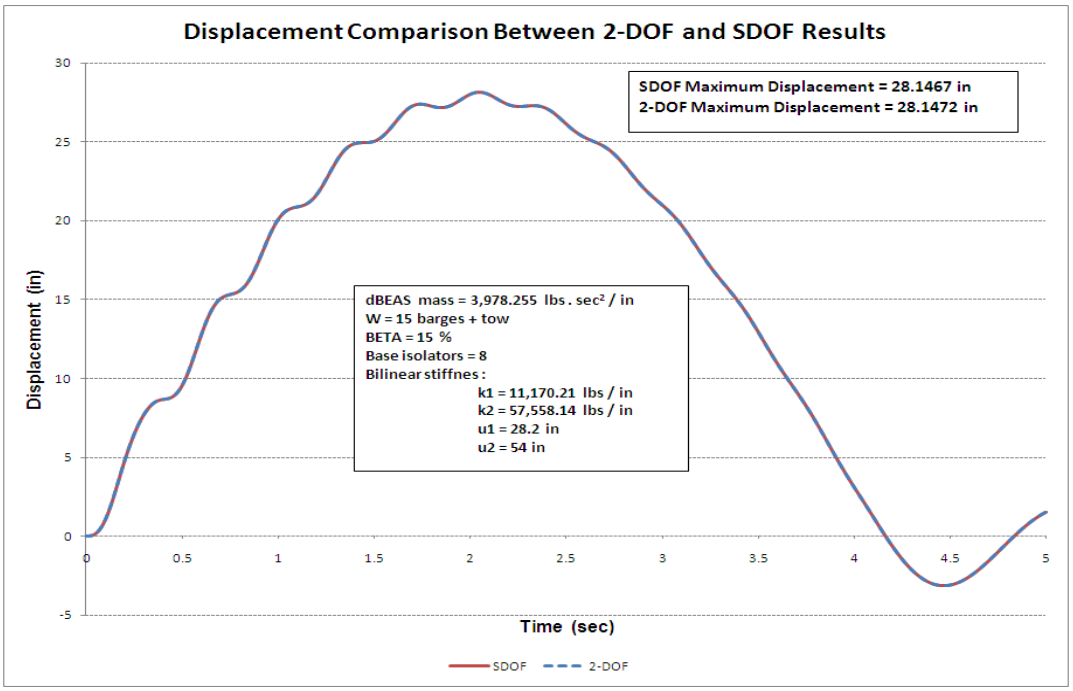

Figure 5.103. Response time-history; dBEAS 2-DOF and Impact_Beam SDOF models, β = 15%, v = 2 ft/s.

A second case was evaluated using dBEAS with $v = 4\,ft/sec$, the impact force from dBEAS as shown in Figure 5.104, with all other parameters of the dBEAS remaining the same. The response of the SDOF system of Impact_Beam and the response of the 2-DOF system of dBEAS computer programs are presented in Figure 5.105. The maximum displacement for the SDOF system and the 2-DOF system was 42.8047 inches and 42.8928 inches, respectively. In both cases, the second slope of the force-displacement relationship of the spring was reached ($x_1 = 28.2\ inches$). It can be observed that the same response was obtained from Impact_Beam and dBEAS.

A third case was evaluated using dBEAS with $v = 6\,ft/sec$, the impact force from dBEAS as shown in Figure 5.106, with all other parameters of the dBEAS remaining the same. The response of the SDOF system of Impact_Beam and the response of the 2-DOF system of dBEAS computer programs are presented in Figure 5.107. The maximum displacement for the SDOF system and the 2-DOF system was 53.952 inches and 54.1416 inches, respectively. In both cases, the second slope of the force-displacement relationship of the spring was reached ($x_1 = 28.2\ inches$) and the base isolator presents failure because the $x_2 = 54\ inches$ was reached. It can be observed that the same response was obtained from Impact_Beam and dBEAS.

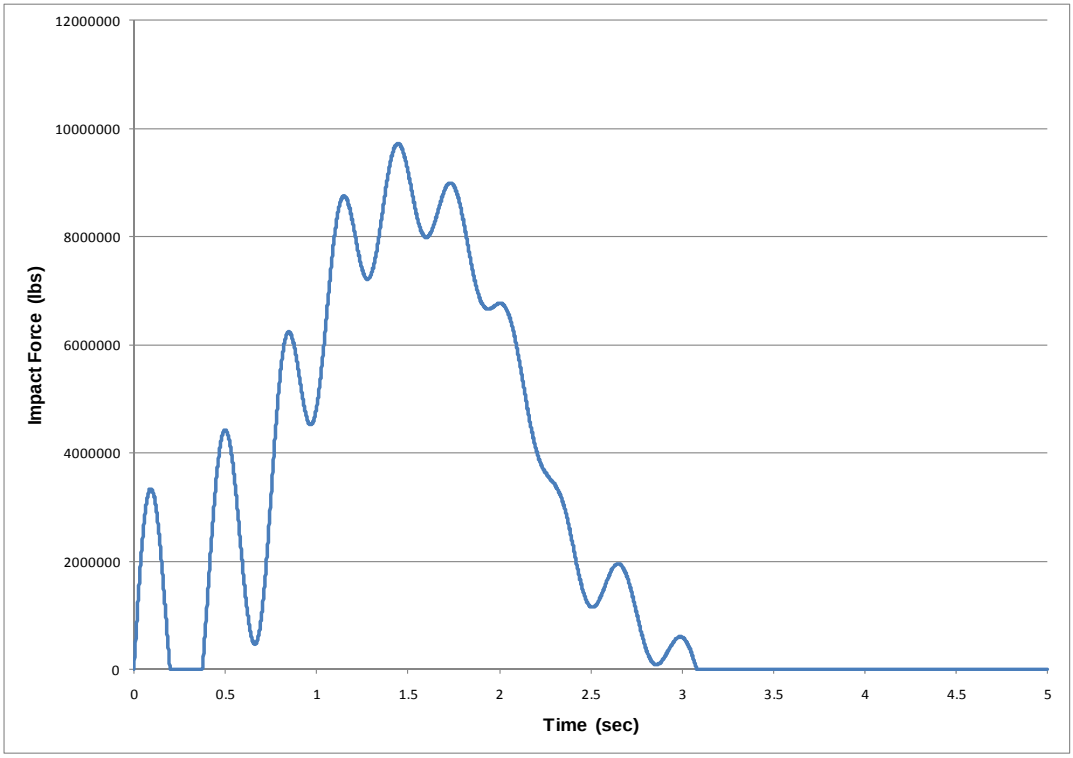

Figure 5.104. Dynamic external force time-history for numerical example in subsection 5.4.5.5 – $\beta = 15\%$, $v = 4$ *ft/s*.

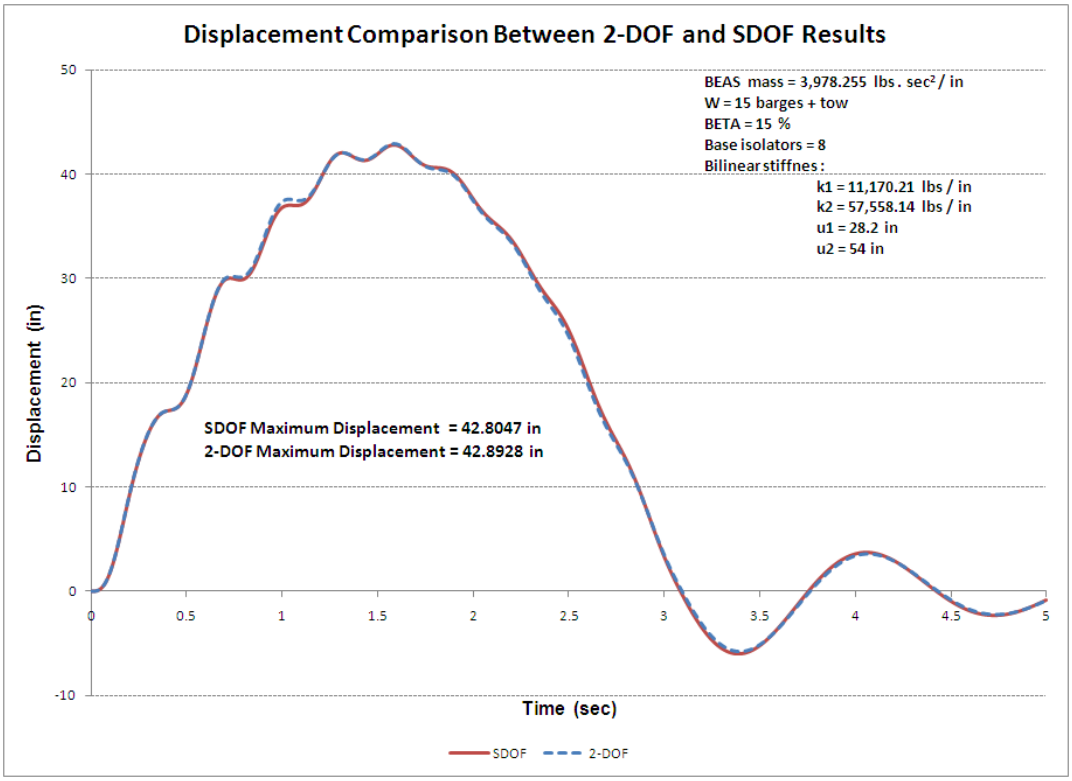

Figure 5.105. Response time-history; dBEAS 2-DOF and Impact_Beam SDOF models, $\beta = 15\%$, $v = 4$ *ft/s*.

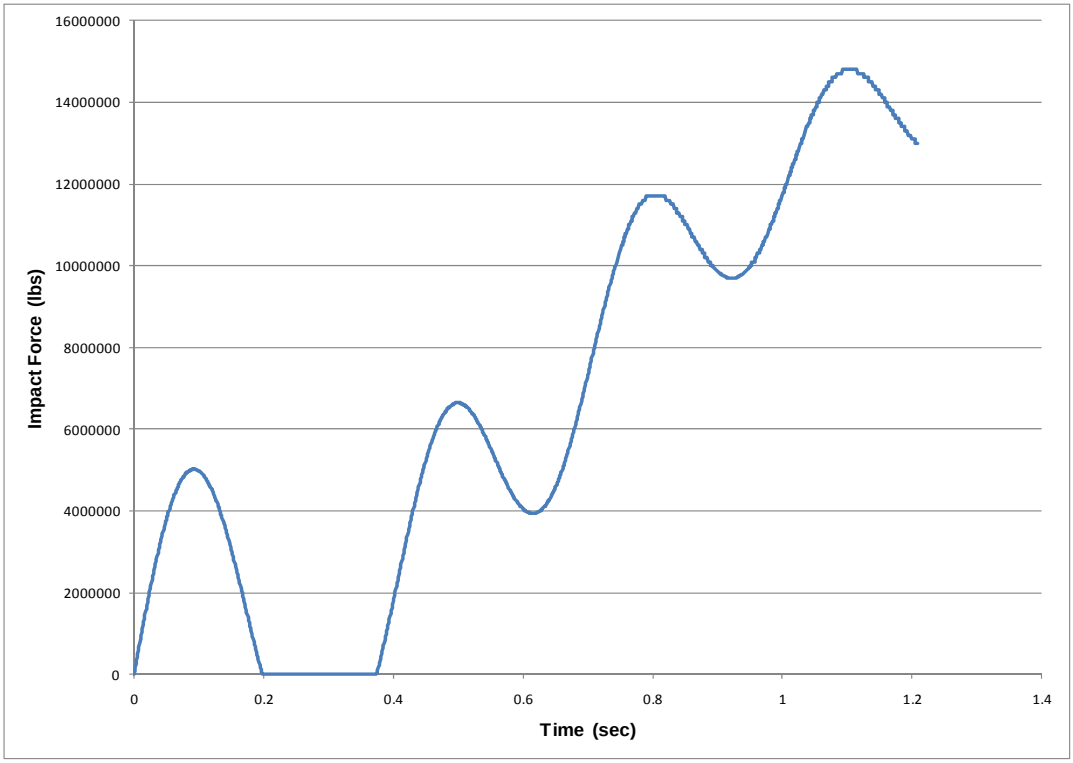

Figure 5.106. Dynamic external force time-history for numerical example in subsection 5.4.5.5 – $\beta = 15\%$, $v = 6$ *ft/s*.

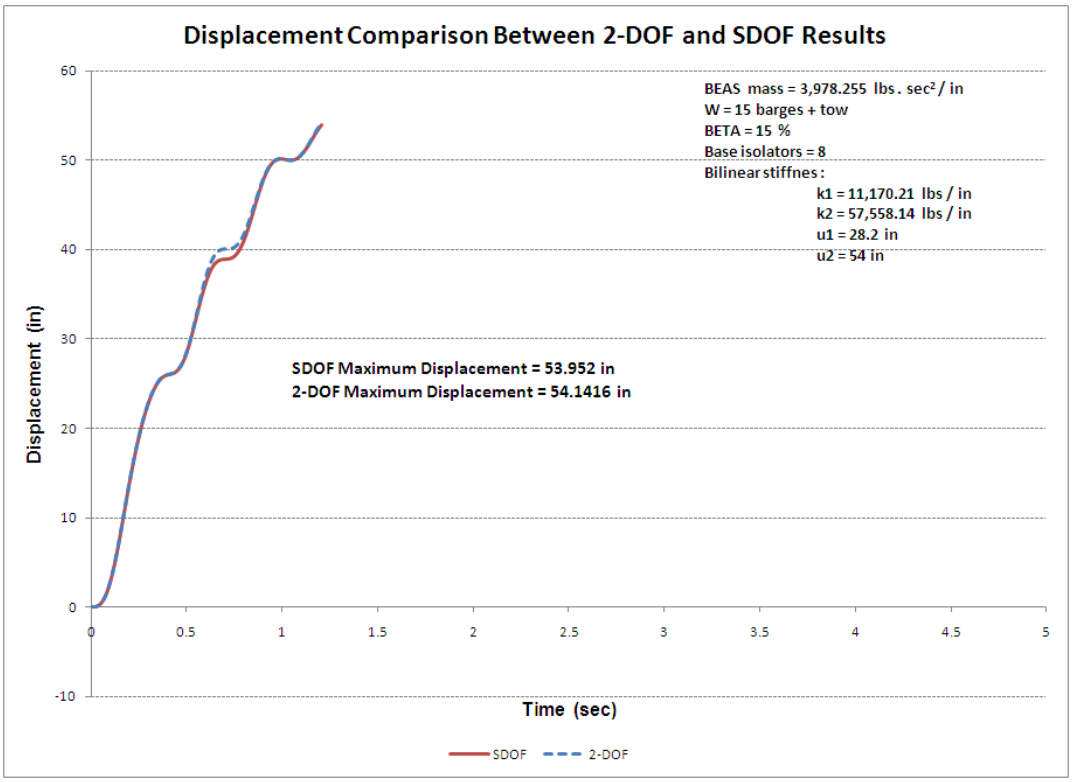

Figure 5.107. Response time-history; dBEAS 2-DOF and Impact_Beam SDOF models, $\beta = 15\%$, $v = 6$ *ft/s*.

5.4.6 dBEAS-SDOF response subjected to force time-history of Winfield Test #10

The SDOF system used in this numerical example represents the behavior of an impacted bullnose supported over *a single* base isolator. The force-displacement relationship of the base isolator is bilinear as shown in Figure 5.108.

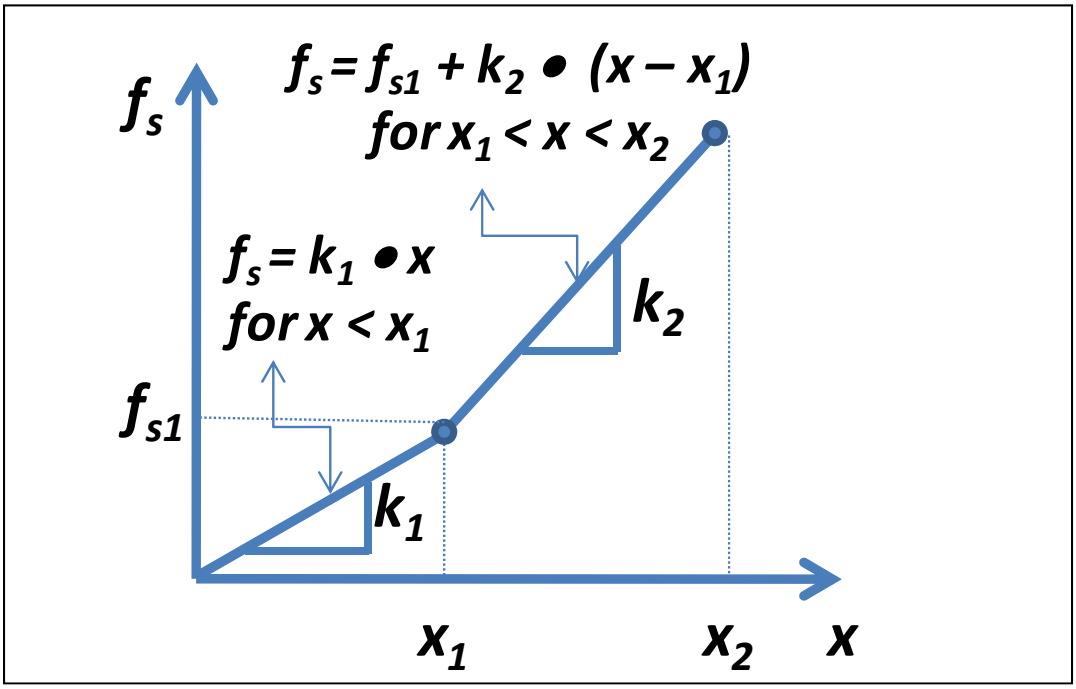

Figure 5.108. Deformable BEAS spring ($k_{base\ isolator}$) bilinear force-displacement relationship.

The force applied to the bullnose is a time-history obtained from the Winfield Test #10 as shown in Figure 5.109. The objective of this example is to show that the use of the SDOF model is comparable to a Deformable BEAS with a impact nosing supported by a single base isolator. The following input data was used in this example:

- Mass (M) = 3,978.255 lbs • s^2/inch
- Stiffness coefficients: k_1 =11,170.21 lbs/in, k_2 = 57,558.14 kips/inch
- Limits for displacement: = x_1 = 28.2 inches; x_2 = 54 inches
- Damping ratio (c) = 15%
- Time step = 0.002

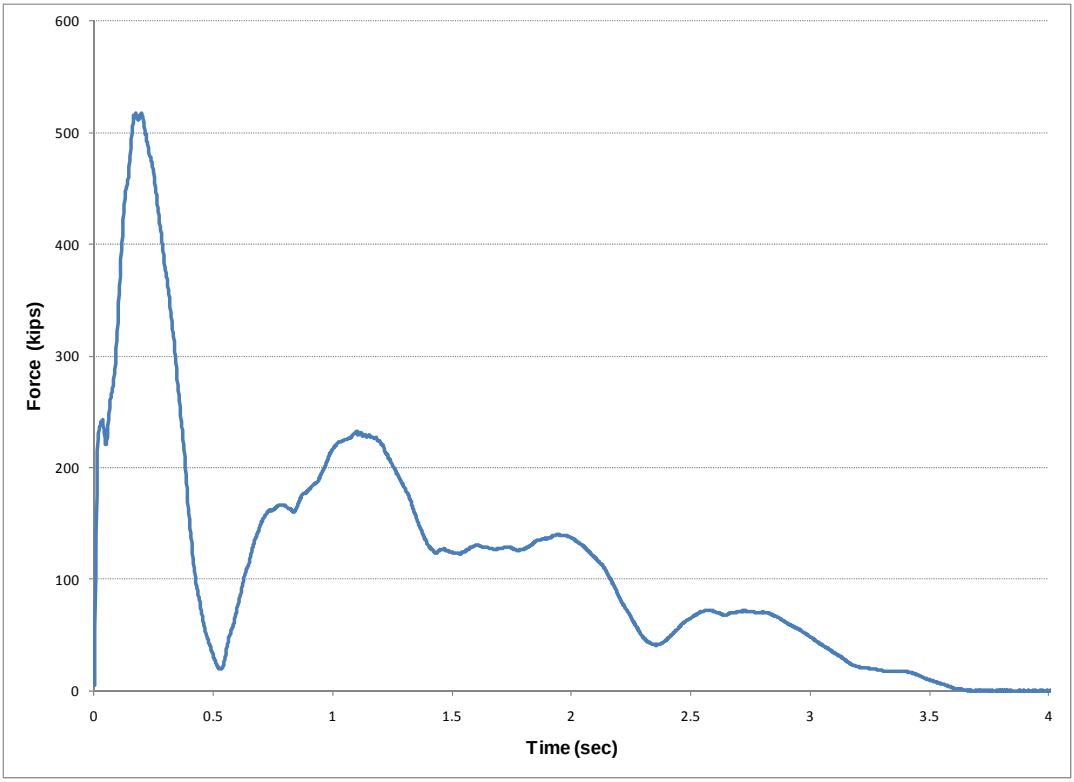

Figure 5.109. Dynamic external force time-history obtained from Winfield Test #10.

The maximum value for the time-history used in this example is 517.4 kips, as was obtained during Winfield Test #10. The maximum value for the dynamic response of the SDOF system was 27.4183 inches. This displacement indicates that the second slope is not reached by the single base isolator if the force time-history obtained from Winfield Test #10 is applied to a deformable BEAS with the properties used in this example.

5.5 Conclusions

In this Chapter, verification and validation for the SDOF solver in the Impact_Beam software were performed using the commercial off-the-shelf (COTS) software SAP2000, full-scale test data from Winfield Test #10, and independently developed software dBEAS, which has been developed to simulate a barge train impact with an innovative flexible bullnose system. Force time-history data were used from an example taken from Paz (1985), from Winfield Test #10 processed by Impact_Force to match a specified barge train configuration, and from simulations performed using the dBEAS software. This series of assessments showed that the results of the Impact_Beam software matched the results from the comparison software and full-scale barge impact tests.

Also, methods to calculate the dynamic modulus of elasticity for a flexible beam from differing sensor data of the full-scale test data have been presented and solved with the data from Winfield Test #10. Determining the dynamic modulus of elasticity as accurately as possible is important for multiple degree of freedom solutions which will be presented in Chapter 6, where moment and shear forces, due to deflection of the beam, will be calculated.

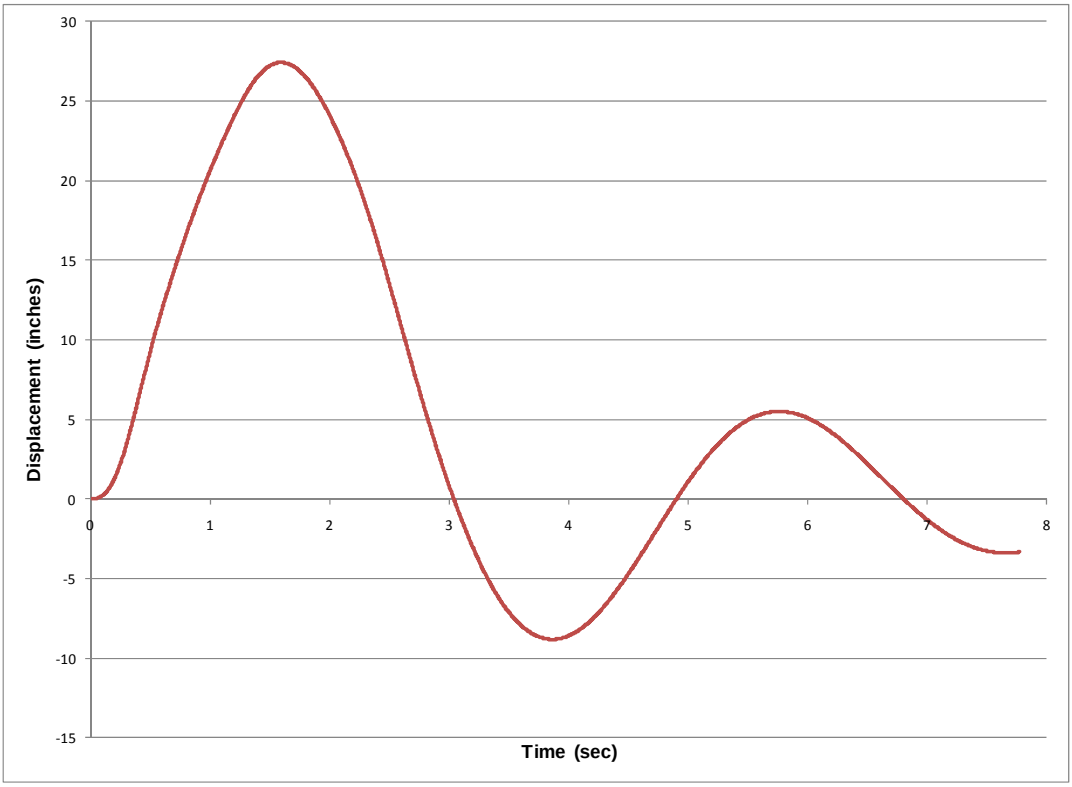

Figure 5.110. Displacement time-history for dBEAS-SDOF response subjected to force time-history of Winfield Test #10.

6 Summary of Interpretation of Full-Scale Impact Test Results Conducted at Winfield Lock and Dam Using Impact_Beam

6.1 Introduction

On the 25th through the 26th of August 2008, a series of full-scale barge train impact experiments with a flexible approach lock wall were performed (Barker et al. 2010). The series of barge train impacts consisted of twenty-three glancing blow impact experiments conducted at the Winfield Lock and Dam at Red House, WV. All experiments were conducted with a 3-by-3 barge train impacting a flexible approach guide wall. A force-measuring load-cell bumper was mounted to the impact corner of the barge. The load-cell bumper measured the amount of force of the barge impacting the lock wall. Of the twenty-three impact experiments, only eighteen were considered to have a sufficient amount of recorded data that could be used for impact analysis. Additionally, four of these impact tests were performed using a "possum" placed between the lock wall face and the load cell bumper. A possum is a knotted section of rope covered with a nylon mesh, used to act as a "shock absorber" between the barge train and the flexible approach wall.

Chapter 5 presented methods for the estimation of the dynamic modulus of elasticity E_{dyn} based on a full interpretation of Winfield Test #10 results. The Winfield impact beam 28-day design, compressive strength was f'_c= *5,000 psi*. For this f'_c the corresponding static modulus of elasticity, E_{st}, was calculated as *4,104.71 ksi*. As presented in Johns and Belanger (1981), multiplying the static modulus of elasticity, E_{st} by a dynamic amplification factor equal to *1.3* gives a dynamic modulus of elasticity. Then, the dynamic modulus of elasticity for the Winfield impact beam results in *5,336.12 ksi*. This dynamic modulus of elasticity value was compared with the resulting values obtained using the calculated beam deflection and normal strains from the Impact_Beam software. This was accomplished by fixing the maximum beam deflection or the maximum curvature at each sensor location as a target value to be matched. Impact_Beam was then executed with the corresponding time-history iterating through values for the modulus of elasticity until the target value was reached. This procedure

guarantees that the maximum experimental response and the maximum simulation response are the same. The average dynamic modulus of elasticity based on the experimental beam deflection using LD3, LD4 and LD5 sensors was 5,574.54 ksi. The average dynamic modulus of elasticity based on the strain sensors (the strains were transformed to curvatures) was 10,525 ksi.

This chapter presents the interpretation of the full-scale impact test results conducted at Winfield lock and dam. The interpretation is done by the use of Impact_Beam computer software. First, a summary of the simply supported elastic beam properties used at Winfield experiments and the summary of the velocities along the beam recorded during the experiments are presented. This is the required input data used by Impact_Beam to generate the simulation results. Then for each test, the maximum beam deflection and maximum curvature (from normal strain) is provided as input and Impact_Beam, with the corresponding force time-history, iterated varying the dynamic modulus of elasticity until the target deflection or curvature is obtained. Based on these calculations, a summary of the values for the dynamic modulus of elasticity for each test and each sensor is presented. The resulting set of calculated values for the dynamic modulus of elasticity for each sensor during each barge impact test is then averaged to produce a best estimate for the comprehensive dynamic modulus of elasticity. This comprehensive dynamic modulus of elasticity is then compared with values of dynamic modulus cited in technical literature. Finally, the interpretation of the dynamic modulus of elasticity values expressed as an amplification factor between field curvature and simulation curvature is presented.

6.2 Summary of the simply supported elastic beam properties and velocities along the beam

Impact_Beam computer program has the capability to calculate the dynamic response of a continuous elastic beam due to a moving transverse concentrated dynamic load. This section presents the basic beam properties used in the interpretation of the impact beam used at the Winfield experiment. The model has the following data;

- effective beam length (from center to center of neoprene pads) is 112.6 ft,
- the moment of inertia of the elastic beam is 517.2 ft^4,
- the cross sectional area is equal to 46 ft^2,

- the total weight per unit length of the beam is 8.2 kips/ft, which considers the hydrodynamic added mass (as discussed in Appendix H).

The force time-history used in the analysis done in this chapter corresponds to the force time-history recorded during the Winfield experiment for each barge impact test. The velocity of the dynamic load, which acts with a force normal to the beam, as it moves along the beam and the initial point of contact of the load on the beam are presented in Table 6.1. The damping ratio assigned was 2% of the critical damping for each of the twelve modes of vibration considered. The locations along the beam where the results need to be known are the same as the positions along the beam where the strain and laser deflections were recorded during the Winfield experiments. These locations for LD3, LD4, LD5, (S1B;S1F), (S2B;S2F), (S3B;S3F), (S4B;S4F) and (S5B;S5F) are the following 71.0425 ft, 56.38625 ft, 41.7196 ft, 80.28208333 ft, 68.2925 ft, 56.3029 ft, 44.31333 ft and 32.32375 ft, respectively.

Table 6.1. Velocity during contact with impact beam (v_x) at Winfield.

Test Number	Angle of the Bow	Velocity at Impact		Location from Target [measured from beam center line]	Velocity during Contact with Impact Beam (Vx)		Notes
		ft/sec	mph	(feet)	ft/sec	mph	
Test 6	15.5	1.55	1.06	7.5	1.55	1.057	
Test 7	20.2	1.53	1.04	9.7	1.53	1.044	
Test 8	10.2	3	2.05	-18.9	2.99	2.041	
Test 9	13.6	2.22	1.51	-9.7	2.21	1.509	
Test 10	15.8	2.99	2.04	7.8	2.97	2.03	
Test 11	6.9	0.8	0.55	35.8	0.78	0.535	
Test 12	6.1	1.41	0.96	15.9	1.4	0.954	
Test 13	10.2	1.5	1.02	5.6	1.5	1.022	
Test 14	11.7	1.48	1.01	-15.2	1.46	0.998	
Test 15	11.3	1.6	1.09	-26.2	1.58	1.079	
Test 16	9.7	3.55	2.42	4.6	3.55	2.42	
Test 17	21.2	1.44	0.98	3.8	1.46	0.998	
Test 18	16.8	2.19	1.5	-18	2.18	1.486	
Test 19	17.3	2.25	1.53	-12.7	2.21	1.507	Possum used between impact beam and load cell bumper
Test 20	13	2.81	1.92	3.8	2.79	1.9	
Test 21	13	2.8	1.91	4.5	2.78	1.892	Possum used between impact beam and load cell bumper
Test 22	9.6	1.61	1.1	-25.1	NA	NA	Possum used between impact beam and load cell bumper
Test 23	13.8	2.87	1.96	4.1	2.74	1.87	Possum used between impact beam and load cell bumper

6.3 Estimation of the dynamic modulus of elasticity based on experimental beam deflection using Impact_Beam

This section will present the results of estimating the dynamic modulus of elasticity for the Winfield impact beam based on the experimental beam deflection. These moduli are obtained by fixing the maximum experimental beam deflection at each sensor (LD3, LD4 and LD5) as a target value. Then, Impact_Beam is iterated, modifying the modulus of elasticity until the target beam deflection is obtained. This procedure guarantees that the peak simulation value is the same as the peak experimental value. The resulting dynamic modulus of elasticity for each case is presented in Figures 6.1 through 6.39.

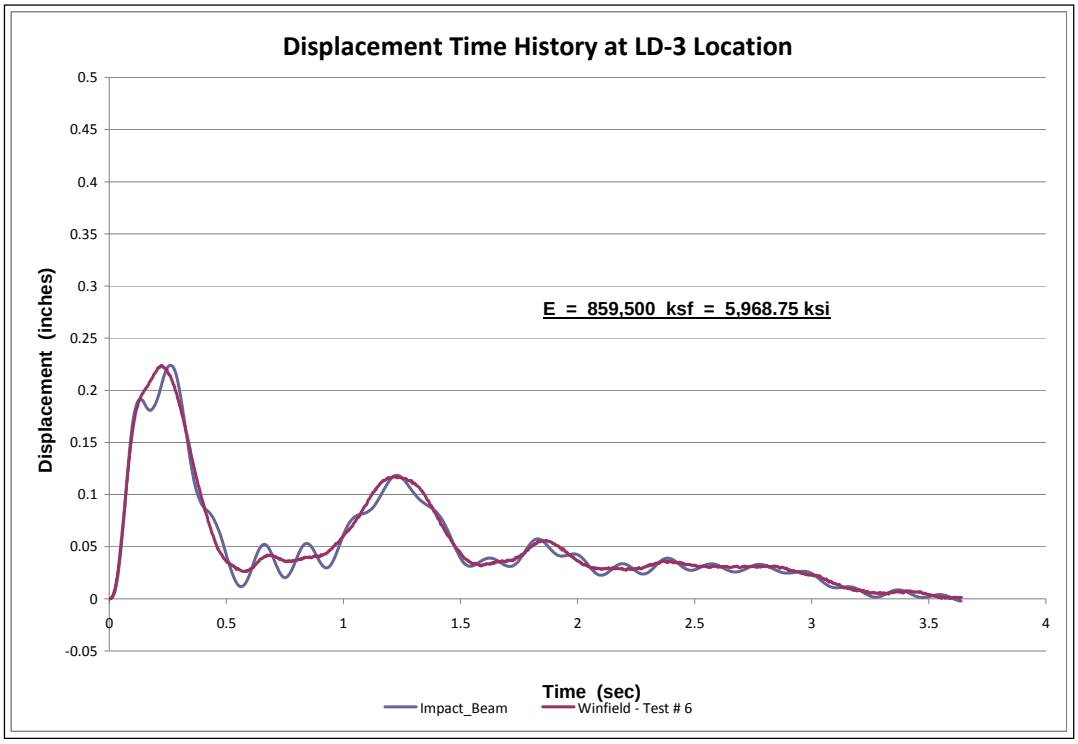

Figure 6.1. E_{dyn} estimation based on experimental beam displacement at LD3-Test #6.

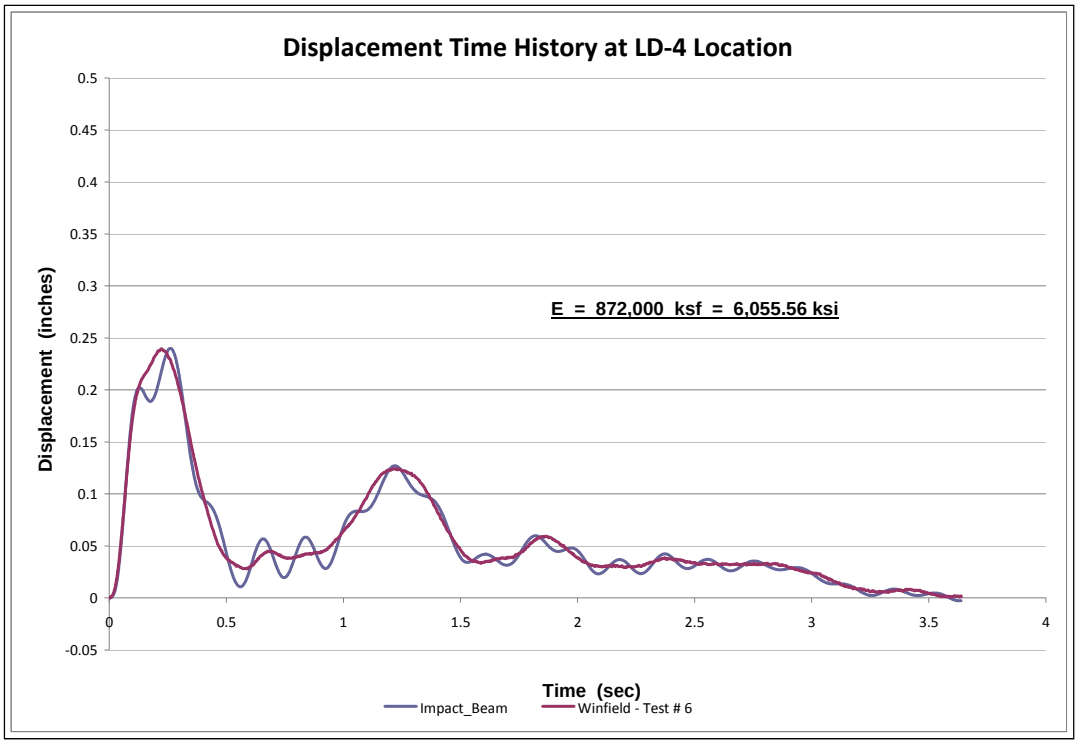

Figure 6.2. E_{dyn} estimation based on experimental beam displacement at LD4-Test # 6.

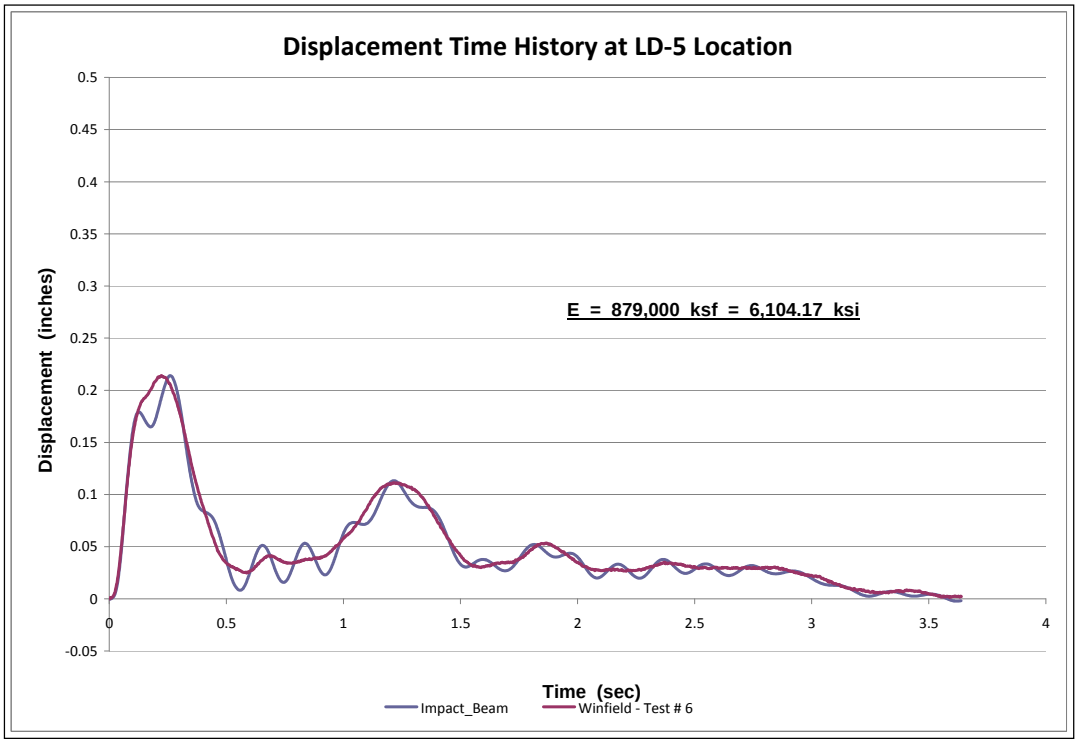

Figure 6.3. E_{dyn} estimation based on experimental beam displacement at LD5-Test # 6.

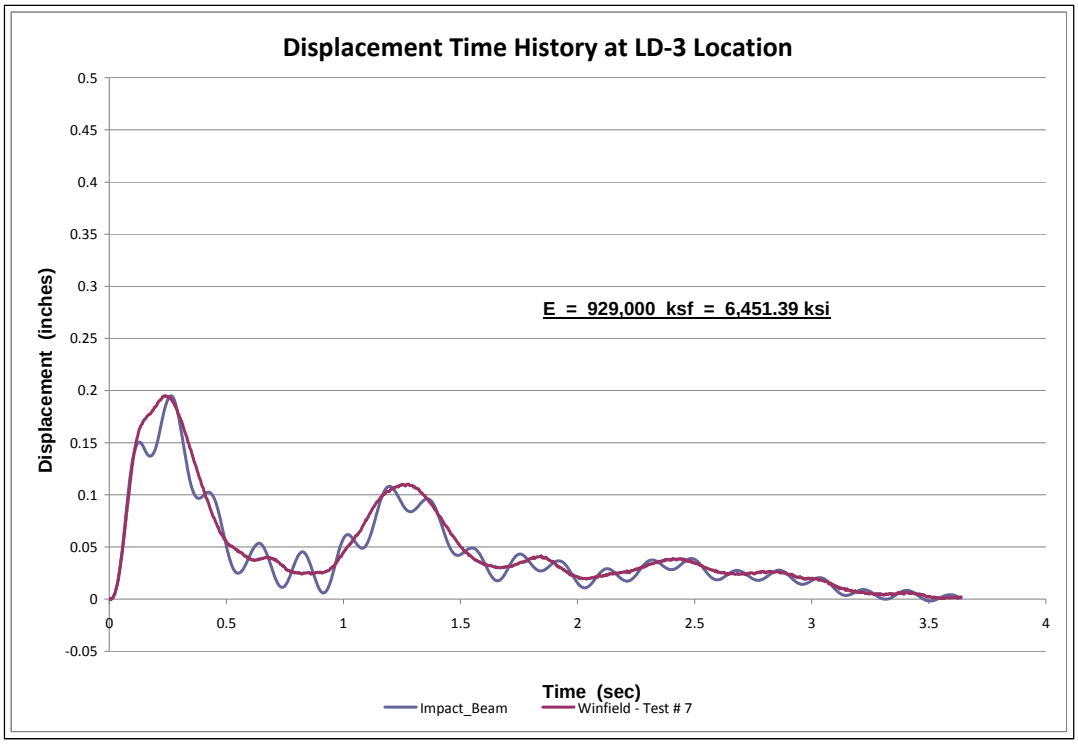

Figure 6.4. E_{dyn} estimation based on experimental beam displacement at LD3-Test # 7.

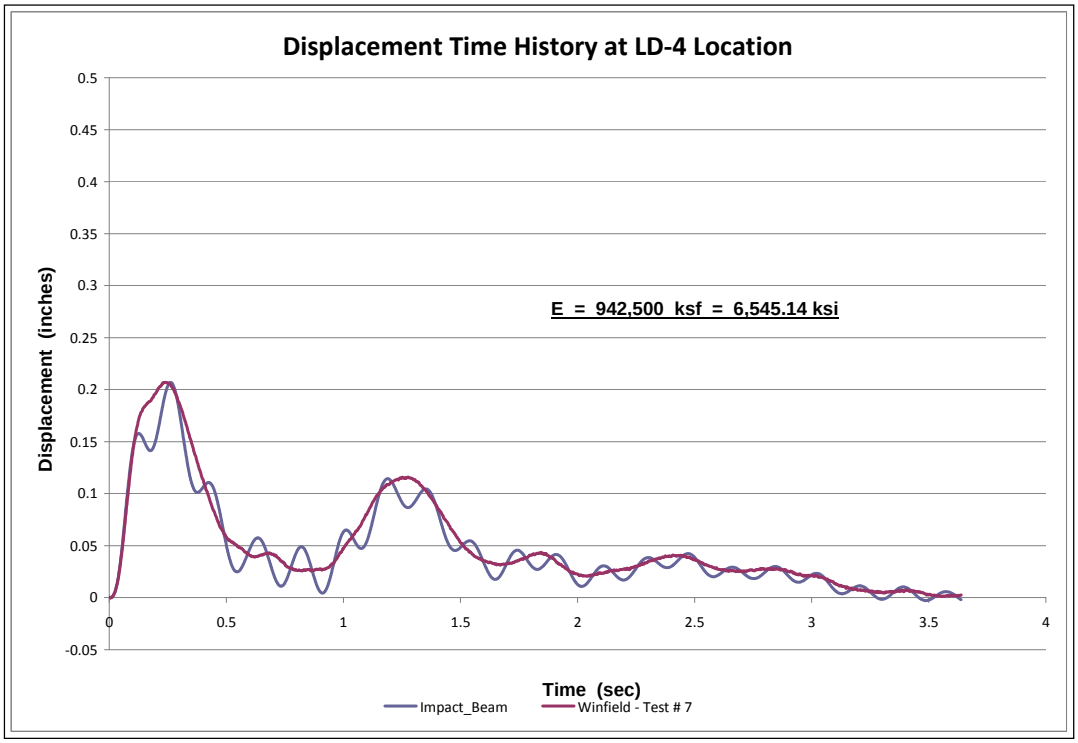

Figure 6.5. E_{dyn} estimation based on experimental beam displacement at LD4-Test # 7.

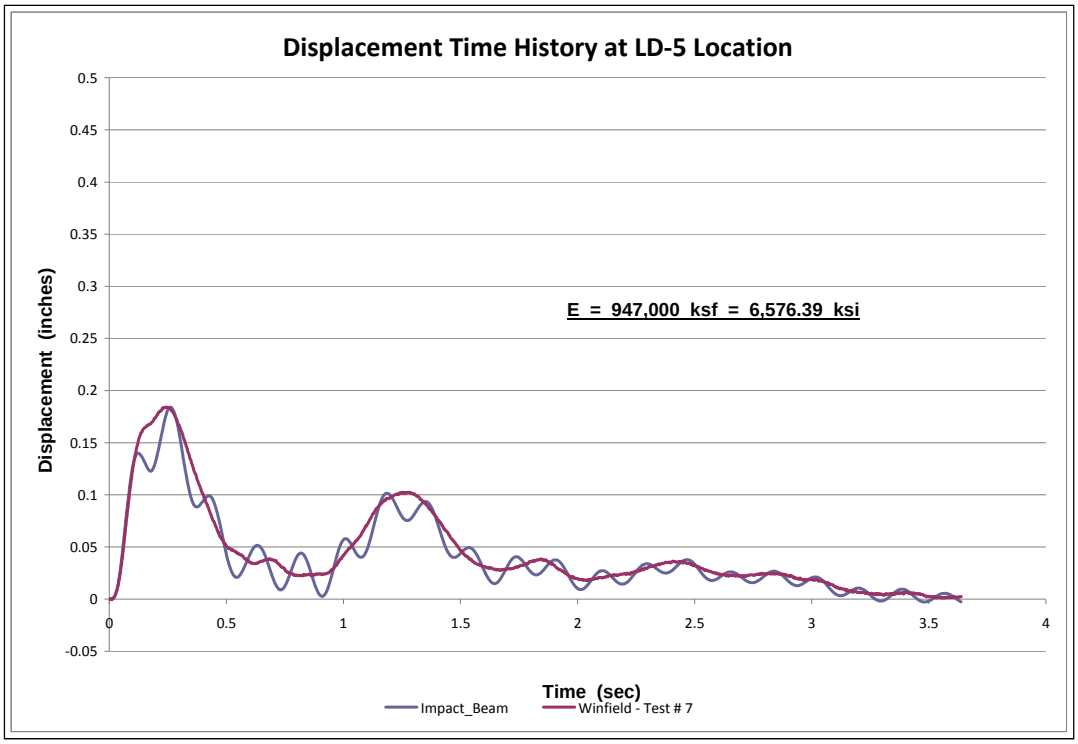

Figure 6.6. E_{dyn} estimation based on experimental beam displacement at LD5-Test # 7.

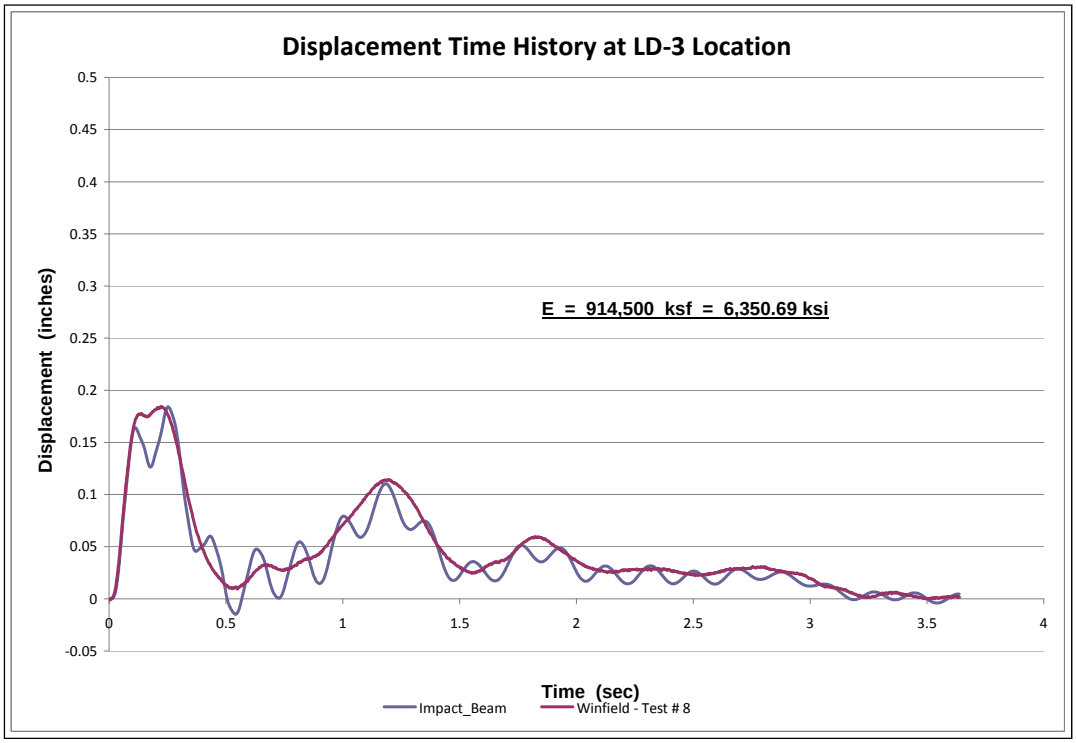

Figure 6.7. E_{dyn} estimation based on experimental beam displacement at LD3-Test # 8.

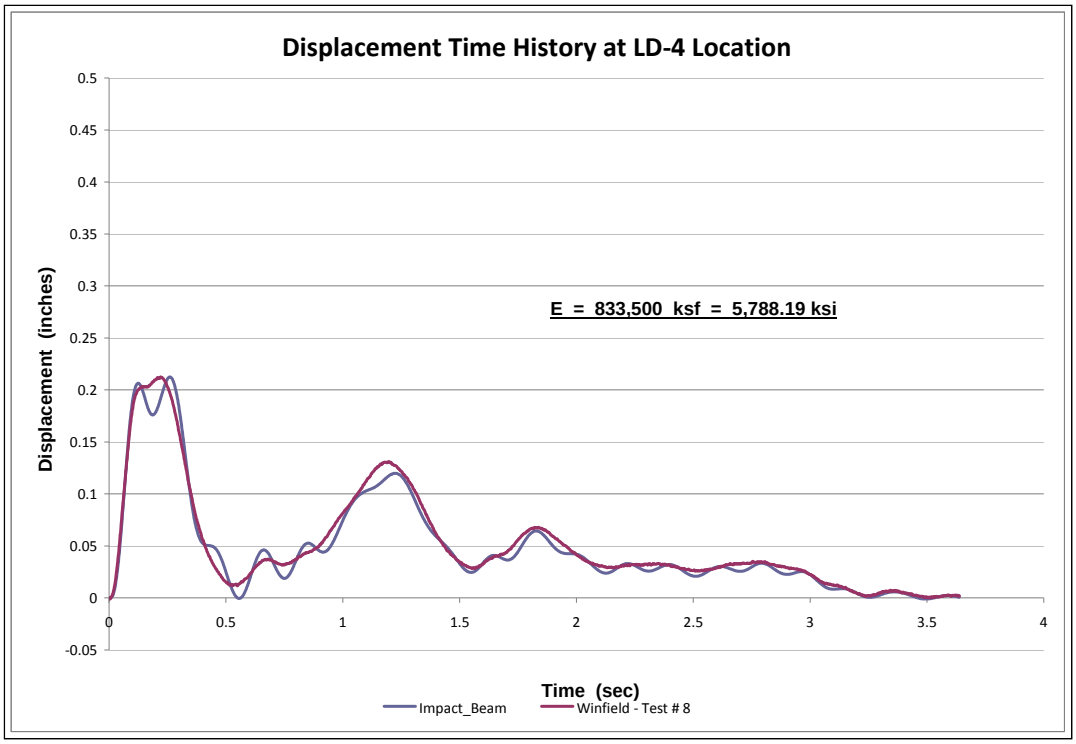

Figure 6.8. E_{dyn} estimation based on experimental beam displacement at LD4-Test # 8.

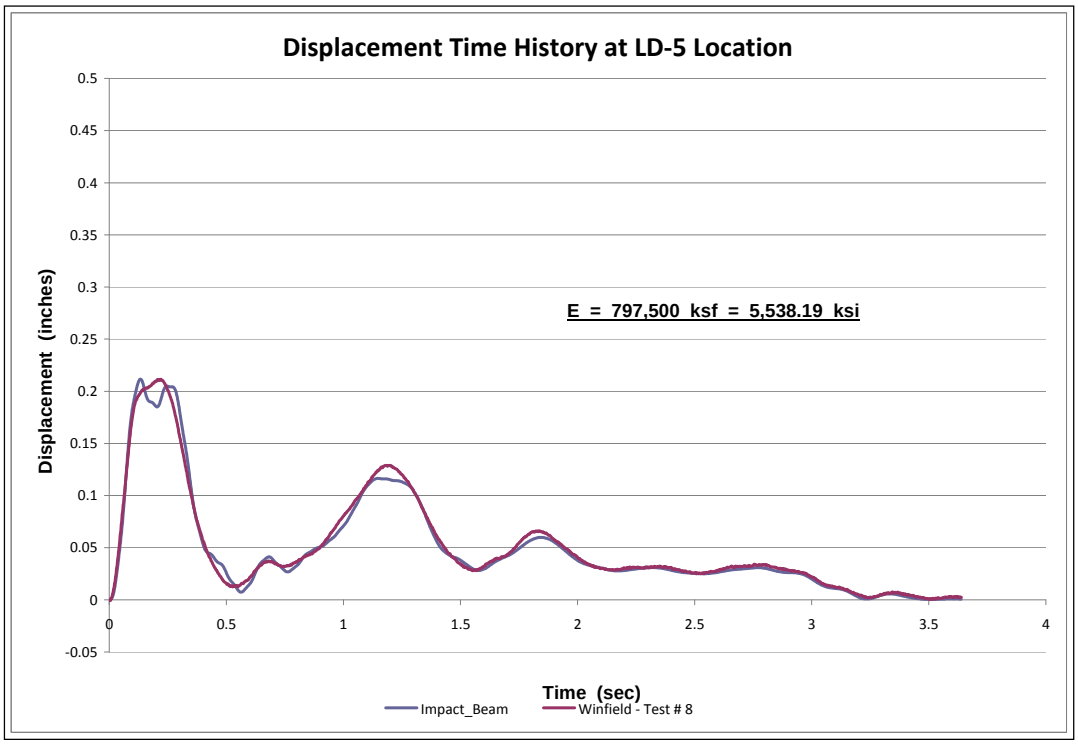

Figure 6.9. E_{dyn} estimation based on experimental beam displacement at LD5-Test # 8.

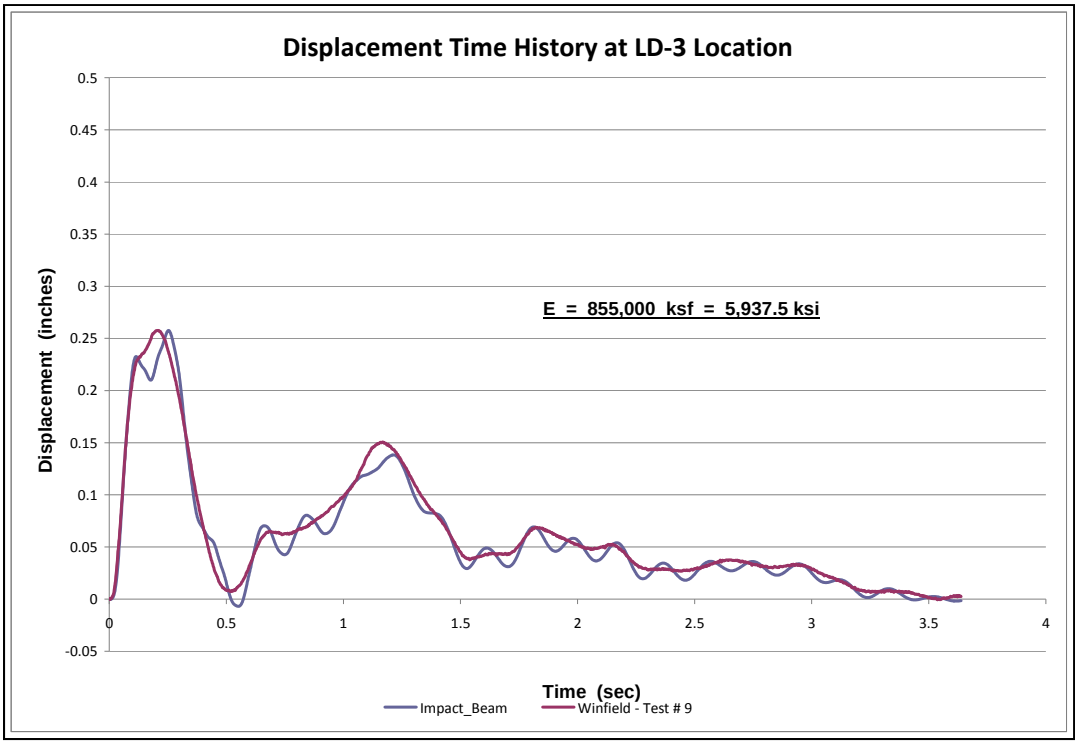

Figure 6.10. E_{dyn} estimation based on experimental beam displacement at LD3-Test #9.

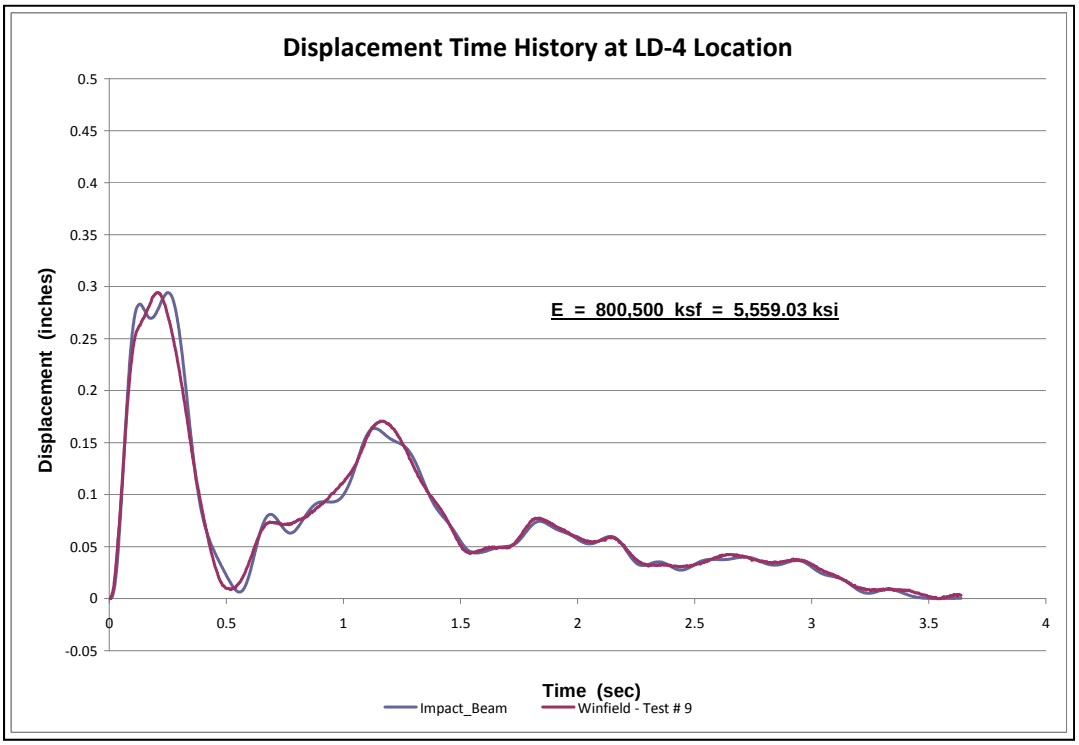

Figure 6.11. E_{dyn} estimation based on experimental beam displacement at LD4-Test # 9.

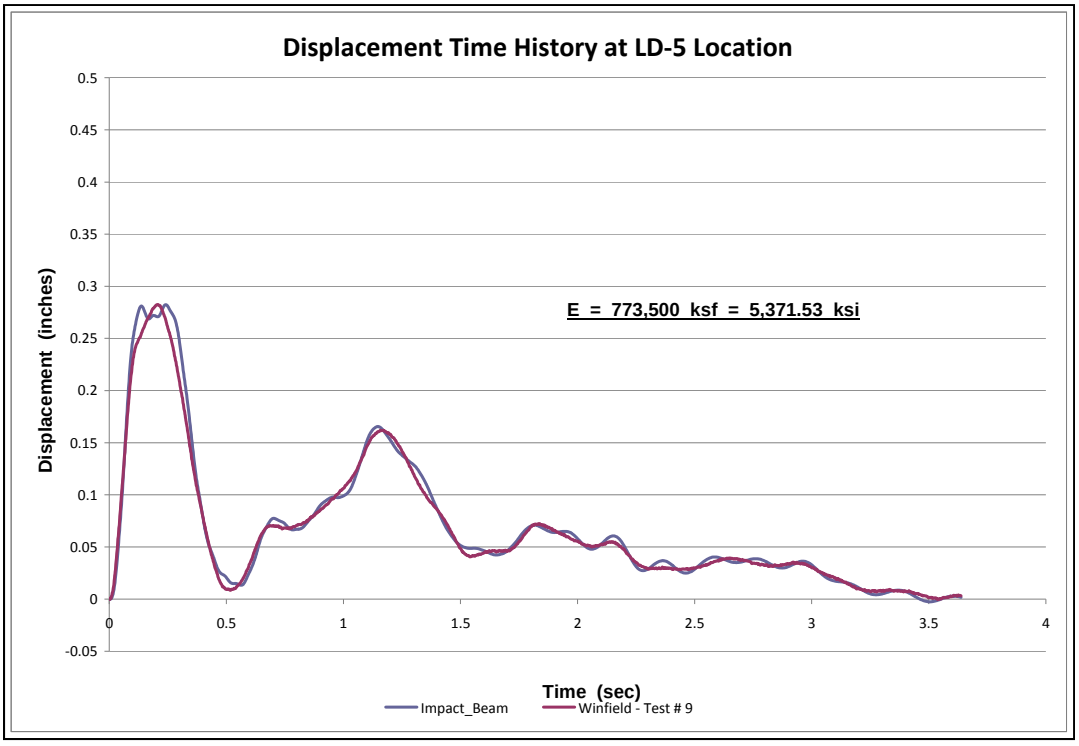

Figure 6.12. E_{dyn} estimation based on experimental beam displacement at LD5-Test # 9.

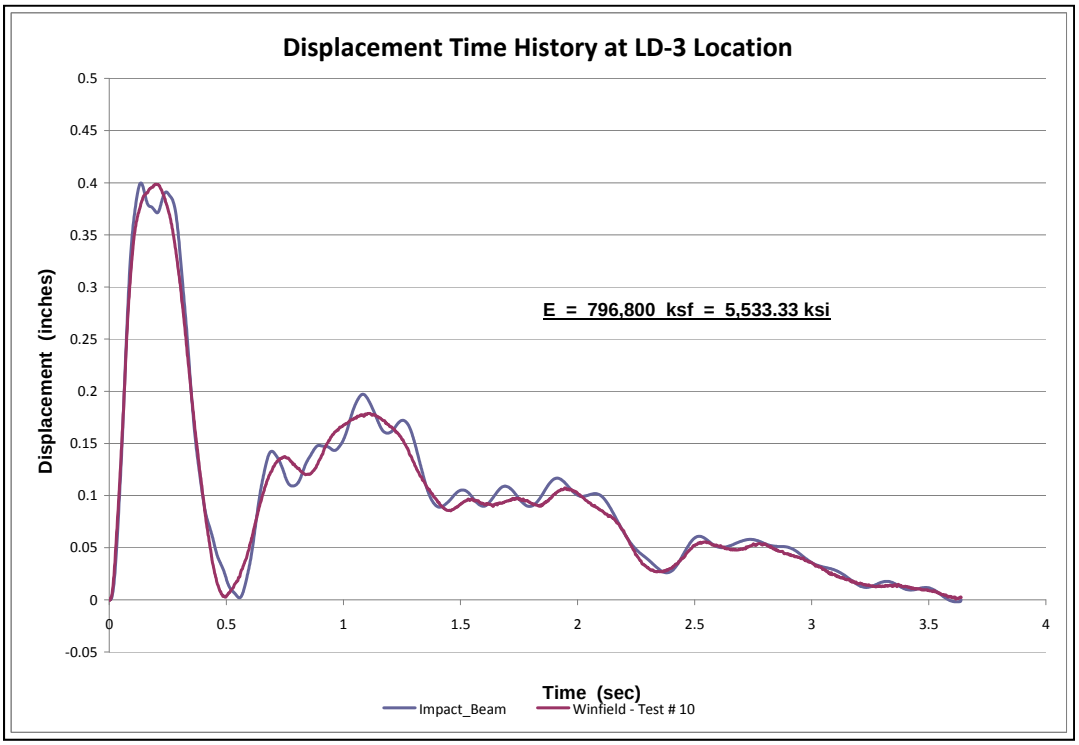

Figure 6.13. E_{dyn} estimation based on experimental beam displacement at LD3-Test #10.

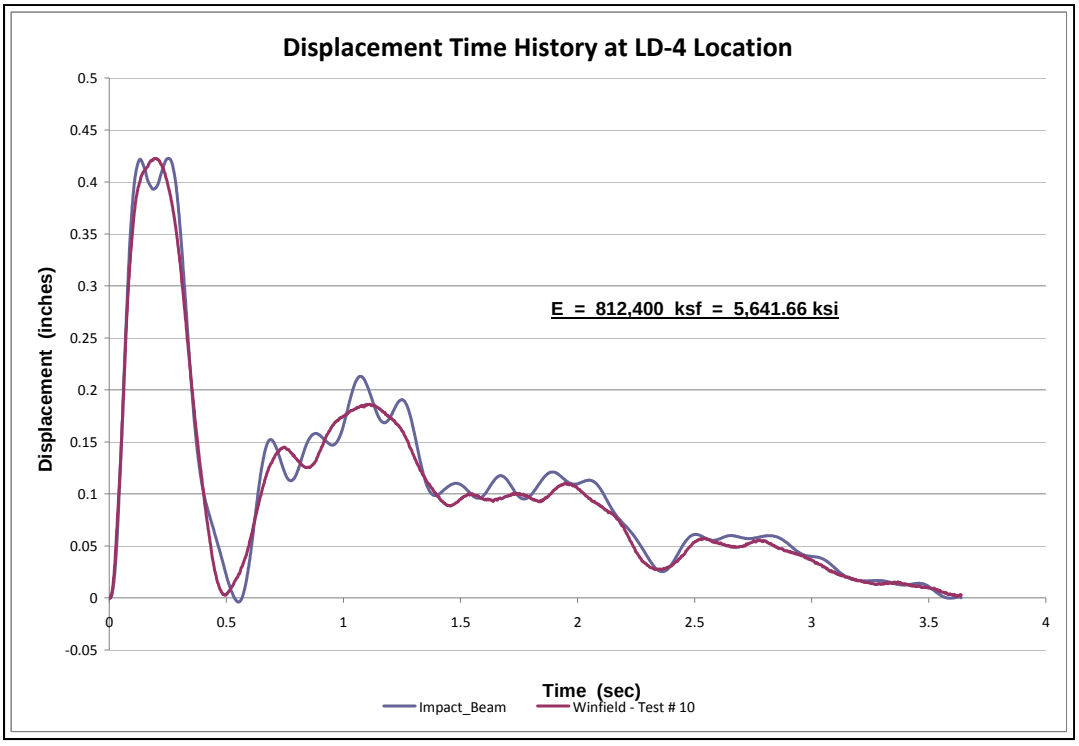

Figure 6.14. E_{dyn} estimation based on experimental beam displacement at LD4-Test #10.

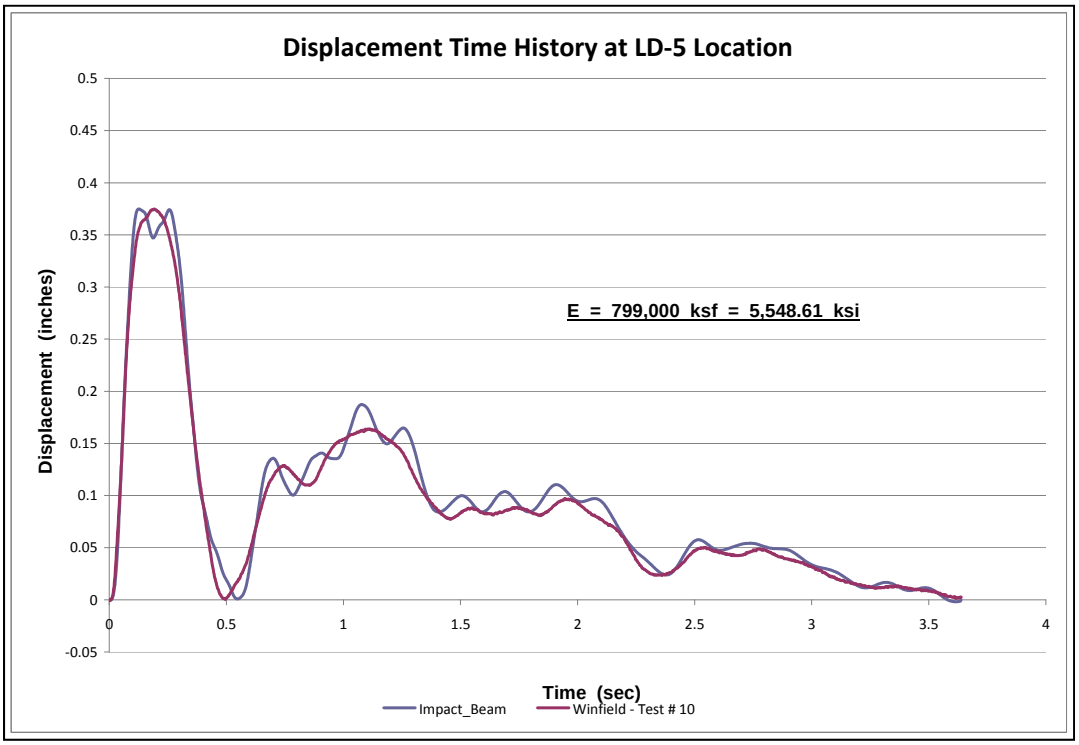

Figure 6.15. E_{dyn} estimation based on experimental beam displacement at LD5-Test #10.

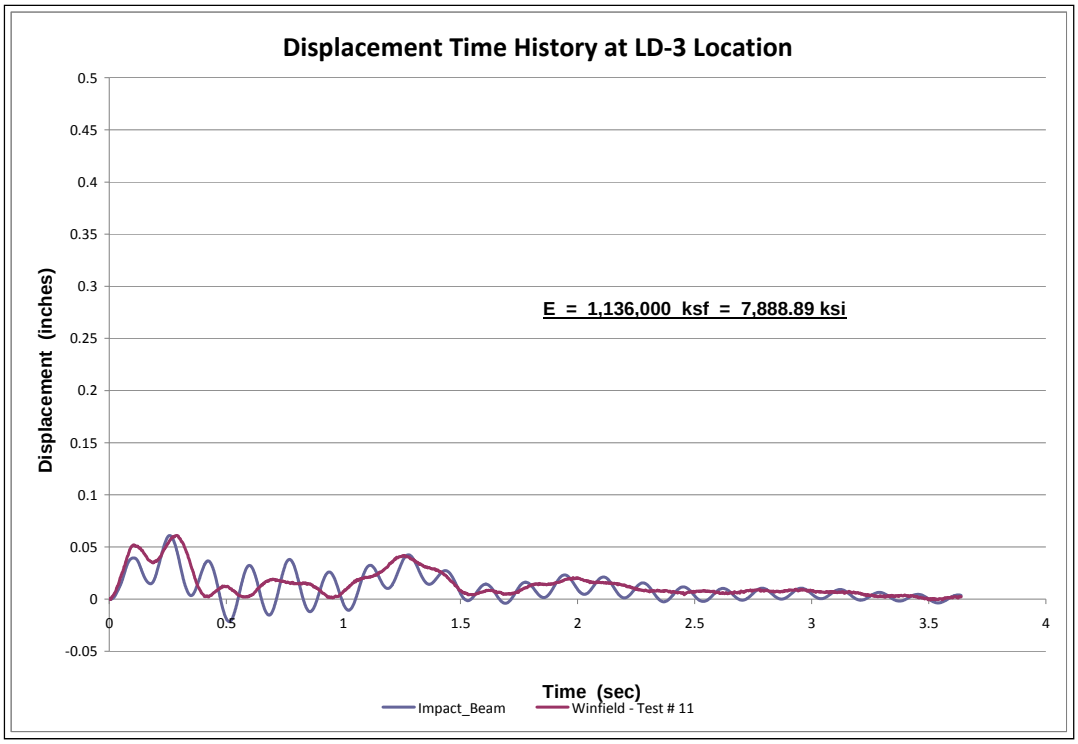

Figure 6.16. E_{dyn} estimation based on experimental beam displacement at LD3-Test #11.

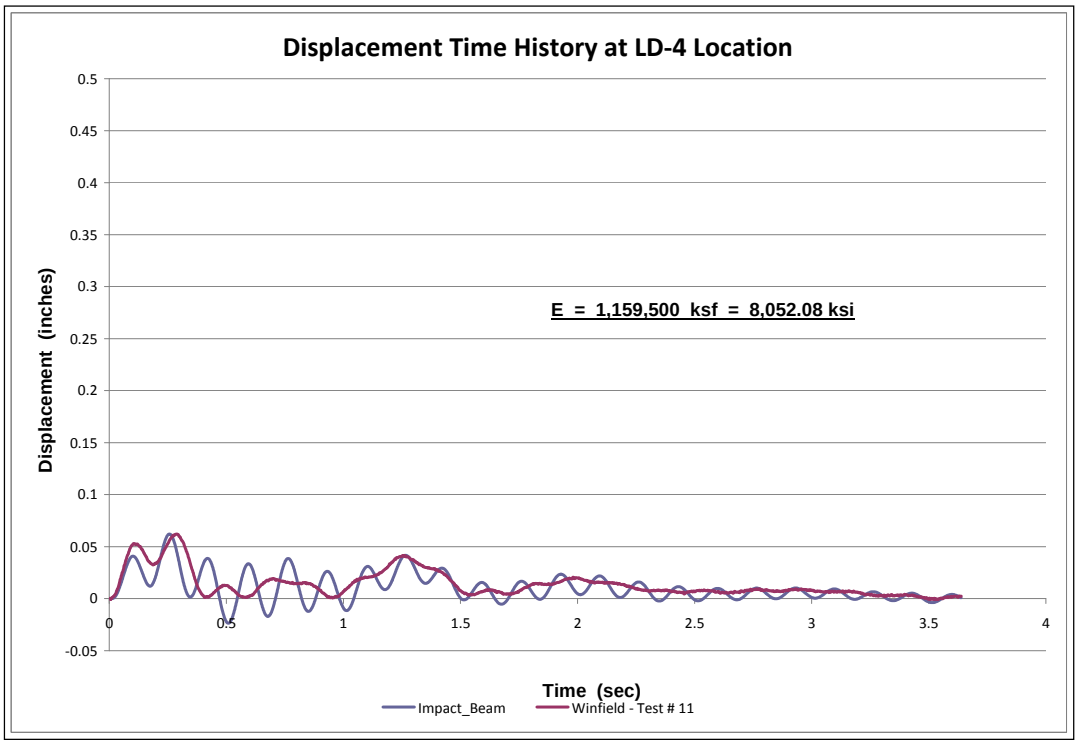

Figure 6.17. E_{dyn} estimation based on experimental beam displacement at LD4-Test #11.

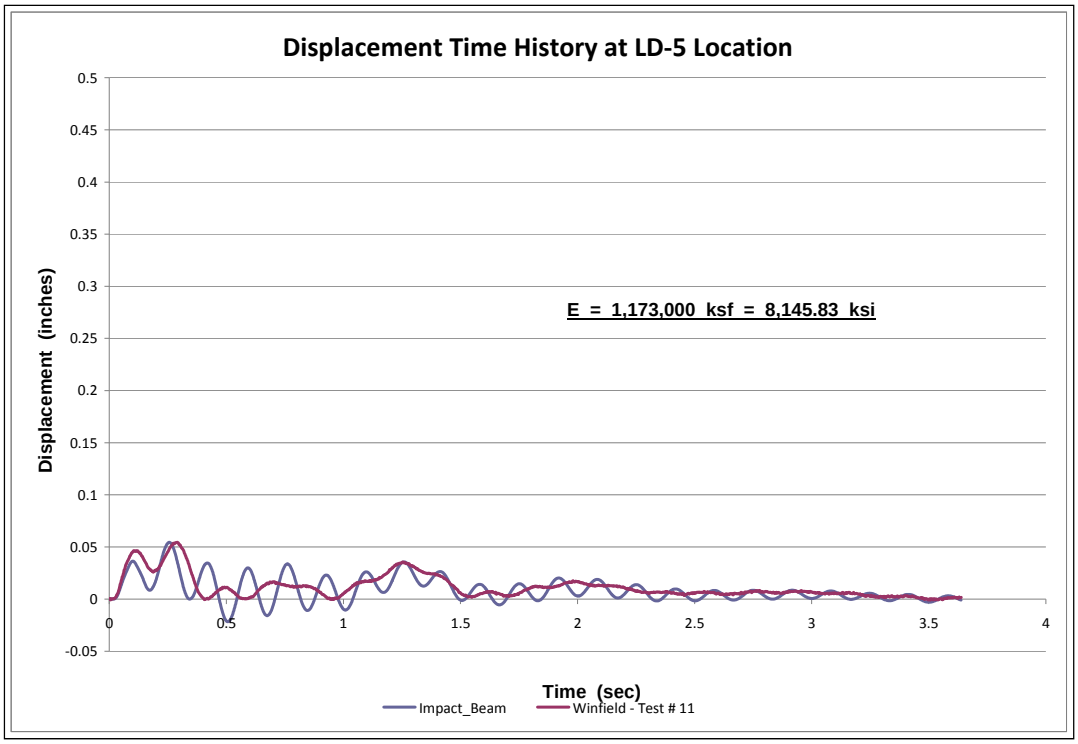

Figure 6.18. E_{dyn} estimation based on experimental beam displacement at LD5-Test #11.

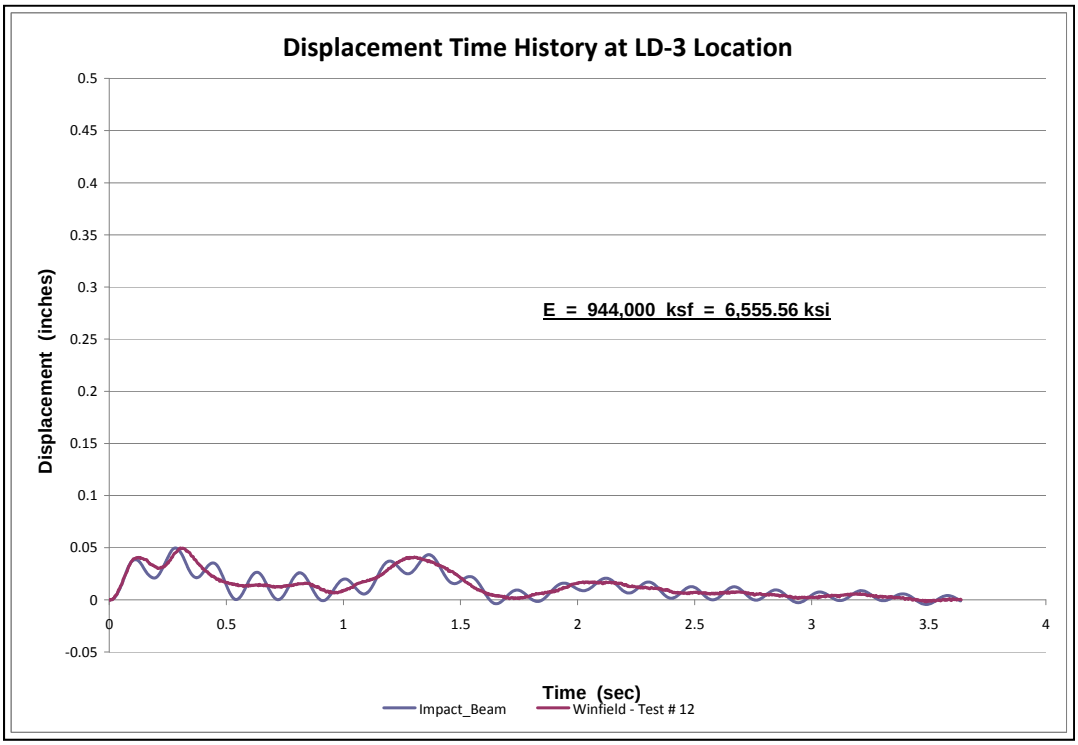

Figure 6.19. E_{dyn} estimation based on experimental beam displacement at LD3-Test #12.

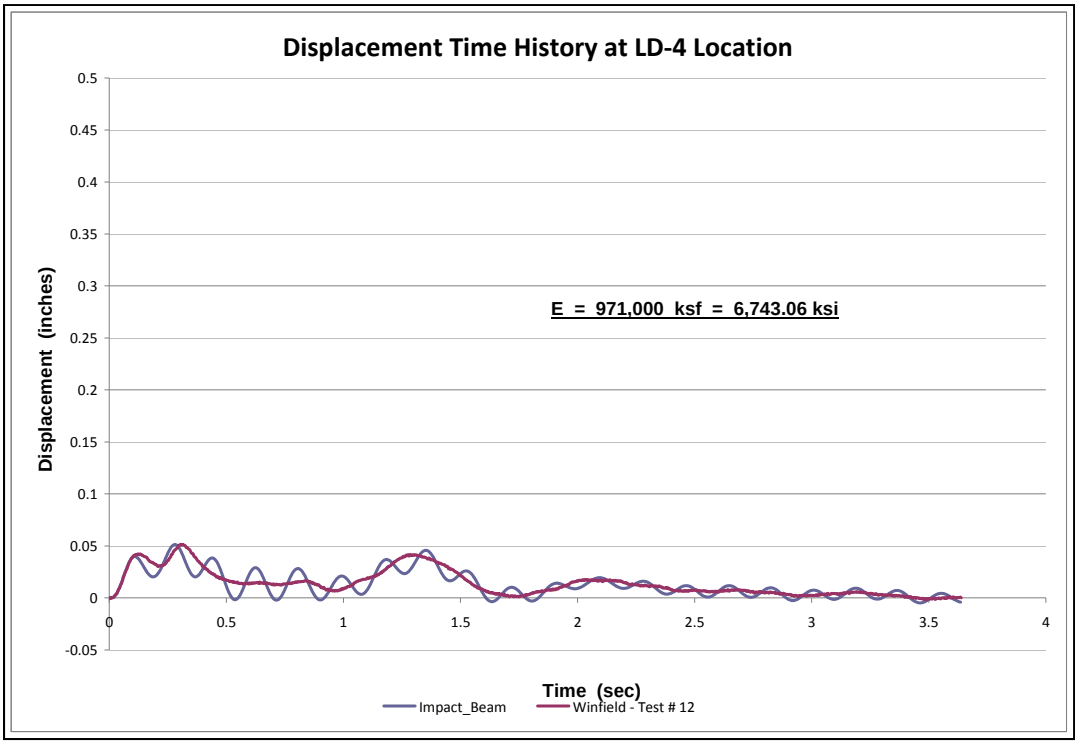

Figure 6.20. E_{dyn} estimation based on experimental beam displacement at LD4-Test #12.

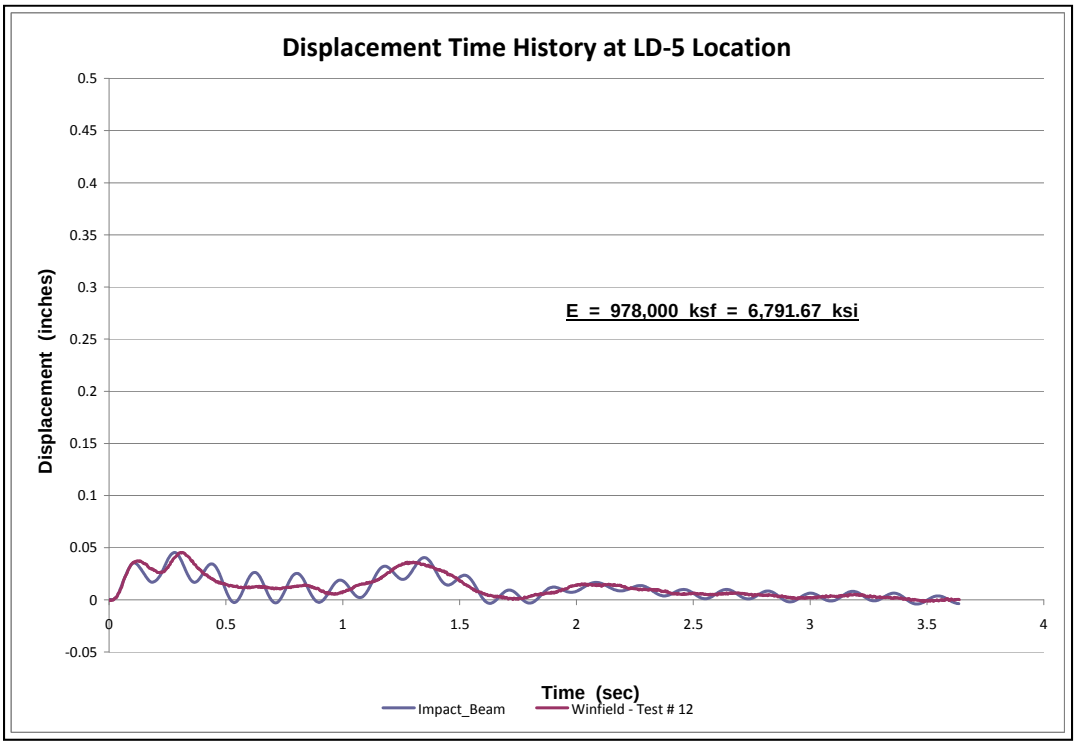

Figure 6.21. E_{dyn} estimation based on experimental beam displacement at LD5-Test #12.

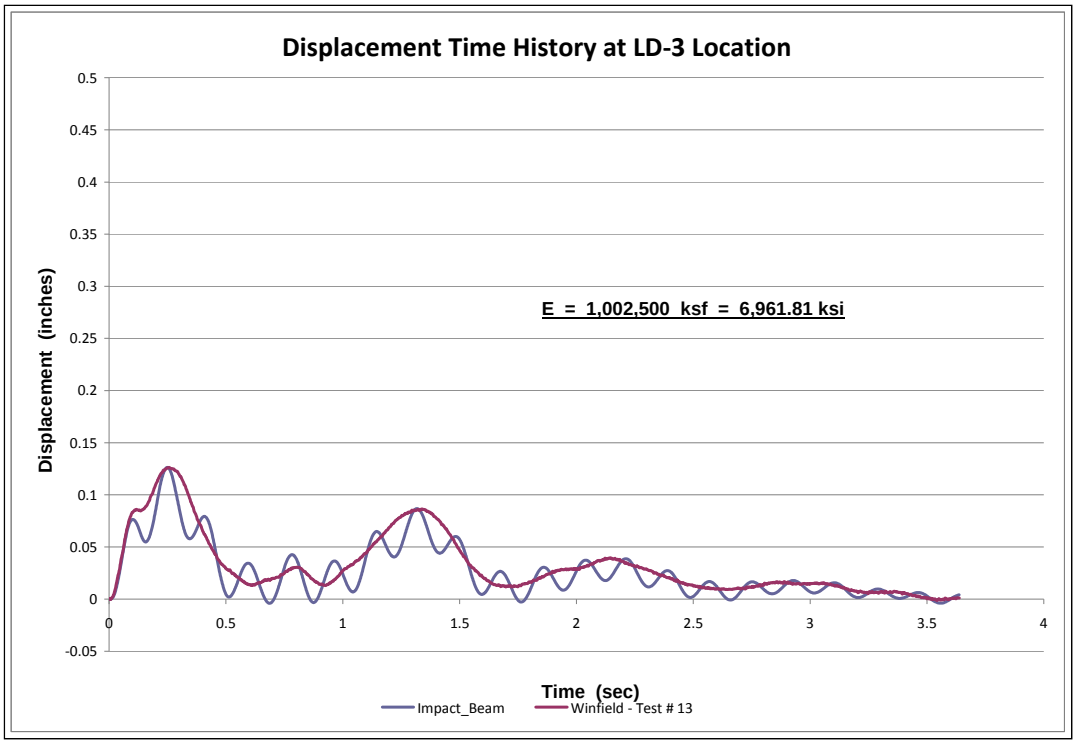

Figure 6.22. E_{dyn} estimation based on experimental beam displacement at LD3-Test #13.

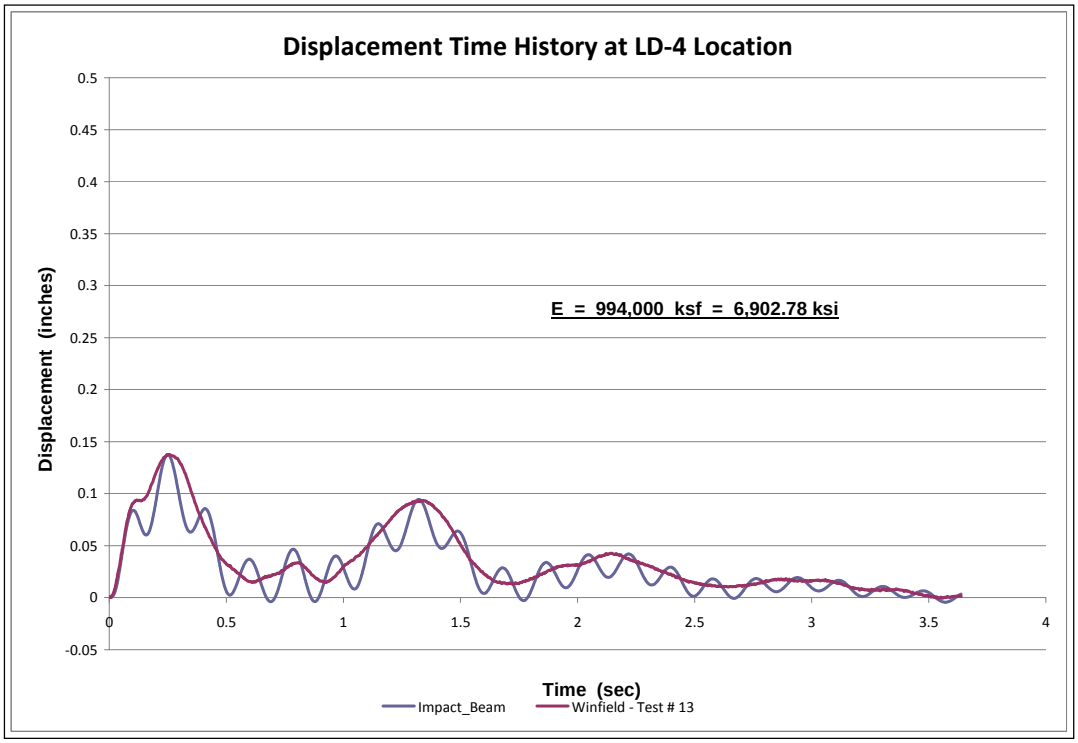

Figure 6.23. E_{dyn} estimation based on experimental beam displacement at LD4-Test #13.

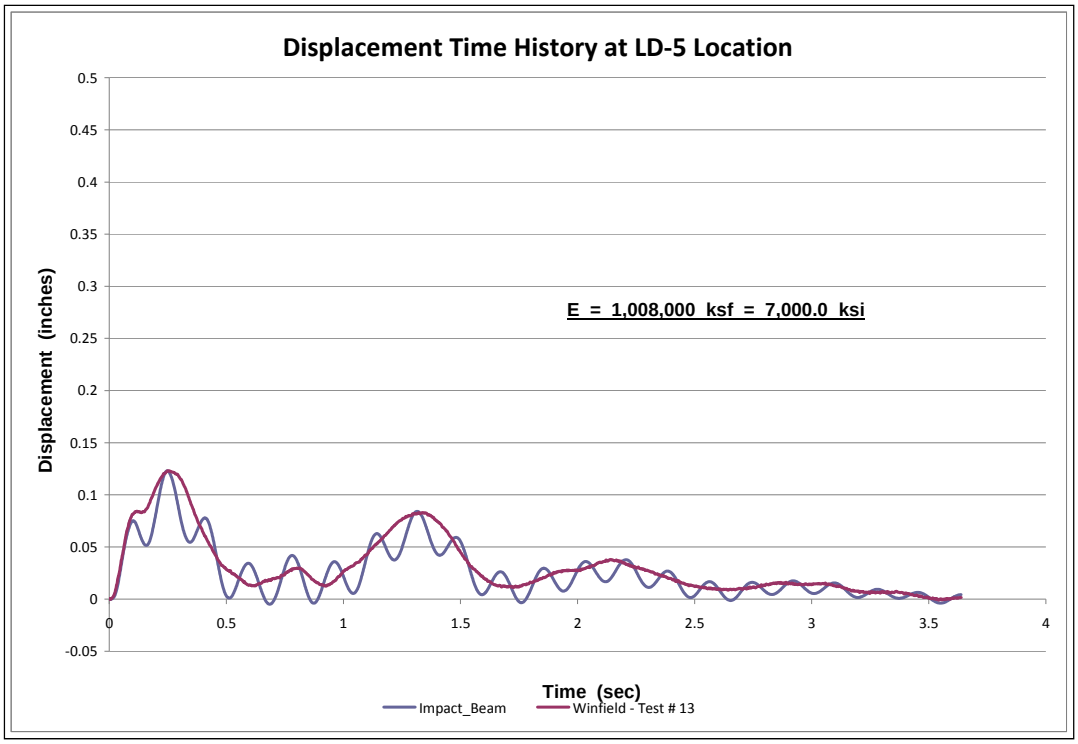

Figure 6.24. E_{dyn} estimation based on experimental beam displacement at LD5-Test #13.

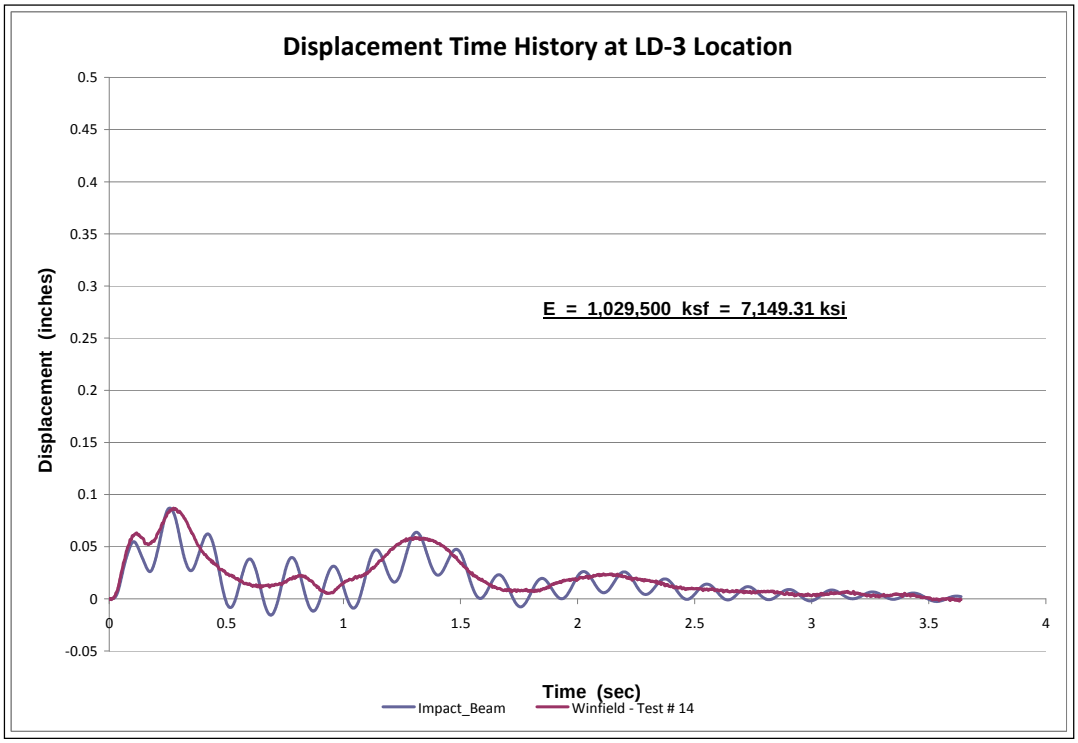

Figure 6.25. E_{dyn} estimation based on experimental beam displacement at LD3-Test #14.

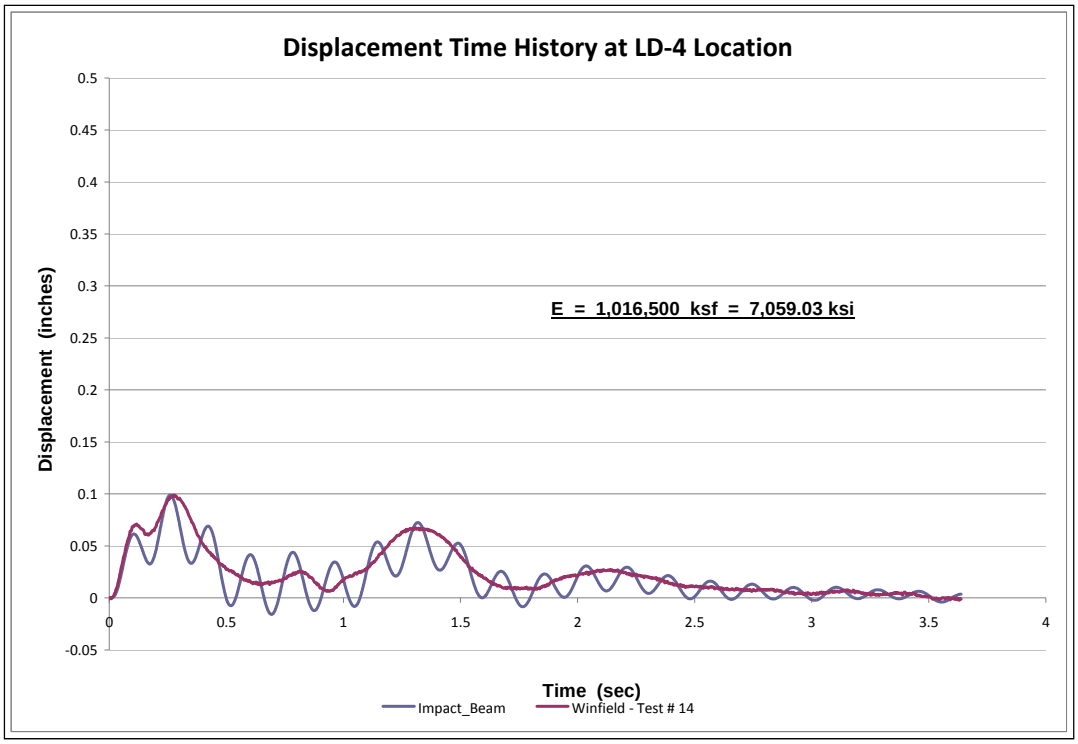

Figure 6.26. E_{dyn} estimation based on experimental beam displacement at LD4-Test #14.

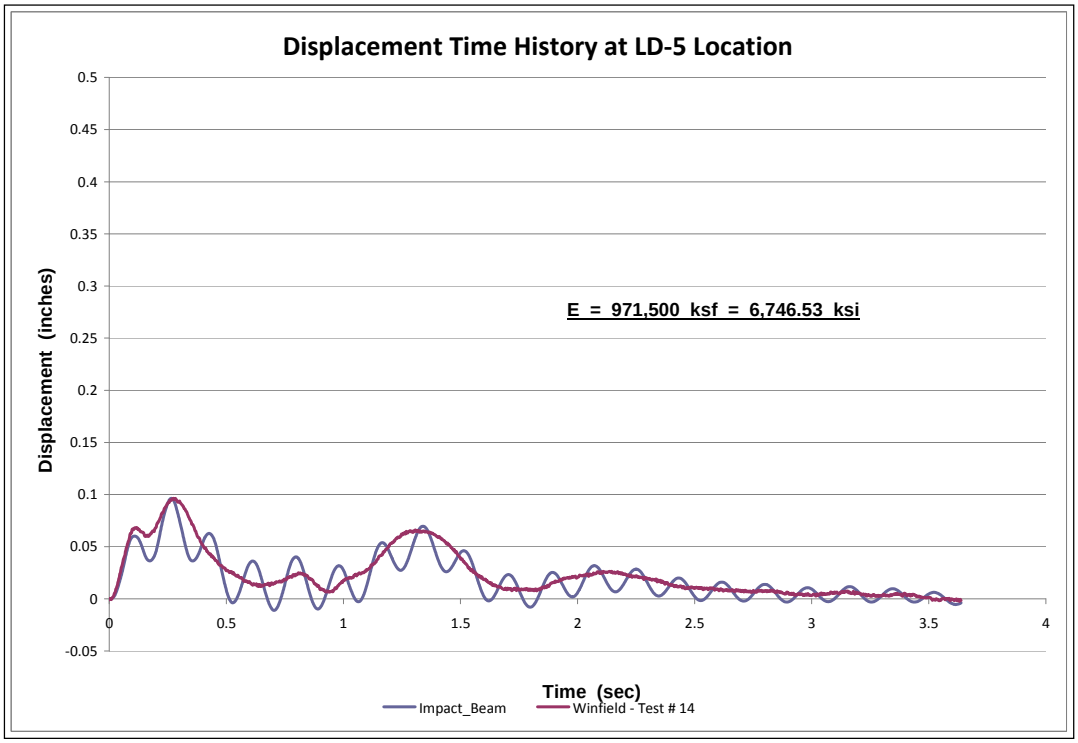

Figure 6.27. E_{dyn} estimation based on experimental beam displacement at LD5-Test #14.

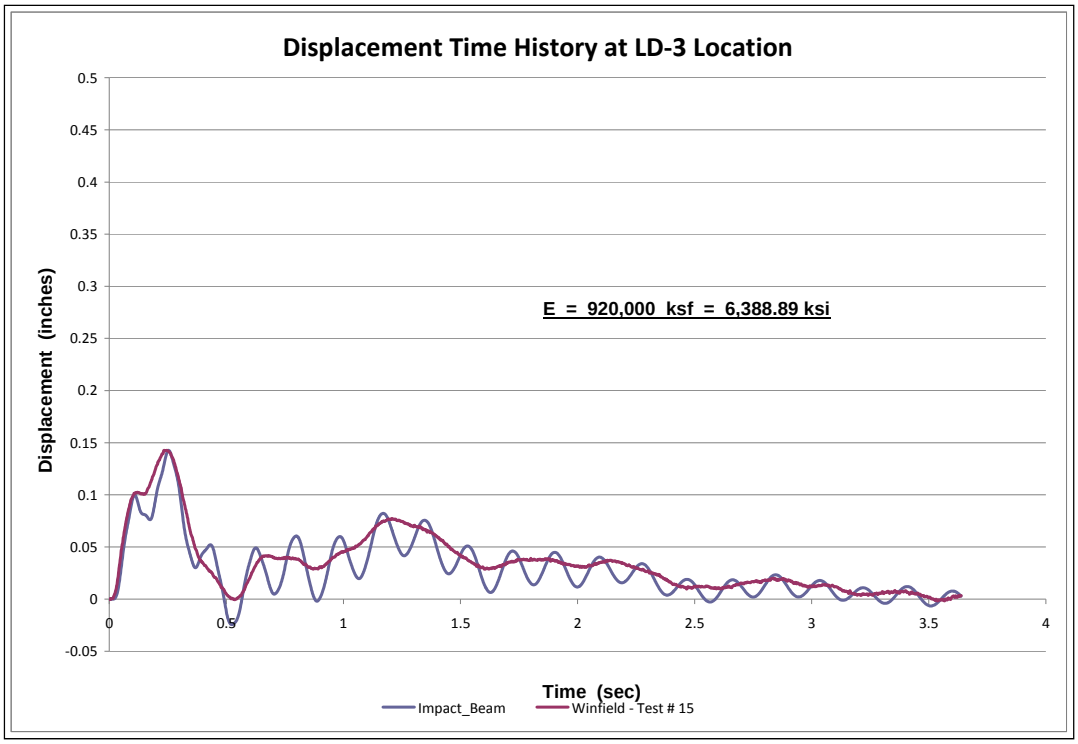

Figure 6.28. E_{dyn} estimation based on experimental beam displacement at LD3-Test #15.

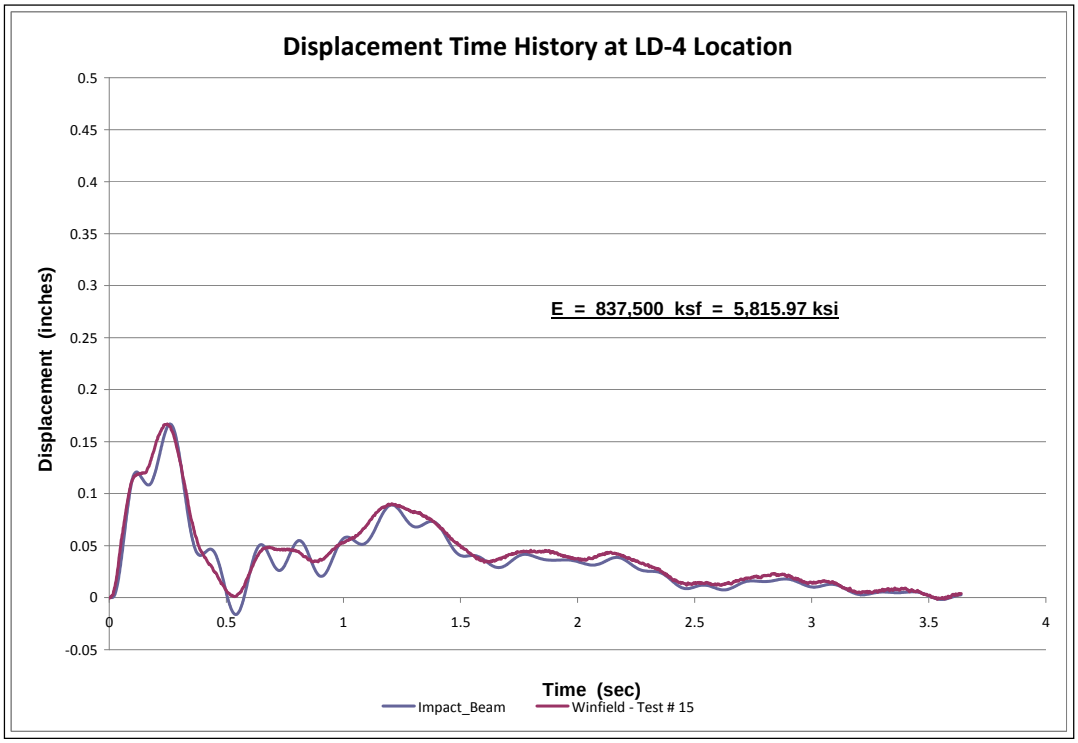

Figure 6.29. E_{dyn} estimation based on experimental beam displacement at LD4-Test #15.

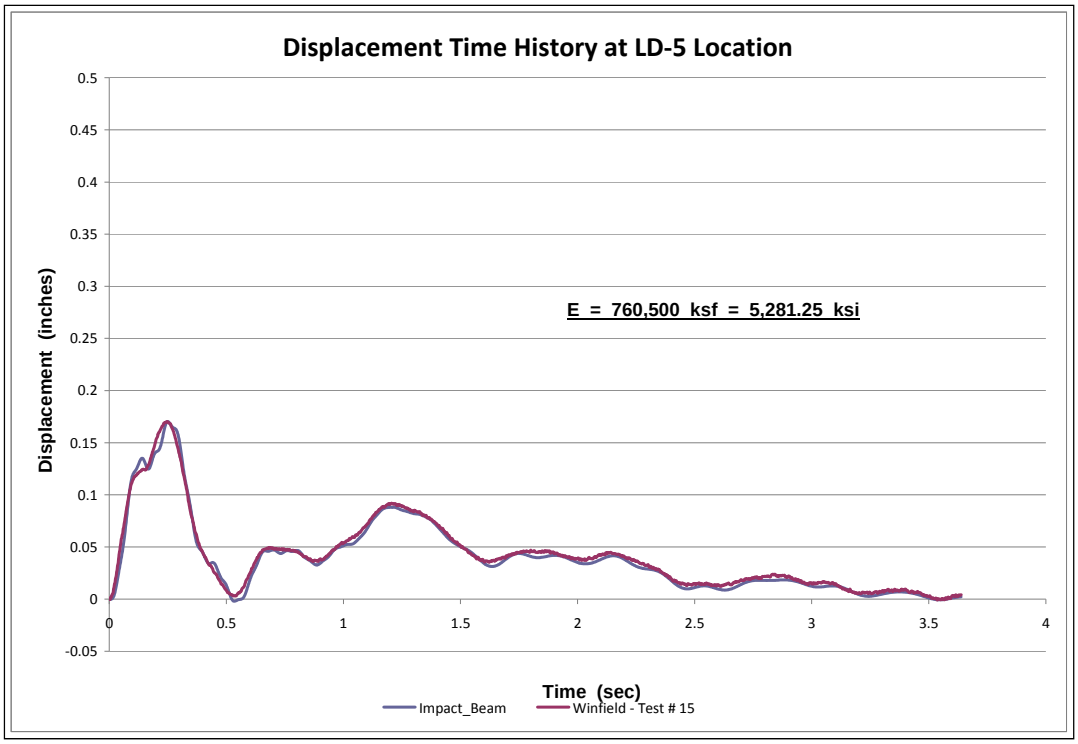

Figure 6.30. E_{dyn} estimation based on experimental beam displacement at LD5-Test #15.

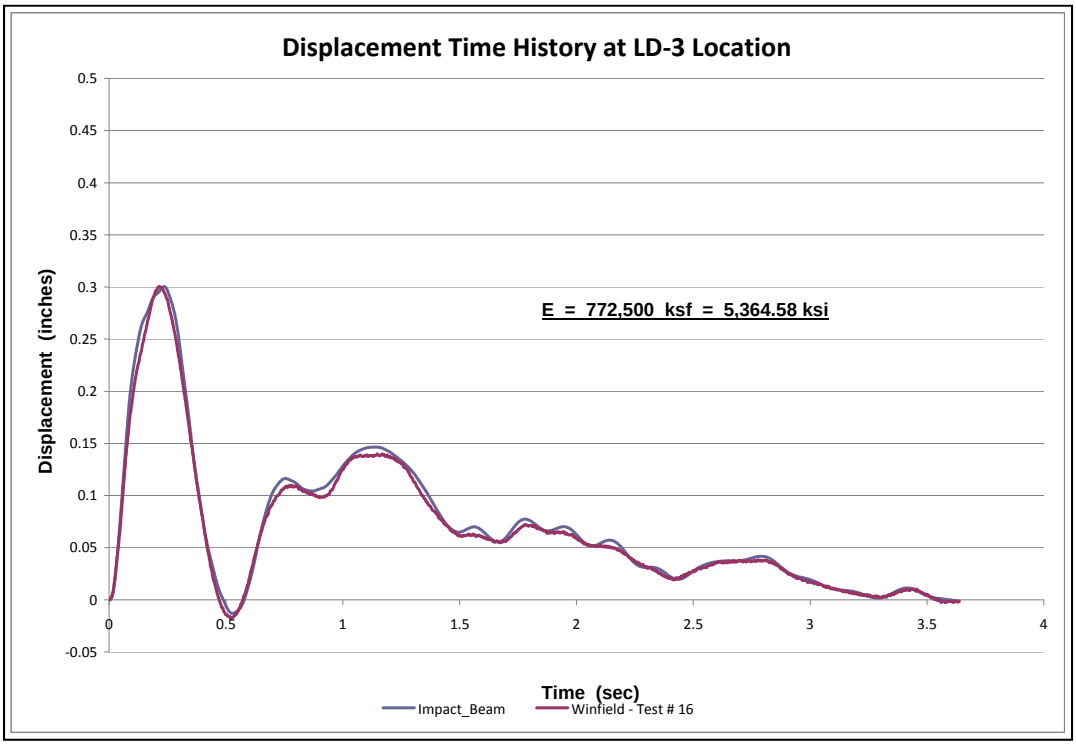

Figure 6.31. E_{dyn} estimation based on experimental beam displacement at LD3-Test #16.

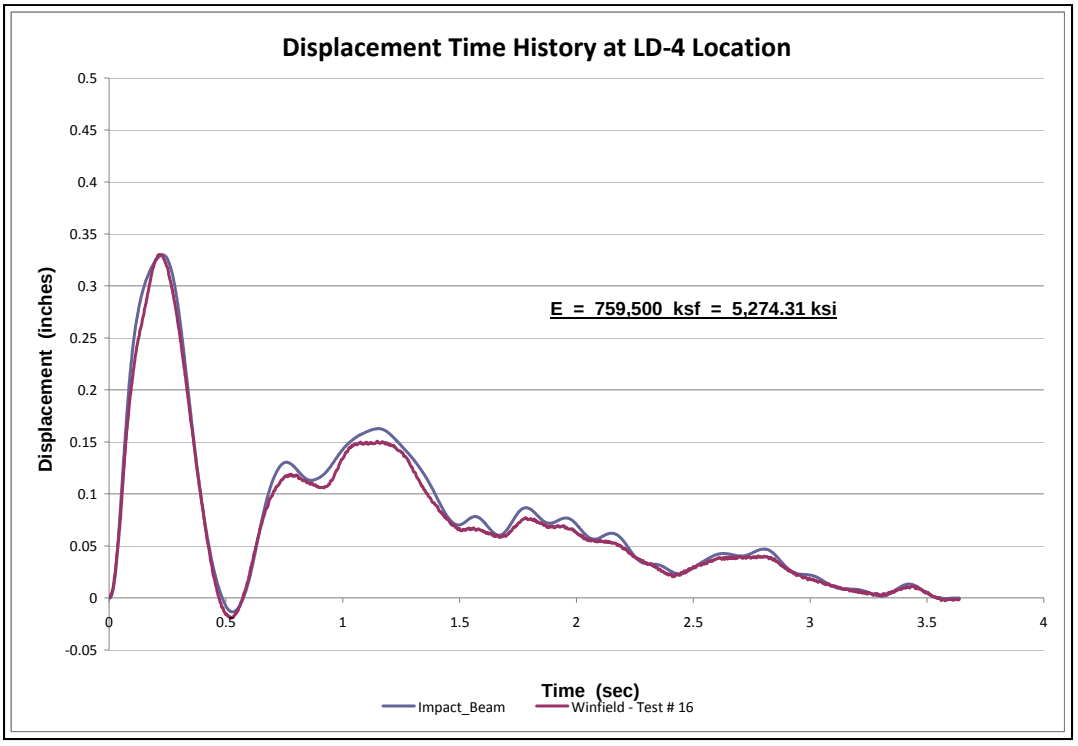

Figure 6.32. E_{dyn} estimation based on experimental beam displacement at LD4-Test #16.

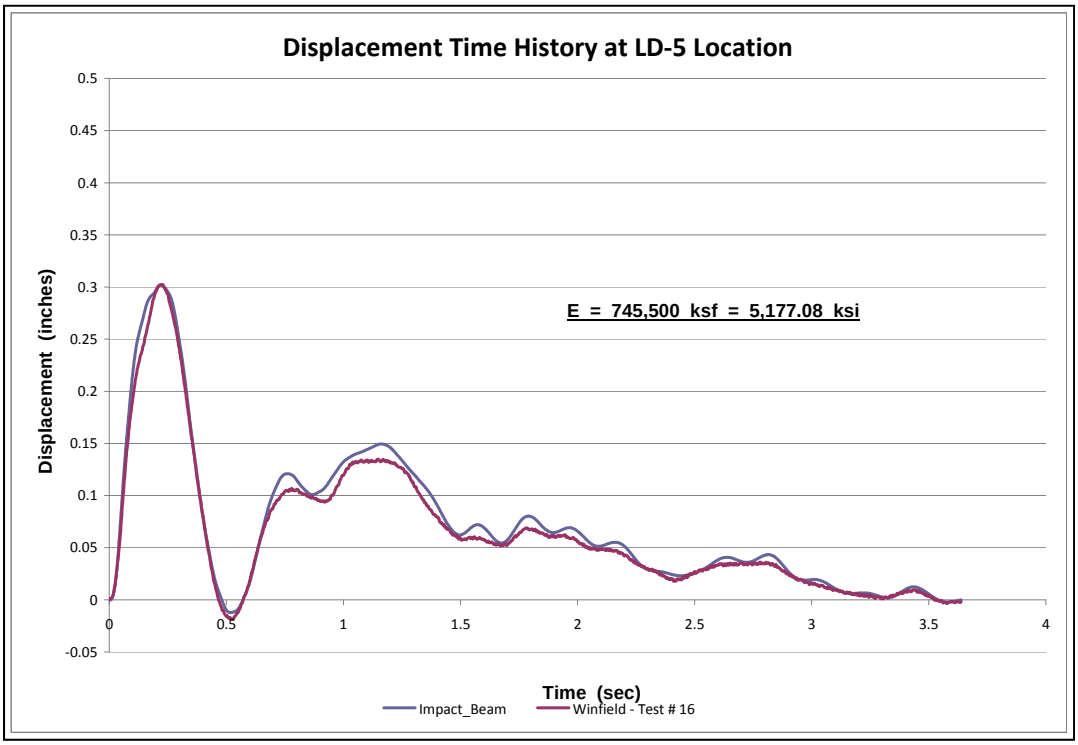

Figure 6.33. E_{dyn} estimation based on experimental beam displacement at LD5-Test #16.

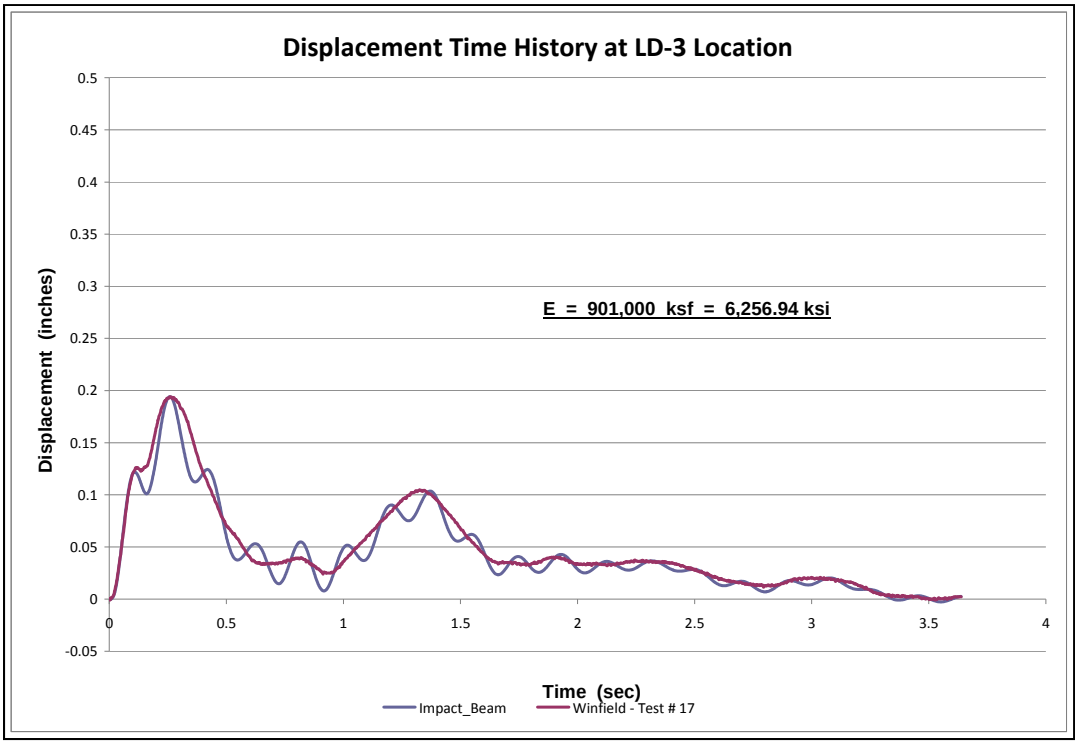

Figure 6.34. E_{dyn} estimation based on experimental beam displacement at LD3-Test #17.

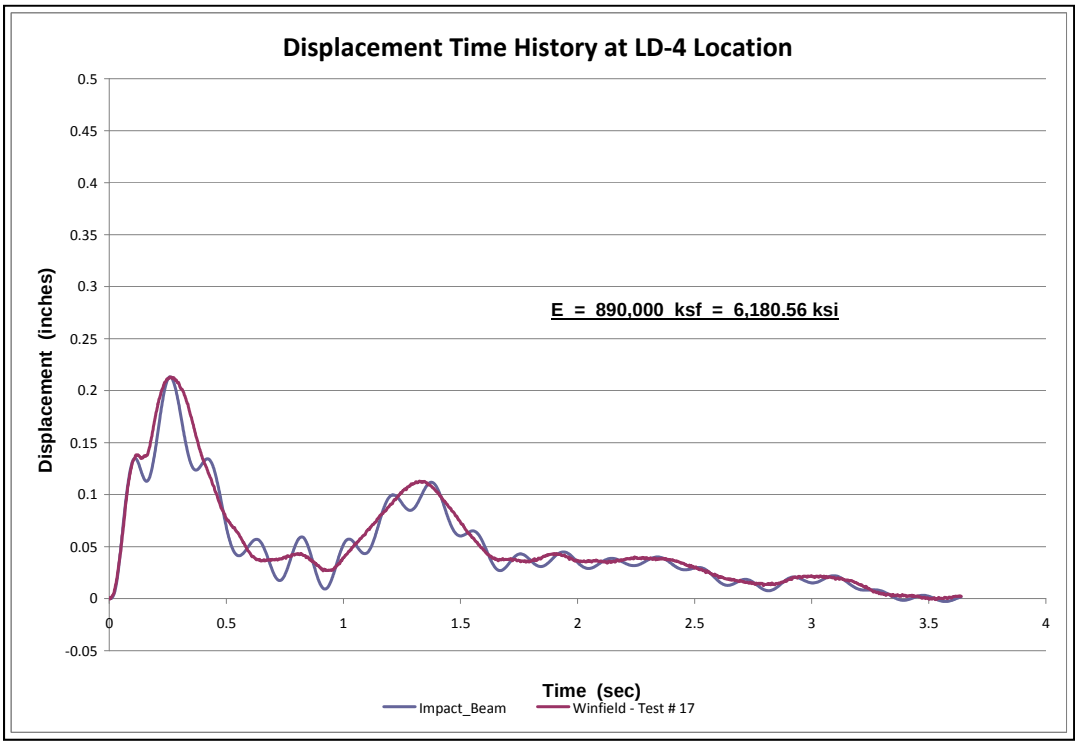

Figure 6.35. E_{dyn} estimation based on experimental beam displacement at LD4-Test #17.

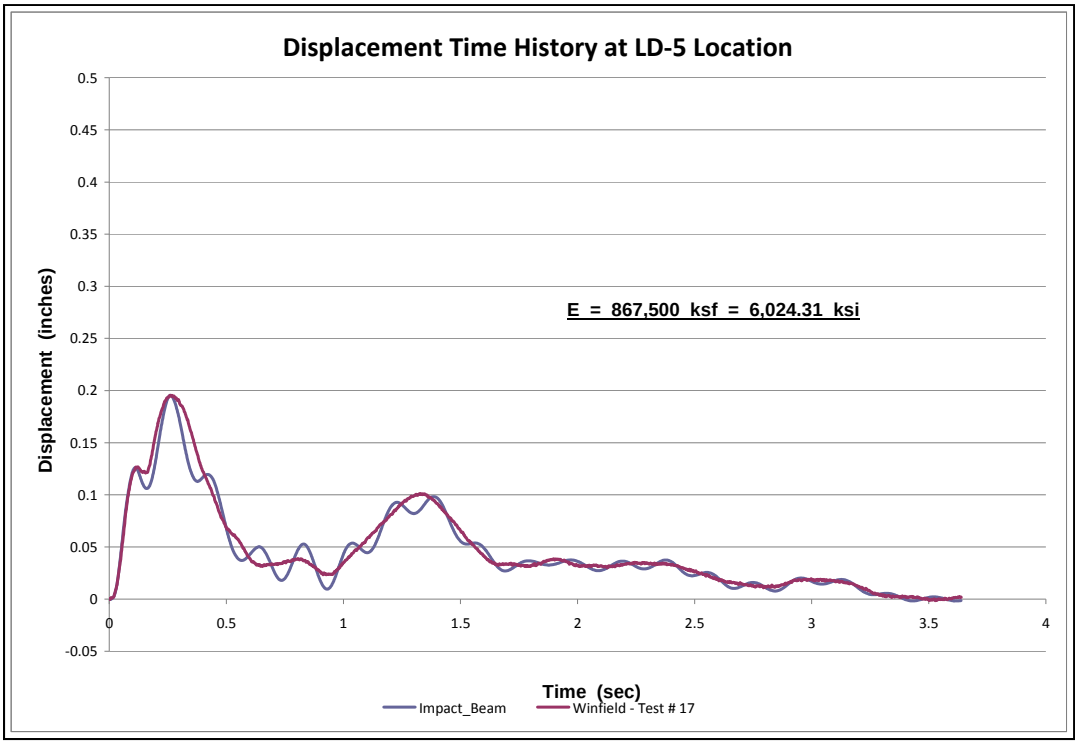

Figure 6.36. E_{dyn} estimation based on experimental beam displacement at LD5-Test #17.

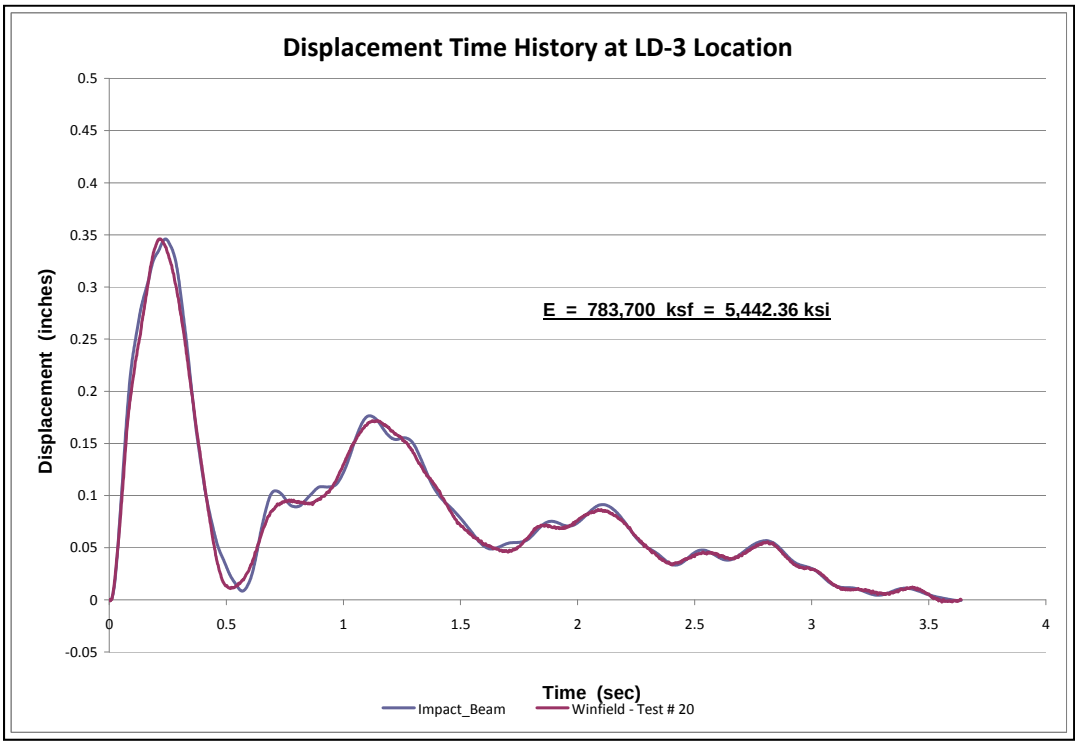

Figure 6.37. E_{dyn} estimation based on experimental beam displacement at LD3-Test #20.

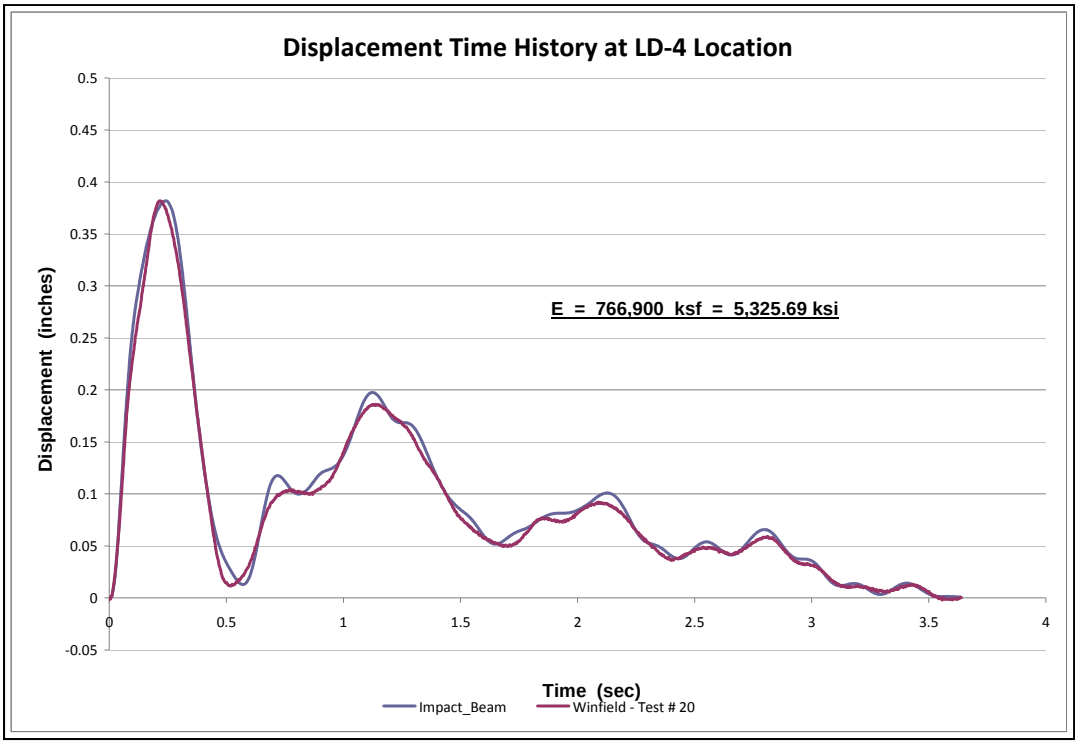

Figure 6.38. E_{dyn} estimation based on experimental beam displacement at LD4-Test #20.

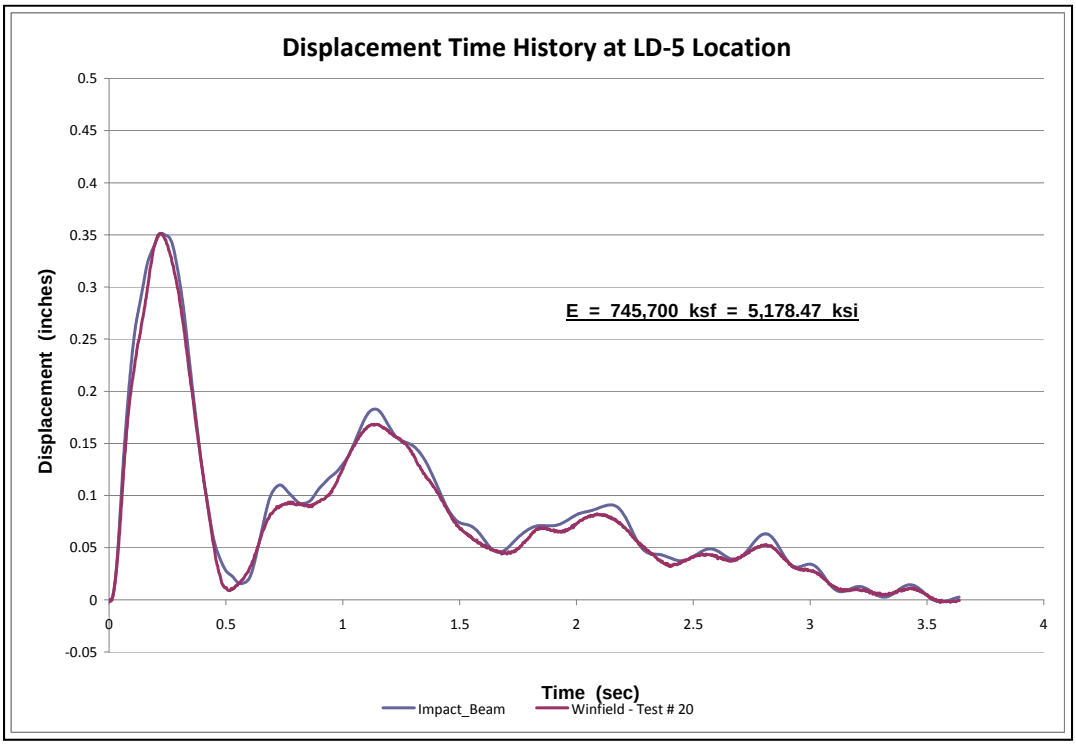

Figure 6.39. E_{dyn} estimation based on experimental beam displacement at LD5-Test #20.

6.4 Summary of the values for the dynamic modulus of elasticity

This section presents a comparison between the experimental internal bending moment and the simulation internal bending moment (from Impact_Beam) based on the average dynamic modulus of elasticity obtained from the beam deflection sensors presented in Section 6.3. The average dynamic modulus of elasticity obtained for Tests 9, 10, 12, 16, 17 and 20 was 5,622.69 ksi, 5,574.54 ksi, 6,696.76 ksi, 5,271.99 ksi, 6,153.93 ksi and 5,315.51 ksi, respectively. The simulation internal bending moment produces a similar shape but with a higher amplitude than the experimental internal bending moment. It can be observed that the shape of the pulse (impact event) was captured by the strain gages but with a difference in magnitude. The analysis of the strain gage experimental data is beyond the scope of this report and needs more research to clarify the essence of the internal moment amplification factor. The behavior between the experimental and simulation internal bending moment is presented in Figures 6.40 through 6.78. Each figure presents the internal bending moment time-history for each strain gage location (back and front sensor) and is compared against the simulation internal bending moment time-history using the average dynamic modulus of elasticity obtained from the beam deflection for each experiment as shown in Section 6.3.

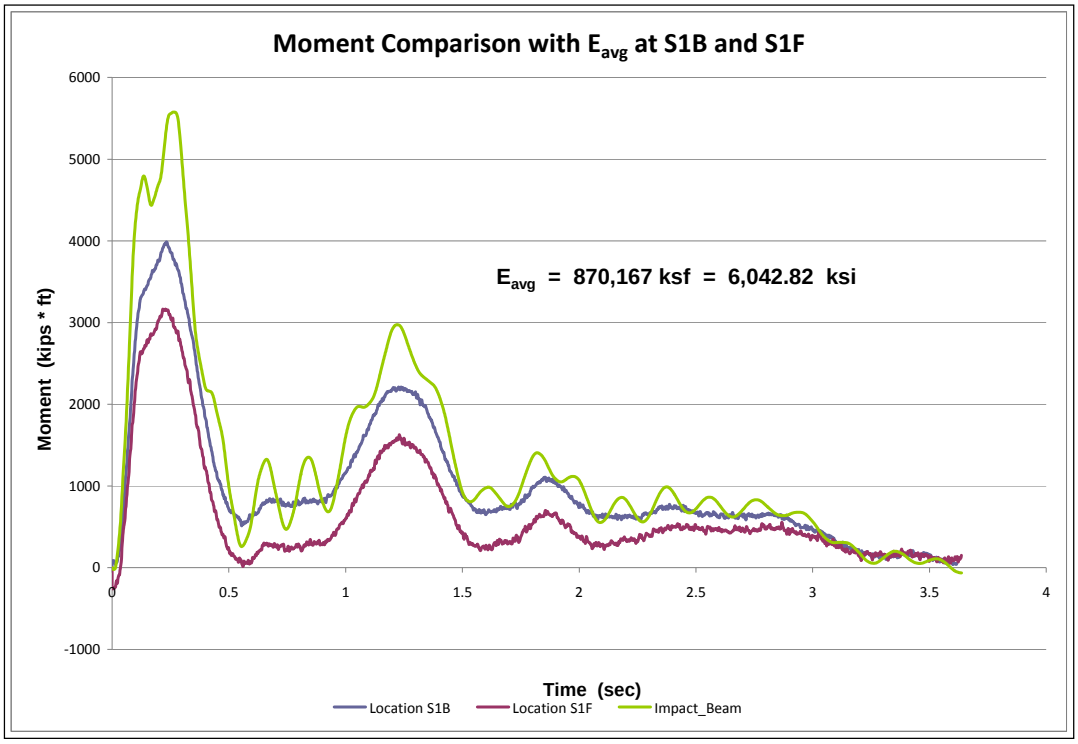

Figure 6.40. Moment comparison with E_{avg} at S1-Test #6.

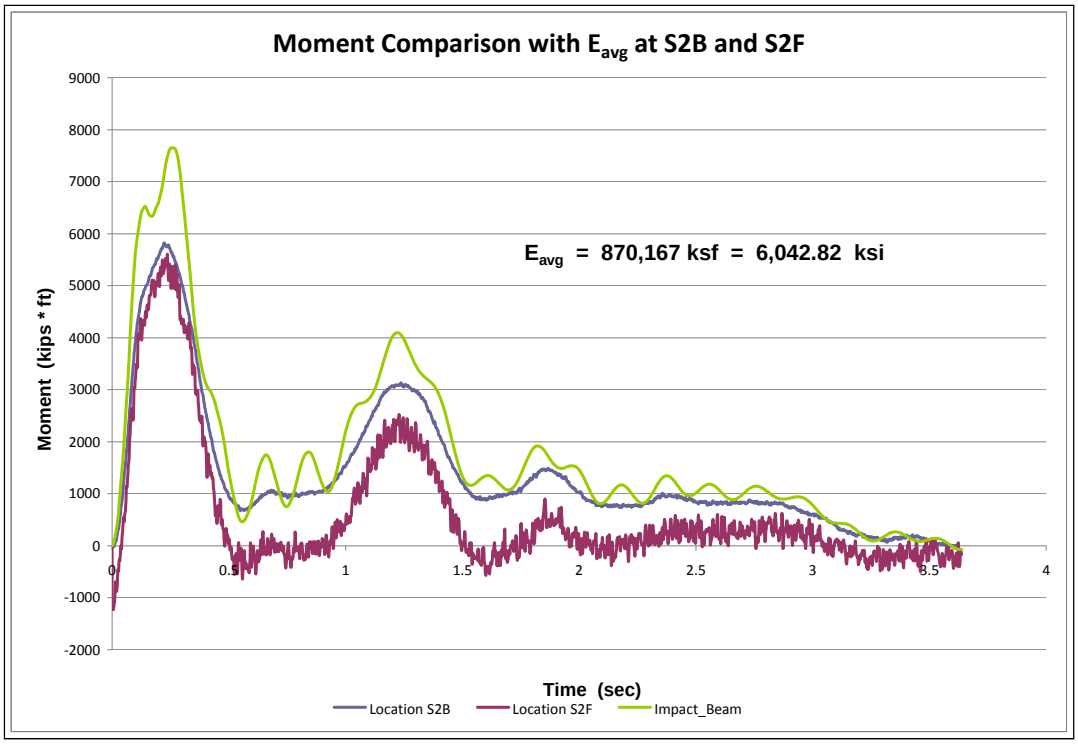

Figure 6.41. Moment comparison with E_{avg} at S2-Test #6.

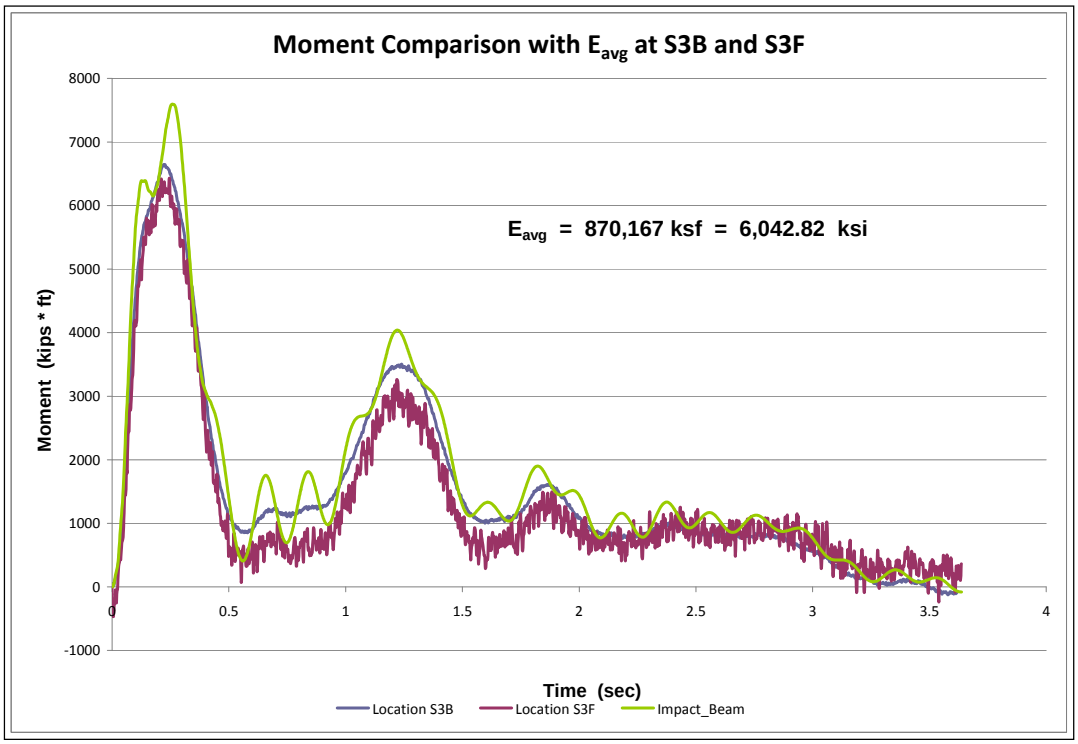

Figure 6.42. Moment comparison with E_{avg} at S3-Test #6.

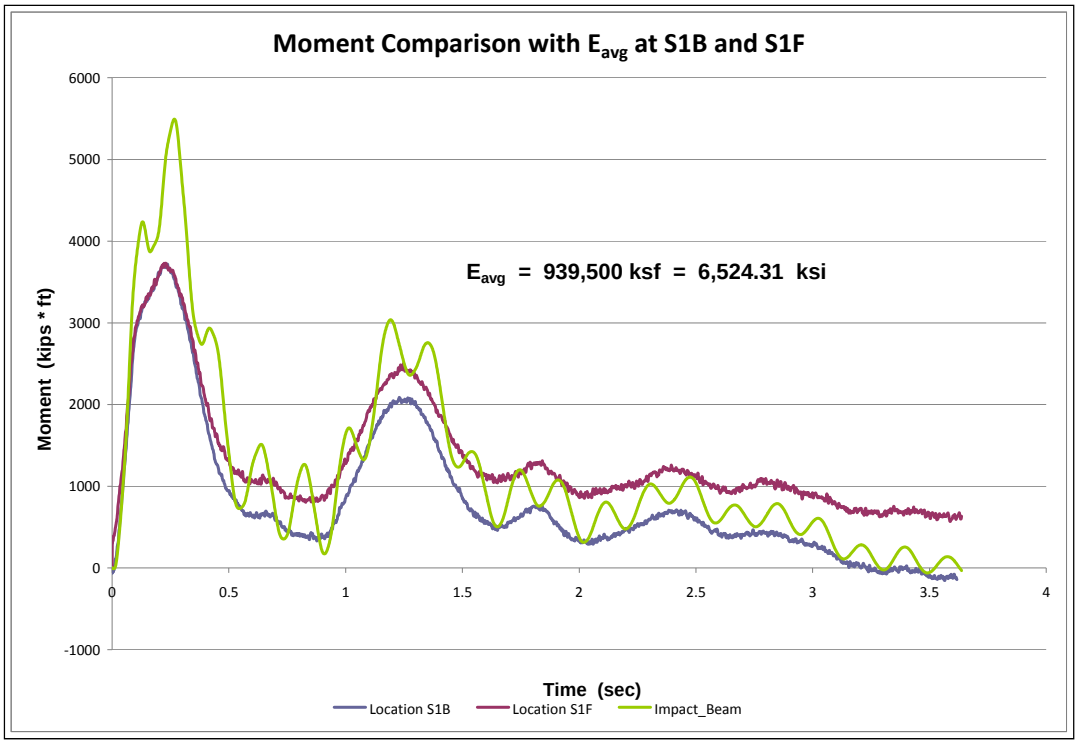

Figure 6.43. Moment comparison with *E*$_{avg}$ at S1-Test #7.

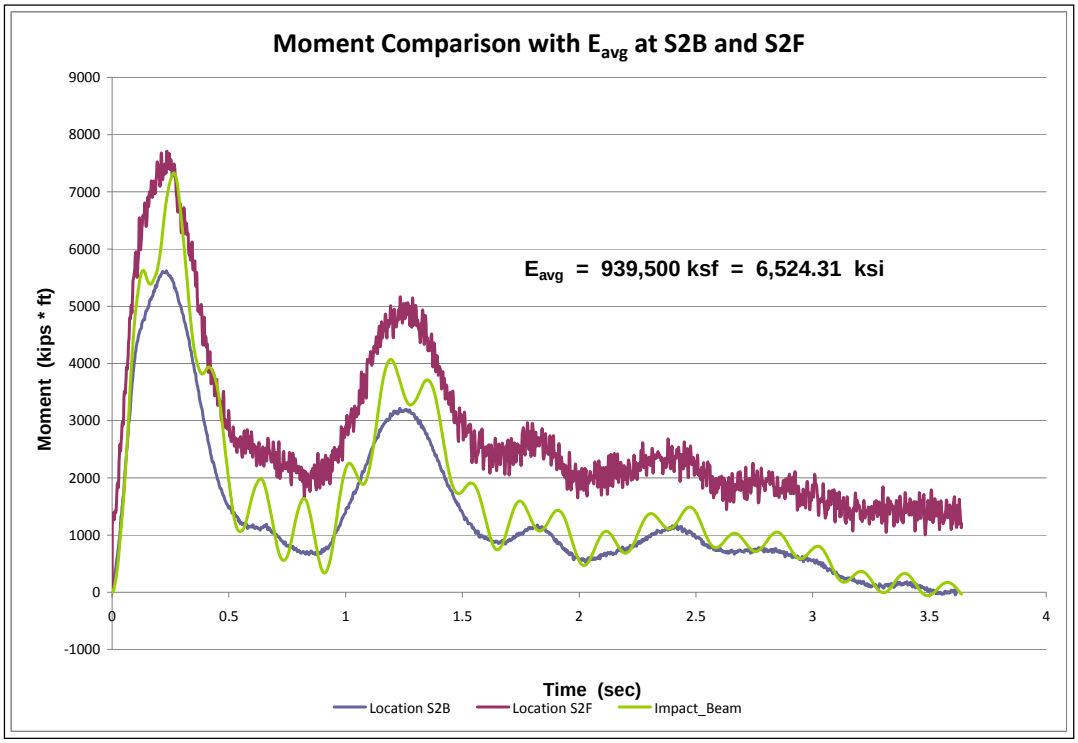

Figure 6.44. Moment comparison with *E*$_{avg}$ at S2-Test #7.

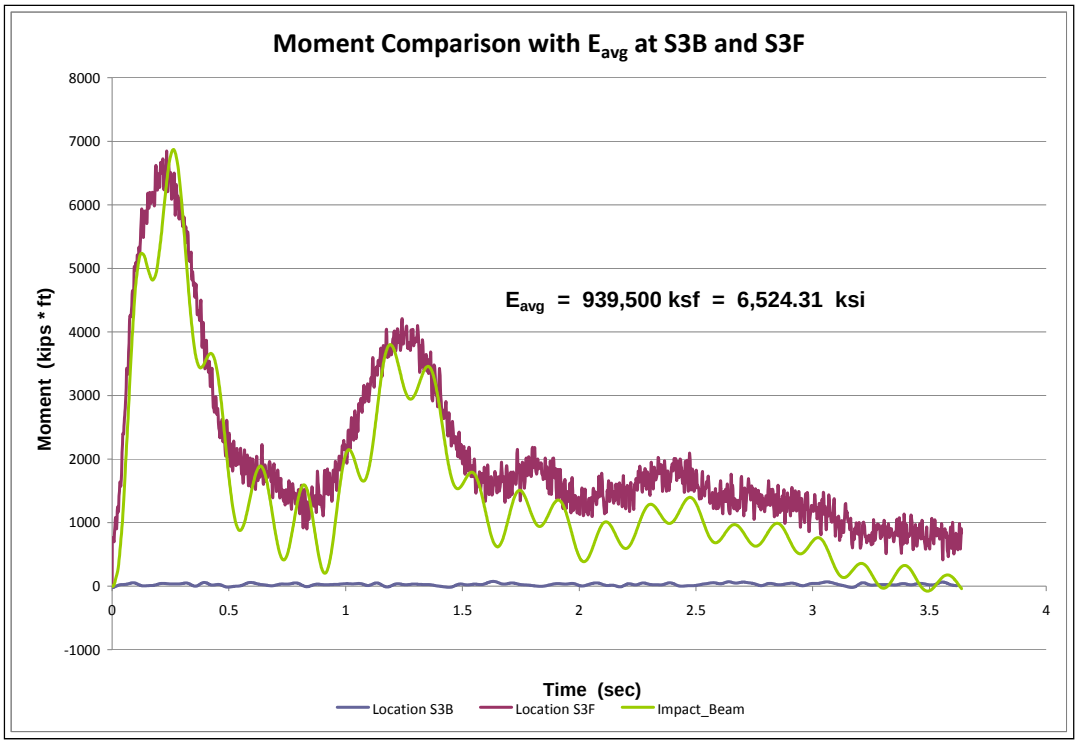

Figure 6.45. Moment comparison with E_{avg} at S3-Test #7.

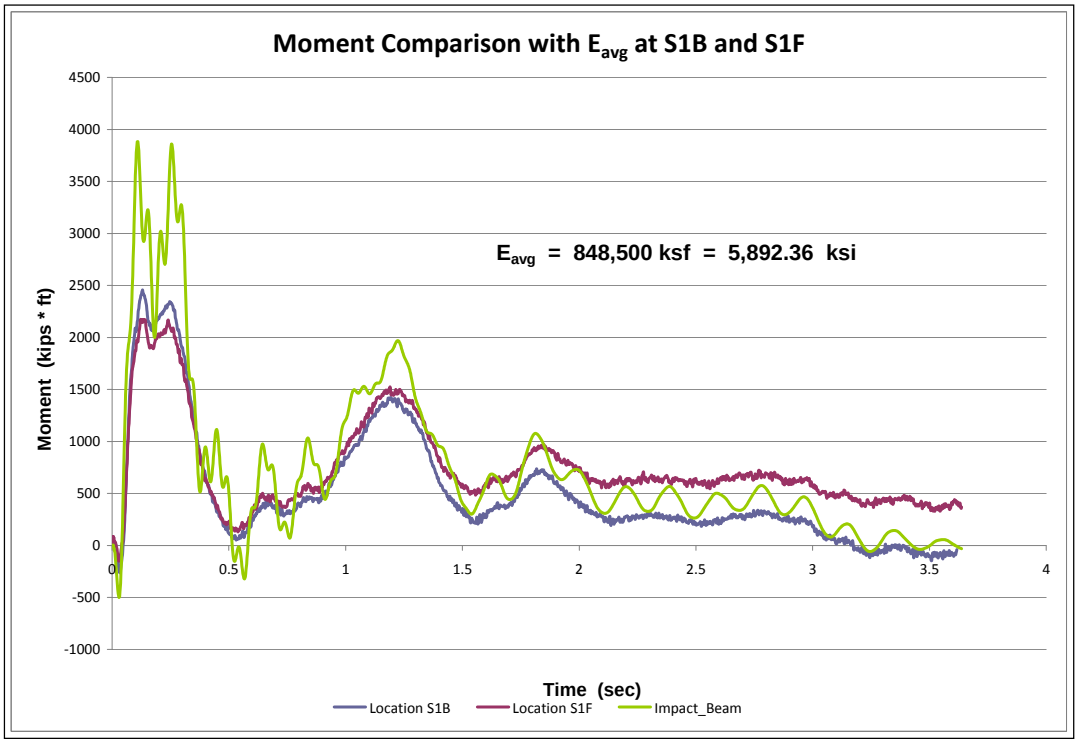

Figure 6.46. Moment comparison with E_{avg} at S1-Test #8.

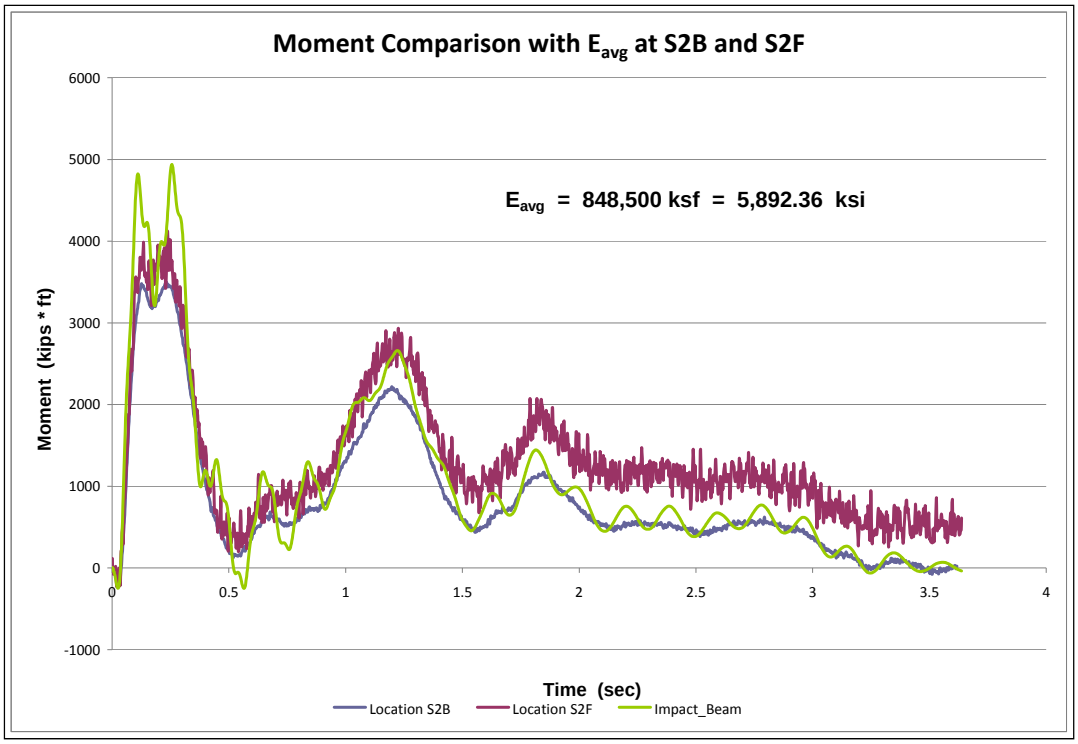

Figure 6.47. Moment comparison with E_{avg} at S2-Test #8.

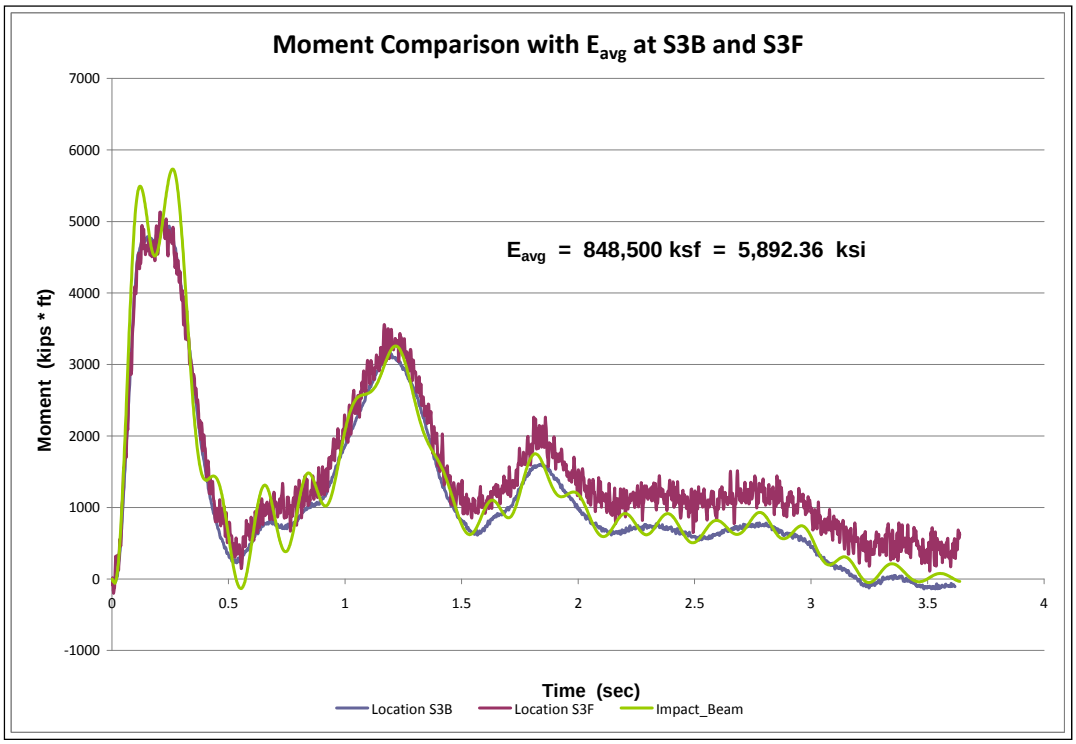

Figure 6.48. Moment comparison with E_{avg} at S3-Test #8.

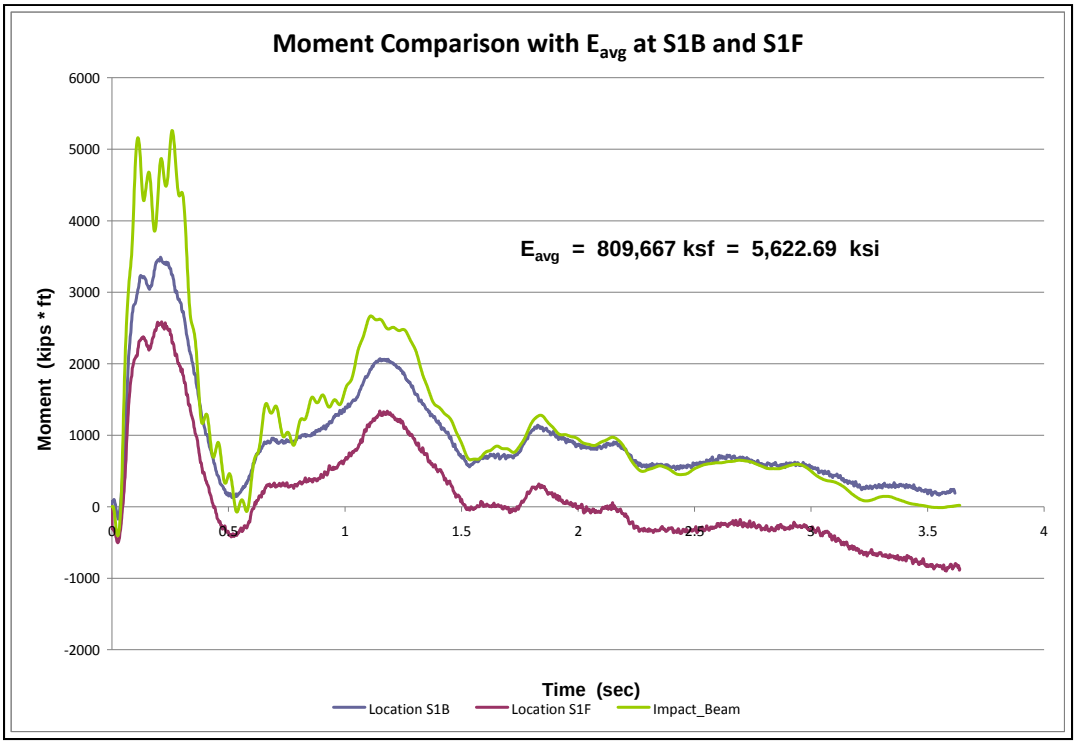

Figure 6.49. Moment comparison with E_{avg} at S1-Test #9.

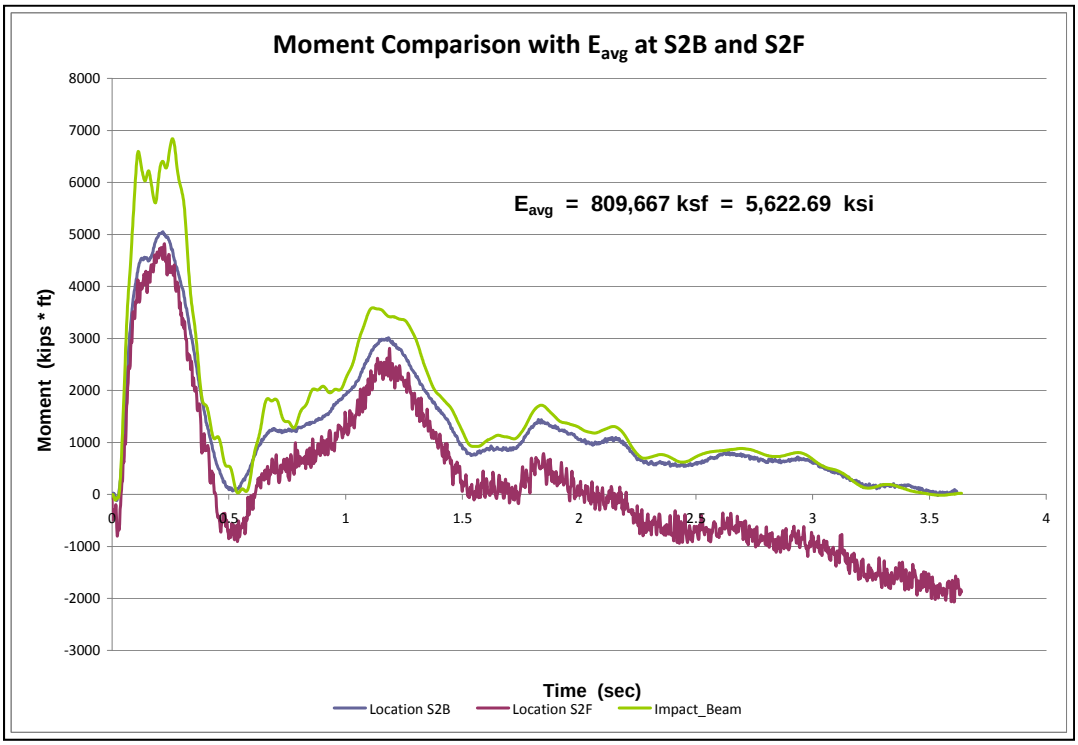

Figure 6.50. Moment comparison with E_{avg} at S2-Test #9.

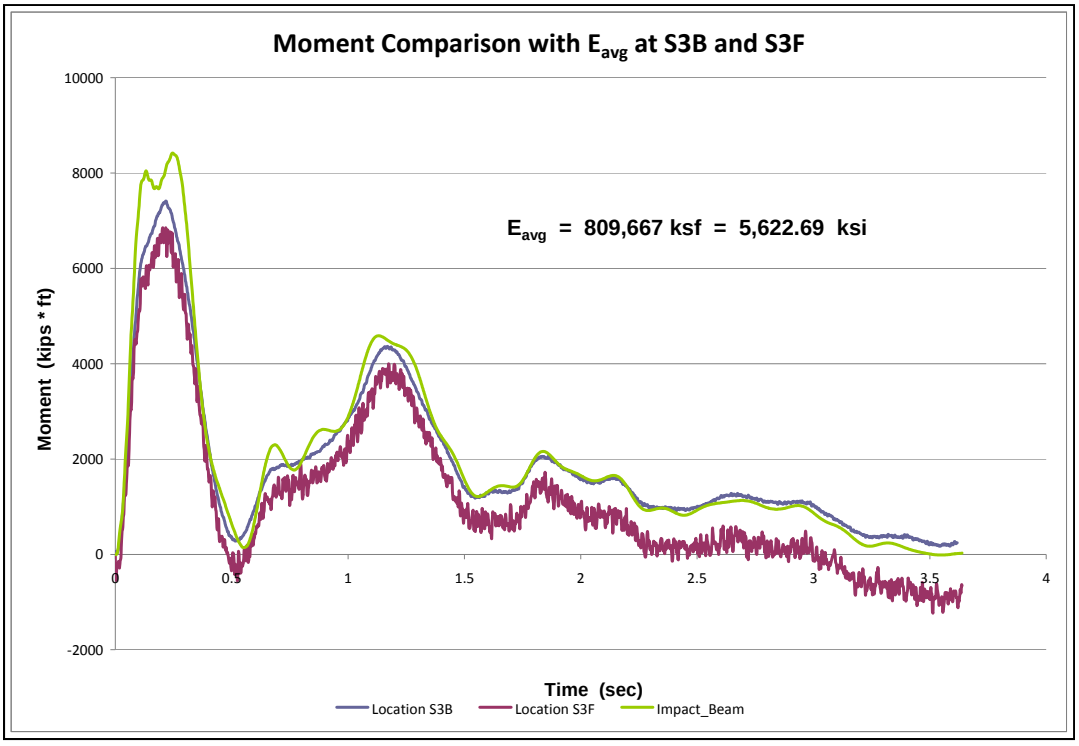

Figure 6.51. Moment comparison with E_{avg} at S3-Test #9.

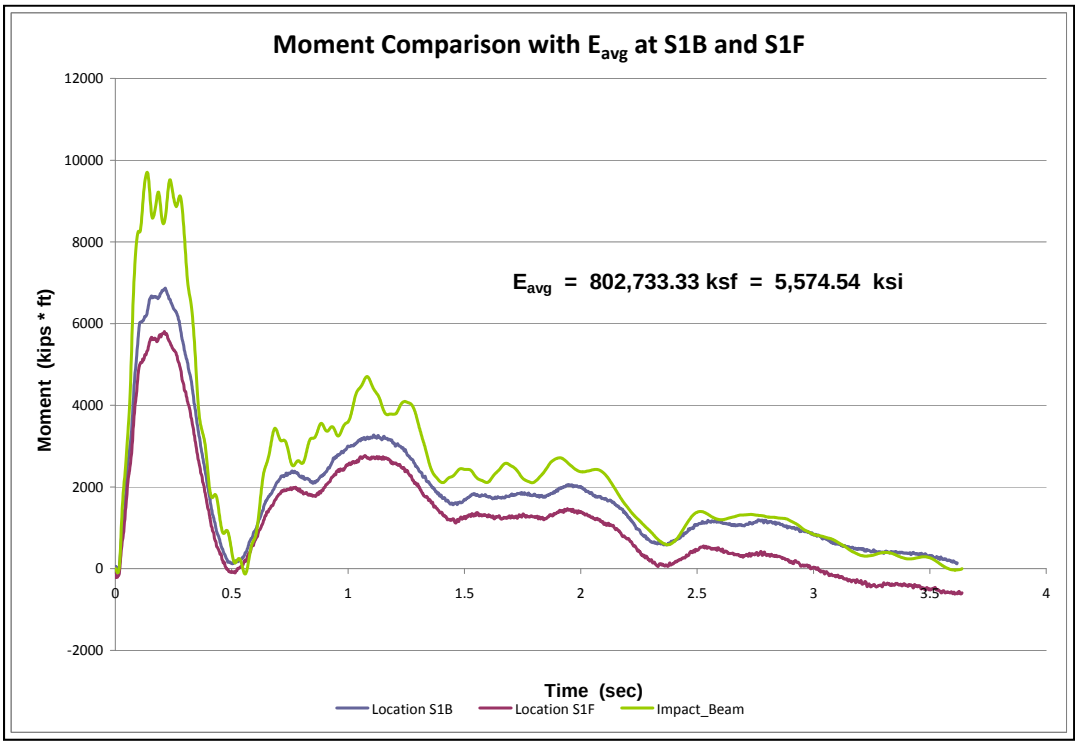

Figure 6.52. Moment comparison with E_{avg} at S1-Test #10.

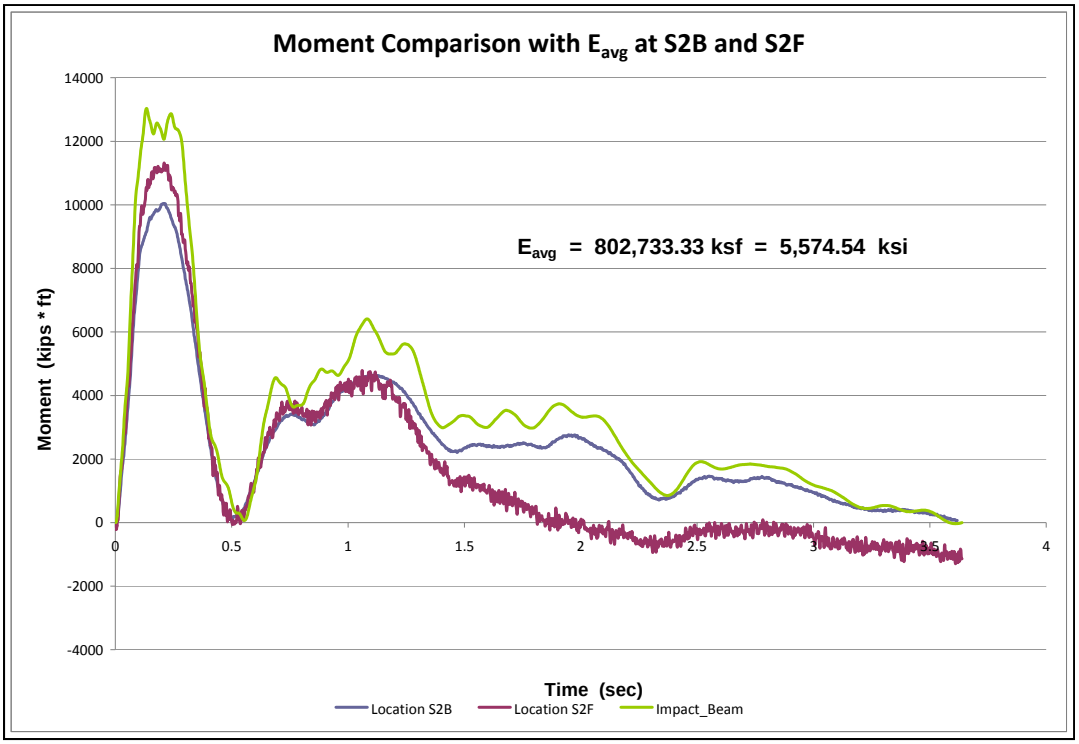

Figure 6.53. Moment comparison with E_{avg} at S2-Test #10.

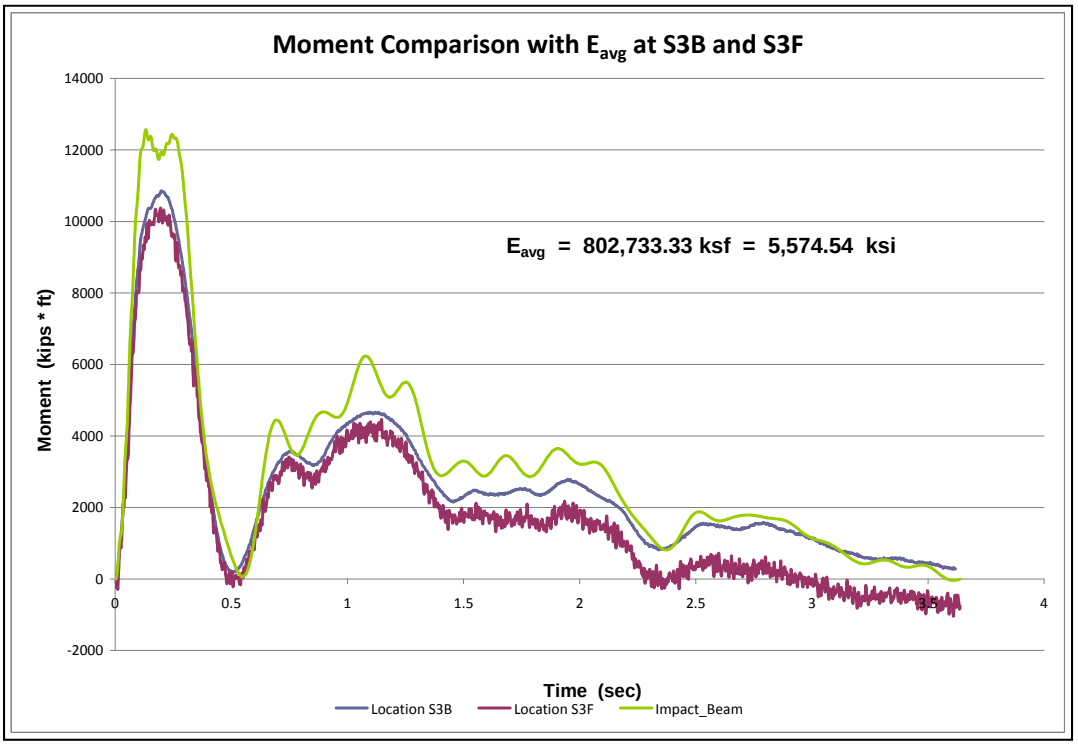

Figure 6.54. Moment comparison with E_{avg} at S3-Test #10.

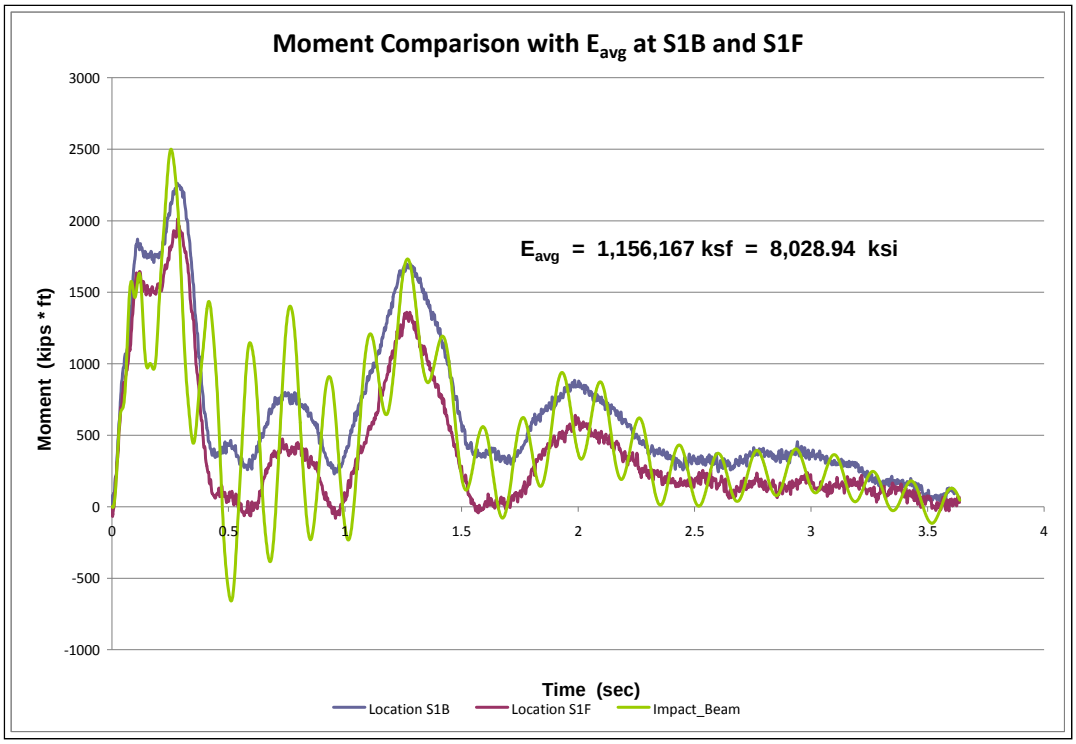

Figure 6.55. Moment comparison with E_{avg} at S1-Test #11.

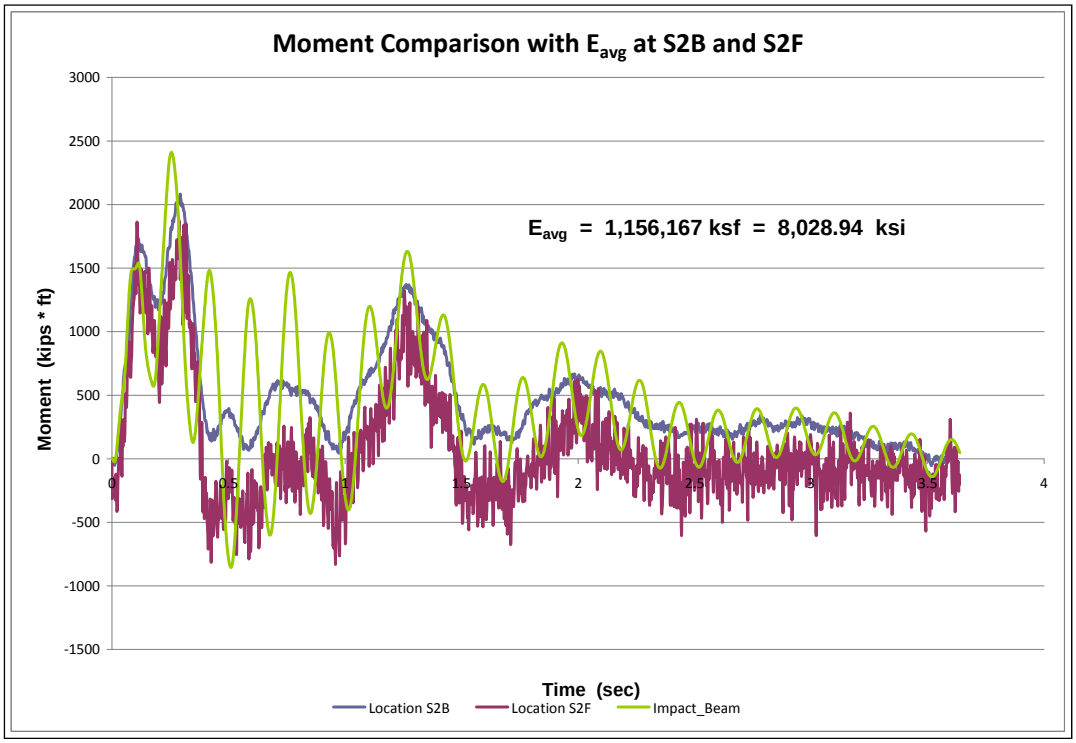

Figure 6.56. Moment comparison with E_{avg} at S2-Test #11.

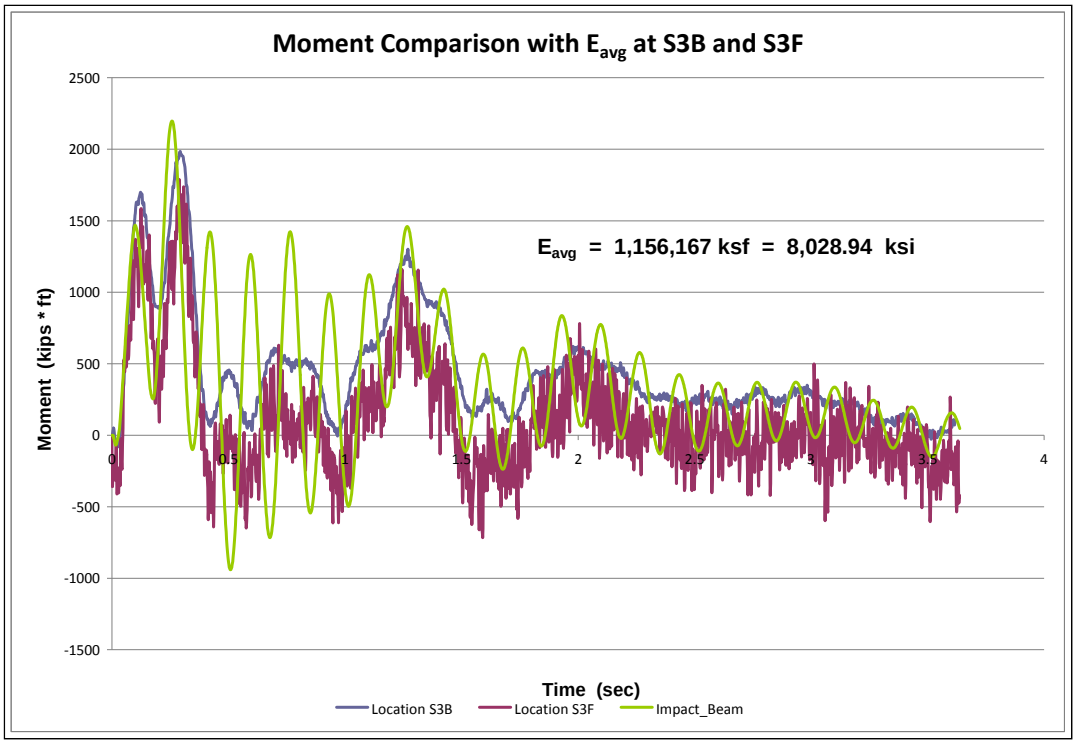

Figure 6.57. Moment comparison with E_{avg} at S3-Test #11.

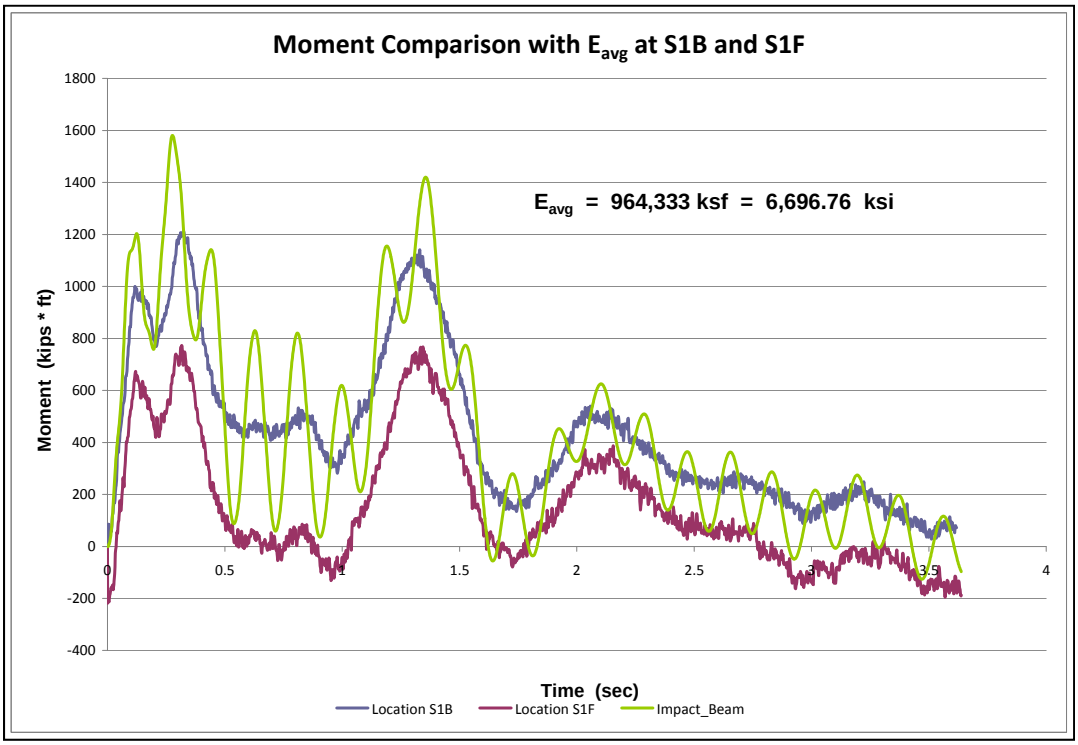

Figure 6.58. Moment comparison with E_{avg} at S1-Test #12.

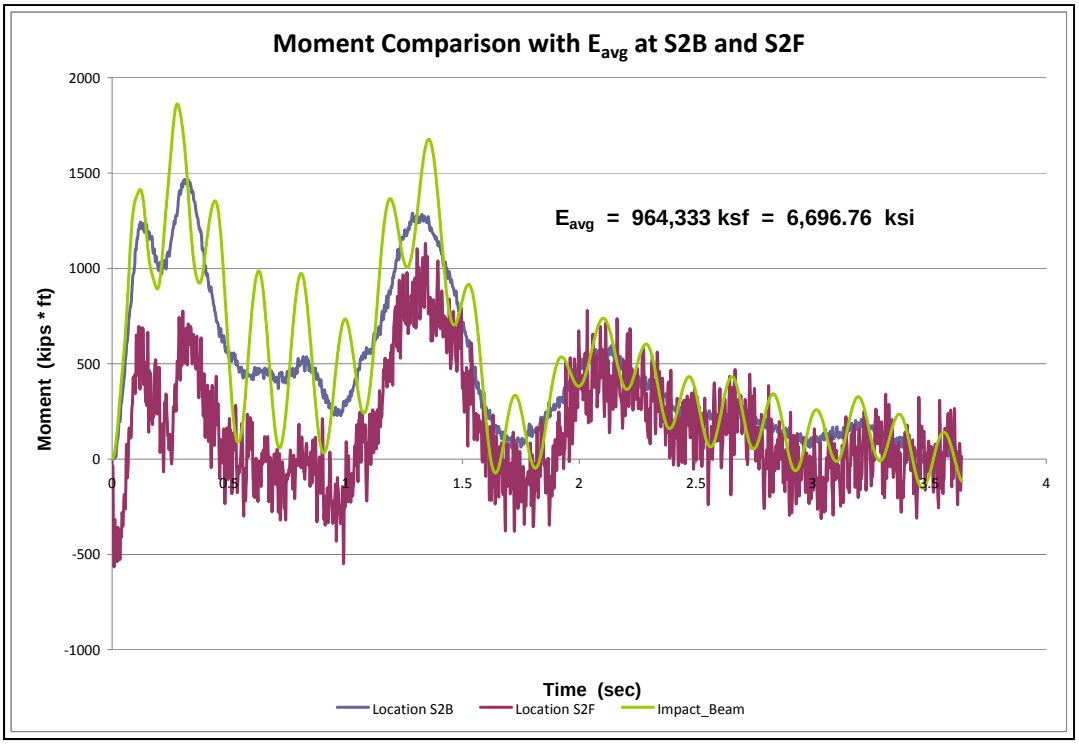

Figure 6.59. Moment comparison with E_{avg} at S2-Test #12.

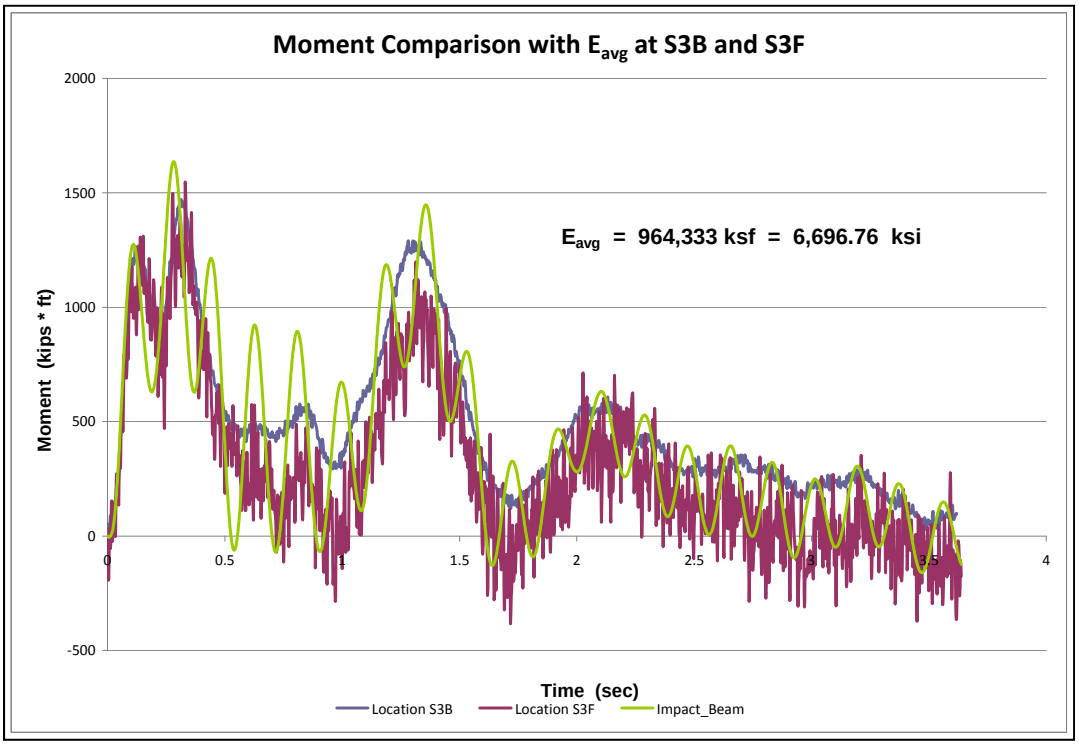

Figure 6.60. Moment comparison with E_{avg} at S3-Test #12.

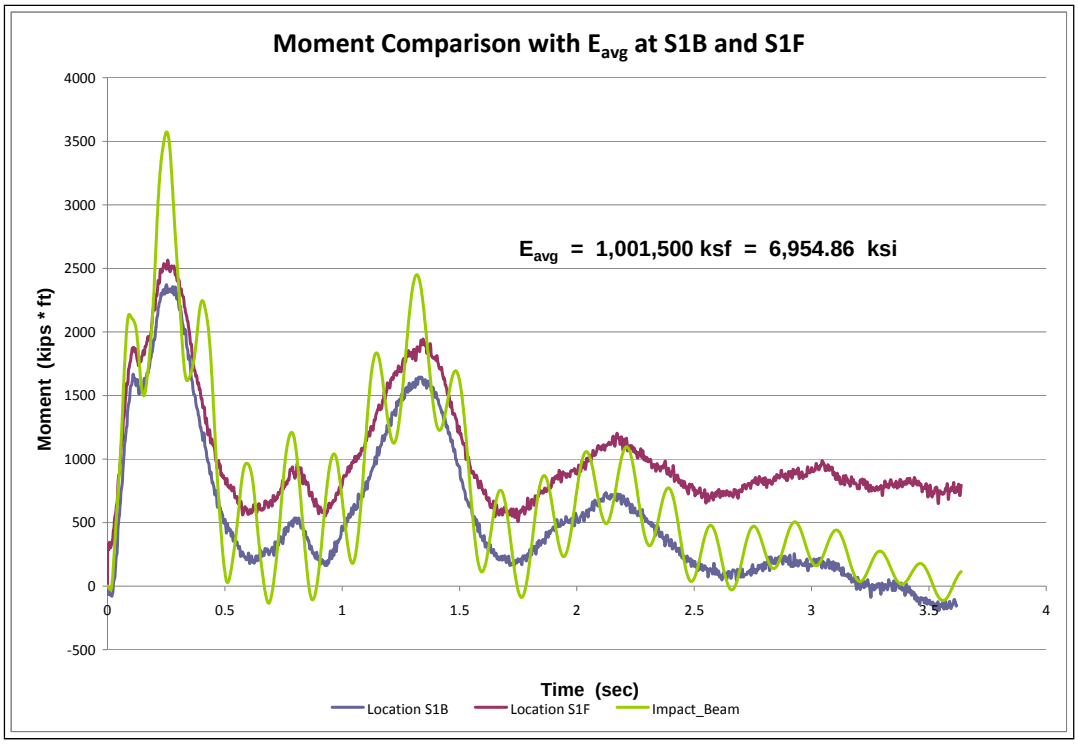

Figure 6.61. Moment comparison with E_{avg} at S1-Test #13.

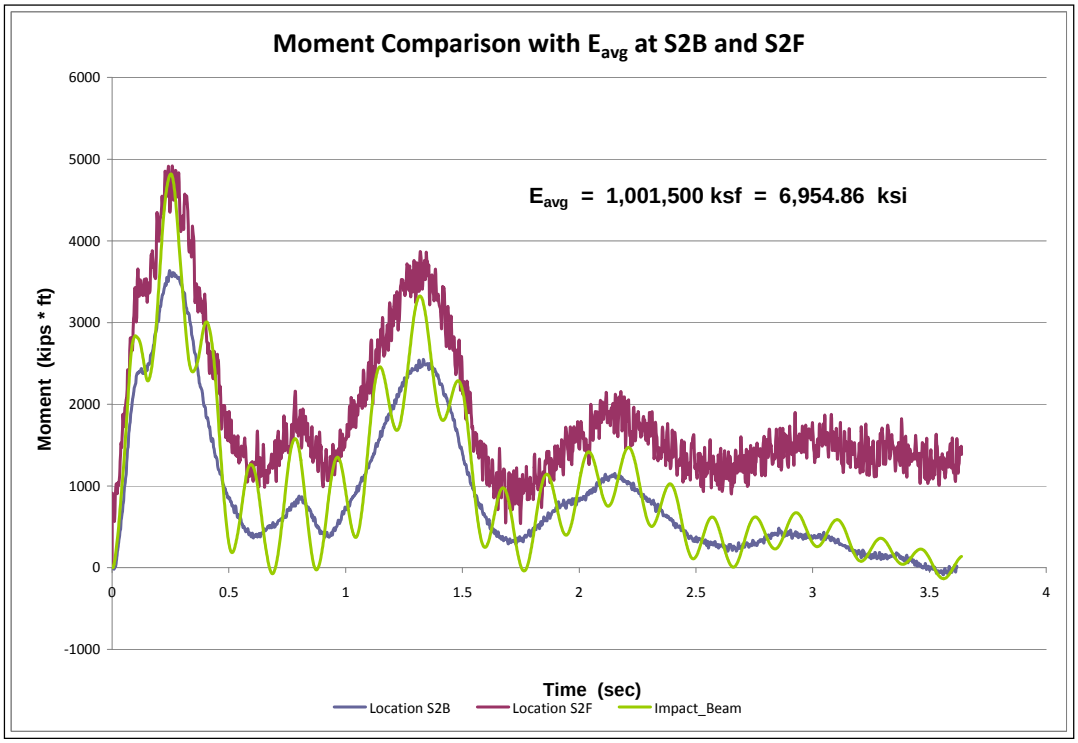

Figure 6.62. Moment comparison with E_{avg} at S2-Test #13.

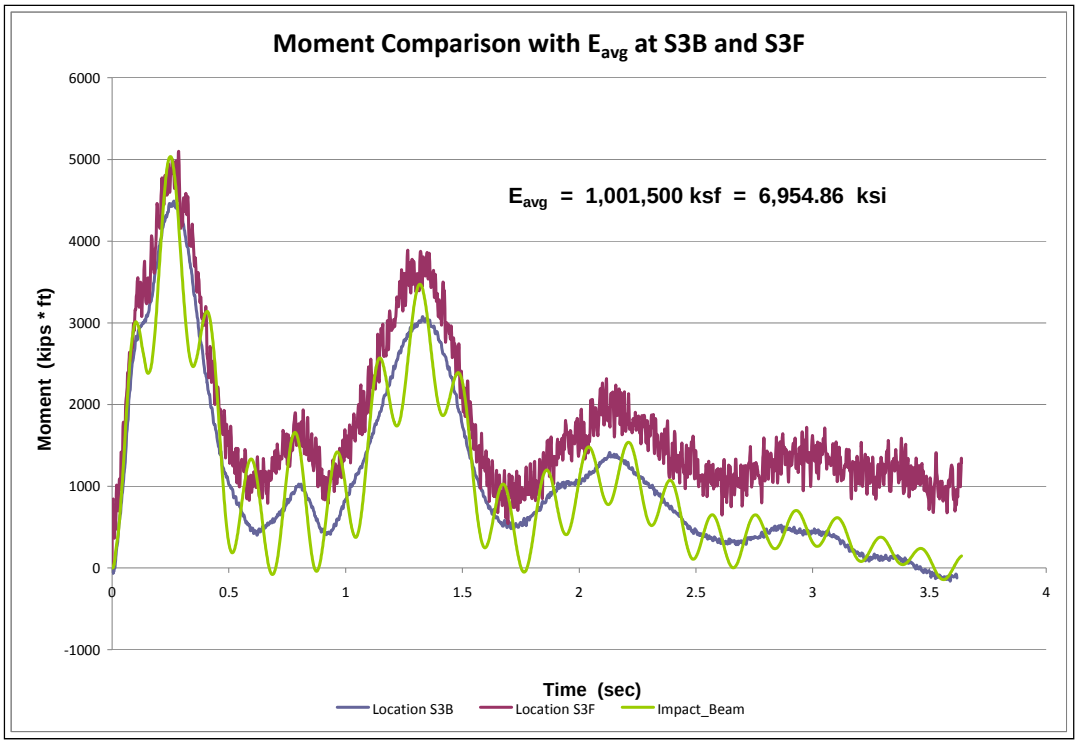

Figure 6.63. Moment comparison with E_{avg} at S3-Test #13.

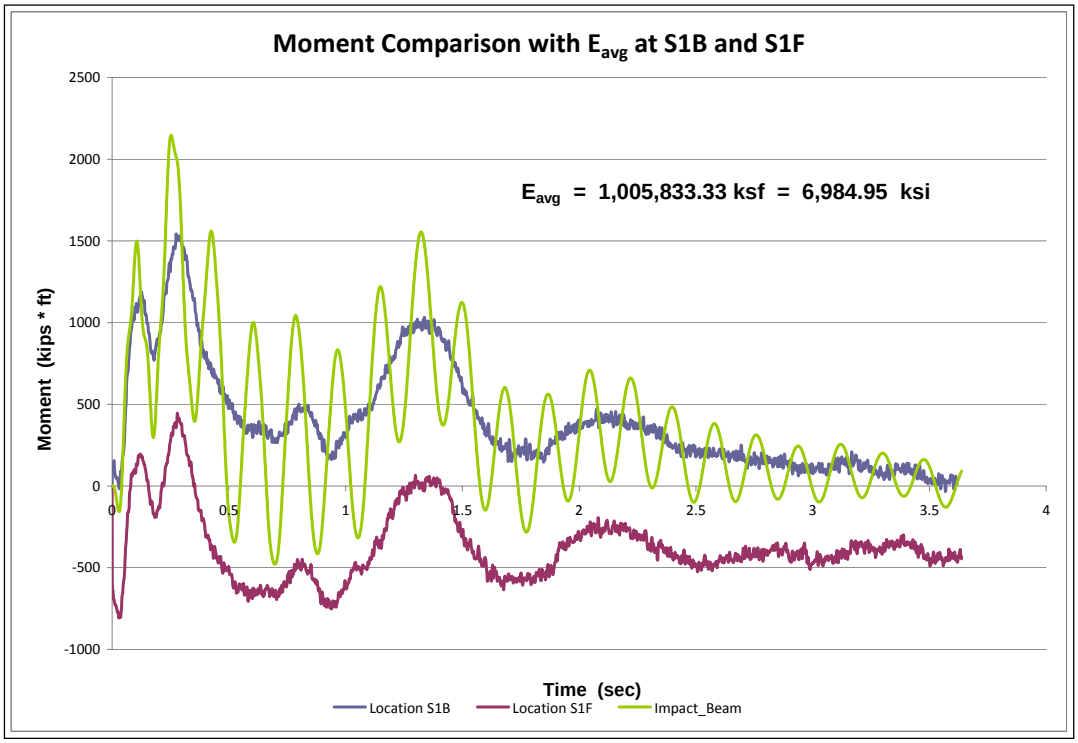

Figure 6.64. Moment comparison with E_{avg} at S1-Test #14.

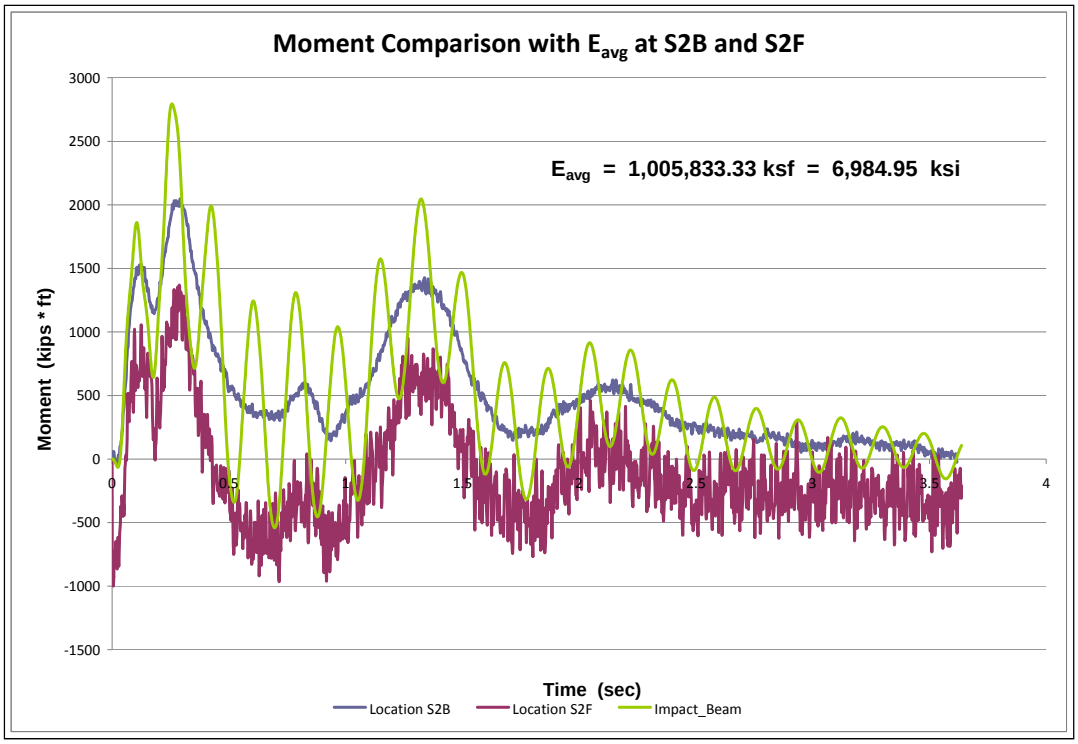

Figure 6.65. Moment comparison with E_{avg} at S2-Test #14.

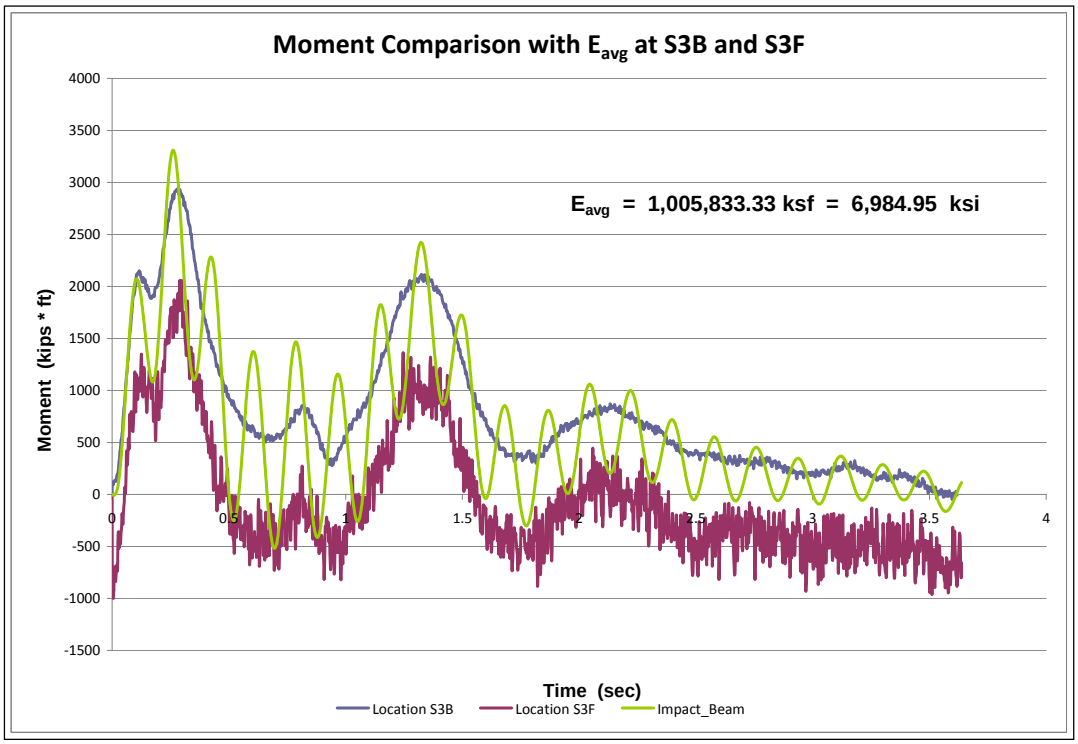

Figure 6.66. Moment comparison with E_{avg} at S3-Test #14.

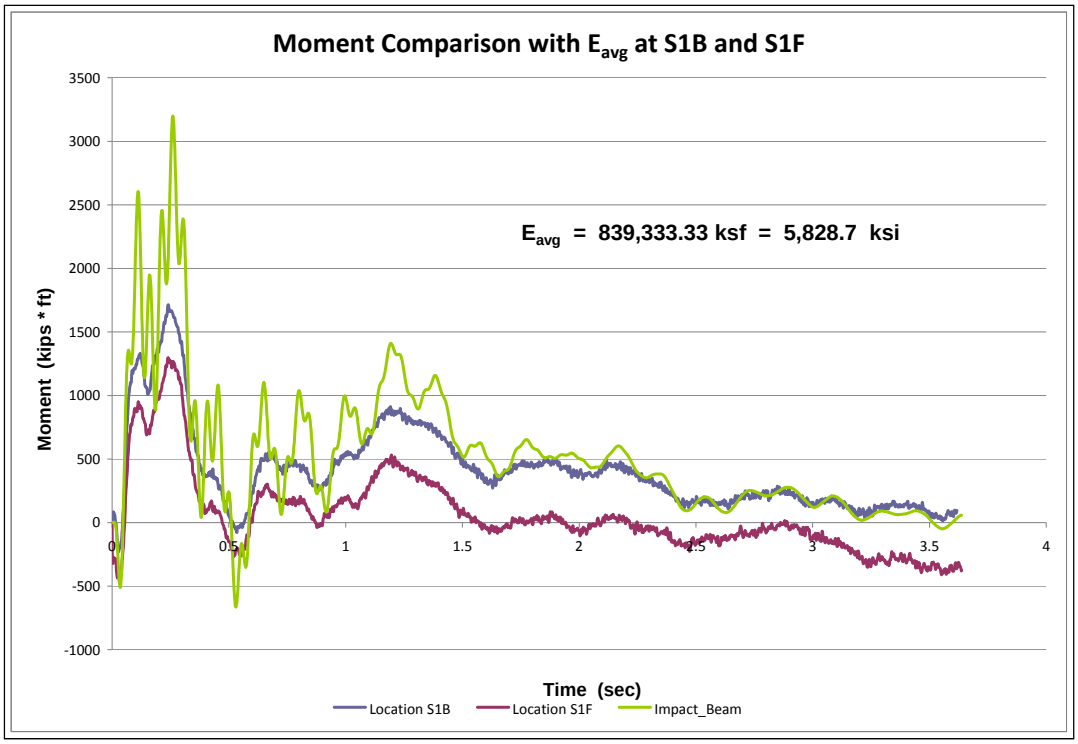

Figure 6.67. Moment comparison with E_{avg} at S1-Test #15.

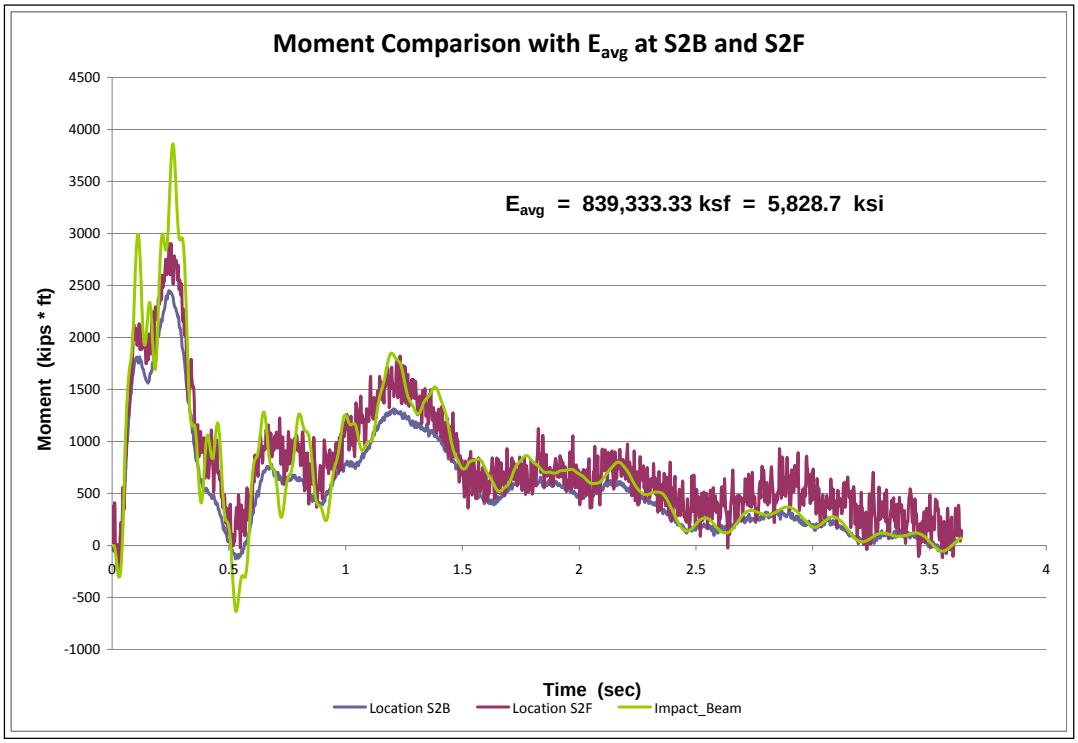

Figure 6.68. Moment comparison with E_{avg} at S2-Test #15.

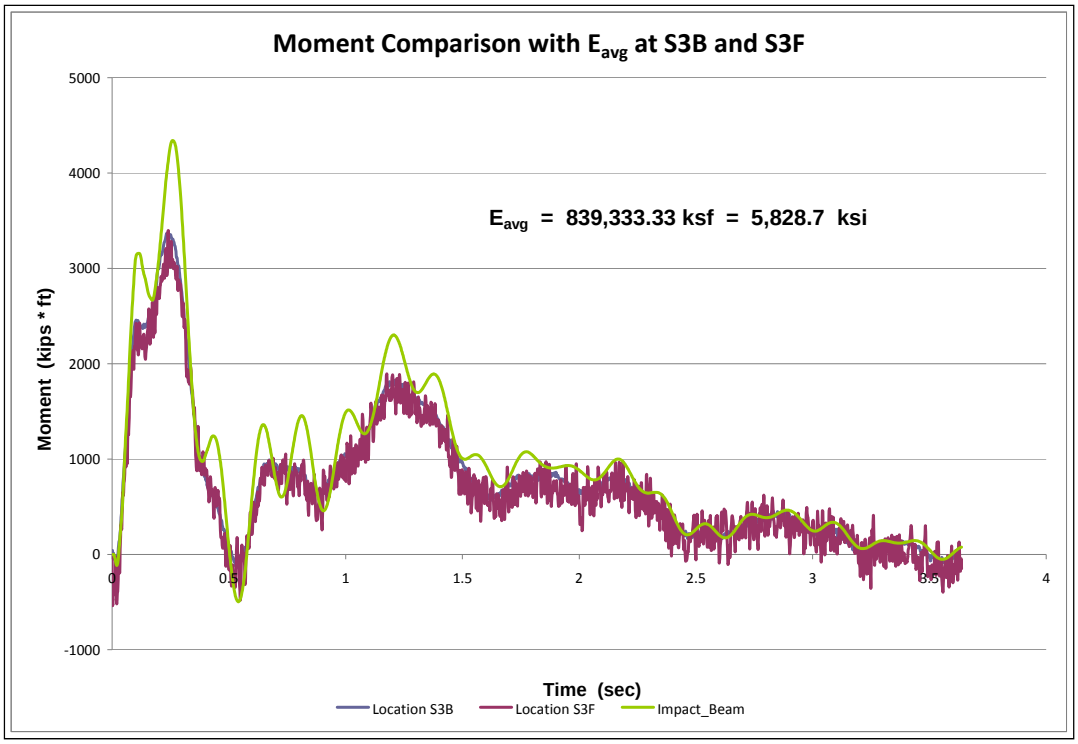

Figure 6.69. Moment comparison with E_{avg} at S3-Test #15.

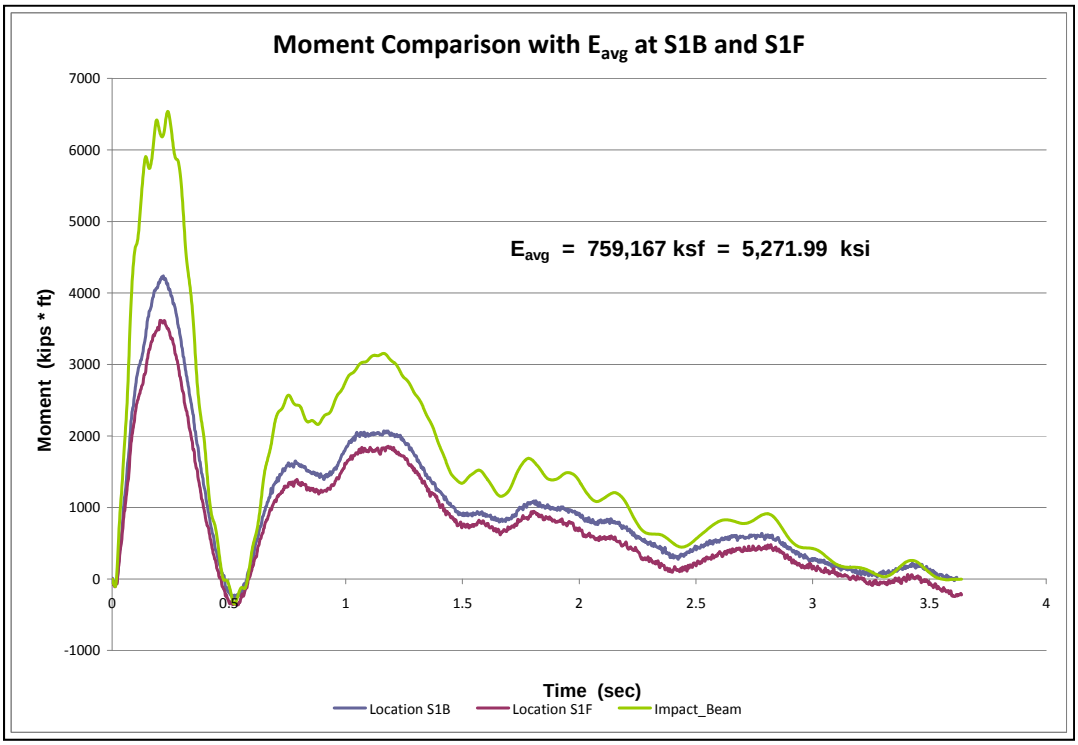

Figure 6.70. Moment comparison with E_{avg} at S1-Test #16.

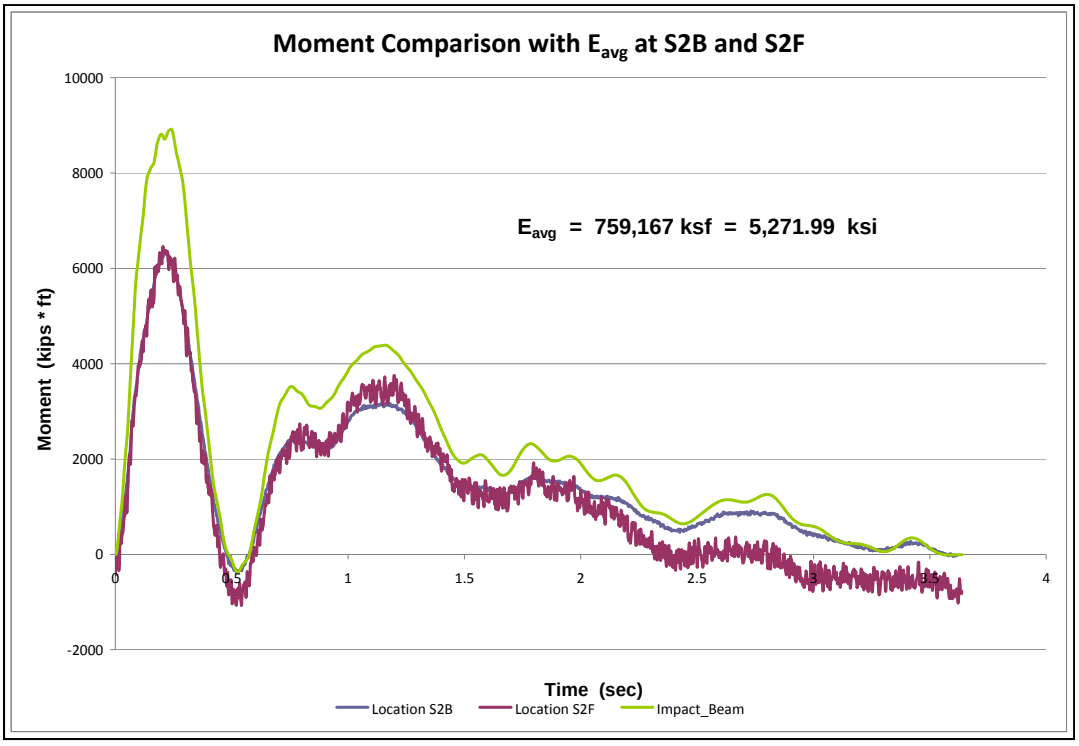

Figure 6.71. Moment comparison with E_{avg} at S2-Test #16.

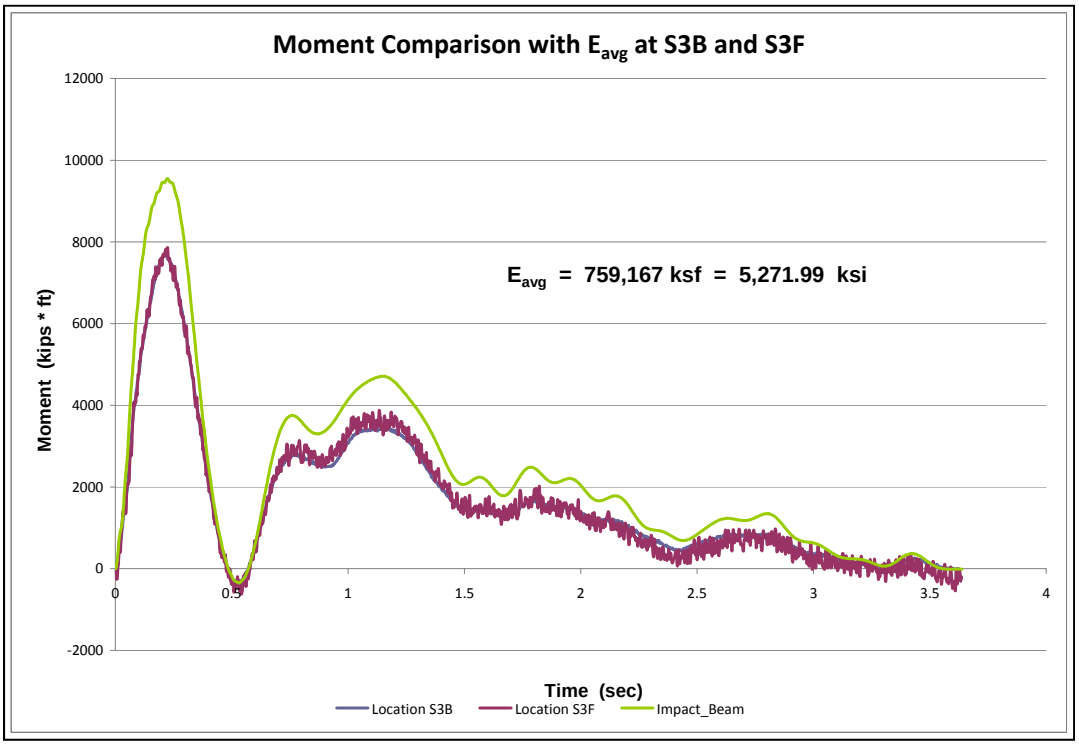

Figure 6.72. Moment comparison with E_{avg} at S3-Test #16.

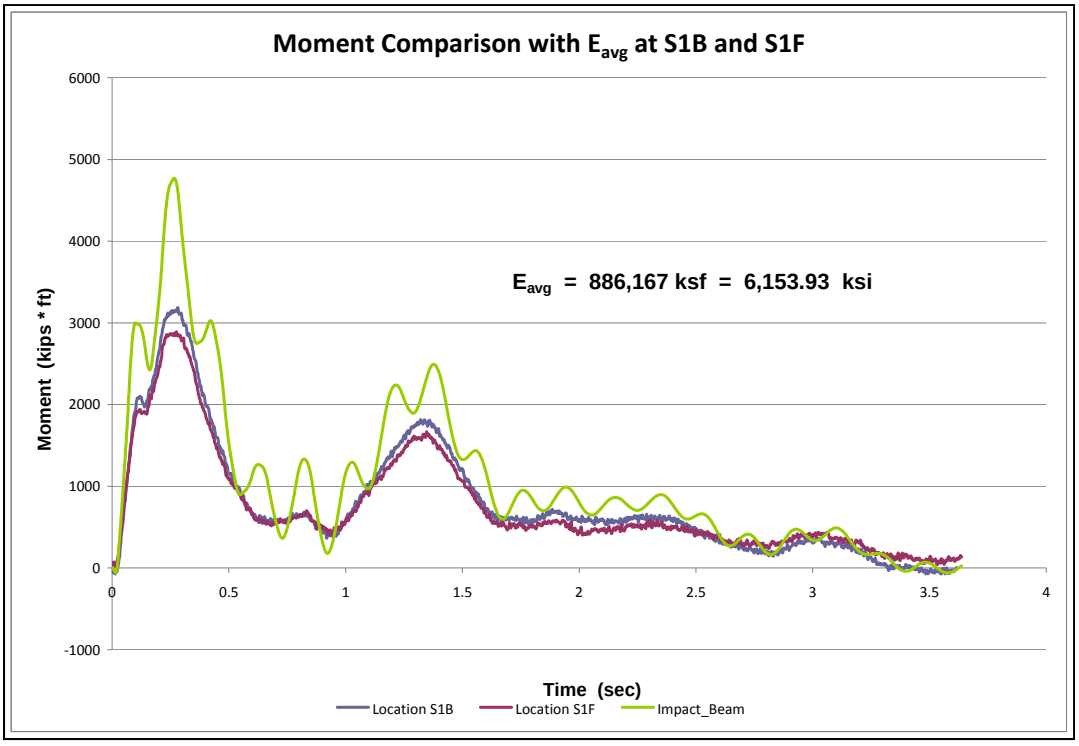

Figure 6.73. Moment comparison with E_{avg} at S1-Test #17.

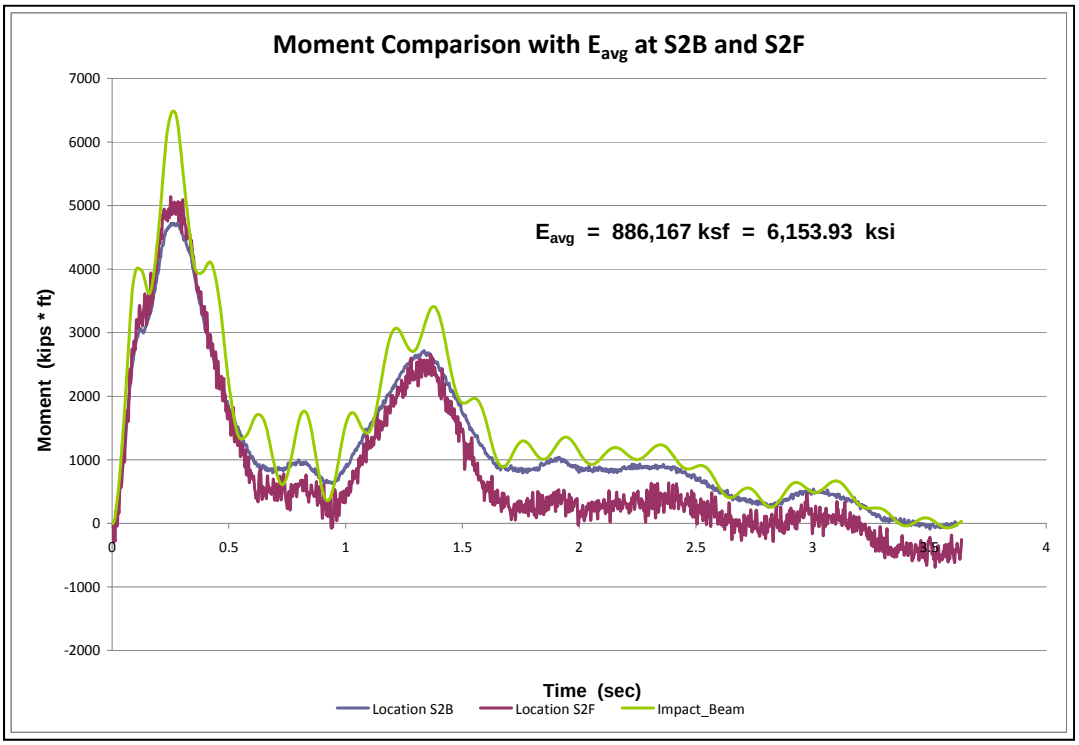

Figure 6.74. Moment comparison with E_{avg} at S2-Test #17.

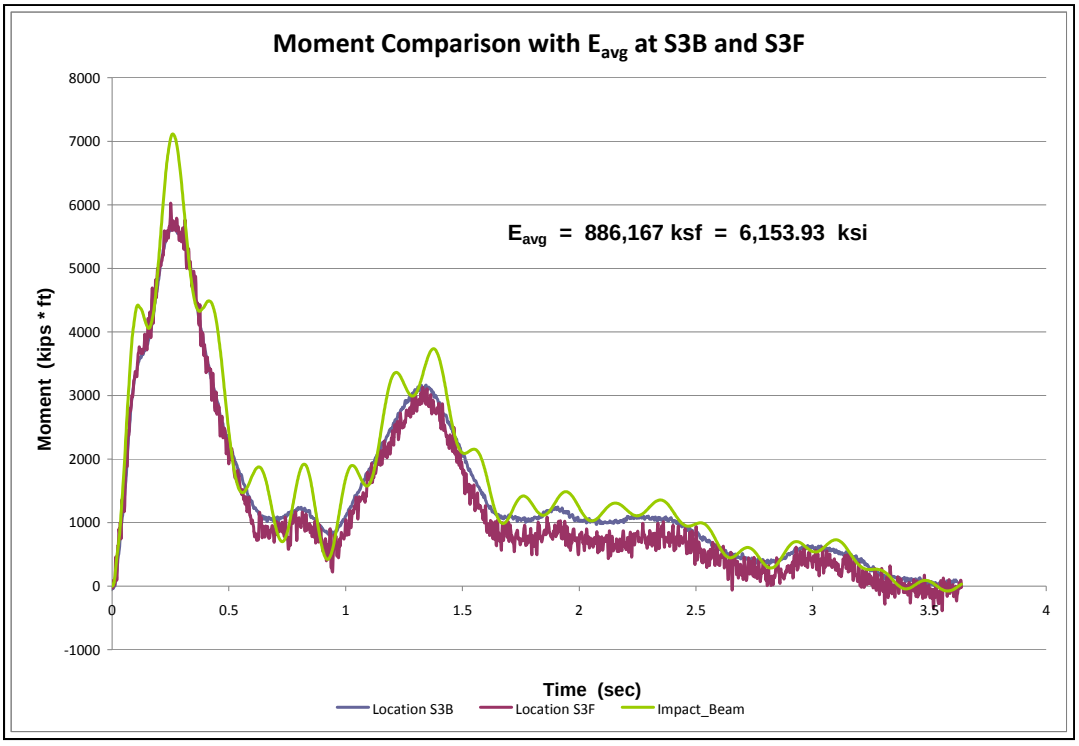

Figure 6.75. Moment comparison with E_{avg} at S3-Test #17.

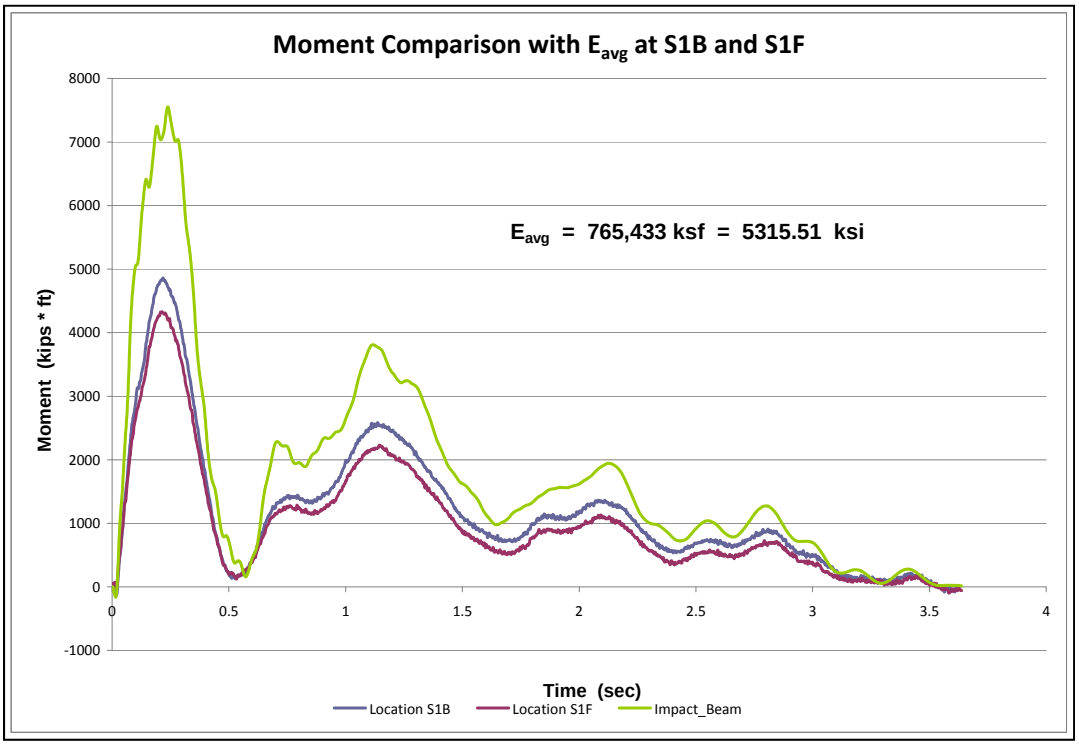

Figure 6.76. Moment comparison with E_{avg} at S1-Test #20.

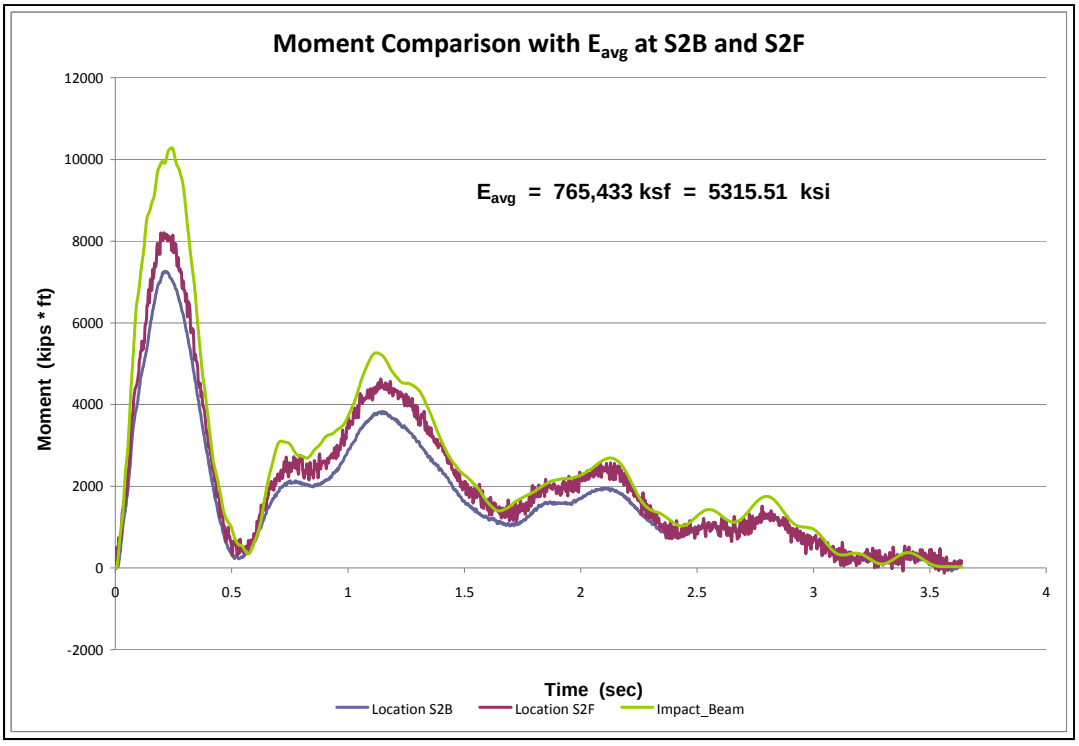

Figure 6.77. Moment comparison with E_{avg} at S2-Test #20.

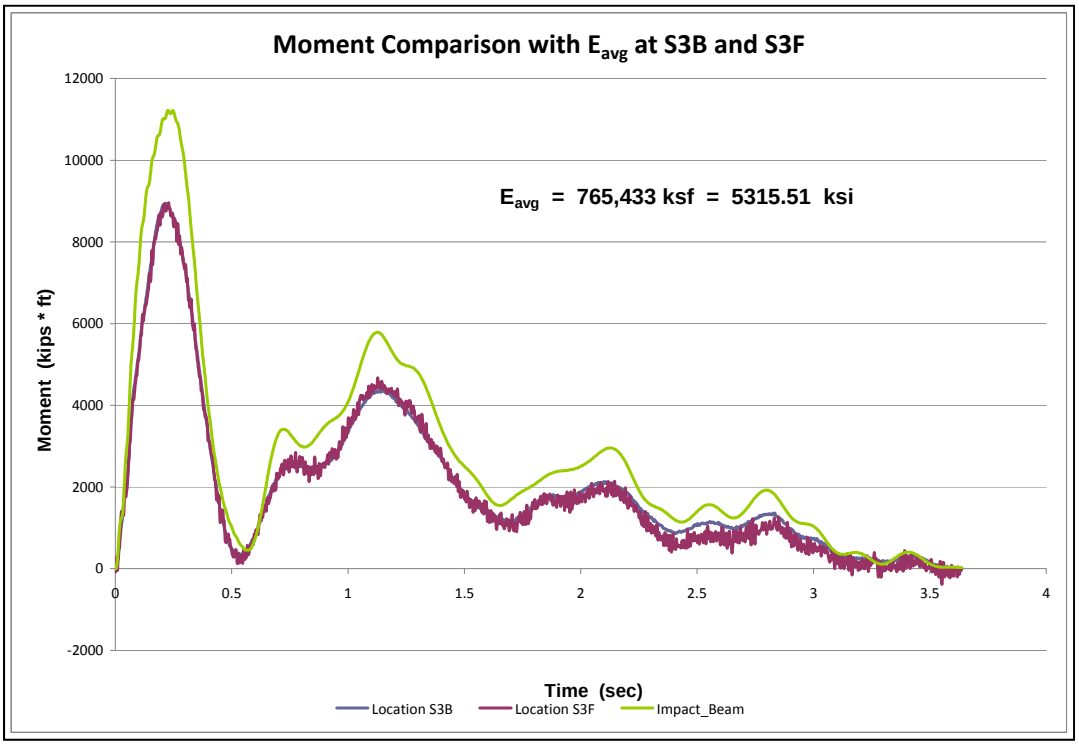

Figure 6.78. Moment comparison with E_{avg} at S3-Test #20.

6.5 Summary of the values for the dynamic modulus of elasticity

This section presents the resulting values for the dynamic modulus of elasticity estimated based on experimental beam deflection and experimental curvatures. The experimental beam deflections for Winfield Test#10 produced values in the range of 5,500 ksi. But the strain gage data for this test, transformed to curvatures as explained in Chapter 5, produces high values of dynamic modulus of elasticity that range to the order of over 10,000 ksi. Both sets of data are repeated for Winfield Test#10 in Table 6.2. The computed value, based on correlations to the unconfined compressive strength defined in the literature with a value of 1.3 times the static modulus of elasticity (as per Nam, Compomanes and Kim, 1977, and Johns and Belanger, 1981), is 5,336.12 ksi (see Section 5.3.2.3). This value is based on the 28-day design compressive strength of 5,000 ksi which is adjusted for long term strength increase. The resulting dynamic modulus of elasticity values for the laser deflection data agrees very well with this definition for Winfield Test #10. The data reduction for the complete set of barge impact tests is summarized in Table 6.2.

In Barge Impact Tests #14-20, complete data for the neoprene displacement for the beam was unavailable due to a loss of sensor information at the end of the beam. For these tests, the neoprene displacement was estimated based on laser displacement sensors near the end of the impact beam and the adjacent beam on the upstream side of the impact beam (LD7 and LD6, respectively). The values for laser deflection for sensors LD3, LD4, and LD5 were determined using the Impact_Beam software for the computed literature dynamic modulus of elasticity and the average dynamic modulus of elasticity discussed below at the target sensor location. A dynamic modulus of elasticity value consistent with the Winfield Test data was then determined for sensors LD3, LD4, and LD5 by performing a linear interpolation/extrapolation using the peak measured deflection from the appropriate Winfield Test and the force acting on the beam at that location and at that time. The resulting values are shown with asterisks in Table 6.2. The extreme dynamic modulus results for Tests 14 and 17 reveal that this method may be error-prone due to the interpolation of the LD6 and LD7 sensor data or the accuracy of measurements for very low deflection or force. These results were calculated but not used to determine the statistics of the chart, or the average dynamic modulus of elasticity value. The positions of the sensor locations are explained in Appendix J.

Table 6.2. Summary of the values for the dynamic modulus of elasticity for each test and each sensor.

	MAXIMUM NORMAL	Laser Deflection Sensors			Strain Sensors									
Test #	FORCE (kips)	LD3 (ksi)	LD4 (ksi)	LD5 (ksi)	S1B (ksi)	S1F (ksi)	S2B (ksi)	S2F (ksi)	S3B (ksi)	S3F (ksi)	S4B (ksi)	S4F (ksi)	S5B (ksi)	S5F (ksi)
6	285.93	5,968.75	6,055.56	6,104.17	11,027.80	14,364.60	9,812.50	10,340.30	7,947.92	8,395.83	10,538.20	10,930.60	12,559.00	12,642.40
7	255.85	6,451.39	6,545.14	6,576.39	11,510.40	11,479.20	9,805.56	5,885.42	N/A	6,565.97	N/A	9,201.39	12,055.60	11,937.50
8	297.2	6,350.69	5,788.19	5,538.19	13,045.10	14,836.80	11,725.70	9,184.03	8,704.86	8,343.75	9,746.53	8,354.17	11,329.90	10,798.60
9	359.84	5,937.50	5,559.03	5,371.53	12,572.90	17,576.40	10,694.40	11,513.90	7,743.06	9,055.56	9,829.86	9,965.28	11,475.70	13,611.10
10	517.42	5,533.00	5,642.00	5,549.00	10,569.00	12,812.00	9,194.00	7,354.00	7,757.00	8,479.00	N/A	11,722.00	N/A	16,313.00
11	124.57	7,888.89	8,052.08	8,145.83	8,868.06	10,024.30	9,388.89	10,486.10	9,100.69	10,128.50	9,468.75	9,100.69	11,697.90	12,361.10
12	59.27	6,555.56	6,743.06	6,791.67	8,774.31	13,496.50	8,621.53	11,069.40	7,555.56	7,156.25	8,409.72	7,541.67	10,347.20	11,642.40
13	150.11	6,962.00	6,902.78	7,000.00	12,288.20	11,305.60	10,434.00	6,718.75	8,315.97	6,812.50	9,906.25	7,576.39	12,128.50	8,086.81
14	111.05	*7,497.74	*7,370.10	*6,978.98	10,972.20	N/A	10,691.00	14,829.90	8,347.22	12,243.10	9,059.03	18,659.70	11,197.90	13,982.60
15	235.27	*8,710.99	*8,560.05	*8,002.82	13,541.70	17,465.30	11,381.90	8,805.56	9,472.22	9,343.75	9,930.56	9,520.83	10,569.40	15,909.70
16	355.03	*6,036.20	*5,998.51	*6,135.10	9,972.22	12,062.50	8,687.50	8,437.50	7,208.33	6,965.28	9,059.03	9,656.25	10,538.20	10,197.90
17	226.07	*7,071.57	*7,102.42	*7,297.67	11,329.90	12,614.60	9,875.00	8,815.97	8,659.72	7,909.72	10,270.80	11,006.90	12,531.30	11,333.30
20	411.44	*6,146.19	*6,129.65	*6,260.43	9,795.00	11,336.00	8,555.00	7,180.00	7,295.00	7,284.00	8,972.22	8,958.00	10,715.30	11,201.00
Minimum	59.27	5,533.00	5,559.03	5,371.53	8,774.31	10,024.30	8,555.00	5,885.42	7,208.33	6,565.97	8,409.72	7,541.67	10,347.20	8,086.81
Maximum	517.42	7,888.89	8,052.08	8,145.83	13,541.70	17,576.40	11,725.70	14,829.90	9,472.22	12,243.10	10,538.20	18,659.70	12,559.00	16,313.00
Average	-	6,455.97	6,410.98	6,384.60	11,097.45	13,281.15	9,912.84	9,278.53	8,175.63	8,360.25	9,562.81	10,168.76	11,428.83	12,309.03
Std. Dev.	-	725.89	836.21	941.33	1,506.00	2,398.61	1,031.16	2,396.78	714.16	1,582.23	632.91	2,842.72	781.82	2,253.41
COV	-	0.1124	0.1304	0.1474	0.1357	0.1806	0.1040	0.2583	0.0874	0.1893	0.0662	0.2796	0.0684	0.1831

* These tests did not have adequate sensor coverage, and data has been estimated for the end-beam deflections

The average dynamic modulus of elasticity using Winfield Barge Impact Tests 6 through 13 for the laser deflection sensor # LD3 is equal to 6,455.97 ksi (Table 6.2). The average values for laser deflection sensors LD4 and LD6 are 6,410.98 ksi and 6,384.60 ksi, respectively. The average for these three laser deflection sensors is 6,417.18 ksi. This average value from all laser deflection sensors is 20.25 percent above the estimated dynamic modulus of elasticity (5,336.12 ksi) from the literature (i.e., 1.3 times the long-term static value). This average value of 6,417.18 ksi that was obtained from the laser deflection sensor data is in the range of 1.56 times the long-term static modulus of elasticity value (4,104.71 ksi). However, the resulting values obtained from the strain gages were not in the same range (see average values cited in Table 6.2). Further research is recommended to determine why the strain gage sensors recorded normal strains lower than expected for the magnitude of the applied load, resulting in the higher than expected dynamic modulus of elasticity.

6.6 Interpretation of the variation of the beam deflection based on fundamental natural period of the Winfield impact beam

The Impact_Beam computer program was validated using the well-known structural analysis computer program SAP2000, as discussed in Chapter 5. The same beam model was analyzed with both programs and the fundamental natural period of the Winfield impact beam was determined. Both software packages produced basically the same results. That is, the fundamental natural period of the Winfield impact beam was 0.2 seconds.

In this section, an interpretation of the variation of the beam deflection is presented based on the computed fundamental natural period. The comparison has to be made by transforming the continuous elastic beam in a SDOF oscillator system. The mass per unit length of the beam is estimated at 0.25486 kips•s^2/ft/ft. The total mass of the beam is the mass per unit length times the total length of the beam of 112.6 ft. The computed total mass is 28.697 kips•s^2/ft. To transform the continuous beam in a SDOF system, it is expected that half of the total beam mass will contribute to the SDOF model and ¼ of the mass goes to each support. Finally, the contributing mass of the continuous beam to the SDOF model is half of the mass and is equal to 14.3486 kips•s^2/ft (= 1.1957 kips•s^2/in). The stiffness of the SDOF oscillator can be calculated based on the maximum experimental recorded normal force and the experimental maximum beam deflection along the beam (LD4). Table 6.3 shows the maximum normal force and the maximum beam deflection which occurs at the LD4 sensor for

each test. It is important to mention that the location of the maximum normal force along the beam and the location of the LD4 sensor are not coincident locations. However, they are close enough to provide a good estimate of the displacement associated to the applied normal force. Based on the SDOF model of the continuous beam, the resulting fundamental natural periods agree perfectly with the fundamental natural period produced by SAP2000 and Impact_Beam. The fundamental natural period of the SDOF model is in the range of $0.196 \leq T \leq 0.211$ seconds. That result means that the fundamental natural period is the predominant mode of vibration for the simply supported beam and that higher modes will have small contribution to the total vibration. The resulting value for each test is summarized in Table 6.3.

Table 6.3. Fundamental natural period based on a SDOF model using experimental peak beam displacement and peak forces.

Test #	F_{max} (kip)	Beam Deflection			$k = \frac{F_{max}}{Beam\ Deflec._{LD4}}$ (kip / in)	ω (rad / sec)	T (sec)
		LD3 (in)	LD4 (in)	LD5 (in)			
9	359.84	0.258	0.294	0.282	1,223.95	31.99	0.196
10	517.42	0.399	0.424	0.376	1,220.33	31.94	0.197
12	59.27	0.497	0.051	0.046	1,162.16	31.18	0.202
16	355.03	0.301	0.330	0.302	1,075.85	29.99	0.209
17	226.07	0.194	0.213	0.195	1,061.36	29.79	0.211
20	411.44	0.346	0.382	0.351	1,077.07	30.01	0.209

6.7 Conclusions

6.7.1 Final remarks on dynamic modulus computation

This chapter presented a summary of the analysis performed to estimate the dynamic modulus of elasticity for each Winfield test. The results are consistent with those presented in Chapter 5. The full-scale experimental beam deflections were used to estimate the dynamic modulus of elasticity which produced a dynamic amplification factor (dynamic modulus over the long-term static modulus) of approximately 1.56. This value is above the range reported in the technical literature, which was an approximate dynamic amplification factor of 1.3. This measured dynamic amplification factor is 1.2 times the literature dynamic amplification factor. For beam normal strain experimental data transformed into curvatures, high values of the dynamic modulus of elasticity resulted from the data processing. It is believed that these values are in error, but more research will need to be done to ascertain the reason for the discrepancy. Also, to demonstrate that

the experimental beam deflection data are satisfactory, an analysis of the fundamental natural period of the continuous beam transformed into a SDOF model was performed. The fundamental natural period of the Winfield impact beam was determined by SAP2000 and Impact_Beam and had similar values of around 0.2 seconds. The calculated fundamental period for the SDOF model, with a stiffness coefficient calculated using the beam deflection and the maximum normal force for each test, produced fundamental natural periods between 0.196 seconds and 0.211 seconds. These results imply that the beam deflection is a good measure of the response of the Winfield impact beam system.

6.7.2 Final remarks regarding Impact_Beam verification

Dynamic Impact_Beam simulations for barge impact were validated against recorded sensor results for a series of full-scale barge impact tests conducted at Winfield lock and dam. Two sets of sensor data were used in this investigation: beam deflections were measured using laser deflection sensors and the in-line displacement of the beam was removed using LVDT and LD sensor data from the adjacent beams, and internal bending strains for determination of moments were measured with strain gages. Computed deflections were a match for recorded deflection sensor data and simulation results from SAP-2000 and dBEAS when an appropriate value of the dynamic modulus is assigned. The simulation bending moment computations had consistent waveforms to the recorded sensor data but differed in amplitude due to the magnitude of dynamic modulus computed from the normal strain sensor data. The reason for this difference is unknown. However, with the correct dynamic Young's modulus, Impact_Beam will provide correct results because the computed wave form is consistent.

Figures 6.79 and 6.80 show the results of processing the inputs that correspond with the Winfield Test #10, and the actual measured values from Winfield Test #10. The value for the dynamic Young's modulus used in the simulation was the value determined from the mean of the three sensor averages, at 6,417.18 kips per square inch. The full beam plot is shown at the time 0.25 seconds that corresponds to the peak deflection of sensor LD3, which is in the region of the moving impact. It is apparent that the magnitudes and trends of the computed deflection histories agree with the Winfield measurements to a significant degree of precision.

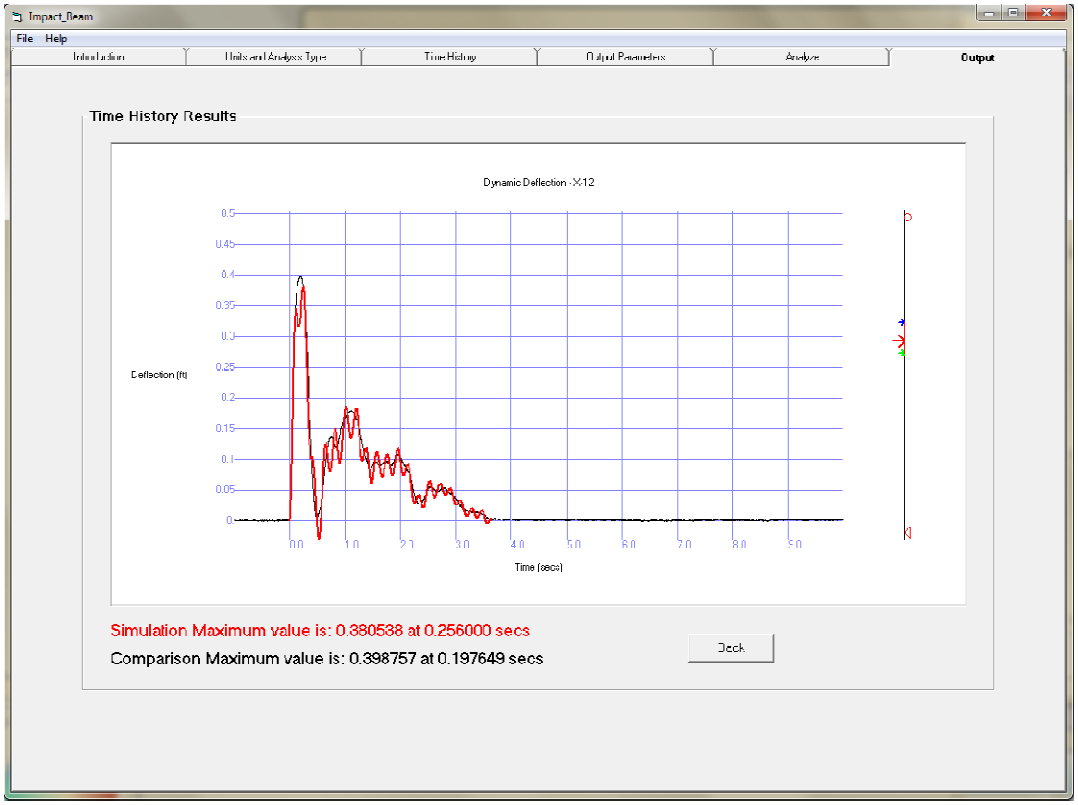

Figure 6.79. Comparison of dynamic deflections at sensor location LD3 for Impact_Beam results and Winfield Test #10 measurements.

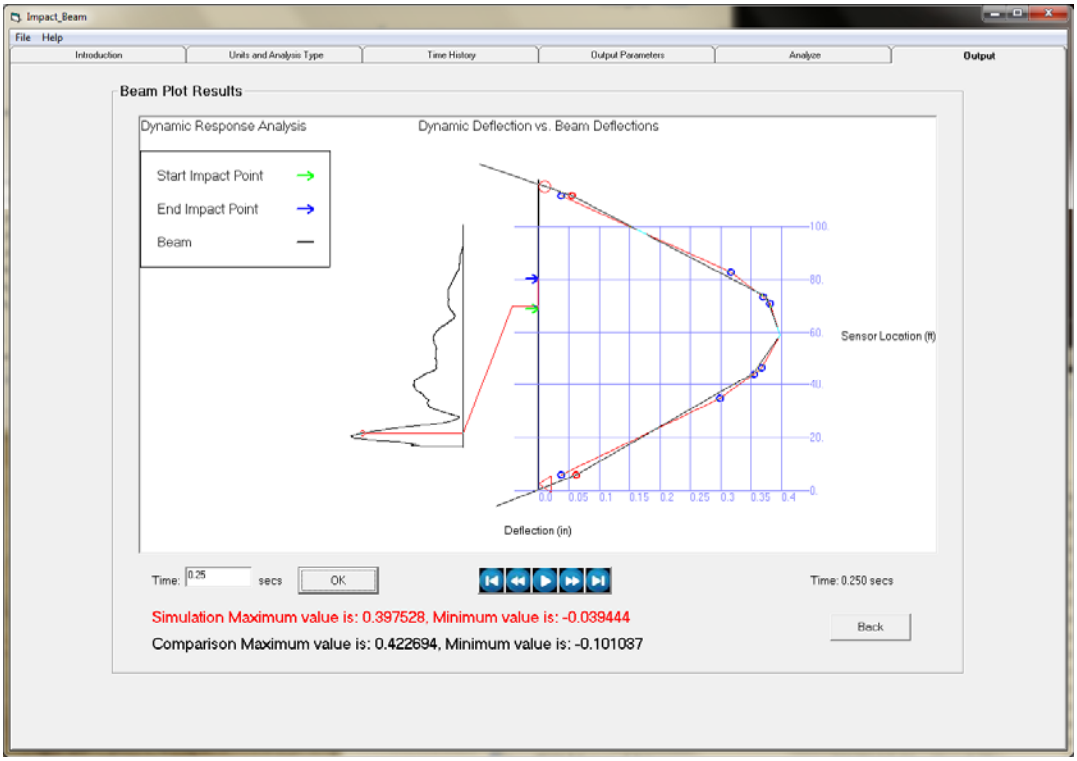

Figure 6.80. Simulated Beam response compared to Winfield Test #10 response at 0.25 seconds.

References

American Association of State Highway and Transportation Officials. 1998. *AASHTO LRFD Bridge Design Specifications: Customary U.S. Units, Second Edition*. Washington, DC: American Association of State Highway and Transportation Officials, Section 14.

Barker, B. C., R. M. Ebeling, C. E. Gray, R. W. Haskins, and T. W. Warren. 2010. *Barge Impact Experiments at Winfield Lock and Dam*, Winfield, West Virginia, unpublished on-site field data collection. Vicksburg, MS: US Army ERDC.

Branson, D. E., *Deformation of Concrete Structures*. New York, NY: McGraw-Hill Book Company.

Carrasquillo, Nilson, and Slate, Properties of High Strength Concrete Subject to Short Term Loads, ACI Journal, May – June 1981, pp. 171 – 178.

Cernica, J. N. 1966. *Strength of Materials*. New York, NY: Holt, Rinehart and Winston, Inc..

Chopra, A. K. 1981. *Dynamics of Structures: A Primer*. Berkeley, CA: Earthquake Engineering Institute.

Chopra, A. K., 1995. *Dynamics of Structures; Theory and Applications to Earthquake Engineering*. Englewood Cliffs, NJ: Prentice Hall.

Chopra, A. K., 2001. *Dynamics of Structures; Theory and Applications to Earthquake Engineering,* second edition. Englewood Cliffs, NJ: Prentice Hall.

Clough, R. W., and J. Penzien. 1993. *Dynamics of Structures*, Second edition. New York, NY: McGraw-Hill, Inc.

Computers and Structures, Inc., SAP2000 Static and Dynamic Finite Element Analysis of Structures Nonlinear 8.2.3, Berkeley, CA, 2003.

Craig, R. R., 1981. *Structural Dynamics, An Introduction to Computer Methods*. New York, NY: John Wiley & Sons, Inc.

Derham, C. J. 1982. *The Design Of Laminated Bearings II*. Hertford, UK: The Malaysian Rubber Producers' Research Association.

Ebeling, R. M. 1992 (June). *Introduction to the computation of response spectrum for earthquake loading*. Computer-Aided Structural Engineering (CASE) Project TR ITL-92-4. Vicksburg, MS: U.S. Army Waterways Experiment Station.

Ebeling, R. M., B. C. White, A. N. Mohamed, and B. C. Barker. 2010. *Force Time-History During the Impact of a Barge Train Impact With A Approach Lock Wall Using Impact_Force*. ERDC/ITL TR-10-XX. Vicksburg, MS: U.S. Army Engineer Research and Development Center.

Ebeling, R. M., B. C. White, R. W. Strom, J. E. Hite, B. C. Barker, and R. W. Haskins. 2011. *Deformable Bullnose Energy Absorbing System (BEAS), Report 2: Head-on Impact with a Deformable BEAS and Introducing a Collapsible Arch*. ERDC/ITL TR-11-XX (in publication). Vicksburg, MS: U.S. Army Engineer Research and Development Center.

El-Tawil, S., E. Severino, and P. Fonseca. 2005, Vehicle Collision with Bridge Piers, *Journal of Bridge Engineering*, ASCE, May/June, pp.345-353.

Headquarters, Department of the Army. 1995. *Gravity Dam Design, Engineer Manual 1110-2-2200*. Washington, DC: Headquarters, Department of the Army.

Inca Engineers, Inc. 1996. *Winfield Lock and Dam Upstream Guard and Guide Walls, Appendix V. Engineering Calculations: Volume 3 of 3*. Inca Engineers Inc. for USACE Huntington District.

Johns and Belanger, Dynamic Stiffness of Concrete Beams, ACI Journal, May-June 1981, pp. 201 – 205.

Kelly, J. M. 1991. Lecture Notes for Corps Base Isolation Workshop, Base Isolation & Energy Dissipation Lecture Series, Lecture 13: Design Process for Multilayer Elastomeric Bearings. Workshop held at US Army Construction Engineering Research Laboratory, Champaign, IL, July 22 - 26, 1991.

Nam, C. H., N. U. Compomanes, and Y. K. Kim. Design of Framed Foundations Subjected to Vibrations, *Computer and Structures*, V.7, 1977, pp. 103-107.

Patev, R. C., B. C. Barker, and L. V. Koestler. 2003. *Prototype Barge Impact Experiments, Allegheny Lock and Dam 2, Pittsburgh, Pennsylvania*. ERDC/ITL TR-03-2. Vicksburg, MS: U.S. Army Engineer Research and Development Center.

Paz, M. 1985. *Structural Dynamics; Theory and Computation, second edition*. New York, NY: Van Nostrand Reinhold Company.

Paz, M. 1991. *Structural Dynamics; Theory and Computation, third edition*. New York, NY: Van Nostrand Reinhold Company.

Podolny, Jr., W., and J. M. Muller. 1982. *Construction and Design of Prestressed Concrete Segmental Bridges*. New York, NY: Wiley-Interscience Publication,

Tabsh, S. W., and A. Aswad. Statistical Properties of Plant-Produced High Strength Concrete in Compression, PCI Journal, July-August 1995, pp. 72-77.

Appendix A: Traditional Single-Degree-of-Freedom System Free Vibration Response

Figure A.1 shows a mathematical model of a single degree of freedom (SDOF) system commonly used in structural dynamics. The mass of magnitude *m* is attached to a fixed reference system with a linear elastic spring and damper. The Figure A.1 SDOF system is subjected to an initial displacement at time equal to zero of magnitude x_o and an initial velocity of magnitude $\dot{x}_o$ which sets the SDOF system in free vibration response.

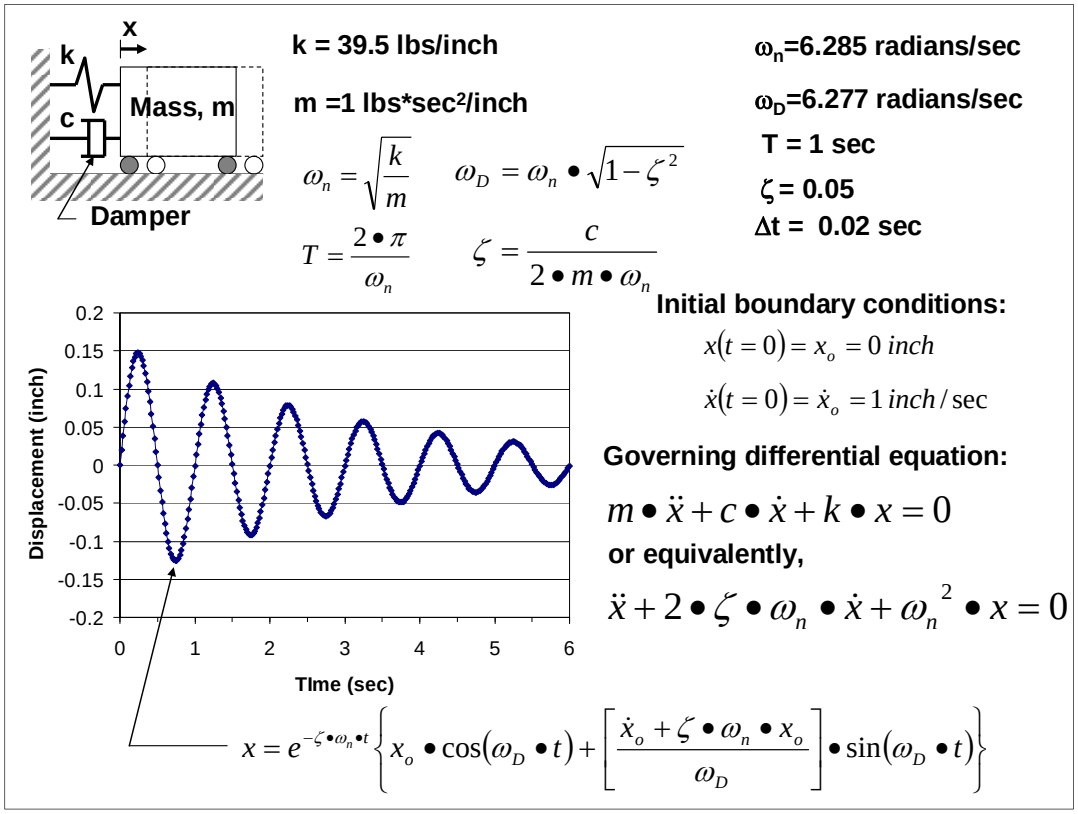

Figure A.1. Free vibration response example of a damped SDOF system with a natural period *T* of 1 second.

The governing differential equation for the free-vibration state for a SDOF system is

$$m \bullet \ddot{x} + c \bullet \dot{x} + k \bullet x = 0 \qquad \text{(A.1)}$$

Note that in free vibration response, the right-hand side of Equation A.1 is equal to zero.[1] Introducing the critical damping ratio ζ, defined as

$$\zeta = \frac{c}{2 \bullet m \bullet \omega_n} \tag{A.2}$$

Equation A.1 becomes

$$\ddot{x} + 2 \bullet \zeta \bullet \omega_n \bullet \dot{x} + \omega_n{}^2 \bullet x = 0 \tag{A.3}$$

The undamped natural circular frequency of the SDOF system is

$$\omega_n = \sqrt{\frac{k}{m}} \tag{A.4}$$

The natural period of vibration (undamped) is

$$T = \frac{2 \bullet \pi}{\omega_n} \tag{A.5}$$

The damped natural circular frequency of the SDOF system is

$$\omega_D = \omega_n \bullet \sqrt{1 - \zeta^2} \tag{A.6}$$

and for completeness, the damped natural period of vibration is

$$T_D = \frac{T}{\sqrt{1 - \zeta^2}} \tag{A.7}$$

The solution to the Equation A.3 differential equation is given in numerous textbooks on Structural Dynamics, including Ebeling (1992), as

$$x(t) = e^{-\zeta \bullet \omega_n \bullet t} \left\{ x_o \bullet \cos(\omega_D \bullet t) + \left[\frac{\dot{x}_o + \zeta \bullet \omega_n \bullet x_o}{\omega_D} \right] \bullet \sin(\omega_D \bullet t) \right\} \tag{A.8}$$

[1] In a forced-vibration response problem, the right-hand side of Equation A.1 would be set equal to a forcing function, e.g. $p(t)$, as discussed in Appendix B.

Example: For a K value of 39.5 inches/sec and a mass m of 1 lbs·sec²/ inch, and with initial values of x_o of zero and $\dot{x}_o$ of 1 inch/sec, the first six seconds of free vibration response computed using Equation A.8 with a time increment of 0.02 seconds and the results shown in Figure A.1. The fraction of critical damping ζ is set equal to 0.05 (or equivalently, 5 percent) in this example.

The undamped natural circular frequency of the SDOF system is 6.285 radians/sec by Equation A.4. The (undamped) natural period T for the SDOF is 1 second, by Equation A.5. The damped natural circular frequency of the SDOF system is 6.277 radians/sec by Equation A.6. The displacement response in free vibration is computed using Equation A.8 and shown in Figure A.1.

Figure A.1 observations regarding the impact of 5% damping specified for the SDOF system;

- the amplitude of the periodic response decays with time, and
- the periodic response of the SDOF in free-vibration is slightly longer than the undamped periodic response by a factor equal to 1.001; refer to Equation A.7 with ζ equal to 0.05.

For this example problem in which the initial displacement x_o is set equal to zero and the initial velocity $\dot{x}_o$ is nonzero, the Equation A.8 free-vibration displacement response relationship reduces to

$$x(t) = e^{-\zeta \bullet \omega_n \bullet t} \left\{ \left[\frac{\dot{x}_o}{\omega_D} \right] \bullet \sin(\omega_D \bullet t) \right\} \tag{A.9}$$

Equation A.9 is of special interest in the solution of a forced vibration problem of a SDOF system by Duhamel's Integral (Appendix B).

Appendix B: Application of Duhamel's Integral to Calculate the Displacement Response of a Single Degree of Freedom System

B.1. General formulation of the Duhamel's Integral.

Figure B.1 shows a mathematical model of a single degree of freedom (SDOF) system commonly used in structural dynamics. The mass of magnitude m is attached to a fixed reference system with a linear elastic spring and damper. The Figure B.1 SDOF system is subjected to a pulse force time-history $p(t)$.[1]

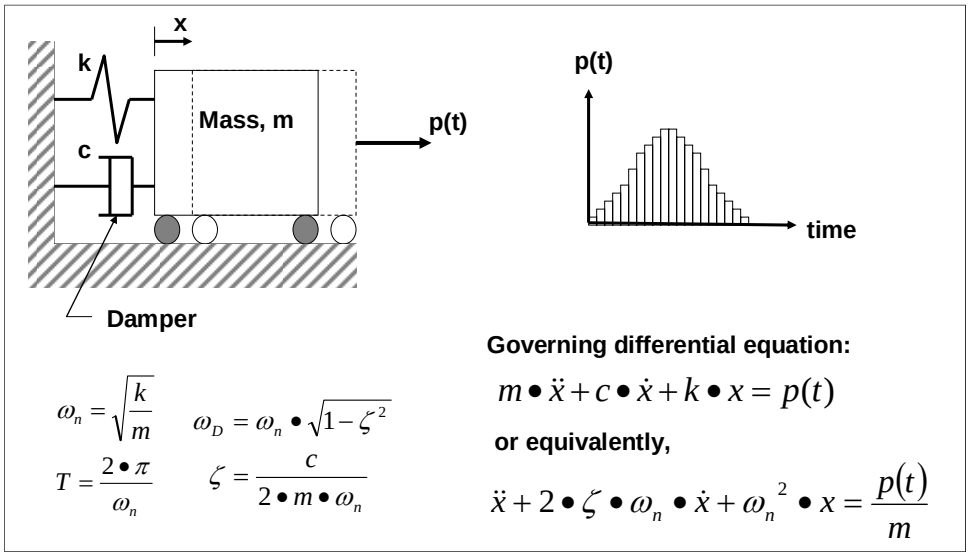

Figure B.1. Damped SDOF system subjected to a pulse force time-history $p(t)$.

The equation of motion is a second order differential equation

$$m \bullet \ddot{x} + c \bullet \dot{x} + k \bullet x = p(t) \tag{B.1}$$

[1] This forcing function could be a constant force of finite time duration, a short duration pulse function that varies in amplitude with time or a harmonic function. See for example, Chopra (1995) Chapter 4 for examples of force-vibration response problems such as a pulse force time-history or Ebeling (1992) for an earthquake time-history applied as a an equivalent forcing function $p(t)$ applied to a SDOF system.

for this SDOF system. One approach for solving for the SDOF system response is application of Duhamel's Integral. It is based on representing the applied force as a sequence of infinitesimally short impulses. The displacement response $x(t)$ of the SDOF system to an applied force that varies in magnitude with time t, $p(t)$, is obtained by adding the responses to all the individual impulses up at a single time t of interest. Note that because superposition is used, application of Duhamel's Integral is limited to linear elastic SDOF systems. Numerous books on Structural Dynamics, including Ebeling (1992)[1] and Chopra (1995)[2], discuss the derivation of the SDOF response relationship to the forced vibration problem.

In summary, the approach is to represent the load time-history $p(t)$ as a series of impulse loadings $p(\tau)$ that are each applied to the SDOF system for infinitesimal time intervals $d\tau$. One impulse (out of the series of impulses) is highlighted in Figure B.2. Using the impulse momentum principle as noted in this figure, the velocity boundary condition at the time t of the application of the impulse is established. (The displacement is zero prior to and up to this single impulse.) This single impulse, converted into an initial velocity boundary condition $\dot{x}_o(\tau) = \frac{p(\tau)}{m} d\tau$ causes a free vibration response from time τ up to time t for the SDOF system.[3] Adapting Equation A.9, the incremental displacement response $dx(t)$ at time t for this single impulse applied at time τ is

$$dx(t) = e^{-\zeta \bullet \omega_n \bullet (t-\tau)} \left\{ \left[\frac{p(\tau) d\tau}{m \bullet \omega_D} \right] \bullet \sin\left(\omega_D \bullet (t-\tau)\right) \right\} \tag{B.2}$$

for $t > \tau$. Equation B.2 would be applied to all remaining impulses shown in Figure B.2 and the final displacement response at time t would equal the sum of these individual responses. The total displacement at time t for all pulses would be

$$x(t) = \int_0^t dx(t) d\tau \tag{B.3}$$

[1] Pages 18-21.

[2] Sections 4.1 and 4.2 on pages 120-123.

[3] Note the equation of motion being solved for the SDOF system is now the homogenous differential equation of Equation A.1.

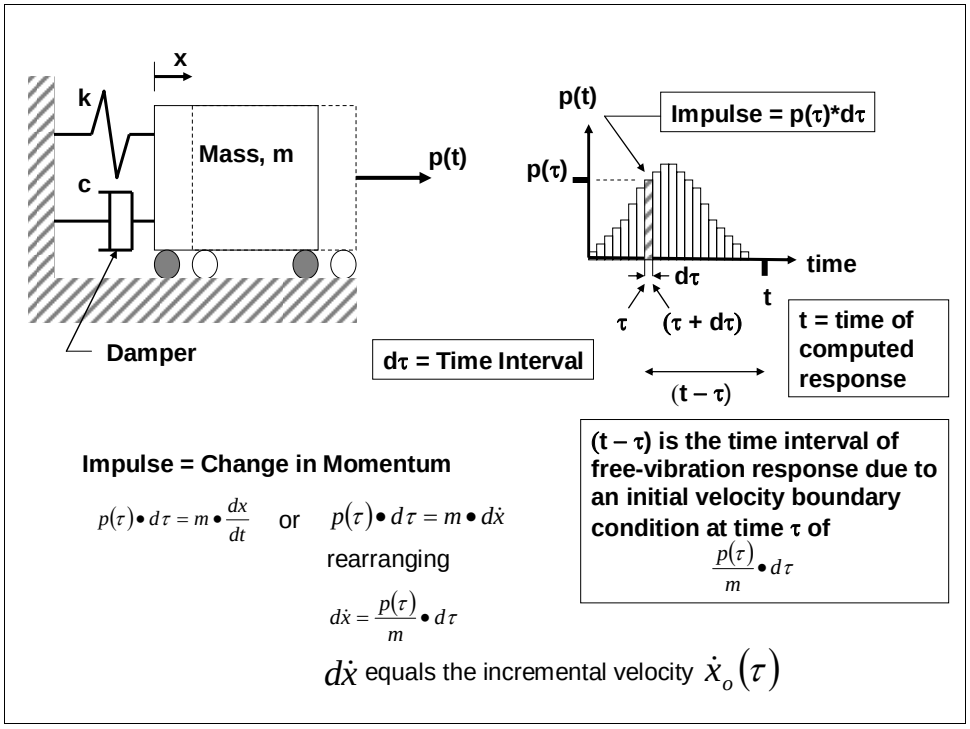

Figure B.2. Conversion of a forcing function time-history to a series of impulses and the response computed at time *t* due to a single impulse in this series of impulses.

Mathematically, this results in Duhamel's Integral expression for a damped SDOF system, as

$$x(t) = \frac{1}{m \bullet \omega_D} \int_0^t p(\tau) \bullet e^{-\zeta \omega_n (t-\tau)} \bullet \sin\left[\omega_D \bullet (t-\tau)\right] d\tau \qquad \text{(B.4)}$$

for a critical damping ratio value β, undamped natural circular frequency ω_n, and damped natural circular frequency ω_D.

Should the SDOF system have an initial displacement x_o and/or initial velocity $\dot{x}_o$ at time *t* equal to zero, the complete equation describing the displacement response of the SDOF system is

$$x(t) = e^{-\zeta \omega_n t} \left\{ x_o \bullet \cos(\omega_D \bullet t) + \left[\frac{\dot{x}_o + \zeta \bullet \omega_n \bullet x_o}{\omega_D} \right] \bullet \sin(\omega_D \bullet t) \right\} + \frac{1}{m \bullet \omega_D} \int_0^t p(\tau) \bullet e^{-\zeta \omega_n (t-\tau)} \bullet \sin\left[\omega_D \bullet (t-\tau)\right] d\tau \qquad \text{(B.5)}$$

B.2. Modification of the equation of motion of underdamped SDOF systems with bilinear elastic spring stiffness

As presented in Section B.1, the equation of motion of a SDOF system with linear elastic spring stiffness as the one shown in Figure B.3 is

$$m\ddot{x} + c\dot{x} + kx = p(t) \tag{B.6}$$

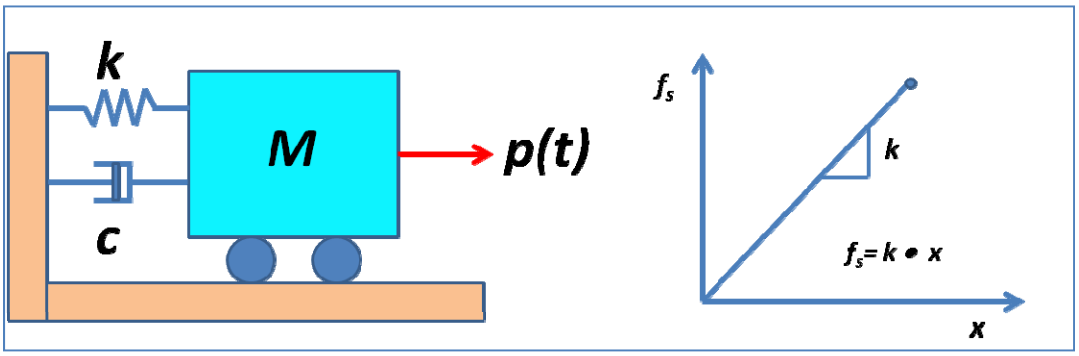

Figure B.3. Single degree of freedom system with linear elastic spring.

In that case, the equation of motion can be solved using the numerical procedures presented in Appendix C. If the single degree of freedom system has a spring with an elastic bilinear stiffness spring, the equation of motion can be modified to account for this elastic bilinear behavior of the spring.

It can be followed easily that for the first slope of an elastic bilinear stiffness, as shown in Figure B.4, the equation of motion that applies is the one presented in Equation (B.6). That is, if the displacement of the mass is equal or below x_1 Equation (B.6) applies. If the displacement of the mass is greater than x_1 and less than x_2 a different equation of motion has to be used. A displacement greater than x_2 indicates a spring model failure.

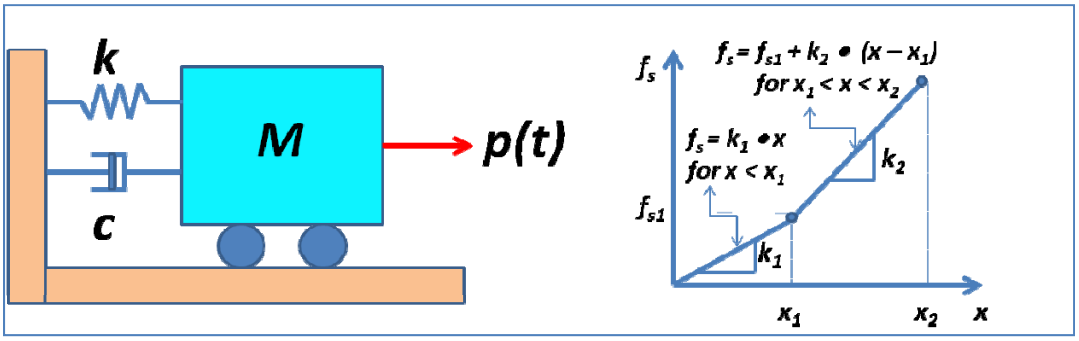

Figure B.4. Single degree of freedom system with bilinear elastic spring.

If the displacement of the SDOF system is greater than x_1 the equation of motion is the following,

$$m\ddot{x} + c\dot{x} + f_s = p(t) \tag{B.7}$$

where the third term to the left (f_s) is the force the spring exerts on the mass. This force is calculated as

$$f_s = k_2 x + f_b \tag{B.8}$$

where f_b is the intercept in the vertical axis, as shown in Figure B.5. Introducing Equation (B.8) into (B.7), a new expression for the equation of motion arrives as

$$m\ddot{x} + c\dot{x} + k_2 x + f_b = p(t) \tag{B.9}$$

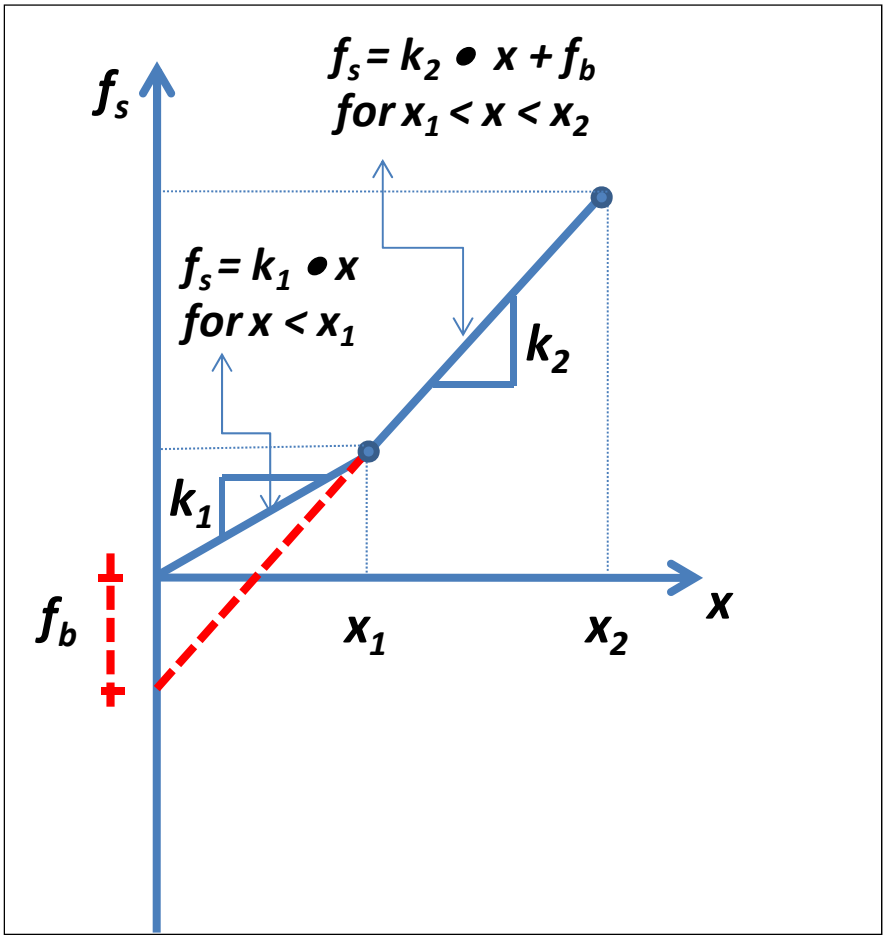

Figure B.5. Modification of the second slope of the force-displacement relationship.

where $x_1 < x < x_2$. Rearranging terms in Equation (B.9), the final equation of motion that is valid for the second slope is

$$m\ddot{x} + c\dot{x} + k_2 x = p(t) - f_b \tag{B.10}$$

or,

$$m\ddot{x} + c\dot{x} + k_2 x = p^*(t) \; for \; x_1 < x < x_2 \tag{B.11}$$

where $p^*(t) = p(t) - f_b$. The equation of motion (Equation B.11) applies if the displacement of the mass is between x_1 and x_2. The equation of motion for the second slope of the elastic bilinear spring is the same as the equation of motion for the first slope of the elastic bilinear spring, Equation (B.6), but with a modification of the excitation.

Appendix C: Numerical Procedure Used to Solve for the Dynamic Displacement of a Generalized Single Degree of Freedom System

C.1. Numerical procedure to solve the Duhamel's Integral

The response of a damped SDOF system expressed by the Duhamel's integral is obtained if the impulse $F(\tau)d\tau$ producing an initial velocity $dv = F(\tau)d\tau/m$ is substituted into the damped free-vibration Equation (C.1).

$$x(t) = e^{-\beta\omega t}(x_0 cos\omega_D t + \frac{v_0 + x_0\beta\omega}{\omega_D} sin\omega_D t) \tag{C.1}$$

Setting $x_0 = 0$, $v_0 = F(\tau)d\tau/m$ and substituting t for $t - \tau$ in Equation (C.1), the differential displacement at time t is

$$dx(t) = e^{-\beta\omega(t-\tau)} \frac{F(\tau)d\tau}{m\omega_D} \sin\omega_D(t-\tau) \tag{C.2}$$

Summing these differential response terms over the entire loading interval results in

$$x(t) = \frac{1}{m\omega_d}\int_o^t F(\tau)e^{-\beta\omega(t-\tau)} \sin\omega_D(t-\tau)d\tau \tag{C.3}$$

which is the response for a damped system in terms of the Duhamel's integral. For numerical evaluation, we proceed with Equation (C.3) as

$$x(t) = \{A_d(t)\sin\omega_D t - B_D(t)\cos\omega_D t\}\frac{e^{-\beta\omega t}}{m\omega_D} \tag{C.4}$$

where

$$A_D(t_i) = A_D(t_{i-1}) + \int_{t_{i-1}}^{t_i} F(\tau)e^{\beta\omega\tau}\cos\omega_D\tau d\tau \tag{C.5}$$

$$B_{D(t_i)} = B_D(t_{i-1}) + \int_{t_{i-1}}^{t_i} F(\tau) e^{\beta\omega\tau} \sin\omega_D \tau d\tau \tag{C.6}$$

For a linear piecewise loading function, $F(\tau)$ is substituted into Equations (C.5) and (C.6) requiring the evaluation of the following integrals:

$$I_1 = \int_{t_{i-1}}^{t_i} e^{\beta\omega\tau} \cos\omega_D \tau d\tau = \frac{e^{\beta\omega\tau}}{(\beta\omega)^2 + \omega_D^2} (\beta\omega \cos\omega_D \tau + \omega_D \sin\omega_D \tau) \Bigg|_{t_{i-1}}^{t_i} \tag{C.7}$$

$$I_2 = \int_{t_{i-1}}^{t_i} e^{\beta\omega\tau} \sin\omega_D \tau d\tau = \frac{e^{\beta\omega\tau}}{(\beta\omega)^2 + \omega_D^2} (\beta\omega \sin\omega_D \tau - \omega_D \cos\omega_D \tau) \Bigg|_{t_{i-1}}^{t_i} \tag{C.8}$$

$$I_3 = \int_{t_{i-1}}^{t_i} \tau e^{\beta\omega\tau} \sin\omega_D \tau d\tau = \left(\tau - \frac{\beta\omega}{(\beta\omega)^2 + \omega_D^2}\right) I_2' + \frac{\omega_D}{(\beta\omega)^2 + \omega_D^2} I_1' \Bigg|_{t_{i-1}}^{t_i} \tag{C.9}$$

$$I_4 = \int_{t_{i-1}}^{t_i} \tau e^{\beta\omega\tau} \cos\omega_D \tau d\tau = \left(\tau - \frac{\beta\omega}{(\beta\omega)^2 + \omega_D^2}\right) I_1' - \frac{\omega_D}{(\beta\omega)^2 + \omega_D^2} I_2' \Bigg|_{t_{i-1}}^{t_i} \tag{C.10}$$

where I_1' and I_2' are the integrals indicated in Equations (C.7) and (C.8) before their evaluation at the limits. In terms of these integrals, $A_D(t_i)$ and $B_D(t_i)$ may be evaluated from

$$A_D(t_i) = A_D(t_{i-1}) + \left(F(t_{i-1}) - t_{i-1}\frac{\Delta F_1}{\Delta t_i}\right) I_i + \frac{\Delta F_i}{\Delta t_i} I_4 \tag{C.11}$$

$$B_D(t_1) = B_D(t_{i-1}) + \left(F(t_{i-1}) - t_{i-1}\frac{\Delta F_i}{\Delta t_i}\right) I_2 + \frac{\Delta F_i}{\Delta t_i} I_3 \tag{C.12}$$

Finally, the substitution of Equations (C.11) and (C.12) into Equation (C.4) gives the displacement at time t_i as

$$x(t_i) = \frac{e^{-\beta\omega t_i}}{m\omega_D} \{A_D(t_i) \sin\omega_D t_i - B_D(t_i) \cos\omega_D t_i\} \tag{C.13}$$

C.2. Numerical evaluation of the response of underdamped SDOF systems subjected to an arbitrary dynamic excitation by using the recursive alternate formulation (explicit formulation)

Because of its convenience, precision, and simplicity, one of the most used methods to calculate in a numerical fashion the response of a SDOF oscillator is based on a recursive equation used to calculate the response at the end of the time interval as a function of the response at the beginning of the time interval and the excitation of the interval. Consider the case of a viscous underdamped oscillator, which means a system with damping ratio β<1. Assume the response $u(t)$ is wanted at the same instant of time t but using another time scale τ as shown in Figure B.2. The expression to calculate the response due to initial conditions and due to an external load for this new time scale is the following:

$$x(\tau)=\left(u_i\cos\omega_d\tau+\frac{\dot{x}_i+\beta\omega_n u_i}{\omega_d}\sin\omega_d\tau\right)e^{-\beta\omega_n\tau}+\int_0^{\tau}f(\tau_1)h(\tau-\tau_1)d\tau_1 \qquad \text{(C.14)}$$

where the integral in Equation (C.14) is known as the Duhamel's Integral and the unit impulse response function for an underdamped system is;

$$h(\tau-\tau_1)=\frac{1}{m\omega_d}\sin\omega_d(\tau-\tau_1)e^{-\beta\omega_n(\tau-\tau_1)} \qquad \text{(C.15)}$$

To solve the Duhamel's Integral in Equation (C.14), a variation for the excitation is assumed. If we adopt a constant variation of the excitation at each time step, then $f(\tau_1) = F_i$, as shown in Figure B.2, and the integral results in;

$$\int_0^{\tau}f(\tau_1)h(\tau-\tau_1)d\tau_1=\frac{F_i}{m\omega_d}\int_0^{\tau}\sin\omega_d(\tau-\tau_1)e^{-\beta\omega_n(\tau-\tau_1)}d\tau_1 \qquad \text{(C.16)}$$

The solution of this integral for a constant load for each time step is;

$$\int_0^{\tau}f(\tau_1)h(\tau-\tau_1)d\tau_1=\frac{1}{m\omega_n^2}\left[1-\left(\cos\omega_d\tau+\frac{\beta}{\sqrt{1-\beta^2}}\sin\omega_d\tau\right)e^{-\beta\omega_n\tau}\right]F_i \qquad \text{(C.17)}$$

Then, substituting Equation (C.17) back into Equation (C.14) and reordering terms, the response in the interval $0 \le \tau \le h$ is;

$$x(\tau)=\left(\cos\omega_d\tau+\frac{\beta}{\sqrt{1-\beta^2}}\sin\omega_d\tau\right)e^{-\beta\omega_n\tau}x_i+\left(\frac{1}{\omega_d}\sin\omega_d\tau\right)e^{-\beta\omega_n\tau}\dot{x}_i \\ +\frac{1}{m\omega_n^2}\left[1-\left(\cos\omega_d\tau+\frac{\beta}{\sqrt{1-\beta^2}}\sin\omega_d\tau e^{-\beta\omega_n\tau}\right)\right]F_i \tag{C.18}$$

The velocity at the same time interval can be obtained taking the first derivative with respect to $\boldsymbol{\tau}$ of Equation (C.18). The resulting expression is;

$$\dot{x}(\tau)=\left(-\frac{\omega_n}{\sqrt{1-\beta^2}}\sin\omega_d\tau\right)e^{-\beta\omega_n\tau}x_i+\left(\cos\omega_d\tau-\frac{\beta}{\sqrt{1-\beta^2}}\sin\omega_d\tau\right)e^{-\beta\omega_n\tau}\dot{x}_i \\ +\frac{1}{m\omega_n^2}\left(\frac{\omega_n}{\sqrt{1-\beta^2}}\sin\omega_d\tau\right)e^{-\beta\omega_n\tau}F_i \tag{C.19}$$

The next step is to obtain the recursive equation for evaluating Equations (C.18) and (C.19) at $\tau = h = \Delta t$, at the end of the interval. In this case $x(\tau) = x_{i+1}$ and $\dot{u}(\tau) = \dot{x}_{i+1}$, resulting in the following expressions for the displacement and velocity at the end of the time interval.

$$x_{i+1}=\left(\cos\omega_d h+\frac{\beta}{\sqrt{1-\beta^2}}\sin\omega_d h\right)e^{-\beta\omega_n h}x_i+\left(\frac{1}{\omega_d}\sin\omega_d h\right)e^{-\beta\omega_n h}\dot{x}_i \\ +\frac{1}{m\omega_n^2}\left[1-\left(\cos\omega_d h+\frac{\beta}{\sqrt{1-\beta^2}}\sin\omega_d h\right)e^{-\beta\omega_n h}\right]F_i \tag{C.20}$$

$$\dot{x}_{i+1}=\left(-\frac{\omega_n}{\sqrt{1-\beta^2}}\sin\omega_d h\right)e^{-\beta\omega_n h}x_i+\left(\cos\omega_d h-\frac{\beta}{\sqrt{1-\beta_2}}\sin\omega_d h\right)e^{-\beta\omega_n h}\dot{x}_i \\ +\frac{1}{m\omega_n^2}\left(\frac{\omega_n}{\sqrt{1-\beta_2}}\sin\omega_d h\right)e^{-\beta\omega_n h}F_i \tag{C.21}$$

Appendix D: Listing and Description of Impact_Beam ASCII Input Data File (file name:Impact_Beam.IN)

This appendix lists and describes the contents of the ASCII input data file to the FORTRAN engineering computer program portion of Impact_Beam. This data file, always designated as Impact_Beam.IN, is created by the graphical user interface (GUI), the visual modeler portion of Impact_Beam. The software performs a dynamic structural response analysis of a simply supported, flexible impact beam of distributed mass to a barge impact event. The collision of a barge train with an approach wall is represented as a short duration pulse force time-history. The impact force time-history to be used in the Impact_Beam analysis is created by the companion PC-based program Impact_Force (Ebeling, White, Mohamed and Barker, 2010). The engineering formulation for Impact_Force uses the impulse momentum principle to convert the linear momentum of a barge train into a pulse force time-history acting normal to the approach wall. Figure D.1 idealizes the problem being solved.

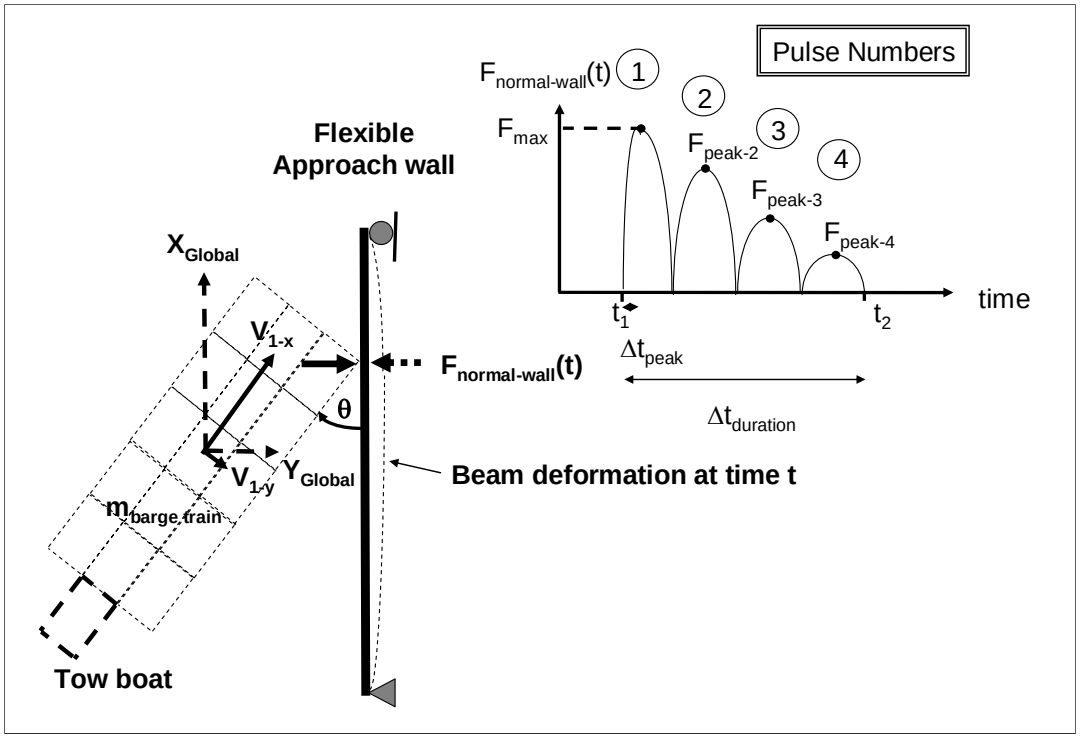

Figure D.1. Impact between a barge train and a simply supported, flexible impact beam that is represented by the user specified pulse force time-history $F_{normal\text{-}wall}(t)$ normal to the beam.

This Impact_Beam software may also be used to compute the dynamic response of a Single-Degree-Of-Freedom (SDOF) system to an external forcing function time-history $p(t)$. Figure D.2 idealizes the problem being solved.

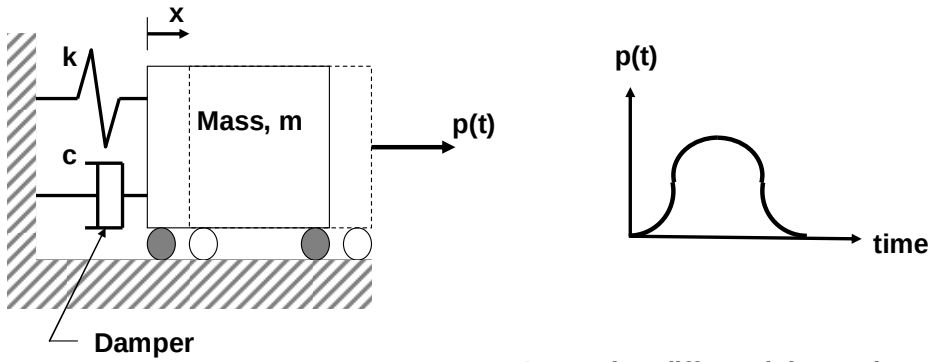

$$c = 2 \bullet m \bullet \omega_n \bullet \zeta$$

$$\omega_n = \sqrt{\frac{k}{m}} \quad \text{in radians/sec}$$

$$T = \frac{2 \bullet \pi}{\omega_n} \quad \text{in seconds}$$

$$f = \frac{1}{T} \quad \text{in Hz}$$

Governing differential equation:

$$m \bullet \ddot{x} + c \bullet \dot{x} + k \bullet x = p(t)$$

or equivalently,

$$\ddot{x} + 2 \bullet \zeta \bullet \omega_n \bullet \dot{x} + \omega_n{}^2 \bullet x = \frac{p(t)}{m}$$

$$\omega_D = \omega_n \bullet \sqrt{1 - \zeta^2} \quad \text{in radians/sec}$$

Figure D.2. The dynamic response problem being solved for a SDOF system subjected to a force time-history $p(t)$.

The ASCII input data to Impact_Force is provided in 7 groups of data for dynamic uniform beam response computations and in 4 groups of data for dynamic SDOF system response computations. They are as follows:

Group #1 – Type of analysis and units for the problem.

KEY_ANALYSIS, Gconstant, Factor_IN

KEY_ANALYSIS = 1 for dynamic response analysis of a simply supported, slender distributed mass beam.

= 2 for a Single Degree of Freedom (SDOF) system.

The values for Gconstant and Factor_IN identify the units of length, acceleration, force (and weight), and mass being used according to the table below.

Value for Gconstant	Value for Factor_IN	Units of Length	Acceleration	Units of Force (and Weight)	Units of Mass
32.174	1000	feet	ft/sec^2	kips	kips-sec^2/ft
386.086	1000	inch	in/sec^2	kips	kips-sec^2/inch
32.174	1	feet	ft/sec^2	lbs	lbs-sec^2/ft
386.086	1	inch	in/sec^2	lbs	lbs-sec^2/inch
9.80665	1	meters	m/sec^2	kN	kN-sec^2/m
980.665	1	centimeters	cm/sec^2	kN	kN-sec^2/cm
9806.65	1	millimeters	mm/sec^2	kN	kN-sec^2/mm

Simply supported, slender flexible impact beam of distributed mass dynamic response problem with KEY_ANALYSIS = 1

Group #2 – Comparison file option of Winfield Barge Impact experimental data

Comp

Comp = 0 for No, a comparison file will not be used in the Impact_Beam analysis

= 1 for Yes, a comparison file will be used in the Impact_Beam analysis

*** Note: The filename of the comparison file is required for Comp = 1. The value for the filename should be placed a line below the value for the Comp variable. A description of the filename is listed directly below. If Comp = 0, then proceed to Group #3.**

Filename

Filename is the full file path name to a Winfield Barge Impact experimental data file. The experimental data file has the beam

deflections, the rigid body deflections, and the strain gages that were recorded on the 25th and 26th August 2008 at the Winfield Lock and Dam in Red House, WV. These experimental data files will be provided to the user under a directory called Winfield_Barge_Impact. The user will select one of these files for comparing the Winfield Barge Impact experimental data results to the results of the Impact_Beam simulation.

An example of specifying the value for Filename would be C:\Temp\filename.dat.

Group #3 – Simply supported, slender flexible impact beam span and properties.

X_Impact, X_Impact_velocity, X_length, Beam_mass, Beam_I, Beam_E, X_Over_Left, X_Over_Right

X_Impact is the point of initial impact along the beam as measured from the support; this distance measurement is in the positive X_{Global} direction (as defined by the direction of the positive barge train approach velocity vector component shown below and parallel to the beam).

X_Impact_velocity is the velocity of the barge train after initial impact as it slides along the impact beam, specified in the positive X_{Global} direction. Note that this global X-velocity may differ from that velocity component of the barge train as it approaches the impact beam and prior to impact. This variable is used to move the user specified impact force time-history along the beam during the impact normal force time-history event. Note: set X_Impact_velocity equal to zero when the impact force time-history is to be specified at a constant position of X_Impact.

X_length is the length of the slender, distributed mass, uniform beam from support center to support center.

Beam_mass is the mass per unit length of the uniform beam.

Beam_I is the moment of inertia of the uniform beam.

Beam_E is the Young's modulus for the beam.

X_Over_Left is the overlap of the beam extending from the left support.

X_Over_Right is the overlap of the beam extending from the right support.

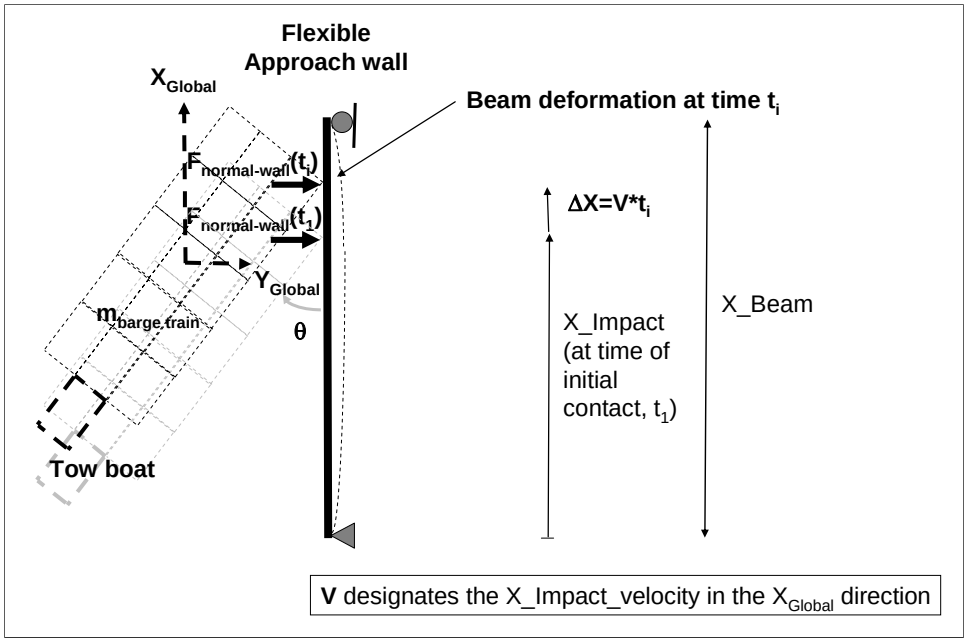

Figure D.3. Definition of the point of initial impact, X_Impact, as measured from the support and the velocity of the barge train, X_Impact_velocity, as it slides along the beam.

Group #4 – Dynamic analysis control information.

No_frequency

XI(j) for j = 1, No_frequency

No_frequency_print

I_out_Frequency(j) for j = 1, No_frequency_print

No_frequency is the total number of beam frequencies to be included in the analysis.[1]

XI(j) is the damping ratio (also referred to as fraction of critical damping) expressed as a decimal fraction for frequency j = 1 through No_frequency.

[1] Accurate dynamic shear force computations typically require more frequencies than dynamic moment computations and accurate dynamic moment computations typically require more frequencies that dynamic displacement computations.

No_frequency_print is the number of SDOF frequencies for which the Duhamel Integral Solution are to be printed.

I_out_Frequency(j) are the frequency numbers for which the Duhamel's Integral solution for the SDOF system output is to be printed, with j = 1 through No_frequency_print.

Group #5 – Dynamic analysis computational output control information.

No_pts_X_out_pt

X_out_pt(j) for j = 1, No_pts_X_out_pt

No_pts_X_out_pt is the number of points along the impact beam that the computed displacements, shear forces and moments (internal to the beam) are reported.

X_out_pt(j) is the coordinate of the point along the beam at which these computations are to be reported, for points j = 1 through No_pts_X_out_pt.

Group #6 – Forcing function time-history *p*(*t*).

DT , No_pts_TH, TMAX, KEY_INT

T_in(i), Force_in(i) for i = 1, No_pts_TH

DT is the incremental time step in seconds.

No_pts_TH is the number of values defining the force time-history $F_{normal\text{-}wall}(t)$ in Figure D.1.

TMAX is the ending time for dynamic beam response in seconds.

KEY_INT is a key to engage interpolation between forcing function p(t) time-history points to match the DT specified for the analysis

= 0 for no interpolation.

= 1 for interpolation.

T_in(i) is the time at time step i in seconds,

Force_in(i) is the user specified pulse force value at time step i, $F_{normal-wall}(t)$ normal to the Figure D.1 beam.

Group #7 – Units for Computed Output.

DISPACC, BMOMACC, Factor_OUT

DISPACC — The value for DISPACC identifies the desired units for the computed dynamic uniform beam displacements.

BMOMACC & Factor_OUT — The values for BMOMACC & Factor_OUT identifies the desired units for the computed dynamic uniform beam bending moments and shear force time histories.

Value for DISPACC	Units of Acceleration	Units of Velocity	Units of Displacement
32.174	ft/sec^2	ft/sec	feet
386.086	in/sec^2	in/sec	inch
9.80665	m/sec^2	m/sec	meters
980.665	cm/sec^2	cm/sec	centimeters
9806.65	mm/sec^2	mm/sec	millimeters

Value for BMOMACC	Value for Factor_OUT	Units of Length	Units of Force	Units of Moment
32.174	1000	feet	kips	ft-kips
386.086	1000	inch	kips	inch-kips
32.174	1	feet	lbs	ft-lbs
386.086	1	inch	lbs	inch-lbs
9.80665	1	meters	kN	m-kN
980.665	1	centimeters	kN	cm-kN
9806.65	1	millimeters	kN	mm-kN

SDOF system dynamic response problem with KEY_ANALYSIS = 2

Group #2 – SDOF model parameters and problem control information.

NTYPE_SDOF, SDOF_M, XI(1), NBASE_ISO

NTYPE_SDOF designates the type of forcing functioning being prescribed.

= 0 for a force time-history $p(t)$ prescribed to the SDOF system mass as shown in Figure D.2

= 1 for a base acceleration time-history $a(t)$; the forcing function $p(t) = -m \bullet a(t)$ as depicted in Figure 10 and discussed in Part IV of Ebeling (1992).

SDOF_M is the mass of the SDOF system.

XI(1) is the damping ratio (also referred to as fraction of critical damping) expressed as a decimal fraction.

NBASE_ISO is the number of base isolators of the SDOF system. The value of NBASE_ISO will determine what kind of slope type will be used in the SDOF analysis.

= 0 for a Linear slope type

= Integer value > 0, for a Bi-Linear slope type

*** Note: The spring stiffness of the SDOF system is required for NBASE_ISO = 0. The value for the spring stiffness should be placed a line below the values for the Group #2 variables mentioned above. A description of the spring stiffness of the Linear case is listed directly below. If NBASE_ISO = 1, then proceed to the next note below in regards to the Bi-Linear slope case.**

SDOF_K

SDOF_K is the spring stiffness of the Linear slope SDOF system.

*** Note: The spring stiffness and the displacement of the SDOF system is required for NBASE_ISO = 1. The value for the spring stiffness and the displacement should be placed a line below the values for the Group #2 variables mentioned above. A description of the spring stiffness and the displacement of the Bi-Linear case is listed directly below. If NBASE_ISO = 0, then proceed to the previous note above in regards to the Linear slope case.**

SDOF_K1, SDOF_K2, SDOF_X1, SDOF_X2

SDOF_K1 is the first spring stiffness of the Bi-Linear slope SDOF system.

SDOF_K2 is the second spring stiffness of the Bi-Linear slope SDOF system.

SDOF_X1 is the first displacement of the Bi-Linear slope SDOF system.

SDOF_X2 is the second displacement of the Bi-Linear slope SDOF system.

Group #3 – Forcing function time-history $p(t)$ or base acceleration time-history $a(t)$.

DT , No_pts_TH, TMAX, KEY_INT
T_in(i), Force_in(i) for i = 1, No_pts_TH

DT is the incremental time step in seconds.

No_pts_TH is the number of values defining the force time-history $p(t)$ or base acceleration time-history $a(t)$.

TMAX is the ending time for SDOF system response in seconds.

KEY_INT is a key to engage interpolation between forcing function $p(t)$ or base acceleration $a(t)$ time-history points to match the DT specified for the analysis

= 0 for no interpolation.

= 1 for interpolation.

T_in(i) is the time at time step i in seconds,

Force_in(i) is the force value at time step i when NTYPE_SDOF equals 0 or the acceleration value expressed as a fraction of g's (a decimal fraction) at time step I when NTYPE_SDOF equals 1.

Group #4 – Units for Output for the problem.

DISPACC, FORCACC, Factor_OUT

DISPACC	The value for DISPACC identifies the desired units of acceleration, computed velocity and computed
FORCACC & Factor_OUT	The values for FORCACC & Factor_OUT identifies the desired units for the computed support forces.

Value for DISPACC	Units of Acceleration	Units of Velocity	Units of Displacement
32.174	ft/sec^2	ft/sec	feet
386.086	in/sec^2	in/sec	inch
9.80665	m/sec^2	m/sec	meters
980.665	cm/sec^2	cm/sec	centimeters
9806.65	mm/sec^2	mm/sec	millimeters

Value for FORCACC	Value for Factor_OUT	Units of Length	Units of Force
32.174	1000	feet	kips
386.086	1000	inch	kips
32.174	1	feet	lbs
386.086	1	inch	lbs
9.80665	1	meters	kN
980.665	1	centimeters	kN
9806.65	1	millimeters	kN

Appendix E: Listing and Description of Impact_Beam ASCII Output Data File (file name: Impact_Beam_Simulation.IBO)

E.1 Description of Output Data File: Impact_Beam_Simulation.IBO

This appendix lists and describes the contents of the ASCII output data file from the FORTRAN engineering computer program portion of Impact_Beam. This data file is always designated as Impact_Beam_Simulation.IBO. The software performs a dynamic structural response analysis of a simply supported, flexible impact beam of distributed mass to a barge impact event.

The ASCII output data from Impact_Beam FORTRAN Code is provided in 2 groups of data. The first group of data contains the general descriptions of the output file. The second group of data contains the results for each of the *output data*, which are; Transverse Displacement (*u*), Dynamic Shear Force (*V*), Dynamic Bending Moment (*M*), Dynamic Impact Factor (*DIF*), Shear Force Impact Factor (*SFIF*) and the Moment Impact Factor (*MIF*). The groups are as follows:

Group #1 – General description

1. **File Identifier Tag** – This line contains a simple string with the value of "Impact_Beam**"**.
2. **Number of Description Lines** – This line presents the number of description lines immediately following. This number can be either 2 or 3. If there are three description lines, a data comparison is being performed.
3. **Description Lines** – These lines contain strings describing the general information about this analysis. If the number of description lines is three, the third line contains the filename of the file used to compare the results against the Impact_Beam results.
4. **Units** – This line contain an echo of the input parameters for unit designation. **KEY_ANALYSIS** – "1" for dynamic response analysis of a simply supported, slender, distributed mass beam and "2" for a SDOF system; **Gconstant** – Floating point value for the constant force of gravity; **Factor_IN** – Floating point factor to determine the units of force;

BEAM_I - Moment of inertia for the beam; **BEAM_E** – Young's modulus for the beam.

5. **Beam Geometry –** This line contains four values. **Beam origin** – A floating point value for the beam simulation reference frame origin; **Effective beam length** – The floating point length of the simulation model from the left reaction to the right reaction; **Left beam overlap** – a floating point value representing the amount of the beam extending beyond the support to the left; **Right beam overlap** – a floating point value representing the amount of the beam extending beyond the support to the right.
6. **Impact Parameters –** This line contains the parameters for the barge train impact with the wall. **Input start point –** a floating point value indicating where the impact occurs along the wall; **Impact Velocity** – a floating point value giving the velocity that the barge train travels along the wall.
7. **Number of output data types** – This line contains an integer number of the different types of output data = 6 (*u, V, M, DIF, SFIF* and *MIF*).

Group #2 – Output data (This data group is repeated six times, one for each output data type as specified in Group #1 - 5)

1. **Description of the output data type –** This line is a string giving the title of the next output corresponding to *u, V, M, DIF, SFIF* or *MIF*.
2. **Total number of locations reporting output along the beam** – This number indicates the total integral number of points along the beam for which results will be reported.
3. **Reporting Beam Location –** This line, which has three values, is repeated for each location reporting output along the beam. **Index of the location of the reported output along the beam** – This integer number identifies the location of each reported output value; **Identifier name for each location** – This non-whitespace string is the name assigned to each location where the results will be reported along the beam; **Location (distance) along the beam for each location** – This is the distance from the beam origin to the location of each reported output value.
4. **Number of connections** – This line contains the integral number of nodes connected from the previous node. At this time, the number is always equal to 1.

5. **Number of connection elements** – This line contains an integral number that is equal to the total number of locations reporting output along the beam.
6. **Index of the location of the reported output along the beam** – This line contains the integral index identifying the location of each reported output value. This line is repeated for the total number of locations reporting output along the beam.
7. **The next two groups are performed for each sensor type:**

- **Analysis Parameters –** This line contains three values. **Start Time** – This floating point value gives the time at which analysis start; **Delta time** – This is a floating point value giving the time step increment for the analysis; **Number of output values for each reported result** – This integral number is the number of available output information for each of the output data types. It is calculated by multiplying the number of time steps by the number of the locations reporting output along the beam.
- **Current Results –** This line is repeated for the number of output values for each reported result. Each line contains the results at a specified time step for specific data at an output reporting point. **Current time step –** The integer index of the current time interval for this step during the analysis**; Index of the location reporting output along the beam** – The number that uniquely identifies the location of each reported output value; **Results** – The floating point data value at this location and at this time step for the output data type.

Group #3 – Reaction Forces (This data group has the shear reactions at the supports for the beam)

1. **Title** – a string reading "Reaction Point Shear"
2. **Number of time steps for reactions –** an integer value giving the number of step 2 reaction force lines below.
3. **Reactions –** one line with two values for each number of time steps. **Left Reaction –** a floating point value for the shear at the left-most support; **Right Reaction** – a floating point value for the shear at the right-most support.

Group #4 – Input Time-History (This data group echoes the input time-history for plotting)

1. **Title** – a string with the title of the section, "Force Time History".
2. **Header lines –** Three lines with the string headers for the time-history.
3. **Time history parameters –** one line with four values. **Time Step Duration –** a floating point value for duration of a time step; **Number of Time Steps –** integral number of time steps for the history; **Time History Duration** – a floating point value with the end time of the time-history; **Interpolation Flag** – an integer telling if the time-history has been interpolated (0 for no interpolation, 1 for interpolation)
4. **Time history lines –** one for each of the number of time steps. **Time –** a floating point value representing the time of the current sample; **Value –** a floating point value with the force for the current time step.

Appendix F: Derivation of the Equations for Deflection of a Simply Supported Beam under a Concentrated Static Load

F.1 Derivation of Equations 3.5 and 3.6

This appendix presents the derivation of Equations (3.5) and (3.6). These equations are used in Impact_Beam computer software to calculate the static transverse deflection of a simply supported beam subjected to a static load as shown in Figure F.1.

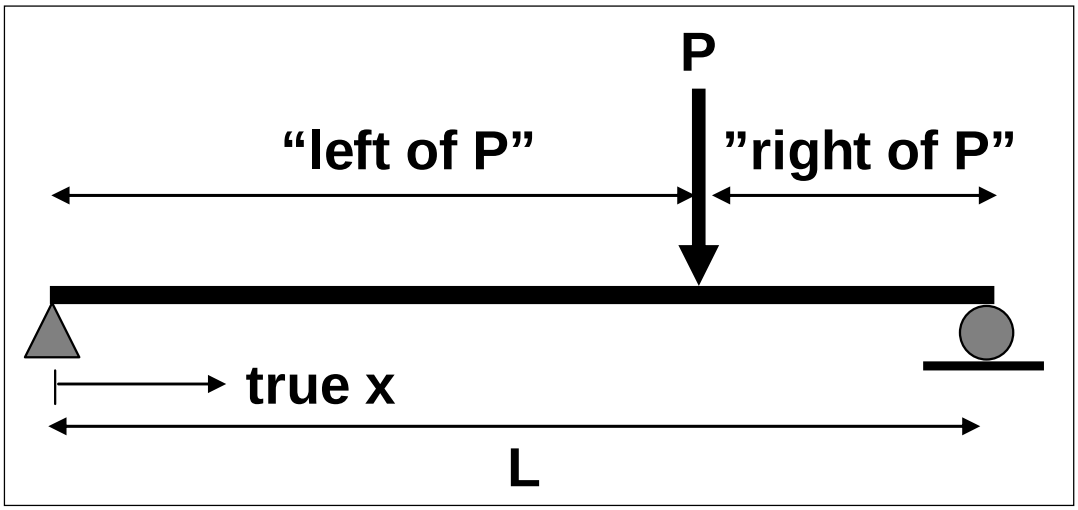

Figure F.1. Simply supported, flexible beam subjected to a static force normal to the beam.

By static equilibrium the left vertical reaction is equal to

$$R_L = \frac{P_b}{L} \tag{F.1}$$

and the right reaction is equal to

$$R_R = \frac{Pa}{L} \tag{F.2}$$

The free body diagram for a segment from $0 \le x \le a$ is presented in Figure F.2.

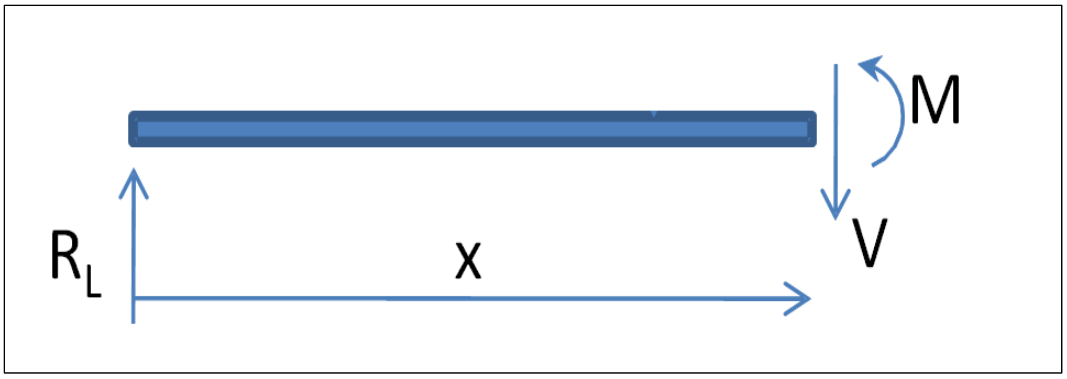

Figure F.2. Free body diagram used to obtain the internal shear force and the internal bending moment from $0 \le x \le a$.

Using this segment of the beam and establishing the equations of equilibrium the internal shear V and internal bending moment M is obtained as

$$V = \frac{Pb}{L} \tag{F.3}$$

$$M = Pb\frac{x}{L} \tag{F.4}$$

The free body diagram for a segment from $a \le x \le L$ is presented in Figure F.3.

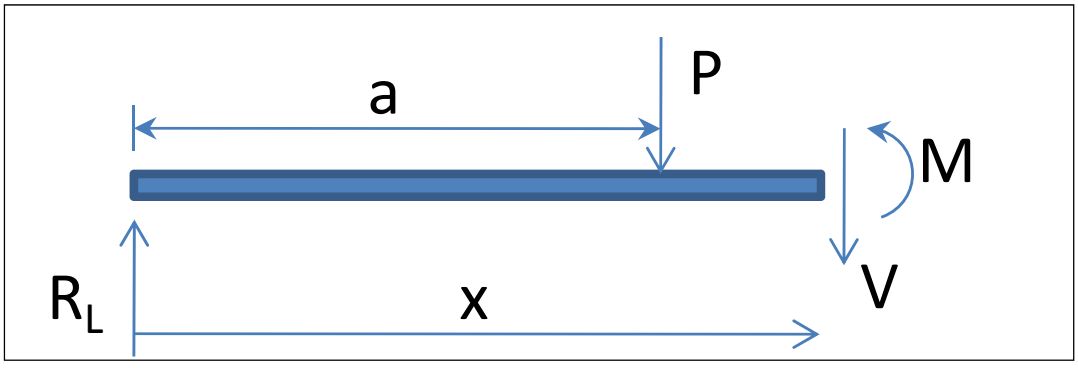

Figure F.3. Free body diagram used to obtain the internal shear force and the internal bending moment from $a \le x \le L$.

Using this segment of the beam and establishing the equations of equilibrium the internal shear V and internal bending moment M is obtained as

$$V = \frac{Pa}{L} \tag{F.5}$$

$$M = P\left(b\frac{x}{L} - x + a\right) \tag{F.6}$$

Now, applying the relationship between moment and curvature $M = EIv''$ for $0 \le x \le a$, using Equation (F.4) and integrating two times, one obtains

$$v' = \frac{1}{EI}\left[\frac{Pbx^2}{2L} + C_1\right] \tag{F.7}$$

$$v = \frac{1}{EI}\left[\frac{Pbx^3}{6L} + C_1 x + C_2\right] \tag{F.8}$$

Proceeding in the same fashion for segment $a \le x \le L$, but using Equation (F.5), one obtains

$$v' = \frac{1}{EI}\left[\frac{Pbx^2}{2L} - \frac{Px^2}{2} + Pax + C_3\right] \tag{F.9}$$

$$v = \frac{1}{EI}\left[\frac{Pbx^3}{6L} - \frac{Px^3}{6} + \frac{Pax^2}{2} + C_3 x + C_4\right] \tag{F.10}$$

Now, applying the following boundary conditions,

$$At\, x = 0, \quad v = 0$$

$$At\, x = L, \quad v = 0$$

And the following continuity conditions,

$$At\, x = a, \quad v^{+} = v^{-}$$

$$At\, x = a, \quad v'^{+} = v'^{-}$$

where the superscript + or – of the transverse displacement (v) or the slope (v') means to the right and to the left of the corresponding variables, respectively. The four integration constant are obtained as,

$$C_1 = \frac{Pa^2}{2} + \frac{PL^2}{6} - \frac{PbL}{6} - \frac{PaL}{2} - \frac{Pa^3}{6L} \tag{F.11}$$

$$C_2 = 0 \tag{F.12}$$

$$C_3 = \frac{PL^2}{6} - \frac{PbL}{6} - \frac{PaL}{2} - \frac{Pa^3}{6L} \tag{F.13}$$

$$C_4 = \frac{Pa^3}{6} \tag{F.14}$$

Finally using the Equations (F.8), (F.10), (F.11) through (F.14), the expressions for the transverse displacement for a simply supported beam under a static load is

$$v = \frac{P}{EI}\left[\frac{bx^3}{6L} + \left(\frac{a^2}{2} + \frac{L^2}{6} - \frac{bL}{6} - \frac{aL}{2} - \frac{a^3}{6L}\right)x\right] \tag{F.15}$$

$$v = \frac{P}{EI}\left[\frac{bx^3}{6L} - \frac{x^3}{6} + \frac{ax^2}{2} + \left(\frac{L^2}{6} - \frac{bL}{6} - \frac{aL}{2} - \frac{a^3}{6L}\right)x + \frac{a^3}{6}\right] \tag{F.16}$$

Appendix G: Estimation of the Dynamic Modulus of Elasticity Considering the Axial and Bending Deformation.

G.1 Estimation of the dynamic modulus of elasticity based on experimental curvature at strain gage S1, S2, S3, S4 and S5 sensor location.

The Impact_Beam computer program has the capability to calculate the dynamic internal moment of a continuous elastic beam affected by a moving dynamic load. This feature allows the use of Impact_Beam to estimate the dynamic modulus of elasticity of the concrete continuous beam used during Winfield Test #10. To perform this analysis, the following Impact_Beam input data are presented. For the Winfield Test #10 the effective beam length (from center to center of the neoprene pads) was 112.6 ft. The moment of inertia of the beam was 517.2 ft^4. The mass per unit length of the beam was 0.25486 kips/ft including the hydrodynamic added mass. The barge train was moving at 2.99 ft/s and the first point of contact was at 64.1 ft from right reaction (right neoprene pads, Figure G.1). The procedure for the estimation of the dynamic modulus of elasticity was as follows. First, the location of each sensor S1B;S1F, S2B;S2F, S3B;S3F, S4B;S4F and S5B;S5F was calculated as 80.28208 ft, 68.2925 ft, 56.30291667 ft, 44.31333 ft and 32.32375 ft, respectively, as shown in Figure G.1.

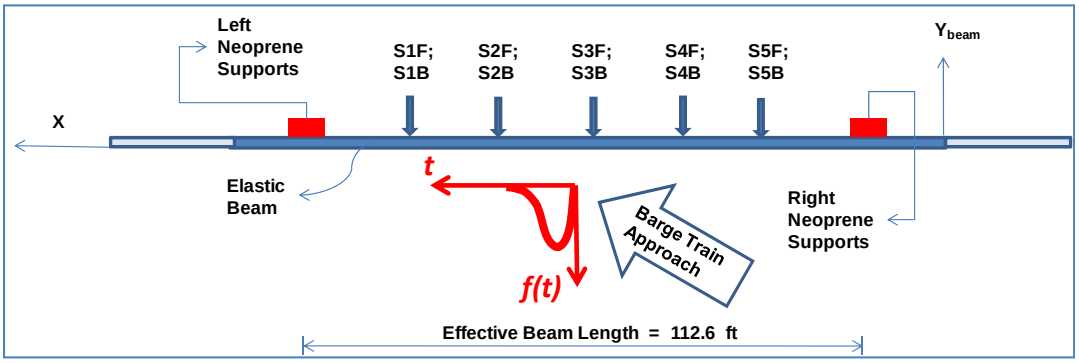

Figure G.1. Location of S1B;S1F, S2B;S2F, S3B;S3F, S4B;S4F and S5B;S5F sensors.

In the input file for the modified Impact_Beam FORTRAN code, each one of these sensor locations was specified as a position where the results were of interest. Ten modes were used and a damping ratio of 0.02 was used for

each mode. The elastic modulus is a variable that needs to be entered as input data in the input file. The initial modulus of elasticity was assigned a value of 790,000 ksf, which is lower than the expected value for the dynamic modulus of elasticity. Then, the modified Impact_Beam FORTRAN software was iterated from this initial modulus of elasticity until the specified curvature at sensor locations S1, S2, S3, S4 and S5 is achieved. Each sensor location represents one run of the computer program and one value for the estimated modulus of elasticity. The maximum curvature at each sensor location was obtained from the experimental curvature time-history. The curvature time-history at each sensor location was obtained from the normal strain recorded during the Winfield Test #10 and divided by the distance to the position of zero normal strain. Due to the fact that this beam was not under pure bending (axial effect was present due to the friction between the barge train and the beam) the centroid of the cross-section cannot be the neutral axis. The neutral axis position, when the axial force is acting, can be determined by similar triangles (assuming plane sections remain planar) as shown in Figure G.2. The equation to calculate the position of the neutral axis (distance y) is the following,

$$\frac{\varepsilon_b}{y} = \frac{\varepsilon_f}{a - y} \tag{G.1}$$

or,

$$y = \frac{a\varepsilon_b}{\left(\varepsilon_b + \varepsilon_f\right)} \tag{G.2}$$

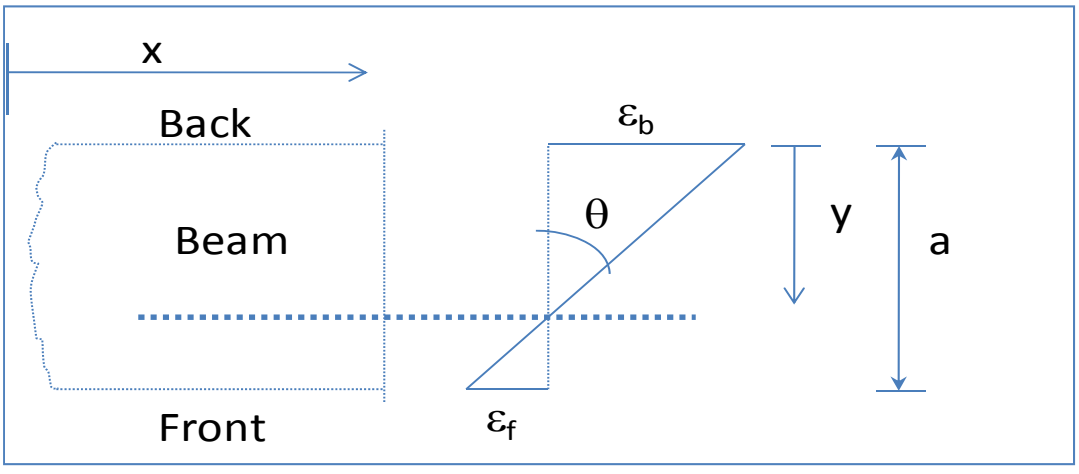

Figure G.2. Experimental curvature calculation at sensors S1, S2, S3, S4 and S5.

After calculating the distance y based on the normal strains in the back and front location at S1, S2, S3, S4 and S5, the curvature θ can be calculated as the back normal strain divided by the calculated distance y, and in mathematical form,

$$\theta = \frac{\varepsilon_b}{y} \tag{G.3}$$

The calculated experimental curvatures (from experimental normal strains) were calculated as; at S1 – 1.57498E-05 rads/ft, S2 – 2.50751E-05 rads/ft, S3 – 2.57593E-05 rads/ft, S4 – 4.86897E-06 rads/ft, and S5 – 2.79889E-06 rads/ft. The Impact_Beam software calculates the dynamic internal bending moment, so the comparison had to be performed against the experimental internal moment. The experimental bending moment is calculated multiplying the curvature at each sensor by the modulus of elasticity and the moment of inertia. The experimental moment and the simulation moment both depend on the modulus of elasticity. Therefore, both values change during the process of increasing the modulus of elasticity. The process ends when the experimental and simulation bending moments reach the same results. The modulus of elasticity at this step is the corresponding dynamic modulus of elasticity based on the curvature at this sensor location.

The resulting values for the dynamic modulus of elasticity for S1, S2, S3, S4, and S5 was 1,618,000 ksf (11,236 ksi), 1,245,000 ksf (8,645.8 ksi), 1,152,000 ksf (8,000 ksi), 5,423,000 ksf (37,659.7 ksi), 6,980,000 ksf (48,472 ksi), respectively. Figures G.3 through G.22 show the experimental and simulation moments and curvature time histories at each specific sensor location. The convergence of the mathematical process to find the dynamic modulus of elasticity at each sensor location is also presented in these set of figures.

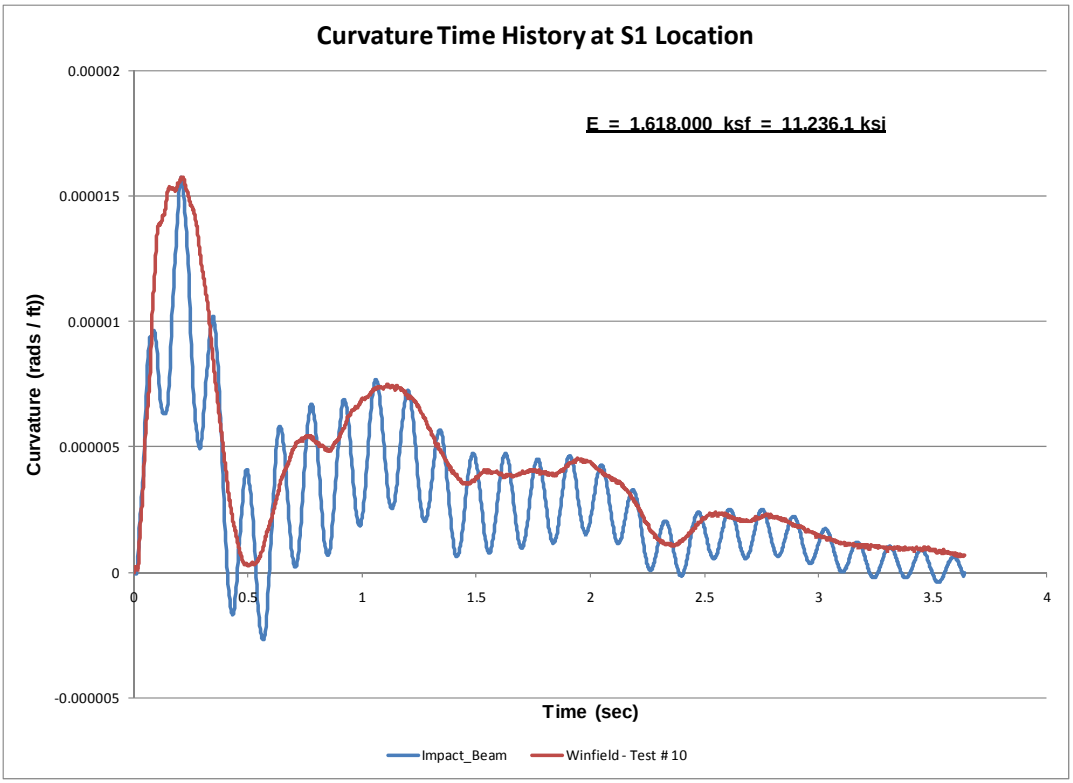

Figure G.3. Curvature time-history at S1 sensor.

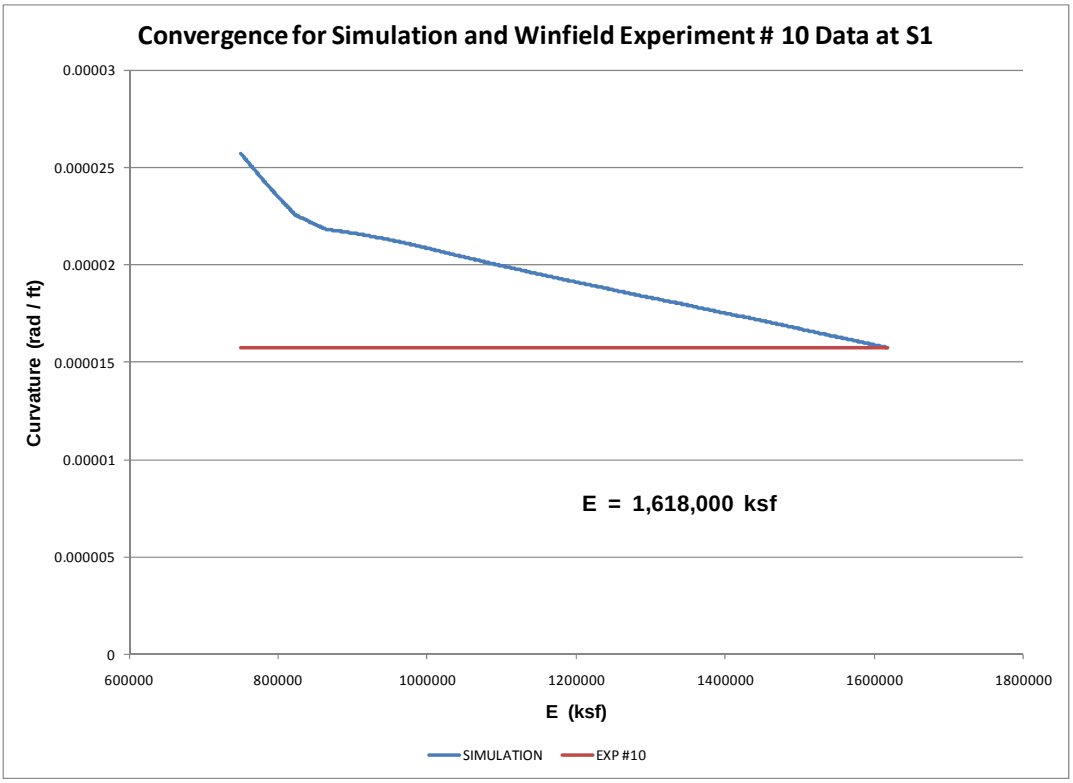

Figure G.4. Curvature convergence at S1 sensor.

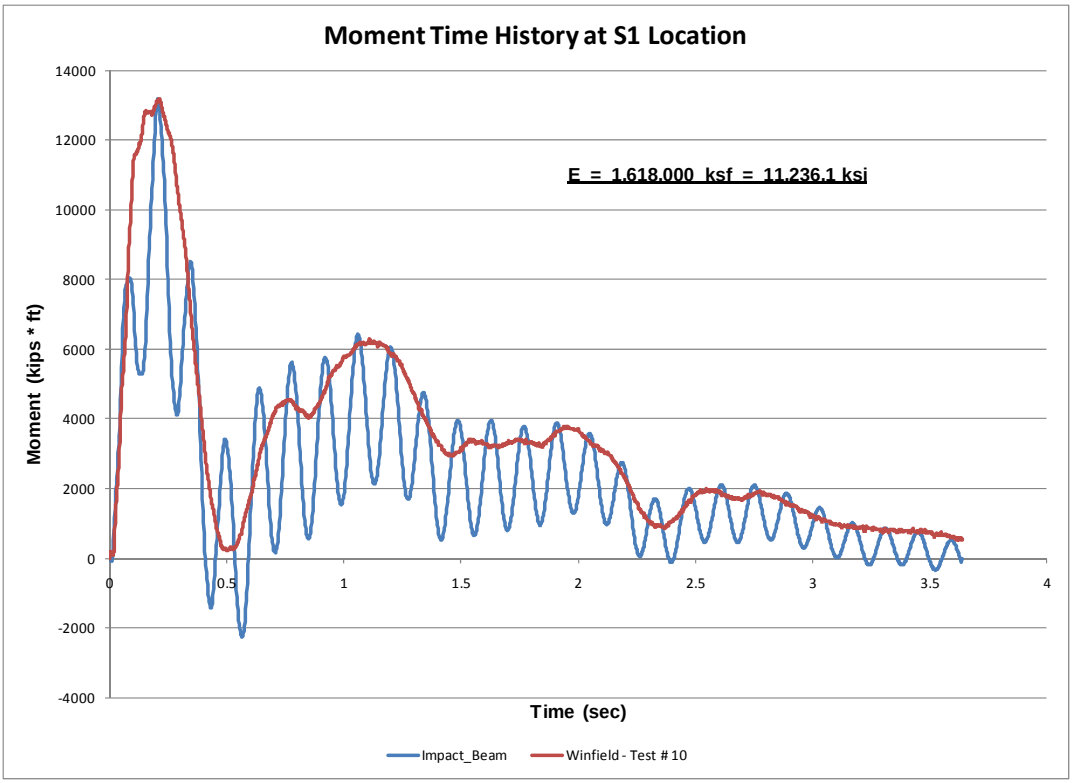

Figure G.5. Moment time-history at S1 sensor.

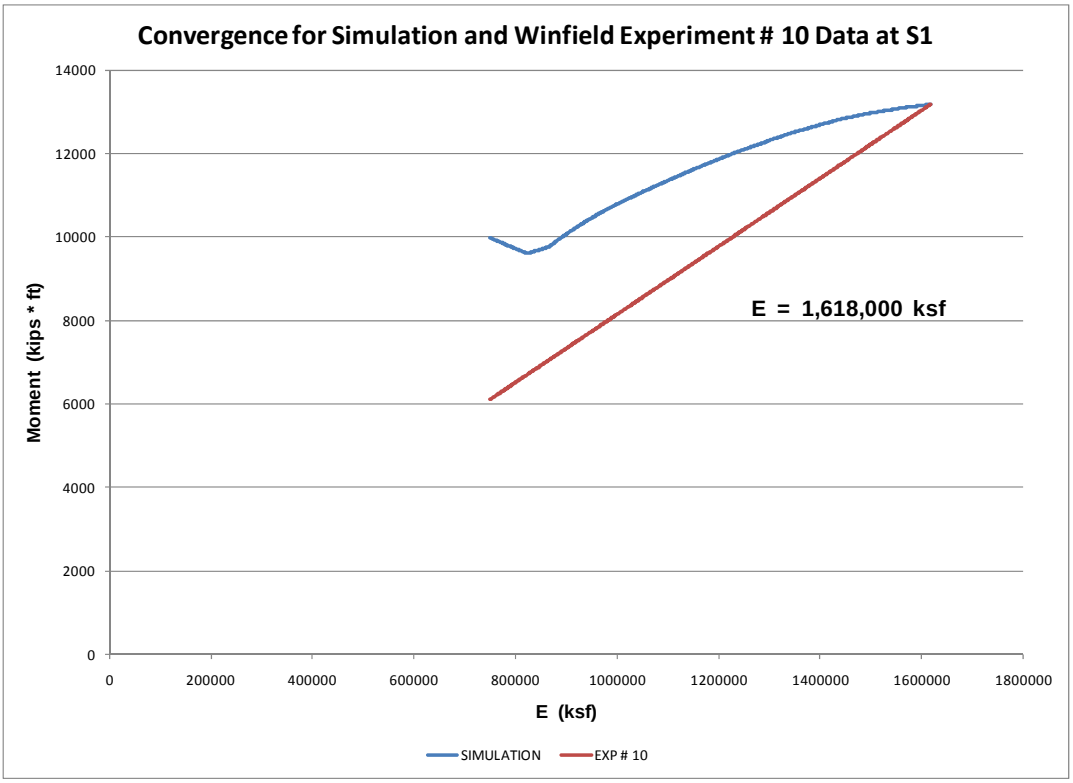

Figure G.6. Moment convergence at S1 sensor.

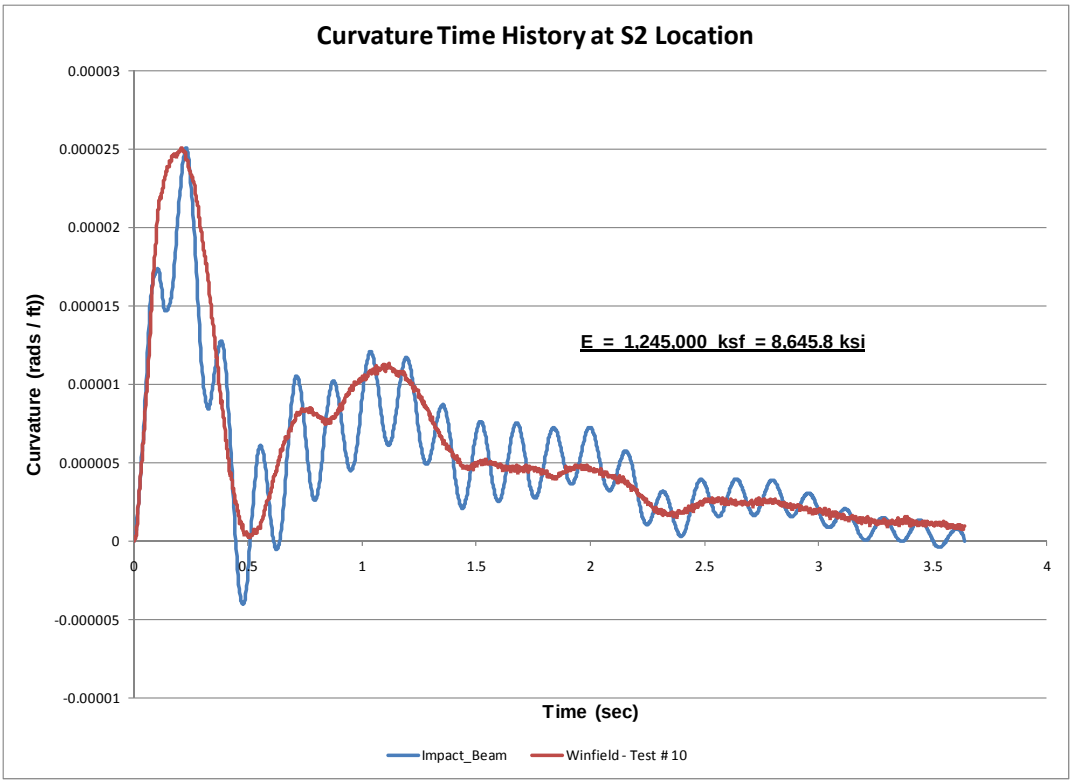

Figure G.7. Curvature time-history at S2 sensor.

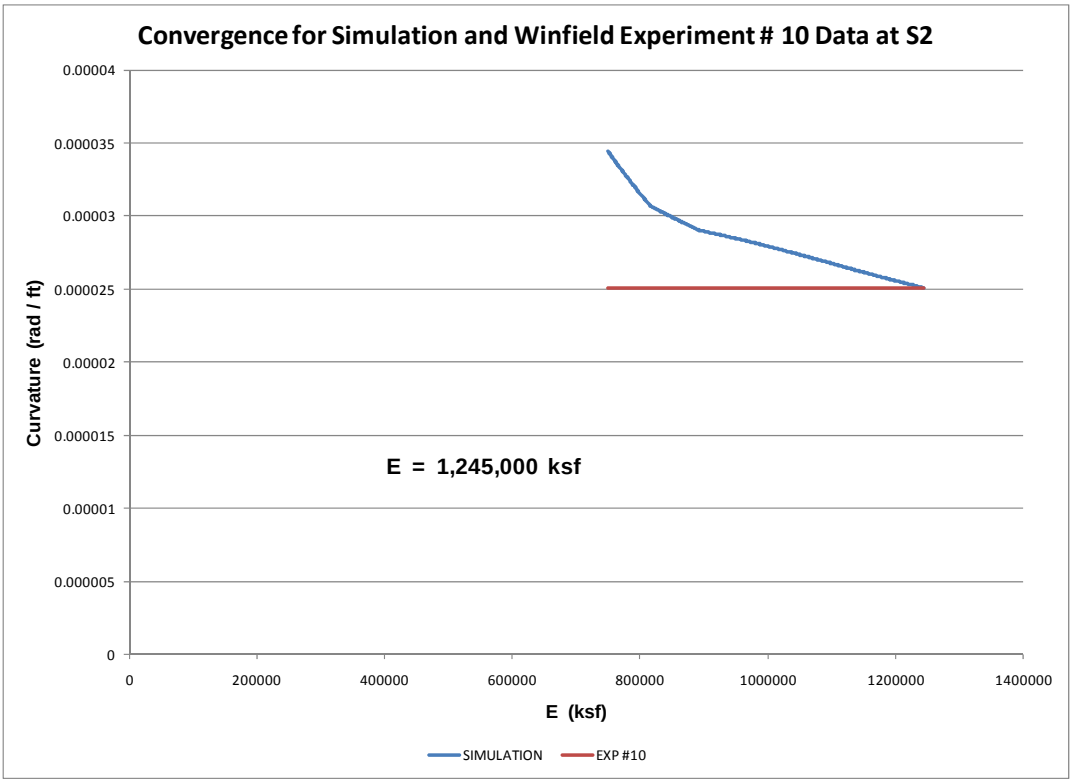

Figure G.8. Curvature convergence at S2 sensor.

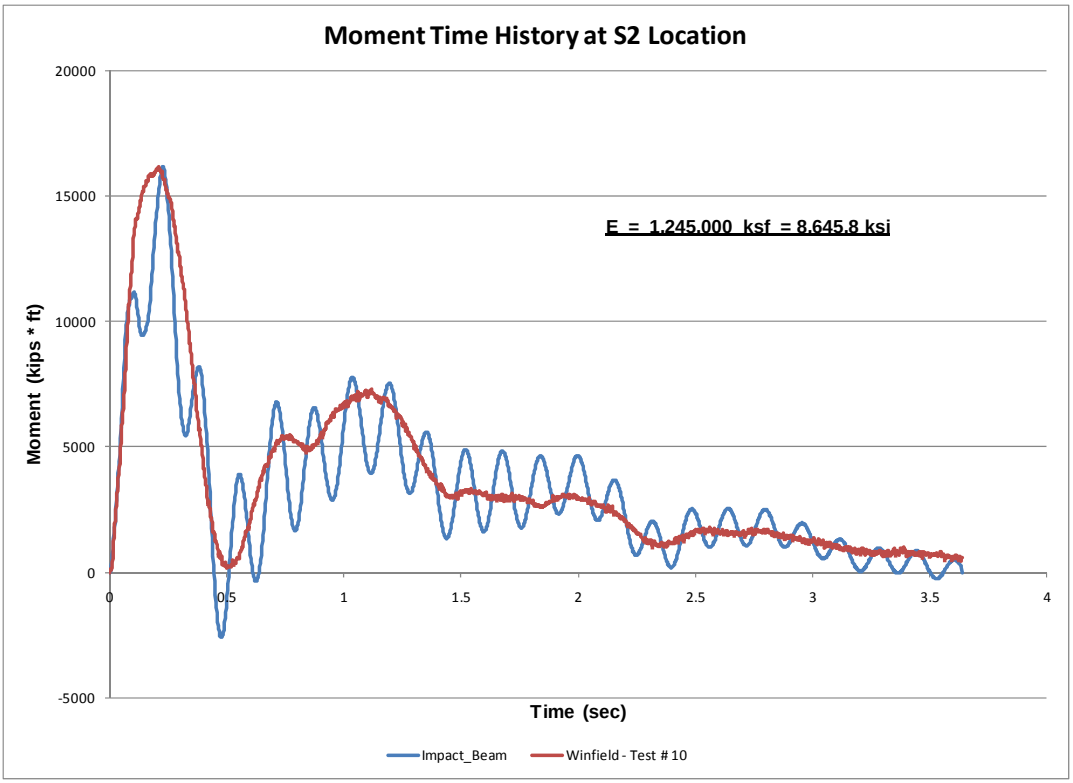

Figure G.9. Moment time-history at S2 sensor.

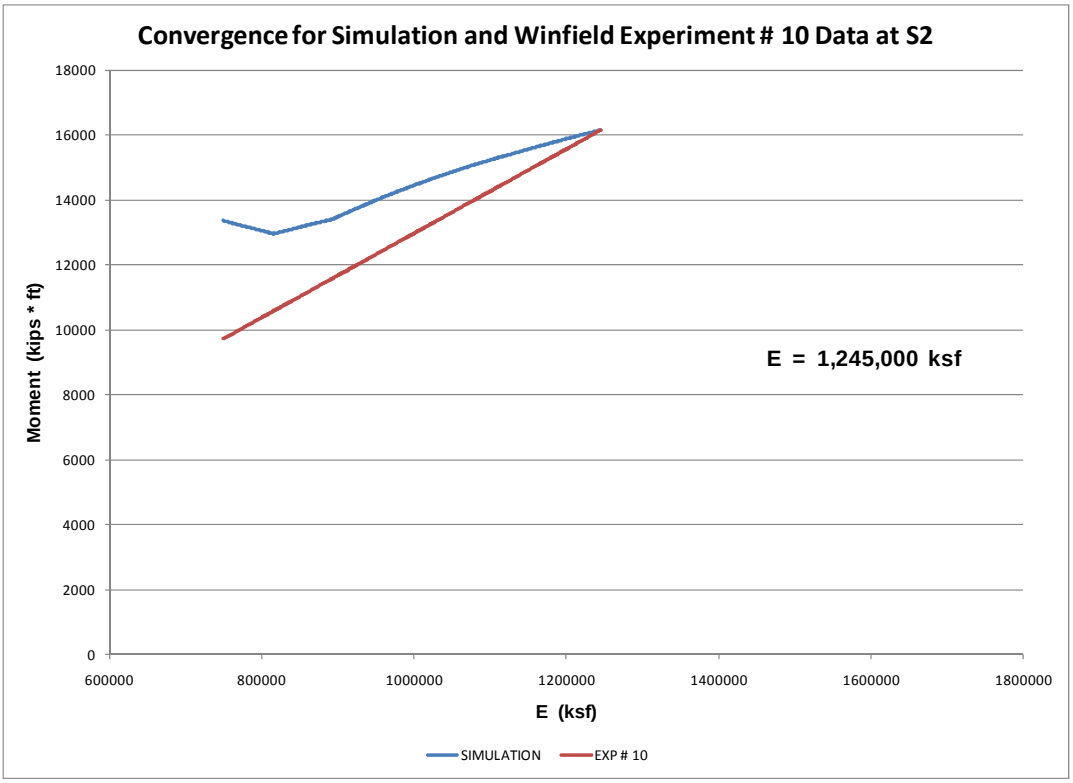

Figure G.10. Moment convergence at S2 sensor.

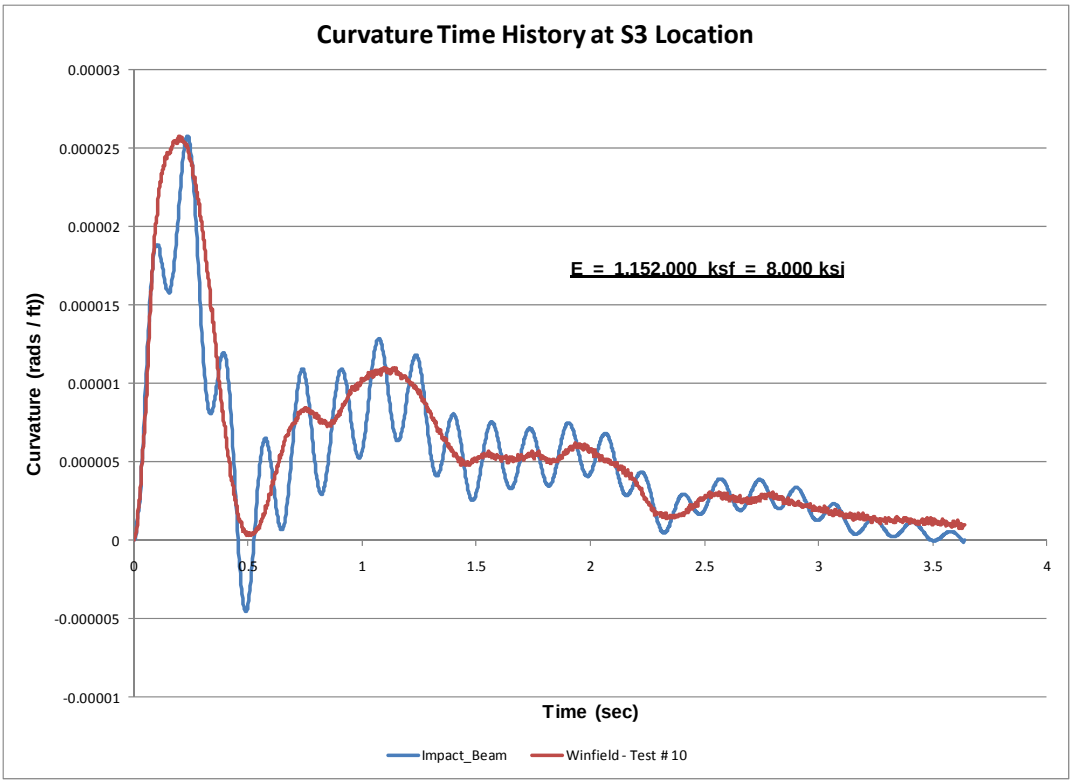

Figure G.11. Curvature time-history at S3 sensor.

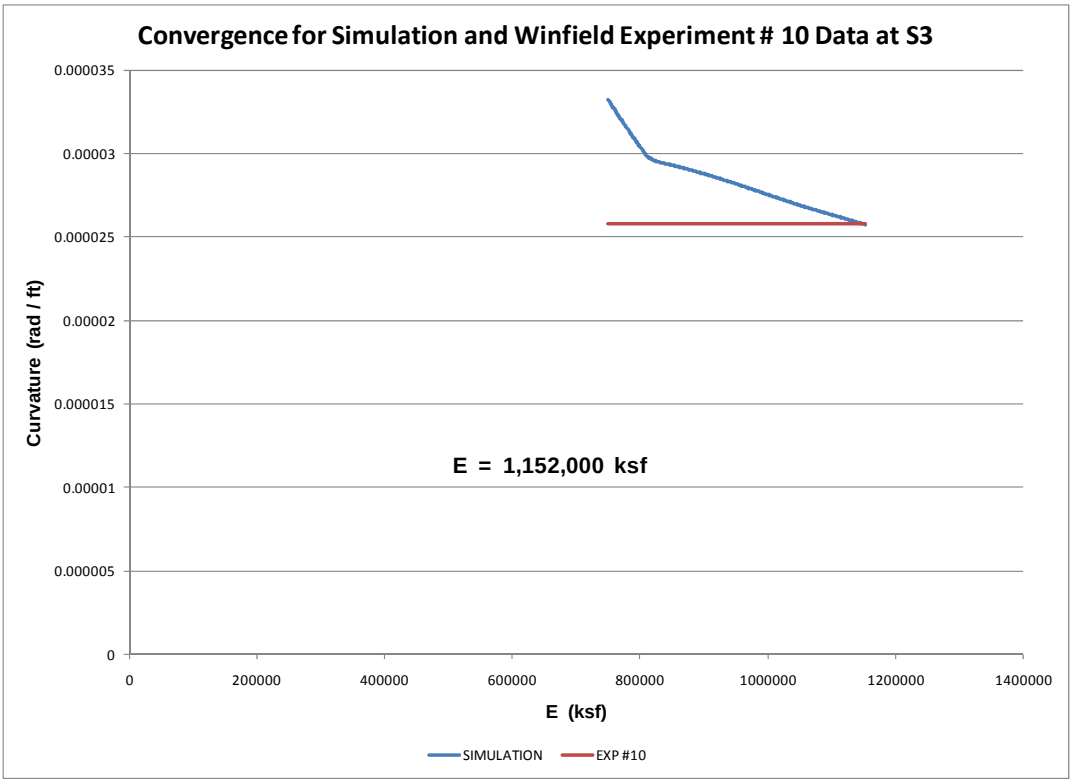

Figure G.12. Curvature convergence at S3 sensor.

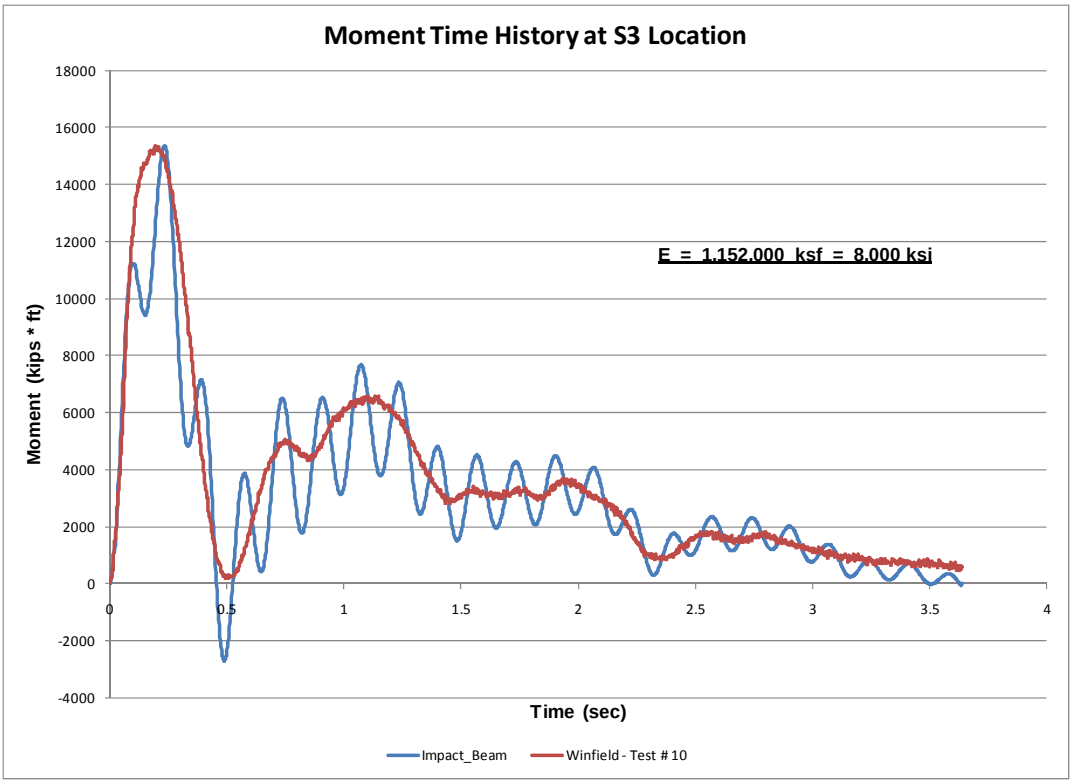

Figure G.13. Moment time-history at S3 sensor.

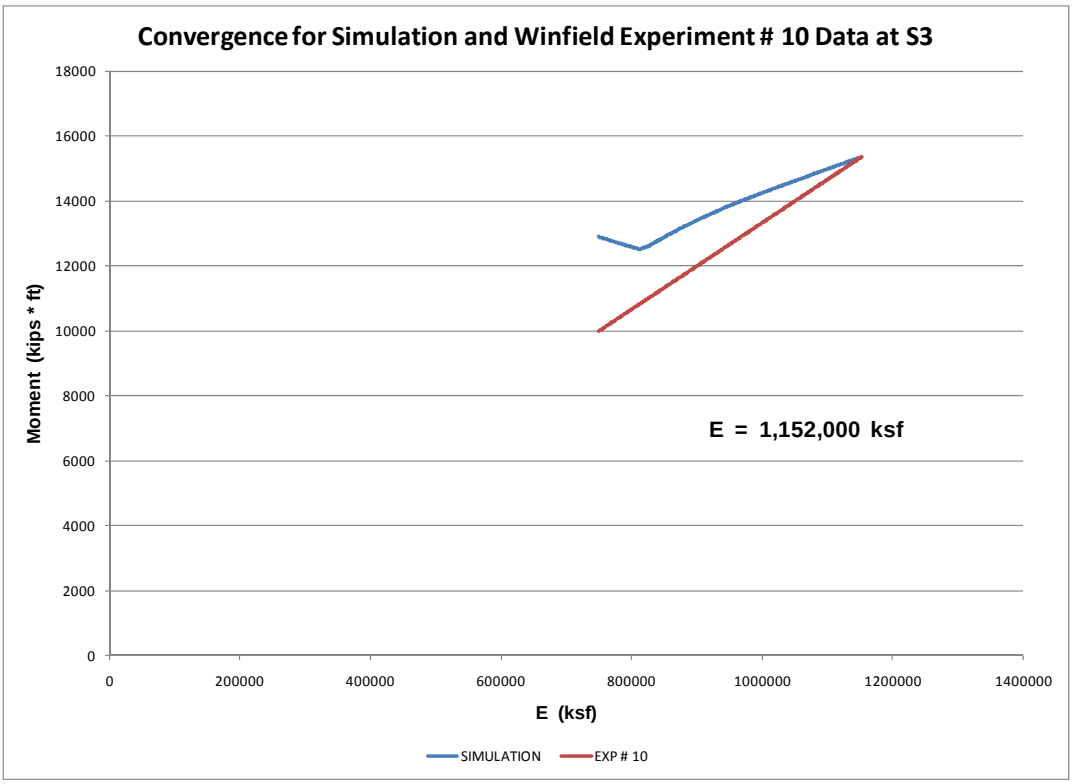

Figure G.14. Moment convergence at S3 sensor.

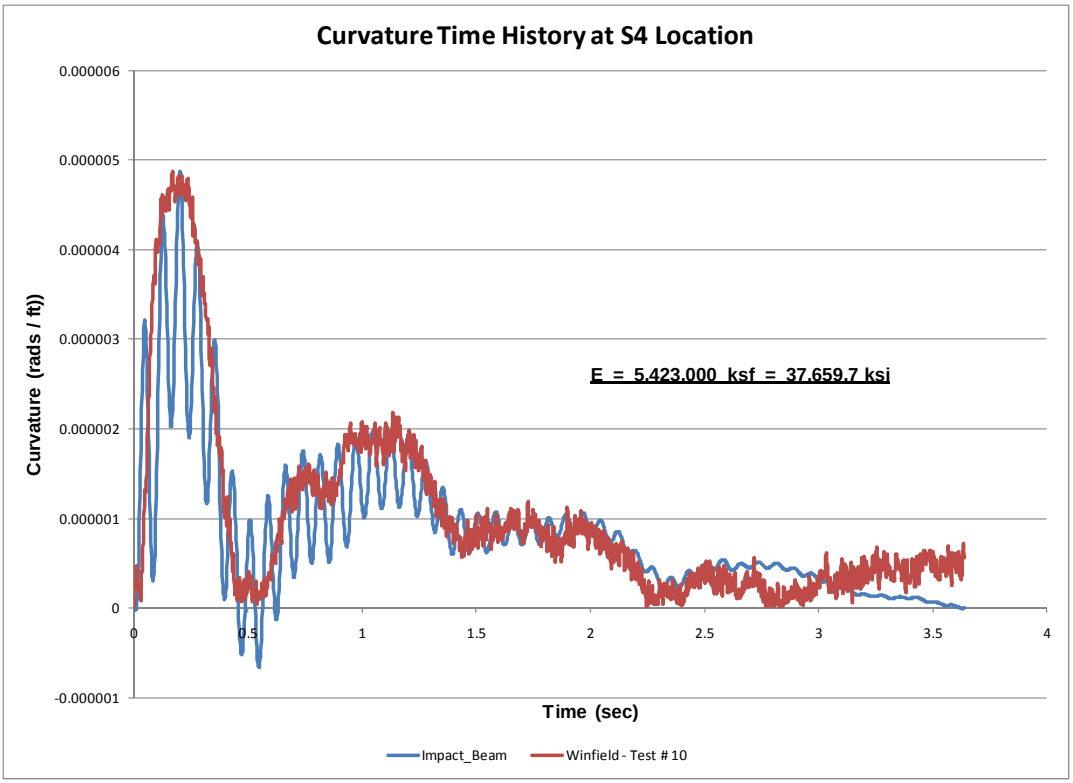

Figure G.15. Curvature time-history at S4 sensor.

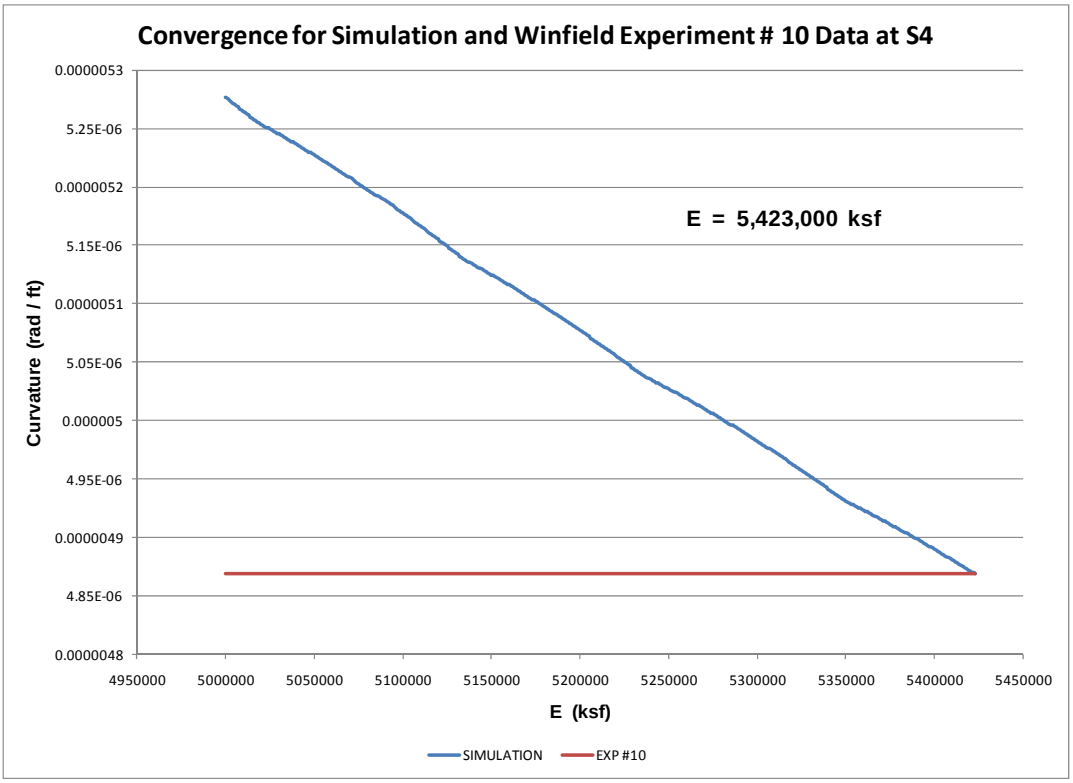

Figure G.16. Curvature convergence at S4 sensor.

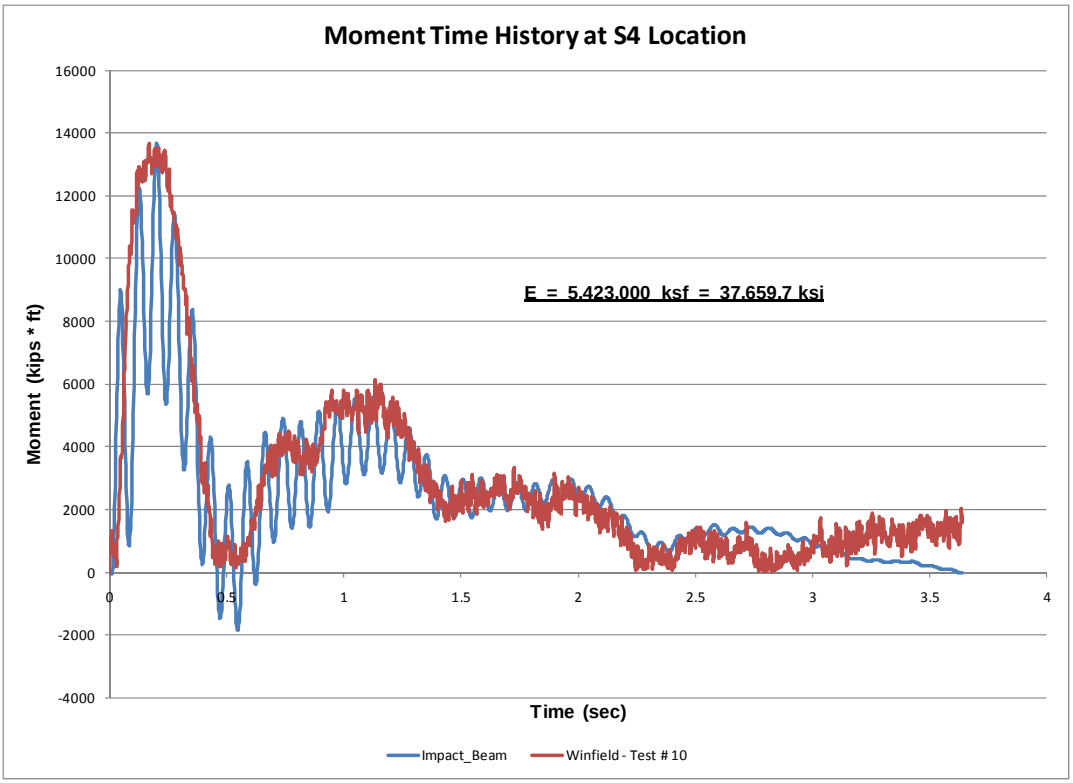

Figure G.17. Moment time-history at S4 sensor.

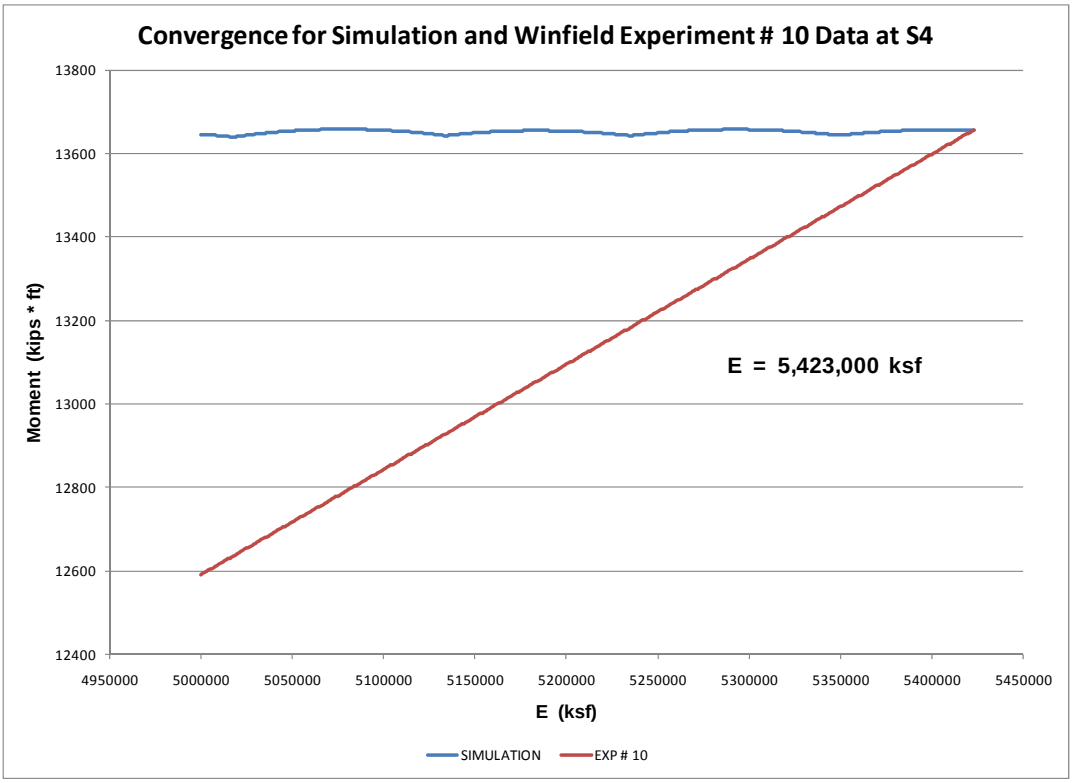

Figure G.18. Moment convergence at S4 sensor.

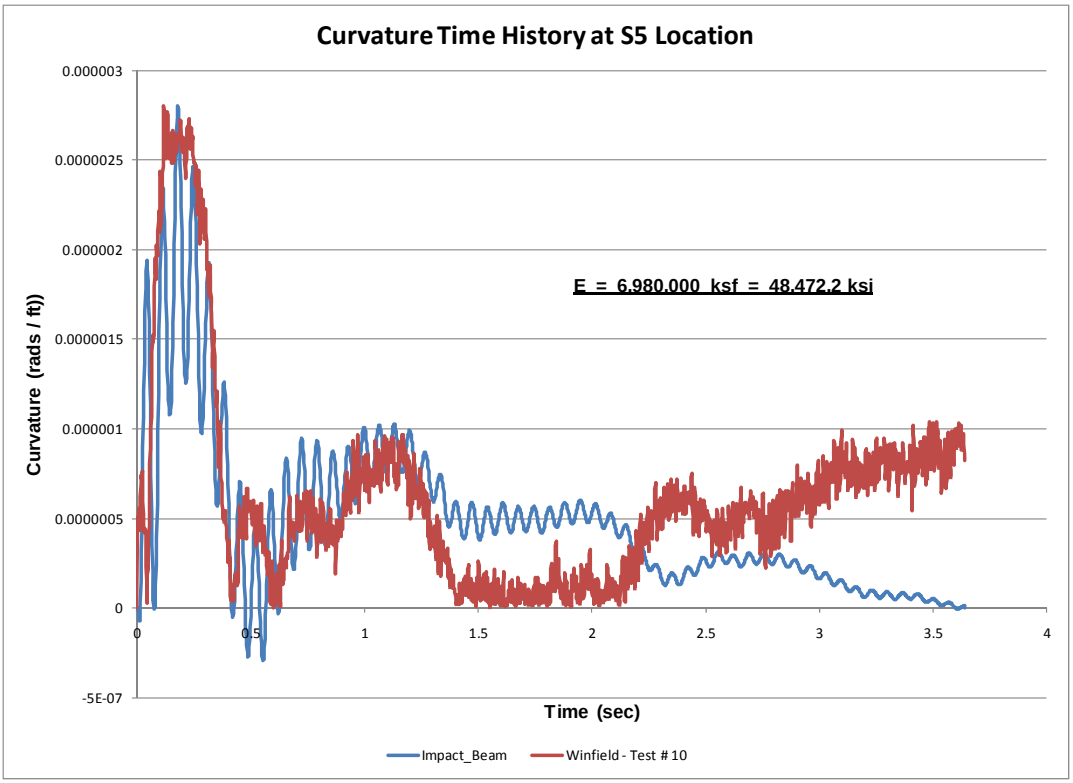

Figure G.19. Curvature time-history at S5 sensor.

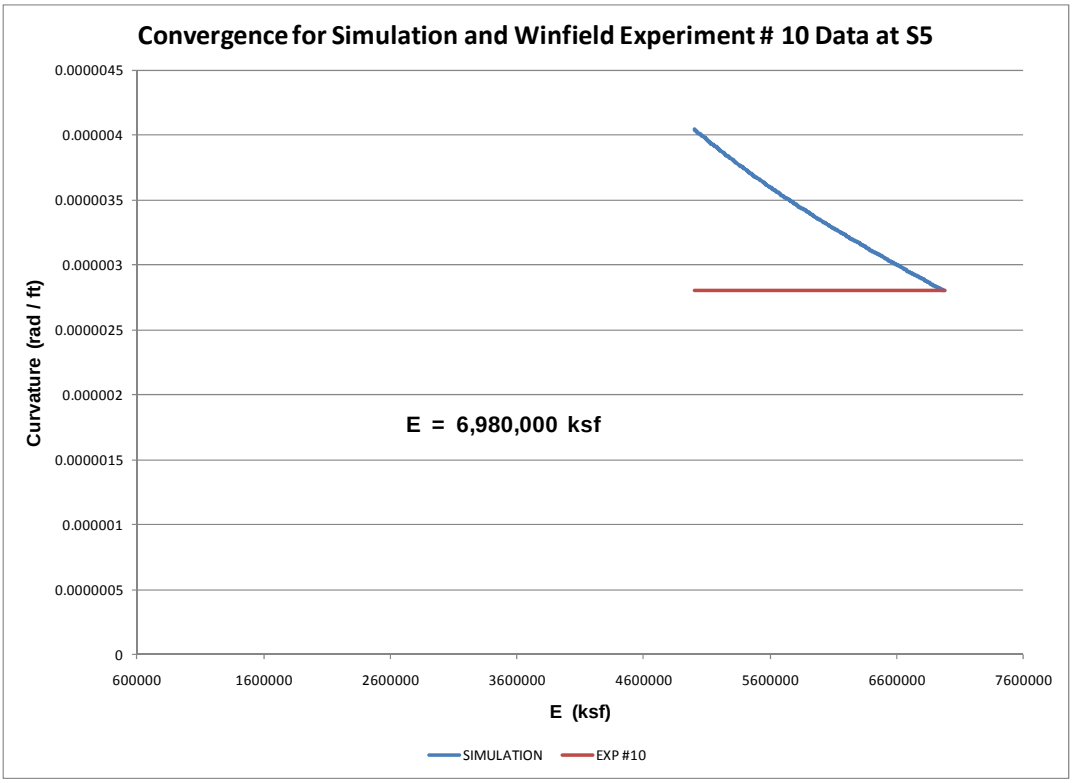

Figure G.20. Curvature convergence at S5 sensor.

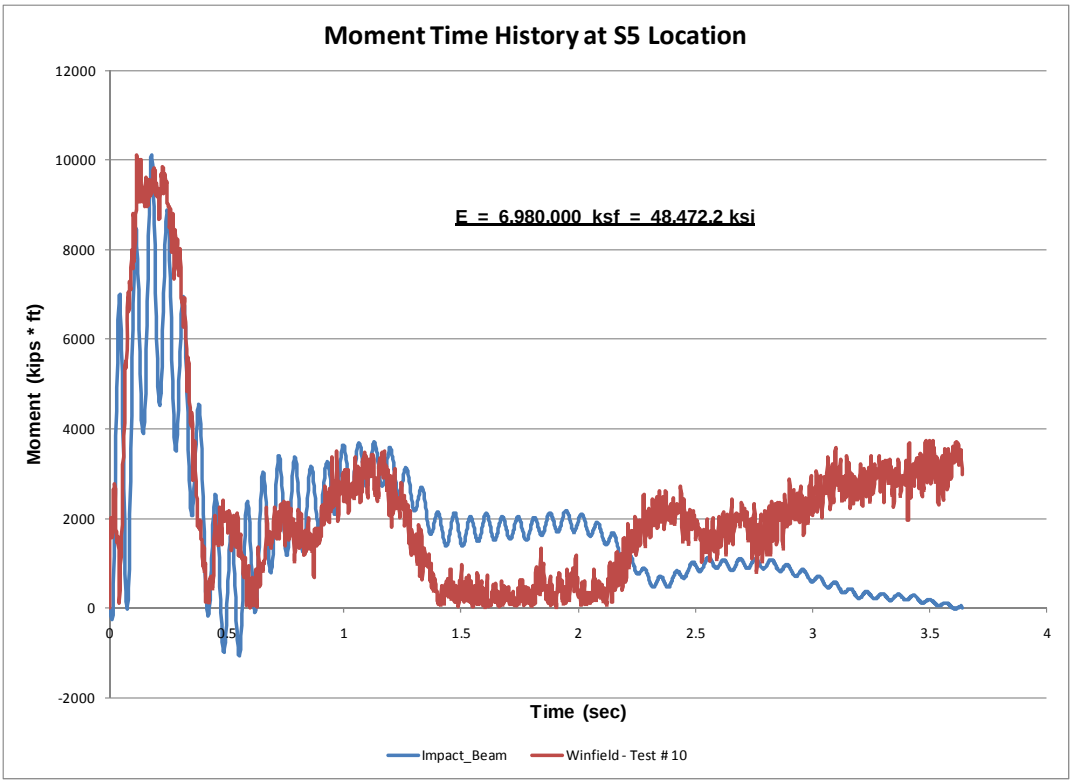

Figure G.21. Moment time-history at S5 sensor.

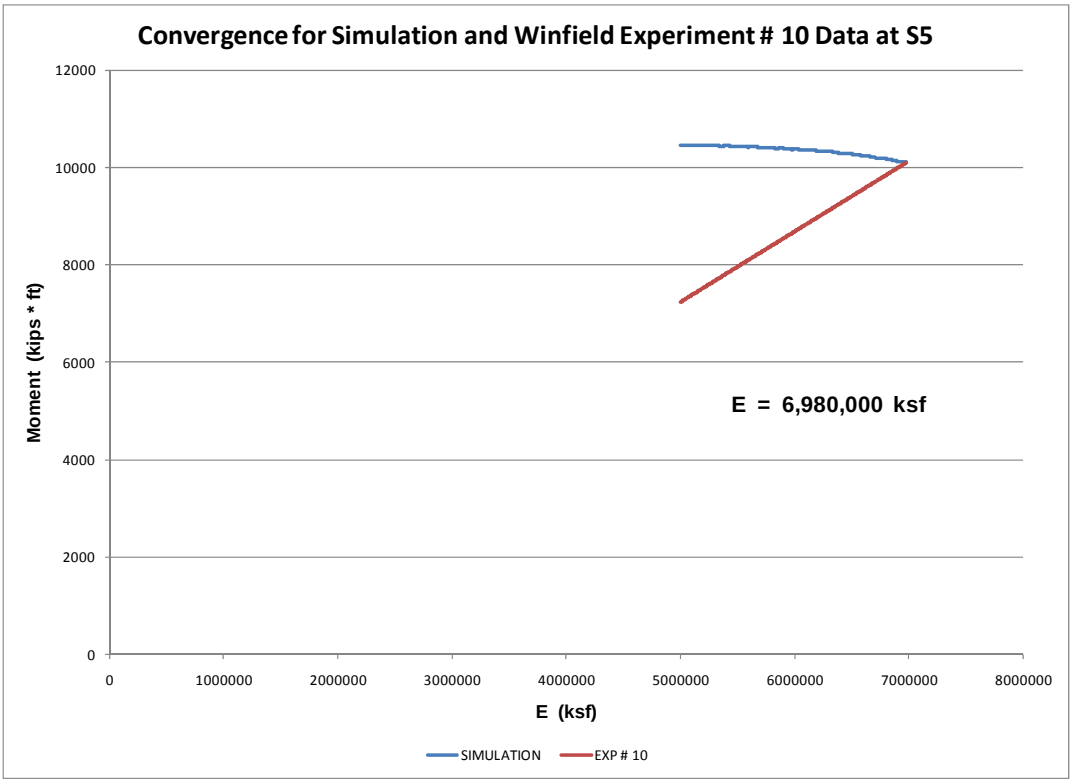

Figure G.22. Moment convergence at S5 sensor.

G.2. Final remarks on the dynamic modulus of elasticity estimation based on axial and bending strains

The resulting values for the dynamic modulus of elasticity based on experimental curvatures obtained from the experimental axial and bending normal strains are presented in Table G.1.

Table G.1. Dynamic modulus of elasticity based on axial and bending normal strains.

Sensor	S1	S2	S3	S4	S5
Dynamic Modulus of Elasticity, ksf (ksi)	1,618,000 (11,236)	1,245,000 (8,645.8)	1,152,000 (8,000)	5,423,000 (37,659.7)	6,980,000 (48,472)
Average Dynamic Modulus of Elasticity = 3,283,600 ksf (22,803 ksi)					

There exists an inconsistency of the dynamic modulus of elasticity obtained from experimental curvature calculated including the axial and bending effects when compared to the dynamic modulus of elasticity obtained from experimental beam deflections in Chapter 5. The dynamic modulus of elasticity obtained from the experimental curvature was greater than the expected values because the experimental curvatures used in the estimation of the dynamic modulus of elasticity were small values. It can be observed that the curvature values at S4 and S5 were 10 times lower than the S1, S2, and S3 curvatures. If these values of curvature are used to estimate the dynamic modulus of elasticity, a very high dynamic modulus is obtained that does not correspond to either the literature recommended value, which is 1.3 times the static modulus of elasticity (Nam, Compomanes and Kim, 1977, Johns and Belanguer, 1981) or the values determined from deflection sensors, as shown in Chapters 5 and 6. The static modulus of elasticity is shown in Equation 5.7 and the dynamic modulus of elasticity is computed in Equation 5.8. The explanation of the behavior of the strain gages (curvatures) during Winfield Test #10 is outside the scope of this analysis. More research will need to be done to accurately process this normal strain data, so that it can be used to estimate the dynamic modulus of elasticity.

G.3. Simulation and experimental moment time-history comparison based on average dynamic modulus of elasticity obtained from experimental beam deflection

This section presents the calculation of the moment time-history using the Impact_Beam software and from experimental curvatures using the average dynamic modulus of elasticity obtained in Chapter 5, which was obtained

from the experimental beam deflection. To perform this analysis the input data for the Impact_Beam software is the following: for the Winfield Test #10, the effective beam length (from center to center of the neoprene pads) was 112.6 ft. The moment of inertia of the beam was 517.2 ft^4. The mass per unit length of the beam was 0.25486 kips/ft. The barge train was moving at 2.99 ft/s and the first point of contact was at 64.1 ft from right reaction (right neoprene pads, Figure G.23). The location of each sensor S1B;S1F, S2B;S2F, S3B;S3F, S4B;S4F and S5B;S5F was calculated as 80.28208 ft, 68.2925 ft, 56.30291667 ft, 44.3133 ft and 32.32375 ft, respectively as shown in Figure G.23.

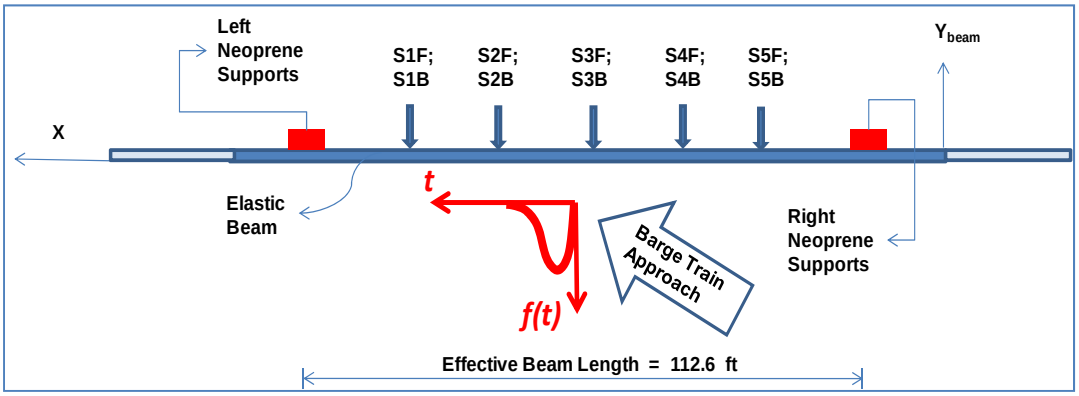

Figure G.23. Location of S1B;S1F, S2B;S2F, S3B;S3F, S4B;S4F and S5B;S5F sensors.

In the Impact_Beam input file, each of these sensor locations was specified as a position where the results were of interest. Ten modes were used and a damping ratio of 0.02 was used for each mode. The elastic modulus was assigned a value of 802,733 ksf, which is the average value obtained from the experimental beam deflection analysis in the previous section. This dynamic modulus of elasticity was multiplied by the moment of inertia and the experimental curvature to calculate the dynamic experimental moment. The results obtained with these values at sensors S1, S2, and S3 are presented in Figures G.24 through G.26. The experimental moment time-history is observed to be similar to the shape of the simulation response. However, the magnitude of the simulation results is higher than the experimental results. This can be explained by considering that the dynamic modulus of elasticity used in these calculations was based on the experimental beam displacement and not on the experimental curvature.

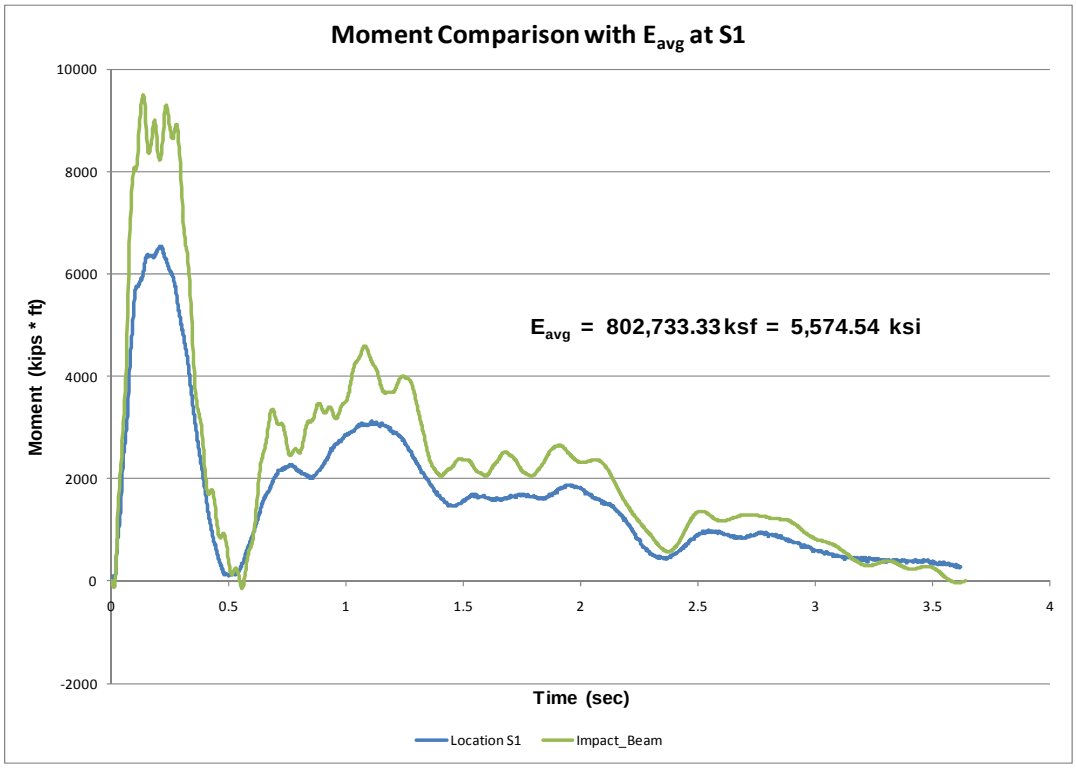

Figure G.24. Moment comparison at sensor S1 using the average dynamic modulus of elasticity obtained from experimental beam deflection.

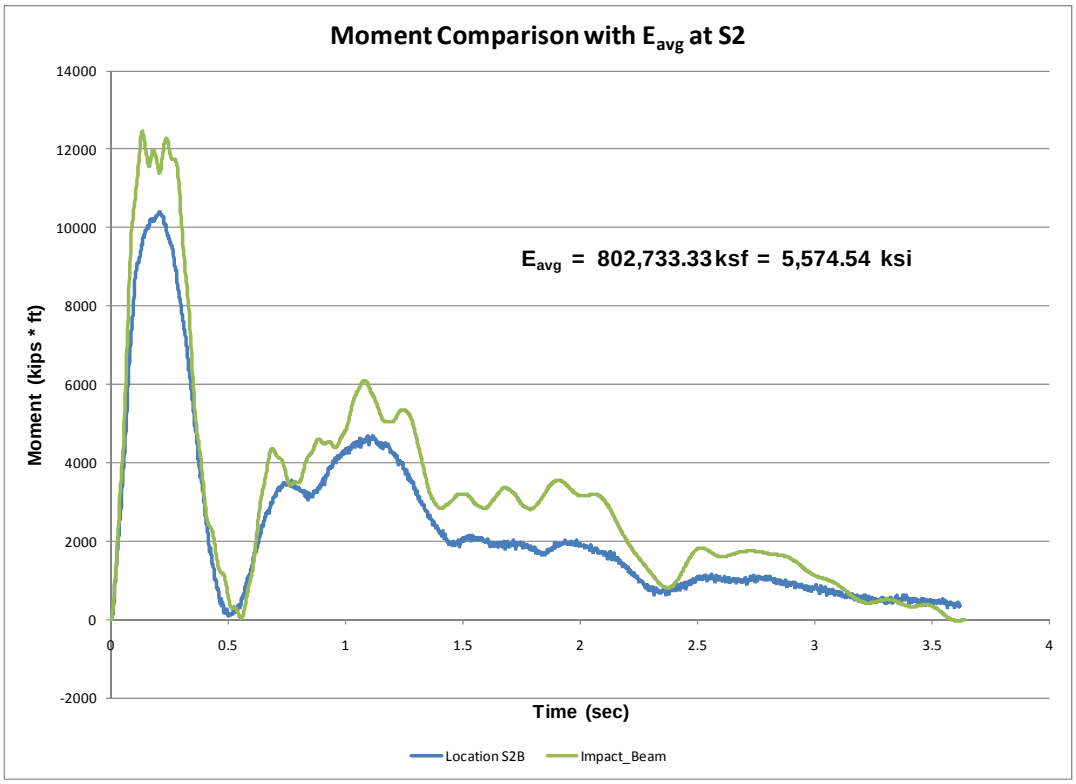

Figure G.25. Moment comparison at sensor S2 using the average dynamic modulus of elasticity obtained from experimental beam deflection.

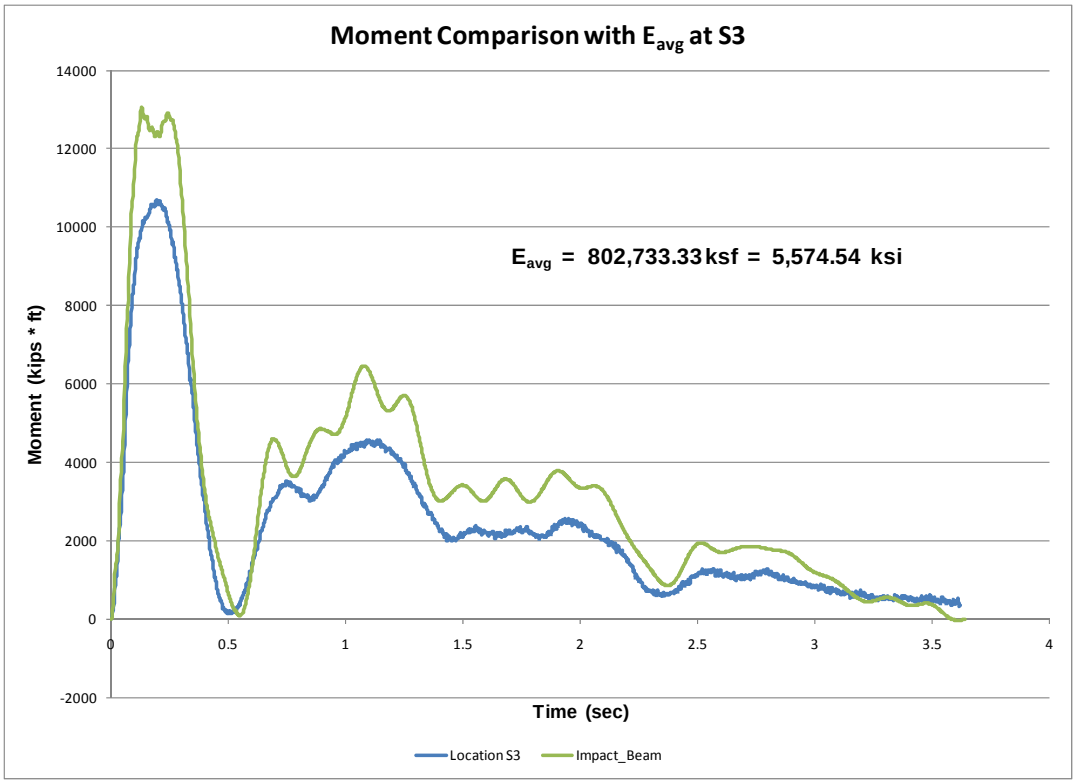

Figure G.26. Moment comparison at sensor S3 using the average dynamic modulus of elasticity obtained from experimental beam deflection.

Appendix H: Mass per Unit Length of the Winfield Beam (Including Hydrodynamic Added Mass)

To process the effects of an impact of a barge train with the beam at Winfield, the mass of the beam per unit length had to be determined. Figure H.1 shows a cross-section of the beam and the additional, hinged concrete skirt that was added to affect the currents flowing around and under the beam. Because the movement was small and the skirt was hinged, the skirt mass was negligible for calculating the motion of the beam along the line of force and therefore not determined, as discussed below. From this cross-section, the volume of the beam can be determined for a unit length and multiplied by the unit weight of concrete. An additional 10% mass was included to account for steel framing, etc., as shown in Figure H.1. The mass of the concrete structure, without hydrodynamic mass, was therefore 7.59 kips per foot along the beam.

This unit weight does not take into account the effects of trying to move the structure while it is sitting in water. These effects are usually accounted for by an additional mass per unit length referred to as the Hydrodynamic Added Mass. Because the skirt is hinged along the length of the beam and swings in the direction opposite to impact, the skirt has negligible impact on the hydrodynamic effects on the beam, as discussed below. The beam is suspended by its supports to a depth of 3.0 feet in the water. Figure H.2 shows the pressures and forces due to inertia of the water in response to loading of the beam (in blue). The force on one side of this structure may be computed by means of the Westergaard formula (EM 1110-2-2200, 1995) using a parabolic approximation:

$$Ke = \frac{2}{3} Ce(\alpha) y(\sqrt{hy}) \tag{H.1}$$

and,

$$Ce = \frac{51}{\sqrt{1 - 0.72(\frac{h}{1000 \cdot t_e})^2}} \tag{H.2}$$

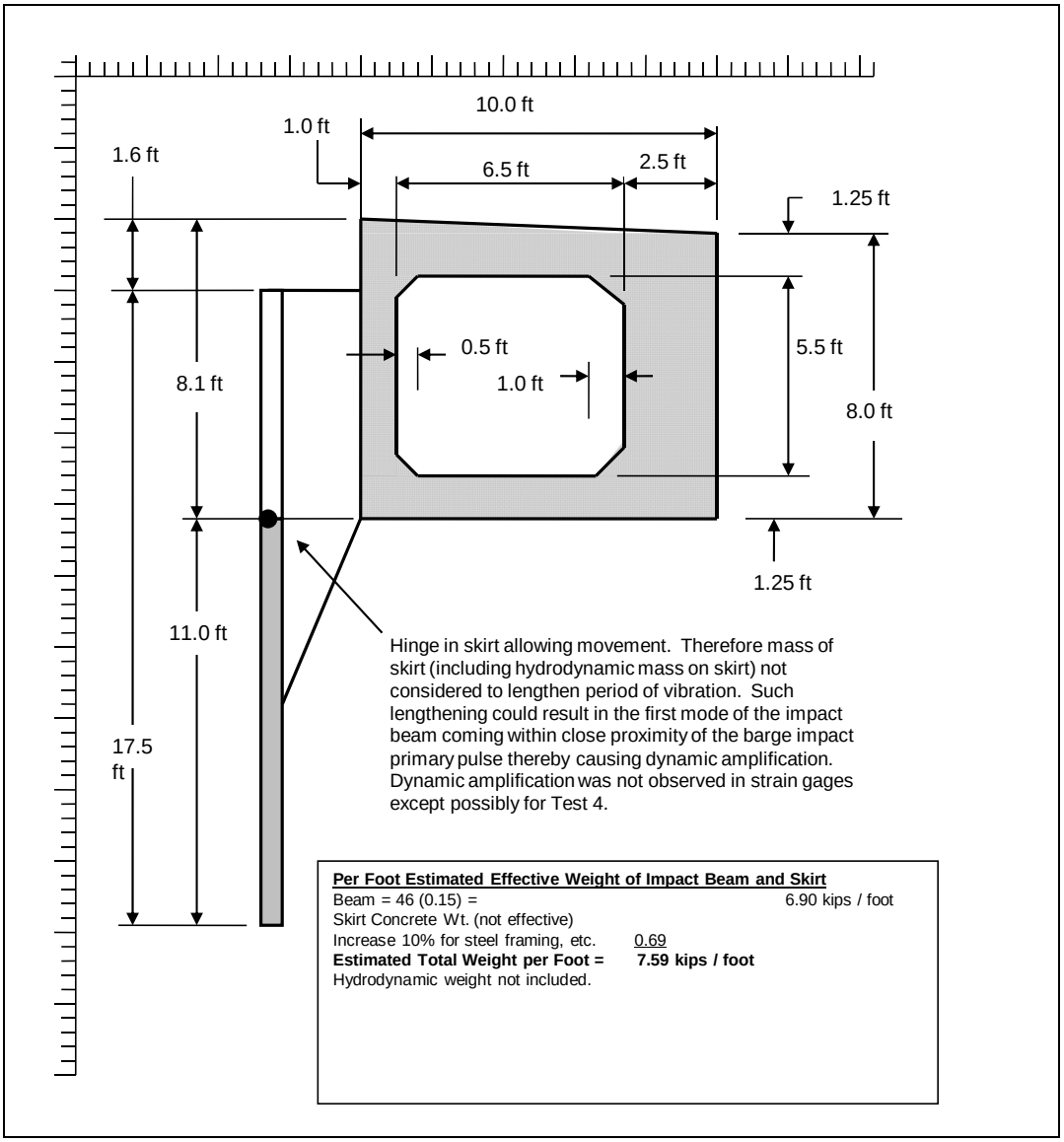

Figure H.1. Computing the area and the weight per foot for the Winfield experiment beam.

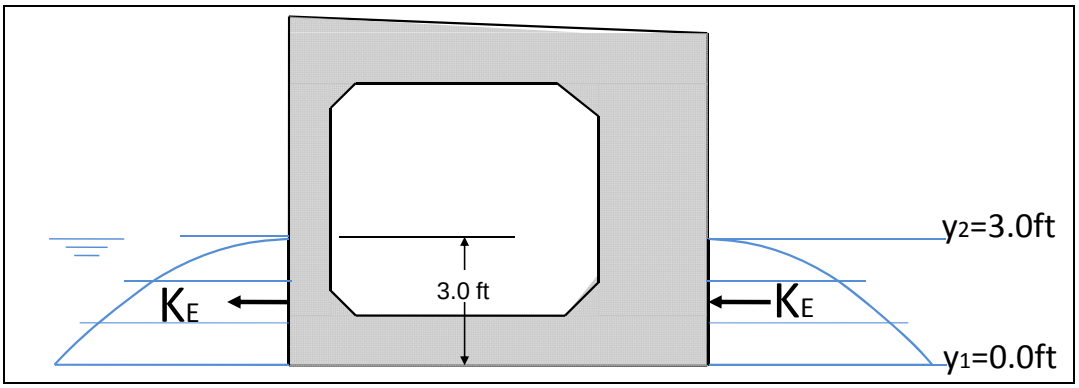

Figure H.2. Hydrostatic added mass is determined by Westergaard equations.

Where K_e is the additional water load acting on the beam, C_e is a factor depending on the depth of the water and the vibration period of the impact, α is the seismic coefficient (which is set to 1.0 for these calculations), and t_e is the period of vibration (which is also set to 1.0 for these calculations).

with

$$h = y_2 - y_1 \tag{H.3}$$

Equation H-2 reduces to

$$Ce = \frac{51}{\sqrt{1 - 0.72(\frac{3.0}{1000})^2}} = 51.0002 \tag{H.4}$$

and, for the whole structure, Equation H-1 returns

$$Ke = \frac{2}{3} \cdot 51.0002 \cdot 3.0\left(\sqrt{3.0 \cdot 3.0}\right) = \frac{2}{3} \cdot 51.0002 \cdot 9.0 = 306.0012 lbs = 0.306 kips \tag{H.5}$$

To account for water on both sides of the structure, the force F_w (along a unit length) is

$$F_W = 2 \cdot Ke = 2 \cdot 0.306 kips = 0.612 kips \tag{H.6}$$

The total force per unit length (F_T) is equal to the sum of the concrete mass force and the hydrodynamic added force:

$$F_T = 7.59 kips + 0.61 kips = 8.2 kips \tag{H.7}$$

Given the total force due to weight and movement in water per unit distance, it is possible to determine the appropriate total mass per unit distance of the structure by dividing the force by the gravitational constant (g):

$$M_{ul} = \frac{F_T}{g} = \frac{8.2}{32.2} \cong 0.25486 \frac{kips \cdot sec^2}{ft} per\ foot\ length \tag{H.8}$$

Initial dynamic beam response analyses were conducted prior to understanding the implications of the connection detail between the skirt and the beam. Hydrodynamic added mass along the front and back faces of the skirt as well as the beam were included in the analyses. A simulation of Winfield Test #10 was then conducted. A comparison of these computed results with Barge Impact Test # 10 field measurements showed poor correlation with the beam response. Additional assessments of the beam and skirt model as well as further investigation into the framing and connection details for the hydraulic skirt to the impact beam led the authors to conclude that the addition of hydrodynamic added mass along the faces of the skirt in the dynamic model is excessive. Subsequent dynamic analyses consider the hinging action of the skirt to the impact beam and therefore exclude hydrodynamic added mass along the faces of the skirt. This modification to the model led to much better agreement with the field data. Consequently, all analyses discussed in this report consider hydrodynamic added mass added to the front and rear face of the impact beam only, as shown in Figure H.2.

Appendix I: The Effects of Selecting the Number of Frequency Modes for the Multi Degree of Freedom Solution

Impact_Beam uses a time-history modal response method of dynamic analysis (Chapter 2). It was shown in Chapter 5, subsection 5.2, for the Winfield Test #10 data, that Impact_Beam was able to replicate the displacement time-history results computed using SAP2000. The Impact_Beam solution was made using 10 modes so as to predict the displacement time-histories accurately. This Appendix describes the effects of choosing the number of modes on the precision of the computed deflections, moments, and shear forces.

The parameters used for the Winfield Test #10 data were chosen to be as close to the physical experiment as possible. The model for determining the effect of varying the number of modes used for a solution has the following input data;

- the effective beam length (from center to center of neoprene pads) is 112.6 ft,
- the moment of inertia of the beam is 517.2 ft^4, the cross-sectional area is equal to 46 ft^2,
- the mass per unit length of the beam is 0.25486 kips / ft, which considers the hydrodynamic added mass (discussed in Appendix H).

The force time-history of Winfield Test #10, which has a maximum force of 517.4 kips was used as the excitation. The total length of the wall (including overlap beyond the neoprene pads) was 117.6458 feet. The initial impact point, measured from the upstream end of the beam, was at 66.6229 along the total beam. This equates to an impact location of 64.1 feet from the upstream neoprene support. The impact travels along the beam in the downstream direction with a velocity of 2.99 feet/second. The unit mass of the beam is 0.25486 kips-sec^2/ft, and the moment of inertia for the beam is 517.2 ft^4. For these tests, the Young's modulus used for the beam was the average Young's modulus of Chapter 6 of 6222.47 ksi, or 896035.7 ksf.

The following example uses the parameters described above and collects the results for a sensor that is 44.083 feet from the upstream end of the beam. This point is behind the impact region. The values collected for this sensor location are the deflection, moment, and shear time-histories for a total number of specified modes from one to seventeen. The peak values for these variables are shown in Table I.1. Figures I.1-I.3 show the change in value for the computed peak values as a function of the total number of modes included in the analysis. For this set of tests, the peak deflections converge when 5 modes or greater were used for a solution. For peak moments, the number of modes required to converge were higher, at approximately 15 modes. The peak shears did not seem to converge with a total of 17 modes attempted.

Table I.1. Peak values for a sensor at a position of 44.083 feet along the beam from the Winfield Test #10 example problem (with average Young's modulus) based on up to 17 modes.

Total Number of Modes	Peak Deflection (ft)	Peak Moment (kip-ft)	Peak Shear (kips)
1	0.371104	11156.33	135.7491
2	0.364783	10412.55	206.2053
3	0.365779	10680.27	271.9839
4	0.3645	10063.91	266.5793
5	0.364465	10037.9	273.831
6	0.364295	9853.798	233.2689
7	0.364357	9945.035	228.2544
8	0.364367	9963.399	199.3272
9	0.364406	10059.35	215.1679
10	0.364414	10082.29	210.5652
11	0.364418	10098.93	238.7279
12	0.364413	10076.4	236.932
13	0.364407	10045.36	253.0412
14	0.364403	10023.96	237.8878
15	0.364401	10005.81	238.8059
16	0.364402	10018.03	220.0577
17	0.364403	10023.19	222.264

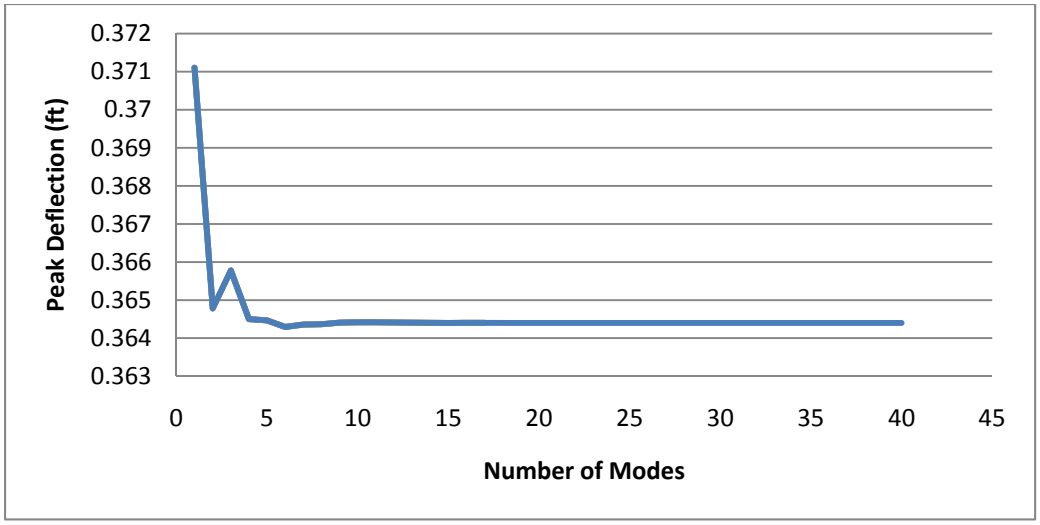

Figure I.1. Peak deflections as a function of the total number modes used for the solution.

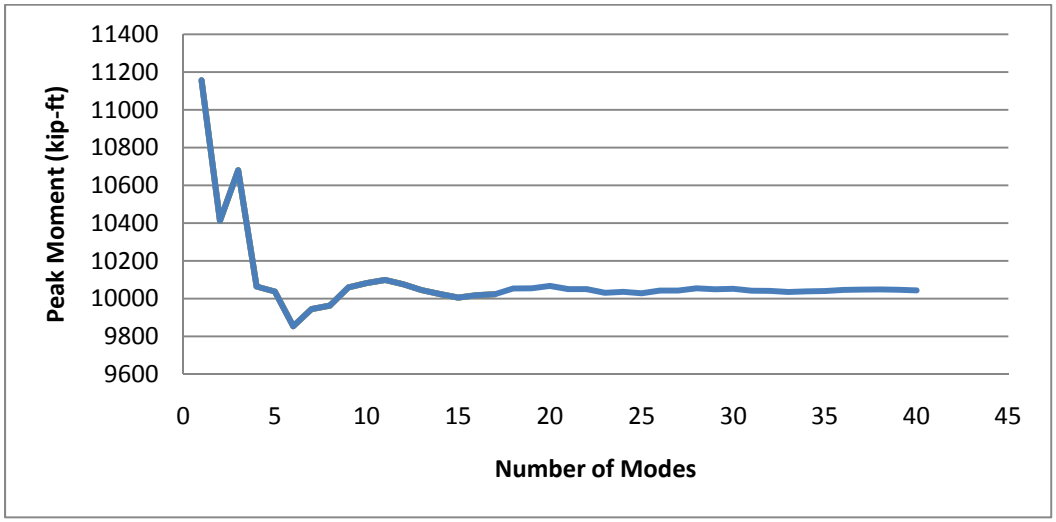

Figure I.2. Peak moments as a function of the total number modes used for the solution.

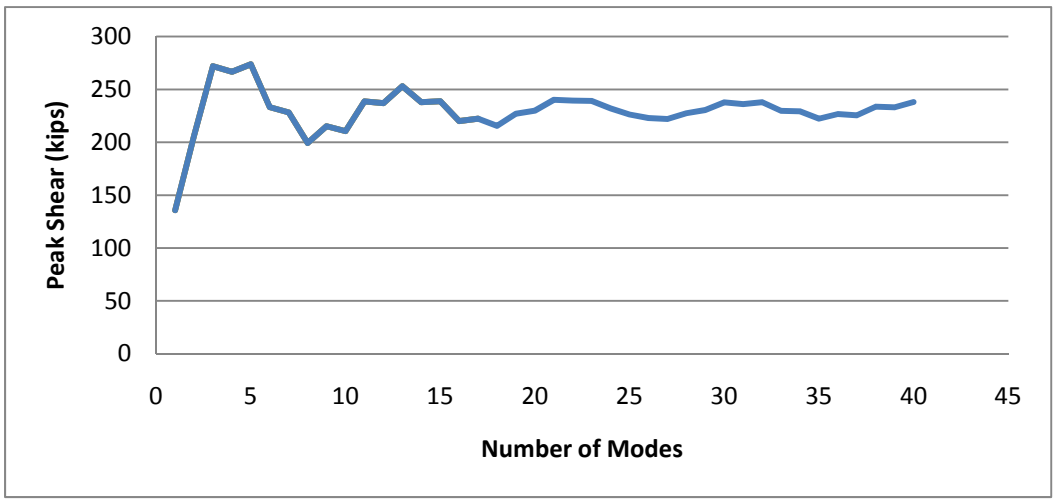

Figure I.3. Peak moments as a function of the total number modes used for the solution.

Figures I.4-I.6 show the total time-history convergence of solutions for deflections, moments, and shear for the sensor located at 44.083 feet downstream from the end of the beam. The results for deflections overlapped within just a few total modes. The moments had very similar curves but took longer to converge, and the shears seemed to be settling in, but still had not converged by a total of 17 modes. Further testing showed that there was a difference of 0.77% between the solution for shears with 30 total modes and the solution with 40 modes. Given the speed of the modal time-history solution method for analysis of the beam, it is desirable to use the maximum total number of frequency modes for a solution for precision, and at least 30 if shear response is of primary concern.

From the test results, it is recommended that the user enter at least 5 frequencies to ensure that deflections have converged to consistent results. For moments to converge to consistent results a total of at least 15 frequencies need to be entered, and for shear forces to converge a total of at least 30 frequencies need to be entered. Fortunately, the analysis occurs rather quickly so, computationally, selecting a large number of frequencies does not take a lot of time.

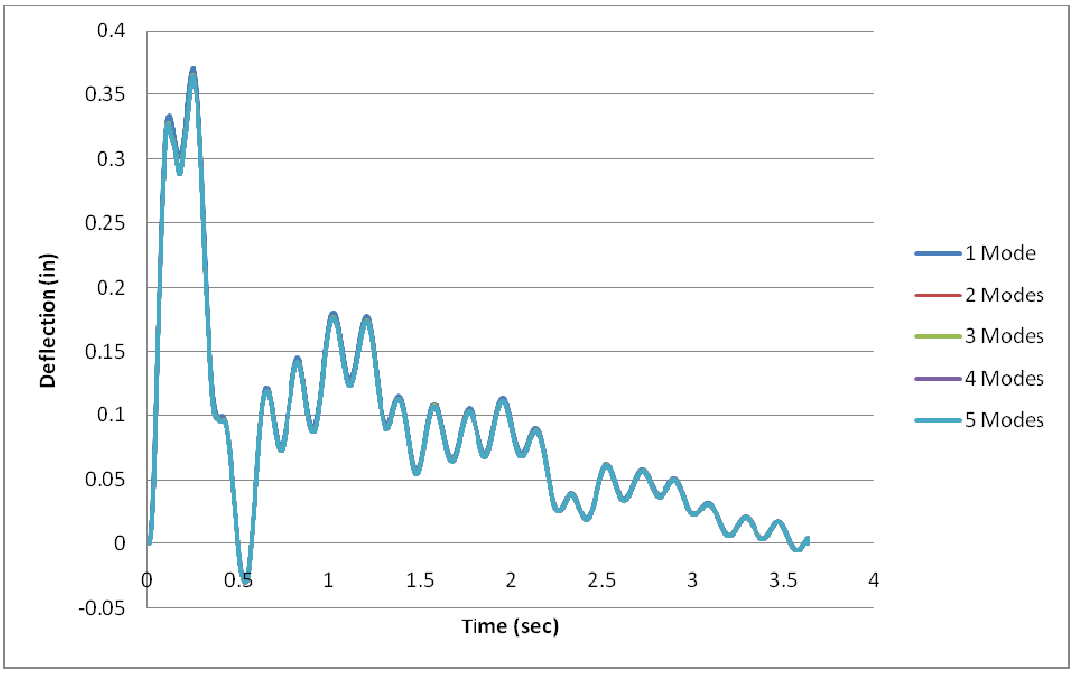

Figure I.4. Deflection time-history responses of a beam solved with different total number of modes at a location 44.083 feet downstream from the end of the beam.

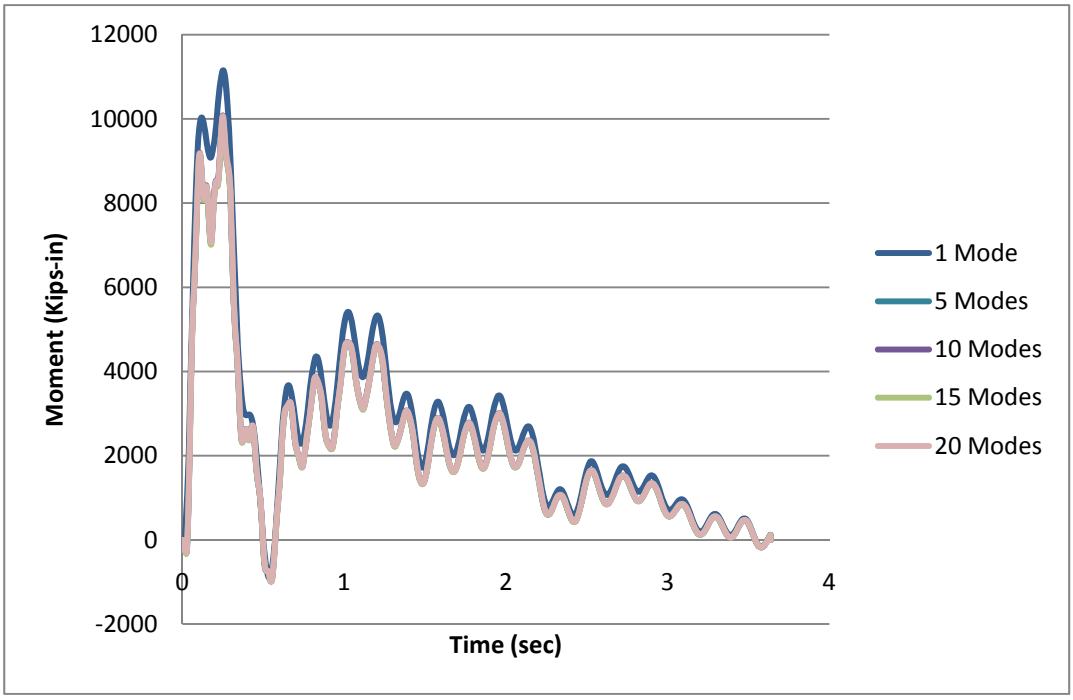

Figure I.5. Moment time-history responses of a beam solved with different total number of modes at a location 44.083 feet downstream from the end of the beam.

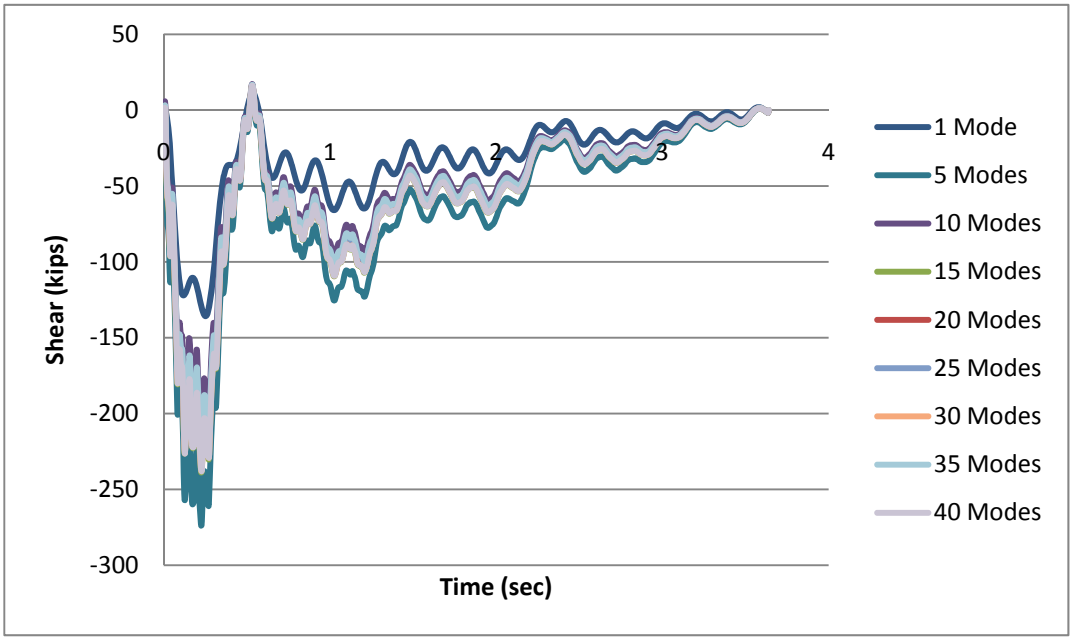

Figure I.6. Shear time-history responses of a beam solved with different total number of modes at a location 44.083 feet downstream from the end of the beam.

Appendix J: Winfield Sensor Locations for Comparison

Throughout this report, sensor positions at the Winfield experiment have been discussed. Shown in Figure J.1 are the positions of the laser deflection sensors, where displacement of the beam is measured. Shown in Figure J.2 are the positions of the strain gage sensors, where moments of the beam are calculated. In Chapter 4, Tables 4.1 and 4.2 show the distances from the upstream support point of the beam to each sensor location. In these diagrams, the barge approach proceeds downstream. The upstream end of the wall is labeled "A" and the downstream end of the wall is labeled "B" for discussion in the report.

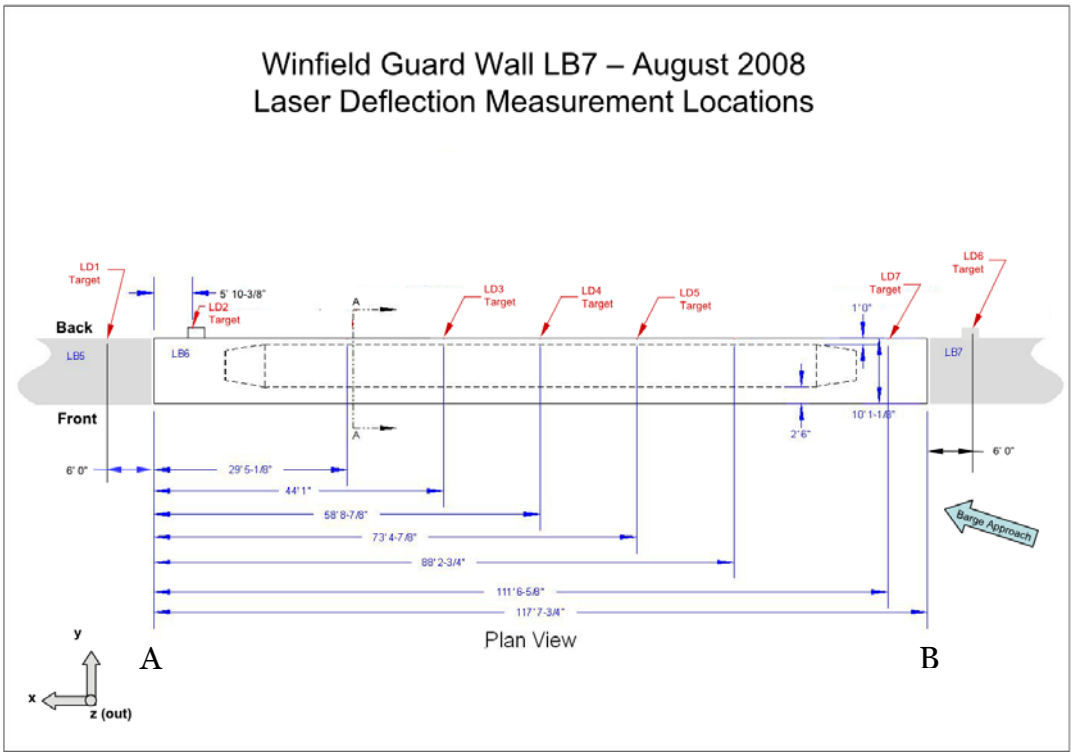

Figure J.1. Positions of the laser deflection sensors.

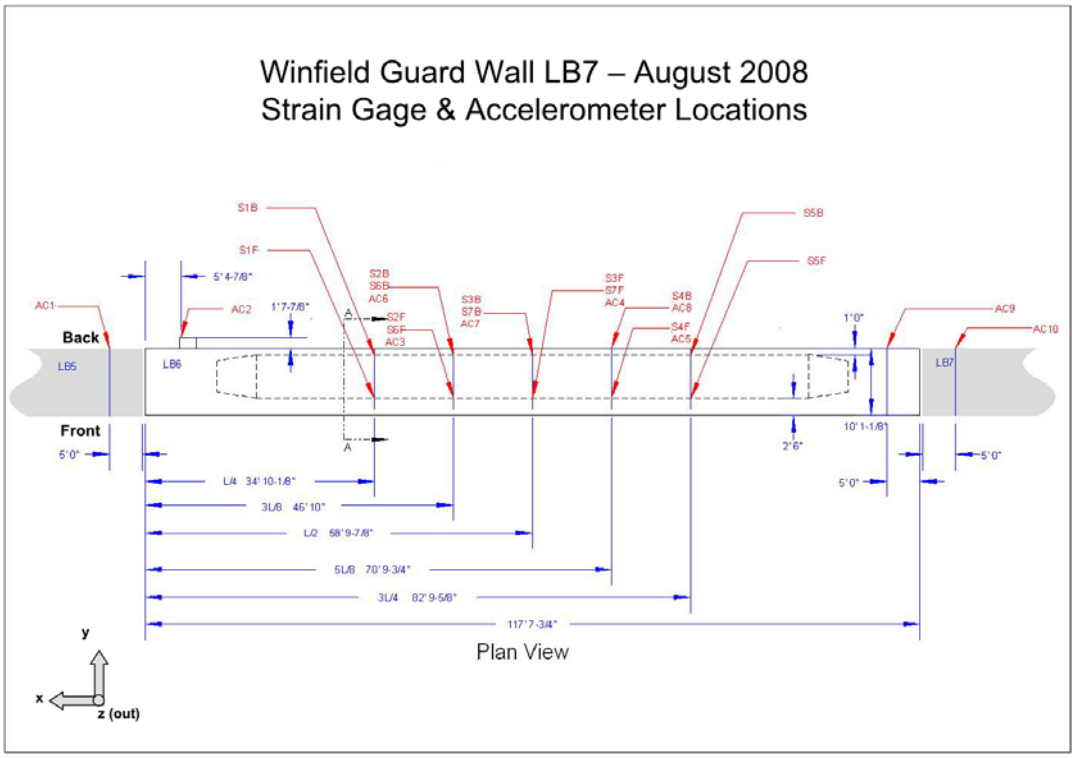

Figure J.2. Positions of strain gages (for moment calculations).

Table 4.1(Bis). Location along the beam of laser deflection sensors used for Winfield barge impact tests.

Sensor	Location from support (ft)
LD2	111.781
LD3	73.5625
LD4	58.906
LD5	44.24
LD7	6.094
LD1 and LD6 are on the adjacent beams	

Table 4.2(Bis). Location along the beam of strain sensors used to determine moments for Winfield barge impact tests.

Sensor	Location from support (ft)
S1	82.802
S2	70.813
S3	58.823
S4	46.833
S5	34.844

Appendix K: Computing the Neoprene Pad compression secant stiffness from Winfield Test results

K.1 Introduction

In the investigation of the Winfield barge impact test results, it became apparent that the back of the Winfield simply-supported beam did not rest directly against the rigid supports of the stop blocks. The impacts of the beam were cushioned at the beam's supports by neoprene pads. Only by subtracting out the neoprene pad displacements could the Winfield beam displacements be compared to the Impact_Beam computed simply supported beam displacements. These elastomeric pads were placed between the stop block for the beam and the beam itself and absorbed energy from the barge train/beam impacts and the support points by compressing and acting as a spring between the beam and the stopper block.

Figure K.1 shows the location and dimensions of the rectangular elastomeric pads used at the Winfield location (as well as other information about the beam supports). These elastomeric pads at Winfield had a length of 42 inches, a width of 18 inches, and a thickness of 2 inches. The thickness was comprised of 4 elastomeric layers of 3/8 inch, ½ inch, ½ inch, and 3/8 inch, respectively. There were 3 layers of material (shims) between the layers that made up the rest of the pad thickness. The pads were made with a 50 durometer hardness elastomer as measured using the Shore A scale (AASHTO 1998). This measure is also known as the IRHD, or International Rubber Hardness Degree. These measurements were specified in Inca (1996).

K.2 Winfield measurements

From the measured deflection data at Winfield and the shear forces computed (using Impact_Beam) at the support points for the beam, where no deflection should occur for rigid supports, a time-history of shear force versus deflection should give a valid approximation of the stiffness (K) of the neoprene pad over time. Because the deflections are very small, the

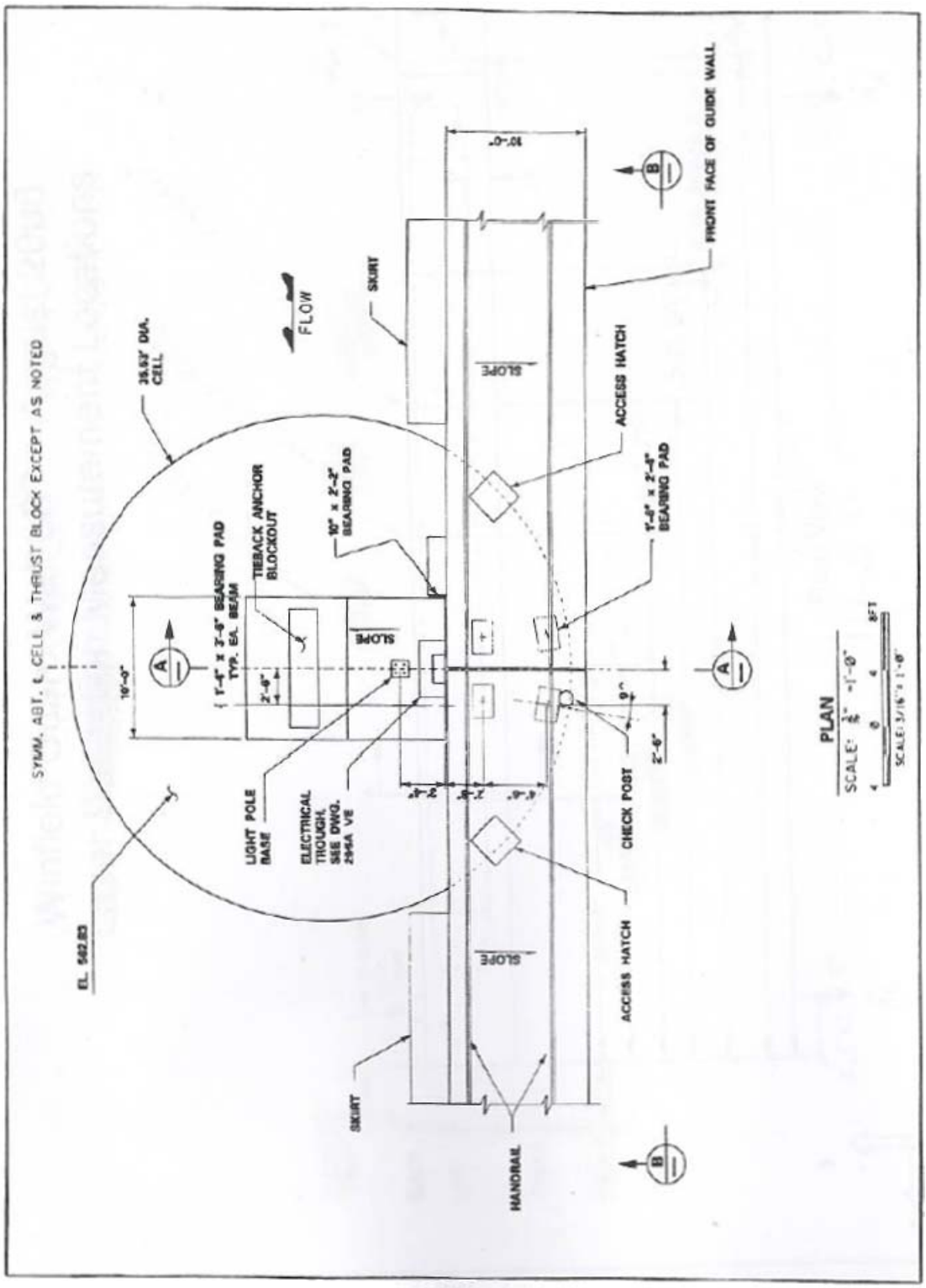

Figure K.1. Plan view of two flexible impact beam supported by a concrete-filled cell and held in place by a concrete stopper block and neoprene pads.

maximum recorded value of deflection was determined and any stiffness value that would be calculated for a deflection of less than 5% of the maximum recorded deflection was discarded from the time-history to prevent extreme values of stiffness due to a division by an extremely small number.

Because deflection sensors were not placed at the support points during the Winfield barge impact tests, the deflections needed to be interpolated between existing sensor data. A linear interpolation was used given the relative deflections at the ends of the beam for each support point, giving an in-line displacement for the beam at the support point. A time-history of deflections at the support points were recorded for each of the Winfield tests. Because LVDT measurements were not recorded at the end of the upstream portion (from the barge approach in Figure J.1) of the beam for barge impact tests after test #13, the relative deflections at that end of the beam were approximated using a linear interpolation between the closest laser deflection sensors on either side of the beam end. Of course, one laser deflection sensor was on the upstream neighboring beam.

The shear forces at the support points of the beam were directly computed using Impact_Beam with output sensors specified at the support points. For each Winfield test, an appropriately scaled time-history (from the Impact_Force software), impact point, and forward velocity along the beam were input into Impact_Beam, as well as the appropriate beam properties. The average dynamic Young's modulus of 6,417.18 ksi for the beam that was determined in Chapter 6 was used in these calculations. The results were stored as a time-history of stresses at the upstream and downstream support points.

A time-history of upstream neoprene support stiffness was created by dividing each computed shear force from the upstream shear force time-history at each time increment by its concurrent deflection from the upstream deflection time-history, discarding values where the deflection was 20% or less of the maximum deflection, to avoid divisions by very small values. A similar process was used to produce a time-history of downstream neoprene support stiffness.

Figures K.2 – K.6 show the process discussed above in action for Winfield Test #10. Figure K.2 shows the input force time-history for Test #10 as it is output from Impact_Force, and the inverse of the summation of the

reactions forces at the support points for the flexible beam. The input force and the inverse sum of the reaction forces is comparable, which implies that the stiffness computation based on the reaction forces divided by the reaction deflections provide for a reasonable approximation for the dynamic stiffness of the neoprene pad. The reaction forces are shown in Figure K.3. The vertical scale has been inverted because the reaction forces are acting against the force of compression. The measured neoprene deflections are shown in Figure K.4 as well as the line delineating the filter below which stiffness values are not computed. For neoprene deflections above the filter line, stiffness values are calculated as discussed above. Figures K.5 and K.6 show the stiffness values calculated for the filtered reaction force divided by the deflection, resulting in stiffness units of kips per inch. A line demarking the average stiffness for upstream and downstream using the filtered values is also shown.

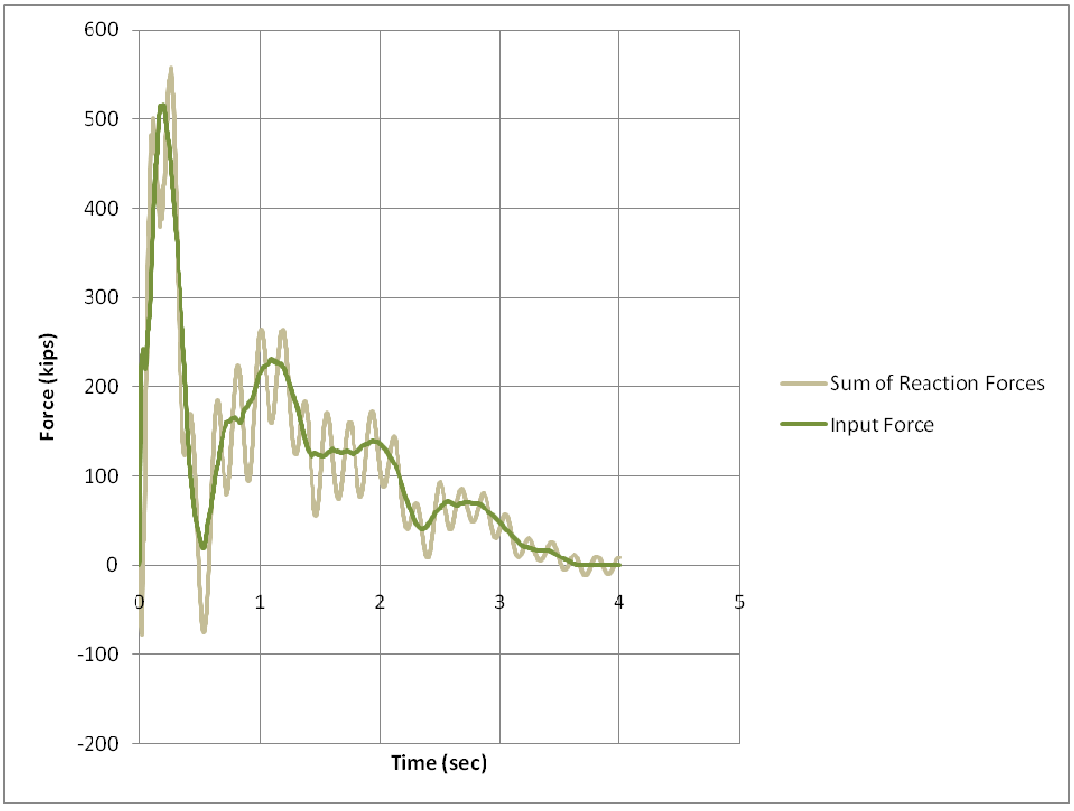

Figure K.2. Input Force and a comparison with the inverse sum of the reactions forces.

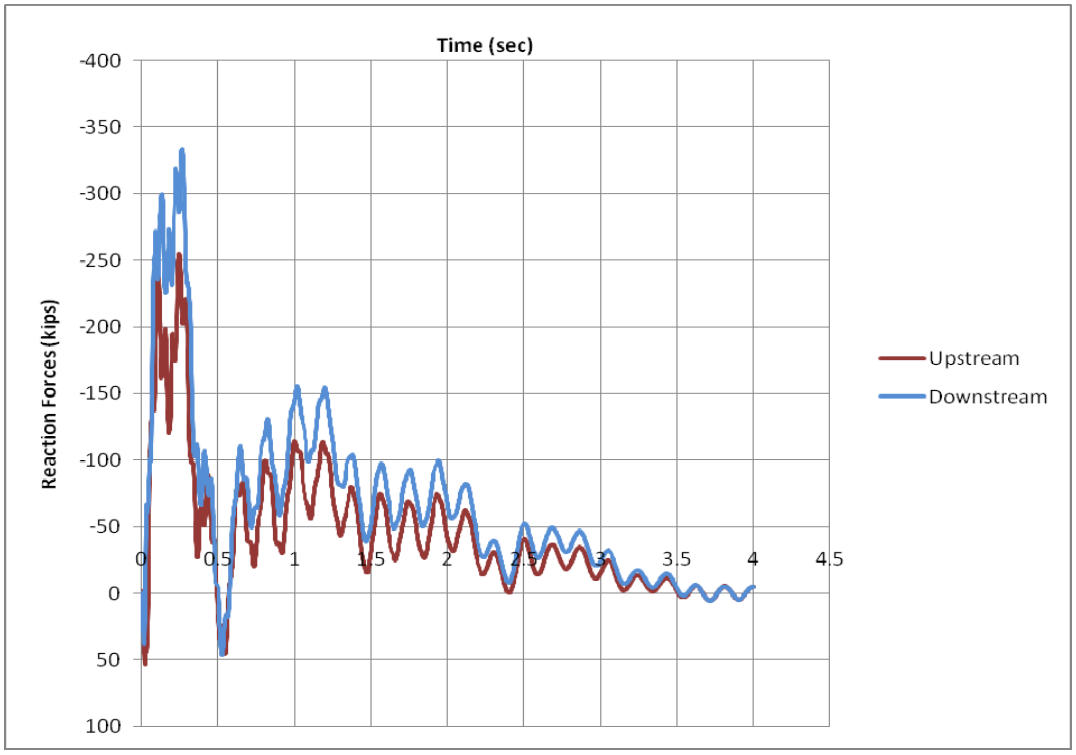

Figure K.3. Reaction forces at the supports for the flexible beam for Winfield Test #10.

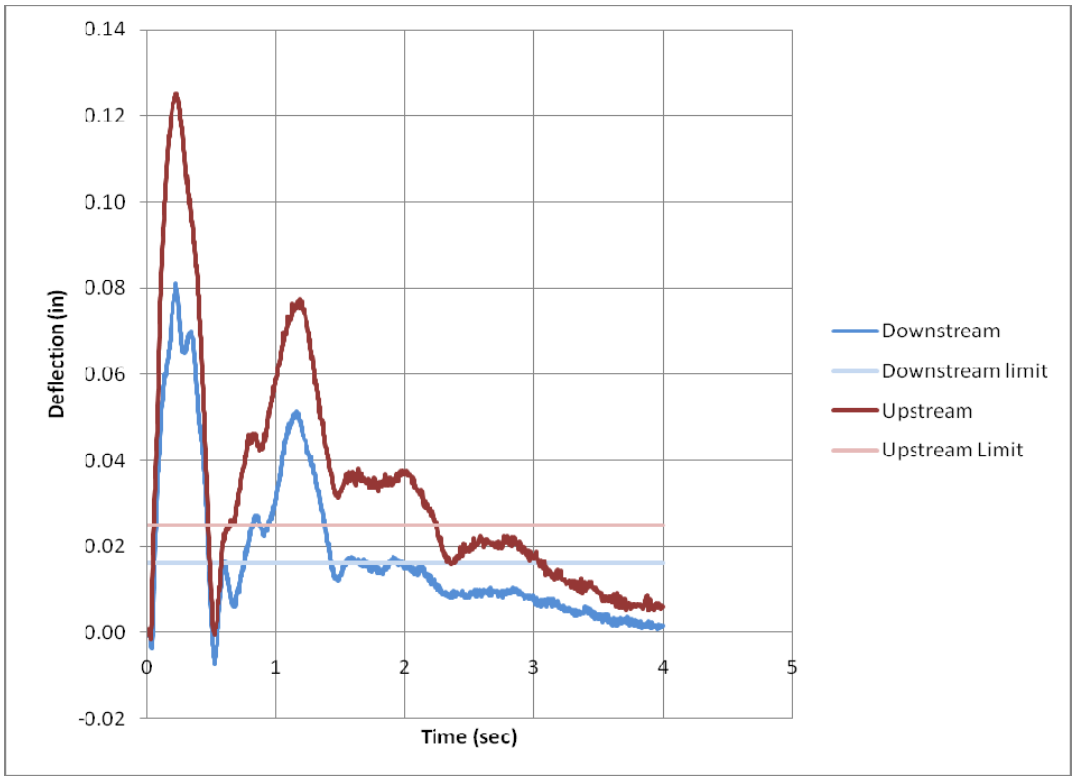

Figure K.4. Neoprene deflections at the support points for the flexible beam for Winfield Test #10. Included are the cut-off limits at 20% of peak value for stiffness computations.

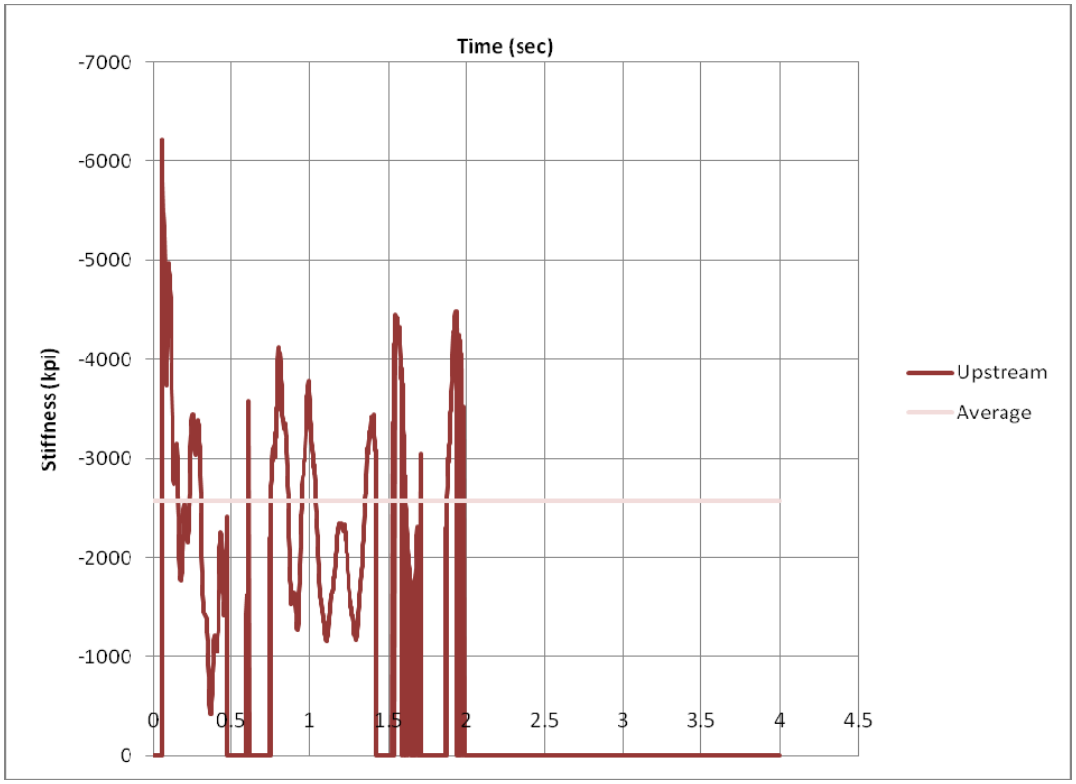

Figure K.5. The measured stiffness of the upstream neoprene pad for Winfield Test #10.

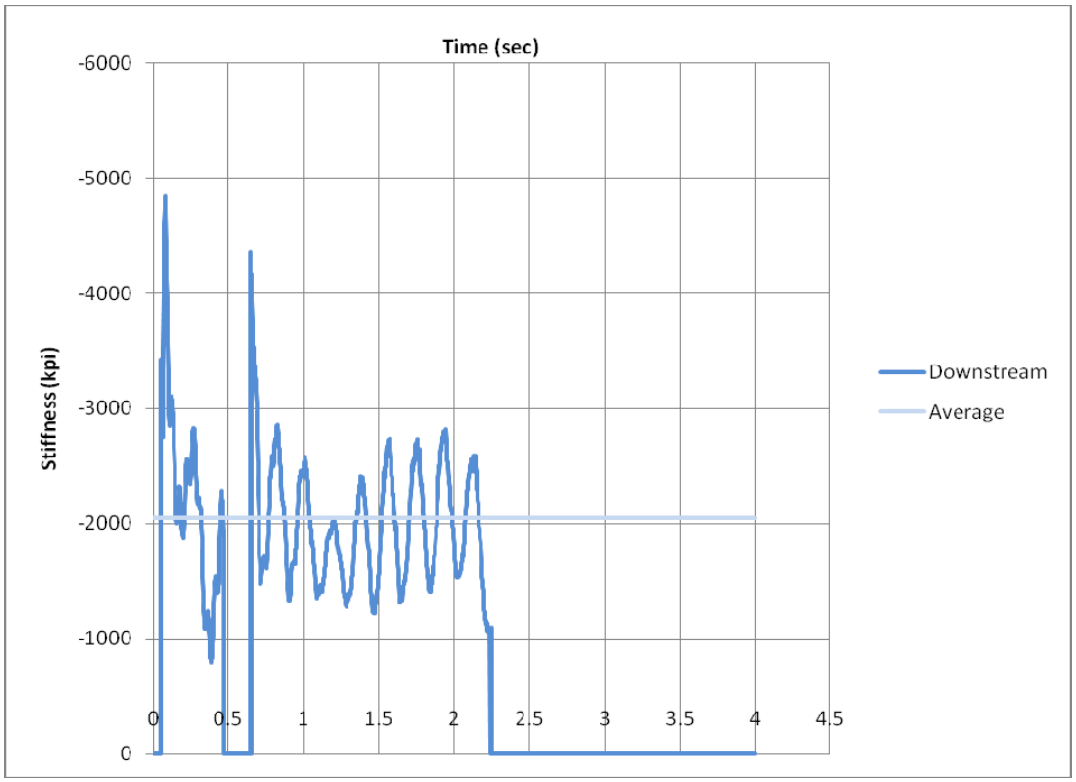

Figure K.6. The measured stiffness of the downstream neoprene pad for Winfield Test #10.

These computations were performed for all of the valid Winfield Barge Impact tests. Table K.1 summarizes the input data and the resulting average stiffnesses and statistical variations for these impact events. The upstream range of average stiffness varies from a minimum value of 2,032.07 kpi to a maximum value of 9,850.37 kpi. The 9,850.37 kpi value seems to be an outlier from the rest of the data, being nearly double the next highest value of 4,858.31 kpi. The coefficient of variation for the upstream stiffness varies from a low of 0.25 to a high of 1.87. The downstream range of average stiffness varies from a minimum value of 2,045.44 kpi to a maximum value of 3,009.20 kpi. The coefficient of variation for the downstream stiffness varies from a low of 0.24 to a high of 0.82.

From the measured averages of Table K.1, it is possible to determine the average values for the upstream *K*, the downstream *K*, and both upstream and downstream *K*. For all of the upstream *K*s, the average stiffness was 3,753 kips per inch. For all of the downstream *K*s, the mean of the average stiffness was 2,623 kips per inch. For both upstream and downstream *K* values, the mean of the average stiffness was 3,189 kips per inch. Given the high uncertainty of some values for *K*, another calculation of average stiffness for both upstream and downstream was calculated by discarding values where the coefficient of variation was greater than 0.6. When these five values were removed, the mean of the average stiffness value for the neoprene pads was calculated to be 2,921 kips per inch.

For Winfield Test #10, the maximum compression of the upstream and downstream neoprene pads corresponds to 0.081 inch and 0.125 inch, respectively, for the Impact_Beam computed peak forces of 255.3 kips and 334 kips. The compressive strains in the 1.75 inch thick elastomer layers of the two neoprene pads are equal to 4.6 percent and 7.1 percent. Because Winfield Test #10 has the greatest impact force applied to the beam, these compressive strains should be the maximums for all of the barge impact tests.

Table K.1. Average neoprene stiffness measured from Winfield Barge Impact Tests and their statistical properties.

Test #	Peak Force (kips)	Velocity (fps)	Angle (degrees)	Impact Location – center = 58.8 (ft)	Peak Deflection Upstream (in)	Peak Deflection Downstream (in)	Average Upstream k (kpi)	Average Downstream k (kpi)	Std Dev Upstream	Std Dev Downstream	COV Upstream	COV Downstream
6	285.66	8.802	16.98	66.30	0.050	0.071	4,059.64	2,659.01	2,659.01	709.13	0.65	0.27
7	255.18	10.269	14.78	68.50	0.043	0.063	4,195.30	2,615.65	1,660.87	707.33	0.40	0.27
8	296.49	11.736	9.58	39.90	0.058	0.063	4,858.31	2,509.34	1,723.94	975.35	0.35	0.39
9	359.3	13.203	14.78	49.10	0.066	0.082	4,381.25	2,240.58	1,422.82	769.76	0.32	0.34
10	516.44	14.670	16.88	66.60	0.081	0.125	2,570.97	2,045.44	1,057.60	613.38	0.41	0.30
11	124.56	16.137	16.98	94.60	0.012	0.031	2,032.07	2,909.61	3,800.28	1,438.78	1.87	0.49
12	58.8	17.604	6.18	74.70	0.006	0.012	2,853.48	3,009.20	2,691.89	1,478.41	0.94	0.49
13	150.17	19.071	11.48	64.40	0.022	0.031	3,493.30	2,973.77	1,563.17	1,058.93	0.45	0.36
14	110.93	20.538	9.08	43.60	0.006	0.016	9,850.37	2,760.96	8,016.26	2,265.83	0.81	0.82
15	235.41	22.005	14.58	32.60	0.058	0.044	3,644.39	2,364.69	1,028.84	1,283.95	0.28	0.54
16	354.97	23.472	9.18	63.40	0.081	0.096	2,346.27	2,651.24	666.19	660.70	0.28	0.25
17	255.87	24.939	15.28	62.60	0.051	0.058	2,288.48	2,802.94	855.46	813.15	0.37	0.29
20	411.03	29.340	13.58	62.60	0.095	0.110	2,221.15	2,555.54	563.80	604.95	0.25	0.24

K.3 Literature review for compression stiffness of laminated elastomer bearing pads

Table K.2 shows the plethora of literature evaluations for the stiffness of a neoprene pad, given the input pad parameters described above for the Winfield beam supports. The primary differences between the calculations are the equations for the shape function (S), which measures the ability of rubber to bulge given the shape of the rubber with loaded areas that are constrained not to spread (usually by vulcanization bonding with shims), and the equations for the compressive modulus (E_c) which is related to but not the same as Young's modulus (E_o) according to Derham (1982).

K.3.1 Shape function calculations

The shape function is used because of the high incompressibility of rubber (Derham 1982). The compression stiffness is therefore determined by the ability of rubber to bulge from the compression point, which is related to the shape of the rubber and how the rubber is laminated with shims. In this case, only the area along the perimeter of each layer of the bearing is allowed to bulge. According to Derham (1982), the shape function is defined by

$$S = \frac{one\,loaded\,area}{total\ force\ free\,area} \tag{K.1}$$

Because the laminated elastomer layers would be acting in parallel, the least stiffness layer would drive the compressibility of the entire laminated structure. Using Equation K.1, it is easy to prove that the thickest layer in an elastomer laminate, with the greatest total force free area, would have the smallest shape function and therefore have the lowest stiffness.

Derham (1982) uses a similar equation as AASHTO (1998) to define the rectangular shape function:

$$S = \frac{WL}{2t(W+L)} \tag{K.2}$$

Table K.2. Table of literature review equations and results given Winfield inputs for compressive neoprene pads.

Variable	value					Units	Equation Reference	Literature Equation Reference	Definition	Notes
width	16					in			plan width	
length	42					in			plan length	
tR	1.75					in			Total rubber thickness in the bearing	
t	0.5					in			thickness of individual layer	4 layers with shims between layers
A	672					in^2			plan area	calculated
a	25.92					in			plan dimension of a square bearing	calculated
Hardness	50								durometer measurement	
G	95					psi			shear modulus of elastomer	50 durometer neoprene
n	4								Number of laminations	
C	1.34							Podolny and Muller (Table 5.2)	Coefficient of restraint on lamination by shims - based on plan dimensions	linearly interpolated from the Table
S	12.96						K.3	Kelly (unreferenced immediately after 13.5)	Shape function (based on individual layer thickness)	based on individual layer thickness (which has been assumed)
		11.59					K.2	AASHTO Section 14		
Ec	107,730	86,082				psi	K.5	Kelly (13.6 square pad)	effective compressive modulus of a single layer	
			76,802				K.4	Derham 1982 Eq. 2		
				73,759			K.6	Derham 1982 Eq. 4		
Kv	41,368	33,055	29,492	28,323		kips/in	K.7	Kelly (13.13)	Vertical stiffness of the entire bearing	
					24,393	kips/in	K.9	Podolny and Muller (Equation 5-2)	(also known as the compressive stiffness)	
Ec/G	1134	906	808	776		unitless		Kelly (second unreferenced after 13.13)		
Kh	36.48	36.48	36.48	36.48		kips/in	K.11	Derived from Kelly (second unreferenced after 13.13)	Shear stiffness of the bearing	
	36.48					kips/in	K.10	Kelly (13.3 converted to kips/in)	This stiffness is based on the input values only	

where W and L are the width and length of the rectangular bearing, respectively, and t is the thickness of the thickest layer of elastomeric material (e.g. neoprene). Kelly (1991) assumes that his bearings are constrained to be square or circular in his shape function calculation(s). For a square bearing, Equation K.2 simplifies to

$$S = \frac{a}{4t} \tag{K.3}$$

where a is the length of the side of a bearing and t is the thickness of the bearing.

K.3.2 Compressive modulus calculations

For Table K.2, the square root of the rectangular area is used as the length a (of an equivalent square) for Equation K.3, to approximate the shape function for the bearing in the first value column of the table. This approximation was to be used in conjunction with the equation for the compressive modulus of a square bearing, discussed below. The more accurate rectangular Equation K.2 is used for the next three value columns.

From Derham (1982), the equation for the compressive modulus (E_c) is

$$E_C = 3G(1 + 2S^2) \tag{K.4}$$

where G is the shear modulus of the elastomer material. E_o should approximately equal $3G$ for a rubber material, which has a Poisson's ratio of nearly one half. For a rectangular pad, Kelly (1991) uses an approximation for the compressive modulus,

$$E_C = 6.75GS^2 \tag{K.5}$$

AASHTO uses a similar approximation for rectangular pads, with a constant of 6.0 instead of 6.75. Kelly's equation for the compressive modulus is used for value columns 1 and 2. Equation K.4 was used for column 3. G was given from tables of the typical values of G for the durometer measure of 50 IHRD.

According to international standards, the compressive modulus can also be defined according to the hardness of the elastomer material measured

with a durometer, and using the units of IRHD. The equation based on hardness is given by Derham to be

$$E_C = \frac{H^{1.9}}{900}\left\{\frac{1+9S^2}{1+4S^2}+2S^2\right\} \tag{K.6}$$

This equation returns units of *MPa*s, and care must be taken to convert to the units of choice. In this case, we are working with psi. Table K.2's fourth value column has the value determined by this equation converted to units of psi.

K.3.2 Compression stiffness and shear stiffness calculations

From the compressive modulus, the compression stiffness can be obtained by

$$K_V = \frac{E_C A}{t} \tag{K.7}$$

where K_V is the compression stiffness of the pad, A is the plan area of the pad, and t is the thickness of the thickest layer. This equation is the same for Derham (1982), Kelly (1991), and AASHTO (1998).

Podolny and Muller [1982] uses a different equation to determine the deflection due to compression of a laminate material,

$$v = C\frac{nt^2}{GA_b a^2}V \tag{K.8}$$

Where v is the compression displacement of the material, n is the number of layers, t is the thickness of the thickest layer, G is the shear modulus, A_b is the area of the pad, a is the length of the shortest side, and V is the applied compression force. Since the compression stiffness is the ratio of compression force to compression displacement, the equation simplifies to

$$K_V = C\frac{nt^2}{GA_b a^2} \tag{K.9}$$

This result is given in the fifth value column of Table K.2. Kelly [1991] also presented two equations for the shear stiffness of an elastomer laminate:

$$K_H = \frac{GA}{t_r} \tag{K.10}$$

where A is the plan area of the pad and t_r is the total thickness of the rubber in the pad, and

$$K_H = \frac{K_V G}{E_c} \tag{K.11}$$

Because K_H could be calculated with or without K_V, these equations were used as a check of the equations for K_V. The values for Equation K.11 are presented above the calculated value from Equation K.10 in Table K.2. Equation K.10 held for each variant of the equations for the compressive modulus (E_C).

K.4 Comparison of compression stiffness between literature review and values computed from measurements at Winfield

AASHTO (1998) provides a limit in any elastomeric bearing layer for bearings subject to shear deformation that the live-load compressive stress is

$$\sigma_L \leq 0.66 \cdot G \cdot S \tag{K.12}$$

where G is the shear modulus, and S is the Shape factor. For Winfield, G has a value of 95 psi for a 50 IRHD elastomer and the shape function S is 11.59 for a pad that is 16 inches by 42 inches, for a shear deformation of 726.7 psi. The largest reaction forces occurred during Winfield Test #10, and had a peak force of 255.3 kips for the upstream reaction and a peak force of 334 kips for the downstream reaction. The compressive stress is the reaction force divided by the area of the neoprene pad. The compressive stress for the neoprene pads during a live load is therefore 379.9 psi and 497 psi for the upstream and down neoprene pads, respectively. These compressive stresses are approximately 0.5 to 0.7 of the limiting compressive stress. Recall that Winfield Test #10 had a peak force value of 517.4 kips, the largest of the Barge Impact Tests. From these calculations we observe that the level of normal live load is significant but less than the AASHTO compression stress limit.

The reduction of the Winfield Barge Impact neoprene displacements combined with the Impact_Beam dynamic response computations for reaction forces, as summarized in Table K.1, indicate that the interpreted "average" value for the Dynamic spring stiffness is on the order of 3,188 kpi. This value is nearly an order of magnitude lower than the compression stiffnesses determined by the literature review, which ranged from 24,393 kips per inch to 41,368 kips per inch. The original INCA (1996) computations provide a compressive stiffness of 9,714 kips per inch for a TRANSU impact load of 680 kips acting on the neoprene pad. This was obtained by using the AASHTO (interim 1994) Figure 14.4.1.2a compressive stress versus compressive strain curve with a shape factor of 11.5. With the TRANSU Load of 680 kips acting on a Neoprene pad cross-sectional area of 672 square inches and the interim AASHTO curve, the corresponding compressive strain is 4%. The deflection of the 1.75 inch thick elastomer layers of the neoprene pad undergoing a compressive strain of 4% equals 0.07 inch. INCA then computed the compressive stiffness as equal to 680 kips divided by the deflection of 0.07 inch, resulting in the value of 9,714 kips per inch. This compressive stiffness computed by INCA is closer to the Winfield Barge Impact test results than the literature values.

In the Section 14 commentary of AASHTO (1998), it is recognized that the load-deflection curve of an elastomeric bearing is nonlinear, and that the compressive modulus (E_C) is load dependent. The authors of this report offer the speculation that the order of magnitude difference in the measured stiffness values and the literature calculated stiffness values is due to the difference in loads between a full barge impact test and the loads typically encountered for bridge bearing pads, which most of the literature covered. This assertion seems to be supported by the INCA calculations based on the usual condition TRANSU Load of 680 kips, where the calculated stiffness is closer to the measured values than the literature review values determined in Table K.2.

The authors also observe that the neoprene pads at Winfield have been in continuous service for approximately 20 years at the time of the Winfield Barge Impact testing. It is also possible that the effects of aging and deterioration on the neoprene pads may have affected their stiffness.

REPORT DOCUMENTATION PAGE

Form Approved
OMB No. 0704-0188

1. REPORT DATE *(DD-MM-YYYY)*	2. REPORT TYPE	3. DATES COVERED *(From - To)*
August 2011	Final Report	

4. TITLE AND SUBTITLE

Dynamic Structural Flexible-Beam Response to a Moving Barge Train Impact Force Time-History Using Impact_Beam

5a. CONTRACT NUMBER

5b. GRANT NUMBER

5c. PROGRAM ELEMENT NUMBER

6. AUTHOR(S)

Robert M. Ebeling, Abdul N. Mohamed, Jose R. Arroyo, Barry C. White, Ralph W. Strom, and Bruce C. Barker

5d. PROJECT NUMBER

5e. TASK NUMBER

5f. WORK UNIT NUMBER

7. PERFORMING ORGANIZATION NAME(S) AND ADDRESS(ES)

U.S. Army Engineer Research and Development Center
Information Technology Laboratory
3909 Halls Ferry Road
Vicksburg, MS 39180-6199

8. PERFORMING ORGANIZATION REPORT NUMBER

ERDC/ITL TR-11-1

9. SPONSORING / MONITORING AGENCY NAME(S) AND ADDRESS(ES)

10. SPONSOR/MONITOR'S ACRONYM(S)

11. SPONSOR/MONITOR'S REPORT NUMBER(S)

12. DISTRIBUTION / AVAILABILITY STATEMENT

Approved for public release; distribution is unlimited.

13. SUPPLEMENTARY NOTES

14. ABSTRACT

To design simply-supported, flexible impact beams spanning between cells or bents for lock approach walls, a dynamic structural analysis of the beam under impact time-history loads for design- specific barge trains is required. At several locks, this flexible structural feature is the primary structural member resisting the glancing-blow impact event of a barge train as it aligns itself with a lock. This technical report describes an engineering methodology used to conduct this dynamic structural analysis and visualize the resulting deflections, moments, and shears. This engineering methodology is implemented with a PC-based FORTRAN program and visual modeler named Impact_Beam. The engineering formulation for Impact_Beam uses time-history force data that are scaled for design specific barge trains to perform a dynamic structural response analysis for either a single degree of freedom system or a modal time-history analysis for the simply supported beam subjected to a impact load that is travelling along the beam. Time-history force data has been collected from the interpretation of the results from the 1997 full-scale barge train impact prototype experiments conducted at Old Lock and Dam 2 just north of Pittsburgh, PA, and of the 2008 full-scale barge train impact experiments conducted at Winfield Lock and Dam, Winfield, WV. This database of pulse time-history can be scaled for site specific design barge trains with approach angle and velocity using the companion software Impact_Force. It is also possible to use force time-histories from other impact simulation software (e.g.. dBEAS). The engineering formulation for Impact_Beam is verified against the original Winfield experiments using modal time-history analysis and dBEAS simulations using single degree of freedom analysis.

15. SUBJECT TERMS				
Barge impact	Dynamic analysis	Force time-history	Guide wall	Impact_Force
Barge train impact	Dynamic structural analysis	Glancing blow	Impact beam	Simply supported beam
	Flexible lock approach wall	Guard wall	Impact_Beam	Time-history analysis

16. SECURITY CLASSIFICATION OF:			17. LIMITATION OF ABSTRACT	18. NUMBER OF PAGES	19a. NAME OF RESPONSIBLE PERSON
a. REPORT	b. ABSTRACT	c. THIS PAGE			19b. TELEPHONE NUMBER *(include area code)*
UNCLASSIFIED	UNCLASSIFIED	UNCLASSIFIED		301	